

NPS ARCHIVE
1998.06
TITLEY, D.

NAVAL POSTGRADUATE SCHOOL Monterey, California



DISSERTATION

INTENSIFICATION AND STRUCTURE
CHANGE OF SUPER TYPHOON FLO AS
RELATED TO THE LARGE-SCALE
ENVIRONMENT

by

David W. Titley

June 1998

Dissertation Supervisor:

Russell L. Elsberry

Thesis
T5565

Approved for public release; distribution is unlimited.

DUDLEY KNOX
NAVAL POSTGRADUATE SCHOOL
MONTEREY, CA

SCHOOL
1

DUDLEY KNOX LIBRARY
NAVAL POSTGRADUATE SCHOOL
MONTEREY, CA 93943-5101

REPORT DOCUMENTATION PAGE

Form Approved OMB No. 0704-0188

Public reporting burden for this collection of information is estimated to average 1 hour per response, including the time for reviewing instruction, searching existing data sources, gathering and maintaining the data needed, and completing and reviewing the collection of information. Send comments regarding this burden estimate or any other aspect of this collection of information, including suggestions for reducing this burden, to Washington Headquarters Services, Directorate for Information Operations and Reports, 1215 Jefferson Davis Highway, Suite 1204, Arlington, VA 22202-4302, and to the Office of Management and Budget, Paperwork Reduction Project (0704-0188) Washington DC 20503.

| | | | |
|---|--|---|----------------------------------|
| 1. AGENCY USE ONLY (Leave blank) | 2. REPORT DATE June 1998. | 3. REPORT TYPE AND DATES COVERED Doctoral Dissertation | |
| 4. TITLE AND SUBTITLE Intensification and Structure Change of Super Typhoon Flo as Related to the Large-Scale Environment | | 5. FUNDING NUMBERS | |
| 6. AUTHOR(S) Titley, David W. | | 8. PERFORMING ORGANIZATION REPORT NUMBER | |
| 7. PERFORMING ORGANIZATION NAME(S) AND ADDRESS(ES) Naval Postgraduate School Monterey CA 93943-5000 | | 10. SPONSORING/MONITORING AGENCY REPORT NUMBER | |
| 9. SPONSORING/MONITORING AGENCY NAME(S) AND ADDRESS(ES) | | 11. SUPPLEMENTARY NOTES The views expressed in this thesis are those of the author and do not reflect the official policy or position of the Department of Defense or the U.S. Government. | |
| 12a. DISTRIBUTION/AVAILABILITY STATEMENT Approved for public release; distribution is unlimited. | | 12b. DISTRIBUTION CODE | |
| 13. ABSTRACT (maximum 200 words) A Multi-Quadric (MQ) analysis is developed and compared with the four-dimensional data assimilation analyses of the structure of Typhoons Flo and Ed during the Tropical Cyclone Motion (TCM-90) field experiment. The MQ analysis has been shown to provide an alternate, plausible depiction of the tropical atmosphere. These analyses are used to compare physical processes leading to rapid intensification of Flo, but not of Ed. Significant documentations include: (i) the existence of a "cyclonic wind burst" extending beyond 1000 km radius at 200 mb during the forcing phase for Typhoon Flo, which appears to be the result of strong, sustained eddy flux convergence of angular momentum (EFC) in the upper troposphere; (ii) a complex EFC vertical structure that evolved with time; (iii) Flo had developed a warmer core near the tropopause, and was less stable than Ed in the upper troposphere prior to the beginning of the rapid intensification period; (iv) a high correlation of the mid-troposphere azimuthally-averaged absolute vorticity with the 48-h future intensity of four tropical cyclones; and (v) the 850 - 200 mb vertical wind shear for Typhoon Ed was less than the vertical shear calculated for Typhoon Flo, which implies that low vertical shear, although necessary for significant storm development is not, by itself, a sufficient dynamic factor to ensure rapid intensification. A conceptual model is proposed for tropical cyclone rapid intensification and subsequent weakening that accounts for varying EFC and vertical shear values. Although based on Typhoons Ed and Flo, this model is also consistent with intensity changes of Typhoons Yancy and Zola. | | | |
| 14. SUBJECT TERMS Tropical Cyclone Intensification, Objective Analysis Method, Multi-Quadric Analysis. | | 15. NUMBER OF PAGES 389 | |
| | | 16. PRICE CODE | |
| 17. SECURITY CLASSIFICATION OF REPORT Unclassified | 18. SECURITY CLASSIFICATION OF THIS PAGE Unclassified | 19. SECURITY CLASSIFICATION OF ABSTRACT Unclassified | 20. LIMITATION OF ABSTRACT UL |

Approved for public release; distribution is unlimited.

**INTENSIFICATION AND STRUCTURE CHANGE OF SUPER TYPHOON FLO
AS RELATED TO THE LARGE-SCALE ENVIRONMENT**

David W. Titley
Commander, United States Navy
B.S., The Pennsylvania State University, 1980
M.S., Naval Postgraduate School, 1991

Submitted in partial fulfillment of the requirements for the degree of

DOCTOR OF PHILOSOPHY IN METEOROLOGY

from the

**NAVAL POSTGRADUATE SCHOOL
June 1998**

ABSTRACT

A Multi-Quadric (MQ) analysis is developed and compared with the four-dimensional data assimilation analyses of the structure of Typhoons Flo and Ed during the Tropical Cyclone Motion (TCM-90) field experiment. The MQ analysis has been shown to provide an alternate, plausible depiction of the tropical atmosphere. These analyses are used to compare physical processes leading to rapid intensification of Flo, but not of Ed. Significant documentations include: (i) the existence of a "cyclonic wind burst" extending beyond 1000 km radius at 200 mb during the forcing phase for Typhoon Flo, which appears to be the result of strong, sustained eddy flux convergence of angular momentum (EFC) in the upper troposphere; (ii) a complex EFC vertical structure that evolved with time; (iii) Flo had developed a warmer core near the tropopause, and was less stable than Ed in the upper troposphere prior to the beginning of the rapid intensification period; (iv) a high correlation of the mid-troposphere azimuthally-averaged absolute vorticity with the 48-h future intensity of four tropical cyclones; and (v) the 850 - 200 mb vertical wind shear for Typhoon Ed was less than the vertical shear calculated for Typhoon Flo, which implies that low vertical shear, although necessary for significant storm development is not, by itself, a sufficient dynamic factor to ensure rapid intensification. A conceptual model is proposed for tropical cyclone rapid intensification and subsequent weakening that accounts for varying EFC and vertical shear values. Although based on Typhoons Ed and Flo, this model is also consistent with intensity changes of Typhoons Yancy and Zola.

TABLE OF CONTENTS

| | |
|--|----|
| I. INTRODUCTION | 1 |
| A. MOTIVATION | 1 |
| B. PREVIOUS WORK ON TROPICAL CYCLONE INTENSITY | 4 |
| 1. Thermodynamic Considerations | 6 |
| 2. Mid-latitude and Tropical Upper Tropospheric Trough (TUTT) Interactions with Tropical Cyclones | 12 |
| 3. Vertical Wind Shear | 21 |
| 4. Identification of Common Predictors for Tropical Cyclone Intensification | 23 |
| C. GOALS AND HYPOTHESES | 24 |
| D. APPROACH | 26 |
| II. DATA ANALYSIS | 29 |
| A. TROPICAL CYCLONE MOTION FIELD EXPERIMENT | 29 |
| B. GRIDDED ANALYSES | 34 |
| C. ANALYSIS METHOD | 34 |
| 1. Background | 34 |
| 2. Method Chosen | 36 |
| a. Multi-Quadric Method | 37 |
| (1) Smoothing. | 39 |

| | | |
|----|---|----|
| | (2) Dynamic Constraints. | 44 |
| b. | Application of the Multi-Quadric Method | 45 |
| | (1) Increment Analysis | 45 |
| | (2) Horizontal Resolution. | 52 |
| | (3) Vertical Resolution. | 52 |
| | (4) Analysis Domain. | 52 |
| | (5) Analyzed Parameters. | 54 |
| 3. | Summary | 54 |
| D. | DATA MANAGEMENT | 55 |
| 1. | Data Preparation | 57 |
| 2. | Quality Control | 57 |
| E. | LOCAL OBJECTIVE ANALYSIS SCHEME | 58 |
| 1. | Observation Quality Control | 60 |
| a. | Horizontal Quality Control Checks | 60 |
| b. | Radiation Error Corrections | 68 |
| c. | DC-8 and LORAN Dropwindsonde Height Observations | 72 |
| | (1) Adjusting the heights to the nearest mandatory pressure level. | 72 |
| | (2) DC-8 and LORAN Dropwindsonde Height Bias. | 73 |

| | | |
|----|---|-----|
| 2. | Dynamic Constraints | 76 |
| 3. | First-Guess Modifications | 81 |
| 4. | Observation Enhancements | 90 |
| a. | Composite Observations | 90 |
| b. | Synthetic Observations | 91 |
| | (1) Zero-bogus Observations. | 91 |
| | (2) Typhoon Depiction Observations.. . . . | 95 |
| 5. | Post-processing the Tropical Cyclone Wind Field | 98 |
| 6. | 0600 and 1800 UTC Analyses | 99 |
| 7. | Summary | 99 |
| F. | VORTICITY, DIVERGENCE, AND VERTICAL VELOCITY CALCULATIONS | 101 |
| 1. | Vorticity | 101 |
| 2. | Divergence | 102 |
| 3. | Vertical Motion | 102 |
| a. | Computing the Surface Pressure | 103 |
| b. | Converting vertical velocity from $\mu\text{bar s}^{-1}$ to m s^{-1} | 105 |
| 4. | Summary | 105 |

| | |
|--|-----|
| III. INITIAL VALIDATION OF THE MULTI-QUADRIC ANALYSES | 107 |
| A. VALIDATION AND COMPARISON OF THE MULTI-QUADRIC ANALYSES | 107 |
| 1. Qualitative Checks | 108 |
| a. Two-Dimensional Plots | 108 |
| b. Comparison With Rucker Hand Analyses | 110 |
| c. Dataset Visualization | 116 |
| 2. Quantitative Checks | 121 |
| a. Root Mean Square Evaluation | 121 |
| (1) Wind RMS Calculations. | 123 |
| (2) Height RMS Calculations. | 135 |
| (3) RMS Summary. | 138 |
| b. Propagation Vector Analysis | 140 |
| (1) Introduction | 140 |
| (2) Typhoon Flo Storm Motion, Large-Scale Steering Flow, and Propagation Vectors. | 143 |
| c. Azimuthally-Averaged Winds in the Vicinity of Typhoon Flo | 148 |
| (1) 850 mb Tangential Wind Speed. | 149 |
| (2) 200 mb Tangential Wind Speed. | 155 |

| | |
|--|-----|
| (3) Vertical Cross-Sections of Tangential Wind | |
| Speed. | 161 |
| (4) 850 mb Radial Wind Speed. | 163 |
| (5) 200 mb Radial Wind Speed. | 168 |
| (6) Vertical Cross-Sections of Radial Wind Speed. | 172 |
| (7) Summary. | 174 |
| B. ANALYSIS CONCLUSIONS | 177 |
| C. FUTURE ANALYSIS WORK | 179 |
| 1. Multi-Quadric Analysis Enhancements | 179 |
| 2. Data Impact and Sensitivity Studies | 180 |
| IV. DISCUSSION OF DYNAMICS OF TYPHOONS ED AND FLO | 183 |
| A. STRENGTHS AND LIMITATIONS OF THE ANALYSES | 183 |
| B. EFFECT OF THERMAL INFLUENCES ON TYPHOONS ED AND FLO | 184 |
| 1. Sea-Surface Temperature | 184 |
| 2. Thermal Structure of Ed and Flo | 186 |
| a. Background | 186 |
| b. Analysis Method | 187 |
| c. Results | 189 |

| | | |
|----|--|-----|
| C. | TIME EVOLUTION OF UPPER-TROPOSPHERIC WINDS IN TYPHOONS ED AND FLO | 190 |
| 1. | Motivation | 190 |
| 2. | Analysis Method | 191 |
| a. | Tangential and Radial Wind Calculations | 191 |
| b. | Vertical Wind Shear Calculations | 193 |
| 3. | Typhoon Flo | 193 |
| a. | Forcing Phase (00 UTC 13 September to 12 UTC 14 September) | 194 |
| | (1) Tangential Wind. | 196 |
| | (2) Radial Wind. | 200 |
| | (3) Eddy Flux Convergence of Relative Angular Momentum. | 212 |
| | (4) Vertical Wind Shear. | 218 |
| | (5) Discussion and Conclusions. | 221 |
| b. | Quiescent Forcing Phase (18 UTC 14 September through 12 UTC 16 September) | 225 |
| | (1) Contraction Phase. | 225 |
| | (2) Rapid Intensification Phase. | 234 |
| c. | Super Typhoon Phase (12 UTC 16 September through 18 UTC 17 September) | 249 |

| | | |
|----|--|-----|
| d. | Mid-latitude Interaction Phase (00 UTC 18 September to 00 UTC 19 September) | 263 |
| 4. | Typhoon Ed | 276 |
| a. | Total Wind Field | 276 |
| b. | Tangential and Radial Winds | 281 |
| c. | Relative Angular Momentum Eddy Flux Convergence | 287 |
| d. | Vertical Wind Shear | 293 |
| D. | CORRELATION BETWEEN PHYSICAL PARAMETERS AND STORM INTENSITY AND INTENSITY CHANGE | 295 |
| 1. | Relative Angular Momentum Eddy Flux Convergence | 298 |
| 2. | Tangential Wind | 302 |
| 3. | Radial Wind | 304 |
| 4. | Absolute Vorticity | 310 |
| E. | WIND SHEAR | 314 |
| F. | SUMMARY | 318 |
| V. | SUMMARY, CONCLUSIONS AND RECOMMENDATIONS | 325 |
| A. | SUMMARY | 325 |
| B. | CONCLUSIONS | 327 |
| 1. | Objective Mesoscale Analysis | 327 |

| | | |
|---|--|-----|
| 2. | Tropical Cyclone Intensification DynamicsNew Findings . . . | 329 |
| a. | Proposed View of Tropical Cyclone Intensification and Weakening | 333 |
| b. | Typhoons Yancy and Zola | 335 |
| 3. | Recommendations | 339 |
| APPENDIX A. QUALITY CONTROL PROCEDURES | | 341 |
| A. | INTRODUCTION | 341 |
| B. | METHOD | 341 |
| C. | SUMMARY | 344 |
| APPENDIX B. INITIAL DATA PROCESSING | | 347 |
| A. | METHOD | 347 |
| 1. | Rawinsonde Data | 347 |
| 2. | Reprocessed Cloud-Tracked Winds | 348 |
| 3. | Operational Cloud-Tracked Winds | 348 |
| 4. | Commercial Aircraft Reports | 348 |
| 5. | DC-8 Flight-Level Observations | 349 |
| B. | FINAL STEP | 349 |
| APPENDIX C. NINE-POINT TROPICAL CYCLONE BOGUS PROCEDURE | | 351 |

| | |
|-------------------------------------|-----|
| LIST OF REFERENCES | 355 |
| INITIAL DISTRIBUTION LIST | 367 |

| | |
|-------------------------------------|---|
| LIST OF CONTENTS | 1 |
| FOREWORD | 1 |
| 1. INTRODUCTION | 1 |
| 2. THE PROBLEM | 1 |
| 3. THE METHOD | 1 |
| 4. THE RESULTS | 1 |
| 5. THE CONCLUSIONS | 1 |
| 6. THE APPENDICES | 1 |
| 7. THE REFERENCES | 1 |
| 8. THE INDEX | 1 |
| 9. THE BIBLIOGRAPHY | 1 |
| 10. THE GLOSSARY | 1 |
| 11. THE ABBREVIATIONS | 1 |
| 12. THE SYMBOLS | 1 |
| 13. THE UNITS | 1 |
| 14. THE FORMULAE | 1 |
| 15. THE TABLES | 1 |
| 16. THE FIGURES | 1 |
| 17. THE PLATES | 1 |
| 18. THE MAPS | 1 |
| 19. THE PHOTOGRAPHS | 1 |
| 20. THE FILMS | 1 |
| 21. THE SLIDES | 1 |
| 22. THE MICROFILMS | 1 |
| 23. THE TAPES | 1 |
| 24. THE DISKS | 1 |
| 25. THE CARTRIDGES | 1 |
| 26. THE MAGNETS | 1 |
| 27. THE COILS | 1 |
| 28. THE RESISTORS | 1 |
| 29. THE CAPACITORS | 1 |
| 30. THE DIODES | 1 |
| 31. THE TRIODES | 1 |
| 32. THE TETRODES | 1 |
| 33. THE PENTODES | 1 |
| 34. THE HEXODES | 1 |
| 35. THE SEPTODES | 1 |
| 36. THE OCTODES | 1 |
| 37. THE NONODES | 1 |
| 38. THE DECADES | 1 |
| 39. THE ELEVENTHS | 1 |
| 40. THE TWELVES | 1 |
| 41. THE THIRTEENS | 1 |
| 42. THE FOURTEENS | 1 |
| 43. THE FIFTEENS | 1 |
| 44. THE SIXTEENS | 1 |
| 45. THE SEVENTEENS | 1 |
| 46. THE EIGHTEENS | 1 |
| 47. THE NINETEENS | 1 |
| 48. THE TWENTYS | 1 |
| 49. THE THIRTYS | 1 |
| 50. THE FORTYS | 1 |
| 51. THE FIFTYS | 1 |
| 52. THE SIXTYS | 1 |
| 53. THE SEVENTYS | 1 |
| 54. THE EIGHTYS | 1 |
| 55. THE NINETYS | 1 |
| 56. THE HUNDREDS | 1 |
| 57. THE THOUSANDS | 1 |
| 58. THE MILLIONS | 1 |
| 59. THE BILLIONS | 1 |
| 60. THE TRILLIONS | 1 |
| 61. THE QUADRILLIONS | 1 |
| 62. THE QUINTILLIONS | 1 |
| 63. THE SEXTILLIONS | 1 |
| 64. THE SEPTILLIONS | 1 |
| 65. THE OCTILLIONS | 1 |
| 66. THE NONILLIONS | 1 |
| 67. THE DECILLIONS | 1 |
| 68. THE UNDECILLIONS | 1 |
| 69. THE DUODECILLIONS | 1 |
| 70. THE TREDECILLIONS | 1 |
| 71. THE QUADRDECILLIONS | 1 |
| 72. THE QUINTDECILLIONS | 1 |
| 73. THE SEXDECILLIONS | 1 |
| 74. THE SEPTDECILLIONS | 1 |
| 75. THE OCTDECILLIONS | 1 |
| 76. THE NONDECILLIONS | 1 |
| 77. THE VIGINTILLIONS | 1 |
| 78. THE TRIGINTILLIONS | 1 |
| 79. THE QUADRIGINTILLIONS | 1 |
| 80. THE QUINQUAGINTILLIONS | 1 |
| 81. THE SEXAGINTILLIONS | 1 |
| 82. THE SEPTUAGINTILLIONS | 1 |
| 83. THE OCTOGINTILLIONS | 1 |
| 84. THE NONAGINTILLIONS | 1 |
| 85. THE CENTILLIONS | 1 |
| 86. THE MILLENTILLIONS | 1 |
| 87. THE BILLYONNTILLIONS | 1 |
| 88. THE TRILLYONNTILLIONS | 1 |
| 89. THE QUADRILLYONNTILLIONS | 1 |
| 90. THE QUINTILLYONNTILLIONS | 1 |
| 91. THE SEXTILLYONNTILLIONS | 1 |
| 92. THE SEPTILLYONNTILLIONS | 1 |
| 93. THE OCTILLYONNTILLIONS | 1 |
| 94. THE NONILLYONNTILLIONS | 1 |
| 95. THE DECILLYONNTILLIONS | 1 |
| 96. THE UNDECILLYONNTILLIONS | 1 |
| 97. THE DUODECILLYONNTILLIONS | 1 |
| 98. THE TREDECILLYONNTILLIONS | 1 |
| 99. THE QUADREDECILLYONNTILLIONS | 1 |
| 100. THE QUINTREDECILLYONNTILLIONS | 1 |
| 101. THE SEXREDECILLYONNTILLIONS | 1 |
| 102. THE SEPTREDECILLYONNTILLIONS | 1 |
| 103. THE OCTREDECILLYONNTILLIONS | 1 |
| 104. THE NONREDECILLYONNTILLIONS | 1 |
| 105. THE VIGINTILLYONNTILLIONS | 1 |
| 106. THE TRIGINTILLYONNTILLIONS | 1 |
| 107. THE QUADRIGINTILLYONNTILLIONS | 1 |
| 108. THE QUINQUAGINTILLYONNTILLIONS | 1 |
| 109. THE SEXAGINTILLYONNTILLIONS | 1 |
| 110. THE SEPTUAGINTILLYONNTILLIONS | 1 |
| 111. THE OCTOGINTILLYONNTILLIONS | 1 |
| 112. THE NONAGINTILLYONNTILLIONS | 1 |
| 113. THE CENTILLYONNTILLIONS | 1 |
| 114. THE MILLENTILLYONNTILLIONS | 1 |
| 115. THE BILLYONNTILLIONS | 1 |
| 116. THE TRILLYONNTILLIONS | 1 |
| 117. THE QUADRILLYONNTILLIONS | 1 |
| 118. THE QUINTILLYONNTILLIONS | 1 |
| 119. THE SEXTILLYONNTILLIONS | 1 |
| 120. THE SEPTILLYONNTILLIONS | 1 |
| 121. THE OCTILLYONNTILLIONS | 1 |
| 122. THE NONILLYONNTILLIONS | 1 |
| 123. THE DECILLYONNTILLIONS | 1 |
| 124. THE UNDECILLYONNTILLIONS | 1 |
| 125. THE DUODECILLYONNTILLIONS | 1 |
| 126. THE TREDECILLYONNTILLIONS | 1 |
| 127. THE QUADREDECILLYONNTILLIONS | 1 |
| 128. THE QUINTREDECILLYONNTILLIONS | 1 |
| 129. THE SEXREDECILLYONNTILLIONS | 1 |
| 130. THE SEPTREDECILLYONNTILLIONS | 1 |
| 131. THE OCTREDECILLYONNTILLIONS | 1 |
| 132. THE NONREDECILLYONNTILLIONS | 1 |
| 133. THE VIGINTILLYONNTILLIONS | 1 |
| 134. THE TRIGINTILLYONNTILLIONS | 1 |
| 135. THE QUADRIGINTILLYONNTILLIONS | 1 |
| 136. THE QUINQUAGINTILLYONNTILLIONS | 1 |
| 137. THE SEXAGINTILLYONNTILLIONS | 1 |
| 138. THE SEPTUAGINTILLYONNTILLIONS | 1 |
| 139. THE OCTOGINTILLYONNTILLIONS | 1 |
| 140. THE NONAGINTILLYONNTILLIONS | 1 |
| 141. THE CENTILLYONNTILLIONS | 1 |
| 142. THE MILLENTILLYONNTILLIONS | 1 |
| 143. THE BILLYONNTILLIONS | 1 |
| 144. THE TRILLYONNTILLIONS | 1 |
| 145. THE QUADRILLYONNTILLIONS | 1 |
| 146. THE QUINTILLYONNTILLIONS | 1 |
| 147. THE SEXTILLYONNTILLIONS | 1 |
| 148. THE SEPTILLYONNTILLIONS | 1 |
| 149. THE OCTILLYONNTILLIONS | 1 |
| 150. THE NONILLYONNTILLIONS | 1 |
| 151. THE DECILLYONNTILLIONS | 1 |
| 152. THE UNDECILLYONNTILLIONS | 1 |
| 153. THE DUODECILLYONNTILLIONS | 1 |
| 154. THE TREDECILLYONNTILLIONS | 1 |
| 155. THE QUADREDECILLYONNTILLIONS | 1 |
| 156. THE QUINTREDECILLYONNTILLIONS | 1 |
| 157. THE SEXREDECILLYONNTILLIONS | 1 |
| 158. THE SEPTREDECILLYONNTILLIONS | 1 |
| 159. THE OCTREDECILLYONNTILLIONS | 1 |
| 160. THE NONREDECILLYONNTILLIONS | 1 |
| 161. THE VIGINTILLYONNTILLIONS | 1 |
| 162. THE TRIGINTILLYONNTILLIONS | 1 |
| 163. THE QUADRIGINTILLYONNTILLIONS | 1 |
| 164. THE QUINQUAGINTILLYONNTILLIONS | 1 |
| 165. THE SEXAGINTILLYONNTILLIONS | 1 |
| 166. THE SEPTUAGINTILLYONNTILLIONS | 1 |
| 167. THE OCTOGINTILLYONNTILLIONS | 1 |
| 168. THE NONAGINTILLYONNTILLIONS | 1 |
| 169. THE CENTILLYONNTILLIONS | 1 |
| 170. THE MILLENTILLYONNTILLIONS | 1 |
| 171. THE BILLYONNTILLIONS | 1 |
| 172. THE TRILLYONNTILLIONS | 1 |
| 173. THE QUADRILLYONNTILLIONS | 1 |
| 174. THE QUINTILLYONNTILLIONS | 1 |
| 175. THE SEXTILLYONNTILLIONS | 1 |
| 176. THE SEPTILLYONNTILLIONS | 1 |
| 177. THE OCTILLYONNTILLIONS | 1 |
| 178. THE NONILLYONNTILLIONS | 1 |
| 179. THE DECILLYONNTILLIONS | 1 |
| 180. THE UNDECILLYONNTILLIONS | 1 |
| 181. THE DUODECILLYONNTILLIONS | 1 |
| 182. THE TREDECILLYONNTILLIONS | 1 |
| 183. THE QUADREDECILLYONNTILLIONS | 1 |
| 184. THE QUINTREDECILLYONNTILLIONS | 1 |
| 185. THE SEXREDECILLYONNTILLIONS | 1 |
| 186. THE SEPTREDECILLYONNTILLIONS | 1 |
| 187. THE OCTREDECILLYONNTILLIONS | 1 |
| 188. THE NONREDECILLYONNTILLIONS | 1 |
| 189. THE VIGINTILLYONNTILLIONS | 1 |
| 190. THE TRIGINTILLYONNTILLIONS | 1 |
| 191. THE QUADRIGINTILLYONNTILLIONS | 1 |
| 192. THE QUINQUAGINTILLYONNTILLIONS | 1 |
| 193. THE SEXAGINTILLYONNTILLIONS | 1 |
| 194. THE SEPTUAGINTILLYONNTILLIONS | 1 |
| 195. THE OCTOGINTILLYONNTILLIONS | 1 |
| 196. THE NONAGINTILLYONNTILLIONS | 1 |
| 197. THE CENTILLYONNTILLIONS | 1 |
| 198. THE MILLENTILLYONNTILLIONS | 1 |
| 199. THE BILLYONNTILLIONS | 1 |
| 200. THE TRILLYONNTILLIONS | 1 |

ACKNOWLEDGMENTS

During the past six years, this dissertation has reminded me each day how fortunate I have been to be associated with so many people, both military and civilian, who have gone out of their way to ensure this project was completed.

This dissertation simply would not have been written without Professor Russ Elsberry's guidance, encouragement, wisdom, (and green editing pen!). Russ asked the right questions at the right time, and demanded critical thinking in every phase of this research. He let me make my own discoveries, and track down my (not infrequent!) dead-ends. He did not give up on this project when it would have been very easy to do so. Thanks, Russ. I would like to thank the other members of my committee, Professors Wendell Nuss, R. T. Williams, Peter Chu of the Naval Postgraduate School (NPS), and Dr. Hugh Willoughby from the Hurricane Research Division, for their time and comments. Their input substantially improved the quality of the final product. I would also like to thank Professors Bob Haney, Chuck Wash, Patricia Pauley, and Richard Franke for their thoughts and constructive comments.

Computation services were provided by the W. R. Church Computer Center at NPS. In addition, Dennis Mar, Helen Davis, Ruth Roy, and Larry Frazier all cheerfully answered my many questions about Job Control Language, DISSPLA, account extensions, and thesis formatting, respectively.

I would like to thank Admirals Art Cebrowski, Mike Bowman, and Paul Gaffney, and Captains Tom Blount Jr. (Ret.), Dieter Rudolph, Larry Warrenfeltz, and Terry

McPherson for their personal interest and encouragement in helping me complete the dissertation while I was stationed at Carrier Group SIX and the Naval Oceanographic Office (NAVOCEANO). Many members of the Warfighting Support Center at NAVOCEANO helped make this dissertation a reality. Mr. Joe Stinus, my Deputy, willingly assumed my duties in addition to his own, while I wrote two-thirds of the dissertation. Ms. Cathy Pope and LT George Moody assisted with copying figures and numerous overnight mailings to NPS, while Ms. Barbara Gibson and Mr. Dave Schneider used their computer abilities to improve selected figures.

LCDR Claudia Whitney helped Quality Control over 30000 individual Rawinsonde observations and provided much assistance with the preparation of the figures and compilation of the final manuscript. Dr. Pat Harr was instrumental in helping load the Eta Model output onto the NPS mainframe computer and answering numerous Tropical Cyclone Motion (TCM-90) field experiment questions, and Ms. Nancy Baker from the Naval Research Laboratory, Monterey taught me the NOGAPS Quality Control procedures. Mr. Paul Dobos helped me with propagation vector calculations, and Dr. Eric Rogers of the Environmental Modeling Center at the National Centers for Environmental Prediction explained the data assimilation process used by the Eta model. Ms. Penny Jones' efforts ensured that an accurate and readable manuscript was distributed to the committee, and LCDR Julia Spinelli of the Naval Oceanographic Office component in San Diego provided facilities to print the final version of the thesis.

The Office of Naval Research Marine Meteorology Program funded the TCM-90 field experiment, and provided ongoing support for the analysis of the results.

Finally, but most importantly, I wish to thank my wife, Kathy, for her incredible patience at tolerating (and still being friends with) me while we undertook this journey. Kathy prepared many of the graphs and all the flowcharts, tables, and schematics, and provided me with hundreds of cups of coffee, dozens of cookies, and unbounded love that kept me going. Kathy, we finally finished! To you, I dedicate this dissertation.

I. INTRODUCTION

A. MOTIVATION

Forecasting tropical cyclone (TC) intensity (maximum wind speed or minimum sea-level pressure) is a problem second only to the forecast of the storm track. Wind damage is very sensitive to the intensity of the TC, because it is proportional to the square, or even the cube, of the maximum sustained wind speed (Southern 1987). Sanders (1984) compared damage assessments for typhoons crossing the Philippines and noted that typhoons with maximum sustained winds between 50-55 m s⁻¹ killed 2.5 times the number of people, and destroyed 16 times as many homes, as minimal strength (33 m s⁻¹) typhoons. TC intensity is also a major factor in determining the amplitude and horizontal extent of the storm surge and wind-waves, which are major causes of damage when a TC makes landfall. For maritime interests, higher wind speeds generate larger swells that propagate ahead of the storm and potentially impede ships attempting to evade the tropical cyclone.

Despite the importance of the intensity forecast, the consensus among operational forecasters and research meteorologists is that operational forecasts are little, if any, better than an intensity forecast based upon persistence and climatology (Elsberry *et al.* 1992). Reasons given in Elsberry *et al.* 1992 for this lack of skill include: poor data resolution, especially near the convective core of the TC in the upper troposphere; lack of a unifying, quantitative conceptual model that relates tropical cyclone intensification

to observed physical processes; and a lack of emphasis placed on the forecast intensity relative to the effort spent on obtaining the TC track. Recent comments from operational forecasters (e.g., Avila 1998) indicate that intensity forecasts have improved little since 1990. Both operational (Avila 1998) and research (Elsberry *et al.* 1992) meteorologists state that the most significant intensity forecast challenge is to understand, and ultimately predict, periods of tropical cyclone rapid intensification.

From an operational forecasting point of view, it is very difficult to make a good forecast (of any parameter) if you do not understand: (1) the current state of the atmosphere (i.e., a good analysis); and (2) a conceptual model of the relevant physical processes.

The goals of this observational study are to improve the analysis procedures used in depicting the upper-tropospheric atmosphere in the vicinity (within 1500 km) of a tropical cyclone, and then use the resulting analyses of Super Typhoon Flo (Figure 1.1) and Typhoon Ed (Figure 1.2) to review the interactions between the large-scale environment and the tropical cyclones. These thermodynamic and dynamical interactions (e.g., upper-tropospheric warming, eddy flux convergence of relative angular momentum, vertical wind shear) are examined in the context of current tropical cyclone intensification theories (discussed below). The objective is to use the high spatial and temporal resolution dataset to determine the relationships and relative importance between these interactions.

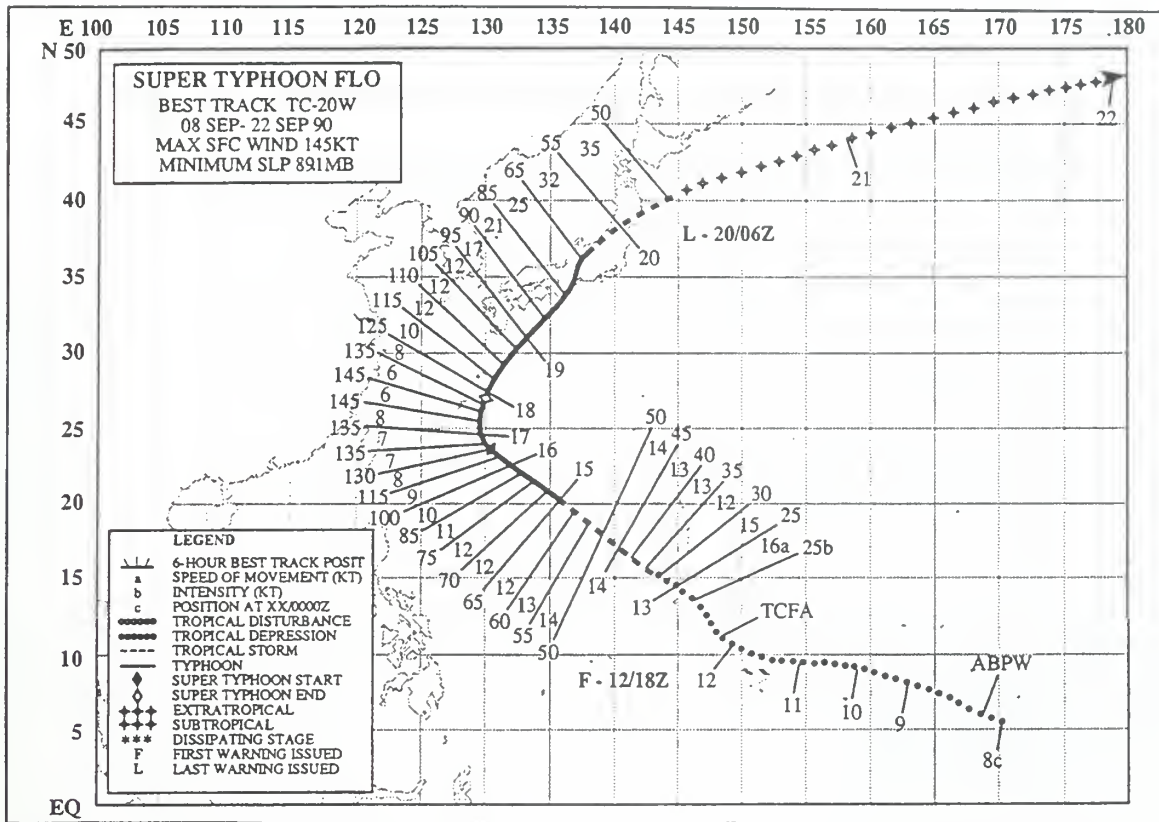


Fig. 1.1. Best track information for Typhoon Flo from Annual Tropical Cyclone Report (JTWC 1990).

Typhoons Ed and Flo were observed during Intensive Observation Periods (IOPs) 5-7 of the Tropical Cyclone Motion 1990 (TCM-90) experiment (Elsberry 1990). This data set (Elsberry *et al.* 1990; Harr *et al.* 1991) is ideally suited to describe the interactions of a tropical cyclone with its surrounding large-scale environment, especially in the upper troposphere.

The remainder of this chapter will provide a background on previous studies relevant to tropical cyclone intensity, this study's primary hypotheses, and the approaches used. Subsequent chapters will discuss the objective analysis of Typhoons Ed and Flo,

the validation of that analysis, the dynamics that interacted with the storms, and the conclusions.

B. PREVIOUS WORK ON TROPICAL CYCLONE INTENSITY

Much of the previous work concerning TC intensity has concentrated on a specific aspect of either the thermodynamics, internal dynamics and convection, or dynamical interactions with the surrounding environment. These aspects of the tropical cyclone have been studied from a theoretical basis, as well as by statistical, composite, individual case study, and numerical modeling approaches.

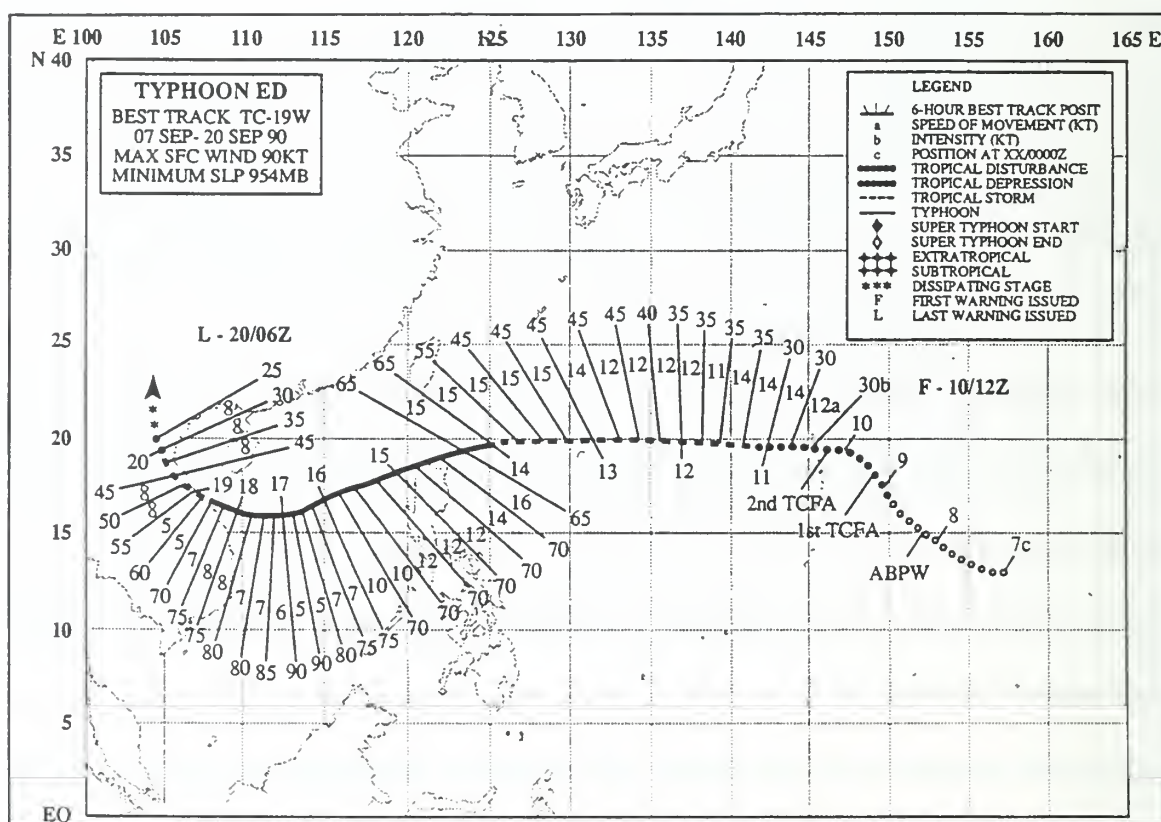


Fig. 1.2 Best track information for Typhoon Ed from Annual Tropical Cyclone Report (JTWC 1990).

While it may be required to compartmentalize the tropical cyclone intensification problem into the above-listed topics to ensure a tractable study, the total processes are not easily separated. Merrill (1989) provided a schematic (Figure 1.3), that qualitatively depicts some of the interactions that govern TC intensification. As illustrated by Figure 1.3, tropical cyclone intensity may be governed by circulations with horizontal scales ranging from the synoptic to the convective element, with multiple positive and negative feedback processes simultaneously occurring.

Recent studies (e.g., Emanuel 1998, Molinari 1998, Holland and Wang 1998, DeMaria and Huber 1998), have stated that several fundamental questions remain. These include: (1) What is the contribution of the ocean surface temperature and mixed layer dynamics to tropical cyclone intensity? (2) How important is the thermodynamic state of the atmosphere? (3) What is the role of transient "lateral dynamical interactions" (Holland and Wang 1998) (e.g., transient mid- and upper-tropospheric systems), and how do they interact with tropical cyclones? What, if any, interaction occurs between these lateral interactions and the tropical cyclone core? (4) What is the role of vertical wind shear? Is the structure of the vertical shear, as discussed by Elsberry and Jeffries (1996) important? How should vertical shear be calculated? (5) Is there an identifiable precursor, or sequence of events, that would enable consistently accurate forecasts of rapid intensification? While Molinari (1998) states that this is the "fundamental forecast problem," there has been little success in achieving this objective, either through

statistical means (Elsberry 1998) or using multiple case studies (Holland and Wang 1998). The following sections provide some background on each of the above-listed topics.

1. Thermodynamic Considerations

Although the strong impact sea-surface temperature (SST) has on tropical cyclone intensity has been known for decades, the degree of control the ocean has on the intensity of a tropical cyclone at any given time is still a controversial topic (Elsberry 1998). Palmén (1948) observed that tropical cyclones typically do not form over SSTs lower than about 26°-27°C. Miller (1958) showed through hydrostatic considerations that the minimum central pressure of a hurricane was determined by the maximum virtual temperature (T_v) that could be sustained in the eye of the TC, and that T_v depends in part on the SST via the surface flux of heat and moisture from the sea. Miller derived an empirical curve describing the minimum sea-level pressure as a function of SST. Miller stated that although the underlying SST is important, the surrounding tropospheric dynamics, low-level relative humidities, and an outflow mechanism also determine the TC intensity.

Charney and Eliassen (1964) proposed that the convective available potential energy (CAPE) in the tropical atmosphere provided the energy source for TC formation. Once the initial convection is triggered by a random perturbation, the latent heat released from the convection would serve to warm the core of the developing system and lower the central pressure. The low-level winds would respond to the inward-directed,

pressure- gradient force by providing more latent heat to the developing storm center, and the disturbance would continue to strengthen. This hypothesis became known as conditional instability of the second kind (CISK).

Emanuel (1986, 1988) questioned this hypothesis. He noted that such a CISK mechanism would result in many more developing cyclones than observed, and these storms would not have to be confined to oceanic regions because Charney and Eliassen did not include a surface source of moisture. Emanuel proposed that the storms developed and intensified based only upon the latent (and to a lesser degree sensible) heat fluxes from the ocean. Emanuel described the TC transverse circulation in terms of a Carnot cycle that provides a relationship for the minimum central pressure of the TC in terms of the temperatures at the surface and at the outflow level, the mean relative humidity, and an average radius of the cyclonic circulation. This theoretical expression gives similar maximum winds as the Miller (1958) empirical relationship for parameters observed on the earth.

While it is generally accepted that SST, or SST in conjunction with the tropopause temperature, provides an upper bound to TC intensity, several recent observational studies highlight the lack of direct correlation between SST and intensity, or even rate of intensification. Evans (1993) analyzed monthly SST data for five ocean basins (North Atlantic, western North Pacific, South Pacific-Australia, northern Indian Ocean, and southwest Indian Ocean) over a 20-year period, and showed that for any given SST value, many different TC intensities may be observed. Evans concludes that SST is not

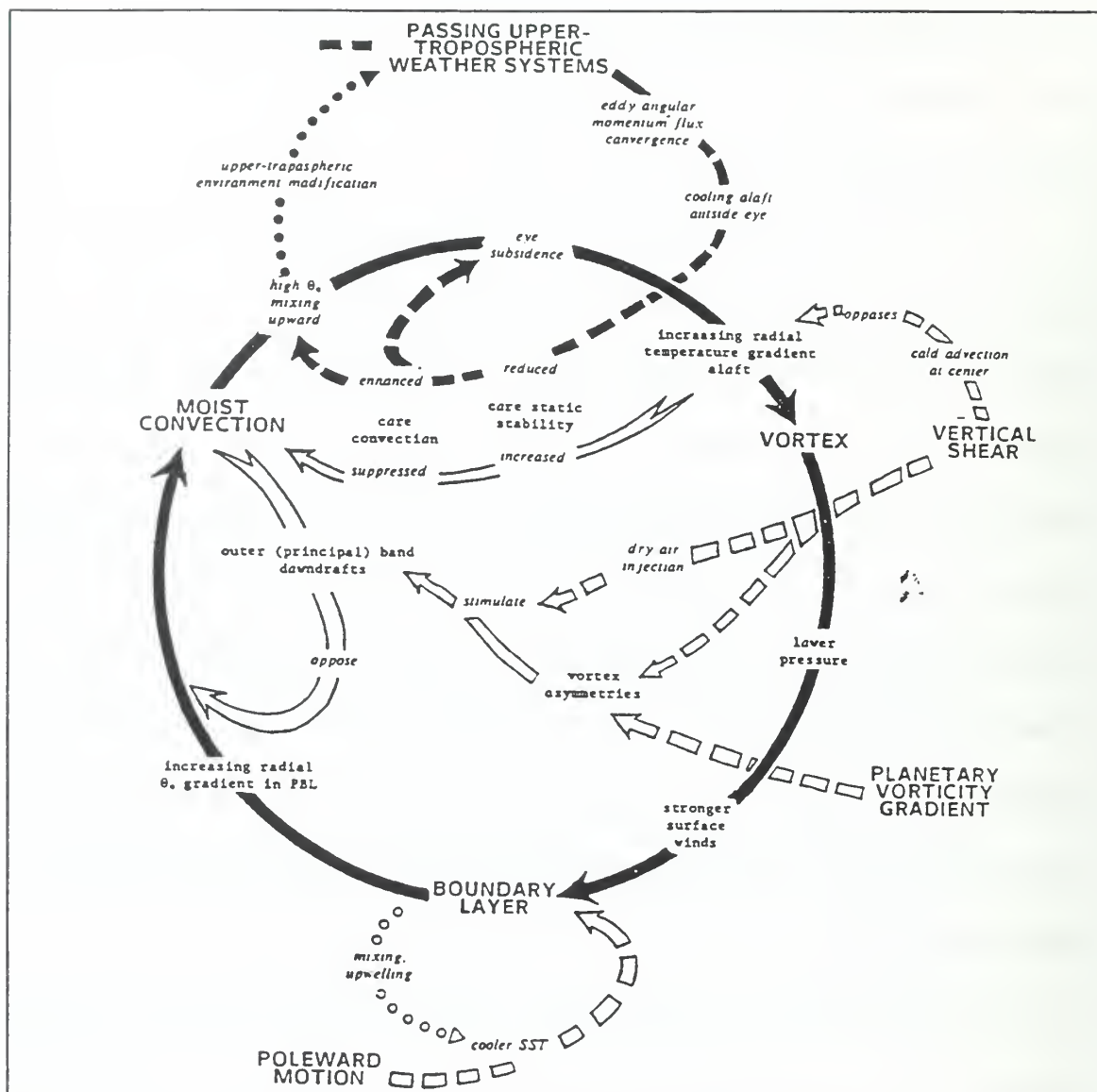


Fig. 1.3. Processes influencing tropical cyclone intensity change. The black circle represents internal positive feedbacks between the vortex, the boundary layer, and moist convection. Negative internal feedbacks are shown as white arrows. Dashed arrows indicate positive (black)/negative (white) environmental influences, and dotted arrows denote modification of the environment by the tropical cyclone (Merrill 1989).

the dominant factor in determining either instantaneous TC intensity, or the maximum intensity for a given storm.

DeMaria and Kaplan (1994) used a 31-year sample of North Atlantic tropical cyclones and climatological SST data to develop an empirical relationship between maximum intensity and SST. The empirical relationship agrees well with Emanuel's (1988) theoretical results, assuming that the tropopause temperature is determined primarily by the SST. Both Merrill (1987) and DeMaria and Kaplan (1994) show that the difference between the actual storm intensity and the upper-bound based on SST (termed the Maximum Potential Intensity (MPI)) provides a better indication of future storm intensification than using SST alone. DeMaria and Kaplan also show that fewer than 20% of storms that are over water have attained at least 80% of their MPI. Finally, DeMaria and Kaplan state that over 70% of the storms examined would require the SST to be decreased by more than 4°C to lower the MPI to the observed intensity. Based on this result, DeMaria and Kaplan argue that factors other than large-scale SST limit storm intensification.

Conversely, Emanuel (1998) argues that our lack of knowledge of the control the ocean surface and mixed layer has on tropical cyclones is a significant factor in the lack of skill in predicting future TC intensity. Specifically, Emanuel states that we must better understand the interactions of air-sea fluxes at hurricane wind speeds and develop high-resolution, coupled air-sea models before we can make appreciable advances in forecasting TC intensity changes.

Holland (1997) provides a comprehensive review of previous research relating the thermodynamic characteristics of the TC environment to the MPI. He also proposes an

alternate theoretical relationship to that submitted by Emanuel (1988). Holland's approach requires an atmospheric sounding, as well as the SST and the local environmental surface pressure. The method accounts for positive oceanic feedback of moist entropy (θ_e) associated with falling pressures and a constant SST, a cloudy eyewall, and a clear eye. Holland's approach is consistent with empirical (e.g., DeMaria and Kaplan 1994), and limited numerical and observational studies, including Typhoon Flo (Merrill and Velden 1996). The approaches advocated by both Emanuel and Holland show the effective minimum SST required to develop tropical cyclones is about 26°C, which is in agreement with observations.

Holland's method is much less sensitive to the environmental and storm relative humidities than the "Carnot Engine" approach of Emanuel, but is more dependent on the specification of the SST. Holland emphasizes that SST values between 26° to 29°C indirectly raise the MPI by creating a more (thermodynamically) favorable atmosphere in *both* the lower troposphere and near the tropopause. That is, the atmosphere warms (cools) in the lower troposphere (tropopause), with little temperature change in the mid levels. This less stable and cooler atmosphere aloft increases the potential for the tropical cyclone to develop an upper-level warm core, which is a feature essential for substantial intensification.

Interest in the role of SST and the associated oceanic mixed layer has recently increased, partly due to Hurricane Opal's (1995) rapid intensification over a warm-core eddy in the Gulf of Mexico, followed by an equally rapid decrease in intensity prior to

landfall in the vicinity of Pensacola, FL (Figure 1.4). Several studies (e.g., Shay *et al.* 1998, Bosart *et al.* 1998, Bracken and Bosart 1998) have noted the interaction of Opal with both the warm-core eddy and the mid-latitude trough to the northwest of the storm. High-resolution SST, satellite-based altimetry, and ocean front location data available from the Naval Oceanographic Office (May *et al.* 1998) may help to answer these questions.

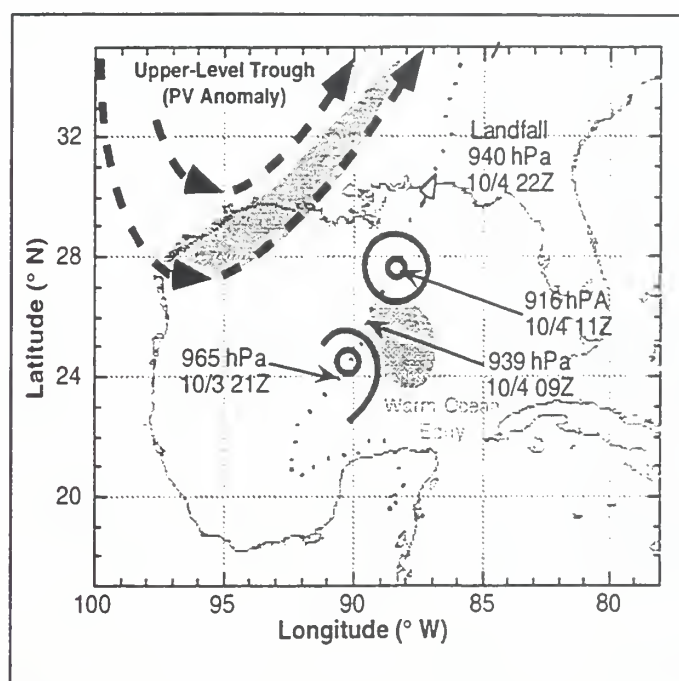


Fig. 1.4. Position of upper-level trough and location of Loop Current warm core eddy based upon TOPEX altimetry data relative to the position of hurricane Opal's track in the Gulf of Mexico from 28 September to 5 October 1995 (Shay *et al.* 1998).

In summary, widespread agreement exists that heat contained in the mixed layer of the ocean, traditionally measured as SST values, provides a strong upper bound to

tropical cyclone intensity. However, researchers have used different methods and assumptions to reach this conclusion. Recent work indicates the environmental surface pressure and upper-tropospheric temperature fields are also significant. Another significant, and difficult to measure, parameter is the relative humidity, especially near the eyewall. Air-sea interactions at hurricane-force wind speeds, and the interactions between tropical cyclones and the oceanic mixed layer are also topics of active research. While the thermodynamics provides an upper bound on tropical cyclone intensity, it does not explain why Ed and Flo, which formed over similar SST's, and in similar surface pressure regimes, displayed very different intensity and intensification characteristics (Figures 1.1 and 1.2).

2. Mid-latitude and Tropical Upper Tropospheric Trough (TUTT) Interactions with Tropical Cyclones

In addition to the strong control exerted by the thermodynamic environment in the vicinity, and as modified by, the TC, substantial theoretical, observational, and modeling evidence exists that TC intensity is influenced by interactions with mid-latitude and upper-tropospheric systems. DeMaria *et al.* (1993) provide an overview of the previous work describing these interactions.

One of the primary difficulties in studying eddy flux convergence of relative angular momentum (EFC) interactions with TCs using "real" observations is that EFC interactions are almost always accompanied by a change (normally an increase) in the vertical wind shear. As will be discussed in the next section, vertical shear is normally considered to be a negative environmental influence on TC intensity. Thus, the vertical

shear may counteract any positive influence the EFC interactions may have. These arguments were articulated by Merrill (1988). The difficulty in isolating the effects of specific environmental interactions on TC intensification is a primary challenge to understanding why some tropical cyclones reach their MPI (usually undergoing at least one period of rapid intensification), while most do not.

Merrill (1988) argues that since few tropical cyclones reach their MPI, the large-scale environment must be an inhibiting influence on the development of tropical cyclones to their full potential. Molinari and Vollaro (1989) argue that Merrill's view of the environment is too simplistic. They state that TC intensification is "a cooperative interaction between previous mesoscale events at the storm core and a favorable synoptic-scale environment." They show that although vertical wind shear appeared to affect the intensity of Hurricane Elena (1985), a simple relationship between shear and intensity did not exist. Molinari and Vollaro also state that the environment can act as a positive influence on a TC, and create conditions in which the storm intensifies more rapidly than it otherwise would, given the same SST and a quiescent mean flow.

Absolute angular momentum concepts have been applied to TCs for over 50 years (e.g., Durst and Sutcliffe (1938)). Sawyer (1947) stated that the cause of upper-level divergence was sustained inertial instability within some upper layer. This instability was to be manifest as an anticyclonic shear, and was possible due to the low values of f at latitudes where TCs formed.

Riehl (1950) noted that although the mechanism proposed by Sawyer (1947) would produce the necessary upper-level divergence to allow the storm to continue to intensify, it was not clear how or why the inertial instability would exist in the free atmosphere for sufficiently long time and space scales to allow the TC to grow. That is, was this inertial instability a cause of tropical cyclone development, or did it simply reflect the existence of the outflow jet? Riehl proposed that the large-scale environment of the TC provides the necessary divergence for TC intensification, rather than dynamics internal to the storm. Riehl stated that TC development occurred when tropical and midlatitude disturbances were favorably aligned in such a manner as to provide upper-level divergence over the tropical disturbance. His paper was significant, because it was the first to recognize the large spatial scales that must be analyzed to determine TC intensification.

Many quantitative studies of the interactions between tropical cyclones and the large-scale environment have been based upon a balanced vortex model that was first described by Eliassen (1951). Eliassen assumes a two-dimensional (radius and height), axisymmetric vortex, with the azimuthally-averaged tangential wind (\bar{u}) in gradient balance with the azimuthally-averaged pressure gradient. Molinari *et al.* (1993) tested this key assumption with European Centre for Medium-range Weather Forecasting (ECMWF) analyses for Hurricanes Allen (1980) and Elena (1985) and found the azimuthally-averaged gradient balance was accurate to within 15-25% outside the core of the storm, including the outflow layer. They conclude that the Eliassen two-

dimensional balanced equations should provide reasonably realistic solutions using analyzed data, even for quickly moving and asymmetric storms.

While a complete derivation of the transverse circulation based upon the Eliassen gradient wind equations in a storm-relative coordinate system can be found in Molinari *et al.* (1993), a summary of the significant terms follows, using the notation found in Molinari and Vollaro (1990) and DeMaria *et al.* (1993). The transverse circulation is

$$L\psi = r \frac{\partial}{\partial p} \left[\left(\frac{2\bar{v}_L}{r} + f \right) M \right] + \left(\frac{r\Pi R}{p} \right) \frac{\partial H}{\partial r}, \quad (1.1)$$

where

$$M = -r^{-2} \frac{\partial}{\partial r} (r^2 \overline{u'_L v'_L}) - \frac{\partial}{\partial p} (\overline{\omega' v'_L}) - \overline{f' u'}, \quad (1.2)$$

and

$$H = -r^{-1} \frac{\partial}{\partial r} (r \overline{\theta' u'_L}) - \frac{\partial}{\partial p} (\overline{\theta' \omega'}). \quad (1.3)$$

In the above equations, r is the radius, p the pressure, u the radial wind, v the tangential wind, ω the pressure vertical velocity, θ the potential temperature, ψ the streamfunction for the secondary circulation, $\Pi = c_p \left(\frac{p}{p_0} \right)^{\frac{R}{c_p}}$, where c_p is the specific heat of dry air at a constant pressure, f the Coriolis parameter, R the gas constant, and L a second-order linear elliptic operator. The overbars and primes are defined as follows for a general variable q :

$$\bar{q} = \frac{1}{2\pi} \int_0^{2\pi} q d\lambda, \quad (1.4)$$

and

$$q' = q - \bar{q}, \quad (1.5)$$

where \bar{q} and q' denote the azimuthal mean and deviation from the mean, respectively. The subscript L indicates the parameter (u or v) is calculated in a coordinate system moving with the storm.

The values M and H in (1.1) represent the eddy momentum and heat fluxes, respectively. Based on observational (Molinari and Vollaro 1990) and modeling (Pfeffer and Challa 1991) work, the heat fluxes (1.3) appear to contribute only about 20% of the secondary circulation forcing. The eddy momentum flux (1.2) has contributions from three terms. For synoptic-scale observations in the atmosphere, the term $\frac{\partial}{\partial P} (\overline{\omega'v_L'})$ is an order of magnitude smaller and is neglected. The third term, $\overline{f'u'}$, accounts for the meridional translations of the axisymmetric storm. This term is proportional to βvr , where β is the northward gradient of the Coriolis parameter. Because of the dependence on the radius, this term is small near the center. DeMaria *et al.* (1993) show that this term is about a factor of five smaller than the magnitude of the first term within a few hundred km of the storm center.

Thus, the first term in (1.2), $-r^{-2} \frac{\partial}{\partial r} (r^2 \overline{u_L' v_L'})$, is referred to as the eddy flux convergence of relative angular momentum (EFC). Physically, when this term is positive (negative), the eddy fluxes are making the upper-level flow more (less) cyclonic. Since EFC has been expressed in units of $\text{m}^{-1} \text{s}^{-1} \text{day}^{-1}$ in several previous studies, this paper will use the same units.

Holland and Merrill (1984) calculated the streamfunction (1.1) using idealized momentum forcing functions. They determined that the high values of inertial stability of the lower TC vortex effectively resists horizontal motion, and therefore precludes significant interaction between the external environment and the tropical cyclone. Conversely, the inertial stability in the upper troposphere (i.e., the outflow layer) is low, which thus allows external forcing to potentially reach the center of the storm. In addition, the transverse circulation (1.1) is not forced by the eddy momentum term, but by the **vertical gradient** of the eddy momentum. For these two reasons, if the EFC increases with height up to the outflow layer, then the transverse circulation will support the "in-up-out" circulation through a deep layer, and should be conducive to tropical cyclone intensification. A deep secondary circulation also implies the warm core will be higher in the troposphere. As described in the previous section, this is favorable for TC intensification, and may demonstrate a positive feedback between dynamic interactions and the TC thermodynamic structure.

As in the studies on tropical cyclone thermodynamics, different researchers have reached different conclusions regarding the effectiveness with which EFC may increase

TC intensity. Numerical modeling (e.g., Pfeffer and Challa 1981, Challa and Pfeffer 1990) experiments in both two and three dimensions indicate that EFCs contribute to enhanced rates of storm intensification and development. Likewise, case studies of Hurricane Elena (1985) (Molinari and Vollaro 1989, 1990) demonstrated the apparent importance of EFCs in storm intensification. A study by DeMaria *et al.* (1993) based upon 1989-1991 Atlantic TC data found a statistically significant (at the 95% confidence level) relationship between EFCs within 600 km of a storm and intensity change in the following 48 h, providing vertical wind shear and SST changes were also accounted for.

However, numerous studies have shown little, if any, relationship between EFCs and TC intensity. In addition to the Merrill (1988) study cited previously, Merrill and Velden (1996) found no apparent relationship between the rapid intensification of Typhoon Flo and EFC. This issue will be addressed in detail in subsequent sections. Fitzpatrick (1997) developed a statistical intensity prediction system for the western North Pacific based upon 1983-1986 climatological, synoptic, and digitized infrared satellite data. The Typhoon Intensity Prediction System (TIPS) is loosely modeled after DeMaria and Kaplan's (1994) Statistical Hurricane Intensity Prediction System (SHIPS), which was developed using North Atlantic data. The 200-mb EFC predictor was determined to be not significant in explaining western North Pacific TC intensity. Zehr (1998) has proposed that the **only** significant interaction between a tropical cyclone and its surrounding environment is vertical wind shear. Landsea *et al.* (1998) use three case studies and SHIPS to demonstrate that while some 1996 North Atlantic storms appeared

to be significantly influenced by EFC (e.g., Bertha), others were mostly influenced by vertical wind shear despite significant EFC values (e.g., Isidore), or rapidly intensified in a low-shear, low-EFC environment (e.g., Edouard). Holland and Wang (1998) summarize the success of applying objective rules or techniques to determine the environmental effects on tropical cyclone intensity change by noting that there are "typically...more failures than successes." This study using the TCM-90 dataset will attempt to determine if this failure is due to a typical lack of high spatial and temporal resolution wind-field data at the outflow level, or if the relationship is as tenuous and complex as previous work indicates. Willoughby (1988) notes that in the TC core, the Rossby number (Ro) is always greater than 1, and may be greater than 100, while L_D may reduce to a value that is the order of the eye radius.

The contracting eyewall process, first described by Willoughby (1988), has been well documented (Willoughby 1990) as a short-term modulation of hurricane intensity. Although the convective and mesoscale motions are not balanced, because their horizontal scales are less than $Ro \left(\frac{v}{f\bar{r}} \right)$, vortex-scale motions will be both hydrostatic and balanced, according to Willoughby. Using the Eliassen balanced vortex equations, Willoughby proposes a model in which the secondary circulation is controlled by the vertical stability, inertial stability, and the baroclinity of the vortex. Inflow near the surface only replaces absolute angular momentum (AAM) lost to frictional dissipation, while the inflow above the boundary layer supplies the TC with an excess of AAM. The secondary circulation, schematically shown in Figure 1.5, consists of direct and indirect gyres. While the direct

gyre has inflow in the lower troposphere, ascent through the eyewall, and outflow in the upper troposphere, the indirect gyre has inflow diverging from the inner eyewall updraft aloft into the eye, and then forced descent near the center of the eye. The adiabatic warming associated with the indirect gyre produces a lower isobaric height just inside the radius of maximum winds (RMW), which from thermal and gradient wind relationships requires a reduction in the RMW. In the Willoughby model, this causes the concentric eyewall to move inward, and the maximum wind speed to increase as AAM is conserved.

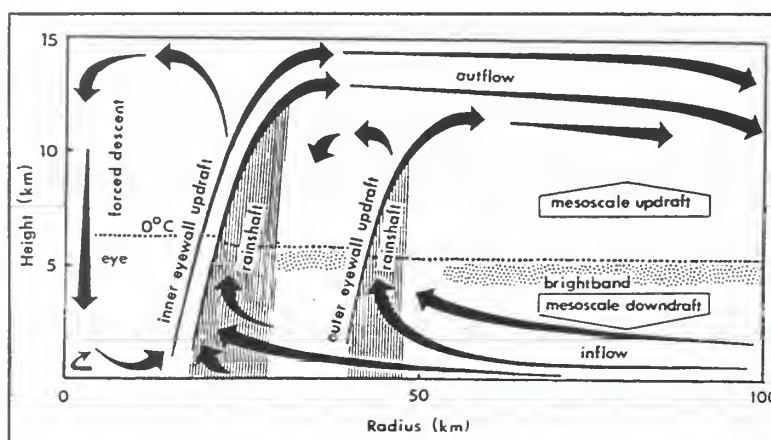


Fig. 1.5. Schematic illustration of the secondary circulation (arrows) and precipitation distribution (shaded) for a $50 - 60 \text{ m s}^{-1}$ northern hemisphere tropical cyclone (Willoughby 1988).

Willoughby (1990) states that the contraction of the convective rings with the subsequent decrease in the RMW may have synoptic precursors such as low-level surges (Molinari and Skubis 1985) or angular momentum influxes (Molinari and Vollaro 1989). He states that if contracting rings are a normal or "preferred" mode of tropical cyclones, then different synoptic forcing may lead to the same inner-core result.

3. Vertical Wind Shear

As mentioned in the previous section, vertical wind shear is closely linked to upper- and mid-tropospheric EFC interaction. A continuing issue is the attempt to "partition" the relative importance of vertical shear and EFC interactions (i.e., Zehr 1998, Landsea *et al.* 1998).

DeMaria and Huber (1998) provide an overview of research relevant to vertical shear interactions with tropical cyclones. DeMaria and Huber note that vertical shear has been related to TC intensity for most of this century, but the first explanation of how vertical shear and TC intensity are related was provided by Simpson and Riehl (1958). Simpson and Riehl proposed that the mid-levels of a vertically sheared storm experienced a relative flow through the vortex, with inflow on one side of the storm, and outflow on the other side of the storm. Gray (1968) used the term "ventilation" to describe the proposed differential advection with height of the release of latent heat of condensation.

Bender (1997), in a numerical study, described patterns of relative inflow and outflow similar to those originally proposed by Simpson and Riehl (1958). In addition, Bender showed that the quadrants of inflow and outflow depended upon the vertical shear profile, and not the direction of storm motion. DeMaria and Huber note that this result implies that the environmental shear affects the tropical cyclone circulation.

DeMaria (1996) proposed an alternate explanation of the effects of wind shear. Using a two-layer diagnostic balance model and a potential vorticity (PV) framework, he reasoned that wind shear vertically tilts the upper- and lower-level positive PV

anomalies. For the mass field to remain in balance, the thermal field adjusts by creating a warm, mid-level potential temperature anomaly. This mid-level warming may reduce the amount and intensity of convection near the storm center, and thus weaken the tropical cyclone. DeMaria also shows that the PV anomalies rotate relative to each other. After one-half of a rotation, the vertical shear reduces the tilt, which in turn reduces the mid-level potential temperature anomaly. This negative feedback acts as a "restoring force" on the system. He shows that the magnitude of this feedback depends upon the Rossby penetration depth. DeMaria shows that the "restoring force" is proportional to latitude and the storm horizontal scale, and is inversely proportional to the static stability. Thus, DeMaria reasons that higher latitude, larger, and more intense tropical cyclones should be more resistant to wind shear than low latitude, small, and relatively weak systems.

Elsberry and Jeffries (1996) use a Multi-Quadric analysis scheme (described in Chapter II) to show that the operational global numerical models may significantly overestimate the "true" vertical shear interacting with a tropical system by not correctly analyzing small-scale upper-level features. Elsberry and Jeffries hypothesize that the numerical models may also misrepresent the depth of shear, which is traditionally measured at 850 and 200 mb, because that was the levels at which conventional wind observations in the tropical atmosphere were located (Elsberry 1987). They propose that some low-latitude vertical shear may be concentrated in a shallow, upper-level layer that may be successfully "deflected" by the tropical cyclone outflow. Elsberry and Jeffries

raise basic questions about the manner in which vertical shear is calculated, and for the first time, question the effect of different vertical profiles of shear. This study, using the TCM-90 dataset, will analyze wind shear over multiple vertical levels for determine any potential effects on the intensification of Typhoons Ed and Flo.

4. Identification of Common Predictors for Tropical Cyclone Intensification

To date little progress has been made in identifying consistently accurate precursors of TC intensification, especially for rapid intensification (e.g., Holland and Wang 1998). Elsberry (1998) states that while the lack of understanding of many aspects of the relevant physics increases the need for accurate empirical and statistical intensity forecast methods, this same lack of understanding hampers the development of any (e.g., numerical, theoretical, observational) intensity forecasting technique.

Both the SHIPS and TIPS statistical techniques are, of necessity, derived from operationally-available data. If there are substantial limitations in the fidelity of the operational wind analyses, as discussed in the previous section, then the vertical wind shear predictors may be inaccurate. Elsberry states that without accurate predictors, it will be very difficult to build a statistical model that will provide forecast skill. The accuracy of the wind field analysis may also affect the calculation of EFCs, although EFC anomalies are usually evident at radii greater than the radius at which vertical shear is a issue. In addition to examining carefully the method by which global models can accurately assimilate (and initialize) mesoscale, upper-tropospheric tropical features, the underlying issue of tropical data availability must be addressed. Methods such as

incorporating water vapor-derived winds (Velden *et al.* 1997) into operational assimilation schemes should allow for more accurate initial analyses. Additional data at levels other than 200 mb will also help describe quantitatively the vertical structure of both the vertical shear and the EFC fields. Both SHIPS and TIPS were derived using EFC values from a single level (200 mb), and did not consider the vertical derivative of EFC.

Elsberry states that more accurate measurements of (at least) vertical wind shear, EFCs, and SST in the vicinity (i.e., 1500 km) of a tropical system are required to build a dataset of more accurate statistical predictors and predictands. Currently, sufficiently accurate objective intensity guidance does not exist to incorporate into a systematic approach method (Carr and Elsberry 1994), such as is used by the Joint Typhoon Warning Center (JTWC) for TC track forecasts.

C. GOALS AND HYPOTHESES

One of the major goals of this study is to develop an independent analysis scheme that may be used to compare with the high-resolution, model-based TCM-90 final analysis. As noted above, numerical model-based analyses may miss significant mesoscale features in the vicinity of a TC outflow layer. The optimum interpolation (OI) scheme and model initialization procedures commonly used in operational numerical analyses may also minimize the amount of divergence captured in the analysis. The goal is to produce a gridded, three-dimensional analysis every 6 h throughout the TCM-90 IOPs 5-7 that faithfully replicates the various types of available observations, especially

the high-quality cloud track winds (to be fully described in the next chapter) contained in the dataset. The analysis should depict the TC (within the resolution of the grid) with only minimal "bogussing."

This study will also test the hypothesis that EFC events are detectable for, and correlated with, rapid intensification events. The belief is that the poor correlation shown in some previous studies is due to the (forced) reliance on operational, low resolution (typically either 1° or 2.5° latitude) analyses that may not adequately capture EFC anomalies. Using the TCM-90 dataset and Multi-Quadric analysis scheme, the objective is to demonstrate a more straight-forward relationship between tropical cyclone intensity and observed upper-troposphere EFC. A goal closely related to this hypothesis is to investigate the EFC variations throughout the troposphere. That is, how does the vertical structure of the EFC evolve with time?

Another goal for this study is to use the TCM-90 dataset to relate the dynamical interactions with the larger scale environment (i.e., EFCs and vertical wind shear) with the storm thermodynamic structure. This goal may be difficult to achieve for two reasons: First, many previous researchers have looked for a "unifying theory" for tropical cyclones without demonstrated success. Second, although there was much enhanced wind data collected during the IOPs, the thermal data were not significantly augmented during TCM-90, with the notable exception of the data collected from the NASA DC-8 aircraft and associated dropsondes.

This study will also test Zehr's (1998) hypothesis that nothing (in the atmosphere) except vertical wind shear influences TC intensity. It was extremely fortunate to have two active typhoons during the period of interest, one of which rapidly intensified (Flo) while the other (Ed) slowly deepened, over very similar SST. The analysis, described above, should help test the above-stated hypothesis. An important goal is to contrast the vertical shear characteristics for a rapidly developing and slowly deepening typhoon active at the same time over similar SST values. Is the shear significantly lower for the rapidly developing system? If so, did the vertical shear decrease prior to rapid intensification, or was the decrease observed as the storm developed?

Finally, can this analysis provide any clues to a "universal predictor" that would help forecasters predict intensification for both rapid and "garden variety" intensifying typhoons? Again, previous research has sought such a parameter, or series of indicators. The quality of the TCM-90 dataset may provide some additional clues to understanding TC intensification.

D. APPROACH

The following chapter briefly describes the TCM-90 experiment, then discusses the Multi-Quadric analysis method, and its application to the TCM-90 dataset. Quality control of the TCM-90 data is then discussed, followed by details of the implementation of the Multi-Quadric objective analysis scheme. Finally, the methods used for calculating vorticity, divergence, and vertical velocity are explained.

Chapter 3 is devoted to validating the derived Multi-Quadric analyses scheme, and comparing the results to the four-dimensional data assimilation method using the Eta model. Results are also compared to the Navy Operational Global Atmospheric Prediction System (NOGAPS).

Chapter 4 is a discussion of the dynamics observed during the intensification of Ed and Flo. Initially, the evolution of Flo is described in terms of calculated thermodynamic and dynamic parameters in four phases: the forcing, quiescent, super typhoon, and mid-latitude interaction phases. The dynamics of Typhoon Ed are then compared to, and contrasted with, those observed in Flo. Correlations between physical parameters and storm intensity (and storm intensity change) are then examined. Chapter 5 contains the study's conclusions and recommendations.

II. DATA ANALYSIS

A. TROPICAL CYCLONE MOTION FIELD EXPERIMENT

In August and September 1990, the Tropical Cyclone Motion (TCM-90) field experiment was conducted in the western North Pacific. As discussed in Elsberry (1990), this experiment was held in conjunction with three other tropical cyclone initiatives that were sponsored by the Economic and Social Commission for Asia and the Pacific/World Meteorological Organization, the former Soviet Union, and Taiwan.

Although each experiment was designed primarily to answer specific hypotheses concerning typhoon motion, the dataset may support additional facets of tropical cyclone research. The primary objective of TCM-90 was to obtain an accurate measurement of the environmental and outer (300-800 km) winds surrounding a typhoon. Accurate wind observations in this region may assist in documenting the existence and character of the hypothesized wavenumber one gyres (*e.g.*, Carr and Elsberry 1992) that determine the tropical cyclone propagation vector, which is defined as the difference between the environmental steering flow and the storm motion. The other TCM-90 experiment goals were to collect an enhanced dataset that would assist in operational tropical cyclone prediction, and to allow researchers to describe the physical mechanisms that cause large track deviations.

These four experiments enhanced the operational dataset by:

- Providing 6-h rawinsonde coverage during Intensive Observation Periods (IOPs).
- Adding over-ocean rawinsondes, such as the four Soviet ships stationed along 20°N. These ships took upper-air, surface, and bathythermograph (BT) observations.
- Arranging for special post-experiment processing of the Geostationary Meteorological Satellite (GMS) cloud-drift winds by the Cooperative Institute for Meteorological Satellite Studies at the University of Wisconsin (Madison). The cloud-drift winds were manually assigned an altitude based upon the temperatures from the enhanced rawinsonde network.
- Adding special observing platforms, such as the NASA DC-8 aircraft. The NASA DC-8 flew three missions in Typhoon Flo. In addition to providing high spatial resolution winds near 200 mb, each DC-8 mission deployed about two dozen dropwindsondes.

A complete list of the data collected unique to each IOP is given in Harr *et al.* (1991), and a summary of the data used in this study is given in Table 2.1. The combined dataset from the four experiments (hereafter referred to as TCM-90) is one of the best ever collected for tropical cyclone research in the western North Pacific. Its particular strength is the DC-8 and reprocessed GMS cloud-track winds (CTW), which provide the opportunity for detailed analysis of the outflow structure of an intense typhoon.

Figure 2.1 contains a typical distribution of 200-mb wind observations for a regular synoptic observation time, but without aircraft reconnaissance. Figure 2.2 depicts the 200-mb wind observations during an off-synoptic time, but with the addition of DC-8 flight-level observations.

| Observation Designation | Description |
|--------------------------------|--|
| RAWIN | Real-Time and delayed Rawinsonde Observations and Pilot Balloon data |
| LDW | LORAN Dropwinsonde observations |
| CTO | Operational Cloud-Track Wind observations from the Japanese Meteorological Agency and, occasionally, India |
| CTW | Reprocessed Cloud-Track Wind data from the satellite data center at the University of Wisconsin |
| AIREP | Real-Time commercial aircraft reports |
| DC8 | NASA DC-8 flight-level data |

Table 2.1. BRIEF DESCRIPTION OF OBSERVATION TYPES USED IN THE MULTI-QUADRIC ANALYSES AND THE ASSOCIATED DESIGNATION ASSIGNED EACH OBSERVATION TYPE.

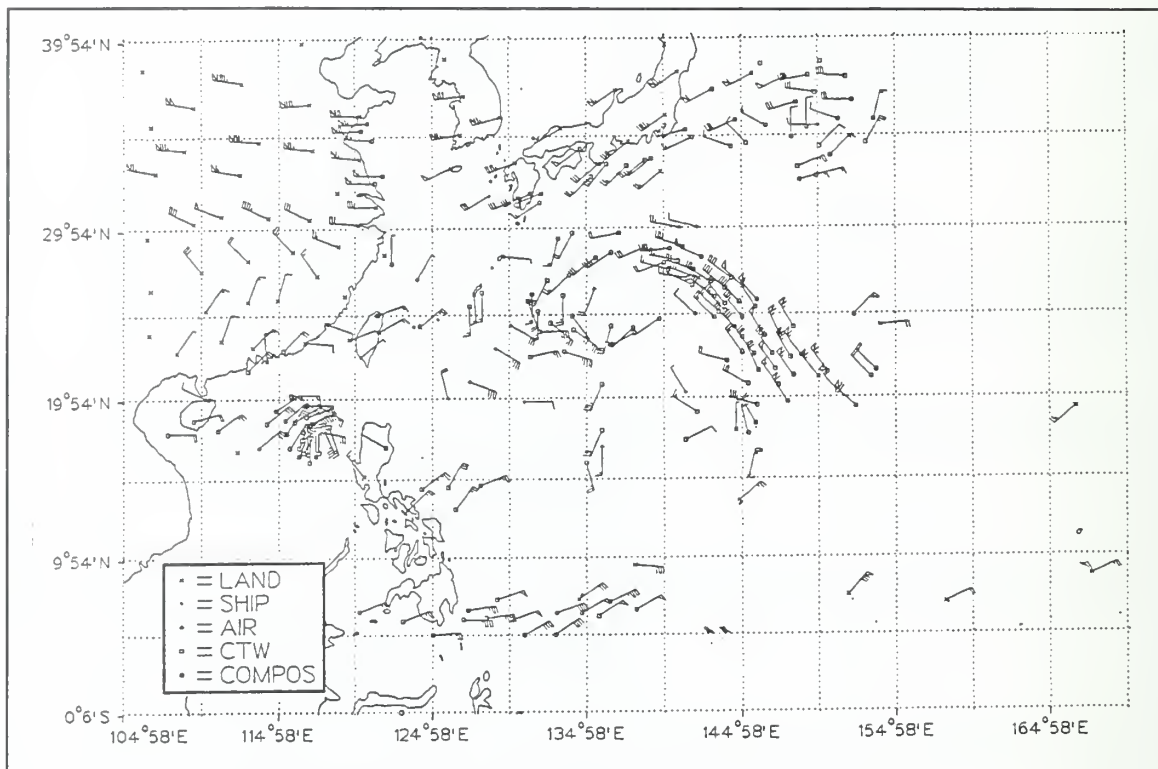


Fig. 2.1. 200 mb observations for 12 UTC 15 September 1990. Type of observations (see inset for symbols) as follows: LAND, land-based rawinsondes; SHIP, sea-based rawinsondes; AIR, commercial Aircraft Reports (AIREPs); CTW, reprocessed cloud-tracked winds; and COMPOS, two or more observations within 25 km linearly averaged in both magnitude and location. Wind barbs aligned in direction from which wind is blowing, with one-half barb = 2.5 m s^{-1} , one full barb = 5 m s^{-1} , and one flag = 25 m s^{-1} .

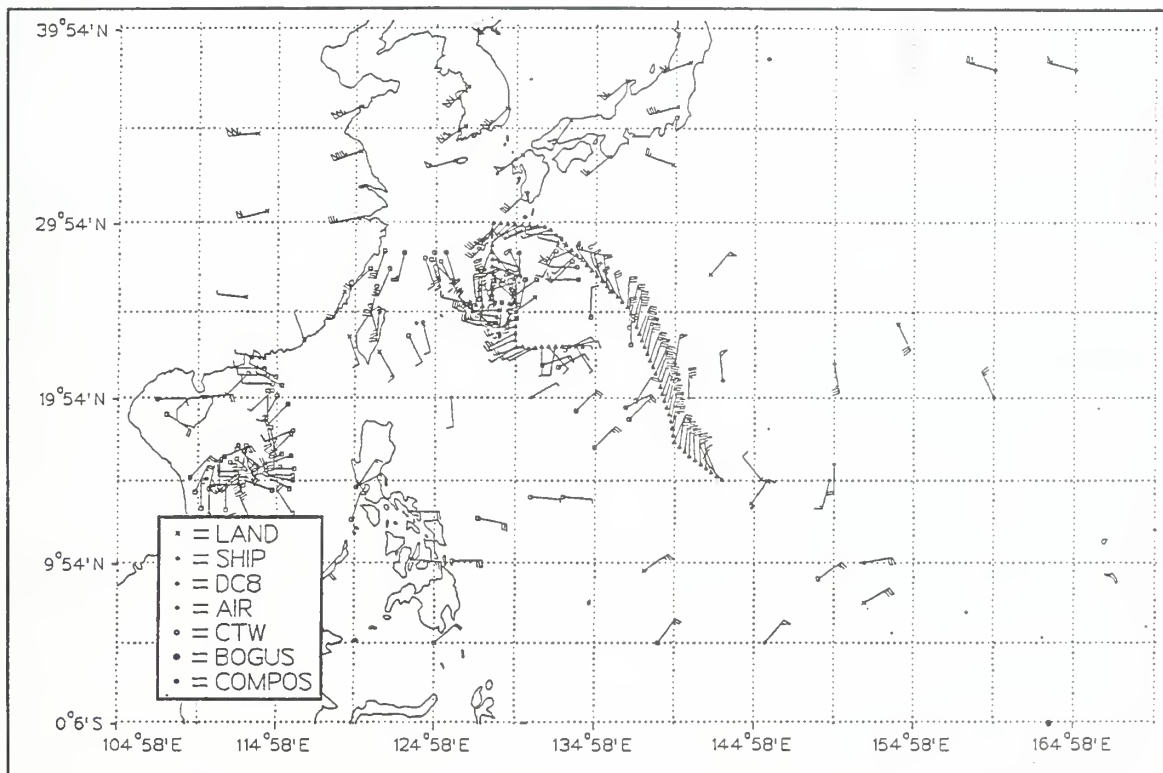


Fig. 2.2. 200 mb observations as in Figure 2.1, except for 06 UTC 17 September. Additional observation types (see inset for symbols): DC8, NASA DC-8 flight-level data; and BOGUS, synthetic observation.

B. GRIDDED ANALYSES

Since a significant effort is necessary to produce gridded analyses from irregularly spaced observations, one can ask are gridded analyses necessary? Rucker (1992) has already performed a hand analysis of the upper-level streamlines and isotachs for TCM-90 IOPs 5-7 (00 UTC 13 September through 00 UTC 19 September). While these analyses provide an alternate description of the atmosphere, Rucker did not do extensive quantitative calculations. Gridded analyses are required for diagnostic calculations involving the vorticity and divergence (*i.e.*, tangential and radial winds around a tropical cyclone), vertical shear, and momentum fields. The intent of this study is to quantify the dynamics in the outflow layer of Typhoon Flo.

C. ANALYSIS METHOD

1. Background

Different methods have been used to analyze meteorological data. Four of the most common are:

- Hand analyze, then manually interpolate the values to gridpoints;
- Locally-performed objective analysis methods, such as successive corrections (*e.g.*, Cressman 1959, Barnes 1973);
- Statistical methods, such as Optimum Interpolation (OI) (*e.g.*, Gandin 1963);
- Four-Dimensional Data Assimilation (4DDA) (*e.g.*, Charney *et al.* 1969, Bergman 1979)

A review of these techniques as applied to objective analysis in an operational environment can be found in Dey (1989).

Each of these techniques has strengths and weaknesses. A human analyst incorporates his or her dynamical knowledge and conceptual models into the analysis, and thus interprets the observations in a multivariate sense, *e.g.*, using height gradient information and satellite imagery in the wind analysis. A hand analyst makes an implicit accuracy determination of each observation based upon the observing platform and neighboring observations in both time and space. A set of hand analyses for TCM-90 IOPs 5-7 winds at 150, 200, 250, and 300 mb has been performed by Rucker (1992). The primary problem with hand analyses is converting the information to a gridded dataset. An analysis at ten vertical levels, with 50 km spatial resolution, and covering the TCM-90 domain represents approximately 1.1 million gridpoints per parameter analyzed, which is not a tractable problem for one person to undertake.

Locally-performed objective analysis schemes efficiently convert irregularly spaced observations onto a regular grid. Previous studies (*e.g.*, Franke 1985, Nuss and Titley 1994) have shown that the type of method has a significant impact on the quality of the final analysis. Analyzing the observations locally gives the analyst greater control over which observations are used and their relative weighting, but dynamical consistency between wind and mass fields is not guaranteed. Assumptions must also be made when transforming asynoptic observations (normally not on a mandatory pressure level) to an analyzed time and/or level. If asynoptic data are not transformed, the analyst must accept the error induced.

A 4DDA scheme using OI or some other statistical analysis method ensures efficient incorporation of asynoptic data, and also dynamical consistency within and between levels. However, the OI scheme depends heavily on assumed statistical relationships between the observations and the dynamical model forecast values. Although these statistics are continually being updated and refined (Dey 1989), many of the statistics are developed over the North American network of stations (Goerss and Phoebus 1992). It is certainly a question whether these statistics are valid in regions with small Coriolis force and low inertial stability such as the outflow layer of a typhoon (Holland 1987) in the western North Pacific Ocean. Another potential problem with a 4DDA/OI scheme is the model parameterization of the tropical cyclone latent heat (Elsberry 1987). If the latent heat release is not correctly modeled, the model will attempt to constrain the observations to a consistent but incorrect balance.

The National Centers for Environmental Prediction (NCEP), (formerly the National Meteorological Center) has completed a 4DDA analysis of the TCM-90 dataset (Rogers *et al.* 1992) using the Eta mesoscale model and an assimilation scheme similar to the Regional Data Assimilation Scheme (Peterson *et al.* 1991). The Eta model is described in Mesinger (1984) and Jancic (1990), and is summarized in Rogers *et al.* (1992).

2. Method Chosen

This study uses an objective analysis scheme that combines information indirectly obtained from the 4DDA and OI methods with an objective analysis technique that has

rarely been used in meteorological applications: the Multi-Quadric (MQ) method. The MQ analyses are then compared qualitatively and quantitatively to the NMC 4DDA and the Navy Operational Global Atmospheric Prediction System (NOGAPS) analyses.

a. Multi-Quadric Method

The MQ method, which was first discussed in Hardy (1971), is a linear combination of hyperbolas (circular hyperboloids) for a one-dimensional (two-dimensional) analysis. Hardy developed the MQ technique to analyze scattered topographic observations in a manner similar to the result produced by an experienced cartographer. This goal is similar to the objective here to produce gridded meteorological analyses that would emulate those of an accomplished synoptic analyst. Because the basic MQ method is fully described in Hardy (1990), it is only briefly summarized here.

Let $H(X)$ be defined as

$$H(X) = \sum_{j=1}^n \alpha_j [(X - X_j)^2 + \Delta^2]^{1/2}, \quad (2.1)$$

where $H(X)$ is the function to be interpolated, α_j are unknown coefficients associated with n nodal locations X_j , and Δ is an arbitrary constant. Therefore,

$$H_i = \sum_{j=1}^n \alpha_j [(X_i - X_j)^2 + \Delta^2]^{1/2}, \quad i = 1, 2, \dots, n. \quad (2.2)$$

where H_i are the observations. In two dimensions, equation (2.2) is modified by substituting circular hyperboloids for the hyperbolas, which results in

$$H_i = \sum_{j=1}^n \alpha_j [(X_i - X_j)^2 + (Y_i - Y_j)^2 + \Delta^2]^{1/2}, \quad i = 1, 2, \dots, n. \quad (2.3)$$

Following Hardy's notation, let Q_{ij} represent any quadric basis function.

Therefore,

$$H_i = \sum_{j=1}^n \alpha_j Q_{ij}, \quad i = 1, 2, \dots, n. \quad (2.4)$$

In matrix notation, equation (2.4) becomes

$$[H_i] = [Q_{ij}] [\alpha_j]. \quad (2.5)$$

The solution for the coefficients is

$$[\alpha_j] = [Q_{ij}]^{-1} [H_i], \quad (2.6)$$

while the function value at any point p (e.g., the grid points) is given by

$$[H_p] = [Q_{pj}] [Q_{ij}]^{-1} [H_i]. \quad (2.7)$$

The free parameter, Δ , ensures that the interpolated function has continuous derivatives. Hardy states that the interpolation is not sensitive to the exact value of Δ relative to the data spacing. To test this assertion, Δ was varied between 0.0025 and 0.200. Apart from the analyses with the larger Δ being slightly smoother,

little effect was noticed. Values of Δ greater than 1.0 produced an ill-conditioned matrix, which had been discovered by Hardy.

The MQ scheme has been shown by Nuss and Titley (1994) to compare favorably with the commonly used successive-correction techniques, such as the Barnes (1973) and Cressman (1959) analyses. Using various data distributions describing an analytical function, Nuss and Titley show that the MQ Root-Mean Square (RMS) errors are 30-50% of those for the successive corrections schemes. The MQ scheme performs particularly well relative to the successive correction methods in regions of sparse data. This is apparently because the linear combination of circular hyperboloids more accurately depicts the underlying function than does an isolated observation in a successive corrections method.

(1) Smoothing. The analysis error consists of two parts: the prediction error (*i.e.*, the error in the first guess) and the observation error (Goerss and Phoebus 1992). Therefore, an analysis scheme should not draw exactly to the observations, but should draw to "smoothed" observations to capture the signal while ignoring the noise. The goal of OI analysis is to minimize the mean squared error over the entire domain. However, the prediction-error correlations must be known to achieve this objective.

A method to reduce the analysis error is to apply the generalized cross validation technique described in Wahba and Wendelberger (1980). Application of this technique to the MQ analysis is discussed in Nuss and Titley (1994). Wahba and

Wendelberger (1980) show that adding an $n\lambda\sigma_i^2\cdot\delta_{ij}$ term to the basis function (Q) controls the smoothing in the vicinity of the observation, where n is the number of observations, σ_i^2 is the mean squared observation error, λ is a smoothing parameter, and δ_{ij} is the Kronecker delta. Wahba and Wendelberger (1980) state that λ can be viewed as the half-power point of a spectral filter, or simply as the parameter that controls the least-squares fit to the observations. An alternate physical explanation is that the $n\lambda\sigma_i^2\cdot\delta_{ij}$ and Δ terms determine how sharply the gradient of the circular hyperboloid changes near each observation. That is, the larger the product of the $n\lambda\sigma_i^2\cdot\delta_{ij}$ and Δ terms, the smoother the analysis.

While Wahba and Wendelberger (1980) determine λ from the observations using a generalized cross validation equation, this study follows the approach of Nuss and Titley (1994), which allows λ to be set by the user. Tables 2.2 and 2.3 list the values used in the MQ analyses for σ and λ , respectively. The values for σ are based upon Goerss and Phoebus (1992), while the λ values were chosen based upon the perceived quality of the different data types, taking into account the research or operational nature of the data. For example, DC-8 flight-level winds and reprocessed satellite cloud-tracked winds are "weighted" more heavily than are commercial AIREPs and operationally-derived satellite cloud-tracked winds.

| Pressure Level (mb) | Height (m) | | u or v wind (m s ⁻¹) | | | | | Temp. (°C) |
|---------------------|------------|------|----------------------------------|-------|-----|-----|-----|------------|
| | RAWIN | DC8 | RAWIN | AIREP | CTO | CTW | DC8 | All Obs |
| 1000 | 6.0 | 15.0 | 2.2 | 3.0 | 2.8 | 2.5 | 2.5 | 1.5 |
| 850 | 6.0 | 15.0 | 2.2 | 3.0 | 2.8 | 2.5 | 2.5 | 1.5 |
| 700 | 6.0 | 15.0 | 2.2 | 3.0 | 3.8 | 2.5 | 2.5 | 1.5 |
| 500 | 9.0 | 15.0 | 2.8 | 3.0 | 4.8 | 3.5 | 2.5 | 1.5 |
| 400 | 10.0 | 15.0 | 3.0 | 3.5 | 4.8 | 4.0 | 2.5 | 1.5 |
| 300 | 12.0 | 15.0 | 3.2 | 4.0 | 6.5 | 4.0 | 2.5 | 1.5 |
| 250 | 13.0 | 15.0 | 3.1 | 4.0 | 6.5 | 4.0 | 2.5 | 1.5 |
| 200 | 14.0 | 15.0 | 3.0 | 4.0 | 6.5 | 4.0 | 2.5 | 1.5 |
| 150 | 15.0 | - | 2.8 | 4.0 | 6.5 | 4.0 | 2.5 | 1.5 |
| 100 | 16.0 | - | 2.8 | 4.0 | 6.5 | 4.0 | 2.5 | 1.5 |

Table 2.2. ROOT-MEAN SQUARE OBSERVATION ERROR (σ) ASSIGNED TO HEIGHT, WIND AND TEMPERATURE OBSERVATIONS ACCORDING TO OBSERVATION PLATFORM AND PRESSURE LEVEL.

| | Height | u or v wind |
|---|--------|-------------|
| RAWIN | 1 | 1 |
| LDW | 10 | 1 |
| CTO | - | 10 |
| CTW | - | 3 |
| AIREP | - | 100 |
| DC8 | 10 | 1 |
| If observation is between (10°N, 105°E) and (35°N, 160°E), $\lambda = \lambda/10$ | | |

Table 2.3. SMOOTHING VALUE λ ASSIGNED TO HEIGHT AND WIND OBSERVATIONS ACCORDING TO OBSERVATION PLATFORM AND LOCATION.

The goal for the MQ analysis was to draw closely to the observations while accounting for the likely observation error, especially in the outflow layer of the TC. While the NOGAPS and 4DDA analyses also attempt to minimize the error between the analysis and the observations, those analyses are constrained by the dynamics and physical parameterizations of the forecast model that provides the first-guess for the analysis. The MQ analysis has no such constraint.

An example of the effect $n\lambda$ has on the analysis is shown in the following test. Increment values (NOGAPS first guess minus the observation values)

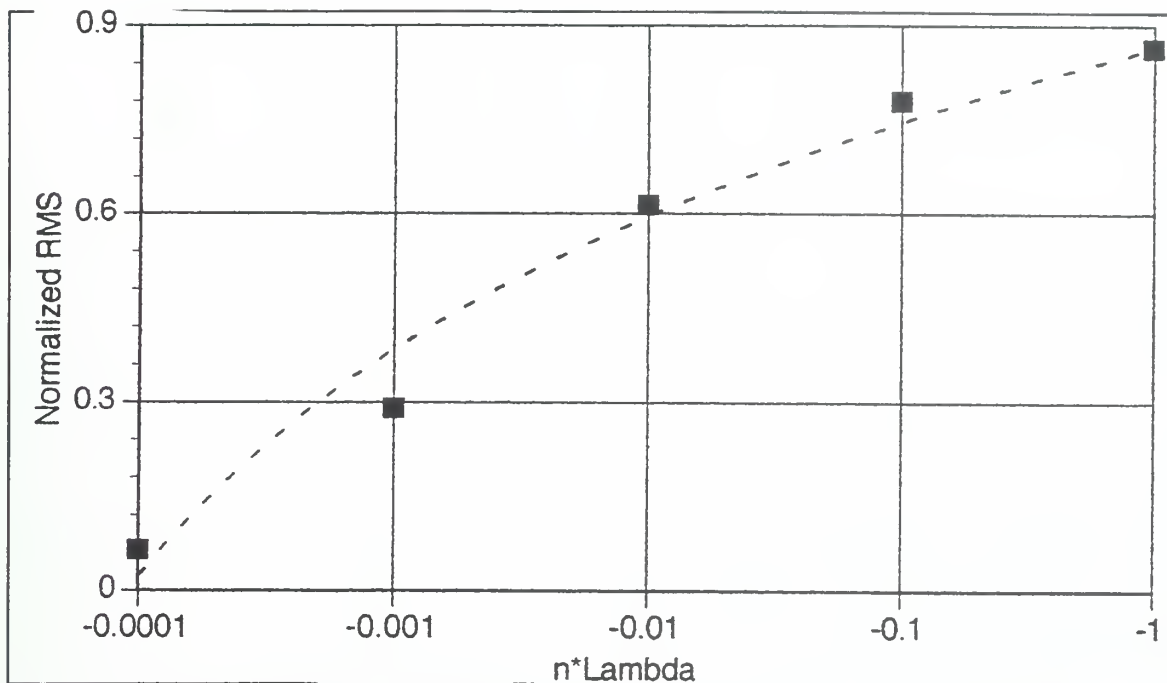


Fig. 2.3. Root-mean square (RMS) values indicating closeness of the fit to the observations as a function of the smoothing parameter $n\lambda$ in the MQ analysis. Calculated data points are indicated by the ■ symbols, and dashed line is quadratic least squares fit to the data.

were calculated for 00 UTC 13 September 1990 1000 mb u (east-west) wind observations ($n=287$). First, a RMS value for no analysis was calculated; *i.e.*, the no-analysis RMS value was the variance of the increments. Then MQ analyses were performed for varying values of λ (keeping n and σ constant), RMS values were calculated, divided by the no-analysis RMS value, and plotted in Figure 2.3. By increasing $n\lambda$ four orders of magnitude, the amount of smoothing clearly changes. Further experiments showed that the basis function could be altered by some factor of λ to control the amount of smoothing based upon the location, level, and type of observation (Table 2.3). This

control over how closely the analysis should fit the observations is analogous to the statistical weights assigned each observation type in the OI methods.

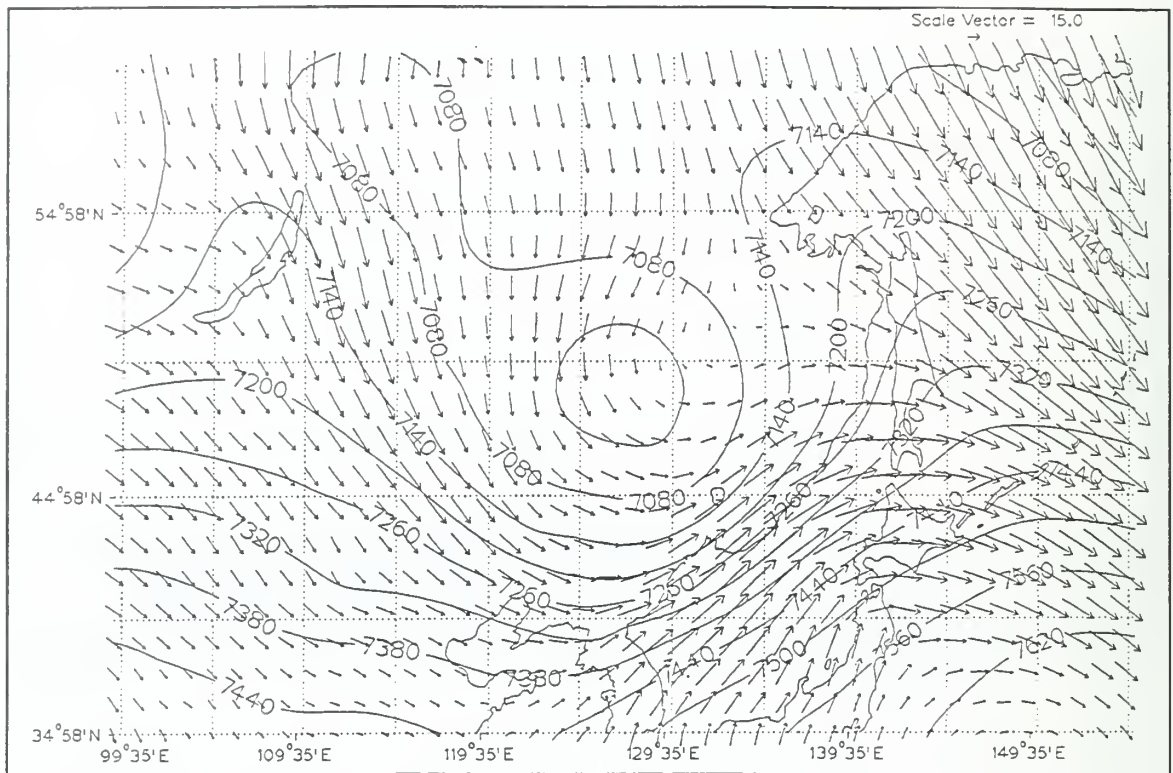


Fig. 2.4. Univariate MQ analyses of the 400-mb heights (solid, contour interval 60 m) and wind vector (m s^{-1} , scale vector in upper right) for 06 UTC 18 September.

(2) Dynamic Constraints. Initially, the MQ analysis was run in a dynamically unconstrained form in which the winds and heights were analyzed independently. An example of an unconstrained analysis that included significant ageostrophic flow is shown in Figure 2.4. Since it is well established that the middle troposphere in the mid-latitudes is in geostrophic balance to first order (*e.g.*, Holton 1979), a method was required to "couple" the winds and heights. Hardy (1990) showed

that a system of MQ basis functions could be set up that would not only analyze the observations, but would also account for the slope in the data. These equations are

$$\begin{aligned}
\sum_{j=1}^n A_j Q_{ij} + \sum_{j=1}^n B_j \frac{\partial Q_{ij}}{\partial X} + \sum_{j=1}^n C_j \frac{\partial Q_{ij}}{\partial Y} &= Z_i, \quad i = 1, 2, \dots, n \\
\sum_{j=1}^n A_j \frac{\partial Q_{ij}}{\partial X} + \sum_{j=1}^n B_j \frac{\partial^2 Q_{ij}}{\partial X^2} + \sum_{j=1}^n C_j \frac{\partial^2 Q_{ij}}{\partial X \partial Y} &= \left(\frac{\partial Z}{\partial X} \right)_i, \quad i = 1, 2, \dots, n \\
\sum_{j=1}^n A_j \frac{\partial Q_{ij}}{\partial Y} + \sum_{j=1}^n B_j \frac{\partial^2 Q_{ij}}{\partial X \partial Y} + \sum_{j=1}^n C_j \frac{\partial^2 Q_{ij}}{\partial Y^2} &= \left(\frac{\partial Z}{\partial Y} \right)_i, \quad i = 1, 2, \dots, n
\end{aligned} \tag{2.8}$$

where Z_i are the height observations, and $\left(\frac{\partial Z}{\partial X} \right)$ and $\left(\frac{\partial Z}{\partial Y} \right)$ are the east-west and north-south height gradients respectively. These gradients are estimated by the geostrophic wind equations (in pressure coordinates)

$$\frac{\partial Z}{\partial X} = \frac{fv}{g} \tag{2.9}$$

$$\frac{\partial Z}{\partial Y} = -\frac{fu}{g} \tag{2.10}$$

where f is the Coriolis parameter and g is the acceleration of gravity.

b. Application of the Multi-Quadric Method

(1) Increment Analysis. In this study, the MQ method is used to analyze increments, which are defined as the observed value minus the NOGAPS value at the location of the observation. The NOGAPS analyses were interpolated to the location of the observations using B-splines as opposed to using a linear interpolation.

As shown by Franke (1985), B-splines minimize the error in the grid-to-observation interpolation, which reduces the error in the final analysis.

Analyzing the increments as opposed to the observed value allows the model (NOGAPS) information to be assimilated into the local analyses in regions of few observations so that the increment tends to zero. Tables 2.4, 2.5, and 2.6 list the number of height, wind, and temperature observations, respectively, included in the MQ analyses. Virtually all the height information was derived from rawinsonde data, while the wind analyses depended upon rawinsonde and satellite cloud-tracked wind data. Although the DC-8 flight-level observations and the associated dropwindsondes produced a relatively small proportion of the total number of observations, their locations were critical to accurately measuring the atmosphere within 1000 km of Typhoon Flo.

The wind observations (Figure 2.5) for IOPs 5-7 had a relative minimum in the middle troposphere (700 - 300 mb), which is common for tropical wind data distributions (Elsberry 1987). The analyzed domain included much elevated terrain (*e.g.*, the Tibetan Plateau). Since 1000-mb height and wind observations were not reported when the station pressure was less than 1000 mb, the number of 1000 mb observations was relatively small. The special data unique to the TCM-90 were also concentrated in the lower and upper troposphere (Figure 2.6). Therefore, the NOGAPS analyses were especially important as a first guess in the mid-tropospheric region.

| Level | RAWIN | LDW | CTO | CTW | AIREP | DC8 | TOTAL |
|-------|-----------------|--------------|-----|-----|-------|-------------|-----------------|
| 1000 | 3284 (247) | 39 (19) | - | - | - | - | 3323 (266) |
| 850 | 3618 (120) | 62 (27) | - | - | - | 6 (6) | 3686 (153) |
| 700 | 3708 (156) | 66 (29) | - | - | - | 10 (10) | 3784 (195) |
| 500 | 3818 (67) | 70 (26) | - | - | - | 9 (9) | 3897 (102) |
| 400 | 3452 (89) | 71 (24) | - | - | - | 9 (9) | 3532 (122) |
| 300 | 3444 (79) | 71 (25) | - | - | - | 9 (5) | 3524 (109) |
| 250 | 3385 (145) | 37 (24) | - | - | - | 39 (1) | 3461 (170) |
| 200 | 3553 (150) | - | - | - | - | 298 (12) | 3651 (162) |
| 150 | 3277 (261) | - | - | - | - | - | 3277 (261) |
| 100 | 3161 (357) | - | - | - | - | - | 3161 (357) |
| SUM | 34500 (1671) | 416 (174) | - | - | - | 380 (52) | 35296 (1897) |

Table 2.4. TOTAL NUMBER OF HEIGHT OBSERVATIONS FOR TCM-90 IOPS 5-7, BY OBSERVATION TYPE AND PRESSURE LEVEL, INCLUDED IN THE MULTI-QUADRIC (MQ) ANALYSIS. VALUE IN () IS THE NUMBER OF OBSERVATIONS REJECTED BY HORIZONTAL QUALITY-CONTROL CHECKS.

| Pressure Level (mb) | RAWIN | LDW | CTO | CTW | AIREP | DC8 | TOTAL |
|---------------------|----------------|-------------|--------------|---------------|--------------|-------------|----------------|
| 1000 | 1772 (9) | 12 (1) | - | - | - | 6 (0) | 1784 (10) |
| 850 | 3823 (23) | 33 (4) | 1902 (3) | 2663 (3) | - | 35 (0) | 8427 (33) |
| 850 | 4023 (15) | 31 (0) | 50 (4) | 182 (0) | 4 (0) | 9 (0) | 4300 (19) |
| 500 | 4091 (17) | 39 (1) | 3 (2) | 734 (0) | 15 (10) | 9 (0) | 4891 (21) |
| 400 | 3732 (10) | 42 (2) | - | 221 (0) | 28 (0) | 3 (2) | 4032 (12) |
| 300 | 3691 (11) | 41 (2) | 123 (13) | 1402 (4) | 255 (6) | 9 (0) | 5521 (33) |
| 250 | 3610 (8) | 33 (1) | 1984 (2) | 1781 (1) | 623 (12) | 39 (0) | 8070 (24) |
| 200 | 3545 (10) | 1 (0) | - | 3425 (3) | 376 (9) | 298 (1) | 7645 (23) |
| 150 | 3399 (12) | - | - | 2159 (0) | 10 (0) | - | 5568 (12) |
| 150 | 3230 (6) | - | - | - | - | - | 3230 (6) |
| SUM | 34916 (121) | 232 (11) | 4062 (24) | 12567 (11) | 1311 (28) | 380 (52) | 53468 (196) |

Table 2.5. AS IN TABLE 2.4, EXCEPT FOR WIND OBSERVATIONS.

| | RAWIN | LDW | CTO | CTW | AIREP | DC8 | TOTAL |
|------|---------------|------------|-----|-----|-------|-----|---------------|
| 1000 | 1901 (3) | 39 (1) | - | - | - | - | 1940 (4) |
| 850 | 3615 (3) | 62 (1) | - | - | - | - | 3677 (4) |
| 700 | 3831 (6) | 66 (0) | - | - | - | - | 3897 (6) |
| 500 | 3949 (7) | 70 (0) | - | - | - | - | 4019 (7) |
| 400 | 3587 (3) | 72 (0) | - | - | - | - | 3659 (3) |
| 300 | 3578 (4) | 70 (0) | - | - | - | - | 3651 (4) |
| 250 | 3513 (6) | 69 (0) | - | - | - | - | 3582 (6) |
| 200 | 3485 (7) | 12 (0) | - | - | - | - | 3497 (7) |
| 150 | 3391 (11) | - | - | - | - | - | 3391 (11) |
| 100 | 3282 (12) | - | - | - | - | - | 3282 (12) |
| SUM | 34132 (62) | 463 (2) | - | - | - | - | 34595 (64) |

Table 2.6. AS IN TABLE 2.4, EXCEPT FOR TEMPERATURE OBSERVATIONS.

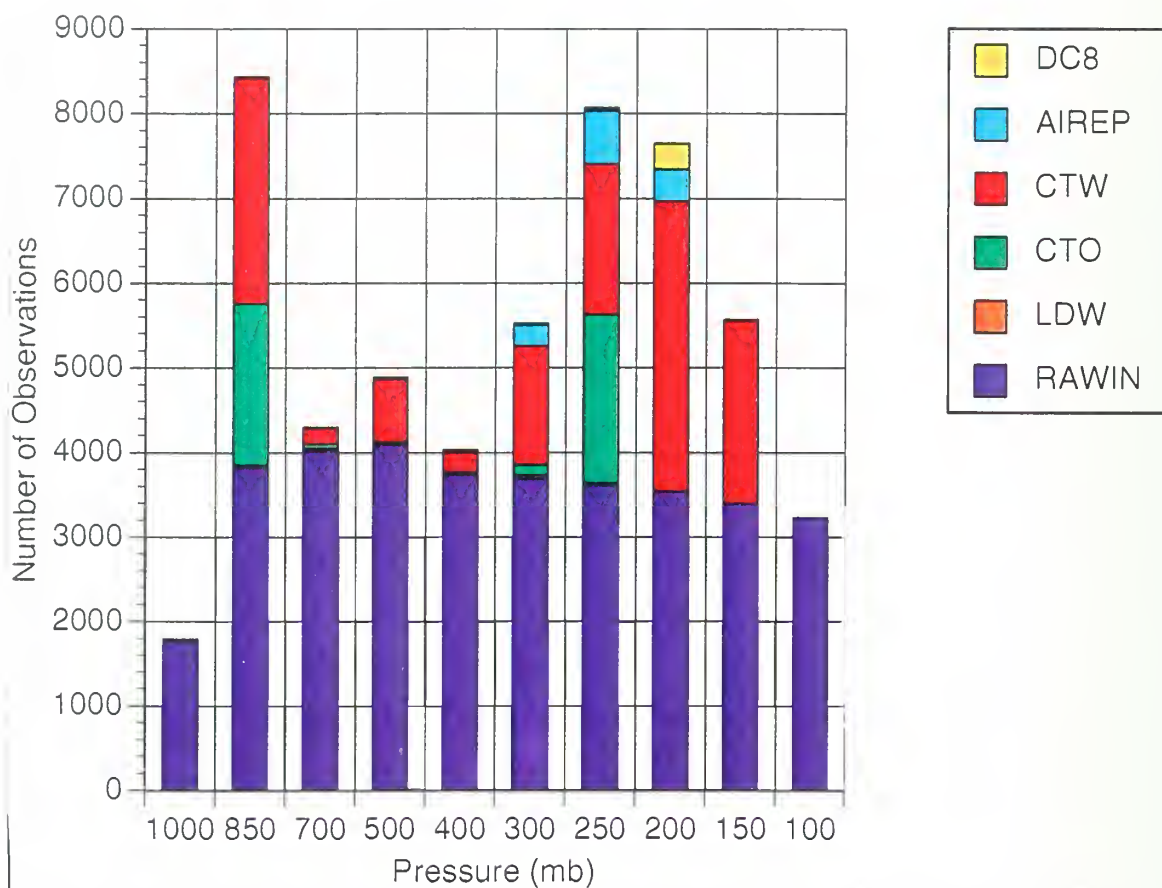


Fig. 2.5. Number of wind observations in TCM-90 dataset for IOPs 5-7 (00 UTC 13 September through 00 UTC 19 September) by type of observation (see inset, with types as in Figures 2.1 and 2.2).

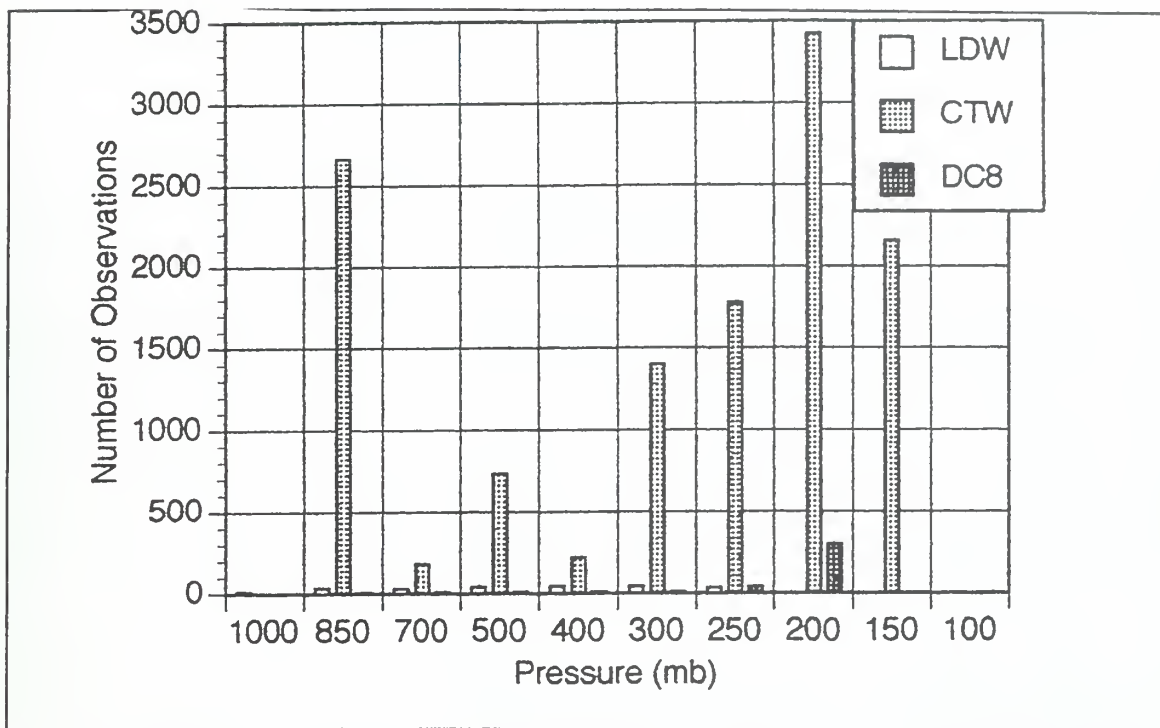


Fig 2.6. Number of delayed wind observations in TCM-90 data set for IOPs 5-7 by type of observation, as defined in Figures 2.1 and 2.2.

Because the NOGAPS analyses received at the Naval Postgraduate School (NPS) were of a 2.5° latitude/longitude (≈ 278 km) resolution, they did not contain the mesoscale details near tropical cyclones. However, they did provide a good synoptic basis from which to commence a higher-resolution analysis. Details on NOGAPS are given by Bayler and Lewit (1992).

In this application, the analyses on mandatory pressure levels were performed on a vertical series of two-dimensional slabs; *i.e.*, no explicit vertical coupling between analyses at adjacent vertical levels was enforced. However, implicit coupling came from the NOGAPS first-guess fields and from a vertical set of observations (*e.g.*,

a rawinsonde observation). Synthetic observations (described later) were added to ensure that the tropical cyclones were vertically aligned.

(2) Horizontal Resolution. Although the data distribution was sparse in certain outlying regions of the TCM-90 domain, it was quite dense in others, especially in the outflow region at 200 mb where there were plentiful cirrus cloud tracers and/or NASA DC-8 flight-level observations (see Figure 2.2). It was on the basis of these high-density upper-level cloud-tracked winds (CTW) and DC8 winds that the entire domain was analyzed at a 50 km horizontal resolution. However, this does not imply that oceanic regions without the high spatial resolution data (*i.e.*, away from the tropical cyclones, especially in the mid-troposphere) support a 50 km horizontal grid. In these regions, the smallest resolvable features may be on the order of several hundred km.

(3) Vertical Resolution. The MQ analysis was performed on mandatory pressure levels extending from near the boundary layer to the lower stratosphere: 1000, 850, 700, 500, 400, 300, 250, 200, 150, and 100 mb. Surface data were not analyzed, since this study was primarily concerned with the response of Flo to any forcing induced by the TUTT cell to the east, the southern outflow region, and the mid-latitude trough to the northwest of Typhoon Flo. Although a sea-surface temperature (SST) analysis was not locally performed, the NCEP-analyzed SSTs on a 0.5° (55.6 km) grid were available from the 4DDA files.

(4) Analysis Domain. A large region from 10°S , 60°E to 60°N , 180° was included in the analysis to ensure that: (i) boundary conditions did not affect

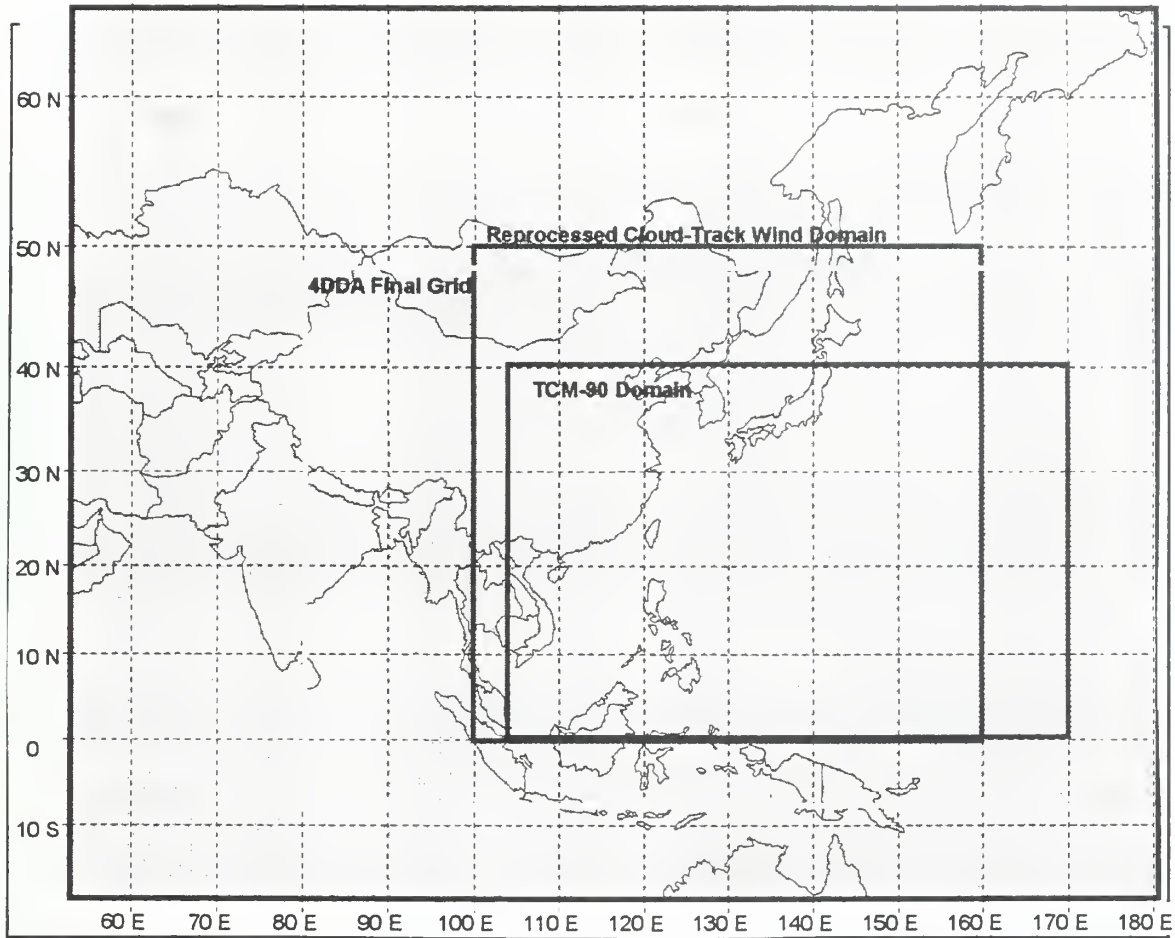


Fig. 2.7. Domains referenced in this study: MQ analysis domain (10°S, 60°E; 60°N, 180°); 4DDA final grid (7.5°S, 80°E; 48.5°N, 172.5°E); Reprocessed cloud-track wind domain (0°N, 100°E; 50°N, 160°E); and TCM-90 analysis domain (0°N, 105°E; 40°N, 170°E) in which MQ analysis will be evaluated, and subsequent diagnostic calculations performed.

any subsequent calculations involving higher-order derivatives; and (ii) any data that might affect the TCM-90 domain analysis were considered. The relationships among the MQ area, the TCM-90 domain (*i.e.*, the region in which subsequent calculations will be performed), and the NCEP 4DDA analysis domain are shown in Figure 2.7.

(5) Analyzed Parameters. Only geopotential heights, winds and temperatures were analyzed in this study. Although it is widely accepted that latent heat release is crucial to the formation and maintenance of tropical cyclones (*e.g.*, Anthes 1982), this study concentrated on the dynamics of the interaction between the tropical cyclone and its adjacent synoptic features. Much of this interaction occurs in the outflow region (*e.g.*, Holland 1987) where vapor pressures are close to zero mb. Vapor pressure analyses would be very important for determining the importance of low-level "surges" into a developing tropical cyclone, but this aspect will not be addressed here.

3. Summary

The MQ method was chosen over more traditional successive-correction schemes based on the results of Franke (1982) and Nuss and Titley (1994). Both studies showed that the MQ method reduced RMS values by 30-50% over the RMS values achieved with successive correction schemes. The MQ method produces fields that are both infinitely differentiable and pleasing to the eye, and thus emulates the work of an experienced synoptic analyst.

Local analyses such as the MQ scheme typically do not contain the dynamic balance constraints found in global or regional analyses. This may be a disadvantage in mid-latitude regions where the dynamics are well known, but the MQ analysis may be more accurate in areas where there are adequate observations, or where the model-predicted first-guess fields are influenced by parameterizations that may not be correct. The outflow region of tropical cyclones may be such an area.

The goal of the locally-produced objective analysis was to depict an alternate representation of the atmosphere in the tropics, especially at levels where there were significant additional observations in the TCM-90 dataset. These analyses will be compared with the 4DDA of the TCM-90 final dataset produced by NCEP, as well as with the NOGAPS analyses. In this study, the NOGAPS analyses should be viewed as a control case, since: (i) the resolution of NOGAPS (received at NPS) is 2.5° latitude/longitude; and (ii) many of the observations unique to TCM-90 were not received in the operational dataset.

D. DATA MANAGEMENT

A key decision in any analysis scheme is what data to include and what data to omit. In general, the more data included, the more accurate the analysis. However, observations with large variability (*i.e.*, operational cloud-track winds (CTO) and AIREPs) may degrade a final analysis if they are weighted too heavily. Harr *et al.* (1991) describe the real-time and delayed-data collection procedures employed in TCM-90. Observations used in the MQ analysis, the NCEP-produced Eta model 4DDA, and the operational NOGAPS analysis are shown in Table 2.7.

The MQ analysis used all of the upper-air observations collected during TCM-90 IOPs 5-7 with two exceptions: (i) Radar profiler data; and (ii) satellite temperature soundings. Each of the radar profiler sites (Taiwan, Okinawa, Japan, Ponape, and Saipan) was co-located with a conventional rawinsonde observation that provided the required mandatory-level height and wind data at 6-h intervals. Although the radar

| Obs Type | Analysis | | |
|--|----------|------|--------|
| | MQ | 4DDA | NOGAPS |
| Real-Time Surface Synoptic Data | | ✓ | ✓ |
| Delayed Surface Synoptic Data | | ✓ | |
| Real-Time Rawinsondes/ PIBALs | ✓ | ✓ | ✓ |
| Delayed Rawinsondes/ PIBALs | ✓ | ✓ | |
| Drifting Buoy Data | | ✓ | |
| Radar Profiler Data | | | |
| AIREP | ✓ | ✓ | ✓ |
| DC-8 Flight Level Data | ✓ | ✓ | |
| LDW | ✓ | ✓ | |
| CTO | ✓ | ✓ | ✓ |
| CTW | ✓ | ✓ | |
| Satellite Soundings | | ✓ | ✓ |
| Special Sensor Microwave/Imager (SSM/I) Data | | | ✓ |
| Moisture Bogus Data | | ✓ | |
| TC Position Data | ✓ | | ✓ |

Table 2.7. TYPES OF DATA INPUT (✓) INTO MULTI-QUADRIC (MQ), 4-DIMENSIONAL DATA ASSIMILATION SYSTEM (4DDA), AND NOGAPS ANALYSES.

profiler winds have a much higher temporal and vertical resolution, they would not add much to the 6-h, mandatory level analyses because of the co-located rawinsonde observations. Television Infrared Observational Satellite (TIROS) Operational Vertical Sounder (TOVS) data were collected by the TCM-90 Satellite Data Center at the University of Wisconsin (Harr *et al.* 1991). These soundings were stored as mean temperatures. Because this format was not directly compatible with the design of the MQ analysis, the TOVS soundings were not used. Since these data were available in real-time to the NOGAPS multivariate optimal interpolation (MVOI) system at Fleet Numerical Meteorology and Oceanography Center (FNMOC), the TOVS data were implicitly included in the first-guess for the MQ analysis.

1. Data Preparation

All data were initially in FGGE-IIB formats described in Harr *et al.* (1991). Data were first converted to GEMPAK format for easy SKEW-T plotting. NASA DC8 height observations were hydrostatically adjusted to the nearest mandatory pressure level, and the DC8 and AIREP wind observations were assigned to the closest mandatory pressure level. After application of the static quality control (QC) checks (described in Appendix A), the mandatory-level height, wind, and temperature observations were transferred to the NPS AMDAHL mainframe for the MQ analysis. The initial data processing is fully described in Appendix B.

2. Quality Control

Quality control (QC) procedures were stringently applied in this study. Much effort was spent in obtaining the best-possible dataset, given the distribution and accuracy of the combined real-time and delayed TCM-90 observations. Since objective analyses typically have no dynamic constraints in the deep tropics (Elsberry 1987), the dynamic consistency can be no better than the observations. Much of the QC is based upon the procedures employed for the real-time NOGAPS database, which are given in Baker (1992). Real-time and delayed data were checked for climatological limits, hydrostatic and adiabatic consistency, and "reasonable" vertical wind shear. Each observation that was flagged as bad or suspect by the QC system was manually checked, and either kept, modified, or discarded. Upon completion of the static QC process, the TCM-90 dataset for IOPs 5-7 was vertically consistent for both the mandatory and significant pressure levels.

E. LOCAL OBJECTIVE ANALYSIS SCHEME

The first MQ analyses were unconstrained analyses of heights, winds, and temperatures. These initial analyses were useful for performing the manual horizontal, or "buddy," QC checks. These first analyses also highlighted weaknesses in the analyses (*e.g.*, inconsistent wind and mass fields, unrealistic TC depiction). As problems were discovered, features were added to the MQ analysis to correct these observed deficiencies. Thus, the MQ analysis scheme as currently implemented was developed in an iterative manner over a period of several months. The final MQ analyses contained the following features:

- Two-dimensional analyses are of the increments (observation - first guess) of geopotential heights, winds, and temperatures at mandatory pressure levels from 1000 mb to 100 mb, where the first guess is the NOGAPS analysis;
- All interpolations are performed with B-splines as opposed to bi-linear interpolations. As shown by Franke (1985), B-splines reduce the error in the grid-to-observation interpolation, which reduces the error in the final analysis;
- Observations separated by less than 25 km are composited into one observation placed at the geometric center of the observation locations. These composite observations are not given any greater weight than individual observations;
- Observations are weighted according to observing platform, observation type, and pressure as shown in Table 2.2;
- Height analysis is geostrophically constrained north of 35°N, unconstrained south of 25°N, and a linear blend between 25°N and 35°N;
- Gradient winds based upon the MQ analyzed height field are the first guess for the wind analysis within 300 km of tropical cyclones and north of 35°N;
- Temperature analysis is unconstrained by any other variables throughout the domain;
- Boundary-layer friction effects are (simply) parameterized in the MQ analysis at 1000 mb;
- Winds and heights within 300 km of a TC are replaced by an azimuthal average (with radial increments of 50 km) in a moving cylindrical coordinate system, and blended with the Cartesian coordinate system between 300 km and 600 km of a TC. The wind field azimuthal-averaging occurs after the final MQ analysis, while the height field azimuthal-averaging occurs during the first guess.

Figure 2.8 provides an overview of the entire objective analysis procedure, and a flow diagram of the steps in the analysis program are shown in Figure 2.9. The analysis enhancements added to correct perceived deficiencies can be divided into five key areas: (i) Observation QC; (ii) Dynamic constraints; (iii) First-guess modifications;

(iv) Observation enhancements; and (v) Post-processing the TC wind field. The following sections describe these enhancements in detail.

1. Observation Quality Control

Although the initial static QC checks determined that the observations were plausible and vertically consistent, adjacent observations at a given pressure level had not been compared. In addition to these horizontal QC checks, the height observations may require a radiation correction (*e.g.*, Julian 1991, Baker 1992). Finally, the NASA DC8 and LDW height observations appeared to have a significant bias. The following sections will discuss the methods of dealing with these problems.

a. Horizontal Quality Control Checks

As in the earlier vertical QC checks, this process was primarily manual. At each pressure level, the increment field plots and output logs were scanned for large or inconsistent increments. If the suspicious increment was determined to be unrealistic, then the time, station number, pressure level, and parameter type were added to the file that would drop that increment from the analysis scheme in future runs. This QC check was an iterative process, with up to three runs required per level to remove all the unrealistic observations. This QC process was analogous to algorithms in use at FNMOC and NCEP that check for observation "unrepresentativeness" and discards those observations. Since the philosophy was to be very cautious in deleting observations, especially in the vicinity of tropical cyclones, some questionable observations were retained.

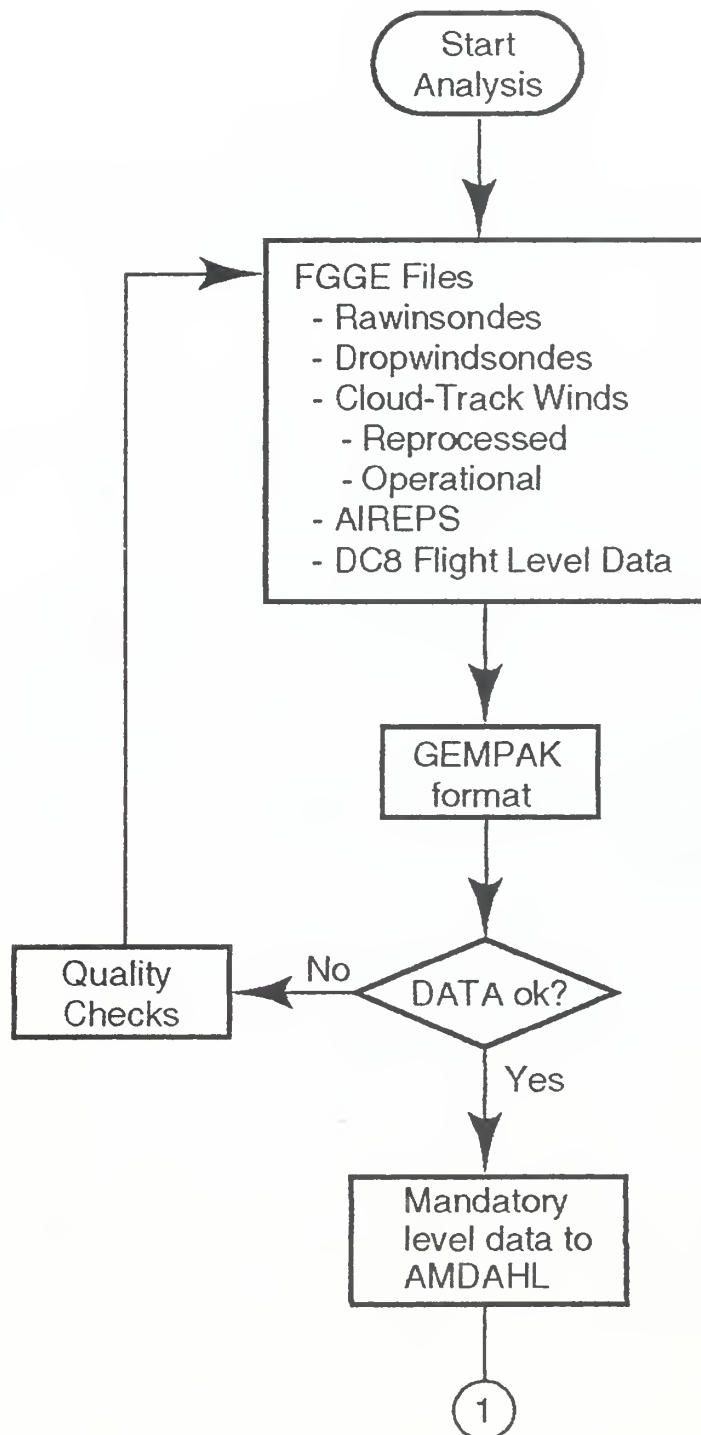


Fig. 2.8. Overall flow diagram of steps in the MQ analysis procedure (see text for description).

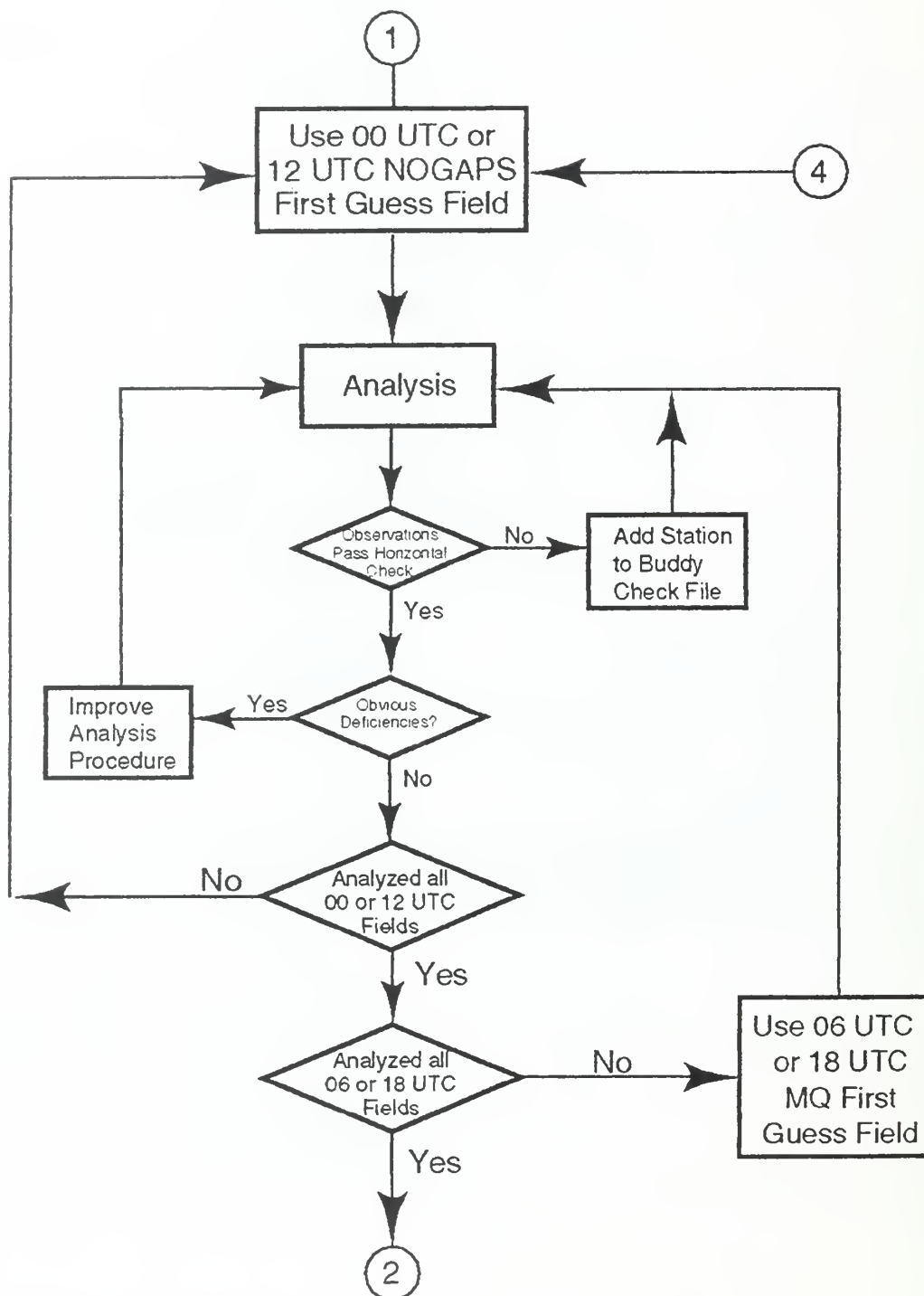


Fig. 2.8. Continued.

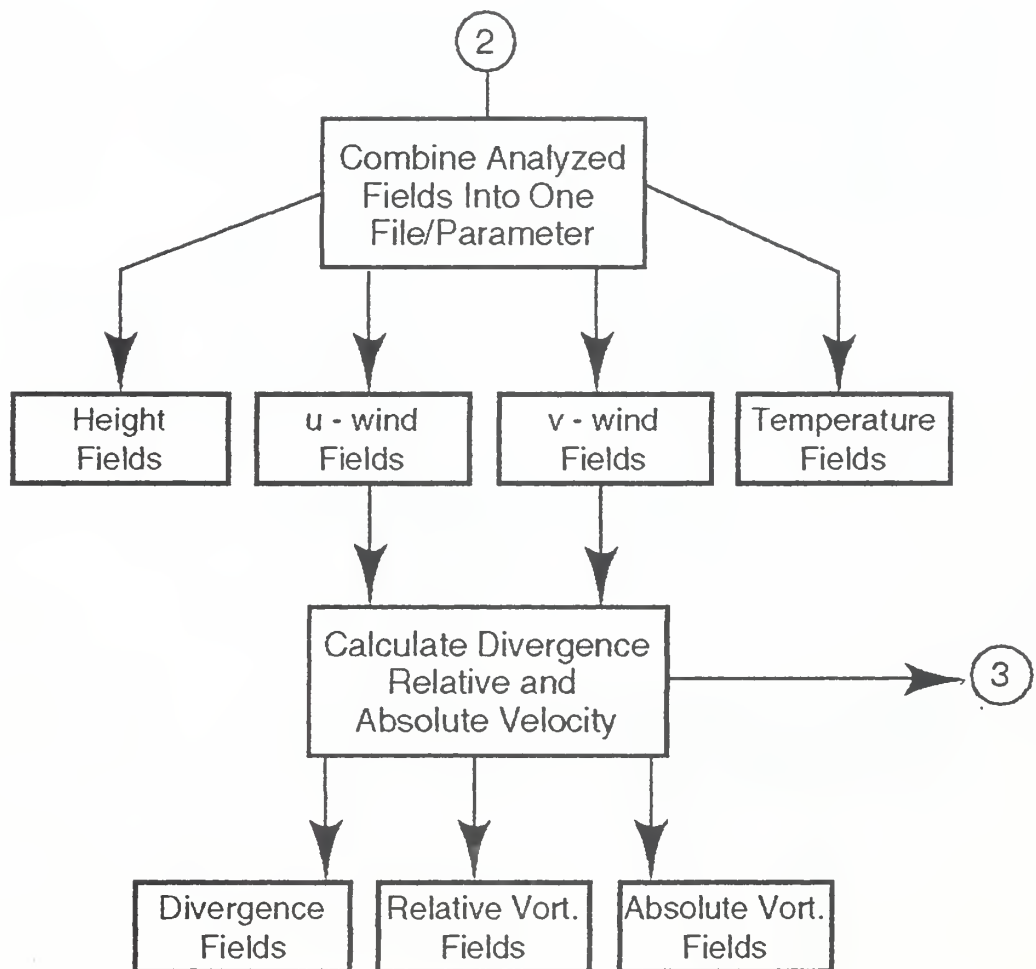


Fig. 2.8. Continued.

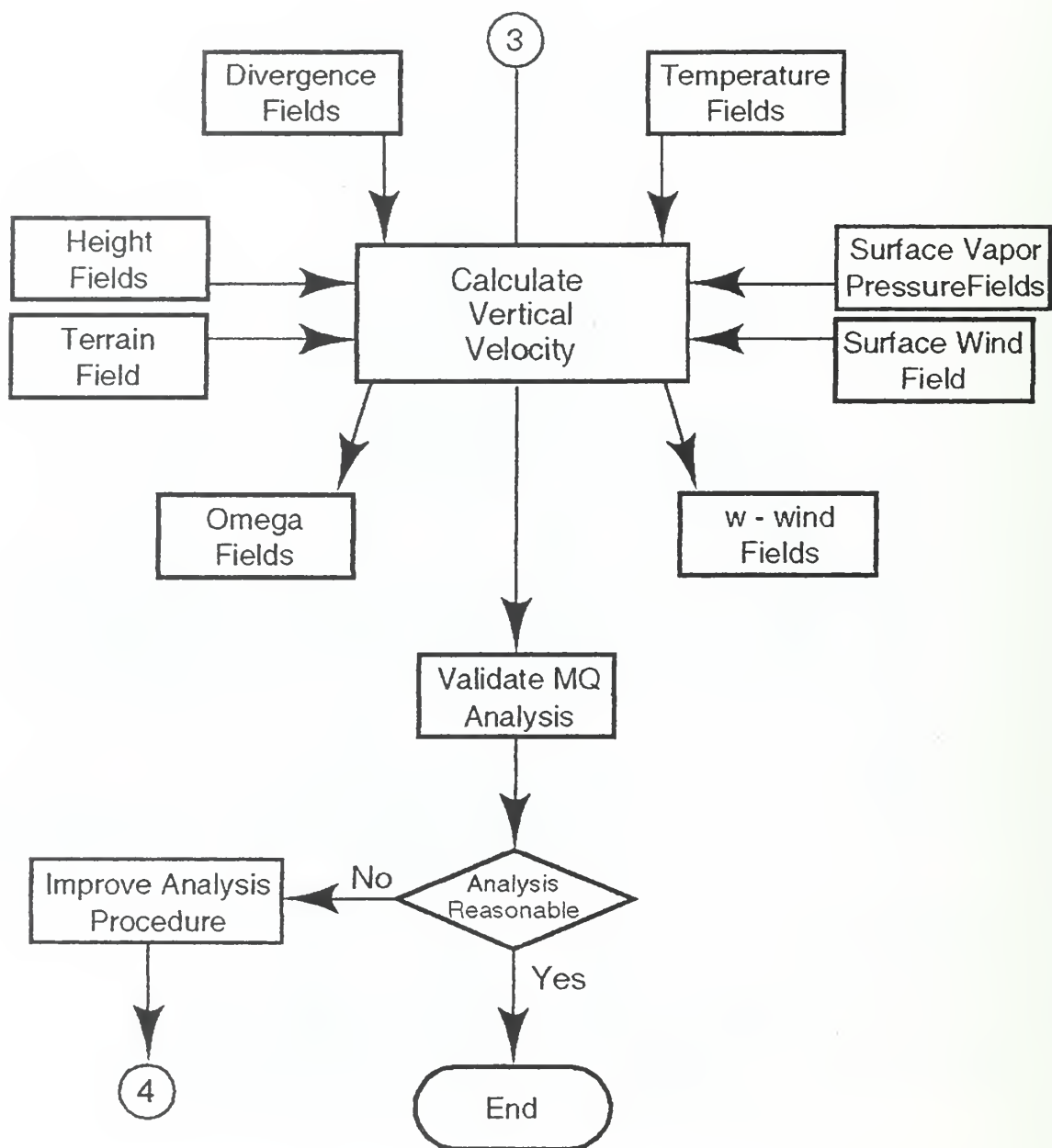


Fig. 2.8. Continued.

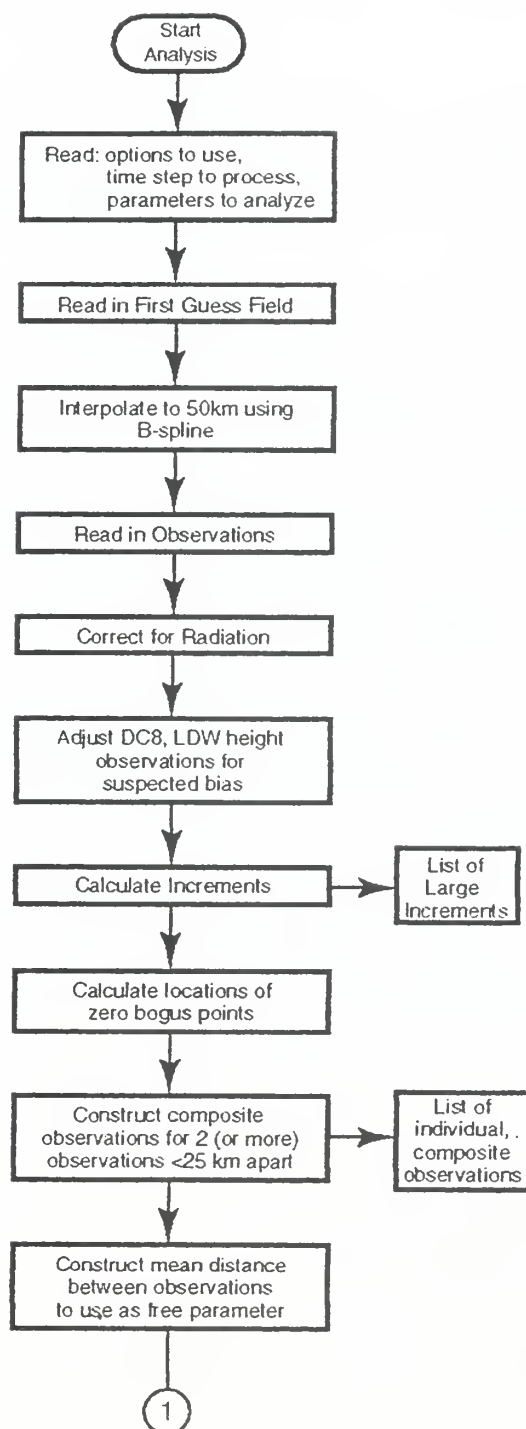


Fig. 2.9. Flow diagram of special processing steps in the Multi-Quadric analysis algorithm (see text for description).

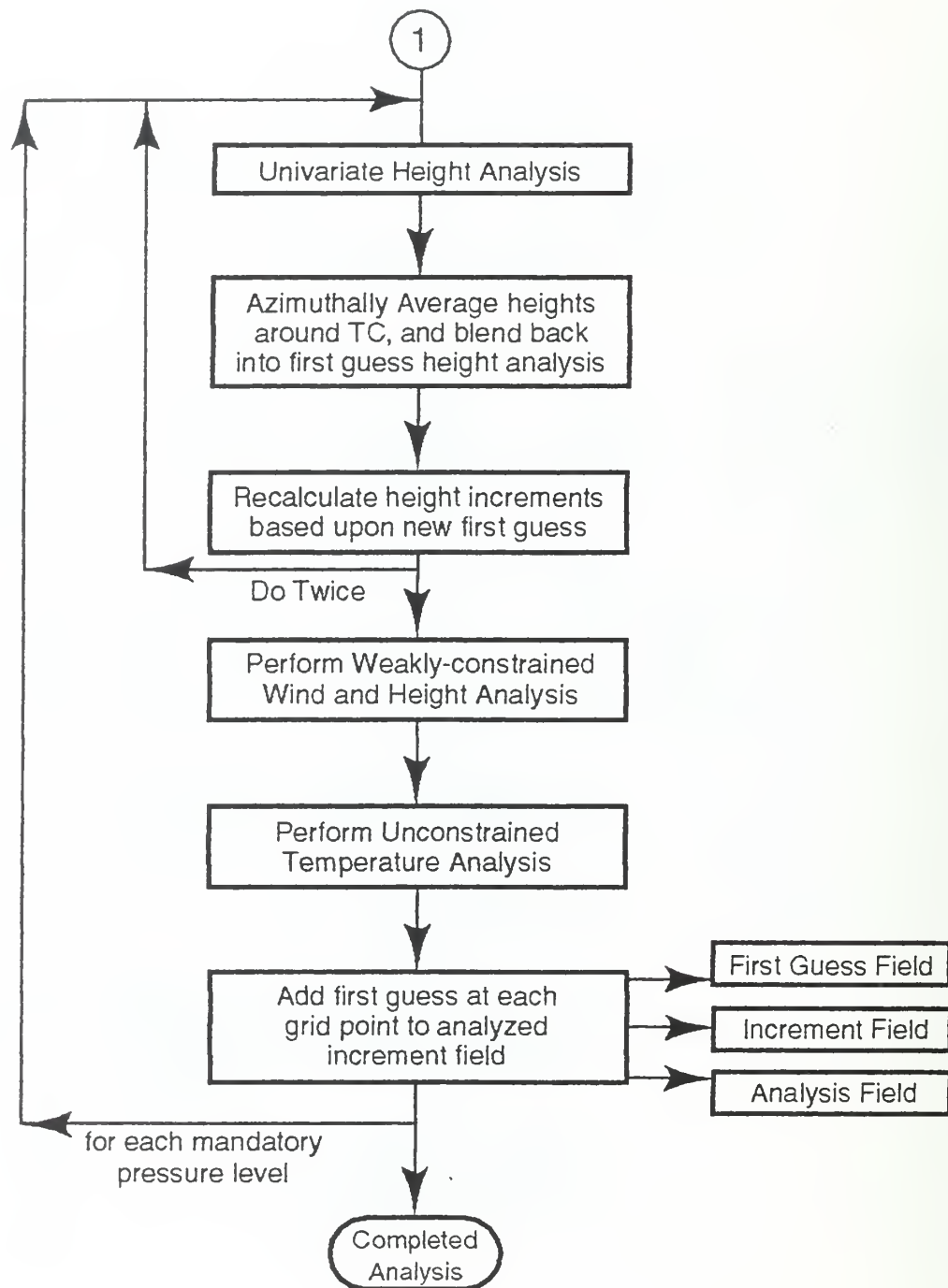


Fig. 2.9. Continued.

Despite this conservative philosophy, nearly 2000 height, 200 wind, and 65 temperature observations were removed from the dataset (Tables 2.4, 2.5, and 2.6, respectively). These numbers represent about 5%, 0.3%, and 0.2% respectively of the total number of observations. Goerss and Phoebus (1992) state that the FNMOC operational real-time QC system typically rejects 2%, and flags as questionable an additional 3%, of the rawinsonde observations, which is consistent with the rejection of about 5% of the rawinsonde data in this study. FNMOC typically rejects 15-20% of the cloud-tracked winds and 4-5% of the AIREP reports. These numbers are substantially higher than the percentage of similar observations rejected here. The lack of model constraints, a willingness to accept potentially greater increments, and the availability of higher-quality reprocessed cloud-track winds throughout much of the domain are probable reasons for maintaining a greater proportion of AIREP and cloud-tracked wind reports than does a typical operational QC system.

Although the distribution of unrealistic wind observations (not shown) normally had little correlation between subsequent time periods, certain stations consistently had questionable height observations. These observations either had a constant bias relative to their surrounding observations, or the magnitude of the bias increased with height. For the first case, it is likely that the station height was incorrectly reported. If the true station height could be determined, then these observations were corrected. If the increment became more positive (negative) with height, then the rawinsonde thermistor likely had a warm (cold) bias. Another possibility

was incorrect observing procedures (Julian 1991). Whatever the cause, these observations were discarded. Most of these types of errors occurred over the former Soviet Union and China. Heights over the Indian sub-continent were not analyzed due to the large number of stations that had very large (> 100 m) increments. About 75% of these observations are routinely rejected in the FNMOC QC system (N. Baker, personal communication).

b. Radiation Error Corrections

It is well known (*e.g.*, Baker 1992; Schmidlin 1991; Julian 1991) that longwave and shortwave radiation on the rawinsonde thermistor may produce significant errors in the computed geopotential height. Baker (1992) states that these errors are strongly dependent upon the specific rawinsonde in use. For example, sharp variations in geopotential height bias (observation minus NOGAPS analysis) often occur across political boundaries when the countries use rawinsondes from different manufacturers. An example of the height increments at 200 mb before adjusting for radiation error is shown in Figure 2.10. The large positive increments in the Chinese data, while the Japanese and Korean stations appear to have only a slight positive bias, are consistent with the findings of Baker (1992).

The calculated geopotential heights were adjusted to account for the radiation error prior to their use in the MQ analysis. For stations in the former Soviet Union, China, and World Meteorological Organization (WMO) blocks 47 (Korea and Japan) and 48 (Southeast Asia), rawinsonde geopotential height bias values for each

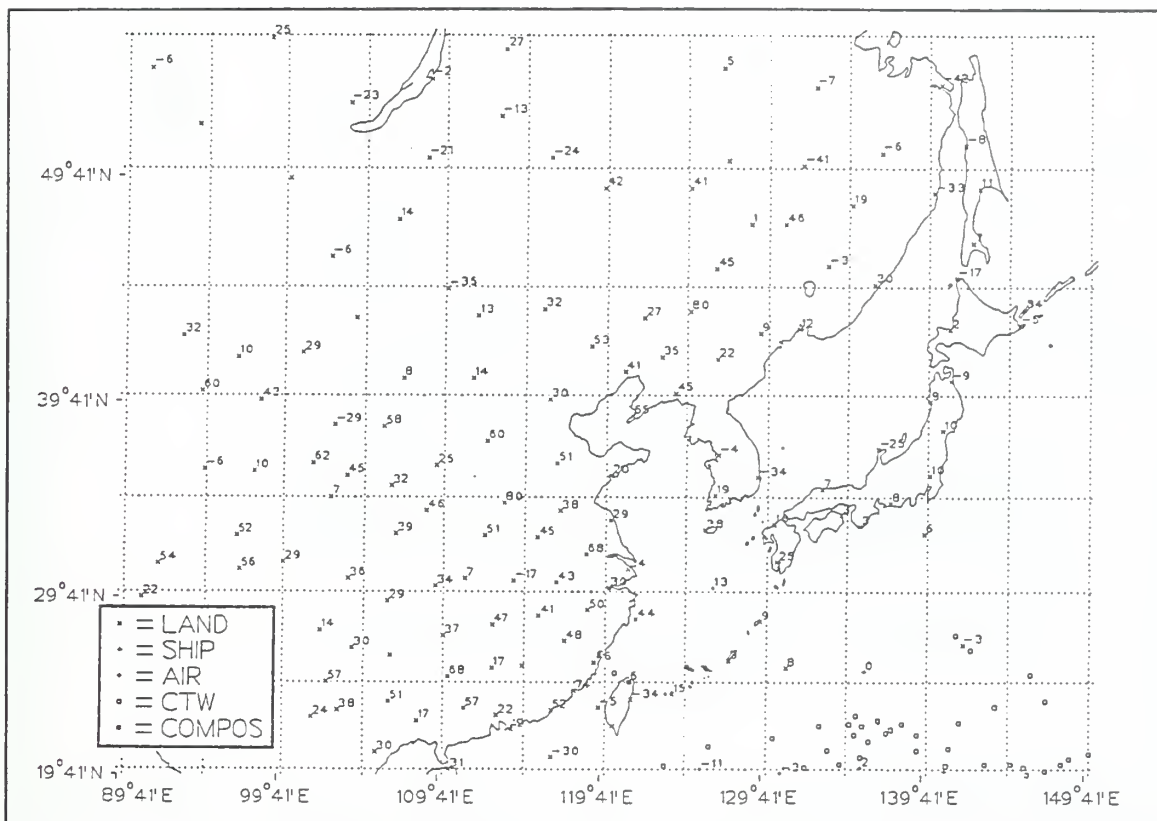


Fig. 2.10. 200 mb height (m) increments (observation minus first guess) for 00 UTC 13 September prior to adjustment for bias due to long- and short-wave radiation on the rawinsondes. Observation types as in Figures 2.1 and 2.2.

analyzed pressure level were obtained from the Naval Research Laboratory (N. Baker). September 1991 data were selected to calculate the radiation error corrections since the September 1990 data were not available. Biases were calculated within each WMO block number. For countries that span multiple WMO block numbers (*i.e.*, China and the former Soviet Union), the biases were averaged to obtain one set of radiation corrections for each country. These biases were calculated separately for 00 UTC (Figure 2.11a) and 12 UTC (Figure 2.11b) for the USSR, China, and Japan. The large positive height

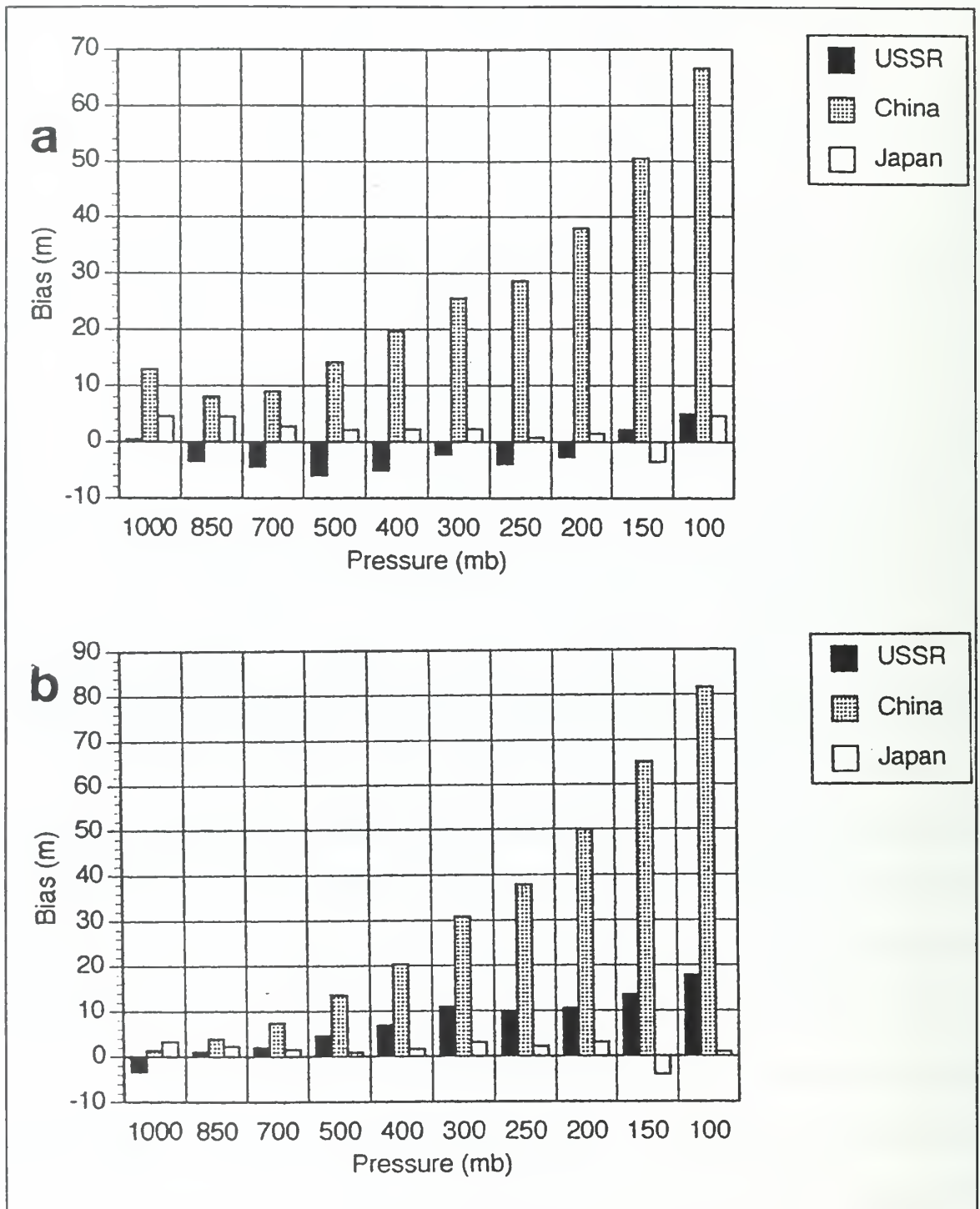


Fig. 2.11 Height (m) bias (observation minus NOGAPS analysis) at mandatory pressure levels for USSR, Chinese, and Japanese rawinsondes (see inset for symbols) for (a) 00 UTC and (b) 12 UTC during September 1991.

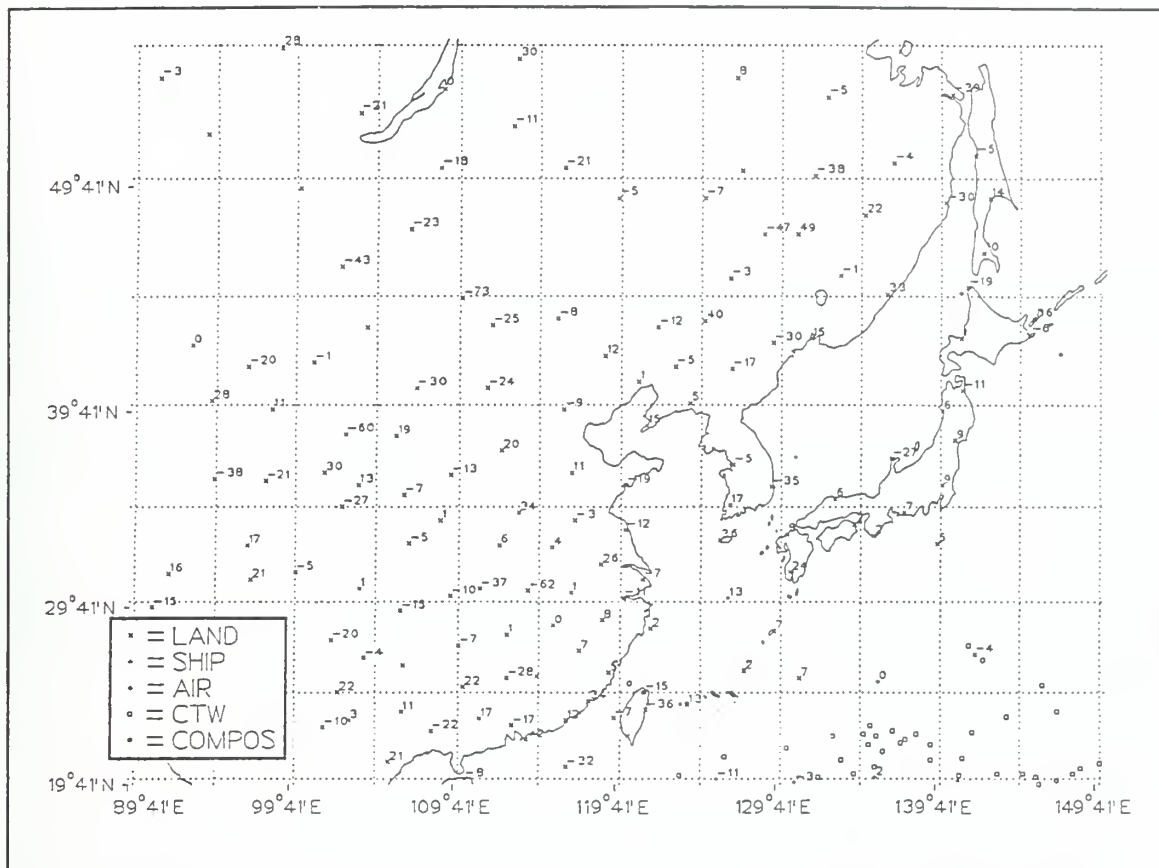


Fig. 2.12. Height increments as in Figure 2.10, except rawinsondes have been adjusted for bias induced by long- and short-wave radiation.

biases found for both morning and evening in the Chinese soundings are similar to the results of Baker (1992).

Prior to calculating the geopotential height increment, the calculated bias was subtracted from the height observation. Height increments after accounting for the radiation bias (Figure 2.12) had typical values over China that were similar to those over Japan. Of course, this correction does not remove the large spatial variability in the

Chinese rawinsonde increments. The objective analysis technique must produce a smooth field that represents the signal in these noisy observations.

For the TCM-90 stations not included in the September 1991 dataset (primarily Philippine, Indonesian, and Pacific Island stations), the observations were adjusted following the method described in Julian (1991). A mean geopotential height error for each analyzed pressure level (for both 00 and 12 UTC) was determined from the tables of various specific rawinsonde types. This number was then combined with the solar angle (determined from the station location, date, and time) to produce the likely bias. This bias was then subtracted from the observation prior to calculating the height increment for the MQ analysis. These biases were generally less than 10 m at pressures greater than 300 mb, and less than 25 m at lower pressures.

c. DC-8 and LORAN Dropwindsonde Height Observations

Two problems were encountered with the DC-8 flight-level and LDW height observations: (i) hydrostatic conversion from the flight-level height to the geopotential height at the nearest mandatory level; and (ii) an apparent negative bias.

(1) Adjusting the heights to the nearest mandatory pressure level.

Initially, the DC-8 flight-level heights were hydrostatically adjusted from the reported flight-level pressure to the nearest mandatory pressure level using a 1976 U.S. standard atmosphere. The adjusted heights raised (lowered) to a standard pressure level were too low (high), since the tropical lower- and mid-troposphere is warmer than the U.S.

standard atmosphere. Therefore, the thickness between the two pressure levels was greater than that based on the standard atmosphere.

The solution was to first run a preliminary MQ analysis without including the DC-8 flight-level heights. Based upon the previously computed MQ temperature analysis, temperatures were interpolated (using B-splines) to every DC8 observation location and time. This synthetic sounding was used in conjunction with the observed flight-level temperature to derive a mean virtual temperature for the portion of the atmosphere between the mandatory pressure level and the flight-level. Although the dropwindsondes report humidity, these data are suspect when environmental values are greater than 50%. Also, no humidity data were reported for the first 100 seconds after the launch (Harr *et al.* 1991). Therefore, the layer was assumed to have a relative humidity of 60%, and the vapor pressure was determined using the method described in Bolton (1980). The adjustment was added to the DC8 height observation, and the corrected height observations were used in the subsequent MQ analyses.

(2) DC-8 and LORAN Dropwindsonde Height Bias. After the DC-8 heights were adjusted to the nearest mandatory pressure level, it was noticed that these heights appeared to have a 30 to 60 m negative bias. A similar negative bias was found in the LDW height observations.

Several independent checks were performed on the observations before concluding that the observations were in error. For example, the DC-8 aircraft may have flown through a previously undetected trough. The Philippine Sea between

Guam and Okinawa has few rawinsonde reports and it was possible (but unlikely) that NOGAPS had missed a mid- and upper-level tropospheric trough. This possibility was rejected for the following reasons:

- The trough appeared to "follow" the DC-8 flight path. On 16, 17, and 18 September, the DC-8 took a variety of flight paths to and from Typhoon Flo. Wherever the aircraft flew, the apparent trough was observed.
- Satellite imagery (not shown) did not support a trough extending over the entire DC-8 flight path.
- DC8 height observations near (in both space and time) Guam, Okinawa, and the Soviet ships differed by 30 to 60 m from the rawinsonde heights. This was true even for flight-level observations within five mb of a mandatory pressure level, thus reducing the chance that the conversion of flight-level heights to mandatory level heights had inadvertently induced the bias.
- The analysis team at NCEP, working independently, also found and documented these height biases (Rogers *et al.* 1992).

After carefully examining the DC8 and LDW height increments, the decision was made to retain these observations in the MQ analysis, but to add 30 m to the LDW observations and 60 m to the DC8 observations. Any DC8 or LDW height observations that still appeared to have abnormally large increments in subsequent horizontal QC checks were discarded. As shown in Table 2.4, many of the DC8 lower-level heights did not pass the subsequent QC checks. The DC8 and LDW height observations were also weighted less heavily than rawinsonde height observations in the MQ analysis, as shown in Tables 2.2 (higher σ values) and 2.3 (higher λ values).

The reason for retaining these observations after adding an empirical correction was to use the height information that appeared reasonable,

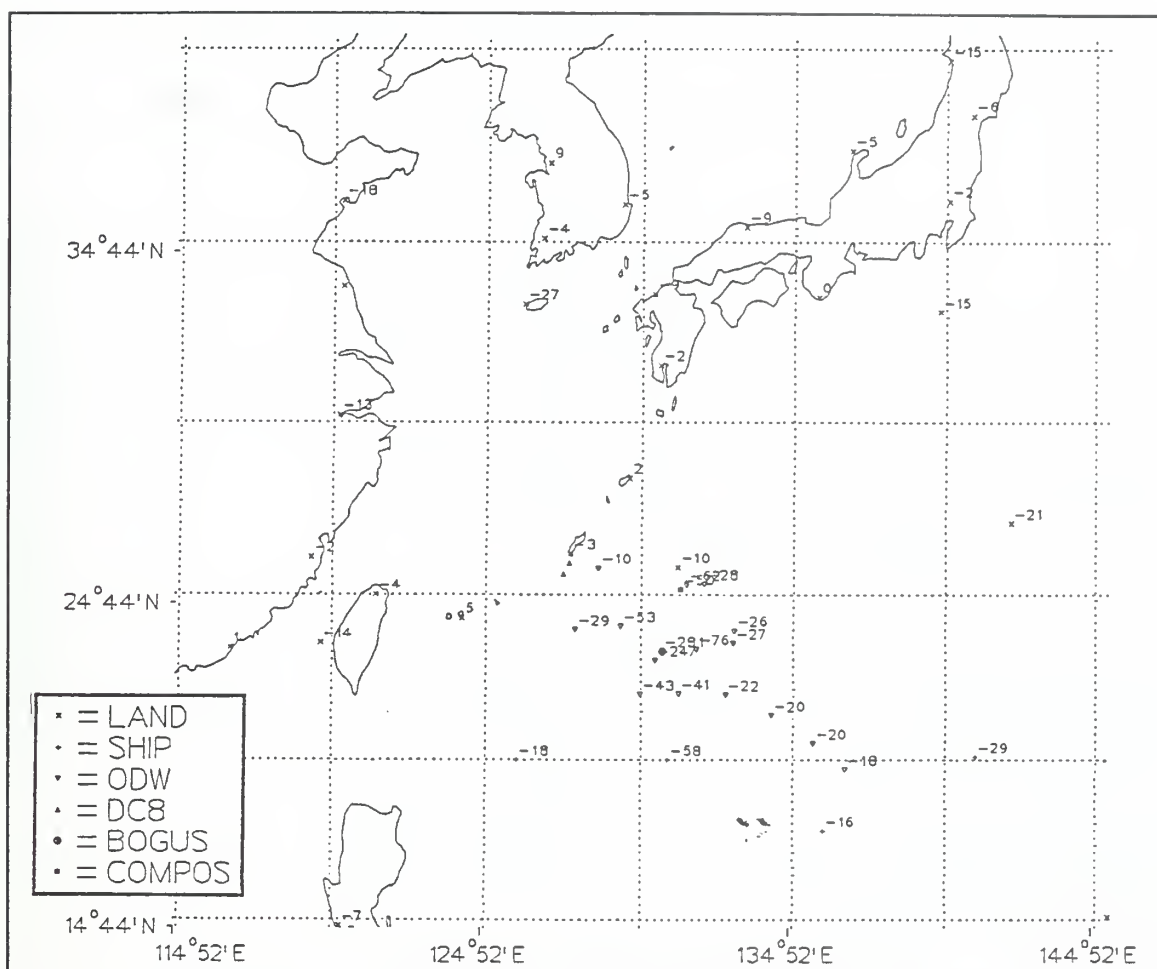


Fig. 2.13. As in Figure 2.12, except for 500 mb at 06 UTC 16 September. Observation types as in Figures 2.1 and 2.2.

especially in the vicinity of Typhoon Flo. Near Flo, the gradients in the increments (or signal) were sufficiently large that the magnitude of the correction was less important, at least relative to the gradients in the quiescent atmosphere away from the typhoon. Height increments at 500 mb in the vicinity of Typhoon Flo at 06 UTC 16 September (Figure 2.13) were as large as several hundred meters. Thus, the (approximate) 30 m bias in the LDW observations was relatively small. Although the true bias in the LDW

and DC8 height observations may never be known, this method retained the available signal from the height observations while avoiding a severe degradation of the MQ height analysis.

While it was disappointing to discover the bias in the NASA aircraft height observations, it is important to note that the DC8 and LDW wind observations were judged to be of high quality and were assimilated well with the adjacent observations into both the MQ and 4DDA analyses.

2. Dynamic Constraints

As discussed above, the MQ analysis can be weakly constrained by the gradient of a field, as well as by the observations. It was quickly apparent (see Figure 2.4) that the height and wind fields analyzed without any dynamic constraints were not in a quasi-geostrophic balance. Therefore, it was decided to impose a weak geostrophic or gradient-wind constraint on the MQ analysis in the mid-latitudes. In the vicinity of tropical cyclones, gradient-wind balance is appropriate, especially in considering an average around the tropical cyclone (Willoughby 1990).

The steps taken to implement a gradient-wind first-guess in the MQ analysis scheme are shown in Figure 2.14. After performing an unconstrained wind analysis, the winds were interpolated using B-splines from the grid to every height observation. Next, the heights were analyzed with the interpolated wind values providing a weak gradient constraint (via the geostrophic relationship) on the height analysis at the point. Using an analysis of the wind field as opposed to the actual wind observations to provide the weak

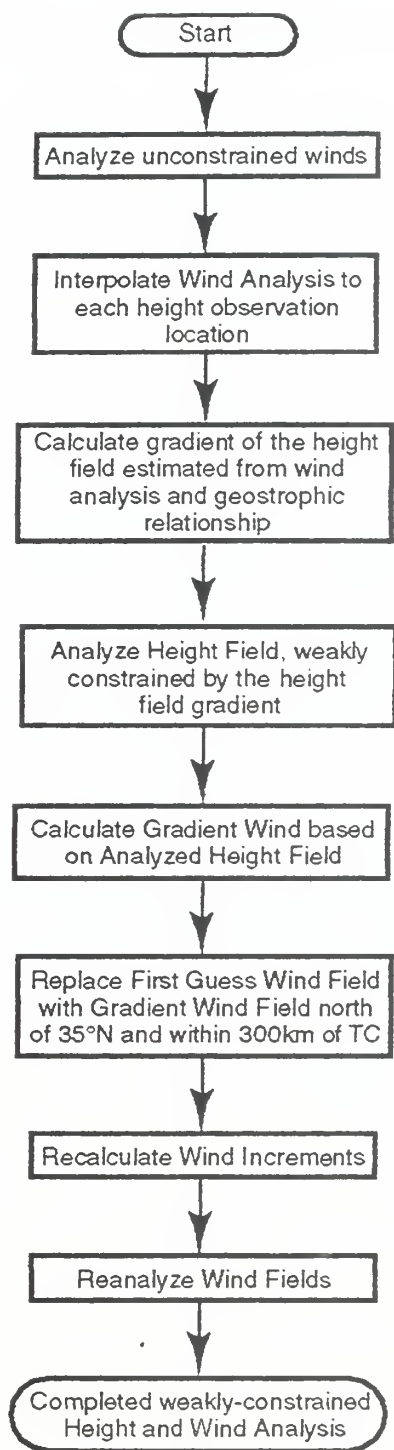


Fig. 2.14. Flow diagram depicting steps to produce constrained height and wind MQ analyses.

constraint had two advantages: (i) The analyzed wind field was smoother than individual observations, so the resulting height analysis was smoother; and (ii) a weak constraint (*i.e.*, a height gradient) could be specified at each height observation even if the wind was not observed at that location. Via these steps, the winds have affected the analysis of the height field.

In the second part of the procedure (Figure 2.14), a gradient wind was calculated based on the analyzed height field. A gradient (as opposed to geostrophic) wind was used because gradient wind balance is more appropriate in the vicinity of a tropical cyclone (see Anthes (1982) for scaling arguments). This gradient wind field became the new first guess north of 35°N and within 300 km of a TC. Between 25°N and 35°N , or between 300 and 600 km from a TC, the gradient wind was blended with the initial NOGAPS first guess. South of 25°N , the wind and height fields were decoupled, and the NOGAPS analysis was used for the wind first guess field. In the final step, the winds were reanalyzed using the new first-guess field. Thus, the height analysis indirectly affected the wind field north of 25°N and within 600 km of a TC, especially in data-sparse regions, because it determined the first guess for the winds.

The 06 UTC 18 September 400 mb height and wind analyses with the application of the weak constraint on the height field and the first-guess gradient wind field are shown in Figure 2.15. In comparison to Figure 2.4 without the dynamic constraints, the wind field is aligned parallel to the height gradient. This is especially apparent near the ridge over Lake Baikal and around the closed low centered near 49°N , 127°E . Since

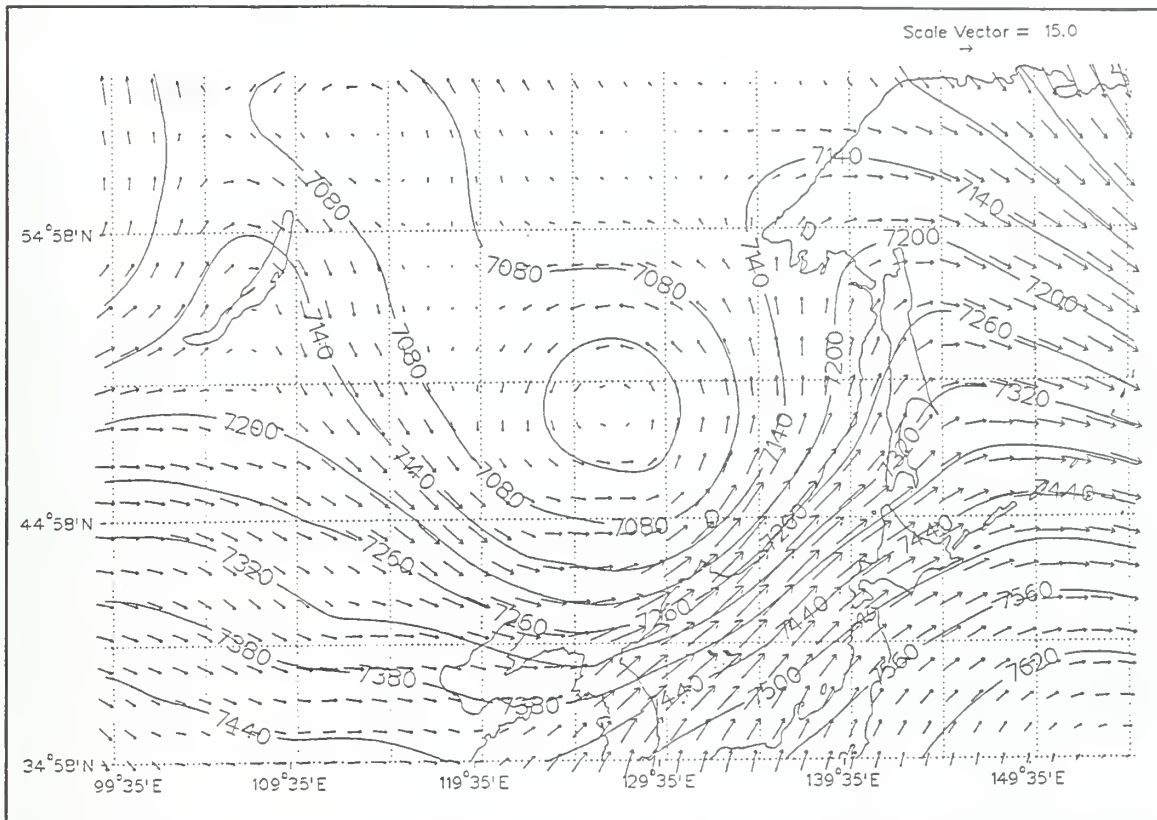


Fig. 2.15. Height and wind MQ analysis as in Figure 2.4, except heights are weakly constrained by geostrophic relationship, and wind analysis has a background field based on a gradient wind derived from preliminary height analysis.

friction is negligible at 400 mb, and quasi-geostrophic balance is generally accepted to apply between 35°N and 60°N, Figure 2.15 appears to be more meteorologically consistent than Figure 2.4. The differences between the dynamically unconstrained and constrained analyses were much more significant at the off-synoptic times, when there were few observations available over the Asian mainland. Even with ample observations, the weakly-constrained analyses appeared to produce more realistic mid-latitude analyses at all times.

The latitudes for the blend zone and for the full implementation of the dynamically constrained analyses (25°N and 35°N respectively) were determined empirically. The 4DDA analysis changes from a multivariate to a univariate height and wind analysis between 20°N and 10°N (Rogers *et al.* 1992), while NOGAPS transitions between a multivariate and univariate analysis at about 20°N (N. Baker, personal communication). It is well known that the correlation between the mass and height field is weak in the tropics (*e.g.*, Elsberry 1987). Extending the weakly constrained wind analysis approach south of 25°N resulted in anomalous circulations in the vicinity of isolated tropical height observations, which is consistent with the weak pressure gradients typically observed in the tropics.

Wind and height fields at 12 UTC 14 September 200 mb with the blend zone and full implementation of the constrained wind and height analyses set at 15°N and 25°N, respectively, are shown in Figure 2.16. Near the ship observation northeast of Luzon, which had a 200 mb height of 12560 m, the wind analysis forced an anticyclonic circulation and anomalously strong winds in the immediate vicinity. The increment chart for that time and level (not shown) indicated the observation had a +75 m increment. Since the gradient wind was used as the first guess, this positive height increment produced an apparent anomalous circulation near this observation. Other times when the weak constraints extended to 15°N had similar localized anticyclonic (cyclonic) circulations around tropical observations with positive (negative) height increments. With the blend zone and full implementation latitudes set at 25°N and 35°N, respectively, a

smooth, flowing analysis (Figure 2.17) is found in the vicinity of the ship observation northeast of Luzon along 20°N. Removing the gradient wind first guess south of 25°N did not hinder the analysis from depicting circulations in the tropics. For example, a weak cyclonic circulation at 23°N over coastal mainland China was consistent with the local CTW and rawinsonde wind observations (Figure 2.17).

While the MQ analysis is weakly dynamically constrained in winds and heights, it does not contain the same degree of sophistication as found in the operational MVOI system in NOGAPS (Goerss and Phoebus 1992) or the NCEP Regional Data Assimilation System (Hoke *et al.* 1989; Petersen *et al.* 1991) used in the 4DDA analysis. The primary reason for the reduced sophistication is the two-dimensional (horizontal) nature of the MQ analysis, as opposed to the three-dimensional spatial analysis in the other schemes. Additionally, calculation of the increments input into the MQ analysis is independent of the background error of the first guess. If the MQ analyses are a valid representation of the atmosphere (to be addressed below), future work should extend the MQ analysis scheme to three dimensions.

3. First-Guess Modifications

The first-guess fields were changed from the real-time NOGAPS analyses in two cases: (i) The wind field first guess was derived from the analyzed height field, as described above; (ii) the height field in the vicinity of a tropical cyclone was modified by the observations to reduce the magnitude of the increments, using a method described below; and (iii) the first-guess wind field at 1000 mb was rotated 20° towards lower

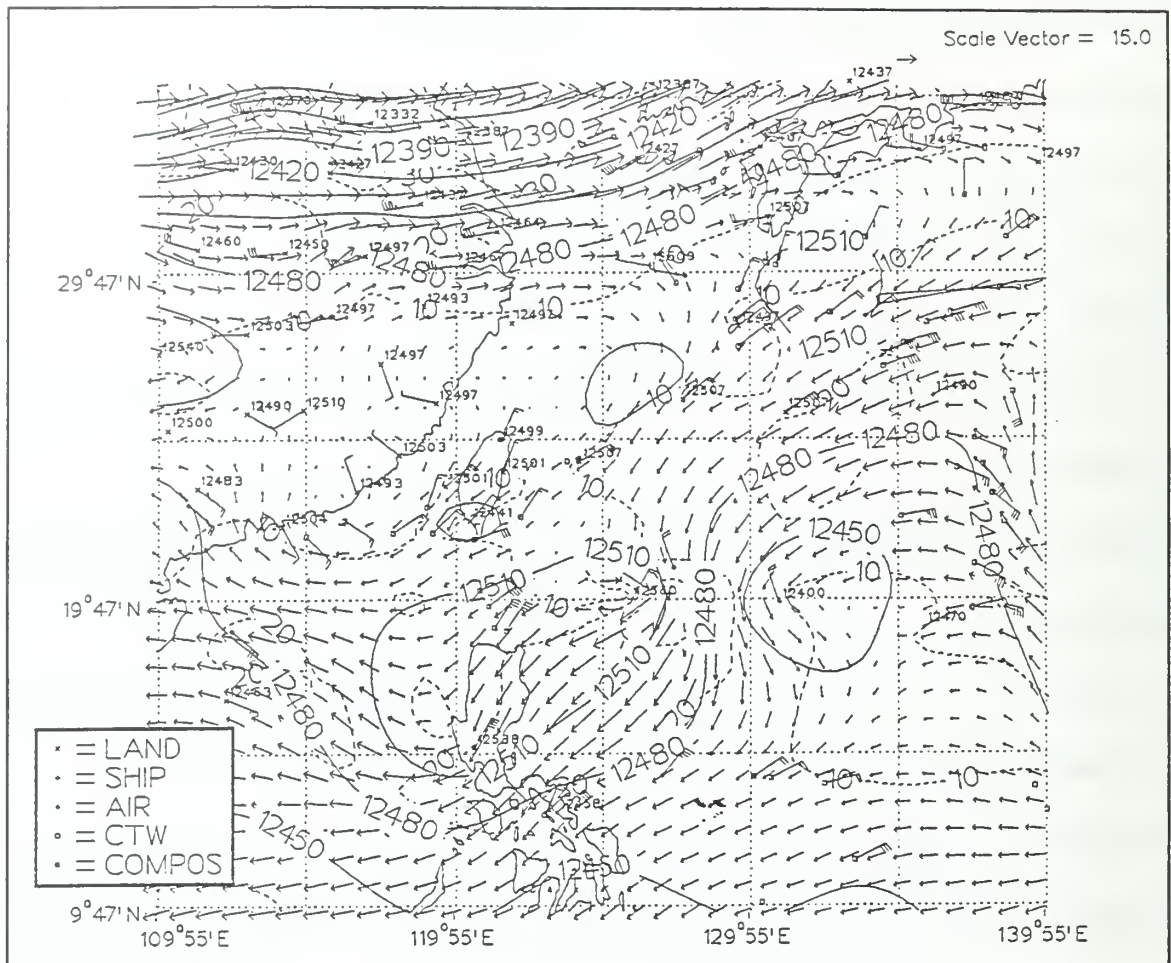


Fig. 2.16. 200 mb height (m, contour interval 30 m) and wind (m s^{-1} , scale vector in upper right) analysis at 12 UTC 14 September with unconstrained analysis south of 15°N , blend zone between 15°N and 25°N , and geostrophic constraint north of 25°N . Observation types as in Figures 2.1 and 2.2.

pressure, and the magnitude was reduced to 90% of the original first guess. This (crudely) parameterized the frictional boundary-layer effects on the 1000 mb wind field.

Analyzing a mature tropical cyclone, even on a 50 km grid, was a challenging task. If the observations were regularly spaced around the storm, then the MQ technique could have produced a plausible pressure field. However, the low-level storm structure

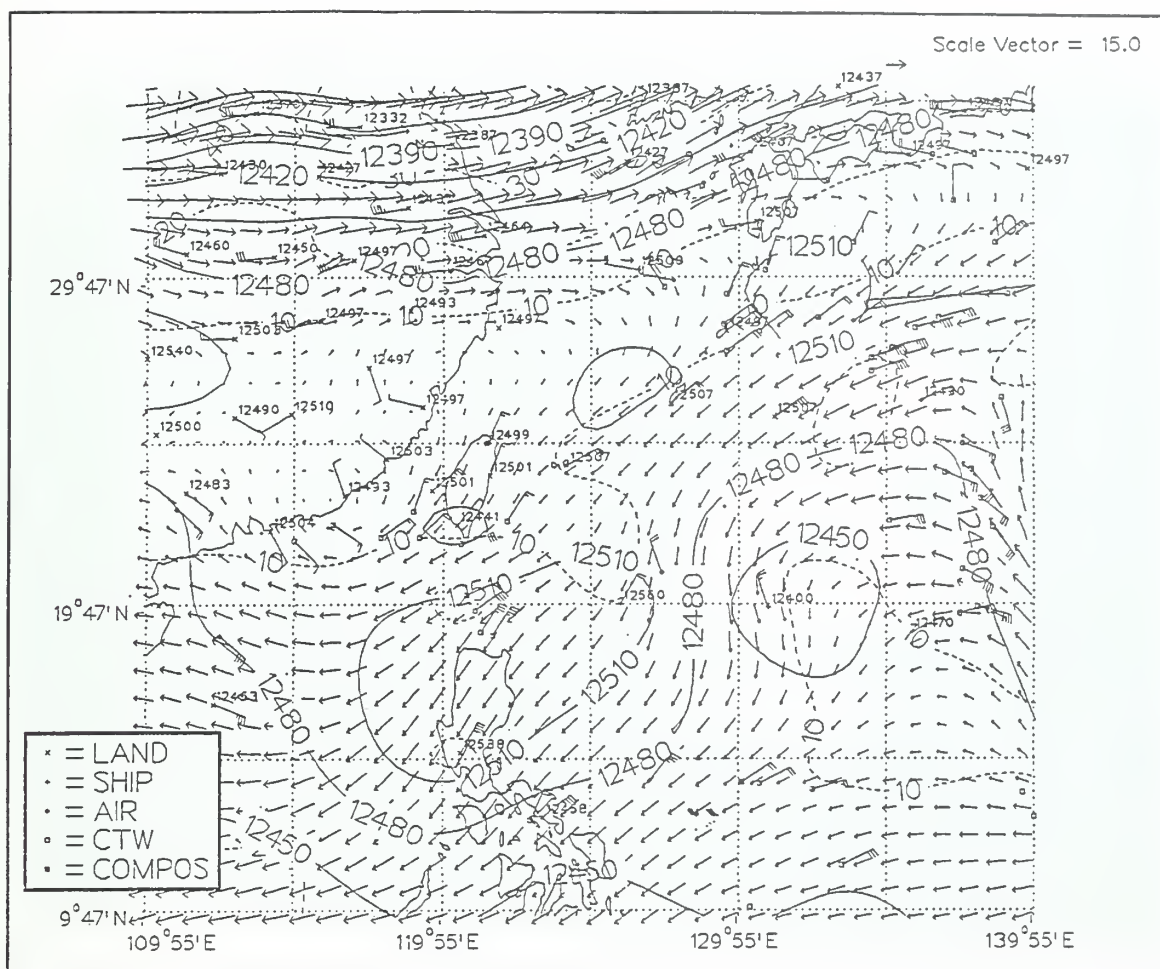


Fig. 2.17 As in Figure 2.16, except unconstrained height and wind analysis south of 25°N, blend zone between 25°N and 35°N, and geostrophic constraint north of 35°N.

was depicted by a few irregularly spaced observations with increments hundreds of meters lower than the first guess from the coarse resolution NOGAPS. The widely-scattered, irregularly-spaced, large-increment observations had the potential to create an unrealistic depiction of a typhoon.

An example of this problem occurred at 12 UTC 18 September. Satellite imagery near this time (Figure 2.18) clearly shows that Typhoon Flo was a moderate-sized, nearly



Fig. 2.18. Geostationary Meteorological Satellite (GMS) visible image of Typhoon Flo at 0503 UTC 18 September.

circular storm as it moved north-northeastward towards southern Japan. The first-guess field at 12 UTC 18 September had only a weak circulation at 500 mb (Figure 2.19). The large increments from the rawinsonde and LDW observations to the immediate north and south of Typhoon Flo did not constrain the increment analysis to the east or west (Figure 2.20). As a result, the increment analysis became very oval-shaped, with the major axis in the unconstrained (east-west) direction. Since this initial height analysis determined

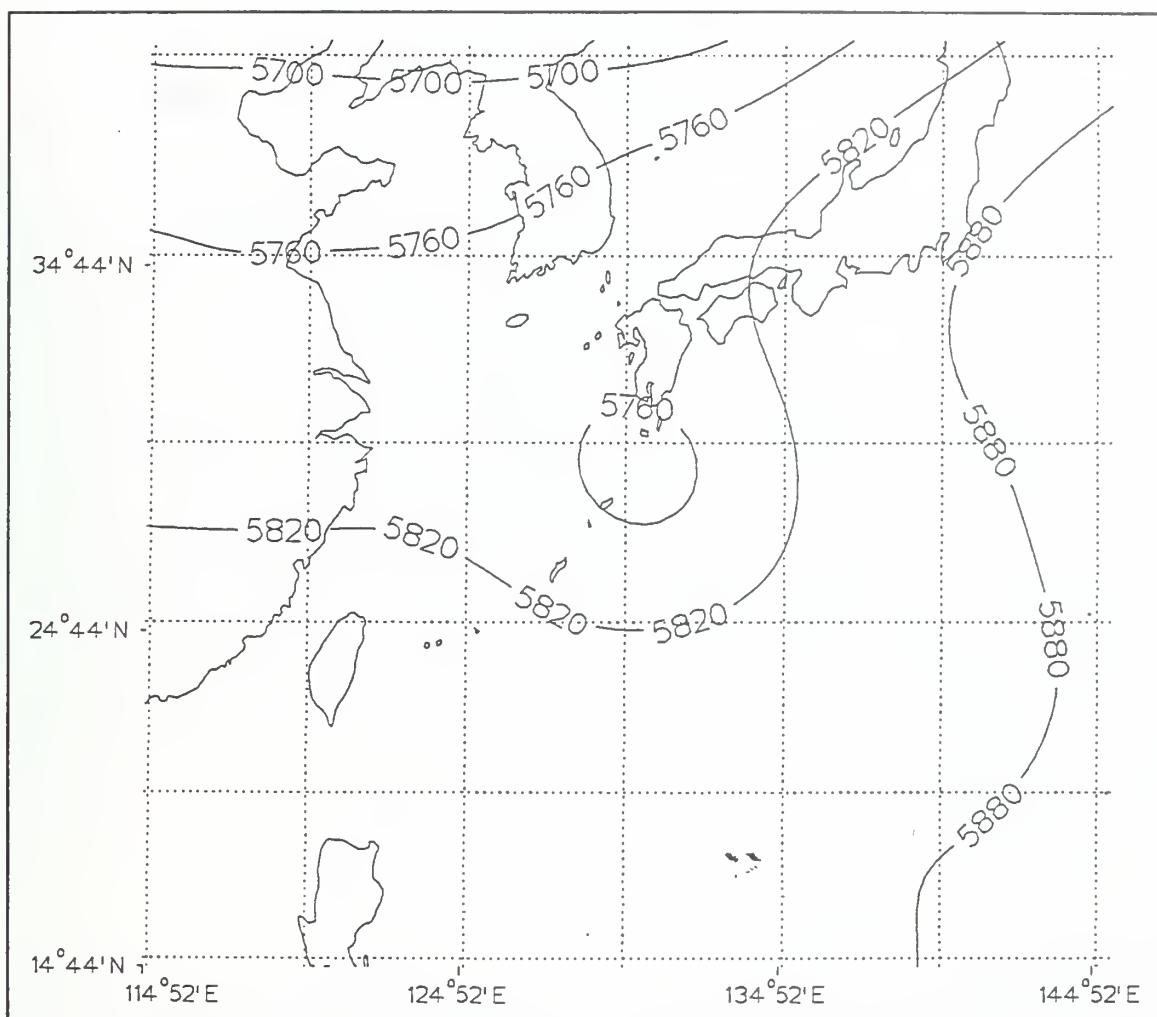


Fig. 2.19. NOGAPS 500 mb height field (m, contour interval 60 m) at 12 UTC 18 September used for the initial first-guess height field for the MQ height analysis.

the first guess for the wind field, the winds around the storm also became oval-shaped, with unrealistically strong cross-isobaric flow where wind reports did occur, such as 500 mb CTW and LDW observations.

The solution was to perform an unconstrained height analysis, and then transform the analysis into a cylindrical coordinate system and azimuthally average the heights

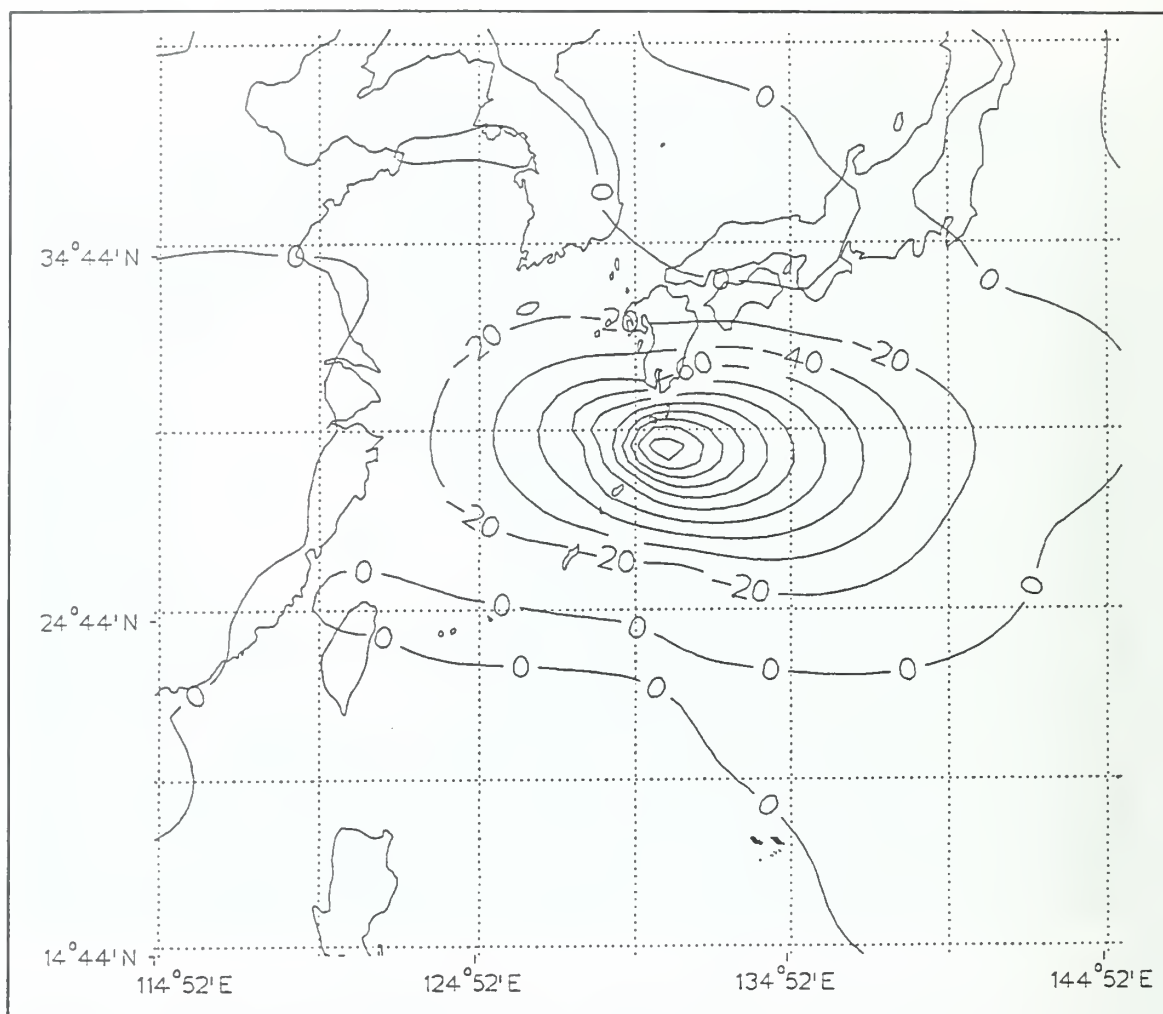


Fig. 2.20. Height increments (m, contour interval 30 m) at 12 UTC 18 September relative to the NOGAPS 500 mb height analysis in Figure 2.19.

within 600 km of the storm. Within 300 km of the TC, the azimuthally-averaged heights became the new first guess. Between 300 and 600 km, the azimuthally-averaged heights and the NOGAPS first-guess heights were blended linearly. This process was repeated twice, and significantly changed the first guess (Figure 2.21). In the final (dynamically constrained) height analysis, the magnitudes of the increments were now much smaller

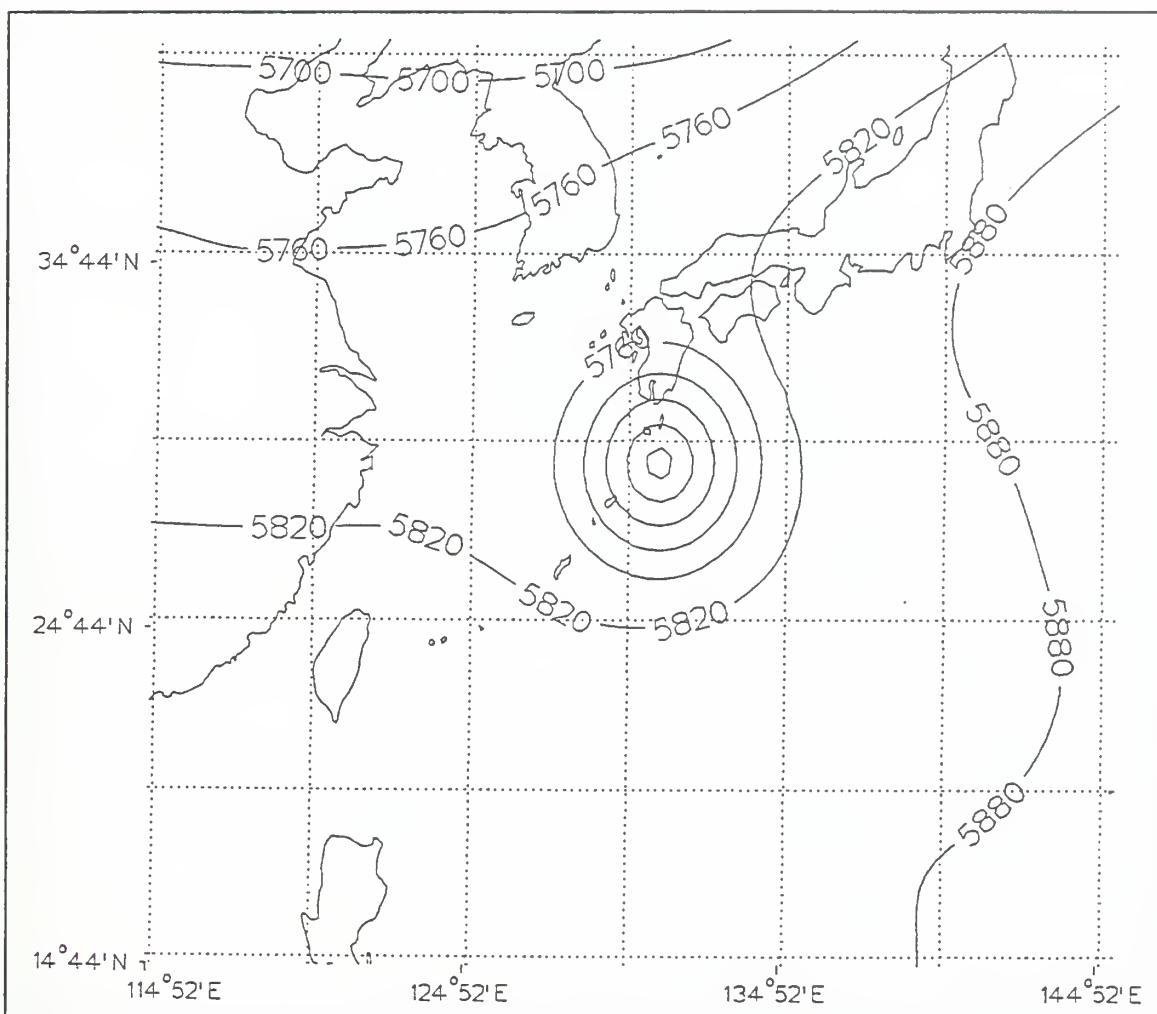


Fig. 2.21. Modified first-guess 500 mb height field (m, contour interval 60 m) at 12 UTC 18 September after azimuthally averaging the preliminary MQ height analyses.

(Figure 2.22). The analysis based on the unmodified first guess (Figure 2.23a) has a distorted typhoon, with significant cross-isobaric flow in the eastern half of the storm. By contrast, the MQ analysis based on the modified first guess (Figure 2.23b), has a smaller, more circular typhoon with little cross-isobaric flow and a central height about 60 m deeper than the analysis of Flo shown in Figure 2.23a. Although the actual storm

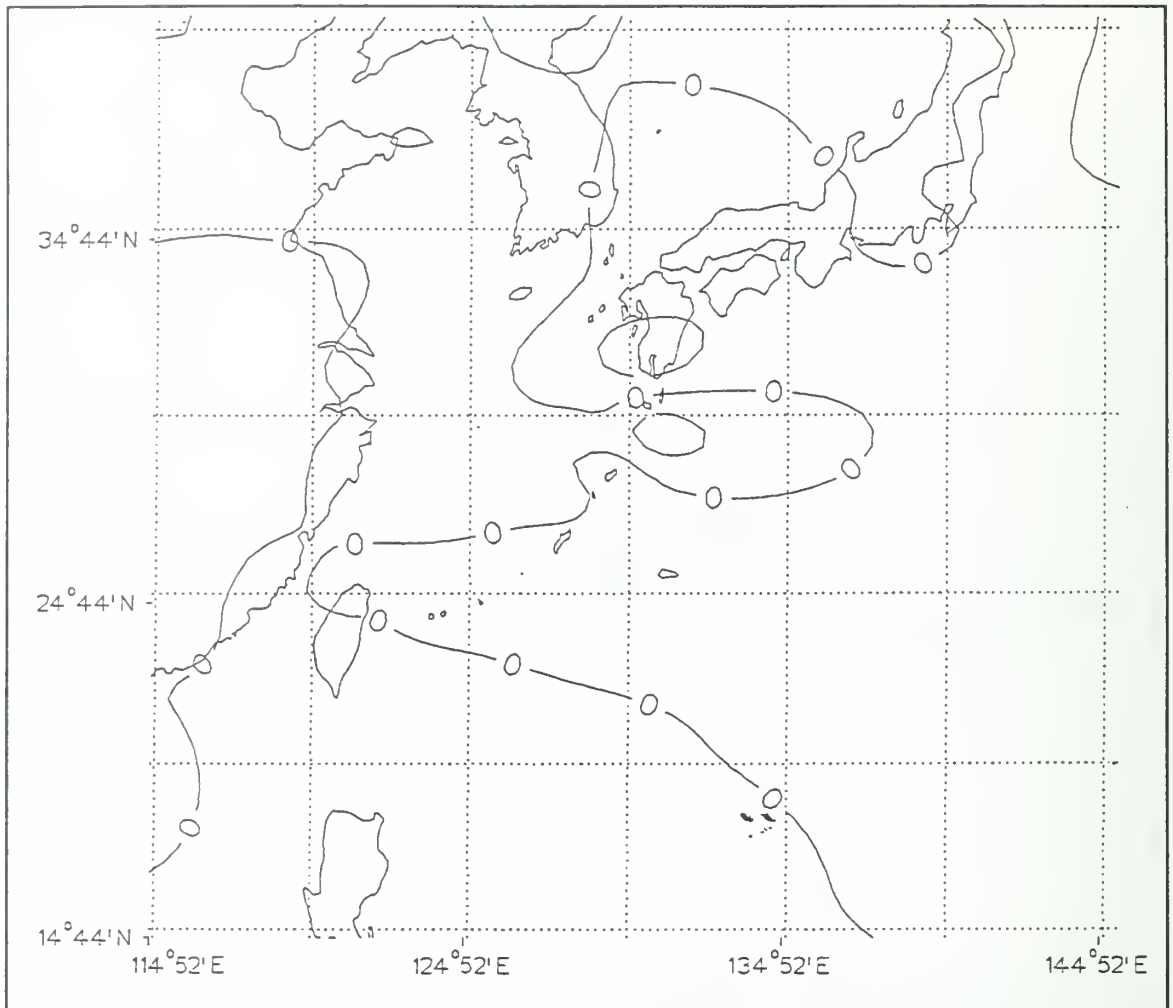


Fig. 2.22. Height increments (m, contour interval 30 m) as in Figure 2.20, except relative to the modified first-guess 500 mb height field analysis in Figure 2.21. Observation types as in Figures 2.1 and 2.2.

may contain asymmetries and not be as circular as the modified first guess, the assumption is much better than allowing the storm to acquire an extreme oval shape. No azimuthal averaging of the height field is performed following the final height analysis, so any asymmetries in the height observations will be reflected in the final analysis.

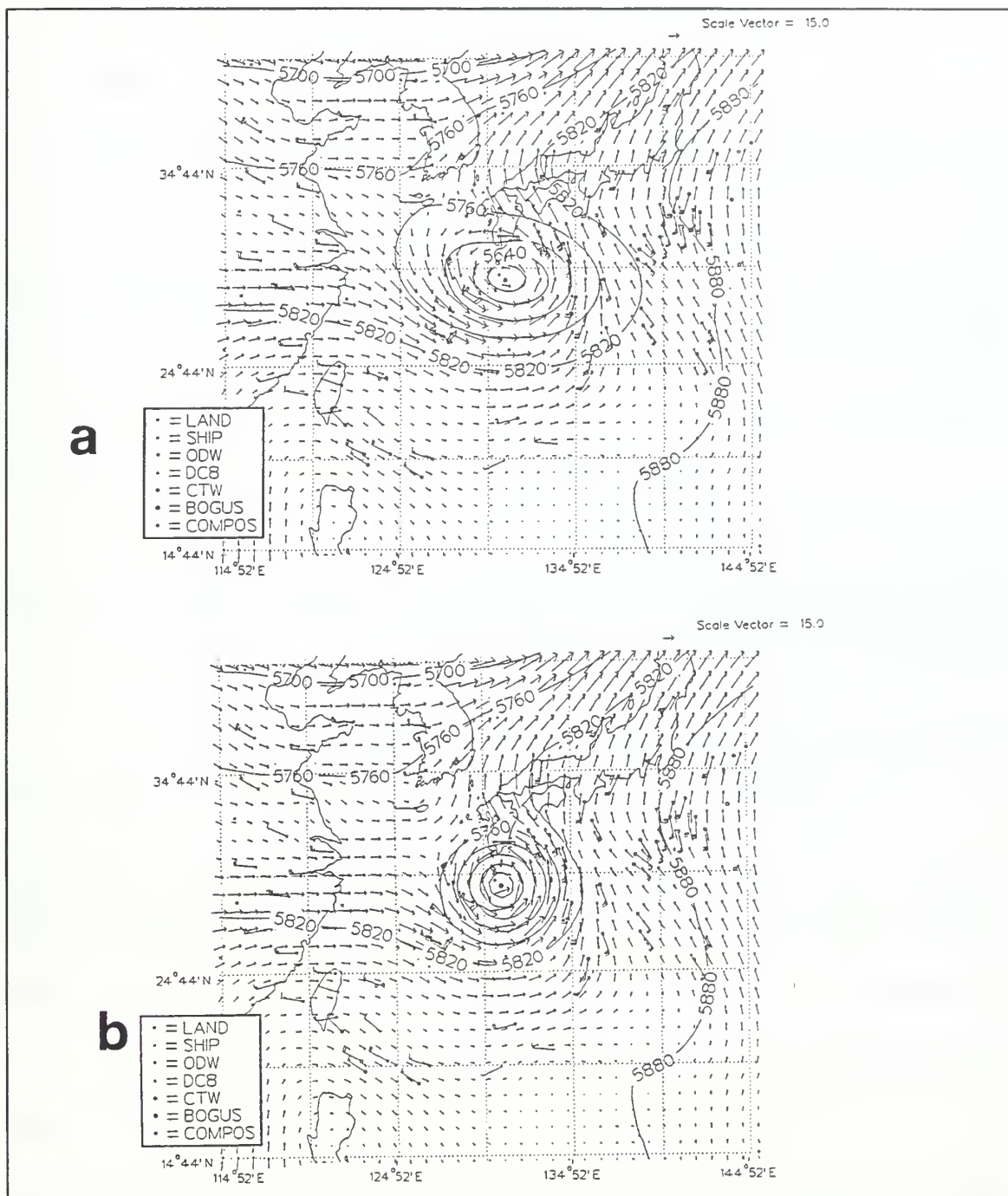


Fig. 2.23. MQ analysis of 500 mb wind (m s^{-1} , scale vector in upper-right) and height (m, contour interval 60 m) at 12 UTC 18 September based on: (a) NOGAPS first-guess height field in Figure 2.19 and (b) modified first guess field in Figure 2.21. Note the cross-contour flow around Typhoon Flo in (a). Observation types as in Figures 2.1 and 2.2.

4. Observation Enhancements

Although the number of observations in the tropics is normally deficient, occasionally there are too many observations for the horizontal grid resolution. This section will describe the procedures for compositing two or more observations that are "too close," *i.e.*, within one-half a grid point (25 km). The use of synthetic or "bogus" observations to improve the representation of the tropical cyclone structure will also be described.

a. Composite Observations

Since the MQ method requires a matrix inversion, there cannot be more than one observation per location in the matrix. In addition, observations too close together will cause the matrix to become ill-conditioned as a result of the numerical precision of the computer, and a reliable solution will not be obtained.

The solution was to composite all observations that were within 25 km. A linear average was applied to both the magnitude of the increments as well as their location. The resulting composite observation was then passed to the analysis algorithm. This observation was not described as a "super-observation," because it was not weighted any more heavily than any other individual observation.

Most analyses during IOPs 5-7 had fewer than ten composite observations. The most composite observations occurred with a combination of five minute DC-8 flight-level observations and plentiful CTW observations. For example, this combination resulted in 14 composite wind observations at 200 mb at 06 UTC 17 September.

b. Synthetic Observations

Synthetic (also called bogus) observations assist the analysis scheme in representing the tropical cyclone structure and in constraining the analysis in data-sparse regions. Synthetic observations of surface conditions are routinely added to some operational numerical models (*e.g.*, Guymer 1978; Goerss and Phoebus 1992). Synthetic wind observations are inserted into NOGAPS in the vicinity of a TC (Goerss *et al.* 1991) to ensure that the model's initial position of the storm is consistent with the observed position.

Two types of synthetic observations were inserted into the MQ analysis:

- Synthetic observations (wind, height, and temperature) that constrain the MQ analysis in regions where no observations were present. These synthetic observations are called "zero-bogus" points.
- Synthetic wind and height observations to assist in defining the TC structure.

(1) Zero-bogus Observations. One weakness of the MQ technique was its characteristic to maintain the gradient of the analysis from the outer-most observation to the edge of the domain. If the outer-most observations were close to the domain boundaries, this was not a serious problem because the analysis would have terminated at the boundary before extreme values were introduced. If no observations are present near the edge of the domain, the analysis scheme may produce completely unrealistic values (Figure 2.24a). The increments over Japan and Korea produced a gradient in the increment field. With no constraining observations, the gradient continued to the edge of the domain. For example, increments in excess of

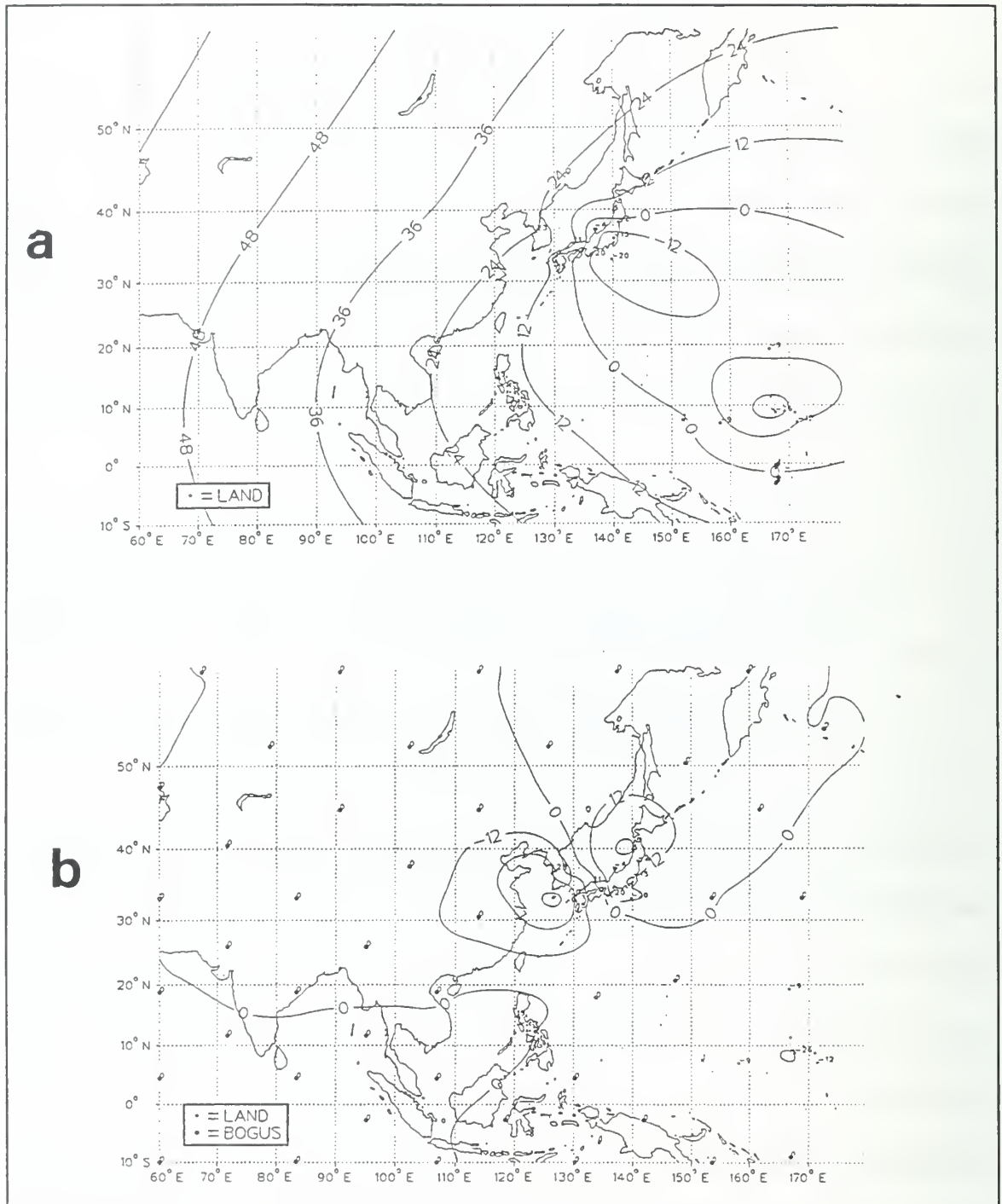


Fig. 2.24. 200 mb height increments (m, contour interval 12 m) at 06 UTC 19 September for (a) without zero-bogus points and (b) with the inclusion of zero-bogus points. Notice the increase in the increment field over central Asia in (a) without zero-bogus points. Observation types as in Figures 2.1 and 2.2.

50 m would have been added to the first-guess field along 60°E, even though no observations supported such a modification to the first-guess field.

A simple solution avoided this problem. In regions where no observations were present, a synthetic observation was created with a value equal to the first guess, so that the increment will be zero (*i.e.*, zero-bogus). The assumption is that the first-guess value is more appropriate than any other synthetic value in the absence of independent information. To implement this scheme, the appropriate distance between zero-bogus observations and actual observations had to be specified. If the distance was too small, the zero-bogus observations would have forced the analysis back to the first guess prematurely; if the distance was too great, erroneous gradients may have degraded the analysis. After several test analyses, a minimum distance between real and zero-bogus observations of 1500 km was established. This produced enough bogus observations in data-sparse regions to keep the analysis well-behaved, but did not interfere with the analysis in areas where there were observations. Also, horizontal prediction-error correlations developed for NOGAPS (Goerss and Phoebus 1992) for height observations separated by 1500 km are less than 0.2. After zero-bogus points were added (Figure 2.24b), the MQ analysis fitted the existing values and the increments now approached zero in regions of no observations.

The average number of height and wind zero-bogus observations are shown in Figure 2.25 for the 850, 500, and 200 mb pressure levels. The number of bogus points was primarily dependent on the analysis time, with fewer (more) zero-point

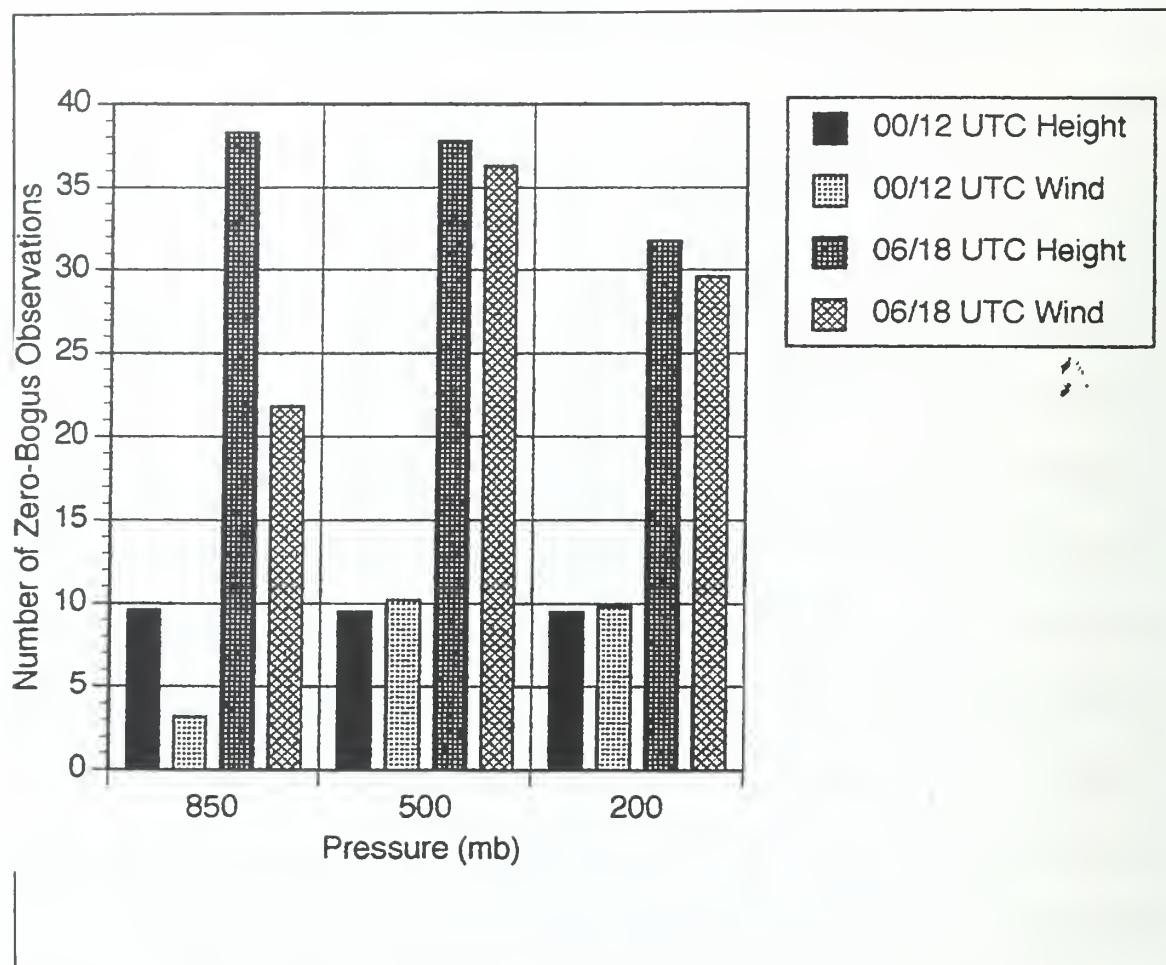


Fig. 2.25 Number of zero-bogus height and wind observations added to MQ analyses at off- and regular-synoptic times at 850, 500 and 200 mb (see inset for times and observation types).

bogus observations at regular (off) synoptic times. The number of 850 mb wind zero-bogus observations were fewer than the number of 850 mb height zero-bogus observations because of operational cloud-track wind observations in the data-sparse Indian Ocean. Although there were many wind observations at 200 mb (Table 2.5), none of the special observations was located in regions where no other (*i.e.*, rawinsonde) data existed. Therefore, the number of zero-bogus observations for 200 mb winds is similar

to the number of zero-bogus observations for 200 mb heights. The conclusion is that the number of zero-bogus observations is determined by the distribution versus the number of available observations.

(2) Typhoon Depiction Observations. Three alternatives were tested to depict the typhoon:

- No synthetic observations, so the typhoon was depicted only through information from the first-guess fields and any observations in the vicinity of the typhoon.
- Alignment bogus observations. Only the location of the typhoon is specified using the JTWC best-track position. At each pressure level where the tropical cyclone circulation is evident, one calm-wind observation is inserted at the best-track location. This one synthetic observation (per pressure level) greatly assists the MQ scheme in maintaining a vertically-consistent tropical cyclone. In the height analysis, a central height observation, if it can be determined, is also inserted at the best-track position. This procedure will be discussed below.
- Full tropical cyclone synthetic observations. Using the JTWC post-storm best-track and intensity estimates, insert synthetic observations of the storm central height, location, and at eight surrounding points along a 300 km radius around the storm. This is similar to the number of points inserted in the NOGAPS TC synthetic observation procedure (Goerss *et al.* 1991), except this MQ alternative includes heights as well as winds, and continues the bogus procedure up to 250 mb (provided there is a defined circulation) rather than 400 mb.

In the no-synthetic observation alternative, the MQ analysis created a vertically-inconsistent typhoon structure, due to the irregular distributions of the observations at the mandatory pressure levels. While Typhoon Flo was intensifying in the northern Philippine Sea and transiting through the sparse data coverage area, the analyzed lowest heights would tend to be equal to the observation closest to the storm,

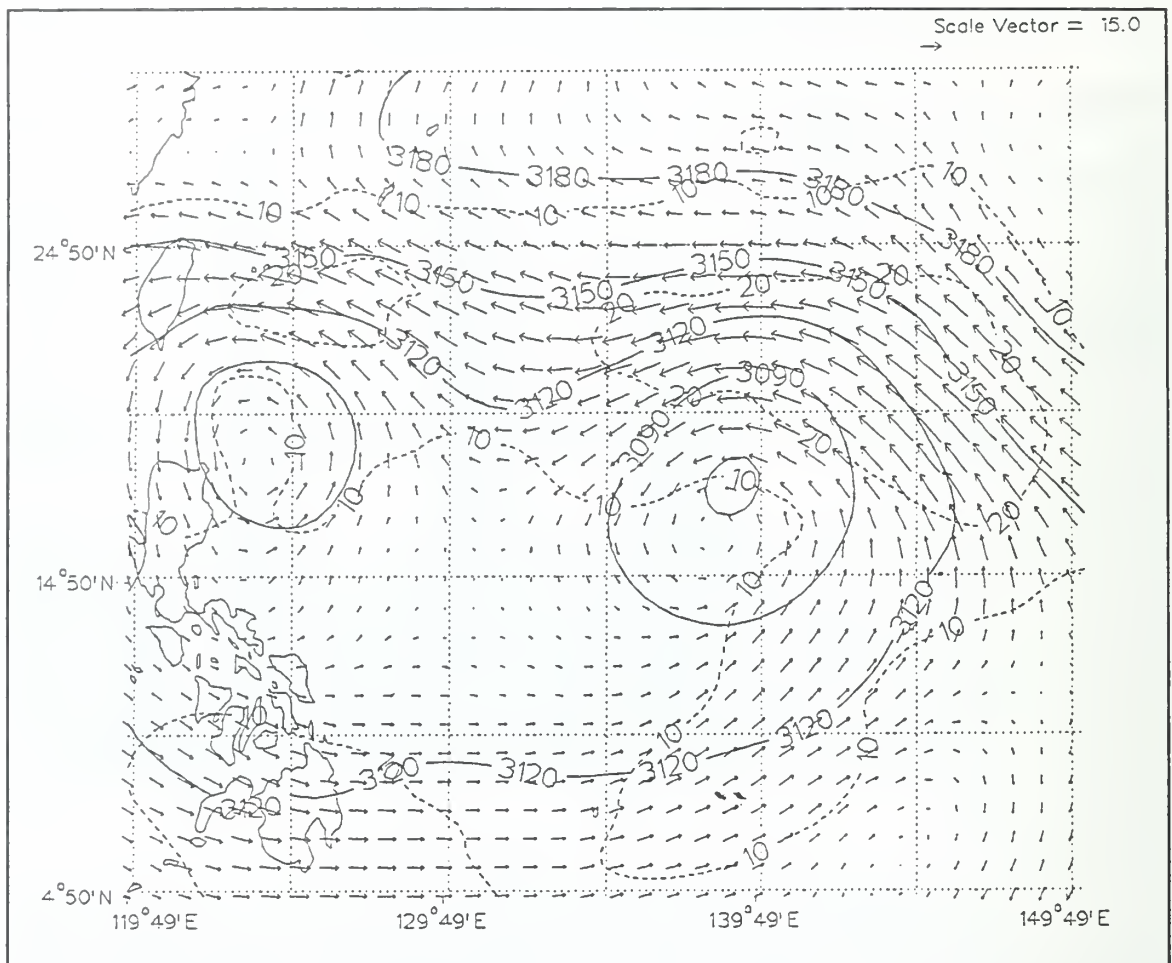


Fig. 2.26. 4DDA analysis of 700 mb wind (m s^{-1} , scale vector in upper right), isotachs (dashed, contour interval 10 m s^{-1}) and heights (solid, contour interval 30 m) at 06 UTC 14 September. Notice mismatch of wind and height fields in the vicinity of Typhoon Flo, which is near 18°N , 139°E .

even though that observation was not in the eye. Another problem was the wind and height centers were then mis-aligned. This mis-alignment problem was also shared by the 4DDA analyses (Figure 2.26), particularly around Typhoon Flo, near 17.5°N 138.5°E , but it also occurred around Typhoon Ed, east-northeast of Luzon.

The alignment-bogus alternative was a compromise between supplying the MQ analysis no information regarding the location of the TC and the full synthetic observation option that explicitly specified the location, intensity, and size. The full TC bogus alternative (described in Appendix C) produced plausible-looking tropical cyclones, but it was counter to the overall philosophy of this analysis scheme, which was to produce an analysis with as few external assumptions as possible. Since the alignment-bogus method also produced reasonable-appearing tropical cyclones, the decision was made to use the bogus procedure that added as few bogus points as possible to the analysis. The alignment-bogus consisted of one calm wind synthetic observation at the JTWC best track position from 1000 mb to the lower of: (i) 250 mb; or, (ii) the level at which no defined cyclonic circulation was present. A central height synthetic observation for these pressure levels was geostrophically calculated using the three closest height observations and the mean wind speed. This minimum height estimate was then checked to ensure that it was lower than the first-guess height at the TC center. If it was, then the height was added to the bogus observation file and used (if requested) on subsequent runs. Although the assumption of a geostrophic balance overestimated the magnitude of the height deviation, the analyzed wind speed near the center of the storm was almost certainly less than the actual wind speed. Rather than attempt to specify the true central height (which is usually not obtainable from the normal observation density), this approach simply ensured that the lowest height relative to neighboring observations was located at the center of the TC. This lower height, in conjunction with the calm

wind bogus, ensured that the winds and heights would be aligned and vertically consistent in the tropical cyclone. This alignment-bogus alternative was used for the final MQ analyses.

5. Post-processing the Tropical Cyclone Wind Field

Before adding the first-guess modifications and alignment-bogus alternative to the MQ analysis scheme, a strong region of low-level divergence was found under the eyewall and central dense overcast of Typhoon Flo between 17 and 18 September. During this time, the storm intensity was $> 60 \text{ m s}^{-1}$, which made the low-level divergence in the analysis extremely doubtful. Although the first-guess modifications and alignment-bogus alternative produced a realistic TC structure (for a 50 km grid), and significantly decreased the magnitude of the analyzed low-level divergence in Flo, divergence values that seemed excessive persisted.

Reasons for this area of divergence were carefully examined using static analyses and a visualization program (VIS5D). The divergence was caused by the irregular spacing of wind observations near (within 300 km) Flo. The wind increments, analyzed on a Cartesian coordinate system, tended to produce a nearly circular increment, rather than a downstream increase in the tangential winds at the radius of the observation.

The solution was to post-process the winds near the TC. After each analysis time, and within 600 km of the TC, the u and v winds were transformed to tangential (v_θ) and radial (v_r) winds. These winds were then azimuthally averaged in a moving cylindrical coordinate system, where the storm motion was determined from the previous

and future best-track positions. After azimuthal averaging, the winds were transformed back to the Cartesian coordinate system. The azimuthally-averaged winds were used within 300 km of the storm, and a blend of the original analysis and the azimuthal average was used 300 to 600 km from the storm. The post-processing virtually eliminated the divergence over Flo, and did not perturb the remainder of the analysis.

This procedure differs from the height azimuthal averaging described earlier to produce a modified first-guess field, which is then analyzed in a Cartesian sense, and the increments are added back to the first-guess field. The azimuthal averaging of the wind field near the TC occurs after the analysis is complete. This forced a symmetric circulation (in the moving coordinate system) near the center of the TC at the expense of drawing as closely to the wind observations in the vicinity of the typhoon.

6. 0600 and 1800 UTC Analyses

As shown in Figure 2.8, the 00 and 12 UTC analyses were completed first. These analyses were linearly averaged to produce the 06 and 18 UTC first-guess fields. These MQ analyses were used since neither 06 and 18 UTC NOGAPS analyses nor 6-h NOGAPS forecasts verifying at 06 and 18 UTC were available. Once the first-guess fields were computed, the 06 and 18 UTC analyses proceeded in the same manner as the 00 and 12 UTC analyses.

7. Summary

This local objective analysis scheme contained procedures for collecting, performing quality control checks, and objectively analyzing much of the total TCM-90

data collected during IOPs 5-7 (00 UTC 13 September to 00 UTC 19 September 1990). Observations were checked for vertical and horizontal consistency. Suspect observations were then manually evaluated, and either accepted, modified, or rejected. Rawinsonde height observations were modified to account for long and shortwave radiation effects, and the DC8 and LDW heights were adjusted to correct a suspected bias in these data.

The objective analysis algorithm was based on the two-dimensional multi-quadric technique, which is a linear summation of circular hyperboloids whose inflection points are coincident with the observation locations. Although no explicit dynamic constraints were imposed in the MQ analysis, the initial analysis of the wind field influenced the height analysis north of 25°N and within 600 km of a tropical cyclone. In addition, the first guess for the final wind analysis north of 25°N and within 600 km of a tropical cyclone was based upon the gradient wind field derived from the height analysis. The effects of friction were simply parameterized in the 1000 mb wind field by rotating the analyzed wind 20° towards lower pressure, and by reducing the magnitude of the wind speed 10%. Synthetic observations were added in data-sparse regions to ensure that the MQ analysis conformed to the first-guess fields where no additional information was available within 1500 km. An alignment bogus point was added at the best-track location of tropical cyclones to ensure vertical consistency in the wind and height fields near the TC. A plausible depiction of TC structure for a 50 km grid was ensured by initially modifying the first-guess height field to minimize the effect of isolated large increments,

and by azimuthally averaging the analyzed wind field in a moving coordinate system within 600 km of the center of the TC.

The first-guess for 00 and 12 UTC analyses was based upon 2.5° latitude/longitude resolution real-time NOGAPS analyses. First-guess fields for 06 (18) UTC analyses are a linear average of the 00 and 12 (12 and the following day 00) UTC MQ analyses.

F. VORTICITY, DIVERGENCE, AND VERTICAL VELOCITY CALCULATIONS

After the height, wind and temperature analyses were computed for IOPs 5-7 (00 UTC 13 Sep through 00 UTC 19 Sep 1990), the analyses were merged into one file per parameter. The relative and absolute vorticity, divergence and vertical velocity fields were calculated as diagnostic tools to evaluate the realism of the wind analyses.

1. Vorticity

The vertical component of relative and absolute vorticity was calculated using the finite difference form of

$$\zeta = \frac{\partial v}{\partial x} - \frac{\partial u}{\partial y} \quad (2.11)$$

and

$$\eta = \frac{\partial v}{\partial x} - \frac{\partial u}{\partial y} + f, \quad (2.12)$$

respectively, where ζ is relative vorticity, η is absolute vorticity, and f is the vertical component of the earth vorticity due to its rotation. Since $f = 2\Omega\sin\phi$, where Ω is the

angular velocity of the earth, and ϕ is the latitude, the absolute vorticity is a function of u , v , and latitude. Although the vorticity was not calculated on the edge of the domain, the TCM-90 analysis sub-domain is well within the outer grid (Figure 2.7).

2. Divergence

The horizontal divergence was calculated using the finite difference form of

$$D = \nabla \cdot \vec{V} = \frac{\partial u}{\partial x} + \frac{\partial v}{\partial y}. \quad (2.13)$$

As in the vorticity calculations, the divergence was not computed on the edge of the grid.

3. Vertical Motion

The vertical velocity was calculated using the kinematic method, that is

$$\omega(p) = \int_{sfc}^p \nabla_p \cdot \vec{V} dp. \quad (2.14)$$

Equation (2.14) was integrated from the surface to 100 mb at each grid point. Following Haltiner and Williams (1980), the lower boundary condition was defined as

$$\omega_{sfc} = -\rho_{sfc} g \vec{V}_{sfc} \cdot \nabla h \quad (2.15)$$

where

$$\rho = \frac{p}{RT} \quad (2.16)$$

and ∇h is the gradient of the topographic surface.

Since the MQ analyses have only been computed at the mandatory pressure levels between 1000 and 100 mb, a method had to be developed to determine the surface pressure. The surface pressure was used to calculate ρ_{sfc} in (2.15) and the initial Δp in (2.14).

a. Computing the Surface Pressure

The surface wind and temperature data were obtained from the NOGAPS analyses (interpolated to 50 km), and the terrain heights were extracted from a global terrain elevation database. This dataset has a $1/6^\circ$ latitude/longitude resolution, so the data were degraded to the 50 km resolution used in this study.

The NOGAPS analyses available at NPS had the sea-level pressure, but did not contain the surface pressure. Thus, a modified form of the hypsometric equation (Holton 1979) was used to calculate the surface pressure

$$p_{sfc} = p(Z)e^{(\Delta Z/H)}, \quad (2.17)$$

where ΔZ is the difference in height between the surface and the mandatory pressure level, and H is the scale height defined as

$$H \equiv \frac{R\bar{T}_v}{g}. \quad (2.18)$$

Here, \bar{T}_v is the mean virtual temperature in the layer, and R is the gas constant for dry air. Using the relationship

$$T_v = \frac{1 + 1.609w}{1 + w} T, \quad (2.19)$$

and the approximation

$$w \approx \epsilon \frac{e}{p} \quad (2.20)$$

from Hess (1979), where $\epsilon = 0.622$ and w is the mixing ratio, the scale height H can be calculated given the layer mean temperature, vapor pressure and pressure. Substituting (2.19) and (2.18) into (2.17),

$$p_{sfc} = p(Z) \exp \left\{ \Delta Z \left[\frac{R}{g} \left(\frac{1 + \bar{e}/\bar{p}}{1 + \epsilon(\bar{e}/\bar{p})} \right) \bar{T} \right]^{-1} \right\}. \quad (2.21)$$

Since (2.21) contains pressure on the right side, an initial mean pressure was required. This value was obtained by first solving (2.18) for a dry atmosphere, using the p_{sfc} value to compute a mean pressure, and then solving (2.21).

After (2.21) was solved at each grid point, the upper boundary condition ($\omega_{100 \text{ mb}} = 0$) was imposed. The correction method described by O'Brien (1970) is applied to remove the kinematically-calculated ω at 100 mb by subtracting a linearly increasing proportion of that vertical velocity at each mandatory pressure level, starting at the surface and proceeding to each mandatory pressure level. The assumption O'Brien made was that the horizontal winds (and therefore the divergence calculation) were most

accurate in the lower troposphere. Therefore, most of the correction to the vertical velocity was applied at upper-tropospheric and lower- stratospheric levels.

b. Converting vertical velocity from $\mu\text{bar s}^{-1}$ to m s^{-1} .

After the O'Brien correction was applied at each grid point, vertical velocities were converted from $\mu\text{bar s}^{-1}$ to m s^{-1} . Holton (1979) shows that for synoptic-scale motions

$$\omega = -\rho g w . \quad (2.22)$$

Substituting (2.22) into (2.16) and solving for w

$$w = -\frac{\omega RT}{pg} . \quad (2.23)$$

ω was then converted to w at each grid point.

4. Summary

The vorticity, divergence and vertical velocity calculations, along with the actual wind and height analyses, will next be used to test the hypothesis that the MQ analyses are a plausible, alternate depiction of the troposphere and lower stratosphere during TCM-90 IOPs 5-7. The evaluation of the MQ analyses will be discussed in the following two chapters.

III. INITIAL VALIDATION OF THE MULTI-QUADRIC ANALYSES

A. VALIDATION AND COMPARISON OF THE MULTI-QUADRIC ANALYSES

The objective of the MQ analyses is to produce an alternate, realistic depiction of the tropical atmosphere in the region of Typhoon Flo. It is therefore important to validate the MQ analyses so that confidence may be placed in any subsequent diagnostic calculations derived from the MQ analyses. Several diagnostic checks were performed and compared with similar calculations using the NOGAPS and 4DDA analyses. These diagnostics, which can be divided into qualitative and quantitative types, are discussed below.

As previously mentioned, the real-time NOGAPS analyses should be viewed as a control case, rather than a detailed final analysis of the TCM-90 domain. Unlike the MQ and 4DDA analyses, the NOGAPS analyses were prepared in a real-time mode, with only the operational dataset available. Although NOGAPS is competitive with other global model analyses and short-range forecasts (Warren 1993; Nelson and Aldinger 1992), no special QC effort or "tuning" of the model took place during the TCM-90 experiment. The horizontal resolution of NOGAPS is 79 zonal wavenumbers with triangular truncation (Rosmond 1992), which corresponds to a grid resolution of approximately 160 km. The NOGAPS fields were further degraded to 2.5° lat. (278 km) resolution prior to archiving. Taking these factors into account, comparisons of the NOGAPS analysis with either the MQ or 4DDA analyses are shown simply to indicate

the value of the enhanced TCM-90 dataset and higher-resolution analysis tools. No implication of deficiencies in the NOGAPS model should be drawn from such a comparison. Since the NOGAPS fields provided the first guess for the MQ analysis, comparisons of these two analyses indicates the "value-added" of the special MQ analysis procedures for this enhanced TCM-90 dataset.

1. Qualitative Checks

Three types of qualitative checks were performed: (i) conventional two-dimensional plots; (ii) comparison with the Rucker (1992) hand analyses; and (iii) computer-aided dataset visualization.

a. Two-Dimensional Plots

Two-dimensional plots were generated for the MQ first-guess, increment, and analysis fields and compared with the NOGAPS and 4DDA analyses. All three analyses had similar depictions of the large-scale features in the TCM-90 domain (*e.g.*, the mid-latitude upper-level trough over Siberia, Mongolia, and China, and the Tropical Upper Tropospheric Trough (TUTT) east of Flo).

The three analysis schemes were slow to intensify (relative to JTWC's post-storm intensity estimates based primarily upon the Dvorak (1984) technique) the low-level circulation of Flo on 14-16 September, as Flo tracked across the northern Philippine Sea towards Okinawa (see Figure 1.1). A typical distribution of observations at 850 mb during this period is shown in Figure 3.1. Although the Soviet ships were

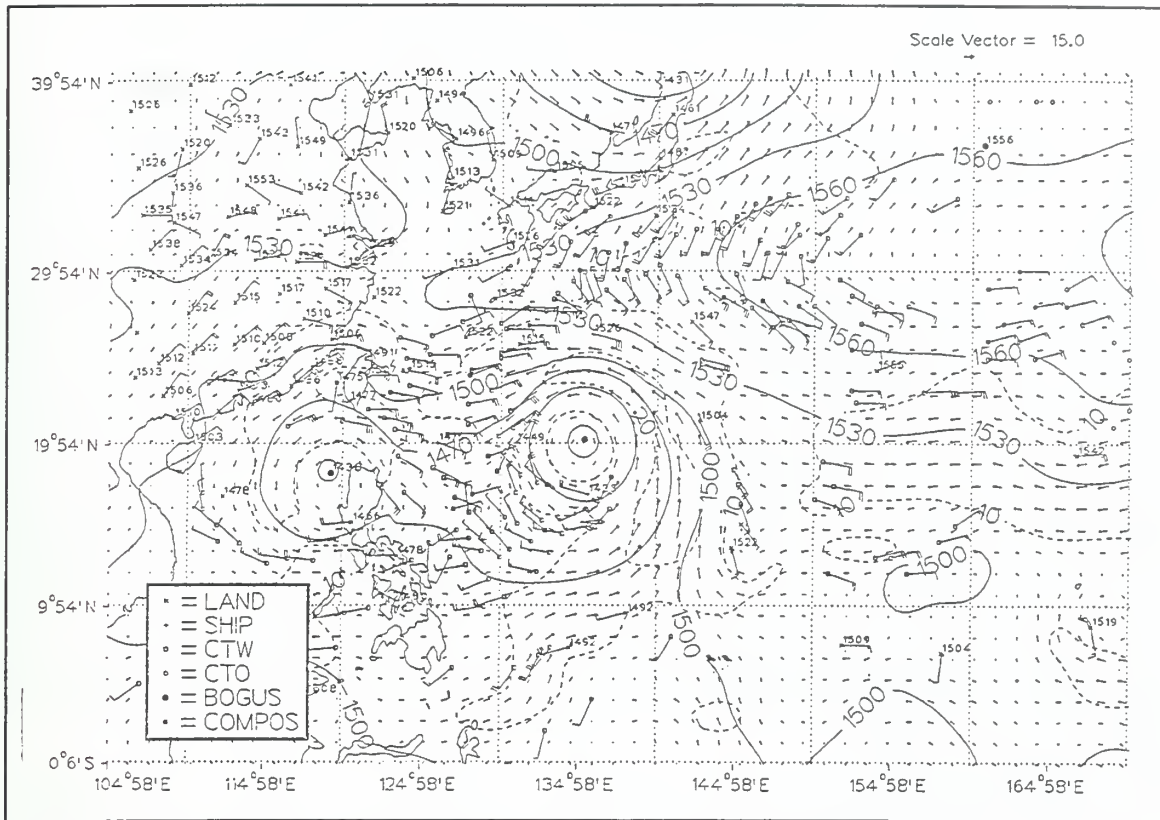


Fig. 3.1. MQ analysis of 850 mb wind (m s^{-1} , scale vector in upper-right), isotachs (dashed, contour interval 10 m s^{-1}) and heights (solid, contour interval 30 m) at 00 UTC 15 September. Note the lack of observations in the immediate vicinity of Typhoon Flo near 20°N , 135°E . Observation types as in Figures 2.1 and 2.2.

located along 20°N , none of the ships observed Flo's inner core, and few other low-level observations were available.

The two-dimensional plots of the increments were especially useful for the QC phase of the MQ scheme because they clearly showed anomalous patterns. Suspect height observations appeared as "bulls-eyes" that were easy to see, while suspect wind observations generated unusually large vectors.

b. Comparison With Rucker Hand Analyses

Rucker (1992) (hereafter referred to as R92) prepared hand analyses at 300, 250, 200, and 150 mb at 6-h time intervals for IOPs 5-7. R92 used the real-time and delayed data, and subjectively weighted the observations accorded to their perceived reliability. Satellite imagery was used extensively for positioning of circulations in the analyses. The 200-mb level was analyzed first because more data were available at that level. The analysis at this level then influenced the analysis at adjacent levels. The analyses of positions of synoptic features were iterated to maximize the spatial and temporal continuity of discrete upper-level features. Based upon these analyses, Rucker constructed "best-track" positions of upper-level cold lows in the environment of Typhoons Flo and Ed.

Initial comparisons of the MQ and R92 analyses were favorable. Both analyses maintained continuity on the large-scale features, and the magnitudes of the upper-level jets (both tropical and mid-latitude) were similar. A typical example of the agreement between the MQ and R92 analyses is shown in Figures 3.2 and 3.3, respectively. Note the 20 m s^{-1} jet about 200 km northeast of Flo, and the excellent agreement on the position of the anticyclone about 500 km east-southeast of Flo and the position of the Tropical Upper Tropospheric Trough (TUTT) cell near 20°N , 129°E ("C2" in Figure 3.3). The positions of "C2" and the anticyclone are in excellent agreement in large part because of the plentiful wind observations that defined these

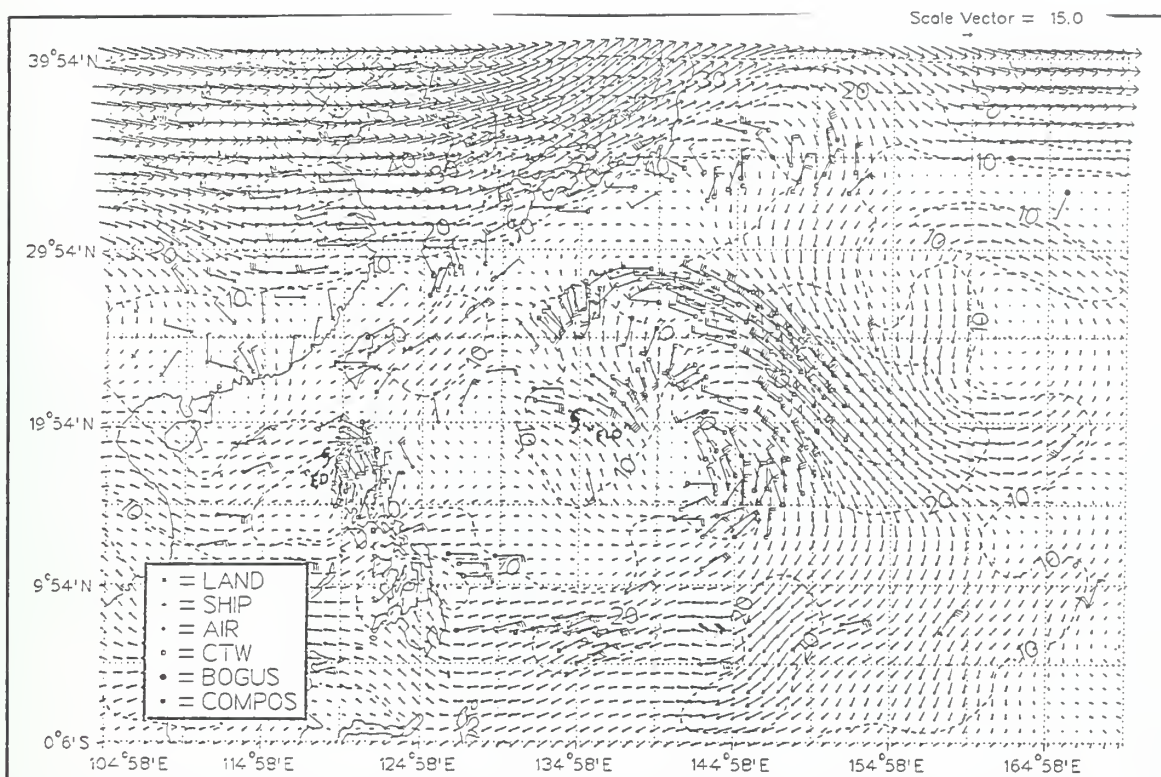


Fig. 3.2. MQ analysis as in Figure 3.1, except for 200 mb and without heights. Locations of Typhoons Ed and Flo given by tropical cyclone symbols.

features. Both analyses were also in close agreement with the depiction of the strong (40 m s^{-1}) jet midway between Flo and TUTT cell "C1." However, there was an approximately 550 km difference between the MQ and R92 analyses in the location of TUTT cell "C1" near 22°N , 160°E . Whereas the R92 "C1" position was based on time continuity and satellite imagery, the MQ "C1" position was based primarily on the first guess, since there were no wind observations within 600 km of the TUTT.

As a further comparison, the positions of the two significant upper-level cold lows ("C1" and "C2" in R92) at 200 mb were subjectively determined for the MQ,

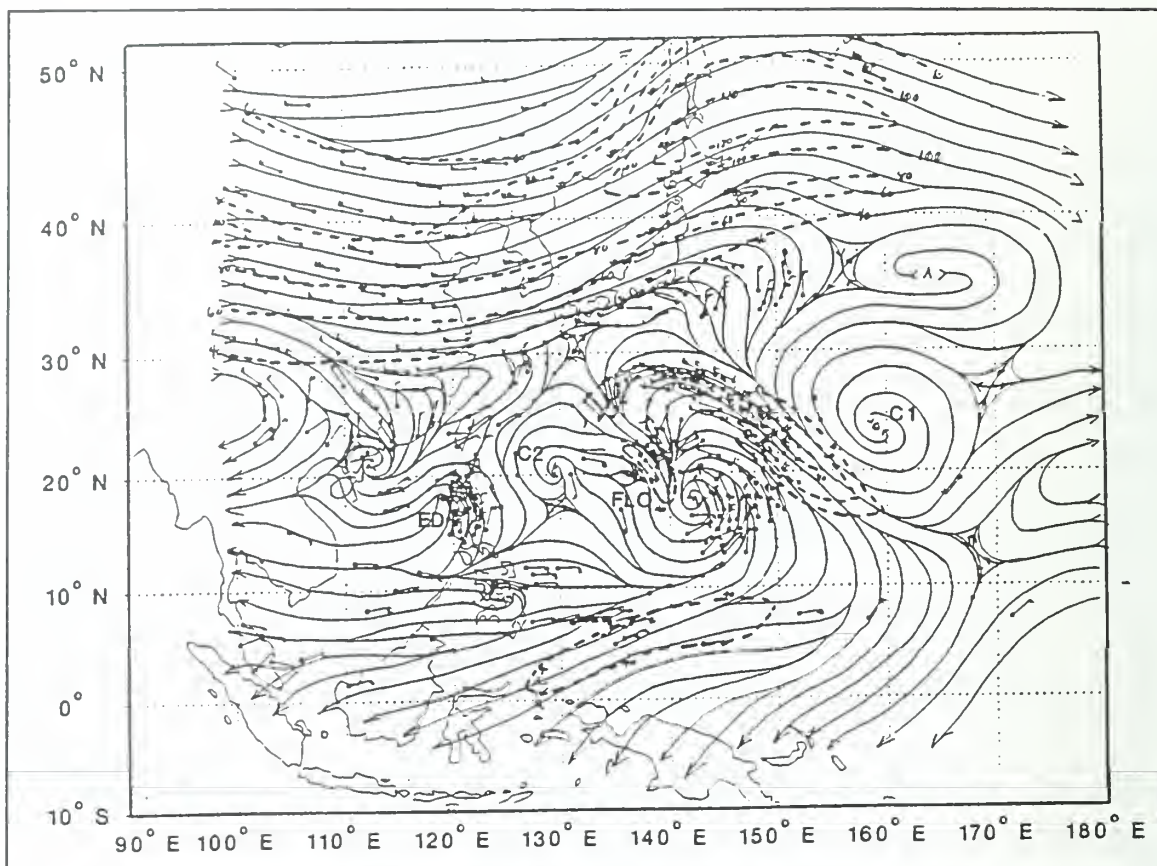


Fig. 3.3. 200 mb streamline (solid) and isotach (dashed, contour interval 20 kt starting at 40 kt) hand analysis at 00 UTC 15 September by Rucker (1992).

4DDA, and R92 analyses. The positions of the MQ and 4DDA TUTT cells "C1" and "C2" relative to the R92 analysis are depicted in Figures 3.4 and 3.5, respectively, and the mean distances and standard deviation values are given in Table 3.1.

TUTT cell "C1" was a large TUTT cell that was located east of Typhoon Flo throughout the IOPs. Although this TUTT cell was large, it was initially in the vicinity of 22°N, 160°E, which was a region of very little data coverage. The MQ

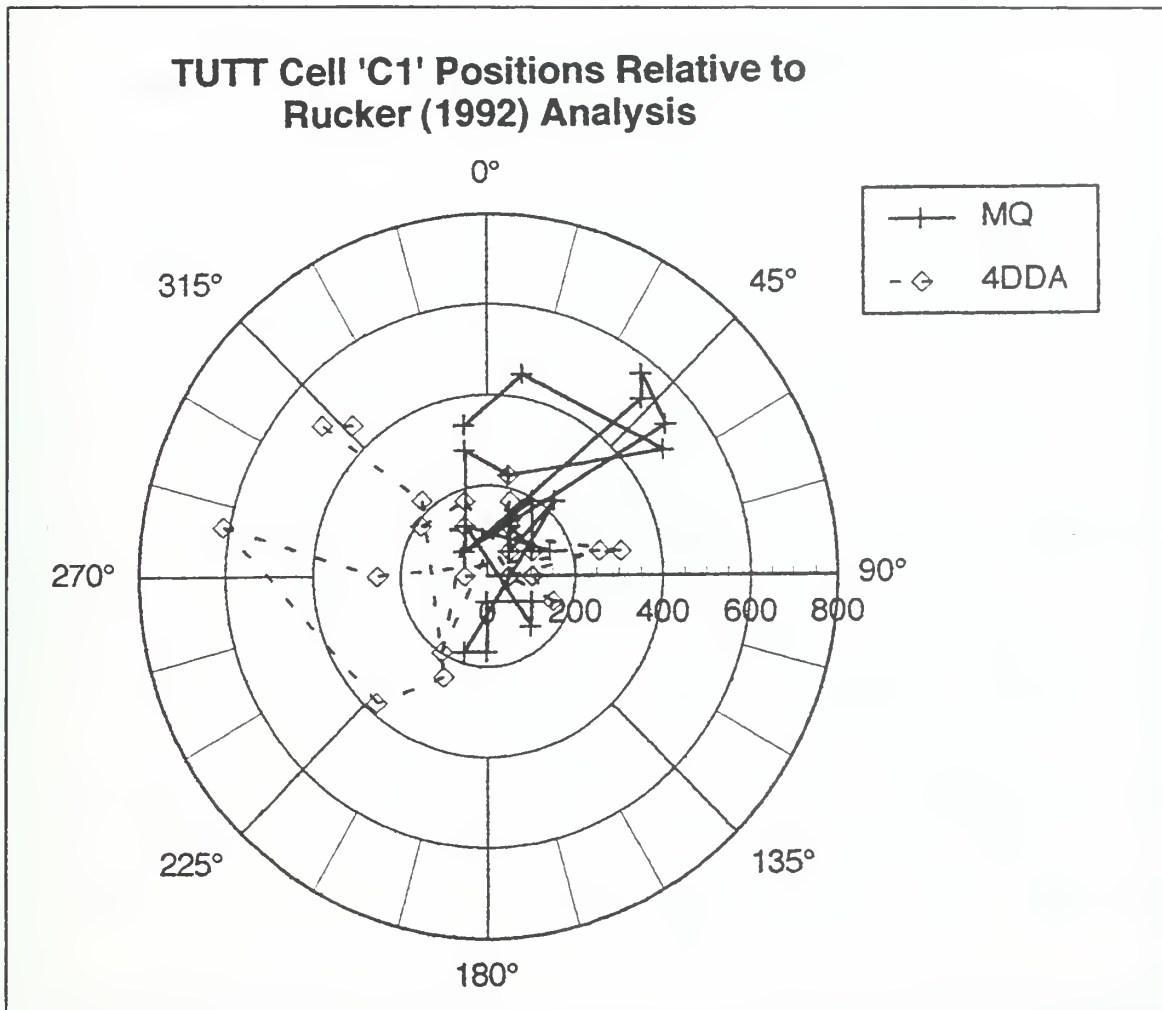


Fig. 3.4. MQ and 4DDA (see inset for symbols) 6-h positions (degrees, km) of the TUTT cell "C1" relative to Rucker (1992) analyses for 00 UTC 13 September through 00 UTC 19 September.

analysis positions "C1" 200-500 km to the north and east of the R92 location from 00 UTC 13 September through 06 UTC 15 September (Figure 3.4). After 06 UTC 15 September, the MQ and R92 "C1" positions were on average only 115 km apart (Table 3.1). Similar results were noted for the relative position of "C1" between the 4DDA and R92 analyses. However, the 4DDA mean position was slightly closer to the R92 "C1"

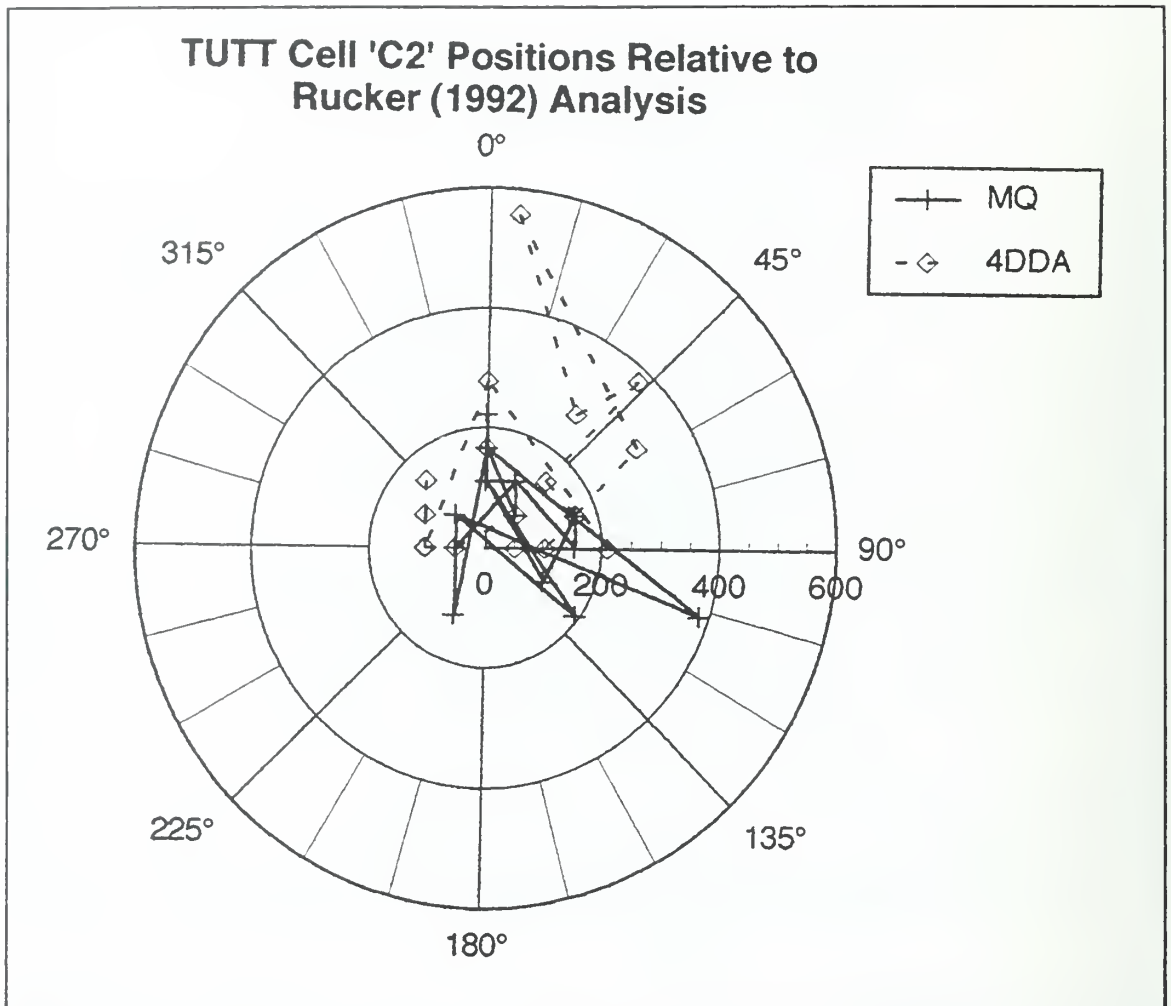


Fig. 3.5. As in Figure 3.4, except for 6-h positions of the TUTT cell "C2" during 00 UTC 13 September through 06 UTC 17 September.

position than was the MQ mean position, perhaps because of the 4DDA assimilation of TOVS data. The reason for the large uncertainty in locating "C1" in the early time periods of the IOP was probably because reprocessed cloud-track wind observations were only available to the west of "C1", *i.e.*, a closed circulation could not be depicted based solely upon the observations. After 06 UTC 15 September, wind observations were

| TUTT cell | Time (day/Hour UTC September) | MQ | | 4DDA | |
|-----------|-------------------------------------|------|--------|------|--------|
| | | mean | st dev | mean | st dev |
| C1 | 13/00-15/06 | 351 | 194 | 335 | 148 |
| | 15/12-19/00 | 115 | 49 | 125 | 68 |
| | ALL | 218 | 167 | 209 | 148 |
| C2 | ALL | 140 | 76 | 190 | 128 |

Table 3.1. MEAN DISTANCE AND STANDARD DEVIATION (KM) BETWEEN MQ OR 4DDA AND R92 DEPICTIONS OF TUTT CELLS "C1" AND "C2".

present that clearly defined the eastern and western quadrants of the circulation. Since all three analyses had this information, the mean differences in the locations of "C1" decreased dramatically.

In contrast to "C1", TUTT cell "C2" was generally located in regions of good data coverage. However, the feature was small, and difficult to detect at all times.

The larger amount of data available contributed to the mean position differences (relative to R92) being less than 200 km for both the MQ and 4DDA analyses (Table 3.1). Although the position differences were smaller than the differences for "C1", "C2" was depicted as a trough 44% and 33% of the time on the MQ and 4DDA analyses, respectively. When this occurred, the center point of the trough was chosen to represent the position of the TUTT cell. The four 4DDA "C2" positions more than 250 km northeast and north-northeast of the R92 analyses (Figure 3.5) occurred when the MQ analysis depicted "C2" as a trough oriented north-northwest to south-southeast. Although the 4DDA analyses had a closed circulation, the circulation was located at the northern extent of the MQ trough. All analyses showed that the circulation was small, with a diameter less than 300 km.

These comparisons between the objective and hand analyses indicate that the objective analyses perform well when there are observations to locate specific features, even when the feature is relatively small. However, caution should be exercised in interpreting any calculations dependent upon the location of TUTT cell "C1" from 00 UTC 13 September through 06 UTC 15 September, since a large variability exists in the positions of "C1" among the three analyses. The wind data alone do not allow a definitive resolution of the "true" location of the TUTT cell.

c. Dataset Visualization

Efficiently evaluating any large dataset is a challenge. Schiavone and Papathomas (1990) summarize methods currently available for visualizing scientific

datasets. These methods include traditional two-dimensional plots in either a horizontal or vertical plane, two-dimensional satellite image data and animation of these depictions. More recently, visualization techniques have included particle-tracing methods, "textured quadric surfaces" to create artificial, but realistic-looking structures such as clouds, and volumetric elements (*i.e.*, isosurfaces) and volumetric animation to observe structure changes throughout the entire volume, rather than only animating a specific feature.

A scientific visualization package called VIS5D (Hibbard and Santek 1989), which is part of the Man-computer Interactive Data Access System (McIDAS), was used to evaluate the MQ, 4DDA, and NOGAPS analyses. VIS5D's features include the use of simultaneous use of depth, motion, and value perception cues by combining color, contours, isosurfaces, particle trajectories, and animation. The analyzed volume can be arbitrarily rotated, and fields on vertical and horizontal cross-sections can be animated and displayed. VIS5D runs on special NPS workstations, and the datasets are easily transferred from the AMDAHL mainframe computer to the appropriate workstation.

Each analysis was viewed in two frames of reference. The first visualization was in geographic coordinates. The second visualization was made in a storm-relative coordinate system, *i.e.*, Typhoon Flo was located at the center of the domain throughout the entire animation. The advantages of using VIS5D included efficiently viewing the entire dataset and seeing four-dimensional relationships between

the data. However, care was required to ensure that small-scale problems in the dataset were not overlooked while viewing such a large domain.

Besides the height, wind, and temperature fields, the absolute and relative vorticity, divergence, and vertical velocity fields were also animated. Since VIS5D provided the efficient means to view these diagnostic fields, it became an integral part of the QC evaluation of the MQ analyses. A videotape of the animations was prepared for repeated viewing. The animation of these initial diagnostic fields was able to reveal deficiencies in the initial MQ analyses that were not immediately apparent in the static wind and height fields. Any suspect regions were then examined in considerable detail using more traditional output. Thus, VIS5D was used to complement existing methods of dataset evaluation. For example, the VIS5D displays revealed clearly the strong low-level divergence over Flo in the preliminary MQ analyses. By using a combination of divergence isosurfaces and color surfaces depicting wind speed, the problem of isolated speed maxima in the wind field near Flo was discovered. As has been described in Chapter II, Section E.5, this deficiency was fixed by azimuthally averaging the winds in a moving cylindrical coordinate system.

Animated vertical cross-sections in the typhoon-relative coordinate system (not shown) show that the single alignment-bogus alternative in the MQ analyses was very effective at maintaining a vertically-aligned storm throughout the IOPs. Between 00 UTC 13 September and 18 UTC 15 September, the MQ analysis had Flo more vertically-stacked than was depicted in either the 4DDA or NOGAPS analyses. Once Flo

reached the vicinity of the Ryukyu Islands (and DC-8 flight-level observations were first available) on 16 September, all of the analyses maintained a vertically aligned storm.

The vertical cross-sections (Figure 3.6) also display one of the MQ analysis' primary weaknesses with respect to the 4DDA and NOGAPS analyses: its two-dimensional character. Horizontal striations caused by the variation in data coverage between levels were clearly depicted. Notice the sharp change in the analysis at 200 mb, which is the result of the DC8 flight-level data. The 4DDA model (not shown) has a

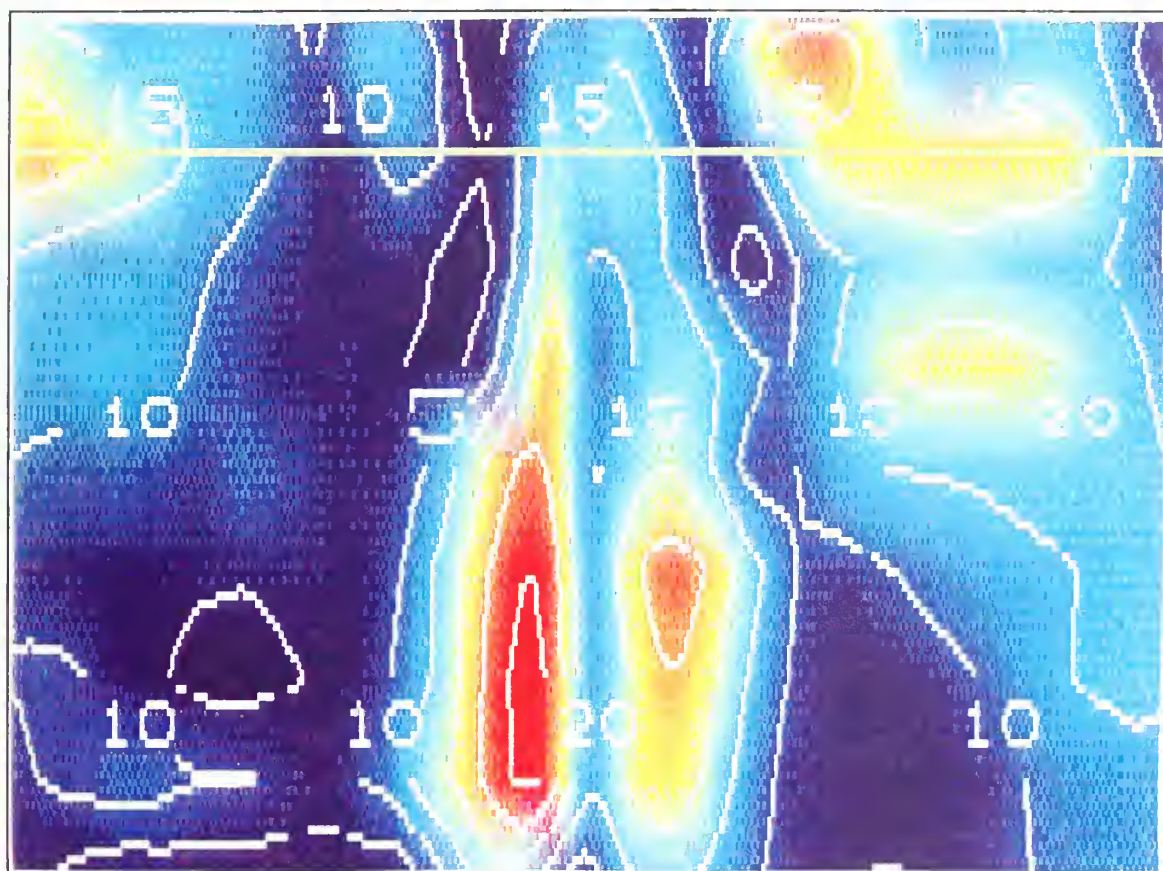


Fig. 3.6. Vertical cross-section of wind speed (m s^{-1} , contour interval 5 m s^{-1}) around Typhoon Flo at 18 UTC 17 September for MQ analysis. Typhoon Flo is at the center of the figure.

much smoother vertical variation in wind speed. This irregular vertical structure will create problems if subsequent calculations involve any vertical derivatives, unless the MQ fields are subjected to some vertical smoothing.

Time continuity between the 6-h analyses appears good in all of the analyses, although each scheme had minor problems. At 00 UTC 15 September, the NOGAPS analysis (and therefore the MQ first guess) changed from a zonal pattern of easterly winds at 200 mb along the equator to a series of four cyclone-anticyclone waves between 110°E and 160°E (not shown). At 12 UTC 15 September, the prevailing easterly flow returned (not shown). The 4DDA model appeared to have intermittent problems with the height analysis over Taiwan, as it produced anomalously low height values about once each 24 h. Animation shows that these negative height values extended southeastward along the eastern coast of Luzon. However, the 4DDA wind field did not appear to be affected by these height perturbations.

Trajectories were calculated using VIS5D, and both the MQ and 4DDA analyses produced an "in-up-out" secondary flow that is expected in tropical cyclones (Shapiro and Willoughby 1982). This feature provided considerable confidence in the 4DDA and MQ wind analyses, since the trajectories depend on the analyzed horizontal and computed vertical components of motion. To produce reasonable trajectories, the MQ horizontal wind analyses at each pressure level, along with the method (kinematic) and assumptions (synoptic-scale flow, O'Brien correction) of obtaining the vertical velocity must also be plausible.

2. Quantitative Checks

The analyses were evaluated using three quantitative methods: (i) RMS calculations; (ii) Propagation vector analysis; and (iii) Azimuthally- averaged wind profile comparisons.

a. Root Mean Square Evaluation

Root mean square (RMS) values were calculated to compare how closely the MQ, 4DDA, and NOGAPS analyses "fit" the observations. Recall that the observation sets being compared were those supplied to the MQ and 4DDA analyses, but the NOGAPS analyses were based only on the real-time observations. As stated earlier, the NOGAPS analyses should be viewed as a control case, while the MQ and 4DDA are enhanced analyses. The RMS values were computed for the height, wind, and temperature observations in the TCM-90 domain (Figure 2.7) for each pressure level and time, and by observation type at each level for the entire time period. The RMS values were also calculated in a similar manner for a domain that encompassed a 1000 km radius around Typhoon Flo.

The time series of RMS values presented in this section are for time intervals of 6 h. Since the NOGAPS analyses were only available at synoptic times, the 00 and 12 UTC (12 and following day 00 UTC) NOGAPS analyses were linearly averaged to produce the 06 (18) UTC NOGAPS analysis. With the smoothing inherent in this averaging, the RMS values for the off-synoptic time NOGAPS field would be expected to be somewhat smaller than those for the main synoptic times.

As discussed in Chapter II, Section C.2.a.(1), observations inherently contain some generally small, but unknown, amount of error. The observations also may have only partially resolved small-scale atmospheric features. Both observation error and sub-grid scale features should be removed from any synoptic analysis. In the MQ analysis, this is accomplished by adding the $n\lambda\sigma_1^2\delta_{ij}$ term to the basis function in Equation (2.4) in Section C.2.a.(1). In the 4DDA and NOGAPS analyses, the observation and representativeness errors are accounted for by analyzing a discrete volume of observations for each analysis point, and applying a summation of weighted corrections to the first guess. A significant difference in the analysis philosophies between the MQ and OI-based analyses is in the amount of weight applied to the first guess. In an OI analysis, the first-guess field can be weighted so that it dominates all, or part of, an analysis. In this MQ analysis, the observations were only weighted based on the type (wind, height, or temperature), observing platform, level in the atmosphere, and location (*i.e.*, close to or far from the typhoons).

Since the RMS values for the MQ analyses were explicitly specified (*e.g.*, draw more closely to CTW and DC8 observations than to CTO and AIREP data), the relative RMS values between observation platforms should be anticipated. It is not known *a priori* what the relative weights between the individual observations, and between the observations and the first-guess field, were for the 4DDA and NOGAPS analyses. These relationships will affect the outcome of the 4DDA and NOGAPS RMS calculations.

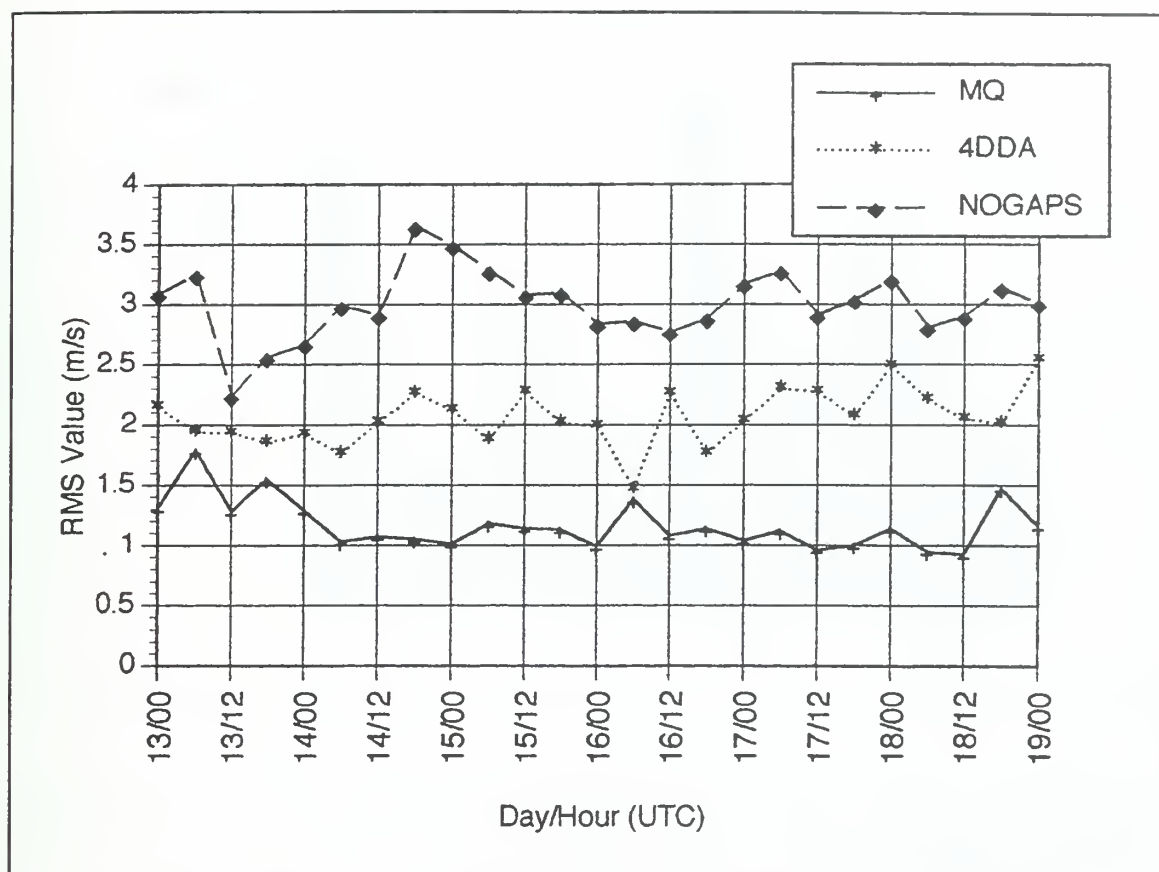


Fig. 3.7. MQ, 4DDA, and NOGAPS (see inset for symbols) Root-Mean-Square (RMS) values (m s^{-1}) for 850 mb winds during 00 UTC 13 September through 00 UTC 19 September.

(1) Wind RMS Calculations. The RMS values for 850 mb winds for IOPs 5-7 are shown in Figure 3.7. Throughout most of the period, the MQ analyses have RMS values of $1.0\text{--}1.5 \text{ m s}^{-1}$, while the 4DDA RMS values range between $1.5\text{--}2.5 \text{ m s}^{-1}$ and the NOGAPS RMS values are $2.0\text{--}3.5 \text{ m s}^{-1}$. Thus, the MQ low-level wind analysis has RMS values about 50% of the 4DDA analysis and 33% of the NOGAPS analysis. Although this result provides no information about the dynamic value of the MQ analysis, it shows that the observations were, on the average, more closely adhered

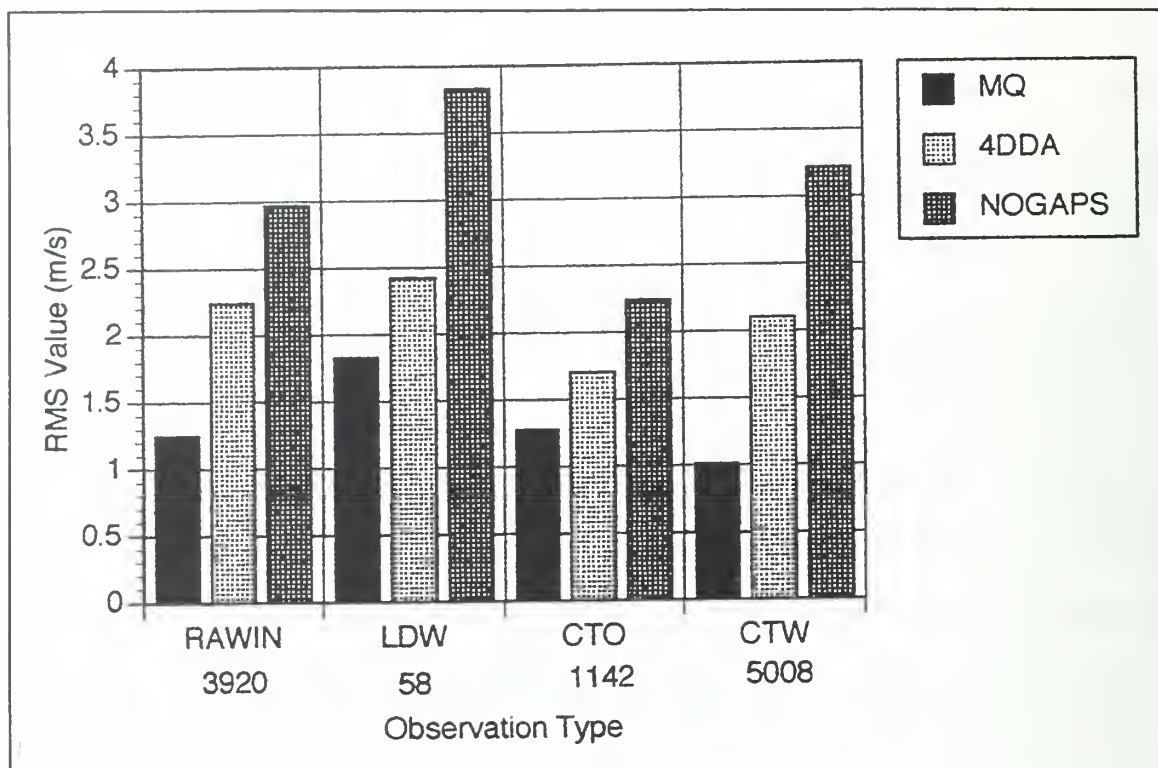


Fig. 3.8. MQ, 4DDA, and NOGAPS (see inset for symbols) RMS values for 850 mb wind observations, by type of observation as defined in Figures 2.1 and 2.2. Number below observation type lists number of observations.

to by the MQ analysis than in the 4DDA analysis. These RMS values provide initial confirmation that the smoothing feature and RMS specification worked as planned in the MQ analyses.

As is shown in Figure 3.8, the MQ analysis produced lower RMS values for all of the different types of low-level wind observations (RAWIN, LDW, CTO, CTW). The relatively large RMS values for LDW and CTW observations for NOGAPS is expected because the operational NOGAPS analyses did not include these delayed-data sources. The most significant difference between the MQ and 4DDA

analyses was the degree to which the MQ analyses conformed to the post-storm analyzed cloud-track wind (CTW) observations. The MQ analyses RMS value for CTW observations is 47% that of the 4DDA analyses, while the MQ analyses RMS value for operational cloud-track (CTO) observations rises to 76% that of the 4DDA analyses. The decrease in the RMS difference of the CTW observations relative to the CTO observations was expected since: (i) The specified σ for the CTW observations was 11% less than that specified for the CTO observations (Table 2.2); and (ii) the specified λ for CTW observations was three versus a λ value of ten for the CTO observations. It is more difficult to understand why the CTO RMS value calculated in the 4DDA analysis is smaller than the CTW RMS value for the same analysis. The 4DDA scheme prescribed a lower RMS value for CTW observations than for CTO observations (E. Rogers, personal communication). It is possible that the relative weighting of the first-guess field was greater than the weight assigned to the CTW observations. Another possibility was that, since the OI system as implemented for the ETA model only uses up to 30 wind increments in each three-dimensional volume (Rogers *et al.* 1992), some of the high spatial density CTW observations were not included in the OI analysis.

The difference between the RMS values for 850 mb winds within 1000 km of Typhoon Flo in the MQ and 4DDA analyses is smaller (Figure 3.9). The RMS values in this region for the 4DDA analyses continue to be $\sim 2 \text{ m s}^{-1}$, but the MQ RMS values now also average nearly 2 m s^{-1} . The MQ analysis has higher RMS values in this region because the winds are first analyzed, then azimuthally averaged in a

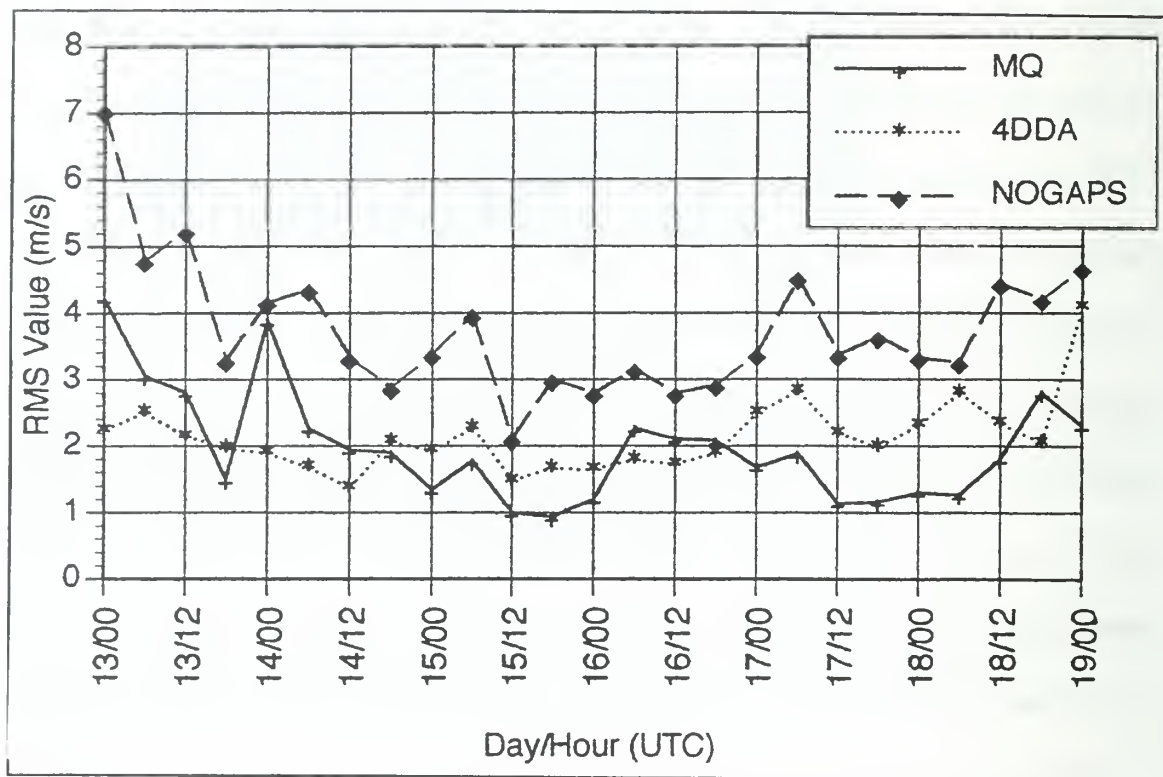


Fig. 3.9. As in Figure 3.7, except for 850 mb wind observations within 1000 km of Typhoon Flo.

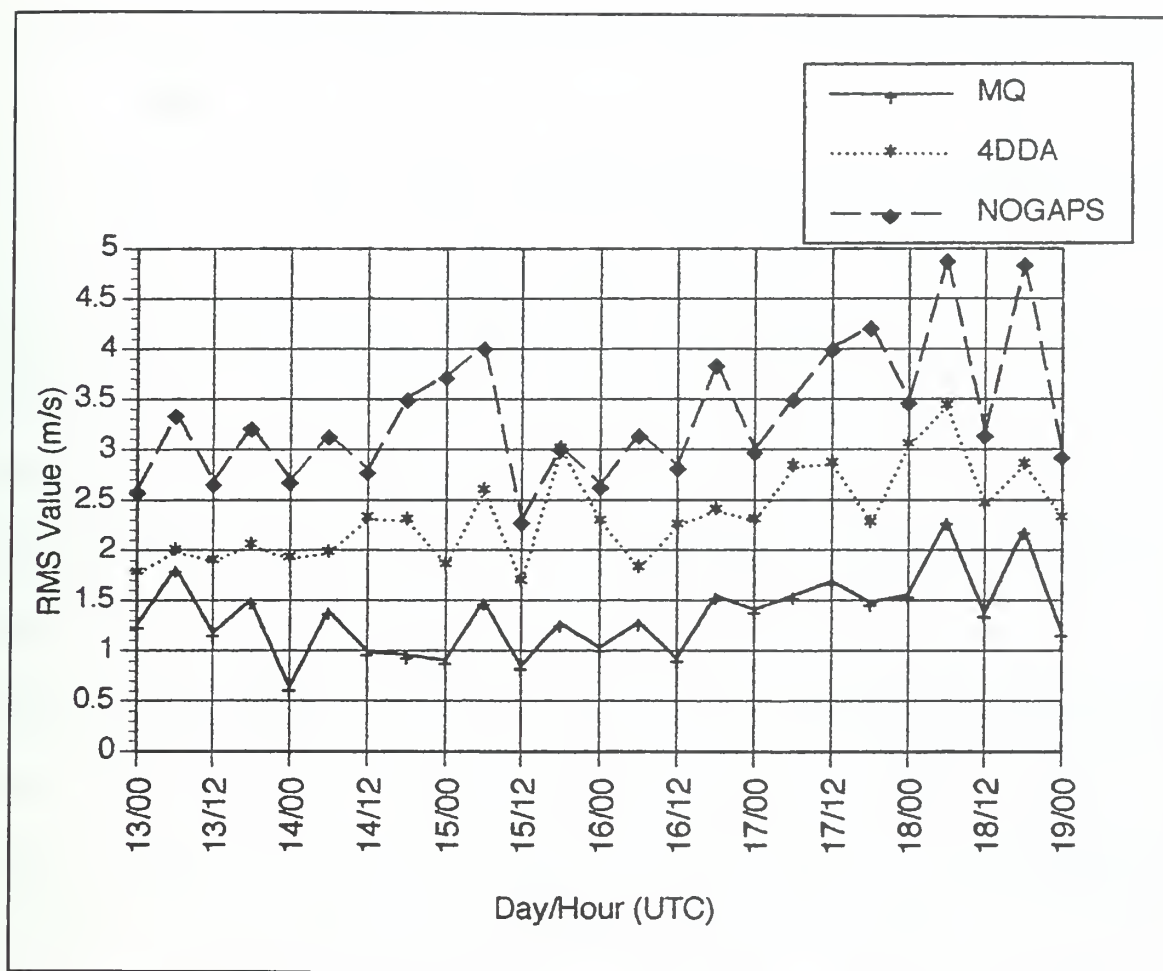


Fig. 3.10. As in Figure 3.7, except for 500 mb wind observations.

moving cylindrical coordinate system, as described above. Although this produces an analysis with greater dynamical consistency (*e.g.*, virtually no low-level divergence over the inner radii of the typhoon), individual wind observations are not "drawn-to" as closely as they are in the rest of the analysis.

Relationships among the 500 mb wind RMS values (Figure 3.10) for the three analyses are similar to the 850 mb wind RMS values. The RMS values for the MQ analysis are about 60% as large as the RMS values for the 4DDA analysis and

about 40-50% as large as the RMS values for the NOGAPS analysis. The MQ and 4DDA RMS values are only slightly larger than those computed at 850 mb. While this is not surprising for the MQ analysis, since the RMS specifications changed little between 850 and 500 mb, the 4DDA analysis might have increased more substantially, since relatively little wind data were available at 500 mb, compared to 850 and 200 mb (Figure 3.11). The mean 4DDA wind RMS value of around 2.5 m s^{-1} implies that the available wind data at 500 mb were fully assimilated, and that the relatively "data-rich" 850 mb and 200 mb levels had limited impact on the 4DDA analysis where there were wind observations at 500 mb. Vertical cross-section plots or a visualization program output would be appropriate tools for assessing the effect of winds (or heights) observed above or below 500 mb in regions of little 500 mb data. However, any comparison of "goodness" of one analysis scheme versus another would be arbitrary without independent observations at adjacent levels that had been withheld from the analyses.

All three analysis schemes have generally increasing RMS values as time progresses (Figure 3.10). This increase is probably caused by the combination of increase in the intensity of Typhoon Flo from about 12.5 m s^{-1} to 75 m s^{-1} , while at the same time moving from a data-poor to a (relatively) data-rich region (the Ryukyu Islands and southern Japan). The saw-tooth pattern in Figure 3.10 starting at 00 UTC 18 September is likely caused by Typhoon Flo being near the sites of many of these off-synoptic time observations, and thus producing relatively large RMS values. The regular synoptic times contain a greater proportion of observations away from the typhoon. The

observations not affected by the typhoon are probably well-handled by all the analysis schemes, and therefore have a lower overall RMS error.

The expected variation in the number of 500 mb wind observations at off-synoptic times relative to the regular reporting times is shown in Figure 3.11. However, an unusual decrease in the number of observations occurred at 18 UTC 18 September. Investigation revealed that the usual number of off-synoptic time rawinsonde stations reported, but the number of reprocessed cloud-track wind (CTW) observations decreased to 271 at this time, which is about one-half that normally reported. The reason for this one-time decrease in the number of CTW observations is not known. The relative lack of CTW observations reduced the number of 500 mb wind observations at 18 UTC 18 September to 74, many of which were located in the vicinity of Typhoon Flo. This significant decrease in the number of observations may assist in explaining the large 500 mb wind RMS values calculated for 18 UTC 18 September.

At 200 mb (Figure 3.12), the RMS relationships among the three analyses are again similar to those at the lower levels. However, the magnitudes are approximately double the wind RMS values calculated at 850 mb. This should be expected, as it is generally accepted (*e.g.*, Goerss and Phoebus 1992) that 200 mb wind data derived from rawinsondes, aircraft, and satellites contain greater errors than similar observations at 850 mb.

The times with DC-8 flight-level observations (0600 UTC 16, 17, 18 September; 1200 UTC 18 September) are evident by an increase in RMS values,

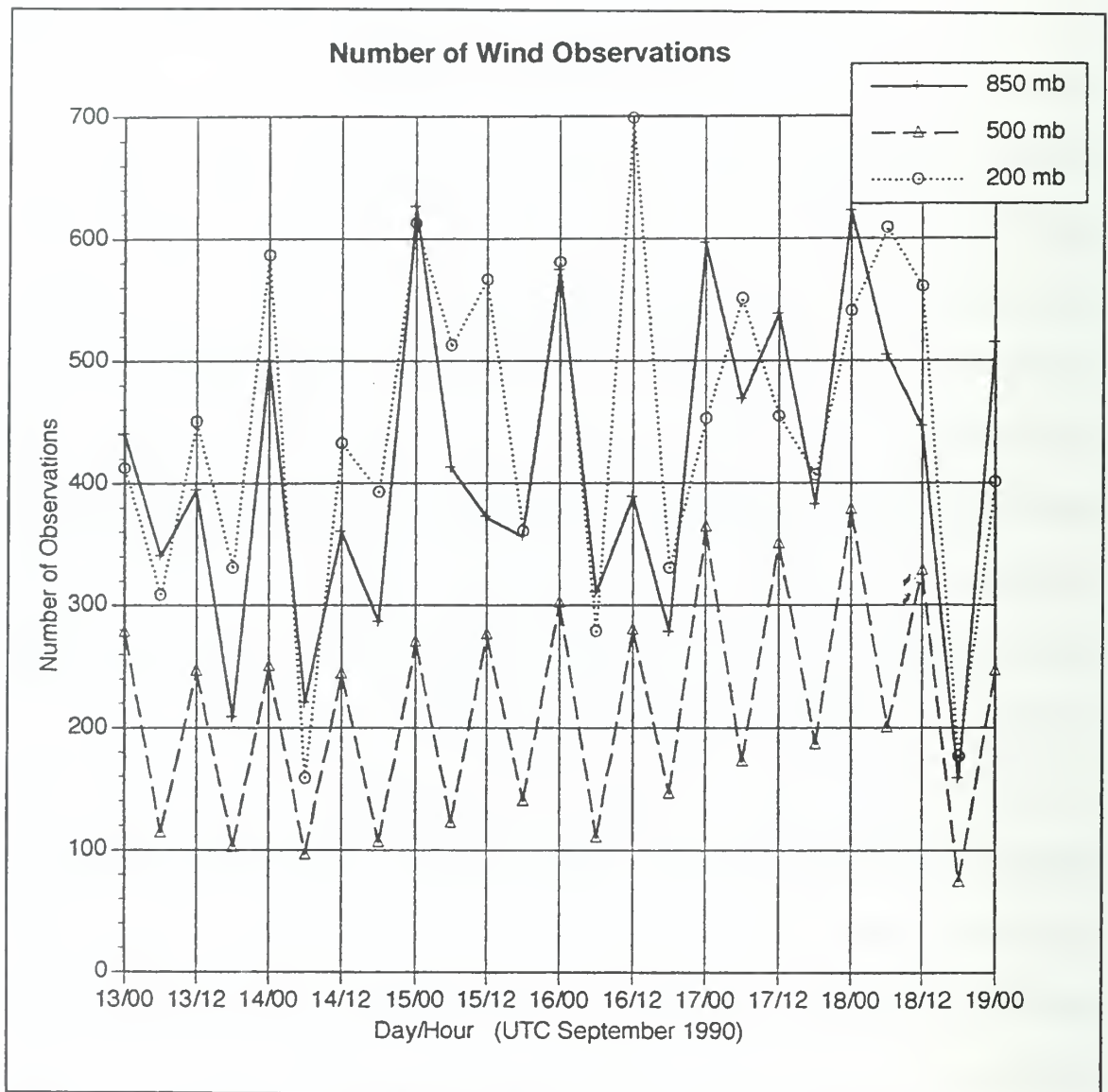


Fig. 3.11. Number of 850, 500, and 200 mb (see inset for symbols) wind observations analyzed by MQ analysis by time from 00 UTC 13 September through 00 UTC 19 September.

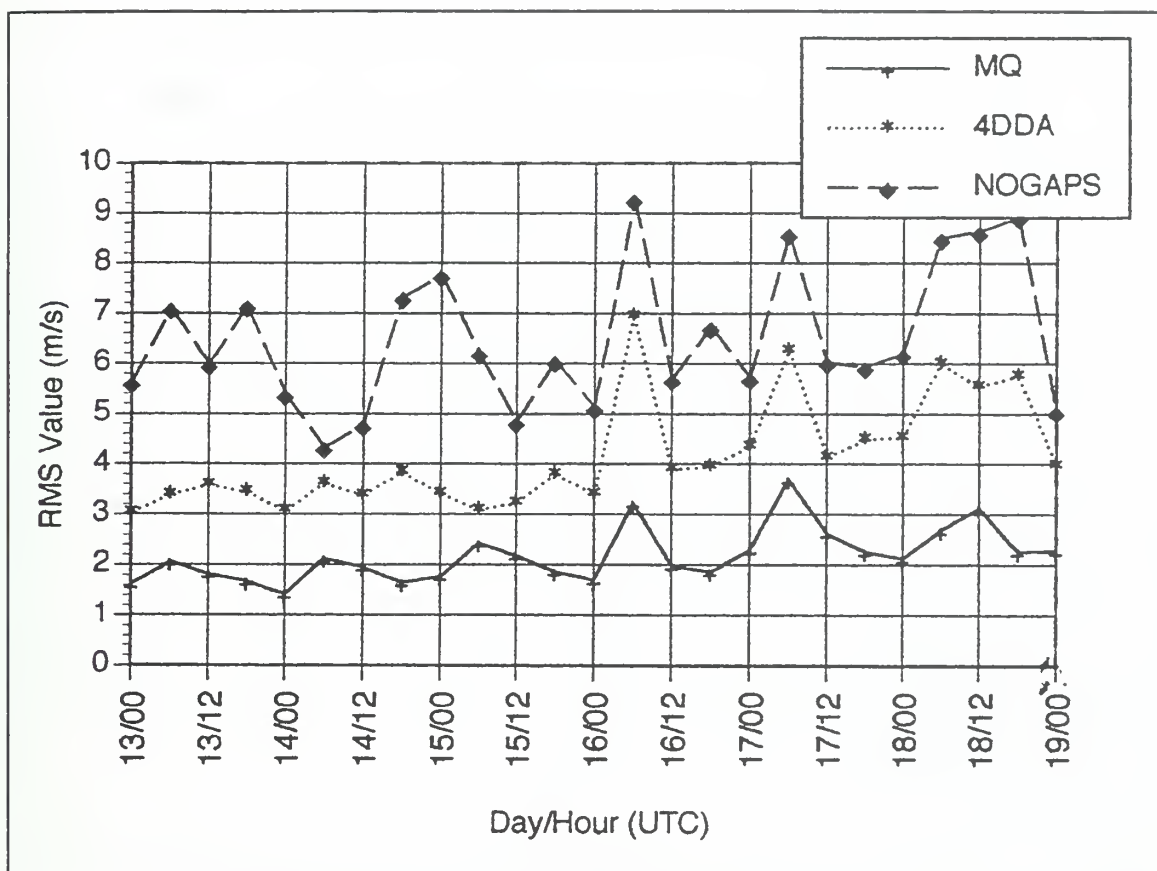


Fig. 3.12. As in Figure 3.7, except for 200 mb wind observations.

especially in the 4DDA and NOGAPS analyses. The 5-minute DC-8 flight-level data at these times provided detailed information on the structure of the 200 mb winds within about 300 km of the center of Typhoon Flo (Figure 3.13). Since the DC-8 typically flew a "figure four" over the center of the storm, many of the DC-8 observations are concentrated in a small geographic area. Thus, the ability to "draw to" these observations may depend upon: (i) the relative weight given to the DC-8 wind observations; (ii) the number of aircraft observations accepted for processing; (iii) the relative weight of the first guess compared to the weighting assigned to the observations;

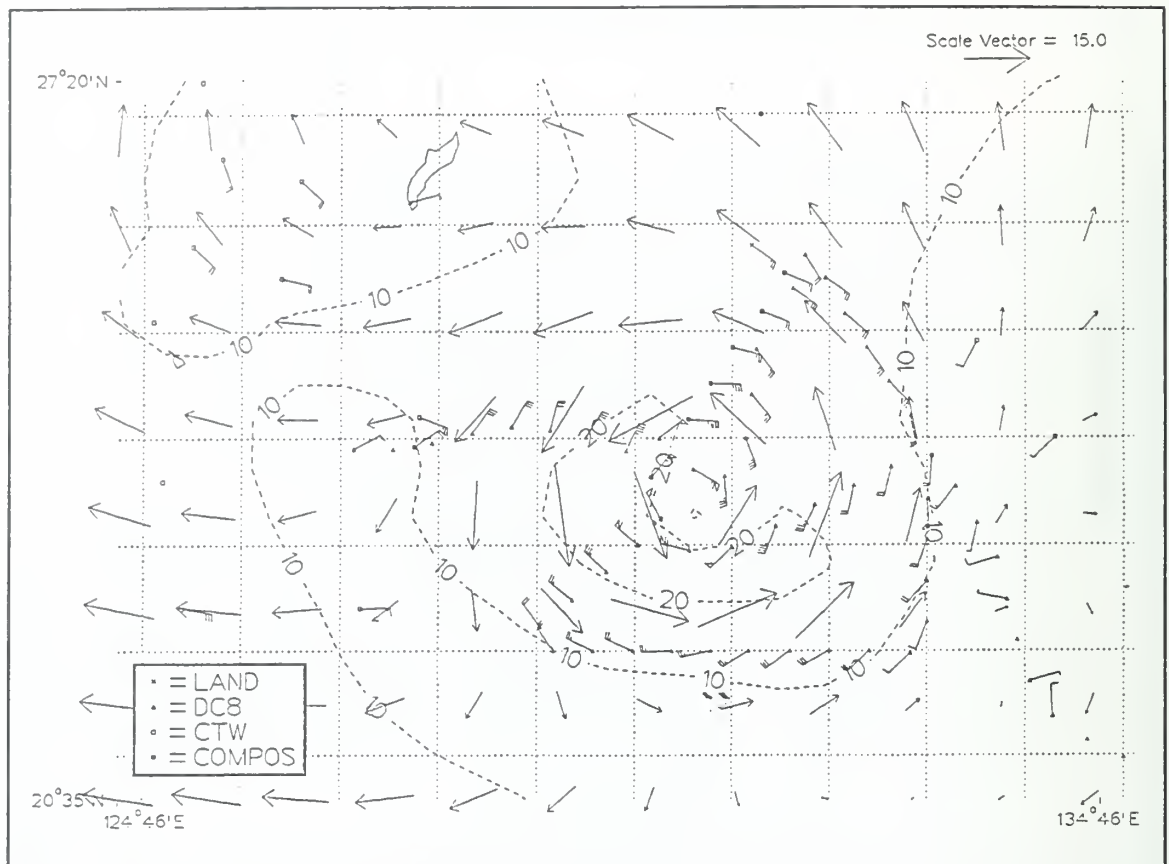


Fig. 3.13. MQ analysis of 200 mb wind (m s^{-1} , scale vector in upper right) and isotachs (dashed, contour interval 10 m s^{-1}) at 06 UTC 16 September.

and (iv) any external dynamic (*e.g.*, gradient, geostrophic wind balance) constraints imposed.

The MQ analysis is only dependent on the first of these factors. As shown in Table 2.2, the DC-8 wind observations had an assigned weighting value two-thirds that of commercial AIREPS. Providing the DC-8 observations were separated by a distance of at least 25 km, all of the observations would be considered by the analysis scheme. No weight is given to the first guess in the MQ scheme, which is a

significant difference from OI systems. The 4DDA analysis weighted DC-8 flight-level winds the same as commercial AIREPS (E. Rogers, personal communication). Since each three-dimensional analysis volume accepts no more than 30 observations (Rogers *et al.* 1992), a portion of the DC-8 flight-level data may not have been incorporated into the OI analysis. Rogers *et al.* do not state what the relative weighting of the first-guess was relative to the weight of the observations. Finally, another difference between the 4DDA and MQ analysis scheme is the dynamic constraints imposed on the aircraft flight-level data. In addition to the OI constraint of the first-guess, the 4DDA is fully geostrophically coupled north of 20°N, where all the DC-8 flights occurred. By contrast, the MQ scheme does not have a geostrophic constraint until 25°N and is not fully coupled until 35°N. Typhoon Flo was located near latitudes 22°N, 24°N, and 27°N on 16, 17, and 18 September, respectively.

These contrasts between the MQ and 4DDA analyses help explain the significant differences between the RMS values for the DC8 and AIREP observations (Figure 3.14). While the MQ analyses produced an RMS values for DC8 observations of 3.5 m s⁻¹, the 4DDA analyses had a DC8 RMS value of 8.0 m s⁻¹, which is only 20% lower than the NOGAPS DC8 RMS value of 10.2 m s⁻¹. Recall again that the NOGAPS analyses did not have access to the DC-8 observations. Conversely, the 200 mb MQ analyses had an RMS value of 5.7 m s⁻¹ for AIREP observations, which is nearly as large as the NOGAPS RMS value for AIREPS, while the 4DDA AIREP RMS value is only 4.0 m s⁻¹. Thus, the MQ analysis closely adheres to the DC8 observations (when

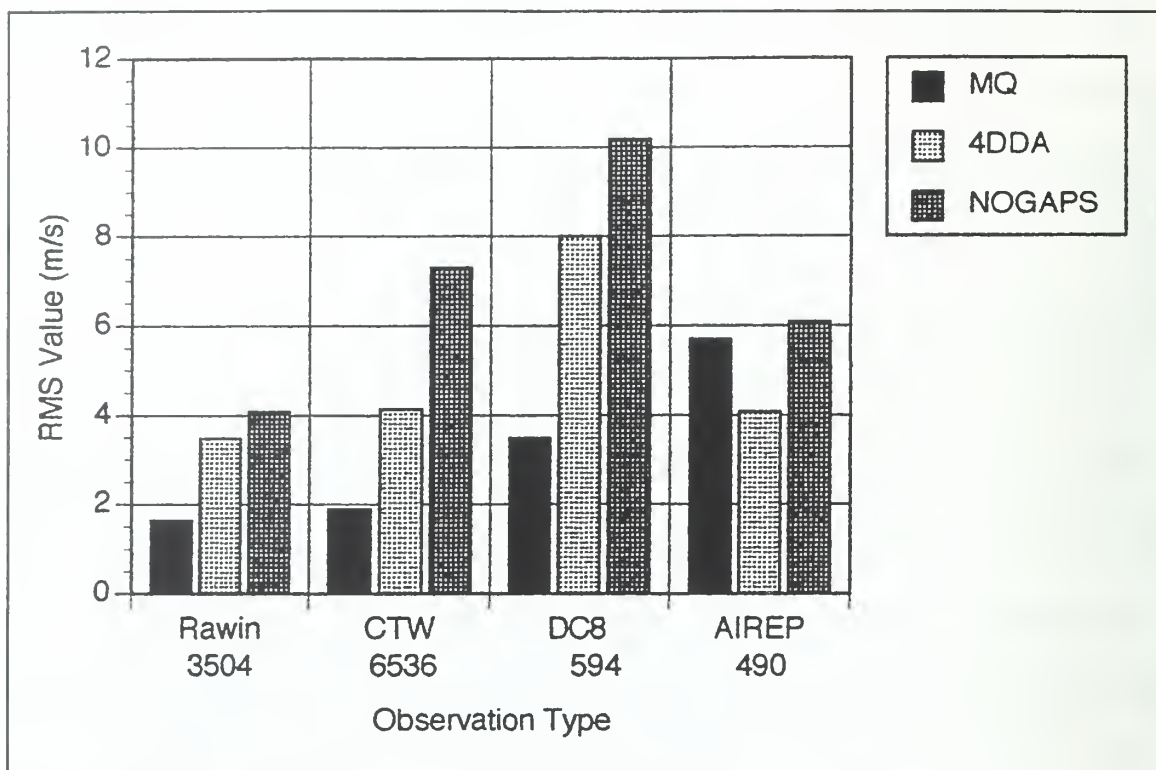


Fig. 3.14. As in Figure 3.8, except for 200 mb wind observations.

available), while not fitting the (presumably) less-accurate AIREPs so closely. By contrast, the 4DDA analysis appears to weight the DC8 wind observations lightly (despite the "keep flag" set on the DC-8 flight-level winds), and instead adheres more closely to AIREP, CTW, and RAWIN observations at 200 mb.

The conclusion is that the MQ and 4DDA offer two alternate representations of the upper troposphere in the vicinity of Typhoon Flo. Both representations are plausible. The 4DDA analysis can be justified by its dynamic consistency, and the ability of its OI analysis to account for a three-dimensional volume of observations, then weight the observations and first guess such that the observational

and background error will have been minimized in a statistically significant ensemble of analyses. The MQ may be considered a valid analysis by its adherence to the research aircraft flight-level data.

Within 1000 km of Flo, the RMS values at 200 mb for the three analyses (not shown) are similar to Figures 3.12 and 3.14. Because no wind-averaging around the storm is used at 200 mb, the MQ scheme closely adheres to all the observations in the domain.

(2) Height RMS Calculations. As in the wind RMS calculations, the height RMS calculations (Figure 3.15) show that the MQ analyses more closely adhere to the data, followed by the 4DDA and NOGAPS analyses. Since all the analyses have obtained the height field using the same method as for the wind field, this result should not be surprising. The MQ analysis has been set up (by the explicit smoothing parameters provided) to draw closely to the height observations, regardless of the dynamic structure involved. The MQ approach differs from the 4DDA and NOGAPS methods in the following ways:

- Multivariate height and wind analyses for the 4DDA and NOGAPS analyses commence north of 10°N and 20°N, respectively.
- The 4DDA and NOGAPS schemes analyze discrete three-dimensional volumes with up to 30 observation-derived increments for each analysis grid point.
- NOGAPS and 4DDA analyses consider not only the observation error of the data, but also the error of the background field.

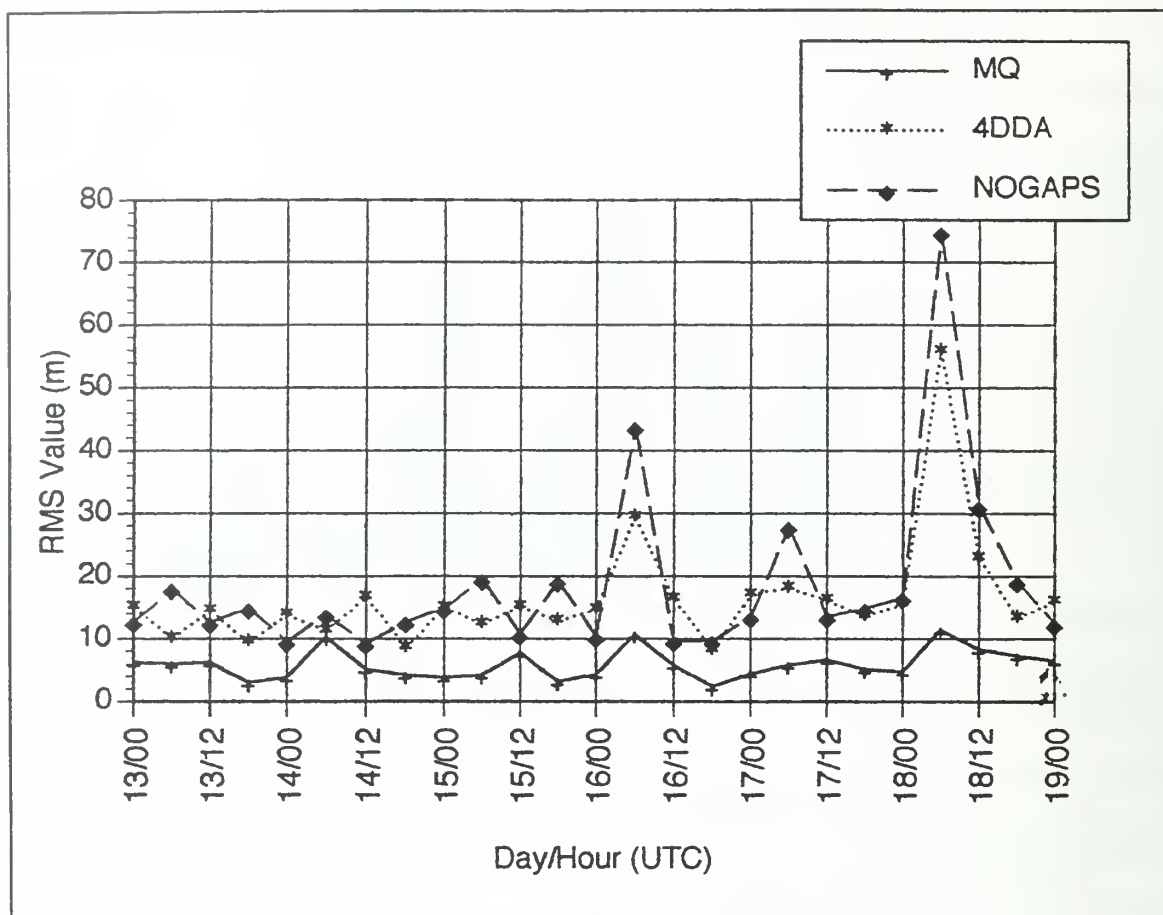


Fig. 3.15. As in Figure 3.7, except for 500 mb height observations (m).

The 4DDA and NOGAPS analyses have very similar RMS values in Figure 3.15 except for time periods when LORAN dropwindsonde (LDW) data were available. This is likely due to two reasons: (i) the availability of rawinsonde data to the operational NOGAPS analysis; and (ii) the relatively coarse horizontal resolution inherent in the rawinsonde database. Harr *et al.* (1991) stated that 85-90% of the rawinsonde data were received in real-time and thus were available to NOGAPS. The horizontal resolution of the data is such that, even when the NOGAPS fields were

degraded to 2.5° horizontal resolution, most of the rawinsonde-based information was retained. This result implies that the quality of the final TCM-90 analyses is more sensitive to the quality and spatial resolution of the delayed data, with perhaps secondary importance placed on the specific model or method chosen to perform that analysis.

The "spikes" in the RMS values at 0600 UTC 16 and 18 September, and to a lesser extent at 0600 UTC 17 September, are caused by the large increments of the LDW observations. These observations near the center of Flo are 200-400 m lower than the surrounding 500 mb heights. Therefore, the RMS values for these time periods are significantly influenced by the degree to which the LDW observations are incorporated into the analysis scheme. As stated above, no constraint prevented these observations from significantly affecting the outcome of the MQ analysis. Ensuring that an OI-based analysis system will accept a specific observation or set of observations is more complicated, especially if that observation has a large increment. Using the NOGAPS MVOI scheme as an example, an observation that exceeds three times the expected error variance will be flagged as a suspect observation (Barker 1992), and confirmation by neighboring observations will be required for it to be accepted. Even if the observation is accepted, it is only one of up to 30 data values that are combined to produce the increment for any specific grid point. Therefore, a typhoon, which has small-scale structure that contains large increments, but is only rarely sampled by more than one or two observations, has little chance of being depicted if no modifications are made to the OI system. The 4DDA analysis had a better depiction of the 500 mb

heights near Typhoon Flo than the NOGAPS analysis (which did not have the LDW data), but the LDW and occasional rawinsonde observations in the vicinity of Typhoon Flo caused the overall 4DDA RMS values to increase from about 15 m to 30-50 m (Figure 3.15).

(3) RMS Summary. The MQ analysis scheme has been shown to produce lower RMS values than either the 4DDA or NOGAPS analyses. This was an intentionally designed feature of the MQ analysis to draw closely to the given observations. Therefore, the conclusion from the RMS data should not be that one analysis is "better." Rather, the RMS values show that both the MQ and 4DDA analyses performed as they were designed. The RMS values for 250 mb winds (Figure 3.16) provide a good comparison of the emphasis placed on different observation types by the MQ and 4DDA analyses. Notice that all the observation types are well represented, as shown by the number of observations in each category. The MQ analysis had significantly lower RMS values than either the 4DDA or NOGAPS analysis for LDW, CTW, and DC8 observations, because it was designed to draw most closely to these delayed data. The assumption was that the delayed, research-quality data would be the most accurate, and when combined with the real-time data, would provide an appropriate depiction of the tropical atmosphere. Conversely, relatively little weight was given to some operational types of data, and the MQ analysis had larger RMS values than the 4DDA analysis for CTO and AIREP observations.

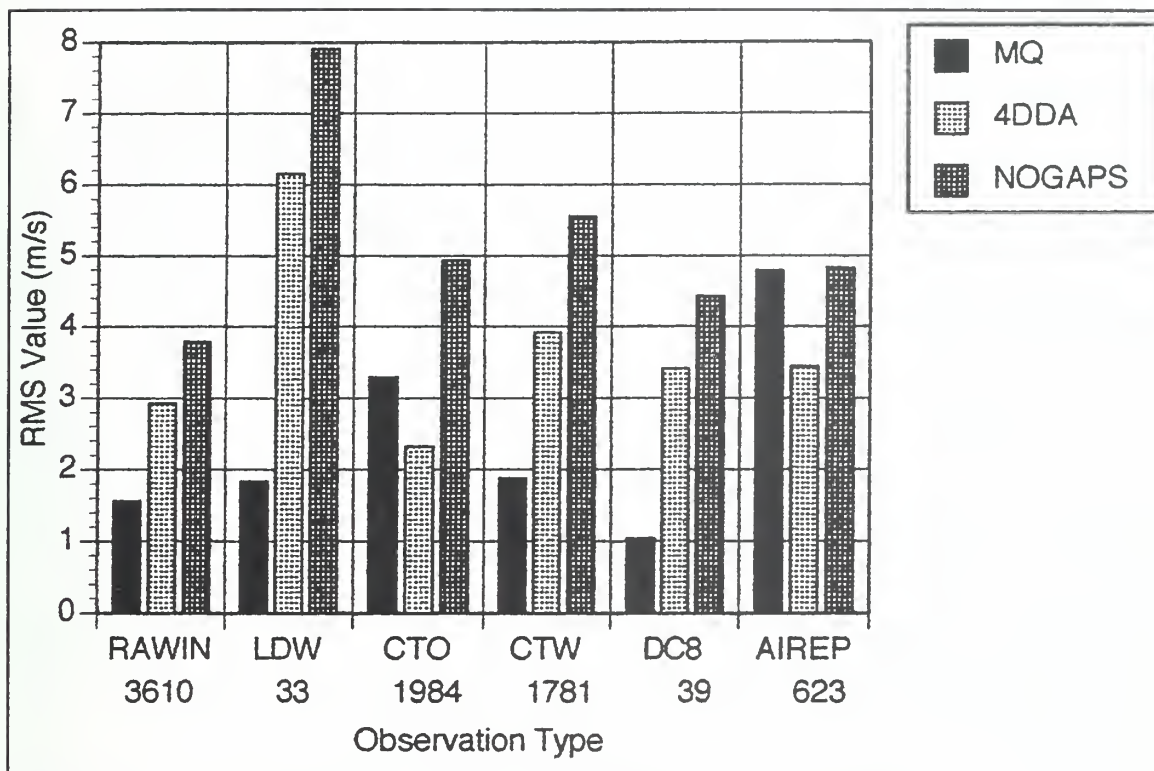


Fig. 3.16. As in Figure 3.8, except for 250 mb wind observations.

Although the MQ and 4DDA analyses appeared to both perform as intended, improvements could no doubt be made to each system. The MQ analysis probably draws too closely to the observations. For example, Goerss and Phoebus (1992) state that the observation wind error for rawinsonde data at 250 mb is 3.1 m s^{-1} , and the MQ analysis had an RMS value of 1.6 m s^{-1} . It is therefore possible that the MQ analysis has noise from the observational error, and/or partially depicted small-scale unrepresentative features in the wind analysis. A future run should increase the smoothing on both winds and heights, but keep the relative amount of smoothing between the observation types similar to the current implementation. In the 4DDA analysis, more

weight should be given to the DC-8 wind data relative to commercial AIREPs, and the reprocessed cloud-track winds should be weighted more heavily relative to the operationally-derived cloud-track winds. As discussed above, altering the weights to achieve this result in an OI scheme is much more complicated than making these adjustments to the MQ analysis.

b. Propagation Vector Analysis

(1) Introduction. Although the track of a tropical cyclone is primarily determined by the large-scale steering flow, observational and modelling studies have consistently indicated that the storm motion deviated from the large-scale environmental flow (Elsberry and Abbey 1991). Carr and Elsberry (1990) defined a propagation vector as this difference between the TC steering vector and the storm motion vector. Elsberry and Abbey (1991) stated that since the TC is observed to coherently track along the sum of the steering and propagation vectors, the mechanism responsible for creating the propagation vector must be of similar scale to the TC (~ 1000 km in diameter). Elsberry and Abbey further state that an atmospheric feature of this magnitude should create irrotational flow over the TC, and thus, through quasi-geostrophic arguments, consist of a cyclonic (anticyclonic) gyre to the left (right) of the propagation vector. The relationships between the storm motion, environmental steering, and propagation vectors, and between the symmetric, asymmetric, and steering components of the total tropical cyclone wind field, are shown in Figure 3.17.

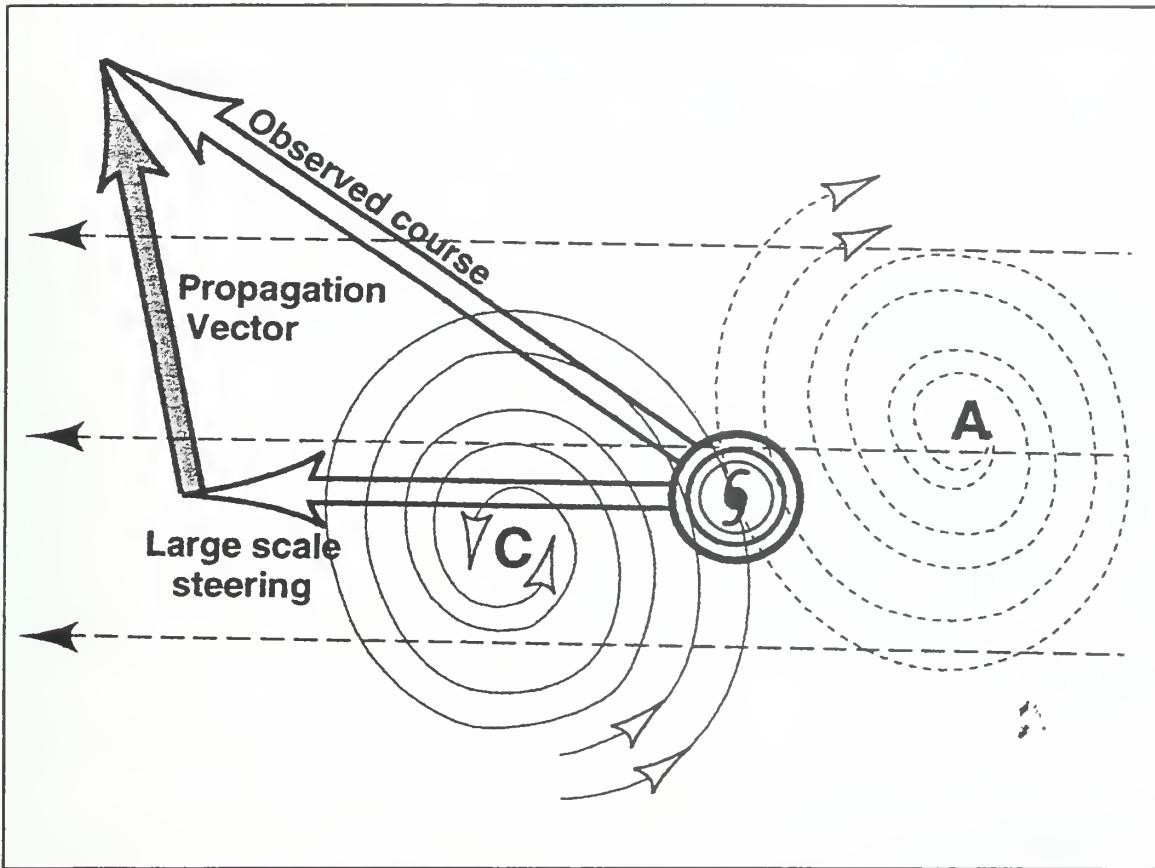


Fig. 3.17. Schematic depicting relationship between large-scale steering flow (long dashed lines), symmetric flow around the tropical cyclone (solid circular lines around tropical cyclone symbol), and cyclonic (light solid lines) and anticyclonic (short dashed lines) gyres. Tropical cyclone motion (observed course vector) depicted as sum of large-scale steering flow and propagation vector (shaded) caused by uniform flow of gyres over the tropical cyclone. See text for further details.

Using a barotropic model, Chan and Williams (1987) showed that the propagation vector could be explained by a nonlinear self-advection process. That is, the advection of the symmetric storm vorticity by the asymmetric wind determines the propagation vector. The asymmetric circulation arises from a meridional gradient in the earth absolute vorticity field. Using a non-divergent barotropic model, Fiorino and

Elsberry (1989) showed that the magnitude of the propagation vector was proportional to the TC outer-wind strength, while the intensity of the TC had little effect on the propagation vectors. Carr and Elsberry (1990) reviewed previously collected composite TC data for the western North Pacific and Australian-Southwest Pacific regions and obtained propagation vectors 1.0 to 2.5 m s⁻¹ in magnitude, and westward and generally poleward in direction. These propagation vectors were generally consistent with the meridional gradient in the absolute vorticity field. Although this gradient is primarily caused by the meridional gradient of the earth vorticity (the β -effect), it is also affected by the positions and strengths of the monsoon trough and the subtropical ridge relative to the TC.

Carr and Elsberry (1992) showed that previously accepted method of defining the environmental steering flow, *i.e.*, averaging a pressure-weighted wind around a specific radial band, was not appropriate. Averaging the total wind field around the TC does not remove the irrotational flow over the tropical cyclone. An ongoing challenge to resolving the "true" propagation vector in an observational dataset is to develop accurate techniques to separate the steering, symmetric and asymmetric wind components. Elsberry and Bohner (1992) proposed a Fourier-decomposition technique in which the 850-300 mb layer-average height or wind field is decomposed into its discrete zonal wavenumbers. The "low" wavenumbers are defined to be the steering flow, while higher wavenumbers are assumed to be part of the TC. Elsberry and Bohner found that wavenumbers 1-15 in the operational NOGAPS analyses produced the most

realistic steering flow for all TC's observed during TCM-90. Other techniques under development include an empirical orthogonal function (EOF) representation of the wind fields (Harr and Elsberry 1993).

(2) Typhoon Flo Storm Motion, Large-Scale Steering Flow, and Propagation Vectors.

The storm-motion vectors for Typhoon Flo were obtained from the JTWC post-analysis best-track by calculating the typhoon mean course and speed \pm 6 h of the 00, 06, 12, and 18 UTC positions, then decomposing the course and speed into x and y components. Typhoon Flo tracked to the north and west until 00 UTC 17 September, when the storm slowed, underwent recurvature, and subsequently accelerated to the northeast.

Elsberry *et al.* (1993) applied the Fourier-decomposition method to calculate Typhoon Flo large-scale steering vectors from the MQ, 4DDA, and NOGAPS analyses. The MQ steering and storm-motion vectors are shown in Figure 3.18a. Until 12 UTC 16 September, the steering vector is to the right of, and has a slightly greater magnitude than the storm-motion vector, which implies a southwestward propagation vector (Figure 3.18b). At 00 UTC 18 September (after recurvature), a dramatic difference occurs in the relationship between the storm-motion and steering vector (Figure 3.18a). While the steering vector is still to the right of the storm-motion vector, the steering vector has a much smaller magnitude than the storm-motion vector, which implies a substantial propagation vector to the north (Figure 3.18b). The propagation vectors suddenly change from south to southwest propagation vectors with

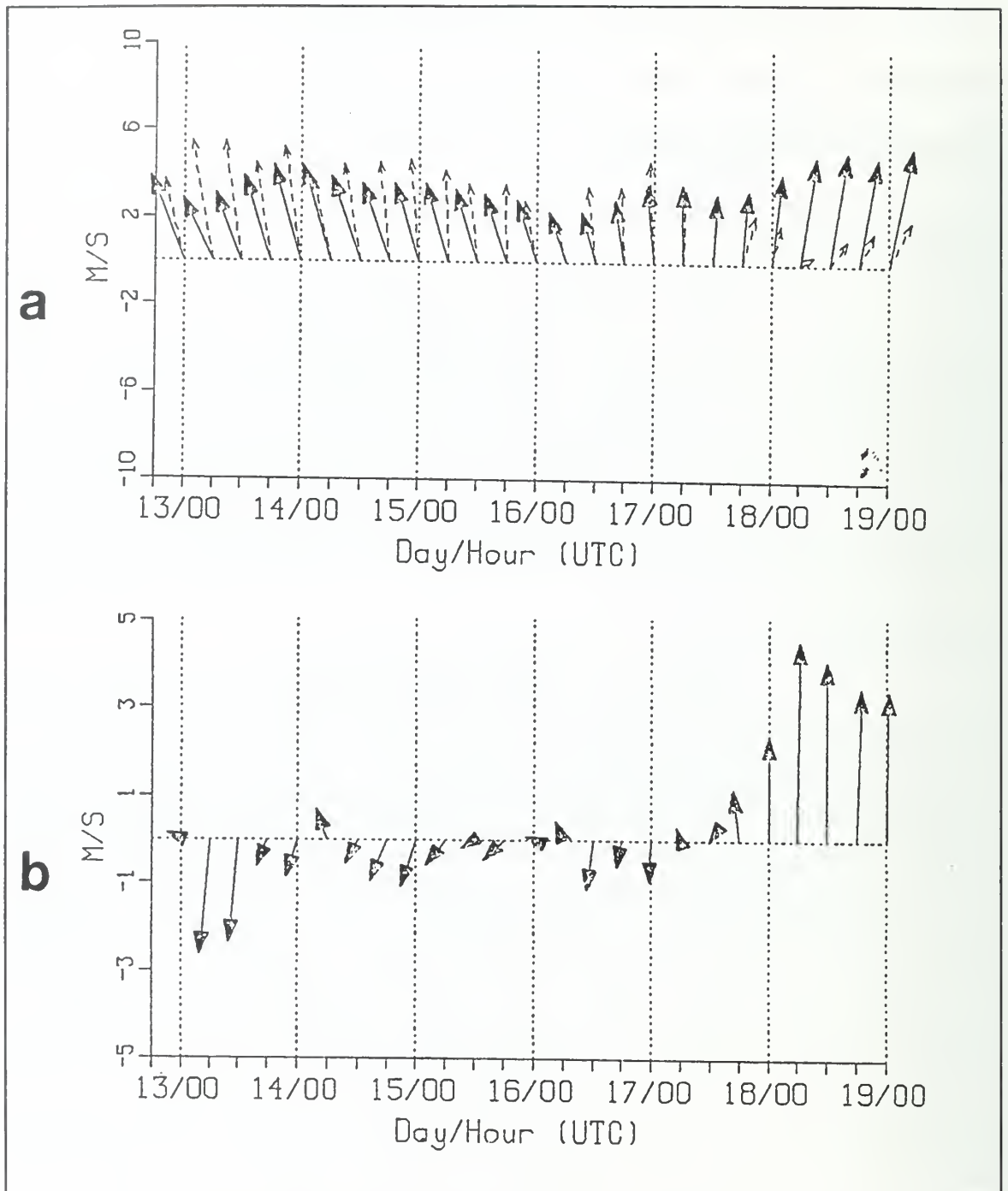


Fig. 3.18. (a) Course (solid), steering (dashed), and (b) propagation vectors (m s^{-1}) every 6 h from 00 UTC 13 September through 00 UTC 19 September. Course vectors from JTWC best-track positions (JTWC 1990). Steering vector is pressure-weighted 850-300 mb average of wavenumber 1-15 winds derived from MQ analyses. Propagation vector is course vector minus MQ steering vector.

a magnitude of 1-2 m s⁻¹ to north-northeast propagation with a magnitude of up to 5 m s⁻¹. These propagation vectors highlight several points.

The MQ wind analysis fields produced a set of propagation vectors that had better temporal consistency than either the 4DDA or NOGAPS analyses wind fields (Figures 3.19a-c). One reason may be the alignment bogus that was used by the MQ analysis. The alignment bogus maintained a vertically aligned typhoon consistent with the JTWC post-analysis best-track position. Although the NOGAPS analyses had a synthetic typhoon bogused into the model, its position was based upon the JTWC working best-track position (Clune *et al.* 1992). The 4DDA analysis did not use TC synthetic inputs, but relied upon the mesoscale model to "spin-up" the TC at the correct location. By 00 UTC 16 September, Typhoon Flo was well-defined in all three analyses. Nevertheless, the MQ analysis continued to have better temporal consistency in the derived propagation vectors. This implies that the temporal consistency of the MQ analysis is competitive with the other two analysis schemes despite each MQ analysis being produced independently of the previous analysis. The better temporal consistency with respect to the NOGAPS analysis indicates the value of the delayed-data TCM-90 observations, especially the reprocessed cloud-tracked winds, which is the primary additional data source in the 850-300 mb layer. Although the higher resolution of the MQ analysis may have introduced additional noise into the analysis, most of this noise appears to have been filtered out by the Fourier-decomposition technique.

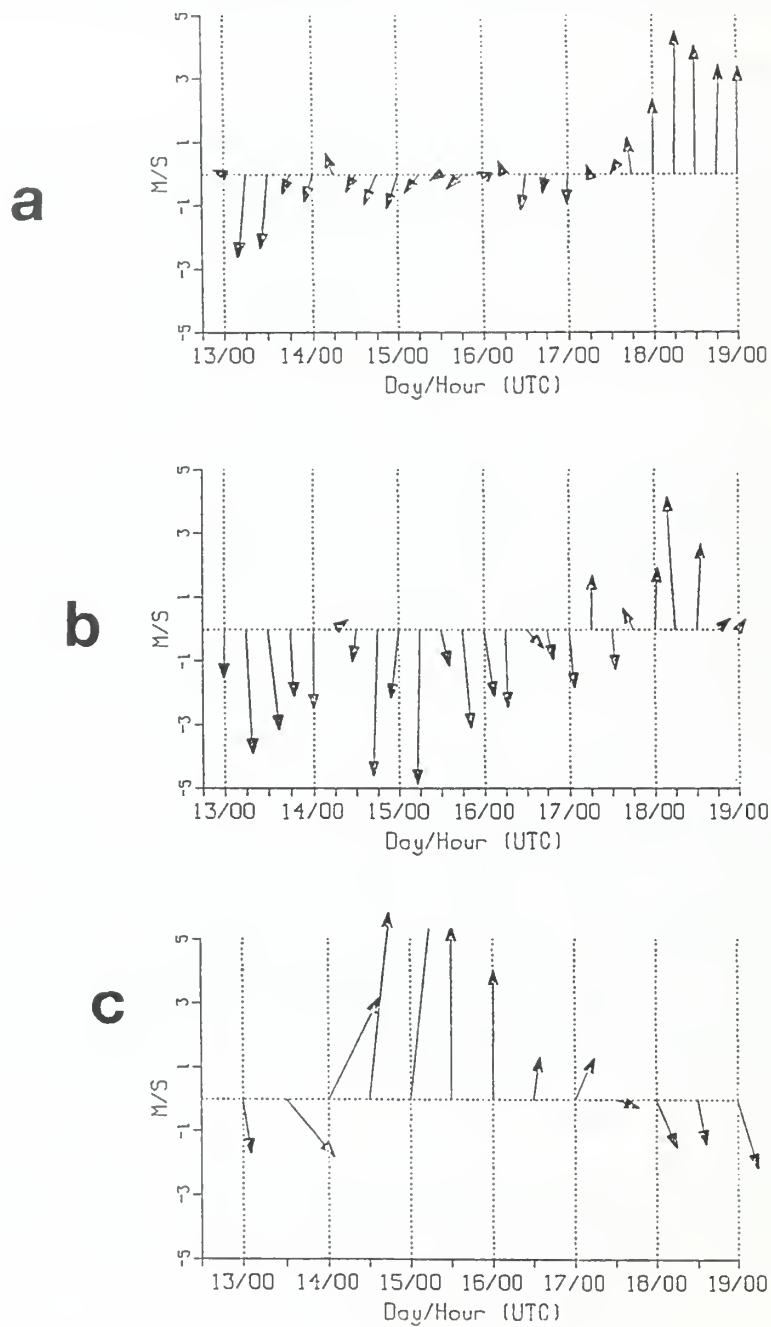


Fig. 3.19. Propagation vectors (m s^{-1}) derived from (a) MQ, (b) 4DDA, and (c) NOGAPS analyses. Propagation vector is course vector (JTWC 1990) minus steering vector derived from respective analysis. Propagation vectors are for every 6 h (12 h) from 00 UTC 13 September through 00 UTC 19 September for MQ, and 4DDA (NOGAPS) analyses.

The magnitude of the MQ propagation vectors (until 00 UTC 18 September) generally agreed with the calculations of Carr and Elsberry (1990) based upon composite datasets, and with previous numerical studies (*e.g.*, Chan and Williams 1987). As Typhoon Flo neared the subtropical ridge, the magnitude of the propagation vector decreased below 1 m s^{-1} , which is smaller than propagation vector magnitudes obtained by barotropic models that only account for the β -effect. The propagation vectors had larger southerly components than were expected. The propagation vectors maintained this southerly component until Typhoon Flo recurved and crossed the subtropical ridge axis (00 UTC 18 September), at which time the propagation vectors rapidly shifted to the northeast and increased in magnitude up to 5 m s^{-1} .

The striking changes over time in the propagation vectors provide conditional observational confirmation of the importance of the environmental relative vorticity gradient in determining the propagation vector. Prior to recurvature, Typhoon Flo was located on the northern edge of the monsoon trough and south of the subtropical ridge. The relative location of the trough and ridge produced a southward increase in the relative vorticity field of Typhoon Flo. A southward increase in the relative vorticity gradient reduces the northwestward propagation β -effect (Elsberry and Abbey 1991). If the relative-vorticity gradient exceeds the β -effect, the propagation vector would be towards the southwest, which is consistent with the MQ-derived propagation vectors.

The purpose of obtaining the propagation vectors for this study was to provide another method of verifying the plausibility of the MQ analyses. If the MQ

analyses had produced unreasonable propagation vector magnitudes, while the 4DDA- and NOGAPS-derived propagation vectors were consistent with previous studies, then serious doubt would have been placed on the value of the mid-level (700-300 mb) MQ analyses. Fortunately, the MQ propagation vectors are both temporally consistent and physically reasonable, which supports the hypothesis that the MQ analyses are a reasonable, alternate depiction of the atmosphere.

Although these results are encouraging, specific interpretations of the propagation vectors should be viewed with some caution, since the Fourier method of Elsberry and Bohner (1992) for decomposing the total wind field may not completely separate the asymmetric circulation from the steering flow. Multi-Quadric-derived propagation vectors should be calculated using the EOF wind technique, once that method becomes available.

c. Azimuthally-Averaged Winds in the Vicinity of Typhoon Flo

The previous quantitative checks (RMS values, propagation vectors) have used data throughout the entire TCM-90 analysis domain to show that the MQ analyses are a viable, alternate representation of the atmosphere. The final quantitative check will be the azimuthally-averaged winds within a 1500 km radius of Typhoon Flo. This is the region of the analysis hypothesized to be the most important for determining the effect of synoptic-scale features on typhoon intensity changes.

Vertical cross-sections of tangential and radial winds for a Pacific composite typhoon are shown in Figure 3.20a-b (Frank 1982). The 850 mb, 200 mb,

and vertical cross-sections of radial and tangential wind components azimuthally averaged around Typhoon Flo will be compared with this composited rawinsonde typhoon structure. The three analysis schemes will be intercompared to show that the MQ and 4DDA analyses both portray reasonable radial and tangential wind profiles. These profiles show more detail than previous composite studies, but contain less structure near the center of the typhoon compared to mesoscale analyses based upon aircraft reconnaissance (Holland 1987).

(1) 850 mb Tangential Wind Speed. Low-level tangential wind profiles were examined for each time period. Figures 3.21-3.23 are representative samples that show the typical relationships of the tangential winds among the three analysis schemes.

The effect in the MQ analysis due to the special azimuthal averaging of the wind in moving cylindrical coordinates and subsequently blending of the wind back into Cartesian coordinates in the MQ analysis is shown in Figure 3.21. This blending caused the increase in wind speed between 450 and 500 km, and then a more rapid decrease in wind speed between 500 and 600 km. This "bump" in the wind profile was most noticeable at 00 UTC 14 September, but was also present at 06 UTC 17 September (not shown). Changes in the slope of the tangential wind speed at 600 km occurred occasionally in the MQ analysis (Figures 3.22 and 3.23). The 4DDA had a smoother variation of the tangential wind speed with respect to radius, although the wind speed maximum and radius of maximum winds (RMW) were generally similar for the

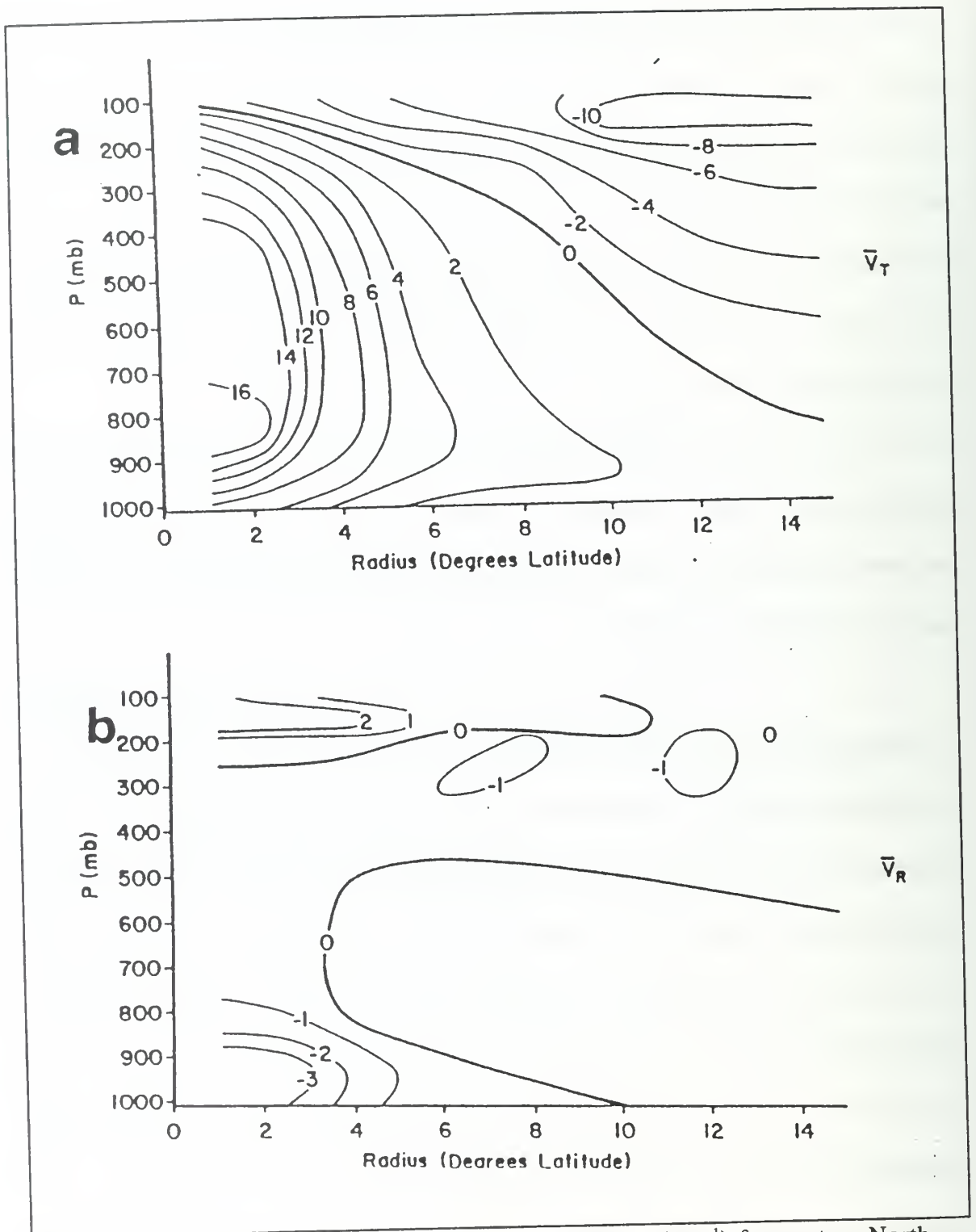


Fig. 3.20. Composite (a) tangential and (b) radial winds (m s^{-1}) for western North Pacific typhoons (Frank 1982).

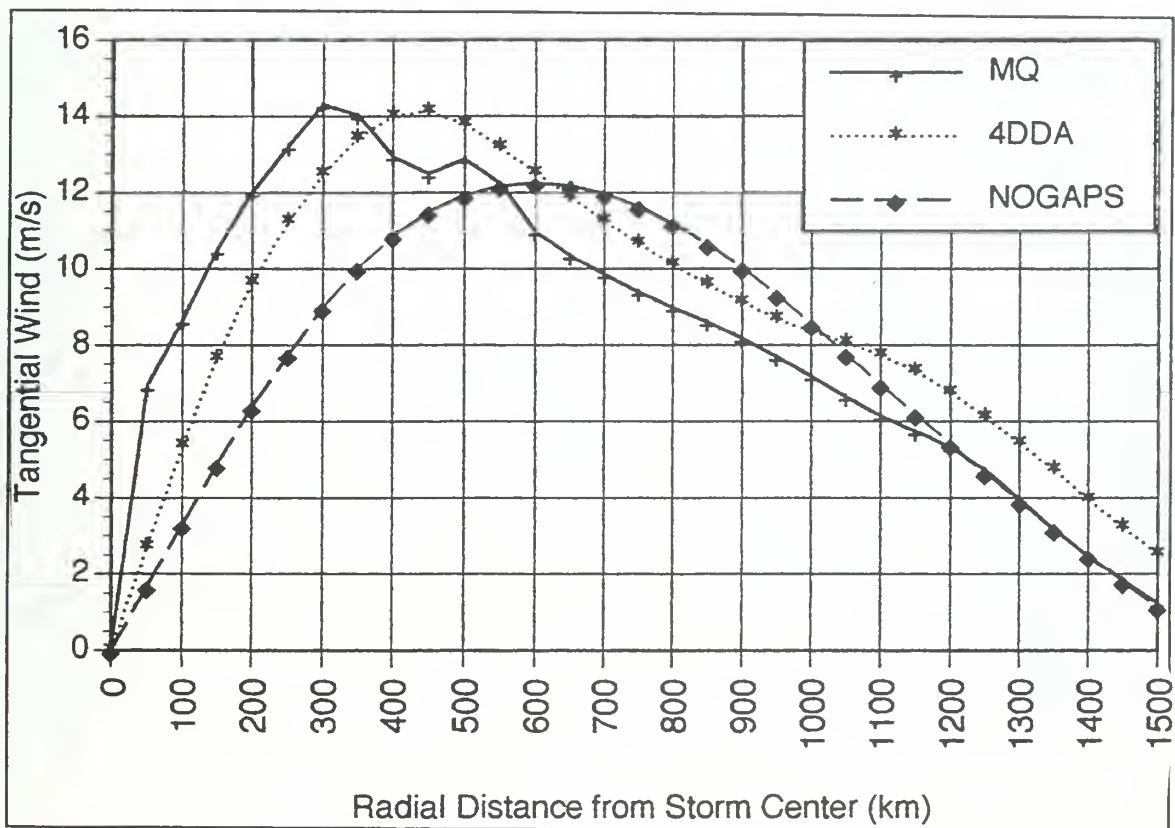


Fig. 3.21. Azimuthally-averaged 850 mb tangential wind (m s^{-1}) versus radius (km) around Typhoon Flo for MQ, 4DDA and NOGAPS (see inset for symbols) analyses at 00 UTC 14 September.

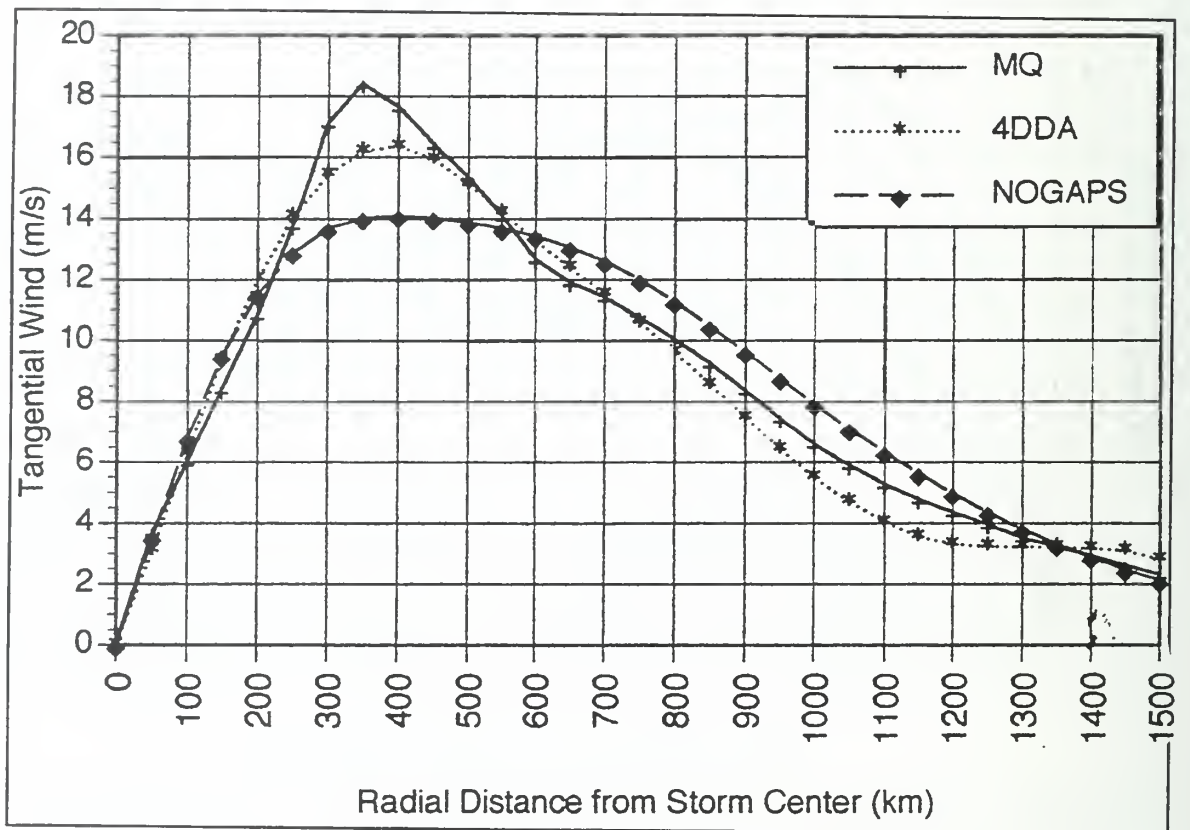


Fig. 3.22. As in Figure 3.21, except at 12 UTC 15 September.

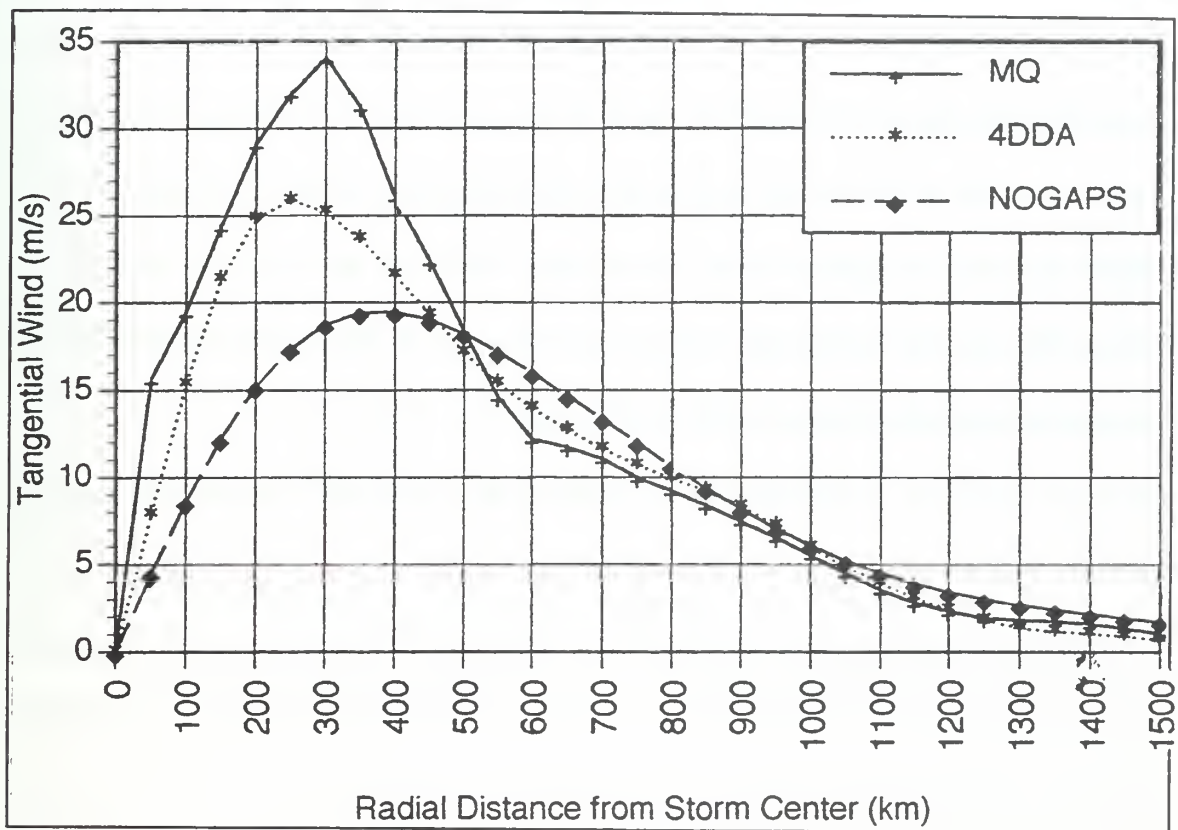


Fig. 3.23. As in Figure 3.21, except at 06 UTC 18 September.

MQ and 4DDA analyses. The exceptions occurred when the NASA DC-8 aircraft launched LORAN dropwindsondes. These observations were assimilated by the MQ analysis, and increased the magnitude of the tangential wind near Typhoon Flo (Figure 3.23).

As would be expected for the 2.5° lat./long. resolution first guess, the NOGAPS analysis has the RMW at 400-600 km, while the MQ and 4DDA analyses typically have the low-level RMW closer to the center at 250-350 km. Notice that the inner structure of Flo is not realistically depicted in any of the analyses. A typical RMW in a mature typhoon is 40 km (Anthes 1982) and the tangential wind speed at about 700 mb for an intense tropical cyclone such as Hurricane Anita based upon research aircraft data had a RMW near 25 km.

Even though the 50 km grid used in the MQ and 4DDA analyses would not have depicted the RMW within 50 km, low-level aircraft reconnaissance would have assisted in accurately measuring the low-level wind structure of Flo. Even when LDW observations were available (*e.g.*, Figure 3.23) the RMW is still depicted at 250-300 km. Perhaps a more nested, higher resolution analysis scheme near the typhoon center would yield a more realistic result.

In summary, the low-level wind analyses within 300 km are suspect. This is not inconsistent with the planning for the data-collection effort of TCM-90, which was to obtain high spatial- and temporal-resolution data 300-800 km from the

typhoon of interest (Elsberry 1990). The effects of this deficiency on this study will be discussed below.

(2) 200 mb Tangential Wind Speed. Good agreement between the MQ and 4DDA analyses is found for the 200 mb tangential wind speed (Figures 3.24-3.26). The MQ and 4DDA analyses have the 200 mb RMW at 200 to 300 km from the storm center for times with no DC-8 flight-level observations, which is likely too far out from the true RMW. However, the 06 UTC 17 September tangential wind speed profile (Figure 3.26) that utilizes the DC8 observations has a RMW at 100 km.

As in the RMS comparisons, the MQ analysis appears to weight these reconnaissance aircraft observations more heavily than the 4DDA analysis. This produces a more realistic RMW (100 km), and larger tangential wind speeds near the center of the storm. However, the remainder of the profiles of tangential wind are similar in the MQ and 4DDA analyses, *e.g.*, the analyses agree within 50 km on the radius at which the tangential winds change from cyclonic to anticyclonic. Other 200 mb tangential wind profiles without DC-8 observations (not shown) are similar at outer radii.

Although the NOGAPS 200 mb tangential wind profiles generally have smaller magnitudes, the profile shape is normally similar to the MQ and 4DDA analyses. One exception is at 00 UTC 15 September, where the NOGAPS tangential wind profile is out of phase with the MQ and 4DDA tangential wind analyses. The 200 mb NOGAPS analysis for 00 UTC 15 September (Figure 3.27) has a series of cyclonic

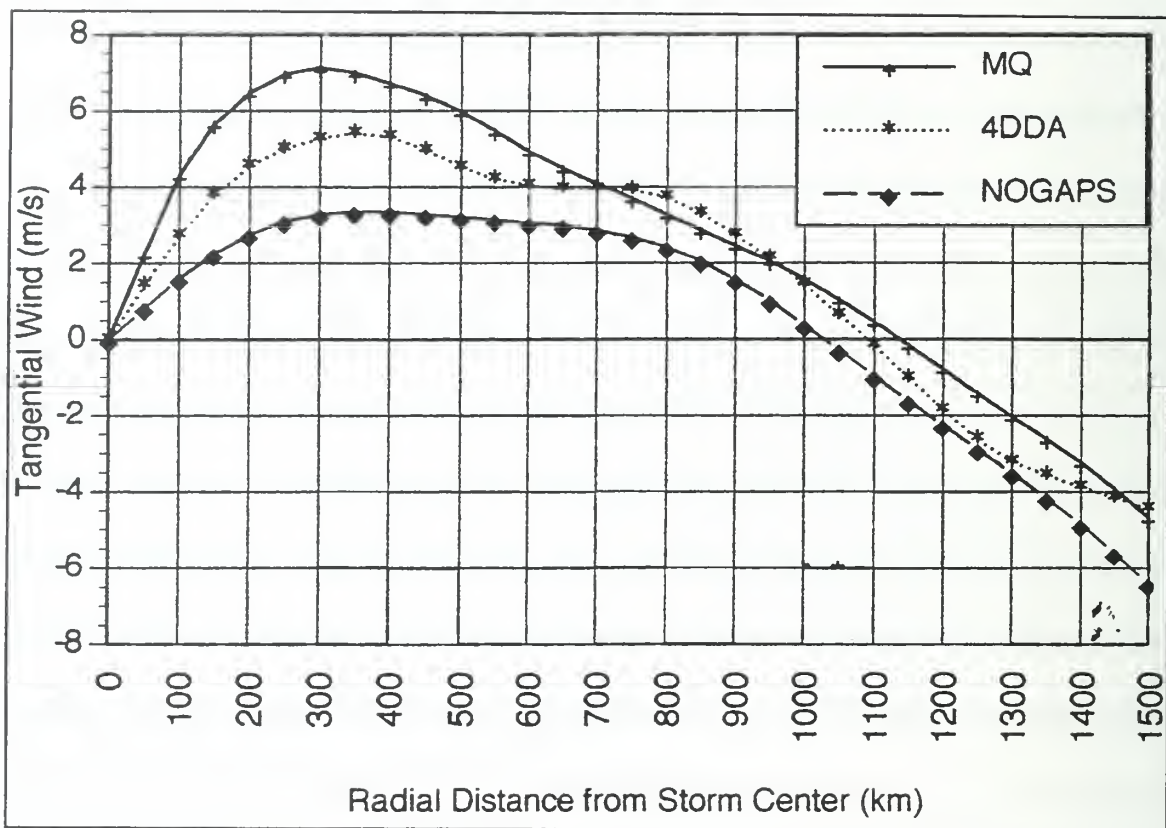


Fig. 3.24. As in Figure 3.21, except for 200 mb at 12 UTC 14 September.

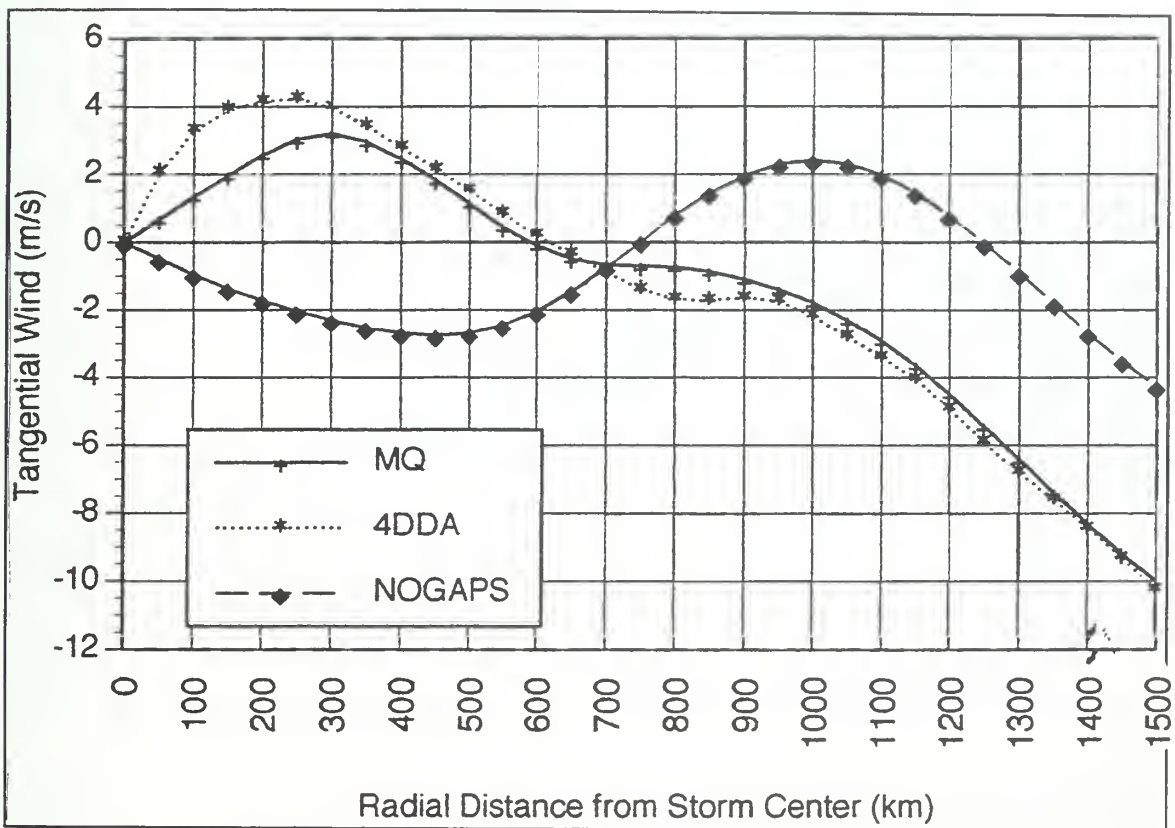


Fig. 3.25. As in Figure 3.21, except for 200 mb at 00 UTC 15 September.

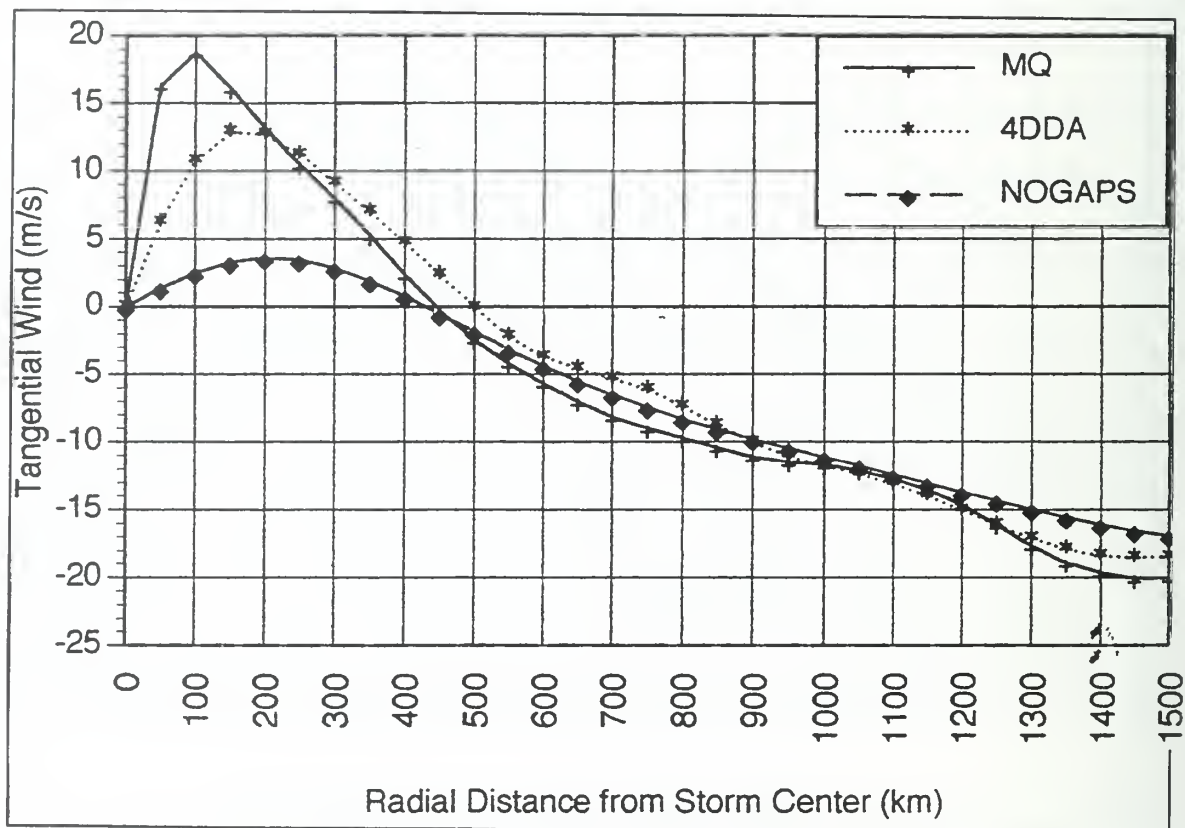


Fig. 3.26. As in Figure 3.21, except for 200 mb at 06 UTC 17 September.

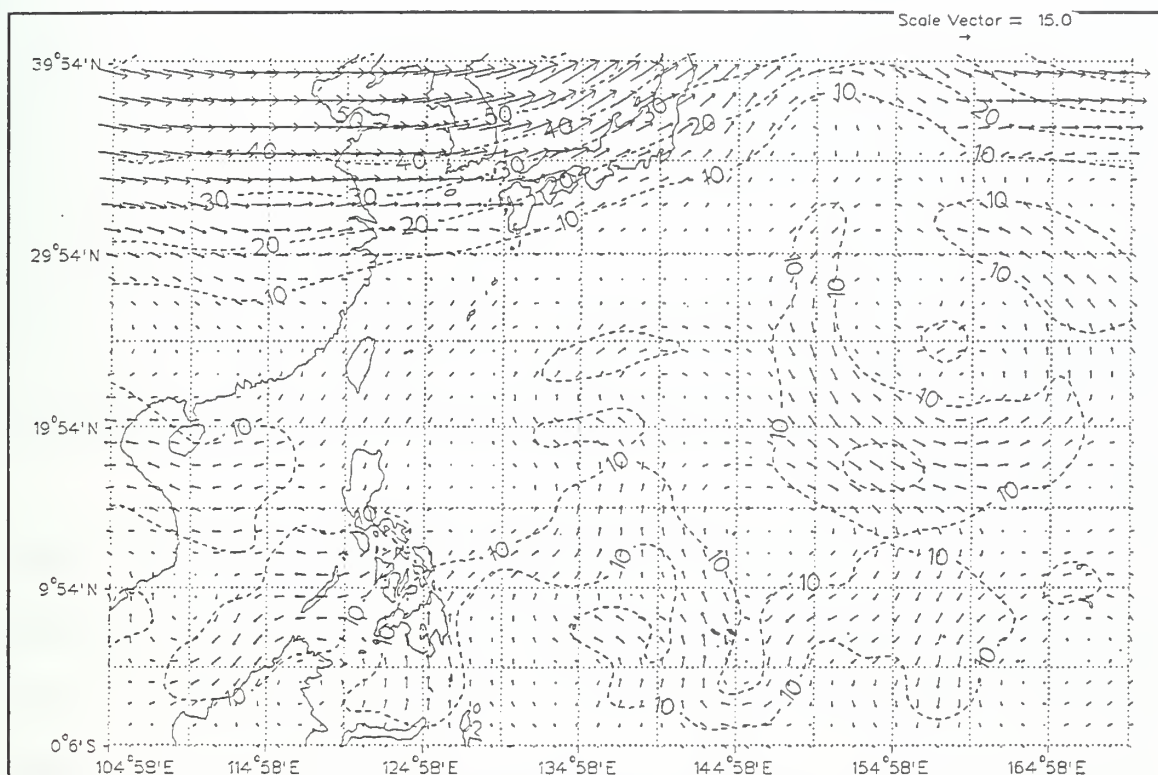


Fig. 3.27. NOGAPS analysis of 200 mb wind (m s^{-1} , scale vector in upper right) and isotachs (dashed, contour interval 10 m s^{-1}) at 00 UTC 15 September.

and anticyclonic circulations centered near 5°N that extend from the Philippines eastward to the dateline. These upper-level circulations have a maximum intensity around 150 mb. Because these circulations influence the upper-tropospheric analysis south of 15°N , they affect the tangential winds around Flo. However, the upper-level flow along 5°N over the western North Pacific 12 h before and after this analysis is a zonal easterly flow (*e.g.*, Figure 3.28). It was determined that the operational NOGAPS series was not run for 00 UTC 15 September (P. Harr, personal communication). Bayler and Lewit (1992) state that previous NOGAPS forecasts are substituted for up to 24 h if NOGAPS is not able to run, but it is not known if that was done in this instance. Recall that the MQ analysis used the NOGAPS analyses as a first guess. Presumably, the delayed TCM-90 data not available to the NOGAPS-backup were able to change the MQ analysis into a more realistic structure.

(3) Vertical Cross-Sections of Tangential Wind Speed. Vertical cross-sections of tangential wind speed (Figure 3.29) generally have good agreement between the MQ and 4DDA analyses, while the NOGAPS analyses usually have smaller magnitude wind speeds. As expected for the coarser resolution NOGAPS analyses, the RMW was located farther from the typhoon center than in either the MQ or 4DDA analyses. The effect of the first guess is shown in the tangential wind cross-sections at 00 UTC 15 September for the MQ and NOGAPS analyses (Figures 3.29a and 3.29c). The NOGAPS analysis had maximum tangential winds between $15\text{--}20\text{ m s}^{-1}$ at 400 to 600 km from the center of Flo, while the 4DDA analysis had maximum tangential winds

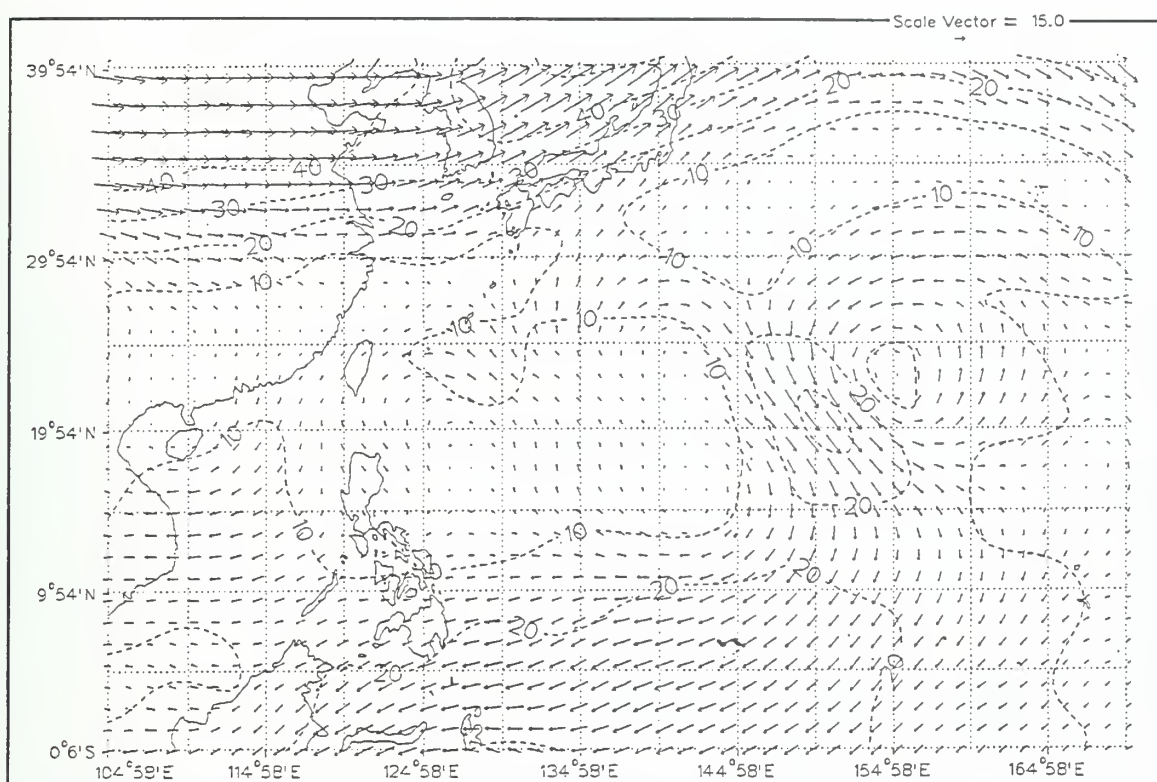


Fig. 3.28. As in Figure 3.27, except at 12 UTC 15 September.

greater than 20 m s^{-1} about 350 km from the center of the TC (Figure 3.29b). The 4DDA analysis also had the level of the maximum tangential winds between 850 and 700 mb, which is consistent with a mid-level wind maximum observed in Flo as the storm passed near Saipan 36 h earlier (Elsberry *et al.* 1990). By contrast, the NOGAPS analysis had near-uniform wind speed between 700 and 1000 mb. The MQ analysis had the mid-level wind maximum between 700 and 850 mb similar to that depicted by the 4DDA analysis, but the MQ analysis winds increased in magnitude below 850 mb at 500–900 km from the typhoon center. The reason for this unusual vertical wind profile was the absence of TCM-90 delayed data at 1000 mb. Consequently, the MQ analysis

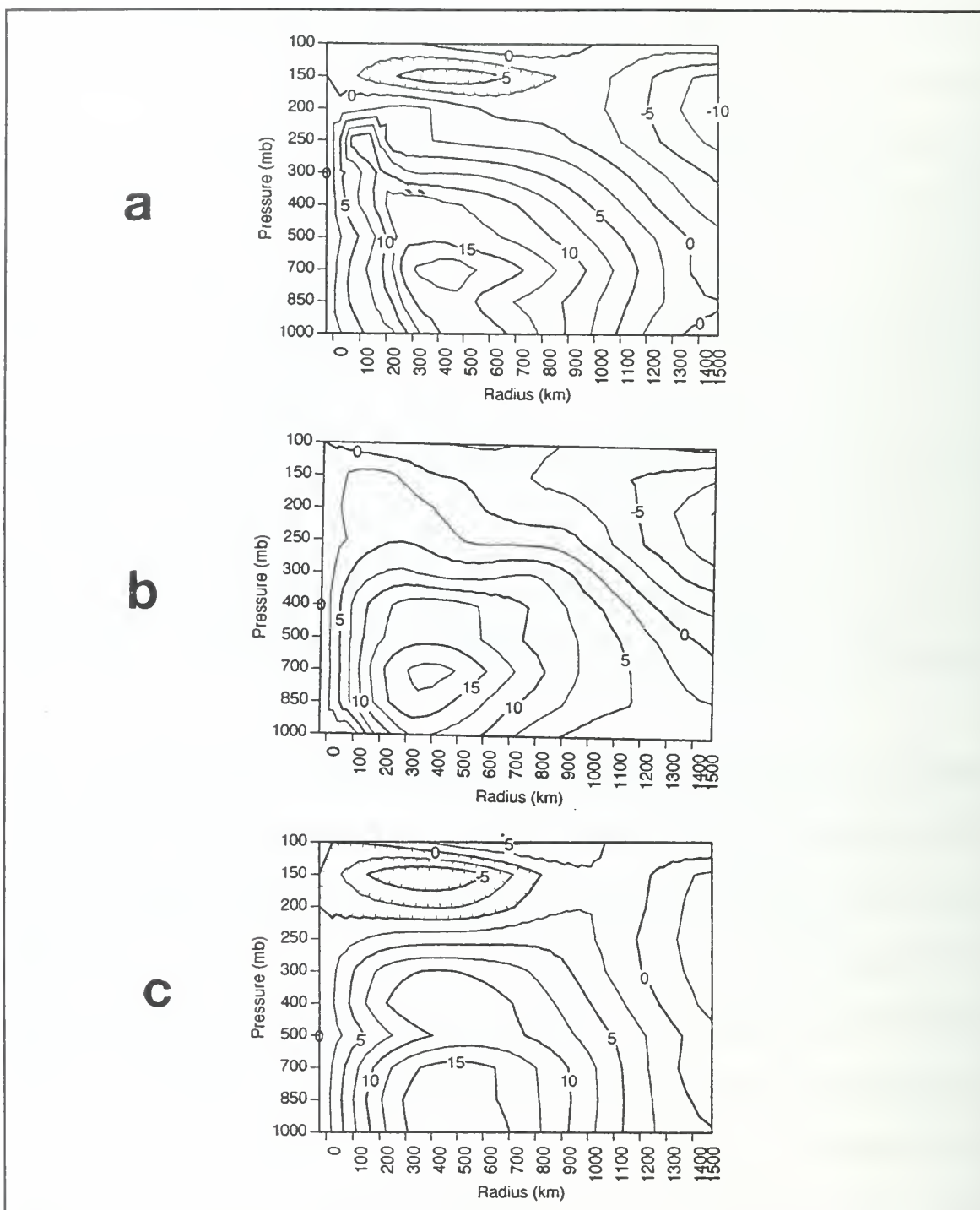


Fig. 3.29. Vertical cross-section of azimuthally-averaged tangential wind (m s^{-1} , contour interval 2.5 m s^{-1} , dashed contours $< 0 \text{ m s}^{-1}$) around Typhoon Flo at 00 UTC 15 September for: (a) MQ analysis; (b) 4DDA analysis; and (c) NOGAPS analysis. Positive values are cyclonic winds, negative values are anticyclonic winds.

appeared very similar to the (NOGAPS) first guess at 1000 mb. This example shows that the MQ 1000 mb winds, and any associated vertical derivatives, may not have significant additional value over the first-guess winds.

An example of a vertical cross-section of tangential winds at an off-synoptic time shows the MQ and 4DDA analyses are in good agreement (Figures 3.30a and 3.30b). Both analyses depict a maximum wind greater than 25 m s^{-1} , with a RMW 200-300 km from the center of Flo. Both analyses have the 0 m s^{-1} contour depicting the outer edge of the TC cyclonic circulation at similar radii for the given pressure levels, and both analyses have anticyclonic winds in excess of 20 m s^{-1} at 150 mb about 1400 km from Typhoon Flo. The vertical consistency in the MQ cross-section is also encouraging, since the analyses are not explicitly vertically coupled.

(4) 850 mb Radial Wind Speed. While Figure 3.20b has weak inflow at all radii at 850 mb, the three analyses depict considerable variability in the low-level flow, both with respect to the other analyses and between time periods (Figures 3.31-3.33). The NOGAPS analysis typically has very little ($< 1 \text{ m s}^{-1}$) radial flow within 400 km of the center, and then usually has weak inflow beyond 400 km. Both the MQ and 4DDA analyses, at different times, have weak outflow from the center of Flo out to 600 km (Figures 3.32 and 3.33). Unfortunately, little agreement is found between the MQ and 4DDA analyses in the shape of the radial wind profile, especially within 600 km of the center. However, the magnitudes of the differences are less than

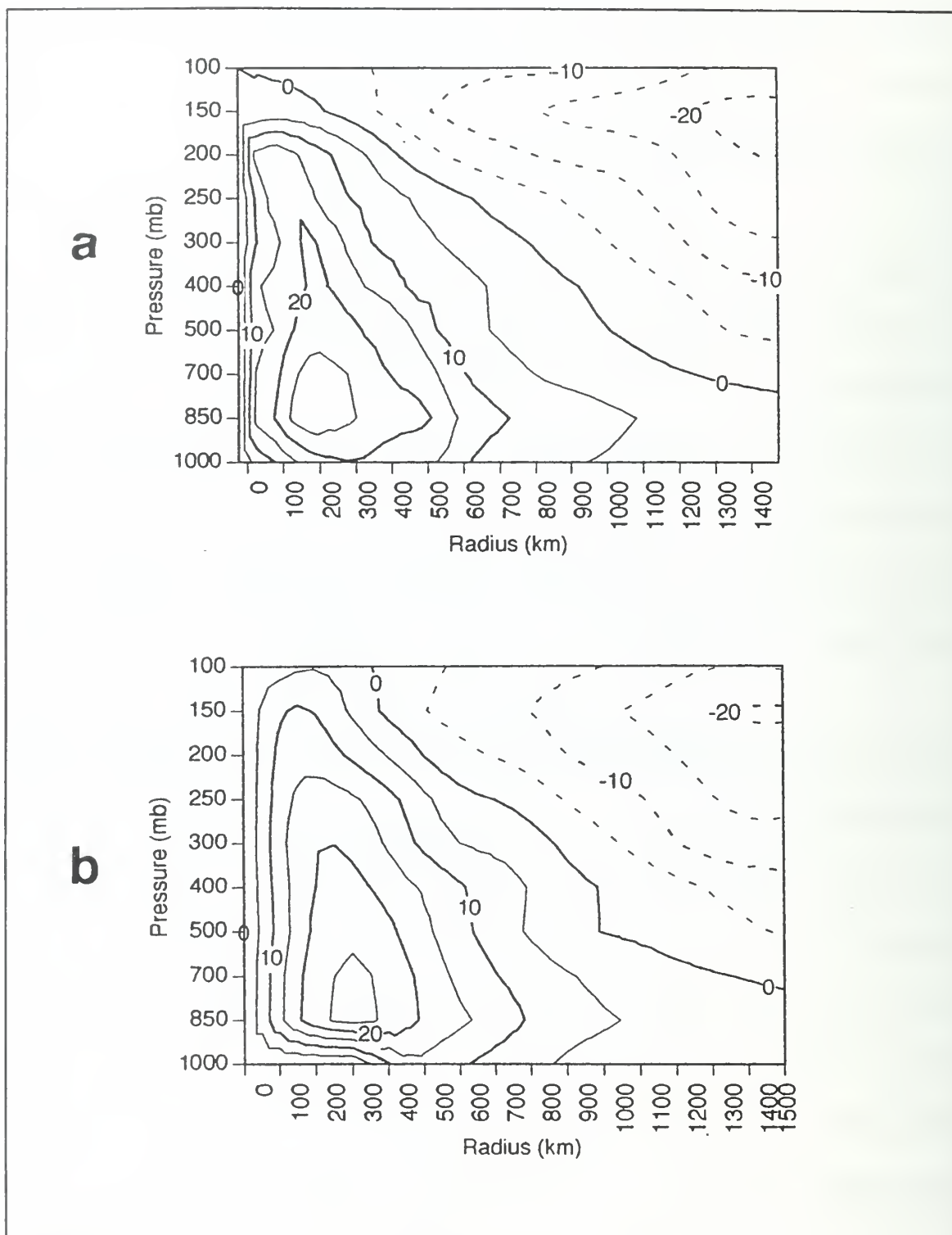


Fig. 3.30. As in Figure 3.29, except contour interval 5 m s^{-1} and at 06 UTC 17 September for (a) MQ analysis and (b) 4DDA analysis.

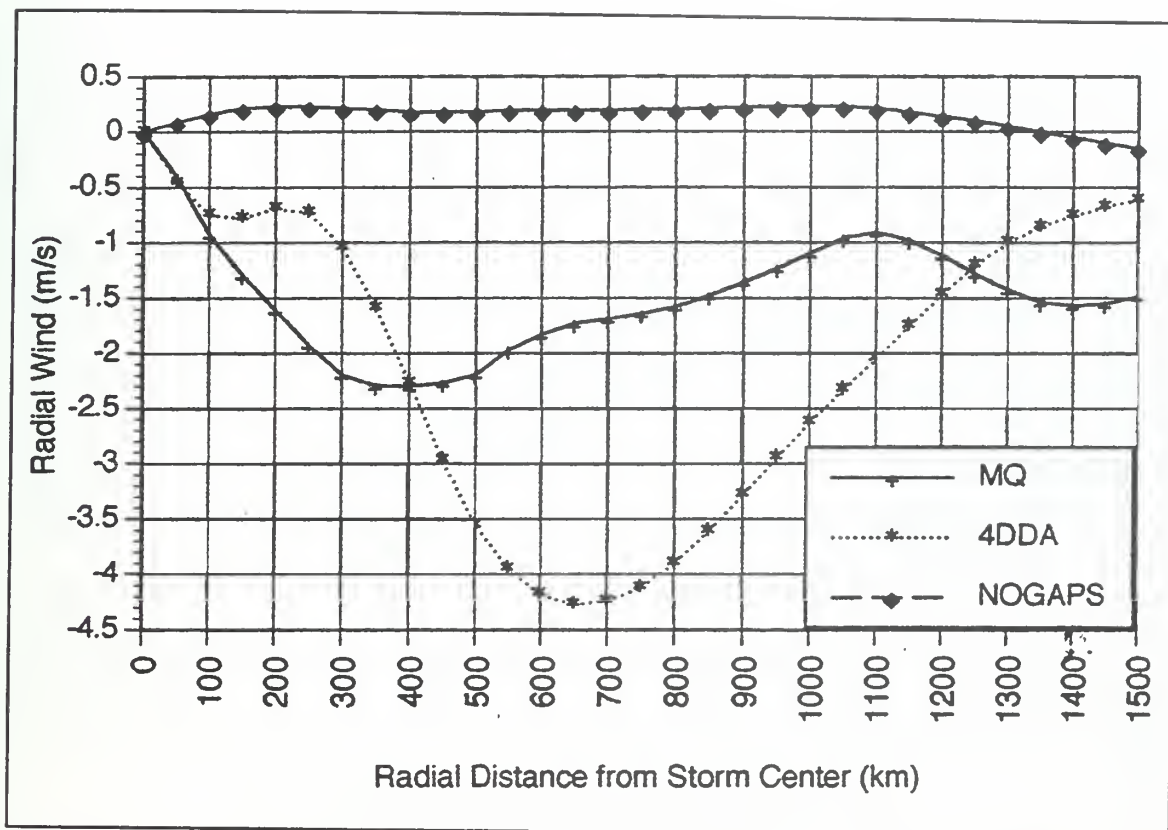


Fig. 3.31. Azimuthally-averaged 850 mb radial wind (m s^{-1}) versus radius (km) around Typhoon Flo for MQ, 4DDA and NOGAPS (see inset for symbols) analyses at 12 UTC 13 September.

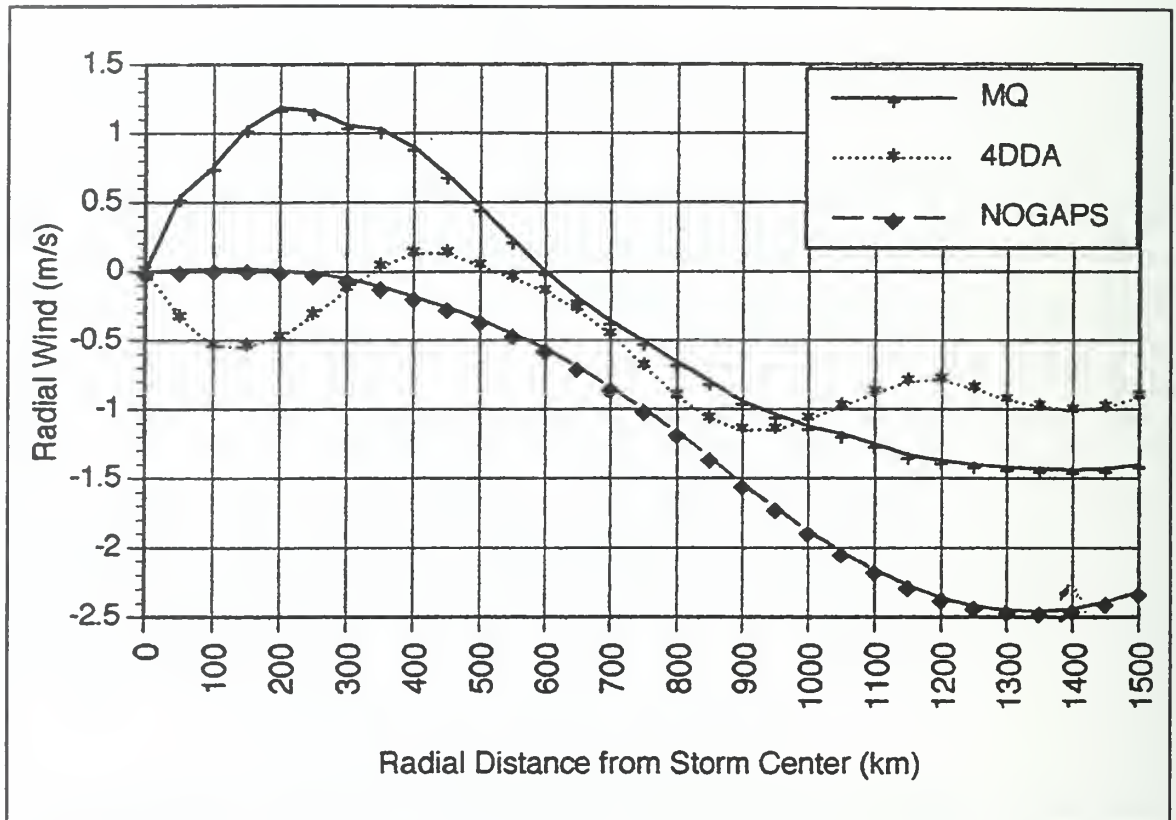


Fig. 3.32. As in Figure 3.31, except at 12 UTC 14 September.

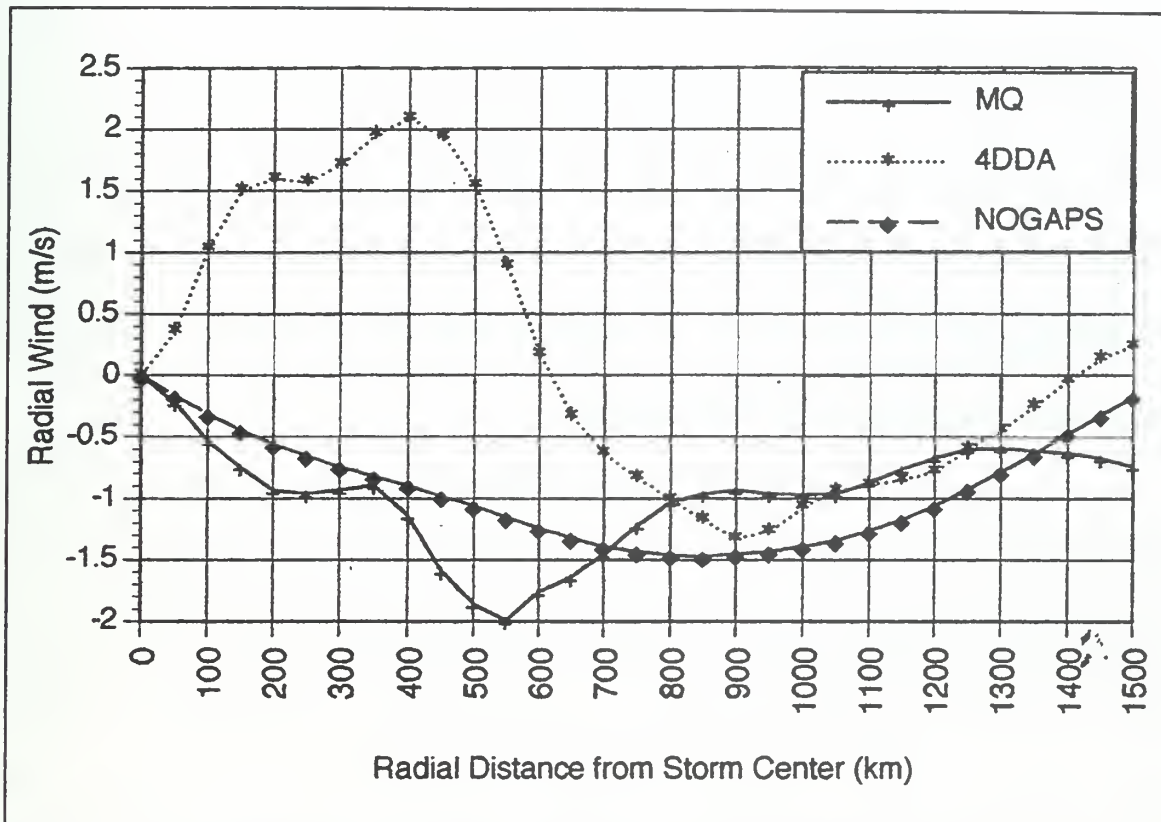


Fig. 3.33. As in Figure 3.31, except at 06 UTC 18 September.

3 m s⁻¹. The low-level radial wind component profiles, and any derived calculations, should be viewed with caution, no matter which analysis is used.

(5) 200 mb Radial Wind Speed . Unlike the low-level radial wind components, generally good agreement is found between the MQ and 4DDA analyses at 200 mb (Figures 3.34-3.36). As expected from Figure 3.20b, these 200 mb profiles are dominated by radial outflow. However, the MQ analysis has slight (< 1 m s⁻¹) inflow within 200 km at 12 UTC 14 September, and within 75 km at 06 UTC 17 September. Notice that the latter period, when DC8 observations were available, again has relatively larger differences between the MQ and 4DDA analyses, presumably due to either the weighting of the DC8 observations, the weighting of the first guess fields, or the imposed geostrophic constraints in the 4DDA analysis.

Whereas the outflow pattern is normally similar to that of the composite typhoon (Figure 3.20b) with the maximum outflow 400-600 km from the storm center (Figures 3.34 and 3.36), the maximum outflow is more than 800 km from Flo at 12 UTC 14 September (Figure 3.35) and 00 UTC 15 September (not shown). This shift in the outflow maximum is present in both the MQ and 4DDA analyses, and appears to be a real feature associated with a 200 mb anticyclone located about 700 km east-southeast of Flo. Although further calculations are required, the working hypothesis is that this unusual radial wind distribution is a precursor to the rapid intensification of Flo that commenced 24 h later.

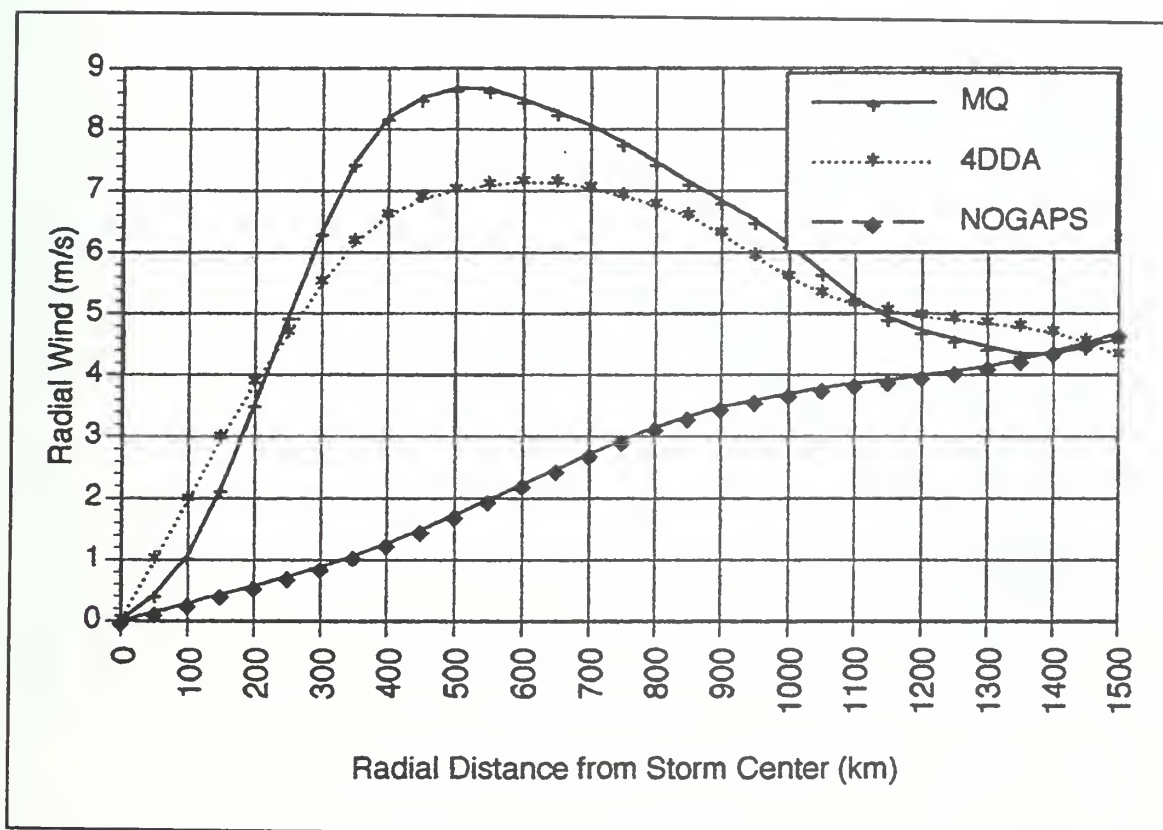


Fig. 3.34. As in Figure 3.31, except for 200 mb at 00 UTC 13 September.

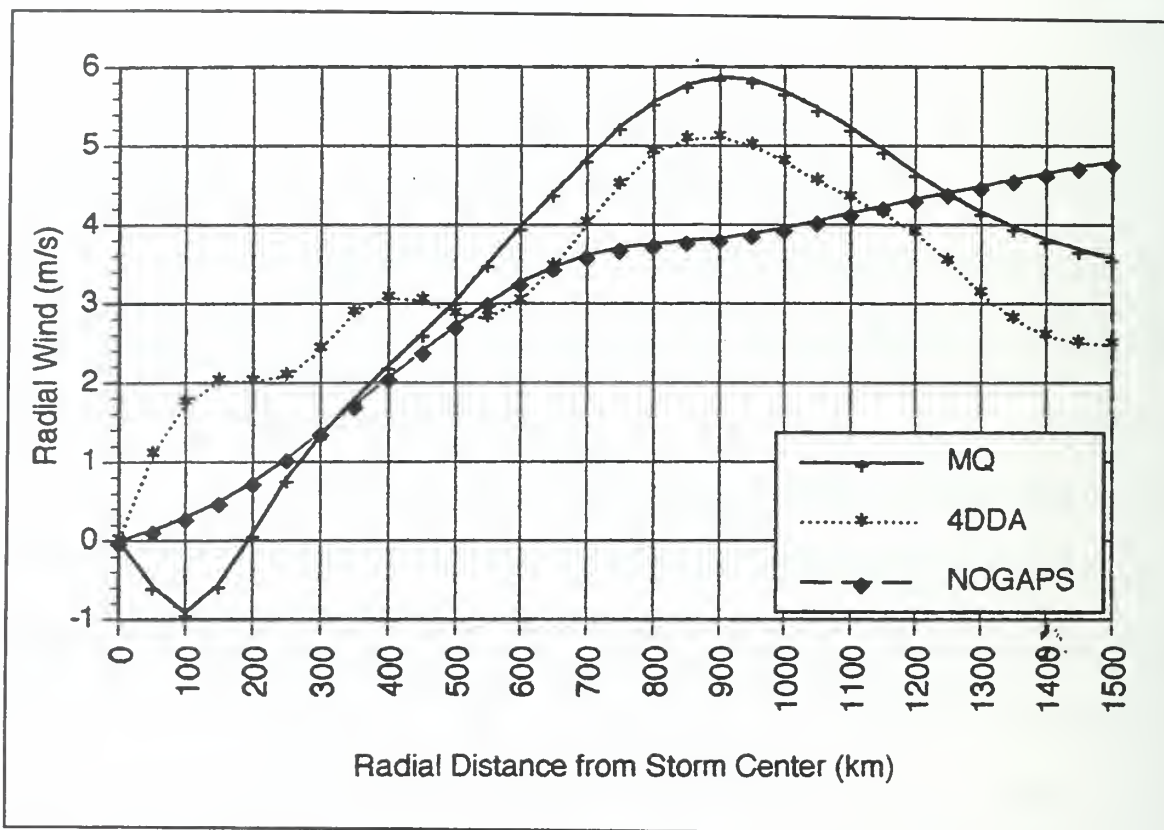


Fig. 3.35. As in Figure 3.31, except for 200 mb at 12 UTC 14 September.

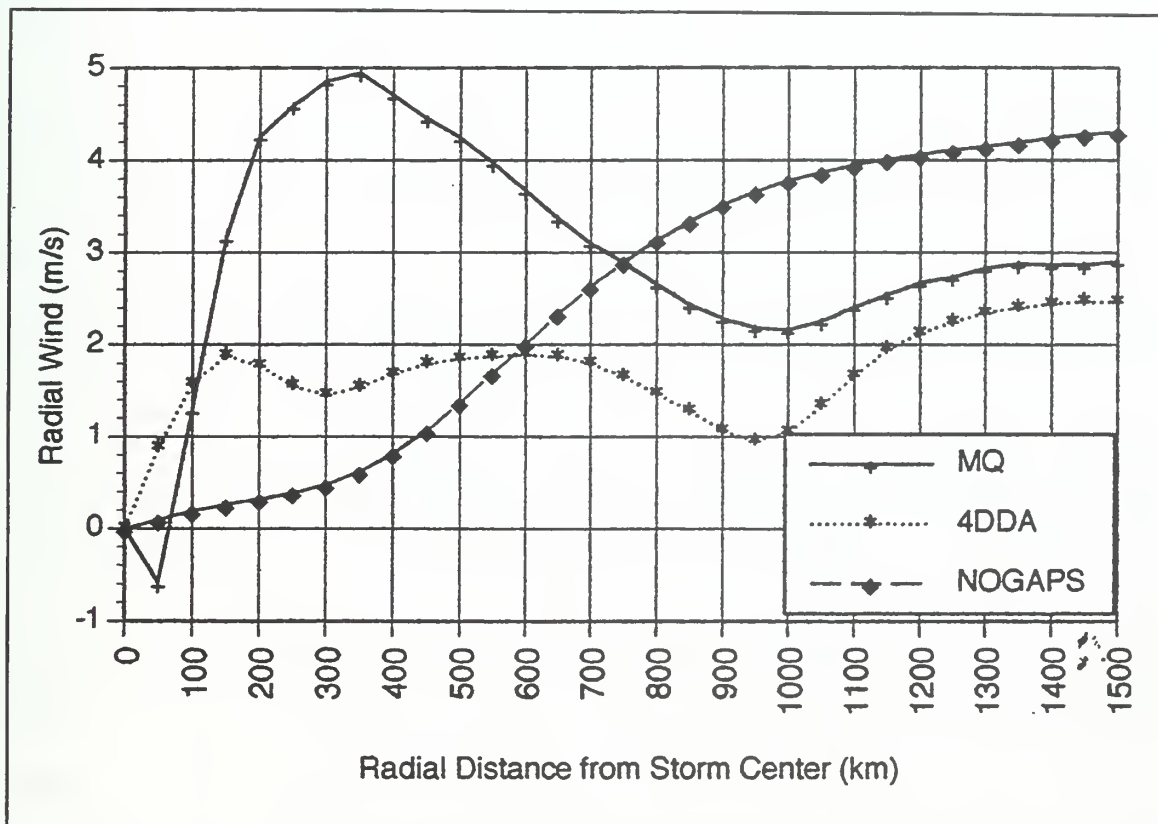


Fig. 3.36. As in Figure 3.31, except for 200 mb at 06 UTC 17 September.

(6) Vertical Cross-Sections of Radial Wind Speed. Although the vertical cross-sections of radial wind speed (Figure 3.37) generally agreed between the MQ and 4DDA analyses, some significant differences occurred. The radial wind cross-sections derived from NOGAPS analyses usually had lower radial wind speed magnitudes and simpler structure than either the MQ or 4DDA analyses. While the MQ analysis (Figure 3.37a) had weak low-level inflow and strong, shallow outflow centered at 200 mb, the 4DDA analysis had more developed inflow, and an outflow structure quite different from the MQ analysis (Figure 3.37b). The 4DDA outflow extended down to 500 mb (versus 300 mb in the MQ analysis), with a secondary outflow maximum at 300 mb about 300 km from the center of the storm. This feature did not appear on the MQ analysis. The better-developed inflow features on the 4DDA analysis probably resulted from the model dynamics "spinning up" the storm and creating inflow, despite a lack of observations. The complex outflow structure is more difficult to explain. Perhaps the model storm had not yet fully "coupled" with the upper troposphere. As described by Holland and Merrill (1984), the circulation driven by the convection near the center of the TC, if not coupled to the upper-troposphere flow, may result in subsidence immediately beyond the TC. The secondary outward radial maximum in Figure 3.37b may be evidence of subsidence just beyond the central convection. The NOGAPS analysis (Figure 3.37c) has the boundary between inflow and outflow located at 400 mb, and the maximum outflow of 3 m s^{-1} about 1500 km from the center of Flo. The near-surface inflow is very weak, becoming a maximum of about 1 m s^{-1} between 350 and 700

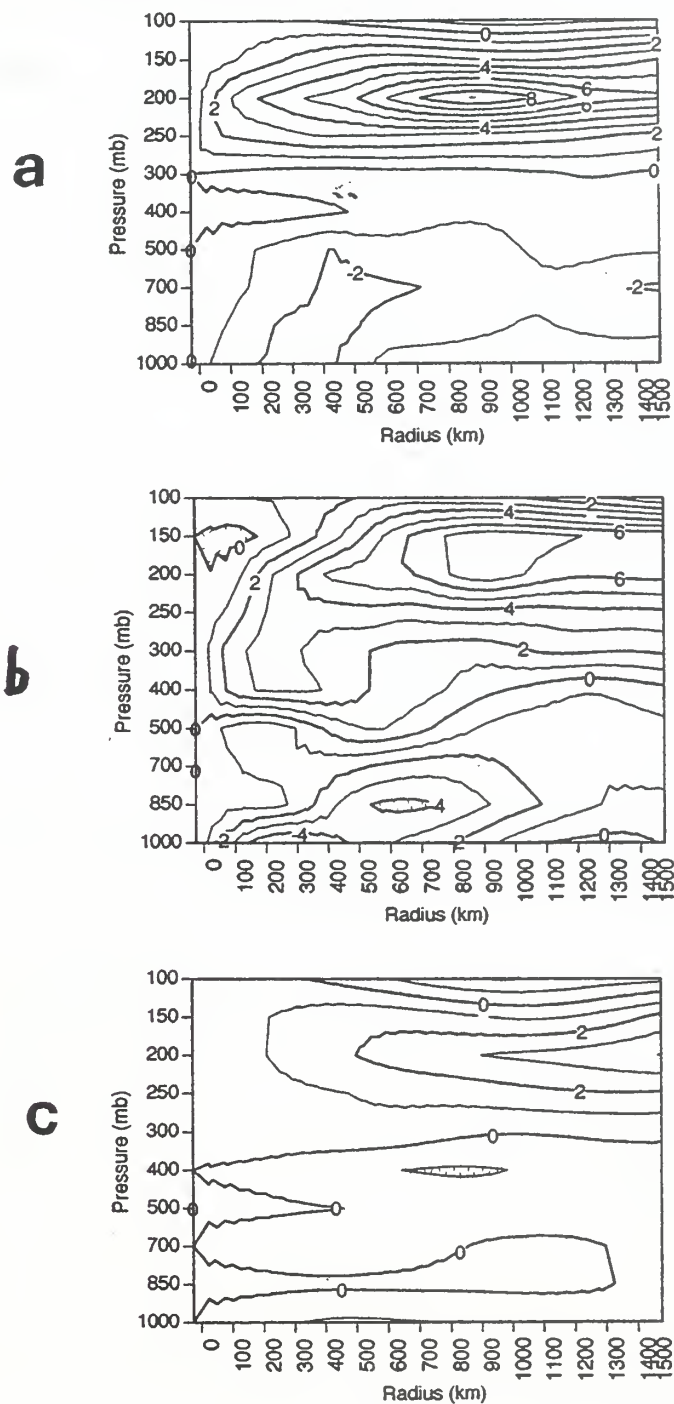


Fig. 3.37. Vertical cross-section of azimuthally-averaged radial wind (m s^{-1} , contour interval 1 m s^{-1}) around Typhoon Flo at 12 UTC 13 September for (a) MQ analysis, (b) 4DDA analysis, and (c) NOGAPS analysis. Positive values are outward winds, negative values are inward winds.

km from the storm center. This weak inflow, contrasted to the 4DDA inflow (Figure 3.37b) implies that the 4DDA has a more developed low-level circulation near Typhoon Flo than does NOGAPS at 12 UTC 13 September.

Differences between the MQ and 4DDA analyses were again evident at 00 UTC 15 September (Figures 3.38a-b). While both the MQ and 4DDA analyses depicted the mid-level inflow and the 4DDA analysis portrayed a more realistic low-level inflow, the MQ analysis showed radial outflow speeds at 200 mb of about 4 m s^{-1} at 1000 km from Typhoon Flo. The 4DDA analysis, by contrast, had a weaker outflow structure with radial outflow speeds generally $2\text{-}3 \text{ m s}^{-1}$, and again depicted a deep outflow layer extending as low as 500 mb. Although this diffuse outflow structure may be correct, Flo attained typhoon strength at 00 UTC 15 September, and would intensify nearly 20 m s^{-1} during the following 24 h. The current intensity and rate of intensification would imply greater organization in the outflow structure than depicted in Figure 3.38b. The 00 UTC 15 September NOGAPS analysis, as previously discussed, appeared not to have been run. The radial winds for the substitute analysis (not shown) were $\pm 0.5 \text{ m s}^{-1}$, implying that the backup analysis used had virtually no outflow structure associated with Flo.

(7) Summary. The low-level, upper-level, and vertical cross-sections of radial and tangential wind profiles provide additional evidence that both the MQ and 4DDA analyses are alternate, plausible, representations of the atmosphere in the vicinity of Typhoon Flo. Whereas the 850 mb profiles suggest that neither the

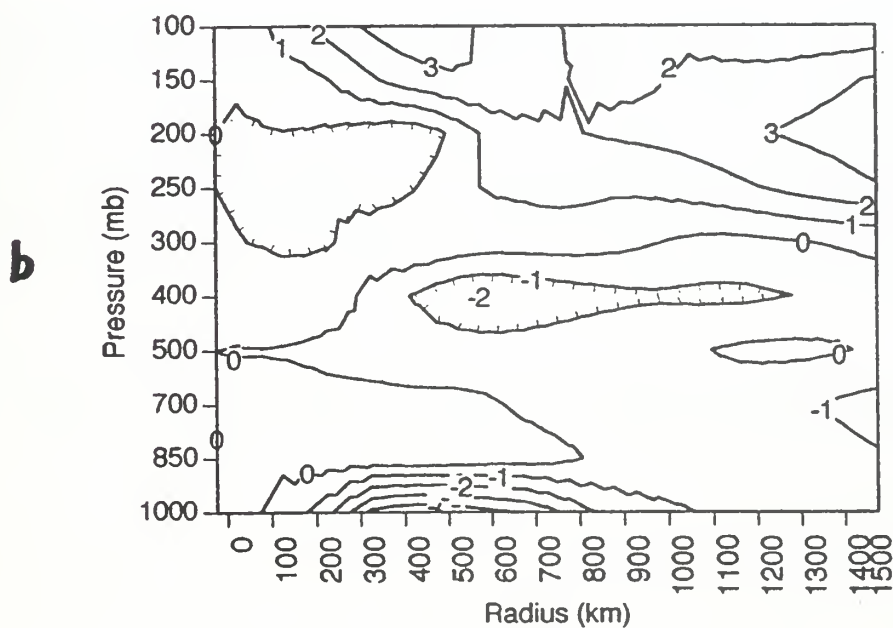
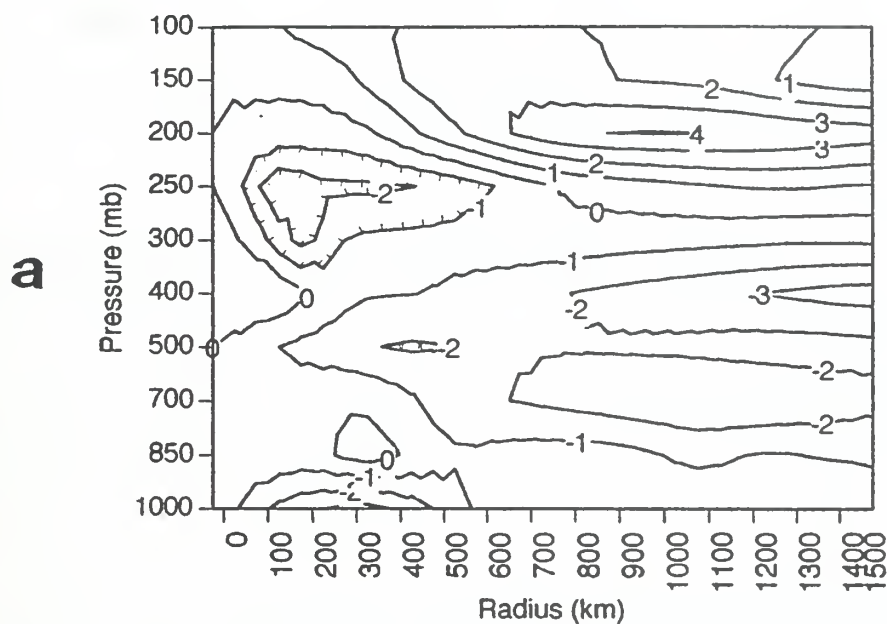


Fig. 3.38. As in Figure 3.37, except at 00 UTC 15 September for (a) MQ analysis and (b) 4DDA analysis.

MQ nor the 4DDA analysis is realistic within 300 km of Flo, both analyses have similar tangential wind profiles beyond 300 km. The radial winds are generally weak, so that the magnitude, or even the sign, is difficult to determine. Any calculations using these low-level radial winds should be viewed with caution.

The 200 mb wind profiles have good agreement between the MQ and 4DDA analyses, and depict the value of the DC8 and CTW observations to the MQ analysis. At times with DC8 observations near the eye of Flo, the MQ analysis may be valid within 100-200 km of Flo. Due to this combination of DC8 and CTW observations, the close agreement between two independent analysis schemes, and the similarity of results with previous studies, high confidence may be placed in the 200 mb wind analyses.

The vertical cross-sections have good agreement between the MQ and 4DDA analyses for the tangential wind profiles, but there is less correlation between the analyses for the radial wind cross-sections. Although both the MQ and 4DDA analyses initially have large values of outward radial flow aloft, followed by a relative minimum at 12 UTC on 14 September (not shown), then increasing outward radial flow between 150 and 200 mb at later times, significant differences are also found between the MQ and 4DDA analyses. The 4DDA analyses generally have a deeper outflow layer, with slightly lower radial wind speeds than in the MQ analyses. The 4DDA radial outflow profiles may have been influenced by the Eta model parameterization of

convection in the vicinity of Typhoon Flo, while the MQ analysis have no such constraint.

Although the wind maximum is normally farther away from the center of the storm and of a lower magnitude, the NOGAPS tangential winds generally have similar profiles as the MQ and 4DDA analyses. The NOGAPS radial winds are normally of small magnitude and are less well correlated with either the MQ or 4DDA radial winds. Moreover, the NOGAPS upper-level analysis at 00 UTC 15 September appears to have a discontinuity in time.

B. ANALYSIS CONCLUSIONS

Most of the weather analysis centers use a 4DDA scheme similar to that of the TCM-90 final analyses (Rogers *et al.* 1992). A key feature of the 4DDA approach is the use of a dynamical model prediction as the first guess field for the analysis, which makes the analysis model-dependent. Although this implementation of a MQ analysis used NOGAPS-derived model data for its background field (*i.e.*, to calculate the increments for analysis), the MQ analysis did not attempt to weight this field in the sense of a first guess.

Based on these preliminary validations, the MQ analysis provides an alternate, plausible depiction of the tropical atmosphere. That is, the MQ analysis compares favorably with the Rucker (1992) analyses, it agrees well with observations as indicated by the small RMS values and has realistic depictions of the azimuthally-averaged wind components. Using the NOGAPS analysis as a first guess and analyzing increments

allows the MQ analysis to retain dynamic information inherent in a competitive global NWP system, and yet extracts information from a high spatial and temporal resolution TCM-90 dataset. Because the MQ analysis lacks the constraints of an OI analysis, it draws more closely to the observations than the 4DDA analysis. If the observations are reliable, this may be an advantage near the tropical cyclone where the dynamical properties may deviate considerably from the type of conditions for which the OI coefficients have been derived.

As implemented here, the MQ scheme is a two-dimensional analysis. Although based upon a three-dimensional NOGAPS first guess, vertical derivatives of analyzed fields may require additional processing to reduce vertical inconsistencies. Based upon the RMS values and the radial and tangential wind profiles around Typhoon Flo, the 200 mb wind MQ analysis, which is based primarily upon reprocessed cloud-track wind and DC-8 observations, appears to be of high quality. The lower- and mid-levels of the MQ analysis are reasonable, as shown by the time consistency of the propagation vector plots. These qualitative and quantitative checks have certainly demonstrated that the MQ analysis adds value to the NOGAPS first-guess fields.

Generating these 50 km analyses covering one-third of the Northern Hemisphere and attempting to resolve features on the scale of a moderate-sized typhoon is far from a trivial task! As the structure of the tropical cyclone is completely different from its environment (*e.g.*, Anthes 1982), the analysis scheme must depict both the large gradients in the tropical cyclone(s) and the smaller gradients of the environment.

Obtaining realistic structure in the vicinity of the TC was possible in this static analysis only after making the decision to analyze the region near the storm in a cylindrical coordinate system, and then blend the azimuthally-averaged winds into the Cartesian coordinate system with increasing distance from the storm.

C. FUTURE ANALYSIS WORK

Although the MQ analysis has produced a realistic depiction of the atmosphere, improvements could be made to the scheme to further enhance the quality of the analysis. Also, several data impact or sensitivity studies could be performed using the TCM-90 dataset.

1. Multi-Quadric Analysis Enhancements

Currently, the most significant drawback to the MQ analysis is its two-dimensional character. In theory, the quadric surface analysis approach could be extended to three, or even four, dimensions. If this were done, the MQ analysis may be competitive with OI schemes in the vertical, as well as in the horizontal. A three-dimensional analysis could use significant-level data, in addition to the mandatory-level data currently being used. That is, any observations between mandatory pressure surfaces (*e.g.*, DC8, AIREP observations) would not have to be adjusted to a mandatory pressure. If the scheme were run in four dimensions, no data cut-off times or time-space adjustments for observations would have to be imposed. The major challenge to extending this scheme to higher dimensions is keeping the matrix of increments (which must be inverted) well-conditioned. Rather than inverting the entire domain's matrix,

as is now done, a system of overlapping volumes similar to the NOGAPS analysis scheme (Barker 1992) might be utilized.

Another significant improvement would be to increase the sophistication of the dynamic constraints used in the MQ analysis scheme. For example, the wind and height analyses could be simultaneously constrained using geostrophic adjustment theory (Haltiner and Williams 1980).

Finally, the manual QC system should be automated. Large-increment observations should be automatically flagged and rejected unless they are near a typhoon or other region with large gradients. The analyses derived from the manual and automated QC systems could be compared to see if the marginally better dataset resulting from manual QC is worth the time invested, even in a research mode.

2. Data Impact and Sensitivity Studies

It has been demonstrated that the MQ analyses have added value to the operationally-derived NOGAPS first guess. This additional value is primarily from the TCM-90 delayed data (*i.e.*, the CTW, LDW, and DC8 observations). If the analyses are valid only at a radius of greater than 300 km from the typhoon center, what would be the impact of removing the DC8 and LDW observations? How will this affect the analyses, especially the 200 mb analyses? That is, are aircraft observations required to obtain the atmospheric structure that determines the rate of typhoon intensification? Obviously, low-level aircraft observations are still desired to determine the actual intensity of a typhoon.

If the CTW observations provide sufficient additional information to analyze the features that determine future typhoon intensity change, how many CTW observations are required? Nuss and Titley (1994) show that one advantage of the MQ analysis is the ability to extract the signal from relatively sparse data. Thus, an MQ analysis may not require all of the CTW observations that were carefully extracted manually after the experiment. If the number of manually-processed CTW observations can be decreased by a factor of two or three, is it realistic for a typhoon or hurricane warning center to locally process a sufficient number of cloud-tracked wind observations around the storm to aid in an objective tropical cyclone intensity forecast? A data impact study with the MQ analysis scheme may be able to answer these questions.

IV. DISCUSSION OF DYNAMICS OF TYPHOONS ED AND FLO

A. STRENGTHS AND LIMITATIONS OF THE ANALYSES

The objective of TCM-90 was to collect a data set to enhance the diagnosis and understanding of tropical cyclone motion. The TCM-90 upper-tropospheric wind data are considered to be the best ever collected for western North Pacific tropical cyclones. Additionally, the high-density, reprocessed GMS cloud-track winds, confirmed by *in situ* open-ocean rawinsonde and NASA DC-8 aircraft observations, provide significant potential to document the interactions between the tropical cyclone outflow and the surrounding environment. These post-experiment satellite cloud-drift winds, which were processed every six hours and at high spatial resolution, provide the key data for spatially and temporally consistent analyses.

As previously described, these data were analyzed by two independent methods: the Multi-Quadric analysis and a four-dimensional data assimilation (4DDA) based upon the NCEP Eta mesoscale model. We have shown that both assimilation schemes provide similar magnitudes for azimuthally-averaged tangential and radial winds, and the environmental steering flow calculations. By using the Multi-quadric analysis as an independent check on the 4DDA, we have confidence in the vertical and temporal depiction by the 4DDA of wind and height fields beyond 200-300 km of Typhoons Ed and Flo.

Another benefit of these particular analyses was the ability to examine simultaneously Typhoons Ed and Flo. While these storms both formed within a few days in the western North Pacific Ocean over nearly identical sea-surface temperatures, their maximum intensities, and their respective rates of intensification were quite different.

While this data set and analysis scheme are believed to be the best-ever description of the interactions between a typhoon outflow layer and its environment, this analysis has several limitations. This analysis lacks high temporal and spatial resolution measurements of the inner-core temperature and winds (except for three NASA DC-8 flights at 195 mb through Typhoon Flo). Few mid-tropospheric wind measurements (apart from the TCM-90 additional rawinsondes) are available, since the geostationary satellite water-vapor imagery (Velden *et al.* 1997) was not available in the western North Pacific during 1990. This lack of high resolution inner-core data prevents the analysis of internal mechanisms that may contribute to rapid intensification.

As in all case studies, caution should be used in generalizing results from these particular cases. It is possible that Typhoon Flo's rapid intensification was atypical, due to the location of the TUTT cell to the east-northeast, or that there may be no "typical" pattern to tropical rapid cyclone intensification.

B. EFFECT OF THERMAL INFLUENCES ON TYPHOONS ED AND FLO

1. Sea-Surface Temperature

As has been demonstrated for decades (e.g., Palmén 1948; Miller 1958), sea-surface temperature (SST) above 26°C is a necessary factor in the formation of tropical

cyclones. Emanuel (1988) and DeMaria and Kaplan (1994) have provided theoretical and empirical relationships, respectively, between the maximum potential intensity of a tropical cyclone and the underlying SST. While DeMaria and Kaplan's relationship between maximum potential intensity (MPI) and SST was derived from Atlantic tropical cyclone data, Evans (1993) shows a similar relationship for western North Pacific tropical cyclones.

The North Pacific SST analysis at 18 UTC 16 September (Figure 4.1) has values of 28.0°C to 28.5°C along both typhoon tracks. These SST values are within 0.5 °C of climatological values (Levitus 1982). Using DeMaria and Kaplan's (1994) MPI relationship, this SST would support a maximum intensity of about 70 m s⁻¹. This value is consistent with Evans' (1993) findings.

As discussed in Chapter I, Typhoon Ed reached a maximum intensity of 46 m s⁻¹, while Flo achieved a maximum intensity of 74 m s⁻¹. While Flo reached its MPI (or at least came very close to that intensity), Ed only achieved about 65% of its MPI. This conclusion, which is consistent with previous studies, is that while sufficiently high SSTs are a necessary large-scale environmental condition for intense tropical cyclones, high SSTs are not sufficient to guarantee either rapid intensification of a tropical cyclone, or even that the storm will eventually reach its MPI.

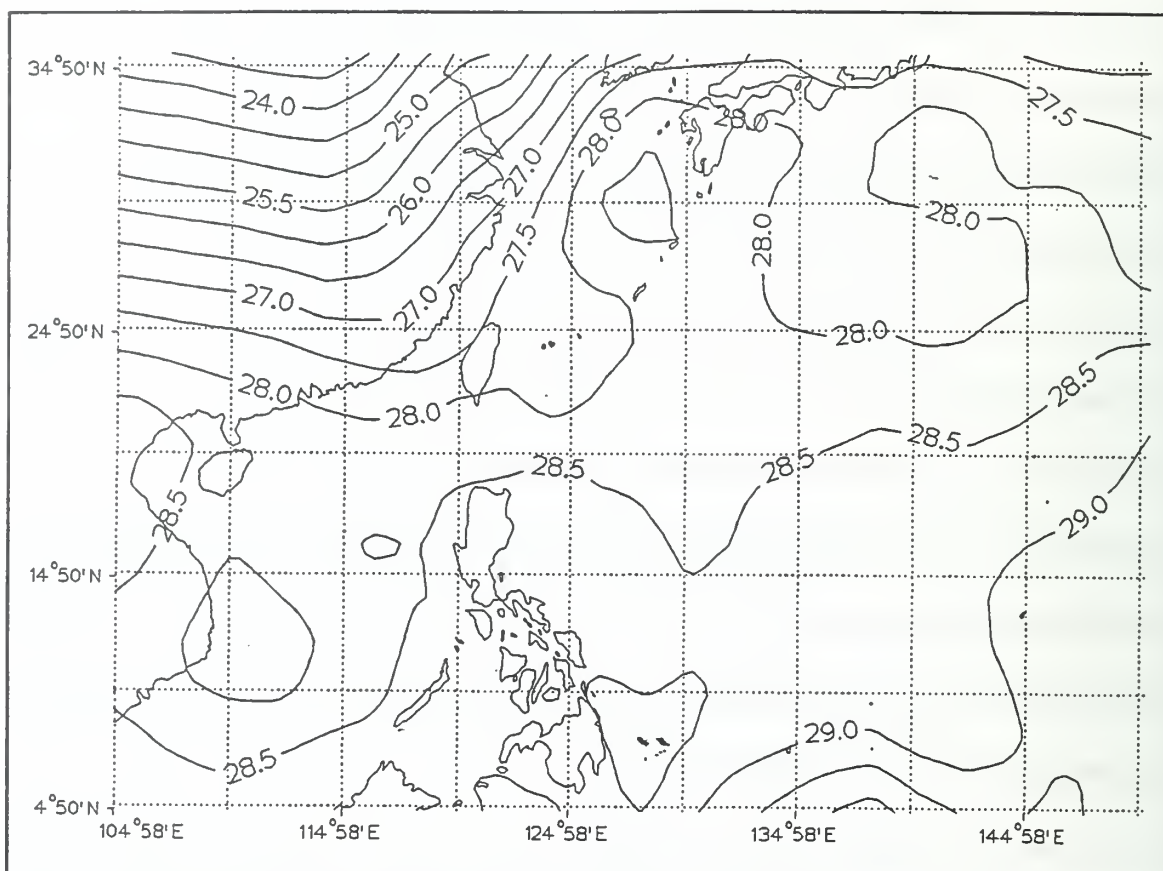


Fig. 4.1. 4DDA analysis of sea-surface temperatures (SST) ($^{\circ}\text{C}$, contour interval 0.5°C) at 18 UTC 16 September. Disregard SST values plotted over land.

2. Thermal Structure of Ed and Flo

As discussed above, detailed temperature measurements of the typhoons' inner-core thermal structure were not available for this dataset. However, a review of the temperature analyses from the 4DDA was enlightening.

a. Background

Using upper-tropospheric temperature data collected from Atlantic hurricane aircraft reconnaissance flights, Gray (1992) proposed that intense tropical

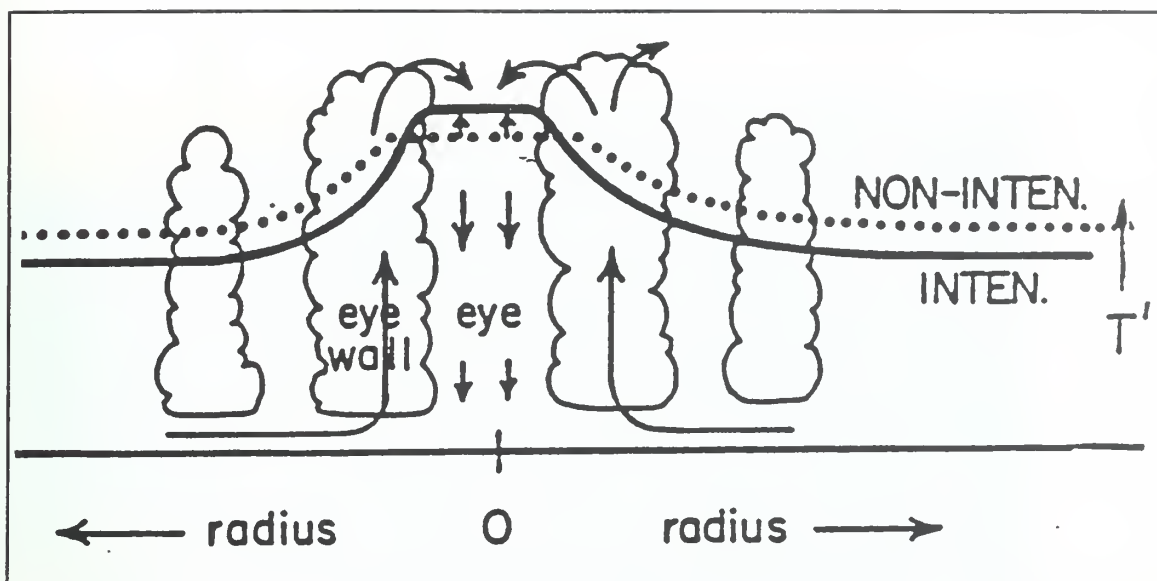


Fig. 4.2. Cross section schematic of upper-troposphere temperatures of intensifying (INTEN.) and non-intensifying (NON-INTEN.) tropical cyclones (from Gray 1992, Figure 8).

cyclones have a greater increase in their upper-tropospheric temperatures than do weaker storms. Gray hypothesized that much of the warming in intense tropical cyclones must occur near the tropopause in the inner eyewall cloud, which satisfies the simultaneous requirements to warm over the entire column and support the low surface pressure (Figure 4.2). In addition, a ring of sufficiently cool upper-troposphere air surrounding the eyewall is desirable to allow for convective instability that will maintain the in-up-out transverse circulation.

b. Analysis Method

The 4DDA temperatures were azimuthally averaged in a storm-centered coordinate system for each 6 h analysis and for both typhoons. The average temperatures were calculated at each analyzed pressure level from the center of each

| Flo | | Ed | |
|--------|-----------|--------|-----------|
| Time | Intensity | Time | Intensity |
| 14/00Z | 45 | 13/00Z | 45 |
| 14/12Z | 55 | 13/18Z | 55 |
| 15/00Z | 65 | 14/00Z | 65 |
| 15/06Z | 70 | 14/12Z | 70 |
| 15/12Z | 75 | 16/00Z | 75 |
| 15/18Z | 85 | 17/00Z | 85 |

Table 4.1. LIST OF TIMES USED AND ASSOCIATED STORM INTENSITY (KT) FOR EACH COMPONENT OF TEMPERATURE DIFFERENCE COMPOSITE BETWEEN TYPHOON FLO AND TYPHOON ED (FIGURE 4.3).

storm to 1500 km radius in 50 km bins. This is the same azimuthal averaging procedure as used for the tangential and radial winds, described in the previous chapter.

Differences in the thermal structure (as analyzed by the 4DDA) for Ed and Flo were calculated for times at which the storms were of similar intensities (Table 4.1). The azimuthally-averaged temperatures of Flo were subtracted from the azimuthally-averaged temperatures of Ed for six times. For five of these times, the storms were at identical intensity (within the limitations of the best-track intensity estimates), and the storms differed by only 2.5 m s^{-1} (42.5 m s^{-1} intensity for Flo versus 45 m s^{-1} intensity for Ed) at one time. The times at which the storms reached these intensities were within 24 h, with an average time difference of 16 h. Typhoon Flo was intensifying at a rate of $2.5 \text{ m s}^{-1} / 6 \text{ h}$ during this time, while Typhoon Ed was either slowly intensifying or

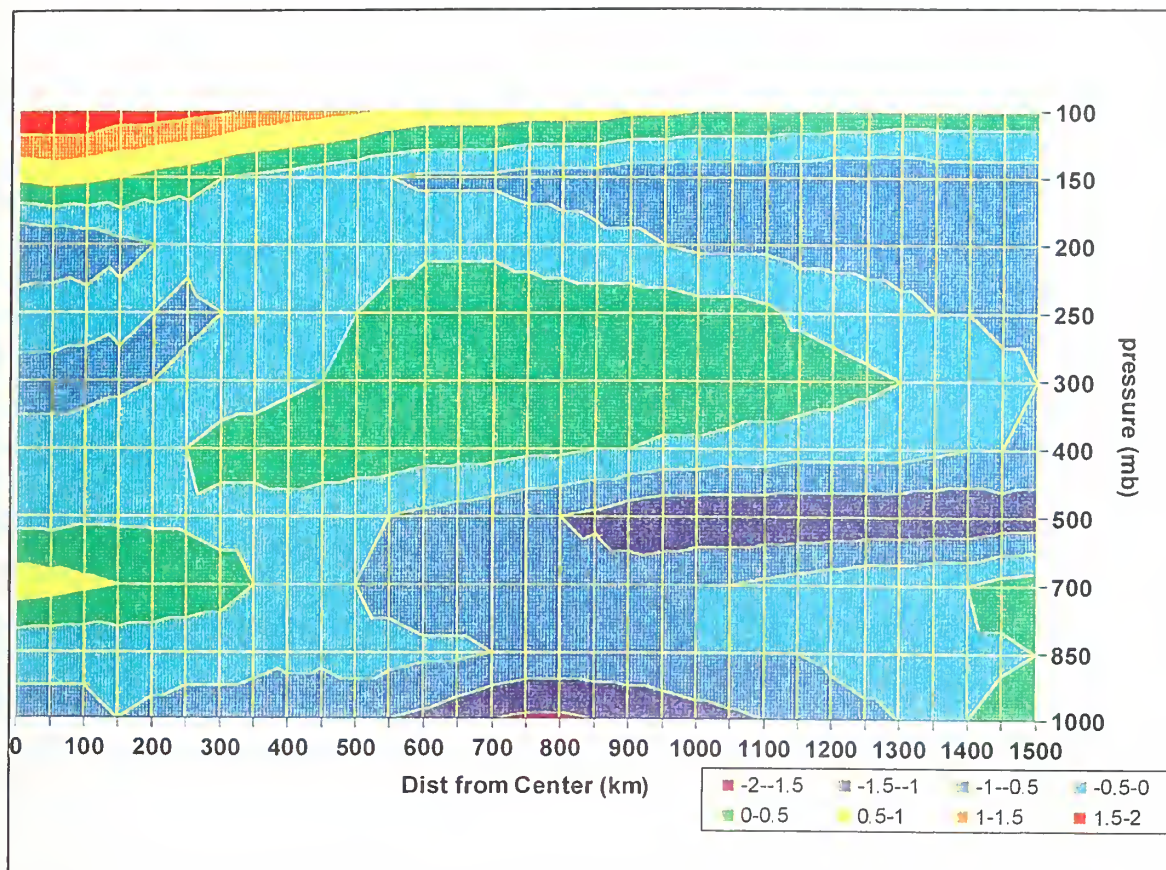


Fig. 4.3. Azimuthally- and time-averaged temperature (°C) difference between Typhoons Flo and Ed versus radius (km). The following times were used in the composite: 00 and 12 UTC 14 September; 00, 06, 12, and 18 UTC 15 September. Positive (negative) values (see inset for colors) indicate regions where the azimuthally averaged temperature of Flo is higher (lower) than the averaged temperature of Ed.

maintaining constant intensity. It is important to note that the times examined were all *prior* to Flo's rapid intensification (Figure 1.1).

c. Results

Rather than examining differences in the temperature structure for the individual times in Table 4.1, the differences from the six times are composited (Figure 4.3). Notice that the azimuthally-averaged temperatures for Flo within 200 km of the

storm center are about 1°C higher than Ed at 700 mb, and about 1°C lower than Ed between 300 and 200 mb. Thus, the inner core of Flo is less stable than that of Ed, which implies the thermal structure of Flo is more conducive to support the sustained convection that produces the in-up-out transverse circulation. While the near-core middle troposphere of Flo appears to be less stable, the upper troposphere (150 - 100 mb) above Flo is 1-2°C higher than Ed. These composited analyses are consistent with Gray's (1992) hypothesis of strong, intensifying storms having greater convective instability in their tropospheric core, and compensating warmer values above the typhoon core. It is emphasized that these temperature differences occurred while Ed and Flo were of the same or very similar intensities, and **prior to** Flo's rapid deepening.

If the tropical cyclones form over similar SST values, but have different thermal structures early in their evolution, then it is reasonable to search for external, dynamic influences that may have caused the differences. The next section will examine the evolution and effects of the outflow layer, tropospheric eddy flux convergence, and vertical wind shear on Typhoons Ed and Flo.

C. TIME EVOLUTION OF UPPER-TROPOSPHERIC WINDS IN TYPHOONS ED AND FLO

1. Motivation

The original hypothesis of this study stated that careful analysis of the high spatial and temporal resolution upper-tropospheric observations available in the TCM-90 dataset for Typhoons Ed and Flo would reveal a high correlation between EFC and future typhoon intensity. The following sections describe the results of this analysis for

Typhoons Ed and Flo. Typhoon Flo, which intensified experienced an 18-h period of rapid intensification between 18 UTC 15 September and 12 UTC 16 September, will be described first and in the greatest detail. Typhoon Ed will be subsequently discussed as a "control case" in that it underwent a typical lifecycle for a western Pacific storm, but only reached a maximum intensity of 45 m s^{-1} , with no rapid intensification.

2. Analysis Method

The upper-tropospheric winds have been examined in depth. In addition to reviewing the objective MQ and 4DDA analyses in geographic coordinates, azimuthally-averaged tangential (\bar{v}_L) and radial (\bar{u}_L) winds were calculated in a coordinate system moving with the storm. The azimuthally-averaged fields are examined as a radius-time plot for each pressure level, as a pressure-radius plot in time, and as a distance-weighted average.

a. Tangential and Radial Wind Calculations

Tangential and radial winds are calculated from the center of the storm outward to 1500 km in 50 km increments at 7.5° azimuthal angles using the following methodology:

1. Determine the location of the storm and from the best track. Convert this geographic position into the (i,j) Cartesian grid position in the analysis;
2. Determine storm motion from best track positions ± 6 -h of the analyzed time;
3. Subtract the north-south component of the storm motion from the north-south (v) wind. Likewise, subtract the east-west component of the storm motion from the east-west (u) wind. The resulting winds (v_L, u_L) are cartesian winds "moving with" the storm.

4. Set up a "key" that records the (i,j) position for each (r,s) point on the cylindrical grid;
5. Using bi-cubic splines, interpolate the value of the east-west (u_L) and north-south (v_L) component of the wind to each r,s point on the cylindrical grid;
6. Calculate the tangential and radial winds as follows:

$$v_{\theta L} = -u_L \sin(\theta) + v_L \cos(\theta), \quad (4.1)$$

$$v_{rL} = u_L \cos(\theta) + v_L \sin(\theta), \quad (4.2)$$

where v_L is the tangential wind (> 0 is cyclonic), u_L is the radial wind, and θ is the angle of the radial wind relative to true north, incremented every 7.5° .

7. Using Eq. (1.4), calculate the azimuthally-averaged tangential and radial winds as follows:

$$\bar{v}_L = \frac{1}{2\pi} \int_0^{2\pi} v_{\theta L} d\lambda, \quad (4.3)$$

$$\bar{u}_L = \frac{1}{2\pi} \int_0^{2\pi} v_{rL} d\lambda, \quad (4.4)$$

where \bar{v}_L is the azimuthally-averaged tangential wind, and \bar{u}_L is the azimuthally-averaged radial wind.

b. Vertical Wind Shear Calculations

Mean 850, 500, 300, 200, and 150 mb \bar{u} and \bar{v} winds are calculated within 800 km of the storm center using the method described in the previous section. Although vertical wind shear is traditionally calculated between 850 mb and 200 mb (Elsberry and Jeffries 1996), the vertical resolution of the mid-tropospheric winds in the 4DDA analysis allowed vertical wind shear to be calculated over five selected layers: 850-500 mb, 850-300 mb, 850-200 mb, 300-200 mb, and 300-150 mb. These calculations provide a check on middle- and upper-tropospheric vertical wind shear, as well as vertical wind shear throughout the troposphere.

The vertical wind shear values are calculated for four pairs of distance-weighted radii (0-600 km, 0-800 km, 200-600 km and 200-800 km), and the results obtained are similar for all radii. It was therefore decided to examine the calculations for the vertical wind shear averaged from 200-600 km in detail. This domain excludes the inner-core region where observations are sparse, but includes much of the storm's significant circulation.

3. Typhoon Flo

Flo's evolution can be described in four phases:

- The "forcing phase" from the beginning of the Intensive Observation Period (IOP) at 00 UTC 13 September to 12 UTC 14 September. During this time, Flo intensified at a steady rate of $5 \text{ m s}^{-1}/12 \text{ h}$. Flo experienced strong, sustained EFC and a cyclonic tangential wind "burst" at 200 mb that will be discussed;

- The "quiescent phase" from 12 UTC 14 September to 12 UTC 16 September. During this phase, Flo intensified at $5 \text{ m s}^{-1}/12 \text{ h}$, until 18 UTC 15 September, then rapidly intensified at $15 \text{ m s}^{-1}/12 \text{ h}$ through 12 UTC 16 September. During this phase, the EFC became small, vertical shear decreased, and the upper-tropospheric cyclonic winds contracted;
- The "super typhoon phase" from 12 UTC 16 September to 18 UTC 17 September. While Flo was a super typhoon, the magnitudes of the vertical shear and EFC were very small; and finally,
- Interaction with the mid-latitude trough from 18 UTC 17 September to the end of the IOP at 00 UTC 19 September. During this period, Flo's intensity decreased from 67 m s^{-1} to about 47 m s^{-1} . The EFC dramatically increased to the strongest magnitude of the lifecycle, but were no longer concentrated exclusively in the upper troposphere, or outflow layer. Also, vertical shear increased to values experienced by the storm in the initial, forcing phase.

The relationships among these four phases and the intensity and rate of intensification of Flo are shown in Figure 4.4.

a. Forcing Phase (00 UTC 13 September to 12 UTC 14 September)

Although Flo's intensity is only 12 m s^{-1} at the commencement of the IOP on 00 UTC 13 September, the upper-tropospheric dynamics are already very active. Strong, sustained diffluence is found over the storm center during this period (e.g., Figure 4.5), with outflow apparent to the east, south, and west. One prominent outflow channel is established to the northeast of Flo. Although some of the outflow in this channel converges into a small upper low about 600 km north of Flo, most of the outflow continues to a larger-developing TUTT cell about 1500 km northeast of Flo. This TUTT is well established by 12 UTC 13 September, and appears to contribute to a sustained outflow channel for most of Flo's existence. Animation of the total wind analyses in a

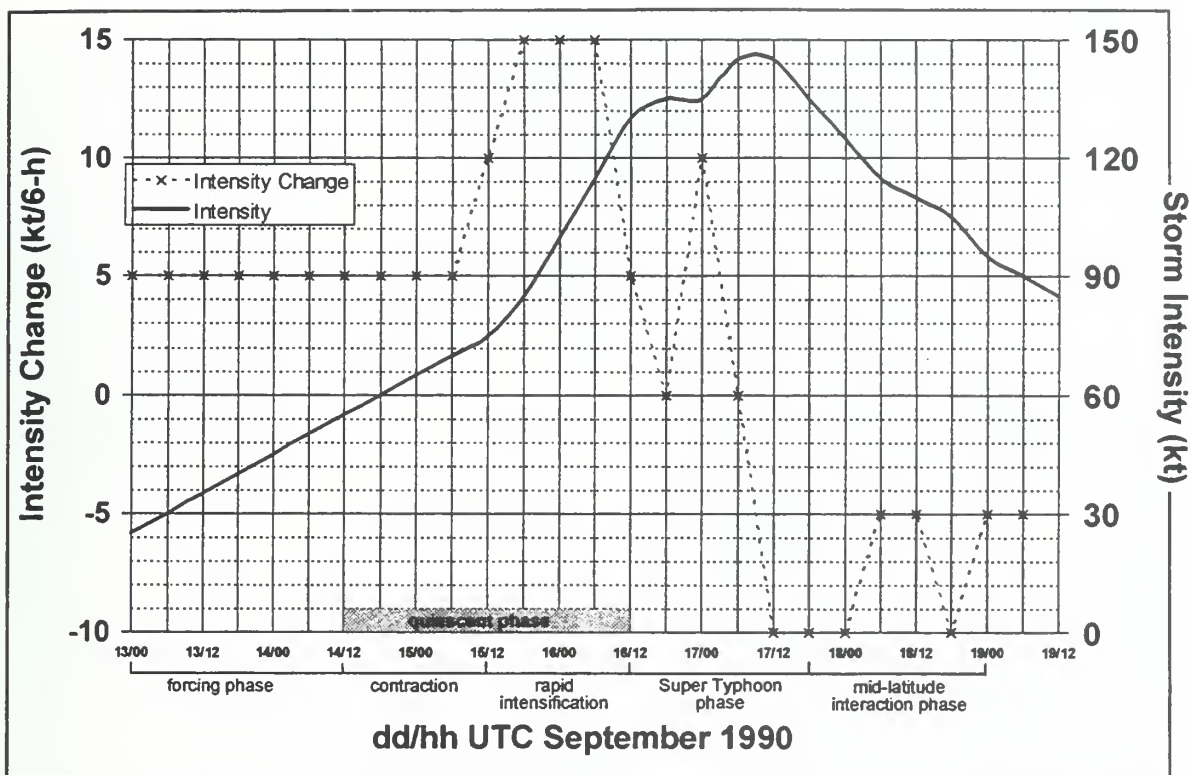


Fig. 4.4 Intensity (kt) (heavy solid line plotted on the right vertical axis) and rate of 6-h intensity change (kt) (dashed line) for Super Typhoon Flo. Annotations indicate the named phase of Flo.

fixed geographic coordinate system using VIS-5D (described in Chapter III) shows a "fountain" of outflow over Flo through 00 UTC 14 September. By 06 UTC 14 September, most of the outflow from Flo is channeled to the north, then curves to the east and southeast around the TUTT, which is still 1000 km to the east-northeast of Flo. A secondary outflow channel flows to the northwest, then cyclonically curves to the southwest and merges with Typhoon Ed's outflow over the central Philippines.

The subsequent sections describe the storm tangential and radial winds, eddy flux convergence of relative angular momentum, and vertical wind shear

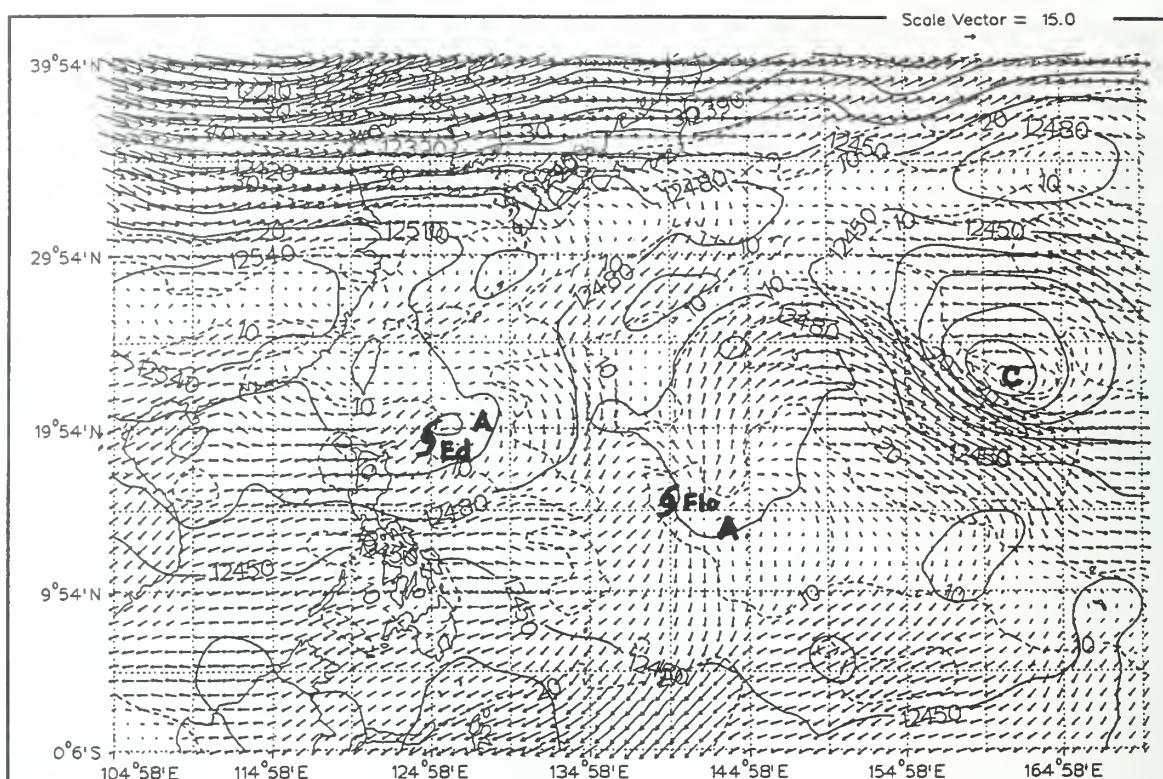


Fig. 4.5 4DDA analysis of 200 mb wind (m s^{-1} , scale vector in upper right), isotachs (dashed, contour interval 10 m s^{-1}) and heights (solid, contour interval 30 m) at 00 UTC 14 September. Surface best-track location of Flo indicated by tropical cyclone symbol. TUTT location (discussed in text) indicated by "C" symbol.

characteristics. The impacts of these characteristics on Flo's intensification are then discussed and summarized.

(1) Tangential Wind. The 200 mb \bar{v}_L in the radius-time plot (Figures 4.6a-c) has a "cyclonic wind burst" during this forcing phase. That is, the tangential, azimuthally-averaged, storm-relative winds are weakly anticyclonic (as expected) at 00 UTC 13 September, then rapidly become cyclonic out to 1200 km from the storm center by 06 UTC 14 September. This phenomenon has not been previously described, perhaps because of the normal paucity of observations in the storm outflow

200 mb Tangential Wind--FLO ET

a

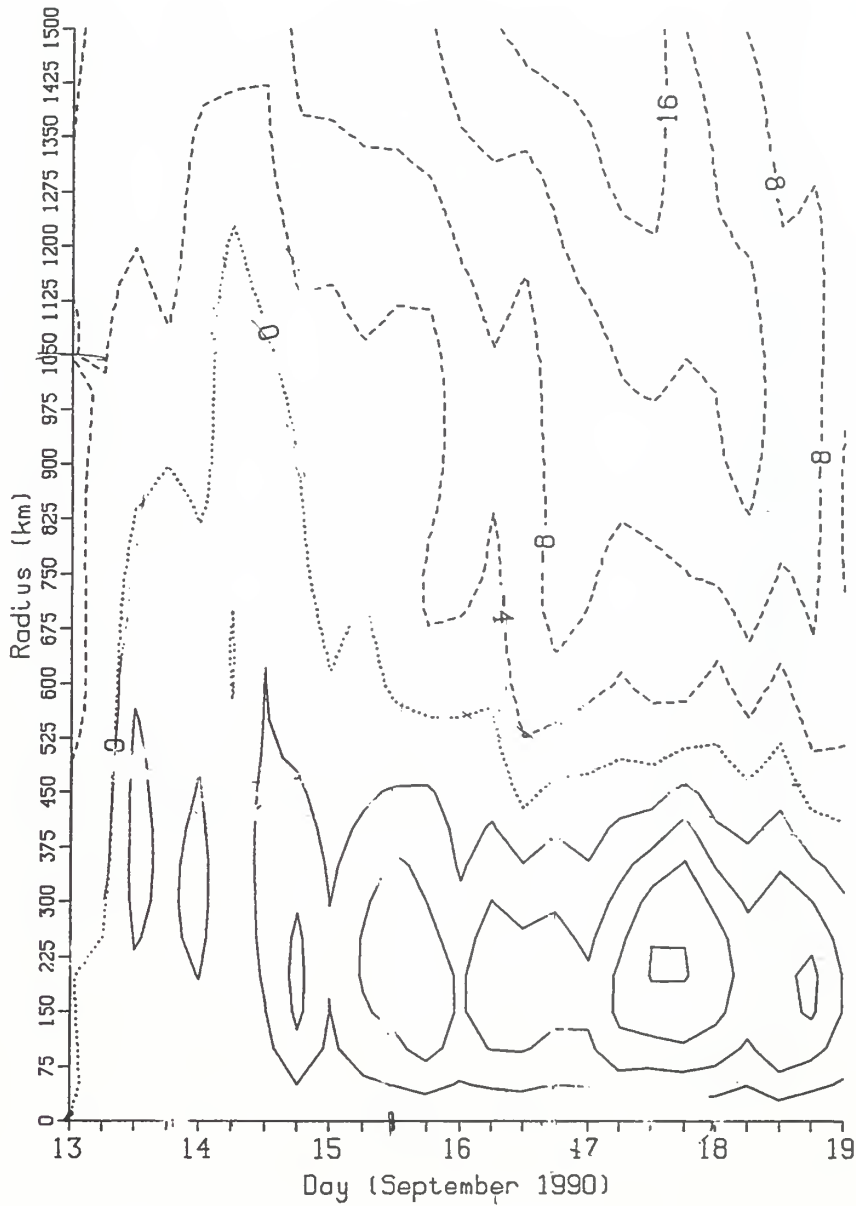


Fig. 4.6. Radial distance versus time plot of \bar{v}_L (m s^{-1} , contour interval 4 m s^{-1} , dashed contours $< 0 \text{ m s}^{-1}$, dotted contour is 0 m s^{-1}) at 200 mb, as calculated by (a) 4DDA analysis, (b) MQ analysis, and (c) NOGAPS analysis.

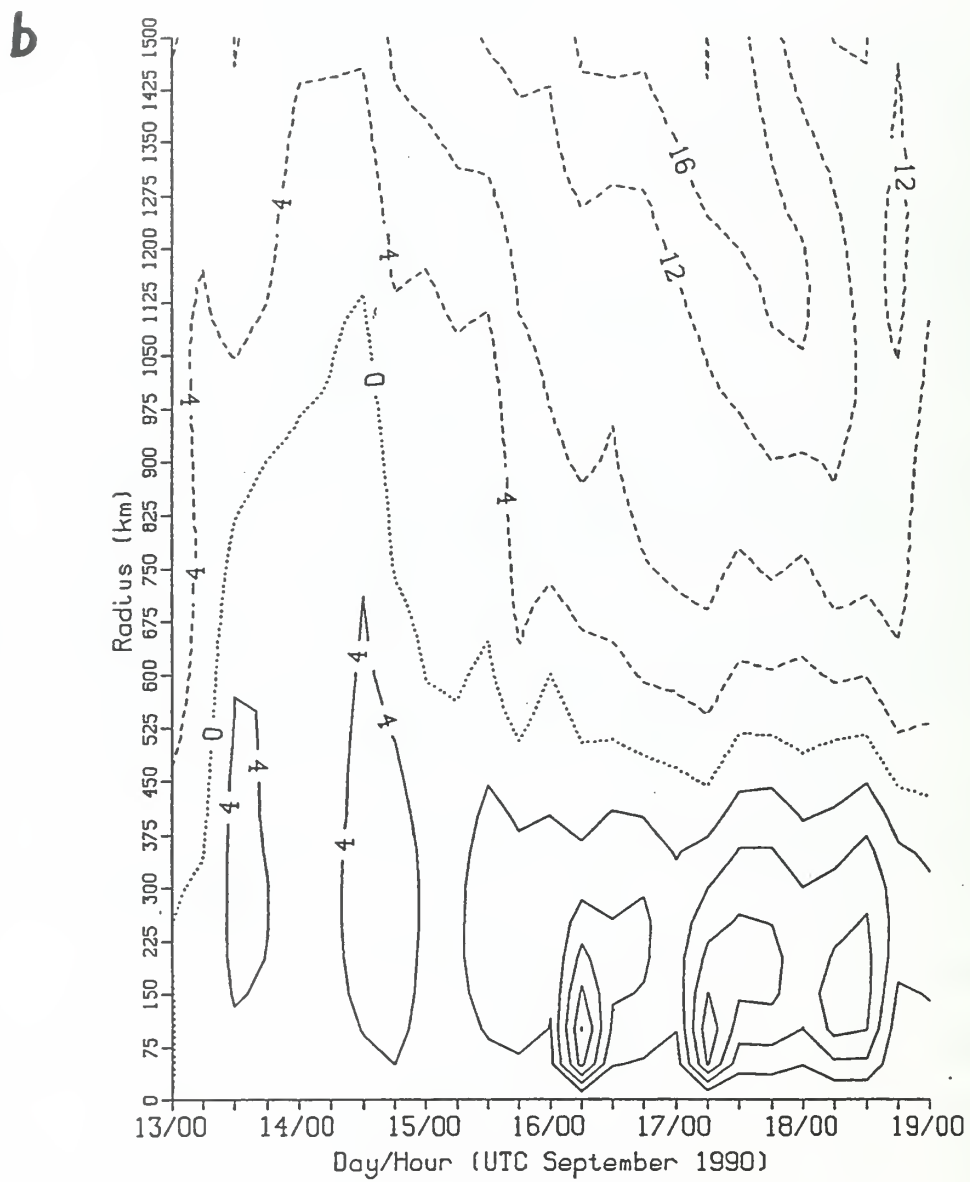


Fig. 4.6. Continued.

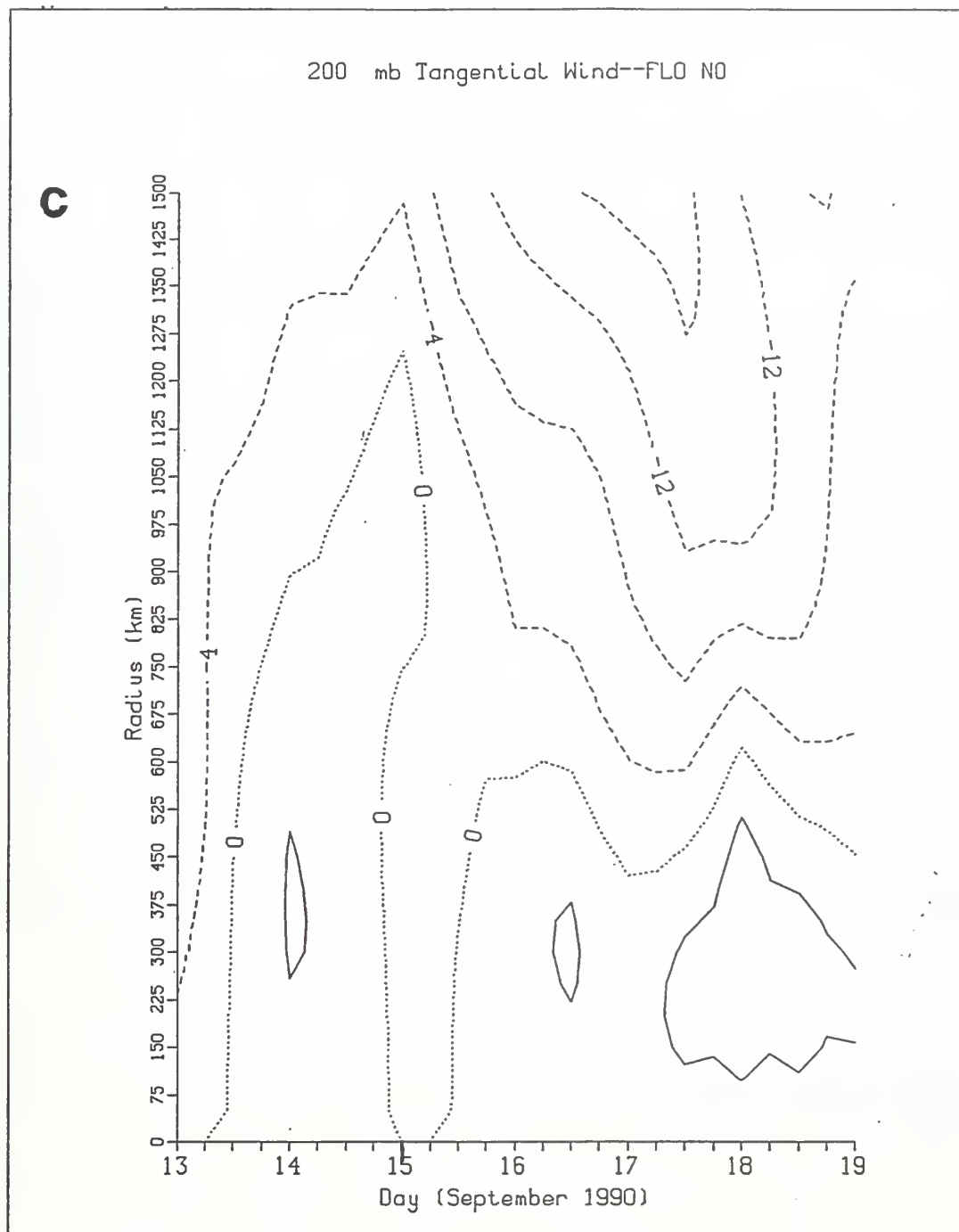


Fig. 4.6. Continued.

layer, and is very different from the accepted composite of \bar{v}_L (Figure 3.20a). This signal is very clear in the 4DDA and MQ analyses, but is only weakly shown in the operational NOGAPS analysis, which again demonstrates the value of high spatial resolution wind observations that depict the typhoon's outflow layer.

The "wind burst" feature is also observed in pressure-radius plots of \bar{v}_L . At 00 UTC 13 September (Figure 4.7a and b), the cyclonic circulation is restricted to below 250 mb in both the 4DDA and MQ analyses. By 12 UTC 13 September, when the intensity was only 17 m s^{-1} , the cyclonic circulation has penetrated to 150 mb (Figure 4.8a and b). This upper-tropospheric cyclonic circulation extends out to 600 km from the center. By 06 UTC 14 September, the cyclonic \bar{v}_L has expanded outward to a radius of 1200 km from the center. This was the maximum outward extent of the "cyclonic wind burst". At 12 UTC 14 September (Figure 4.9a and b), the cyclonic \bar{v}_L contracted to 1000 km radius from the storm center, and would further contract into a radius of 600 km in the following 24 h. A proposed mechanism that explains the occurrence of this feature will be explained in subsection (5) below.

(2) Radial Wind. The radius-time 4DDA analysis of 200 mb \bar{u}_L (Figure 4.10a) has strong ($6\text{--}8 \text{ m s}^{-1}$) outflow through 00 UTC 14 September beyond 300 km of Flo's center. After 00 UTC 14 September, the outflow remains strong, but decreases to $4\text{--}6 \text{ m s}^{-1}$. The Multi-quadric analysis (Figure 4.10b) has a similar pattern, with outflow in excess of 10 m s^{-1} between 600 and 850 km at 06 UTC 13 September. Such outflows are consistent with the "fountain" of outflow mentioned in subsection 3a

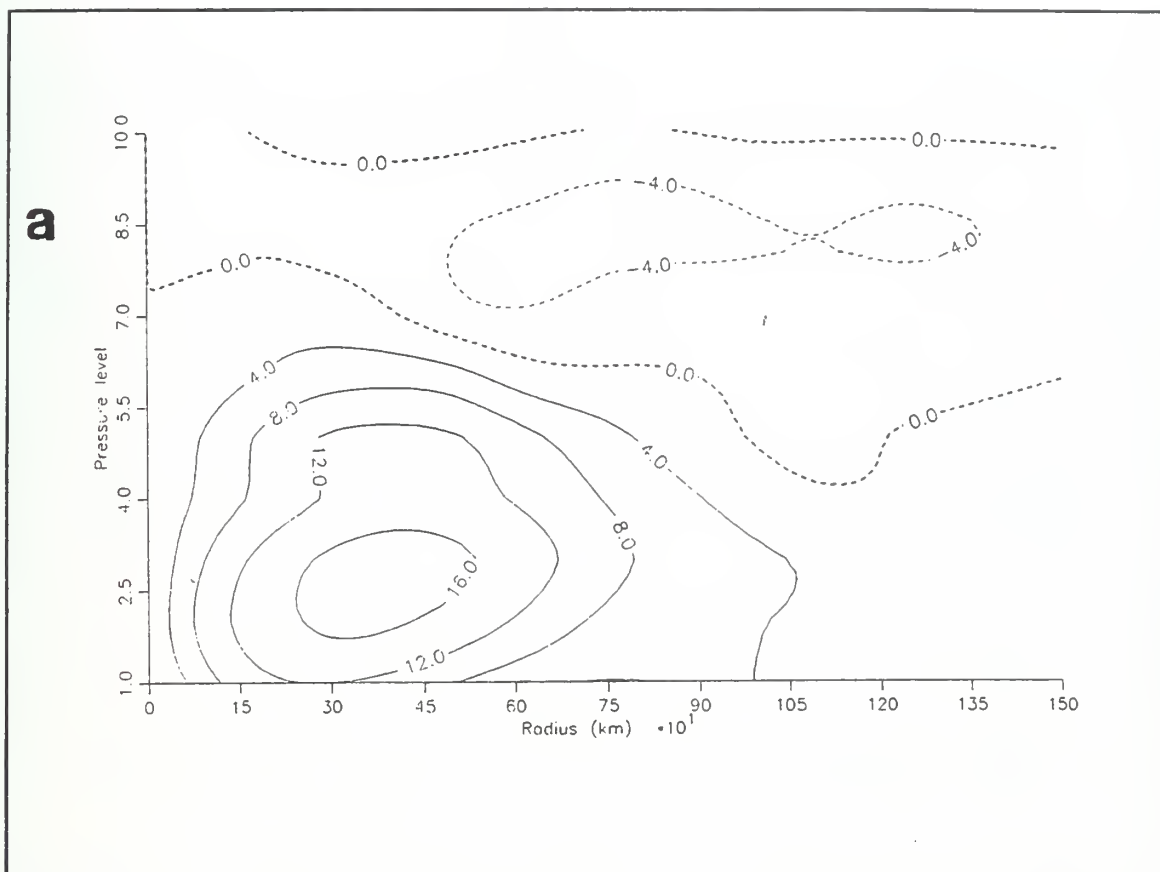


Fig. 4.7. Pressure versus radial distance plot of \bar{v}_L (m s^{-1} , contour interval 4 m s^{-1} , dashed contours $< 0 \text{ m s}^{-1}$, heavy dashed contour is 0 m s^{-1}) at 00 UTC 13 September, as calculated by (a) 4DDA analysis and (b) MQ analysis. Pressure levels are: level 1 = 1000 mb, level 2 = 850 mb, level 3 = 700 mb, level 4 = 500 mb, level 5 = 400 mb, level 6 = 300 mb, level 7 = 250 mb, level 8 = 200 mb, level 9 = 150 mb, and level 10 = 100 mb.

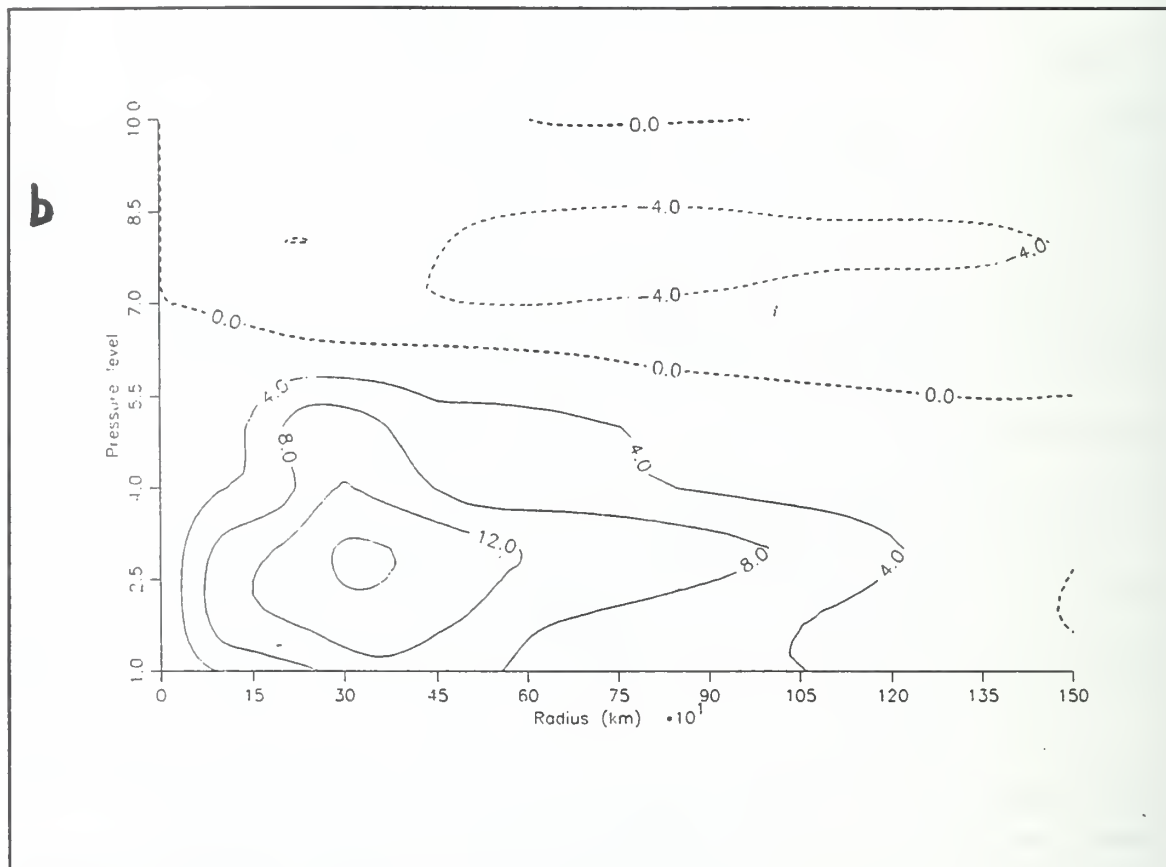


Fig. 4.7 Continued.

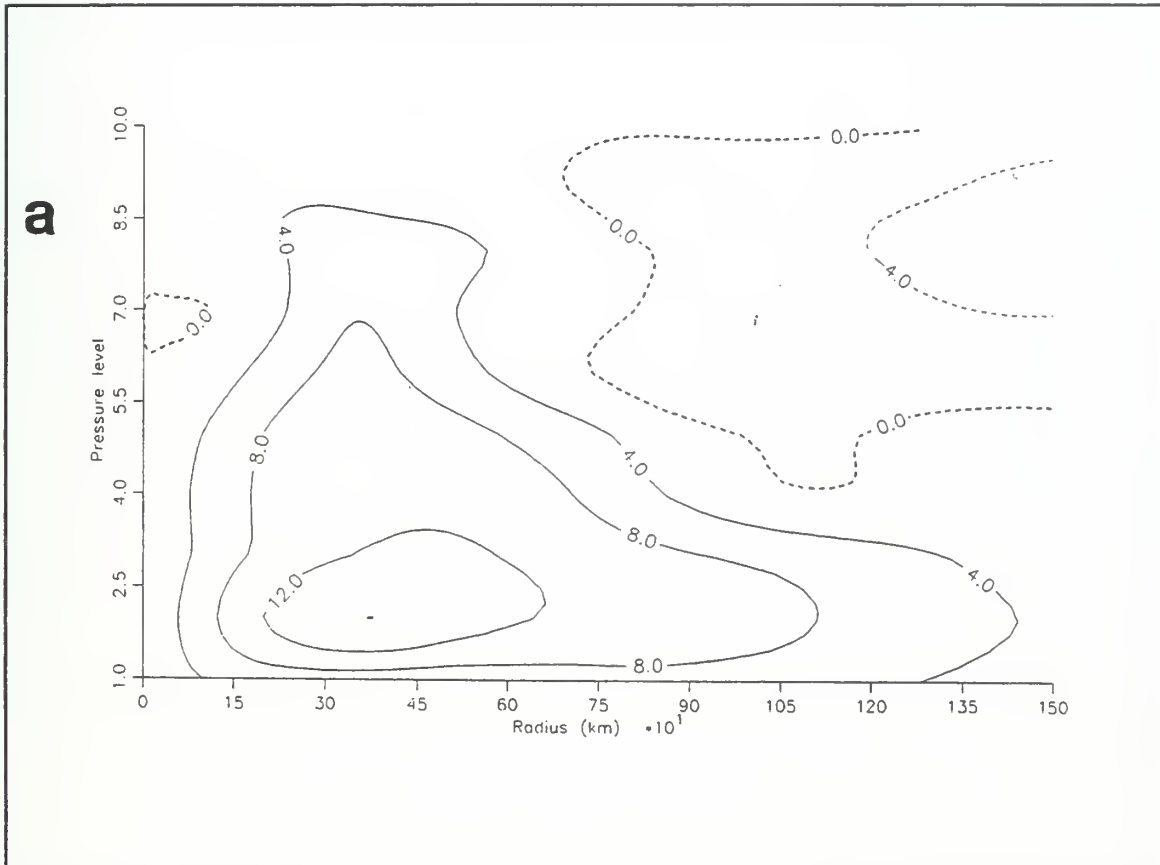


Fig. 4.8. Tangential winds as in Figure 4.7, except at 12 UTC 13 September, as calculated by (a) 4DDA analysis and (b) MQ analysis.

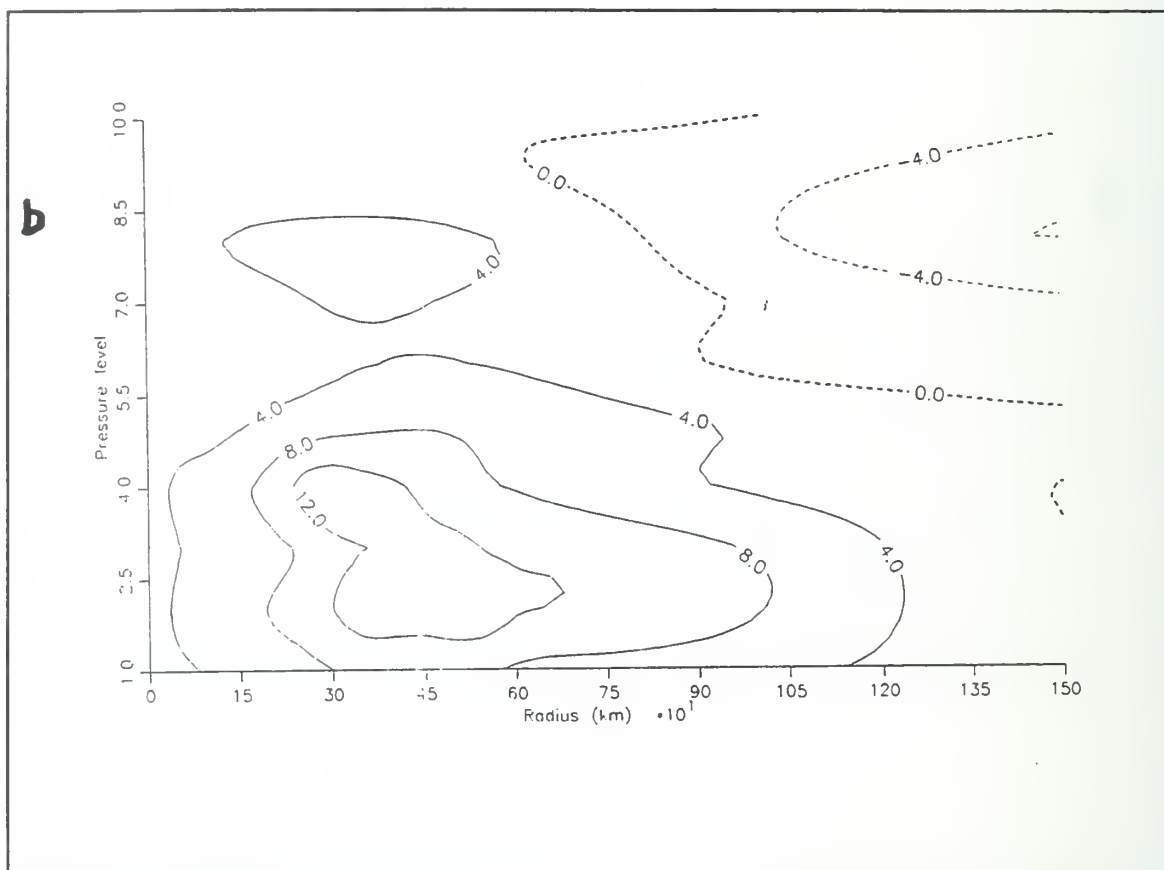


Fig. 4.8. Continued.

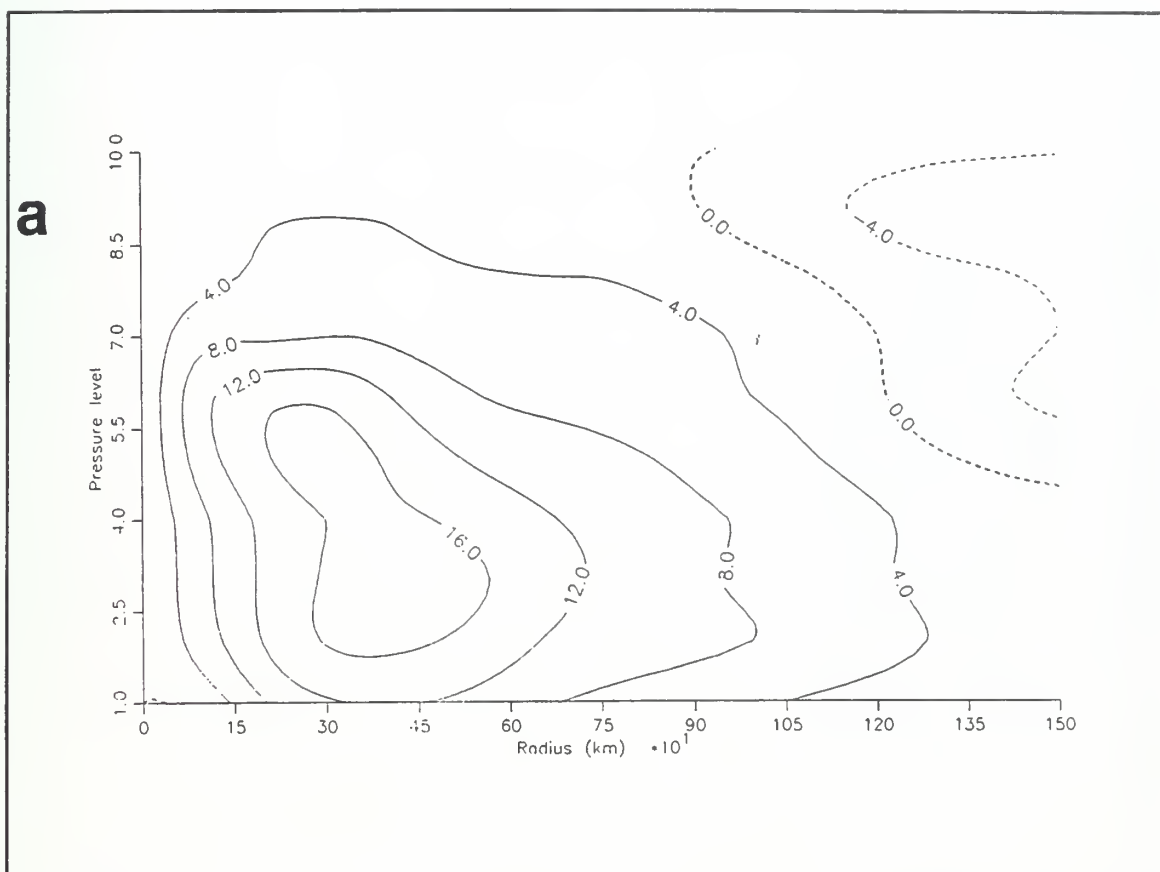


Fig. 4.9. Tangential winds as in Figure 4.7, except at 12 UTC 14 September, as calculated by (a) 4DDA analysis and (b) MQ analysis.

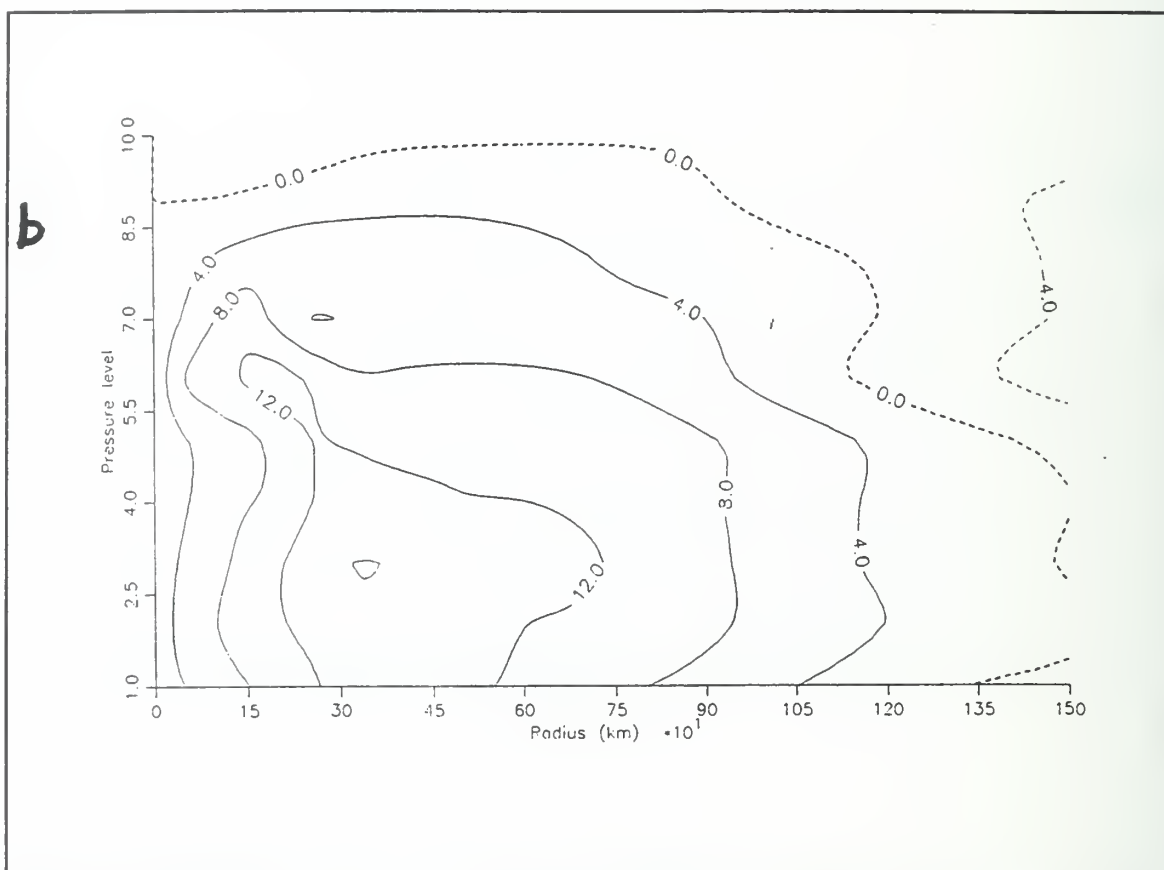


Fig. 4.9. Continued.

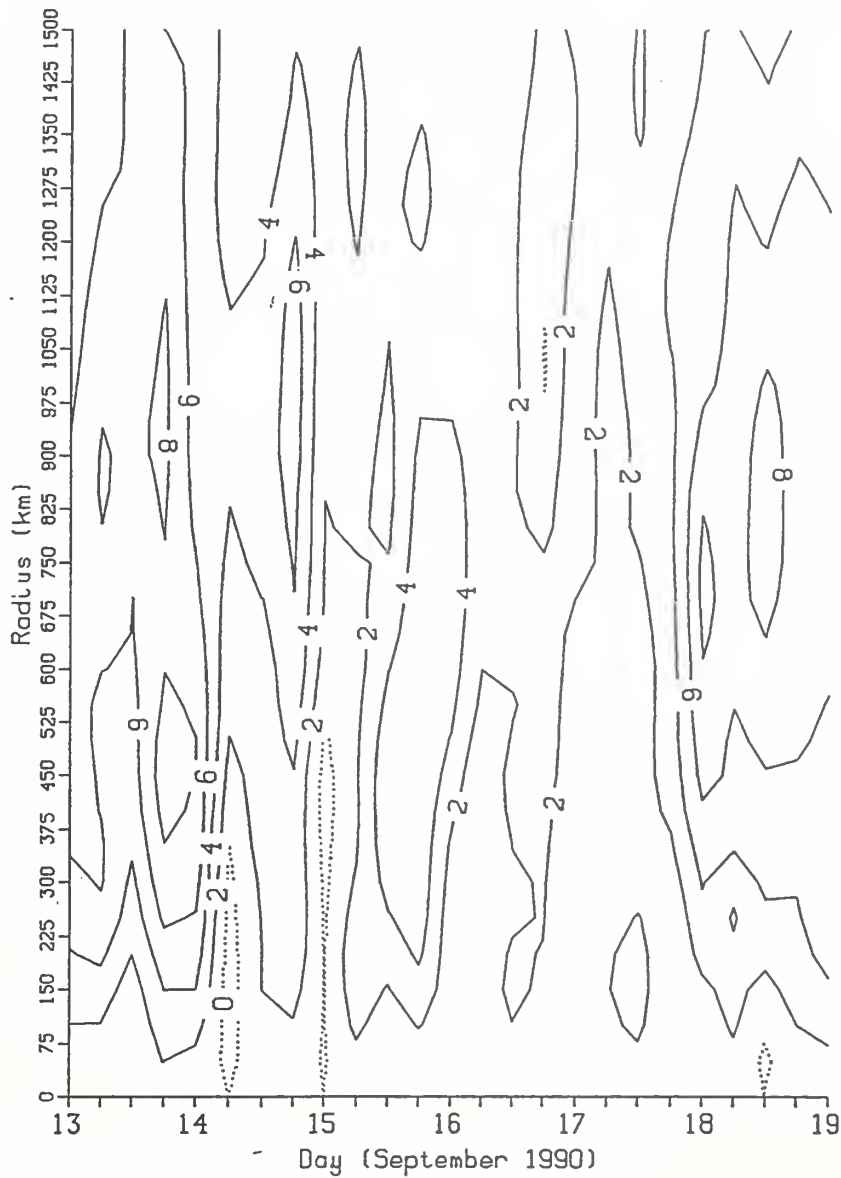
a

Fig. 4.10. Radial distance versus time plot of radial wind \bar{u}_L (m s^{-1} , contour interval 4 m s^{-1} , dashed contours $< 0 \text{ m s}^{-1}$, dotted contour is 0 m s^{-1}) at 200 mb, as calculated by (a) 4DDA analysis, and (b) MQ analysis.

b

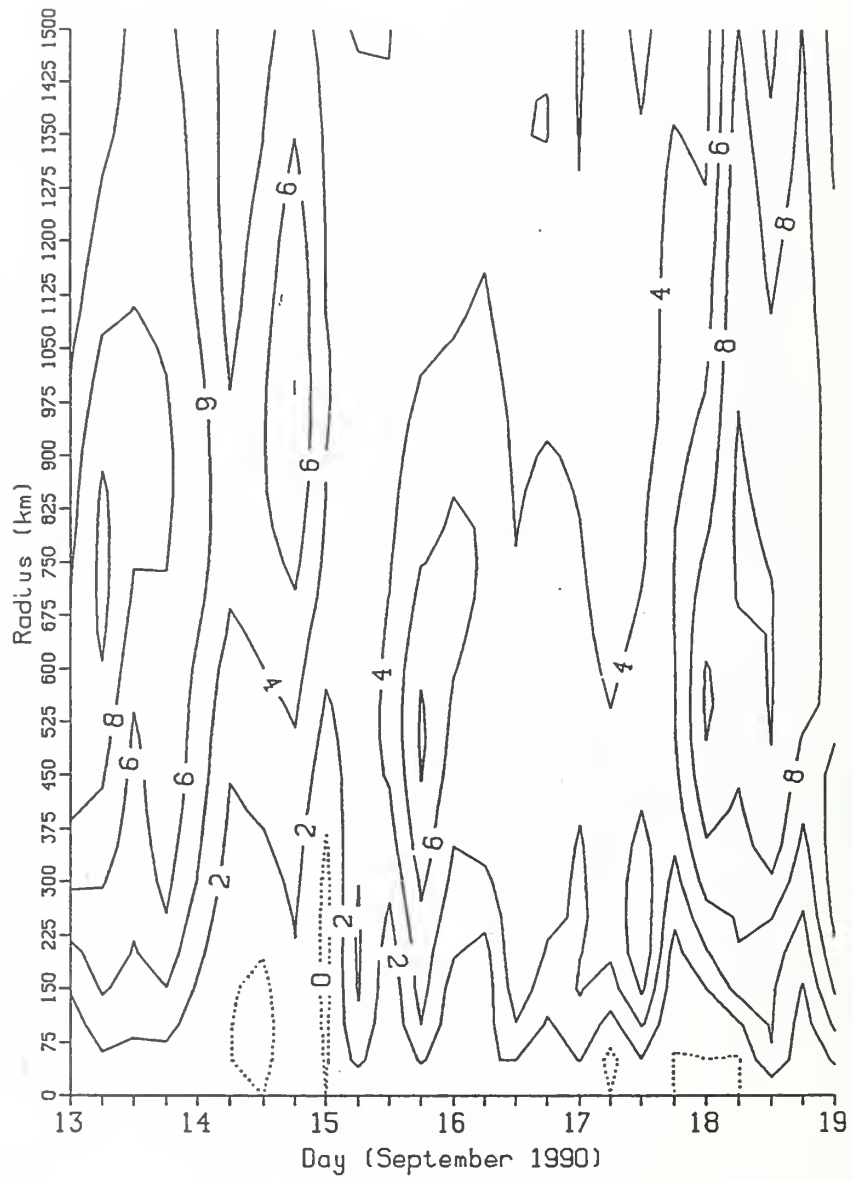


Fig. 4.10. Continued.

above and illustrated in Figure 4.5. By contrast, the NOGAPS analysis of \bar{u}_L (not shown) depicts a broad, weak outflow of 2-4 m s⁻¹ beyond 500 km of the center through 12 UTC 17 September; the NOGAPS analysis then has outflow of about 4 m s⁻¹ for all radii through 00 UTC 19 September. This result demonstrates the caution that must be used when interpreting divergent or radial winds from the operational numerical analyses from the early 1990's. This is the same conclusion reached by Molanari and Vollaro (1990) using European Centre for Medium Range Forecasting (ECMWF) analyses from 1985.

Pressure-radius 4DDA and MQ plots of \bar{u}_L have strong upper-tropospheric outflow at all radii out to 1500 km. The maximum outflow (8-11 m s⁻¹) moves out from about 650 km radius at 00 UTC 13 September to 900 km by 12 UTC 13 September. At 18 UTC 13 September (Figure 4.11), a secondary maximum in the outflow develops at 450 km radius, which moves inward to 400 km radius 6 h later (Figure 4.12).

A narrow band of strong (2-3 m s⁻¹) inflow develops by 18 UTC 13 September between 700 and 500 mb (Figure 4.11). By 00 UTC 14 September (Figure 4.12), this inflow jet has risen to between 500 and 400 mb. Again, this feature does not fit the "typical" axisymmetric radial wind conceptual model for a 20 m s⁻¹ tropical storm (Figure 4.13).

While the outflow maximum initially is located at the 200 mb level, the strongest outflow rises to 150 mb within 400 km of the storm center at 00 UTC 14

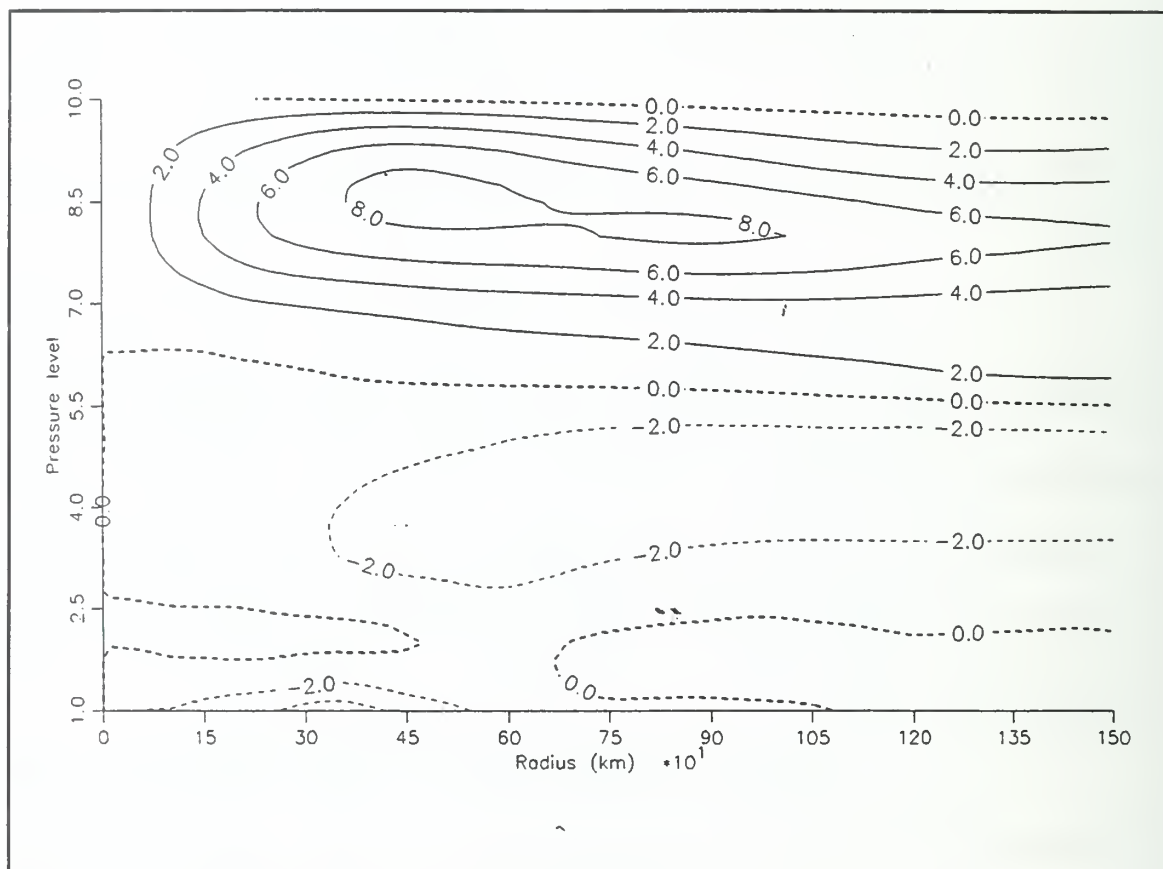


Fig. 4.11. Pressure versus radial distance plot of \bar{u}_L (m s^{-1} , contour interval 2 m s^{-1} , dashed contours $< 0 \text{ m s}^{-1}$, heavy dashed contour is 0 m s^{-1}) at 18 UTC 13 September, as calculated by MQ analysis. Pressure levels are given in Figure 4.7.

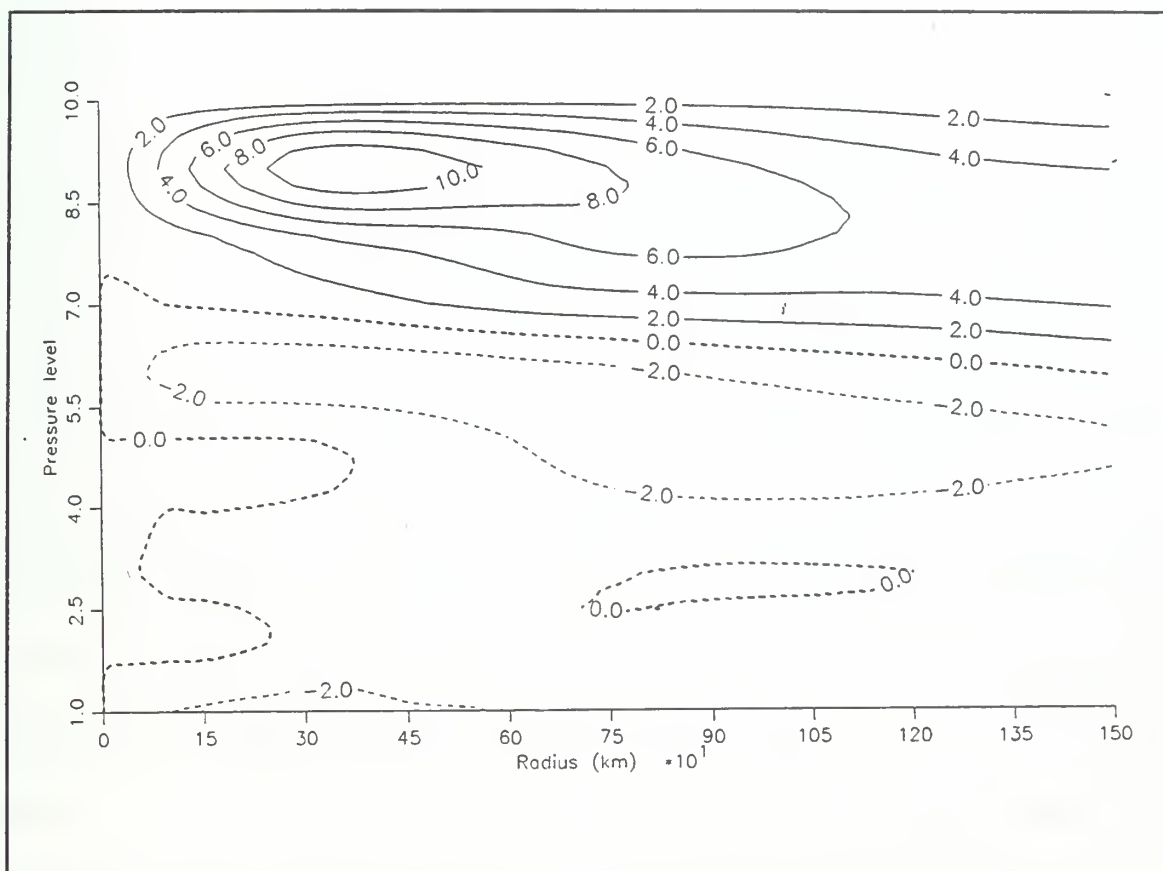


Fig. 4.12. Radial winds as in Figure 4.11, except at 00 UTC 14 September.

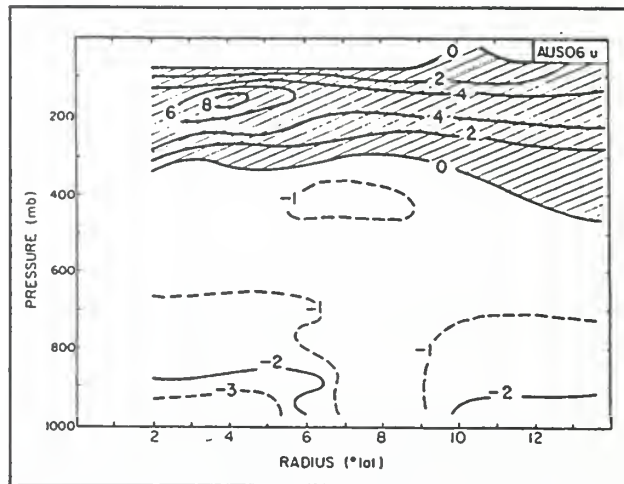


Fig. 4.13. Axisymmetric, vertical cross-section of radial winds (m s^{-1} , shaded regions are outward) for a composite intensifying tropical storm (From Holland and Merrill 1984, Figure 4).

September (Figure 4.12). The core of the outflow jet remains at 150 mb for 6 h, then lowers to 200 mb by 12 UTC 14 September. While this vertical oscillation of the outflow layer was documented in the super typhoon stage of Flo (Merrill and Velden 1996), this phenomenon has not previously been reported for a developing tropical storm.

(3) Eddy Flux Convergence of Relative Angular Momentum. A major focus of this study was to relate the EFC values to intensification. Molinari and Vollaro (1989) showed the rapid intensification of Hurricane Elena (1985) was preceded by EFC values in excess of $25 \text{ m s}^{-1}/\text{day}$. With the high spatial depiction of Flo's outflow layer, it is hypothesized that large EFC values would clearly precede Flo's rapid intensification. That is, EFC values derived from high resolution data, and objective

analyses that "drew" to the observations, could be used as a forecasting tool to predict rapid intensification events.

The 4DDA EFC radius-time plot for 200 mb (Figure 4.14a) shows two regions of $\text{EFC} > 30 \text{ m s}^{-1}/\text{day}$ between 900 and 1000 km radius during the forcing phase. The first maximum develops at 06 UTC 13 September at about 1100 km radius, and appears to propagate to within 100 km of the center by 12 UTC 14 September, which represents a propagation speed of about 9 m s^{-1} . The second EFC maximum develops at a radius of 1250 km at 18 UTC 13 September, and possibly reaches the center of Flo by 06 UTC 16 September. However, the signals for both these maxima are not continuous. The first maximum is most difficult to assess in the "off-time" (i.e., 18 UTC 13 September and 06 UTC 14 September) analyses, and the second maximum becomes extremely tenuous within 500 km of the center. Given the previous discussion of variations in the level of the outflow, the radius-time plot for 150 mb EFC is also examined (Figure 4.15). While positive EFC is calculated at 18 UTC 13 September and 00 UTC 14 September, and an isolated maximum of $25 \text{ m s}^{-1}/\text{day}$ is found at 200 km radius at 12 UTC 15 September, it is not possible to track a coherent signal of the second EFC maximum into the center. Thus, this study is not able to link directly inward EFC propagation to Flo's rapid intensification.

The EFC during the forcing period (e.g., Figures 4.16 and 4.17) is consistent and strong ($> 20 \text{ m s}^{-1}/\text{day}$) throughout the upper troposphere, with several regions having EFC values greater than $30 \text{ m s}^{-1}/\text{day}$. While the 4DDA analyses (not

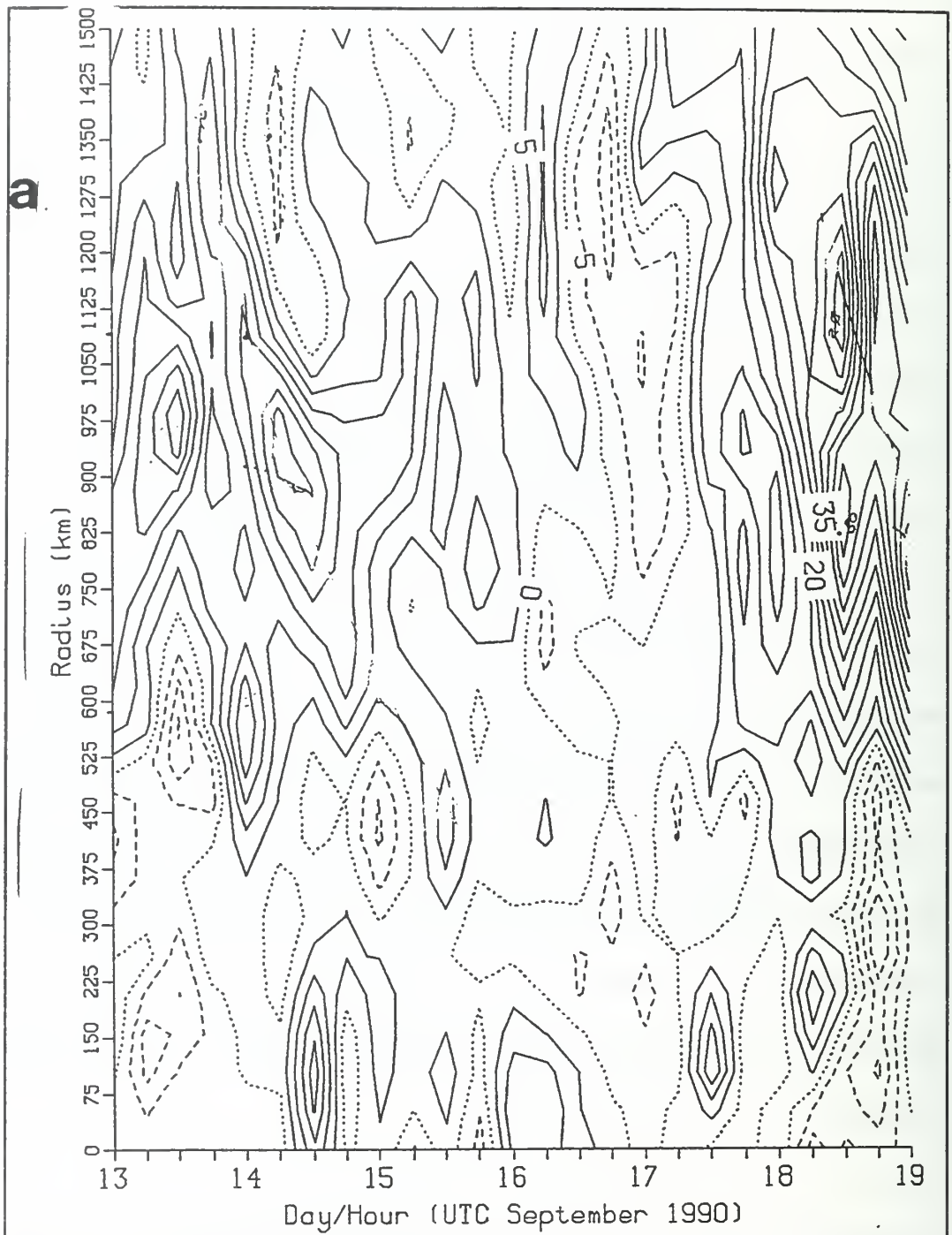


Fig. 4.14. Radial distance versus time plot of EFC ($\text{m s}^{-1}/\text{day}$, contour interval $5 \text{ m s}^{-1}/\text{day}$, dashed contours $< 0 \text{ m s}^{-1}$, dotted contour is 0 m s^{-1}) at 200 mb, as calculated by (a) 4DDA analysis, and (b) MQ analysis.

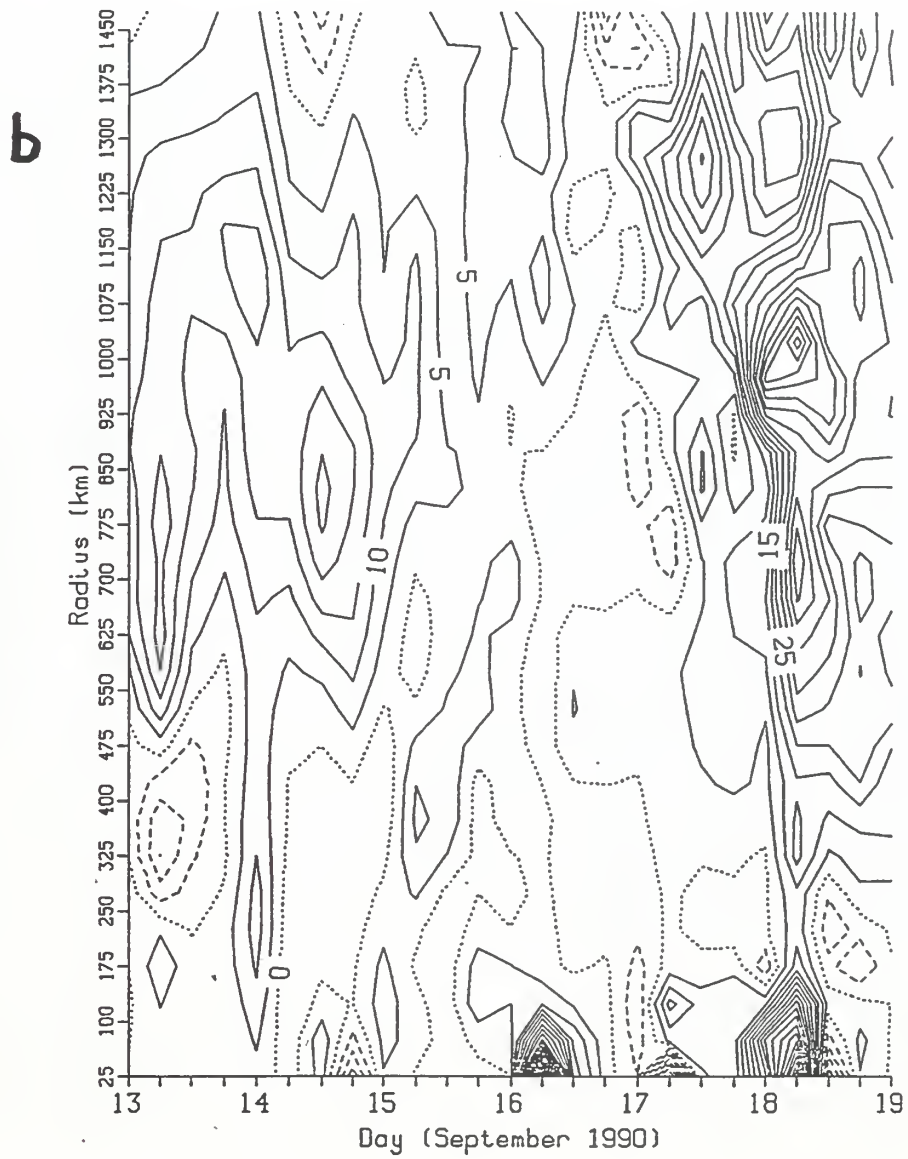


Fig.4.14. Continued.

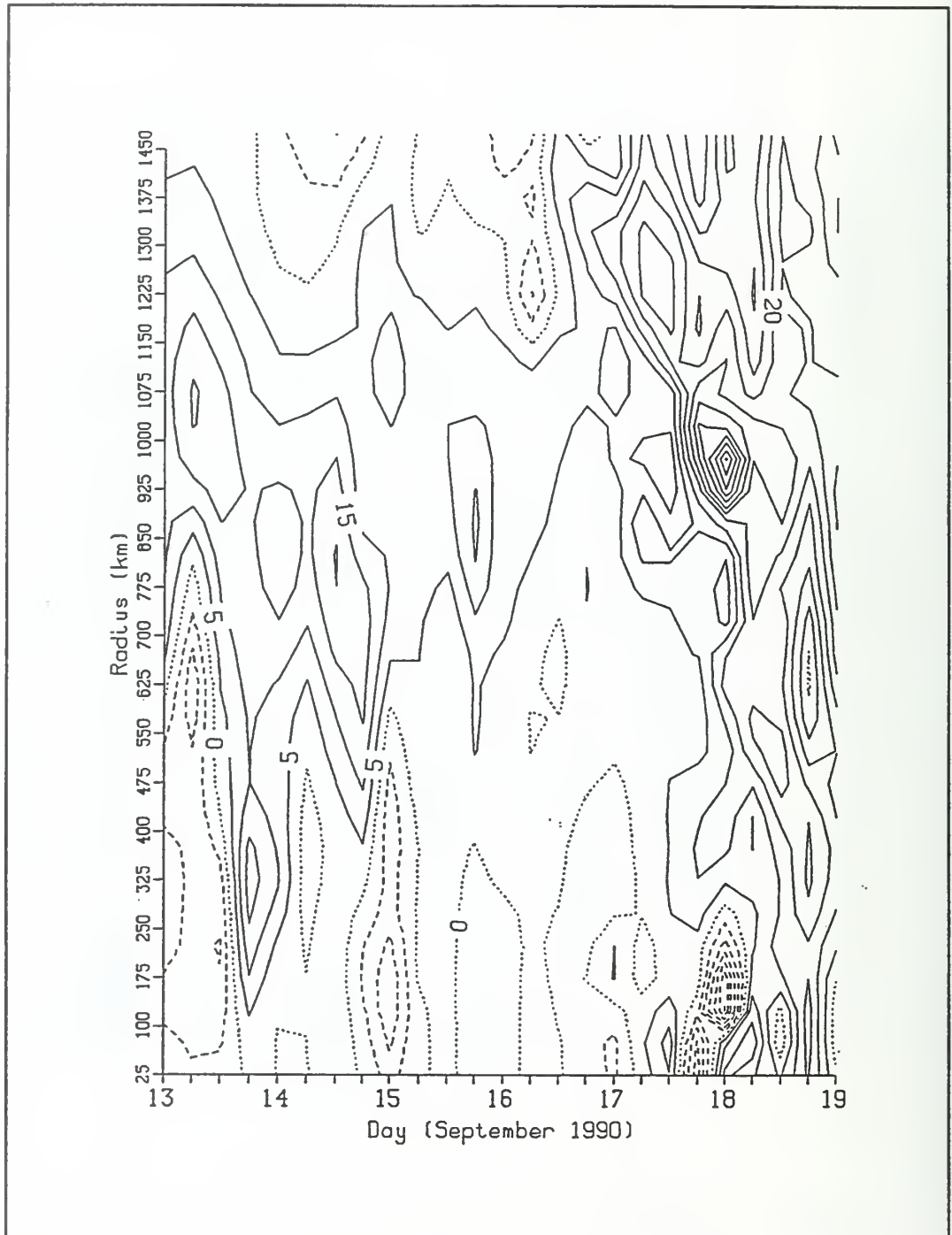


Fig. 4.15. As in Figure 4.14, except at 150 mb, as calculated by 4DDA analysis.

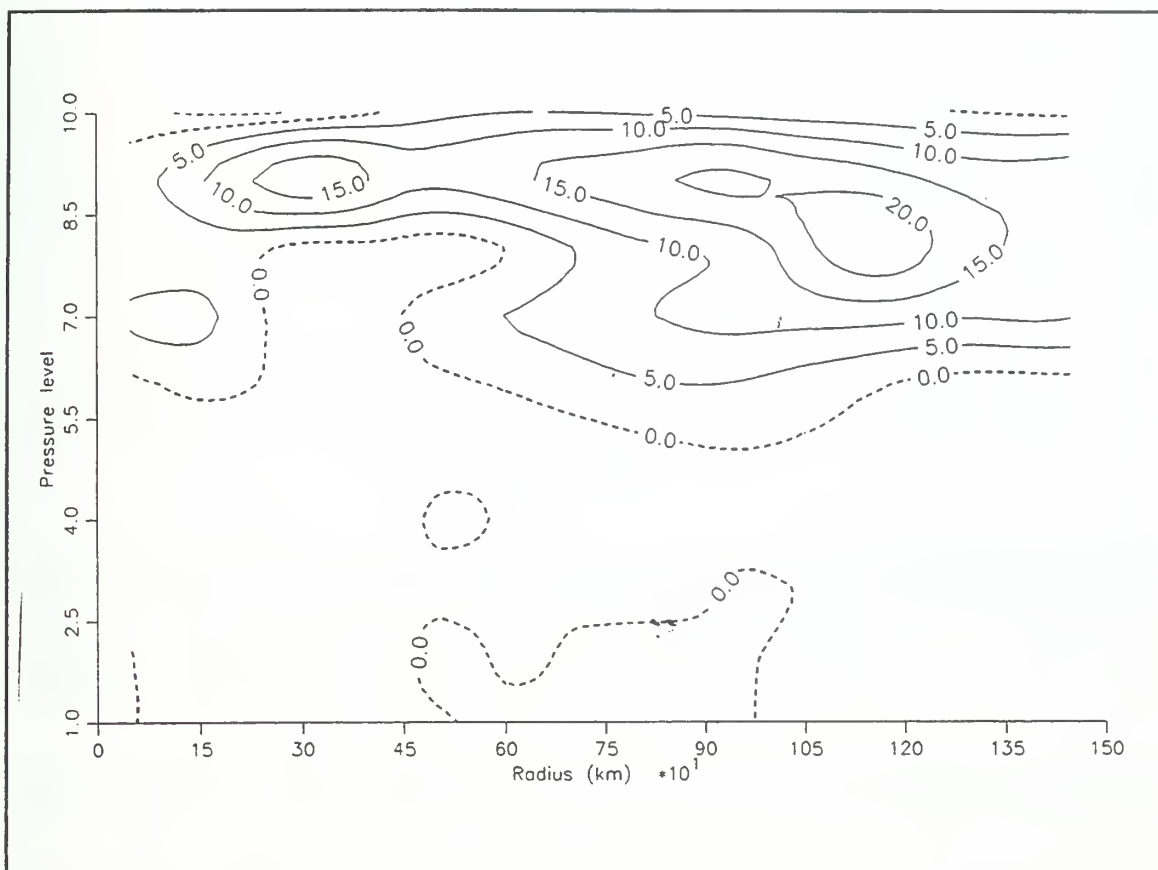


Fig. 4.16. Pressure versus radial distance plot of EFC ($\text{m s}^{-1}/\text{day}$, contour interval $5 \text{ m s}^{-1}/\text{day}$, dashed contours $< 0 \text{ m s}^{-1}$, heavy dashed contour is 0 m s^{-1}) at 18 UTC 13 September, as calculated by MQ analysis. Pressure levels are given in Figure 4.7.

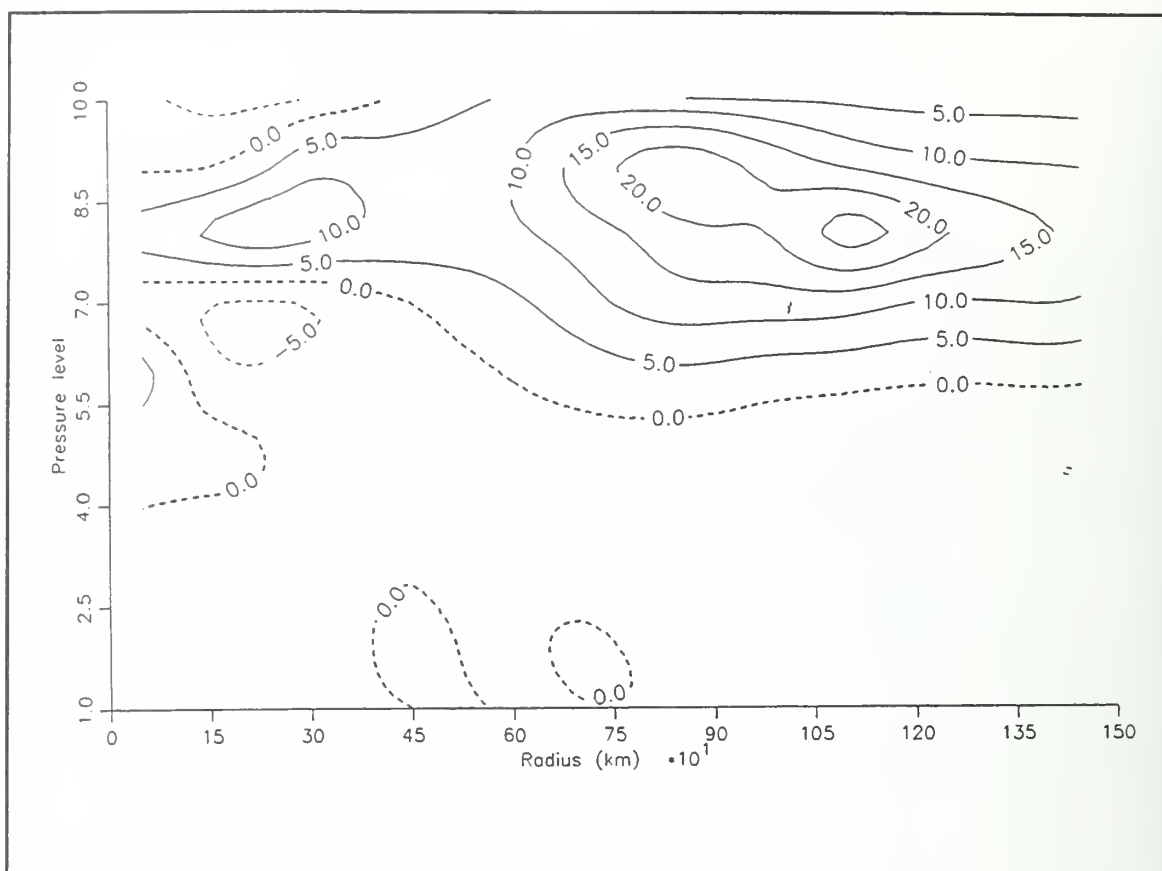


Fig. 4.17. EFC values as Figure 4.16, except at 00 UTC 14 September.

shown) depict slightly more vertical EFC structures than the Multi-quadric analysis EFC calculations, both have the strong, positive upper-troposphere EFC pattern throughout the forcing period. At 12 UTC (not shown) and 18 UTC 13 September (Figure 4.16), the maximum EFC rises to 150 mb in both analyses. This is 12 h prior to the observed rise in the height of maximum radial outflow previously discussed.

(4) Vertical Wind Shear. It has long been known (e.g., Gray 1968) that excessive vertical wind shear inhibits tropical cyclone development and intensification. Zehr (1992) determined that the maximum vertical wind shear between

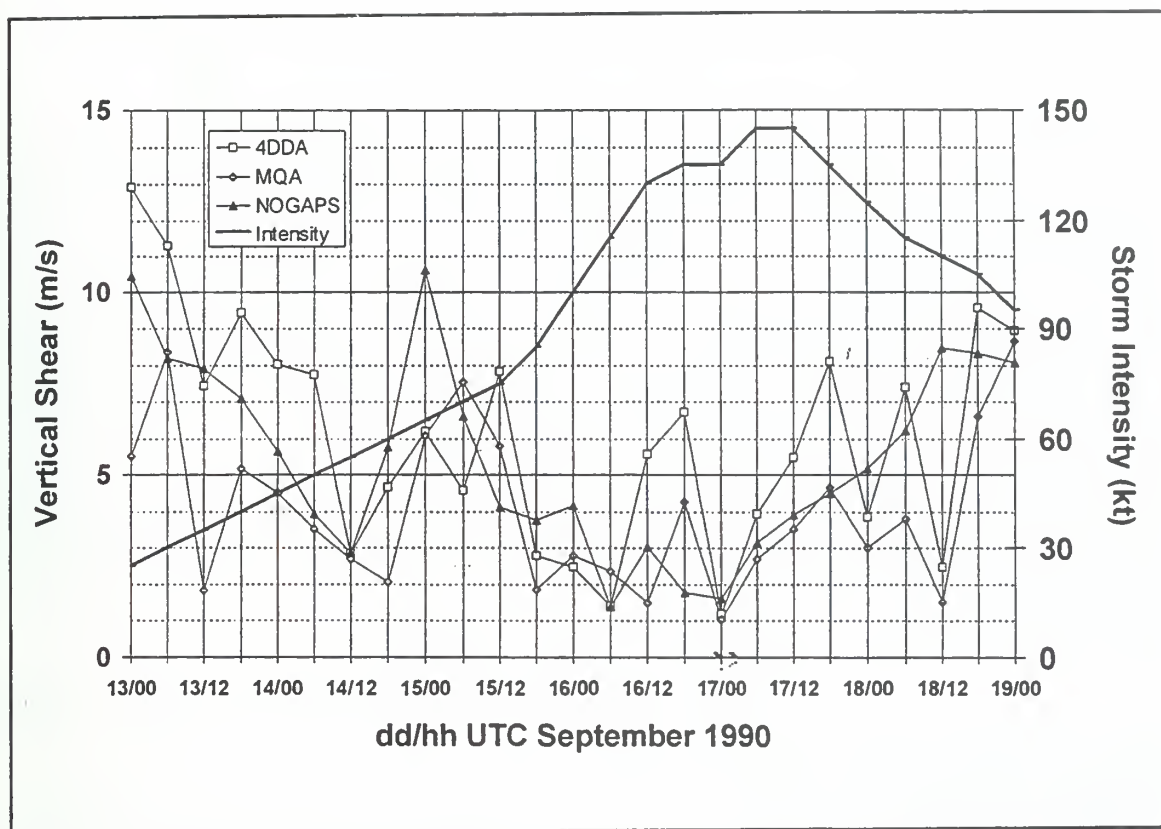


Fig. 4.18. Vertical wind shears between 850 mb and 200 mb, azimuthally-averaged between 200 km and 600 km around Typhoon Flo as calculated from 4DDA, MQ, and NOGAPS (see inset for symbols) analyses. Storm intensity (heavy solid) is given on right vertical axis.

the 200 mb and 850 mb wind averaged over the tropical cyclone for intensifying western North Pacific Ocean storms is less than 12.5 m s^{-1} . As previously described, the magnitude of the 850 mb - 200 mb vertical shear between 200 km and 600 km was calculated for each analysis scheme (Figure 4.18).

A comparison of the three vertical shear analyses reveals a significant difference in the vertical shear magnitude between Multi-quadric analysis calculations and the 4DDA and NOGAPS analyses through 00 UTC 14 September. The

Multi-quadric analysis has a (temporally-averaged) vertical shear magnitude of about 5 m s^{-1} for the initial 24 h of the analysis. By contrast, the 4DDA (NOGAPS) analysis has vertical shear values of nearly 10 (8) m s^{-1} , with the 00 UTC 13 September 4DDA vertical shear nearly 13 m s^{-1} . The observed robust intensification of Flo by 5 $\text{m s}^{-1}/12$ h would indicate the lower value of vertical shear calculated in the Multi-quadric analysis is more likely to be correct. This finding is consistent with Elsberry and Jeffries (1996), who concluded that the operational NOGAPS analysis sometimes does not represent well the mesoscale outflow structure in intensifying cyclones. They found this structure is typically better represented by the Multi-quadric analysis.

Another noteworthy feature is the significant decrease in vertical shear calculated between 300 mb and 150 mb throughout the forcing period (Figure 4.19). Although observational coverage is only fair (good) at 150 (200) mb, and observations are relatively sparse in the vicinity of Flo at 300 mb, both Multi-quadric analysis and 4DDA analyses depict a greater than 35% decrease in this vertical shear during this time. Additionally, both (independent) analyses are in close agreement regarding the decrease in this vertical shear. It is hypothesized that this rapid decrease in upper-tropospheric shear indicates the early stages of the upper-troposphere being coupled to the storm circulation. If this decrease in upper-tropospheric shear is observed in other tropical cyclones that subsequently rapidly intensify, this calculation could serve as a useful forecasting tool.

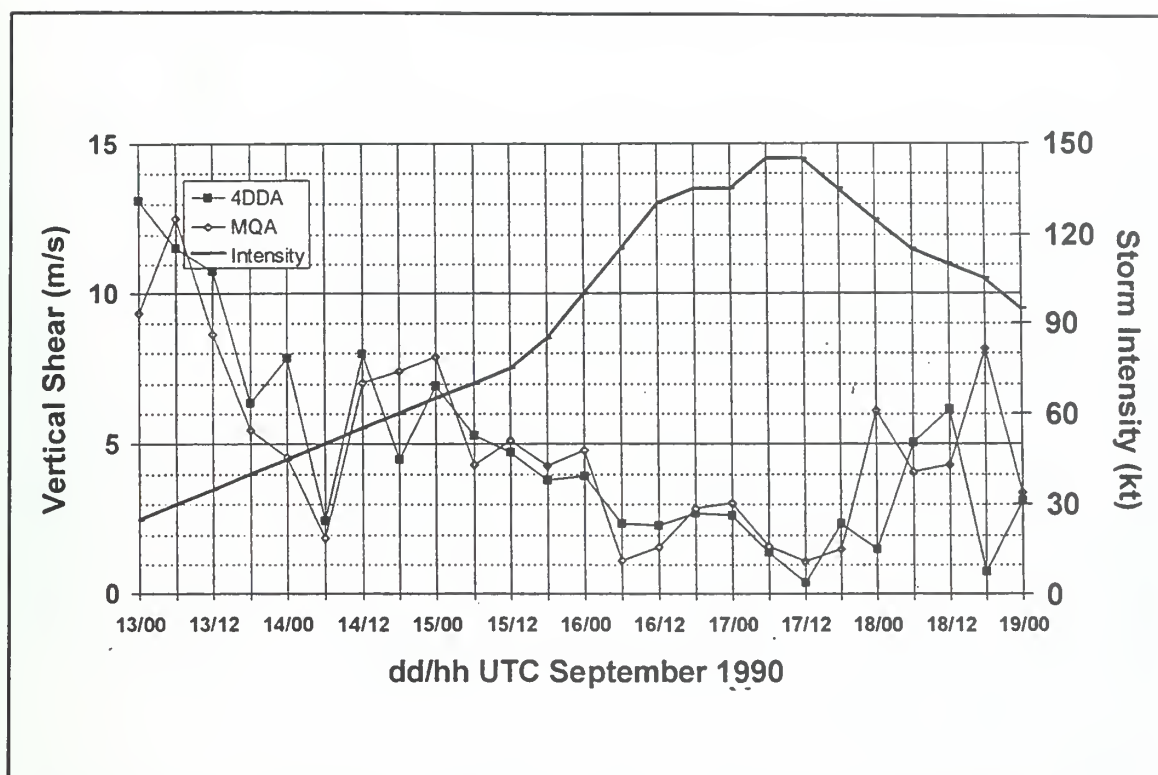


Fig. 4.19. Vertical wind shears between 300 mb and 150 mb, azimuthally-averaged between 200 km and 600 km around Typhoon Flo for 4DDA and MQ (see inset for symbols) analyses. Storm intensity (heavy solid) is given on right vertical axis.

(5) Discussion and Conclusions. It is initially disappointing to note

that the storm intensity changes are not directly related to EFC values, despite the high spatial and temporal resolution of the upper tropospheric wind data set. However, the combination of the thermal composite, tangential and radial winds and associated vertical shear structure, and EFC calculations, provide evidence that the environmental dynamics acting on the Flo altered the storm thermal structure to a mode that would be conducive for future rapid intensification. That is, the large-scale environment "pre-conditioned" the storm to enhance the potential for future rapid intensification.

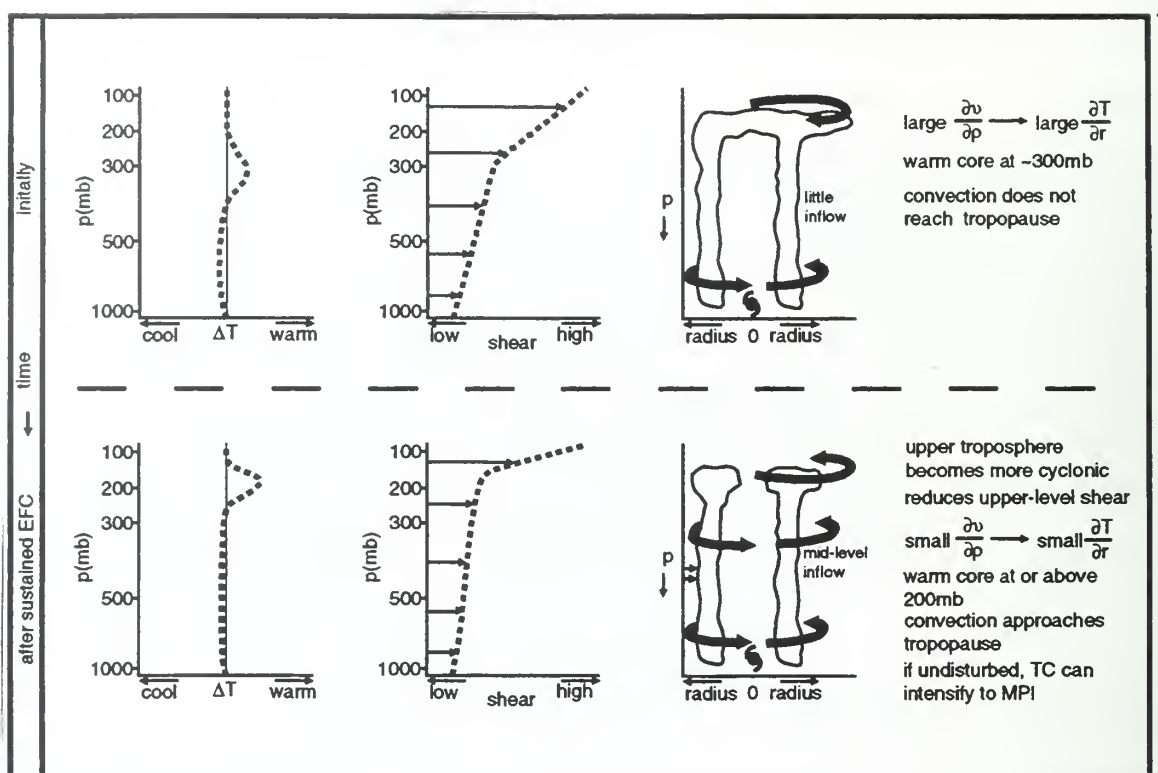


Fig. 4.20 Conceptual model of the relationship between EFCs, increased cyclonic winds, reduced vertical shear, and subsequent thermal implications. See text for details.

The proposed relationships among the above-listed parameters is shown in Figure 4.20. The hypothesis is that strong, sustained upper-tropospheric EFC acting on a weak storm increases (decreases) the cyclonic (anticyclonic) component of \bar{v}_L (Figure 4.21). That is, sustained, positive EFC causes the "cyclonic wind burst" at 200 mb previously described in subsection (I). In addition, the increase in the cyclonic component of \bar{v}_L decreases the storm vertical shear in the upper troposphere. From thermal wind considerations, $\frac{\partial \bar{v}_L}{\partial p} \propto \frac{-\partial \bar{T}}{\partial r}$, this implies that a relatively small horizontal thermal gradient exists. However, the storm is intensifying throughout this period, so

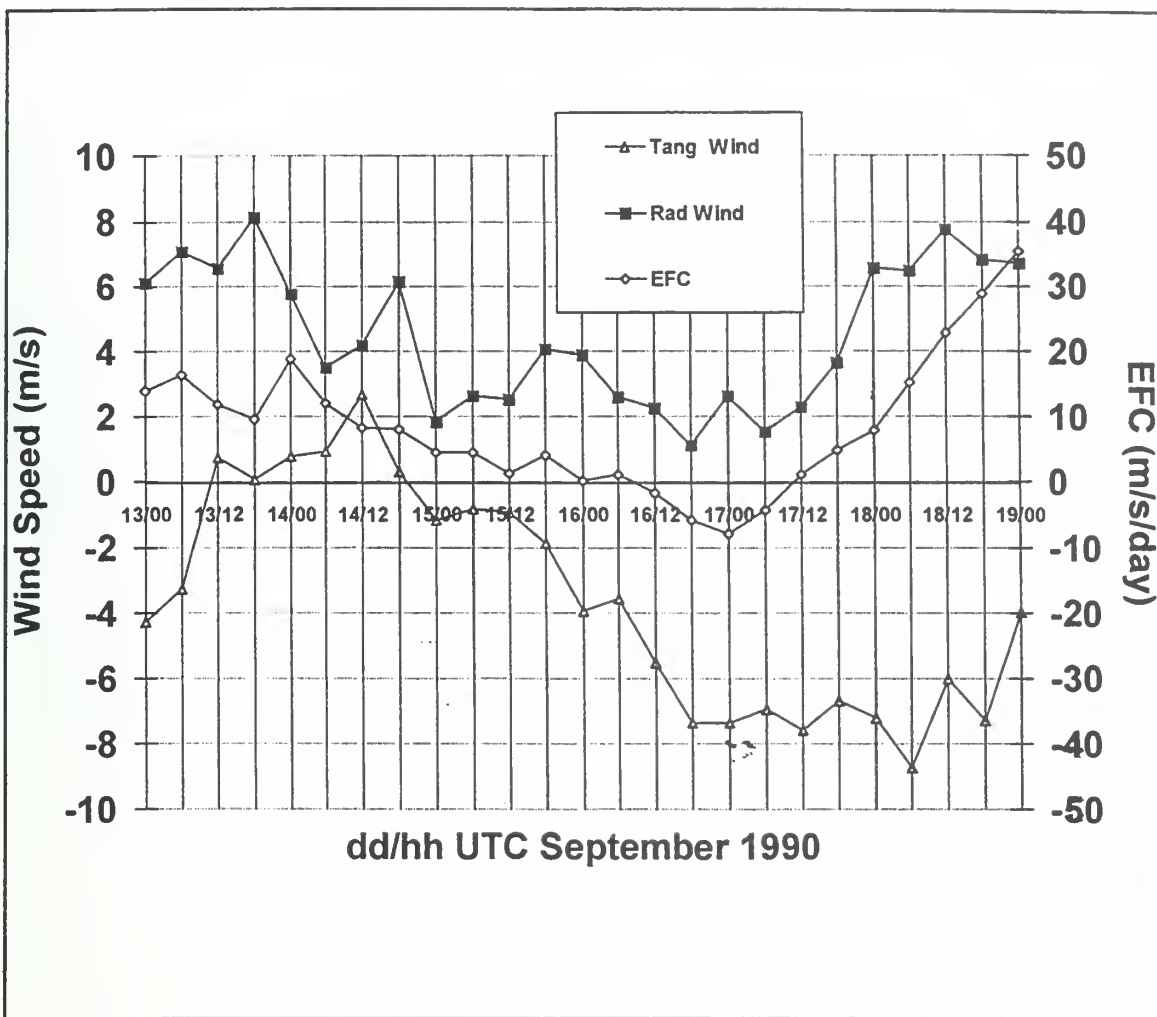


Fig. 4.21 Azimuthally-averaged 200 mb \bar{v}_L , \bar{u}_L , and EFC averaged over an annulus between 400 km and 1200 km around Typhoon Flo. The \bar{v}_L , \bar{u}_L values are displayed on the left vertical axis; EFC values are displayed on the right vertical axis. Calculations are based on the 4DDA analysis.

the additional required warming to balance the lower central pressure must be concentrated near the tropopause, above the region of small $\frac{\partial \bar{v}_L}{\partial p}$. Therefore, the "cyclonic wind burst" may mark the transition of Flo's thermal structure from that of a typical tropical cyclone to one that would support rapid intensification.

The conclusion is that a strong, sustained EFC environment acting on a tropical storm can, through the process described above, alter the thermal structure of the storm such that the majority of the storm's warm anomaly is concentrated higher in the upper troposphere than normal. Such a structure provides a less stable environment that is more conducive to deep, sustained convection than that found in a typical tropical cyclone. While this process alone does not guarantee subsequent rapid intensification, it does provide an indirect mechanism to allow rapid intensification of the storm in the future.

Another mechanism that may be assisting storm development is the enhanced inflow in the mid-troposphere produced by the upper-level EFC forcing, as proposed by Pfeffer and Challa (1981) and Holland and Merrill (1984). That is, the inflow below and in direct response to the EFC, could spin up the storm by enhancing the transverse circulation. While some evidence of enhanced inflow exists, especially at 500 mb at 18 UTC 13 September (Figure 4.11) and at 400 mb at 00 UTC 14 September (Figure 4.12), the sparcity of mid-troposphere observations makes this conclusion tentative. Improved methods of determining mid-troposphere winds (e.g., Velden *et al.* 1997) may allow future testing of this hypothesis with observational data.

This study is also consistent with the results of Elsberry and Jeffries (1996), who showed that operational objective analysis schemes may not capture the mesoscale outflow structure of a developing tropical system. These details can be

important when determining the amount of vertical wind shear the storm is actually encountering.

b. Quiescent Forcing Phase (18 UTC 14 September through 12 UTC 16 September)

This phase is named quiescent for the distinct lack of strong external forcing that was observed around Flo throughout this period, despite a dramatic change in the storm intensity. The quiescent phase consists of two parts: a contraction of the "cyclonic burst" of \bar{v}_L observed at 200 mb and the rapid intensification of Flo. During the contraction phase, the radius of cyclonic \bar{v}_L decreases from about 1100 km to 600 km by 12 UTC 15 September. In the rapid intensification phase, Flo's intensity increased by 23 m s^{-1} in 18 h, from 44 m s^{-1} at 18 UTC 15 September to 67 m s^{-1} by 12 UTC 16 September.

(1) Contraction Phase. The 200 mb total wind fields are very similar for both the MQ (not shown) and 4DDA (e.g., Figure 4.22) analyses. The dominant outflow channel is toward the north for about 500 km, then curves anticyclonically to the southeast and flow between a strengthening anticyclone 600 km southeast of Flo and the large TUTT now 2600 km east of Flo. Wind speeds in the gradient between the anticyclone and the TUTT are in excess of 40 m s^{-1} through 06 UTC 15 September. A secondary outflow channel is to the north-northwest of Flo, and then the flow curves cyclonically around a small cyclone 450 km west-northwest of Flo, and finally merges with the deep tropical easterly flow over the Philippines south of 15°N . A schematic (Figure 4.23) based upon observations and objective and satellite

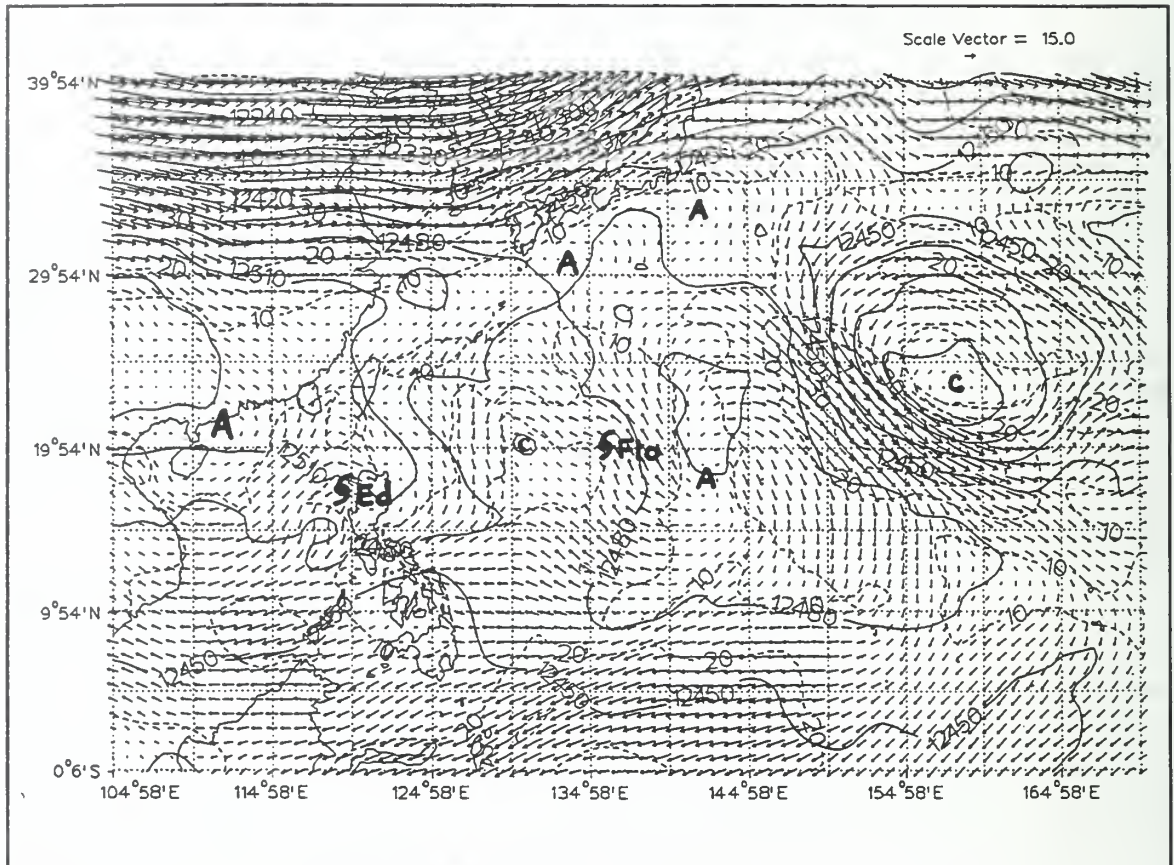


Fig. 4.22. 4DDA analysis of 200 mb wind (m s^{-1} , scale vector in upper right), isotachs (dashed, contour interval 10 m s^{-1}) and heights (solid, contour interval 30 m) at 00 UTC 15 September. Surface best-track location of Flo is indicated by the tropical cyclone symbol. TUTT location is indicated by "C" symbol. Anticyclone location is indicated by "A" symbol.

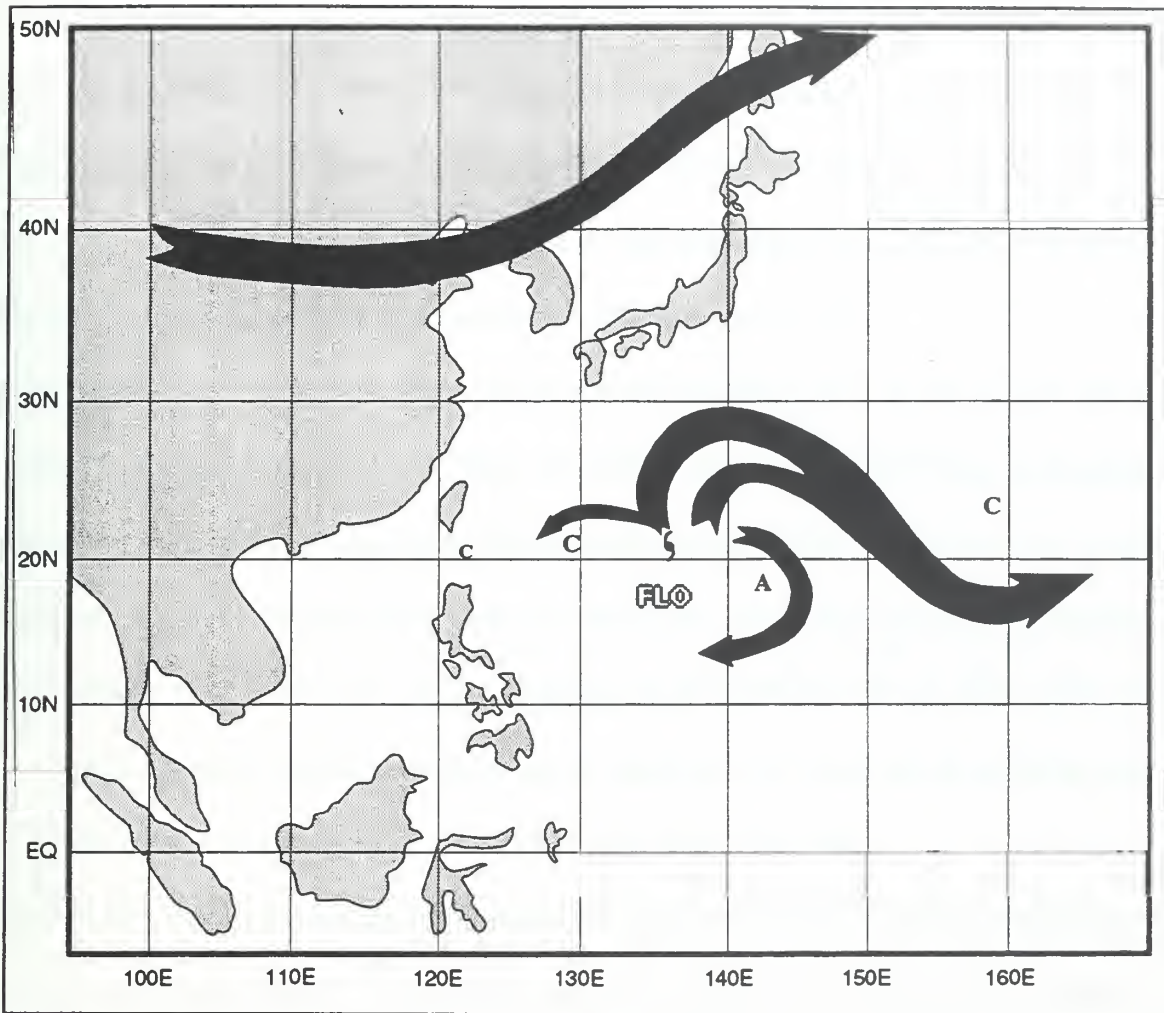


Fig. 4.23. Schematic of the trajectories of the outflow jet (light stipple) of Typhoon Flo and the midlatitude jet (dark stipple) at 00 UTC 15 September.

analyses shows the relationship between Flo's outflow channels and the mid-latitude jet to the northwest.

This outflow pattern is maintained through 06 UTC 15 September as Flo continues to move to the northwest at 6 m s^{-1} . By 12 UTC, the dominant features affecting Flo's outflow are still the anticyclone and TUTT 800 km and 2200 km,

respectively, to the east. The 4DDA analysis depicts a cyclonic turn to the outflow within 200 km of the typhoon. For the first time some of the outflow also appears to be interacting and merging with the strong southwesterlies south of Kyushu. This flow is ahead of a mid-latitude trough over the Yellow Sea.

The outflow appears qualitatively weaker at this stage of Flo than in the forcing phase. The dominant features of the upper-troposphere circulation are the anticyclone and TUTT to the east. While the outflow is eventually channeled between these two systems, a substantial gradient would be present between the two systems without the typhoon's presence. However, Flo may have contributed to the strength of the anticyclone via the subsidence in the typhoon's wake. The "fountain of outflow" that was prevalent in the early forcing phase, is now a uni-directional southerly flow.

The radius-time plot of 200 mb \bar{v}_L (Figure 4.6a and b) shows the contraction of the cyclonic wind burst first observed in the forcing phase. In the 24 h commencing 12 UTC 14 September, the radius of cyclonic winds decreases from 1000 km to 550 km. The 4DDA pressure-radius plots through this period (e.g., Figure 4.24a) show the cyclonic circulation extends above 150 mb within 400 km of the storm center. Both the 4DDA and MQ analysis (Figure 4.24b) depict the developing upper-troposphere anticyclone beyond 600 km from Flo.

By 18 UTC 14 September, much of the upper-tropospheric outflow is concentrated between 200 and 150 mb, especially within the inner 600 km of the storm. In particular, the MQ analysis depicts the outflow as rising over a ridge between

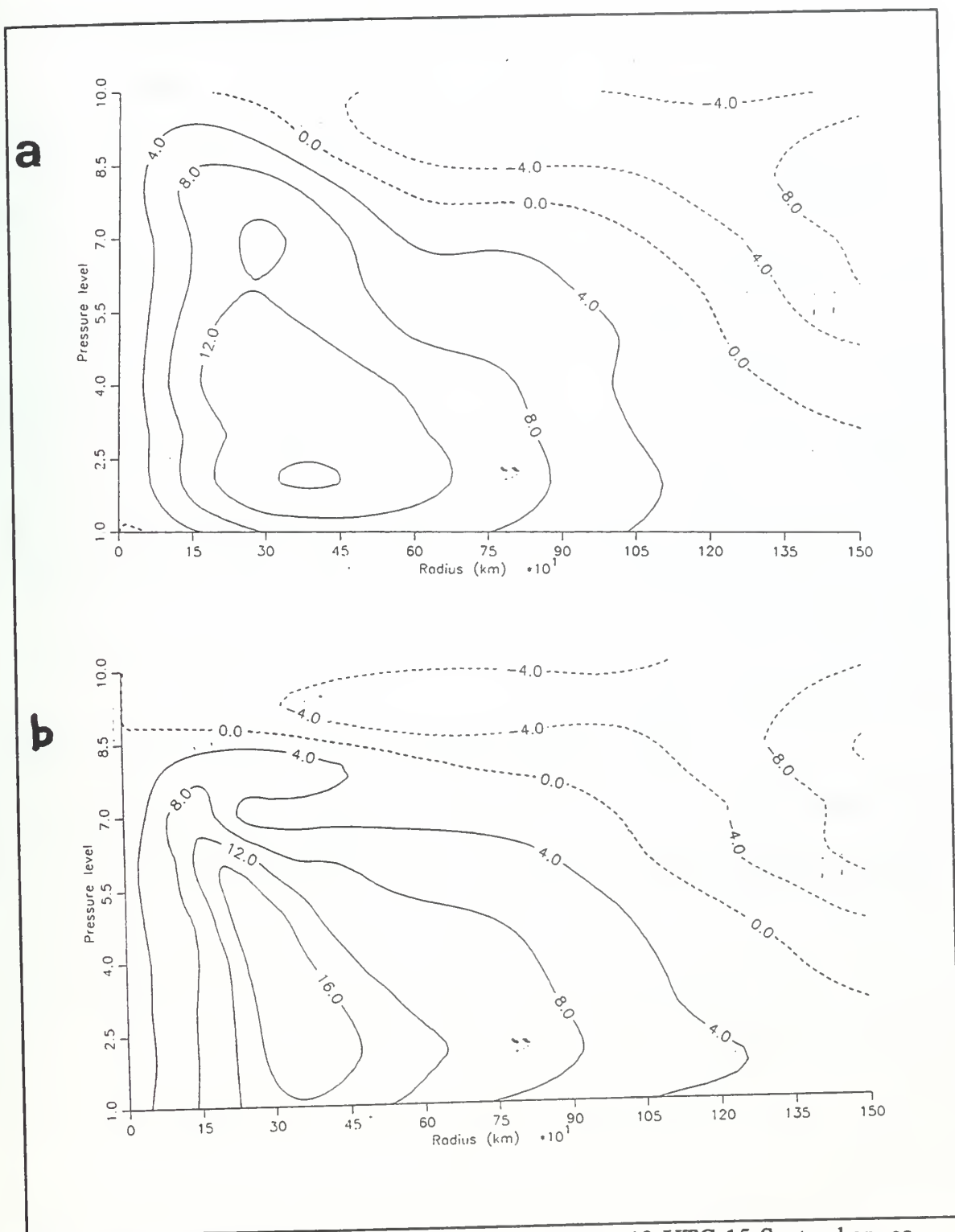


Fig. 4.24. Tangential wind as in Figure 4.7, except at 12 UTC 15 September, as calculated by (a) 4DDA analysis and (b) MQ analysis.

300-600 km from the storm center, and then gradually descending to 200 mb at outer radii. At 00 UTC 15 September, when Flo reaches minimum typhoon intensity, both the 4DDA (Figure 4.25a) and MQ (Figure 4.25b) analyses show the outflow layer extending to 150 mb near the center. However, the magnitude of the radial outflow has decreased from the forcing phase, with maximum \bar{u}_L generally 3-5 m s⁻¹ in this phase.

The analyses (especially the MQ analysis) show strong (2-3 m s⁻¹), deep (up to 250 mb) inflow at 18 UTC 14 September through 00 UTC 15 September (Figure 4.25). The 4DDA (Figure 4.26) and MQ (not shown) radius-time plots of the 400 mb \bar{u}_L also depict this mid-level inflow maximum. This strong, high-level inflow may be caused by the enhanced EFC in the forcing period, and, as proposed by Pfeffer and Challa (1981), may have contributed to strengthening the transverse circulation, and the subsequent storm intensification.

The pressure-radius pattern of the EFC changes significantly during the contraction phase. Whereas the EFCs in the forcing phase were strongly positive in the upper troposphere out to 1500 km, the regions of positive EFC become "patchy" and isolated after 00 UTC 15 September (e.g., Figure 4.27). Regions that are positive are generally weaker than the values observed during the forcing phase. The radius-time plot of 200 mb EFC (Figure 4.14a) shows the inward propagation of an EFC maximum from 600 km at 18 UTC 14 September to within 350 km of the storm center by 12 UTC 15 September.

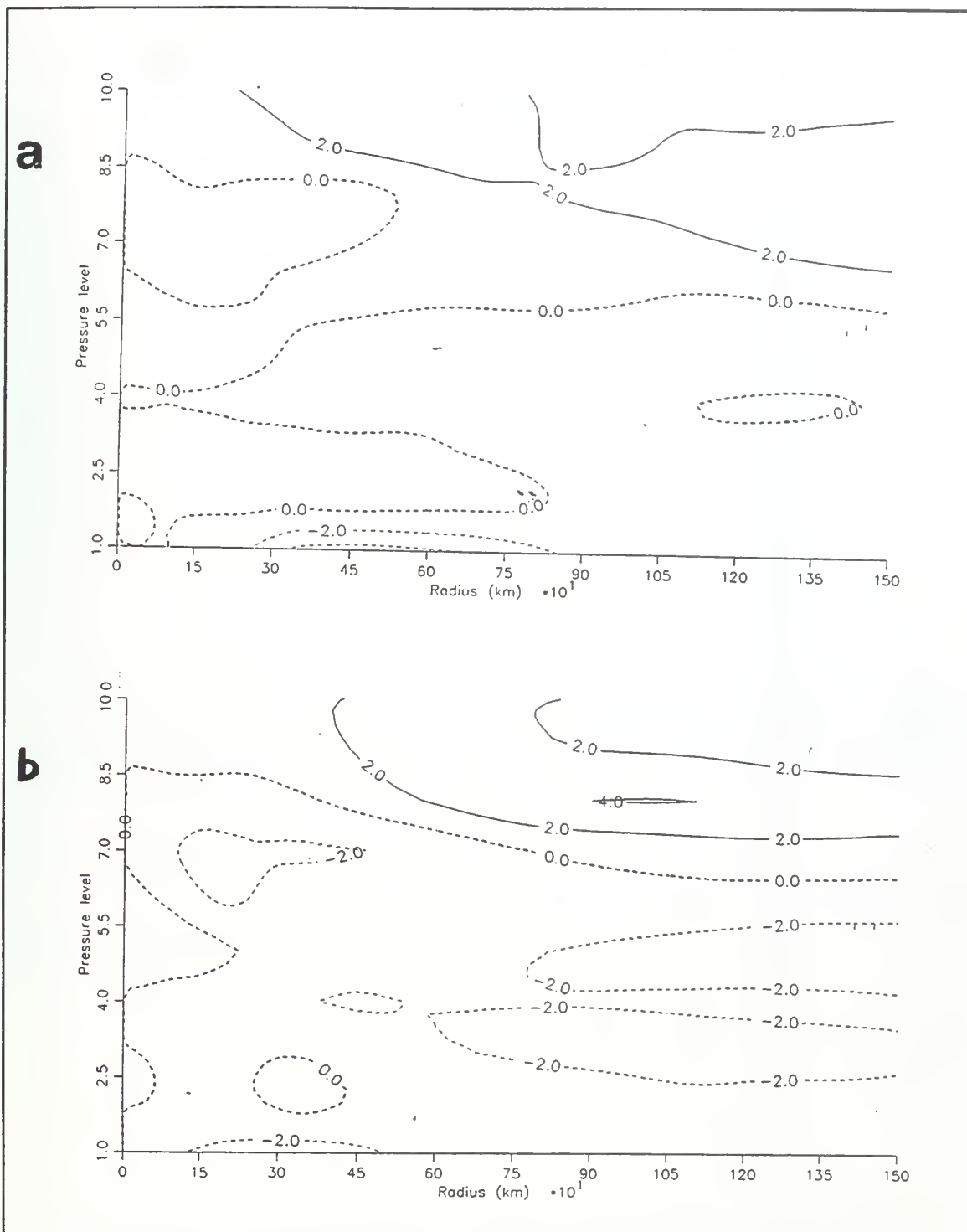


Fig. 4.25 Radial wind as in Figure 4.11, except at 00 UTC 15 September as calculated by (a) 4DDA analysis and (b) MQ analysis. Note the unusually high levels of both inflow and outflow.

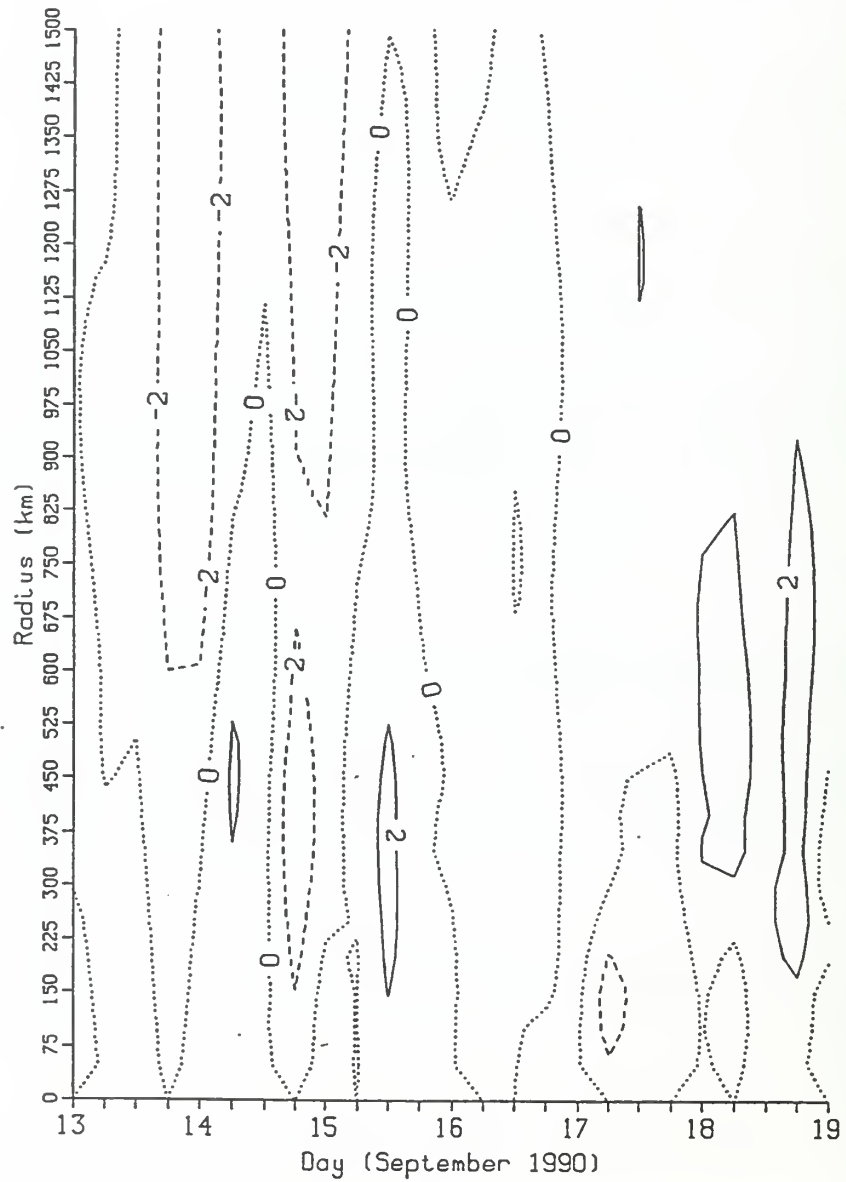


Fig. 4.26 Radial wind as in Figure 4.10, except at 400 mb, as calculated by MQ analysis.

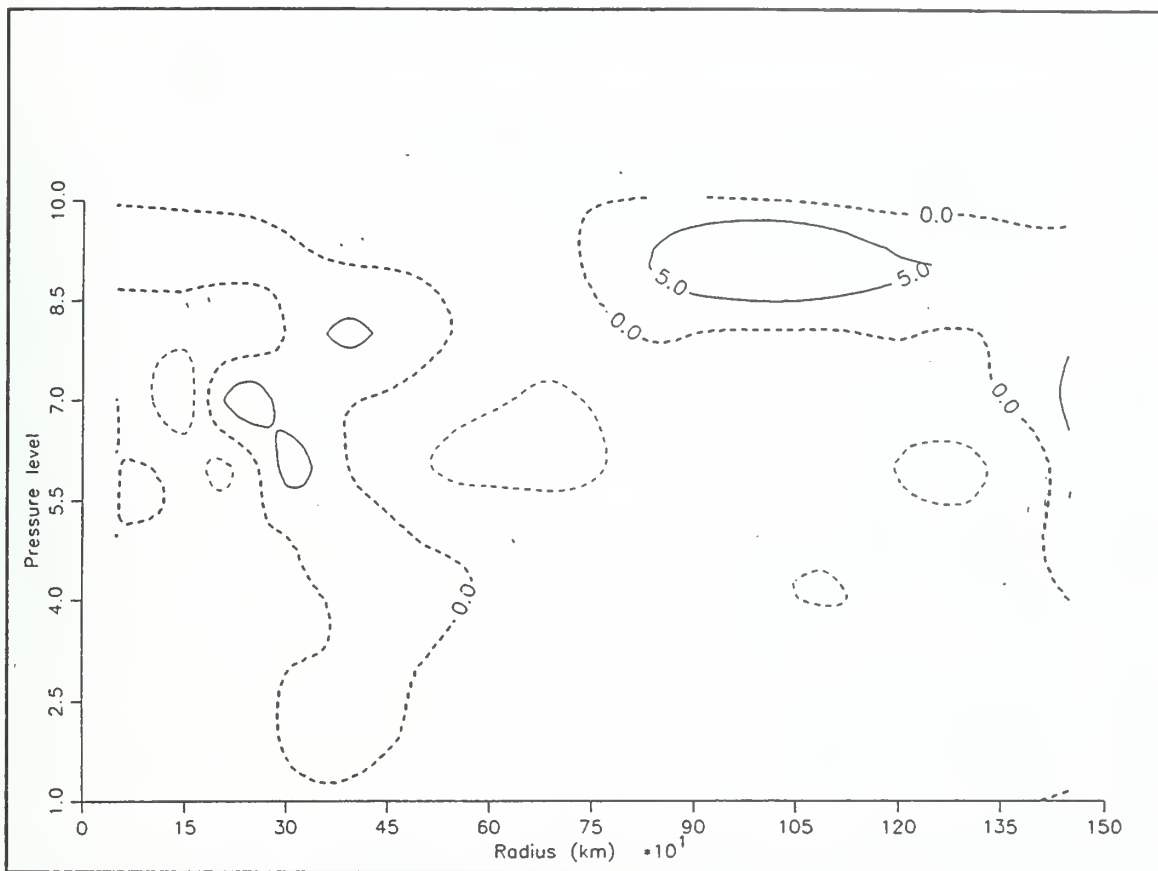


Fig. 4.27 EFC values as in Figure 4.16, except at 12 UTC 15 September as calculated by MQ analysis.

The vertical wind shear between 850 and 200 mb (Figure 4.18) actually **increases** throughout this period, although the magnitude remains well below the 12.5 m s^{-1} threshold discussed by Zehr (1992). The vertical wind shear magnitude increases from 3 m s^{-1} to about 7 m s^{-1} by 12 UTC 15 September. Despite the difficulties in precisely measuring vertical shear magnitudes, neither the MQ nor 4DDA analyses show the anticipated decrease in wind shear immediately prior to Flo's rapid intensification. This observation provides evidence that wind shear, once below a given

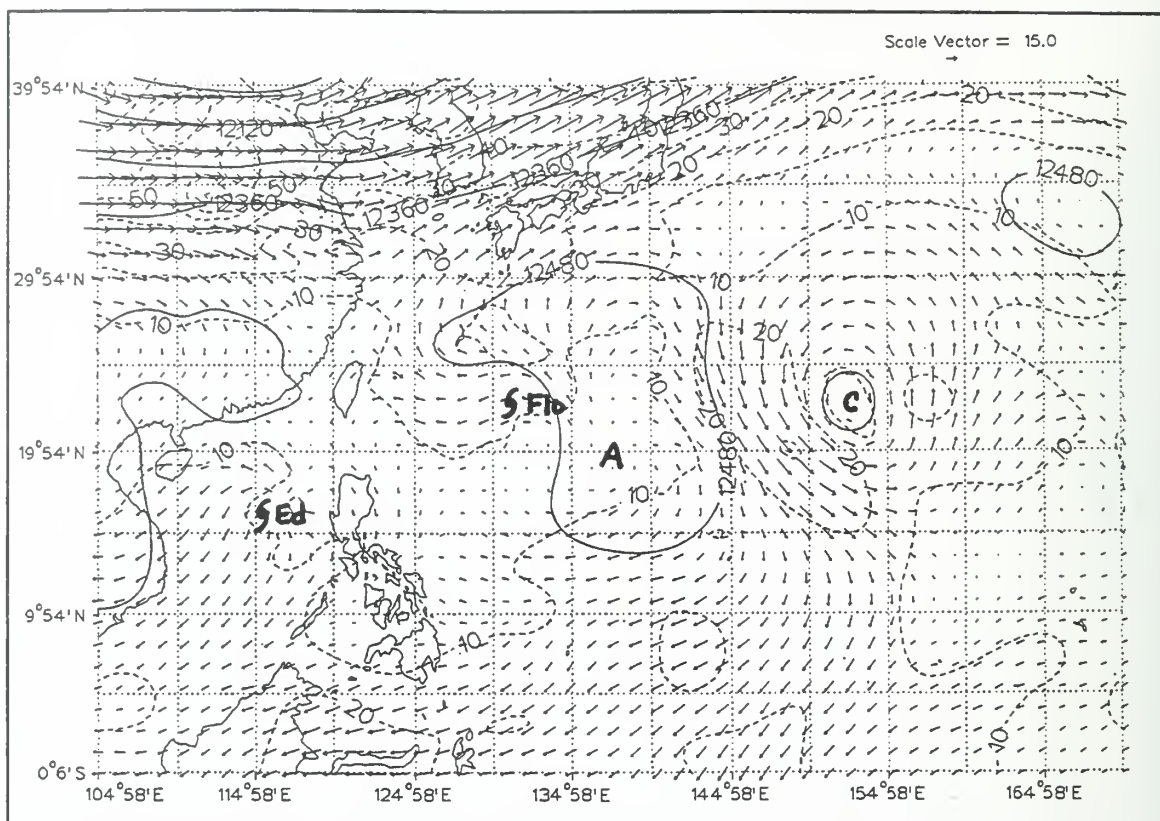


Fig. 4.28. MQ analysis of 200 mb wind, isotach, and height fields at 00 UTC 16 September. Symbols and contour intervals as in Figure 4.4.

threshold, may not be the significant factor in the likelihood of a tropical cyclone to intensify rapidly .

(2) Rapid Intensification Phase. Between 18 UTC 15 September and 12 UTC 16 September, Flo rapidly intensified from 44 m s^{-1} to 65 m s^{-1} . That is, Flo intensified 48% in 18 h. Surprisingly, little evidence is found of upper-tropospheric dynamic reaction to this significant increase in surface wind speed.

The 200 mb total wind fields, as depicted in both the 4DDA (not shown) and MQ (Figure 4.28) analyses, show little variation through 00 UTC 16

September. The dominant features remain the TUTT cell now 2200 km east-southeast of Flo, an anticyclone 700 km southeast of Flo, and the mid-latitude jet over the Yellow Sea and Korean Peninsula. After 00 UTC, the interaction between Flo's outflow and the mid-latitude jet 1000 km to the north increases significantly, and the flow from the typhoon to the TUTT cell east of Flo becomes more meridional.

Previous research (e.g., Sadler 1978) has suggested that relative position of a tropical cyclone to either a TUTT or mid-latitude trough may be important for intensification. These larger scale features would provide an efficient outflow channel(s) to remove mass and heat from the upper-troposphere near the storm core.

While the mid-latitude trough may be providing an outflow "channel of opportunity" for Flo, it is difficult to find quantitative evidence in the wind or EFC fields of the mid-latitude trough impact on Flo at 12 UTC 16 September, 18 h after the commencement of rapid intensification. The 4DDA \bar{v}_L , \bar{u}_L , and EFC fields (Figures 4.29b, 4.30, 4.31, respectively) do not show any change in their quiescent character at the radius of the mid-latitude trough (~ 1000 km). The winds are anticyclonic with uniform $2\text{--}4\text{ m s}^{-1}$ outflow above 250 mb and the EFC values are mostly less than $4\text{ m s}^{-1}/\text{day}$.

Fortunately, the NASA DC-8 aircraft observed Flo's outflow layer at 06 UTC 16 September. The 200 mb wind observations, (Figures 3.13, 4.32) depict a well-defined cyclonic circulation with winds in the eyewall up to 33 m s^{-1} . Such upper-tropospheric measurements are consistent with aircraft observations in strong tropical

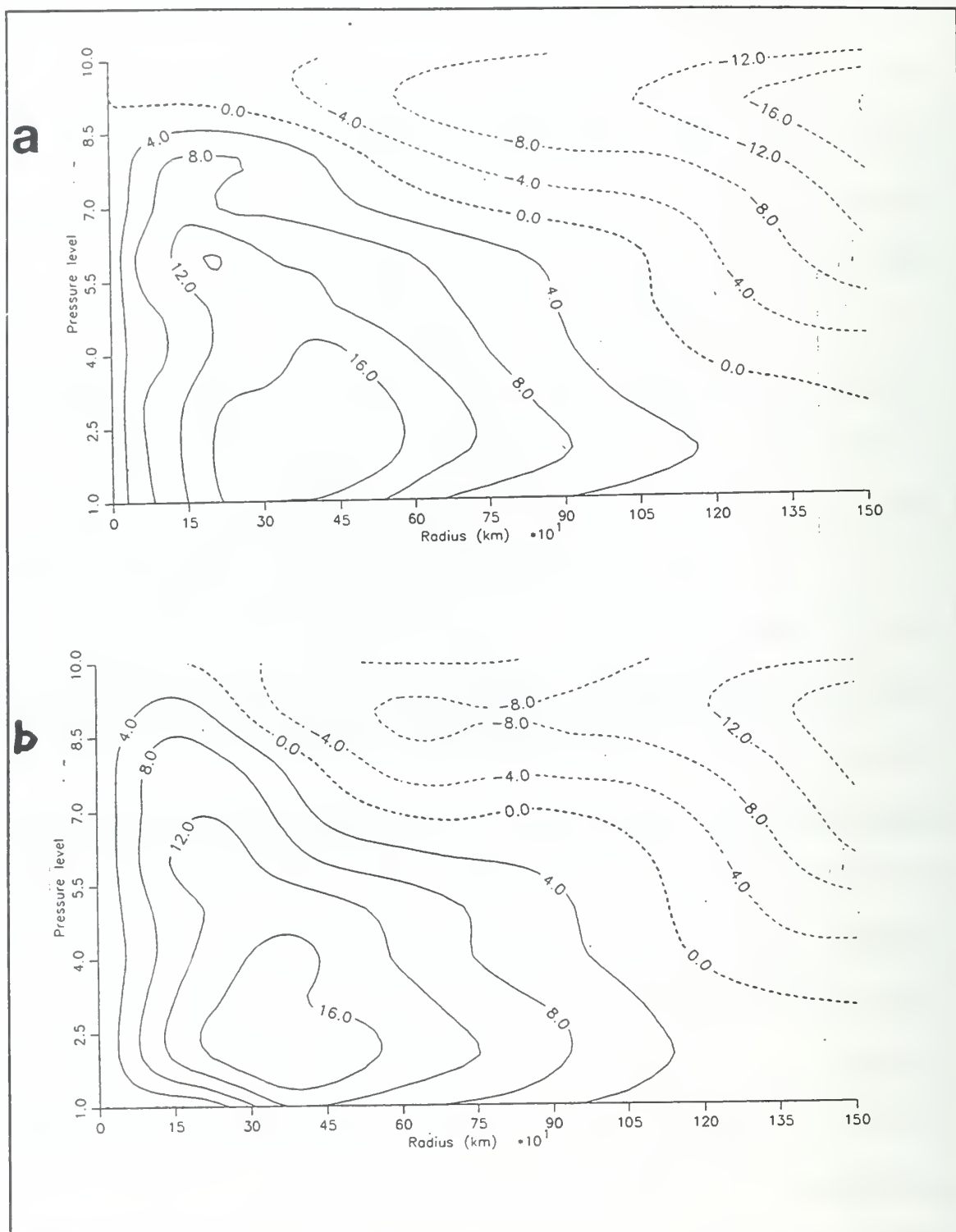


Fig. 4.29. Tangential winds as in Figure 4.7, except at 12 UTC 16 September, as calculated by (a) MQ analysis, and (b) 4DDA analysis.

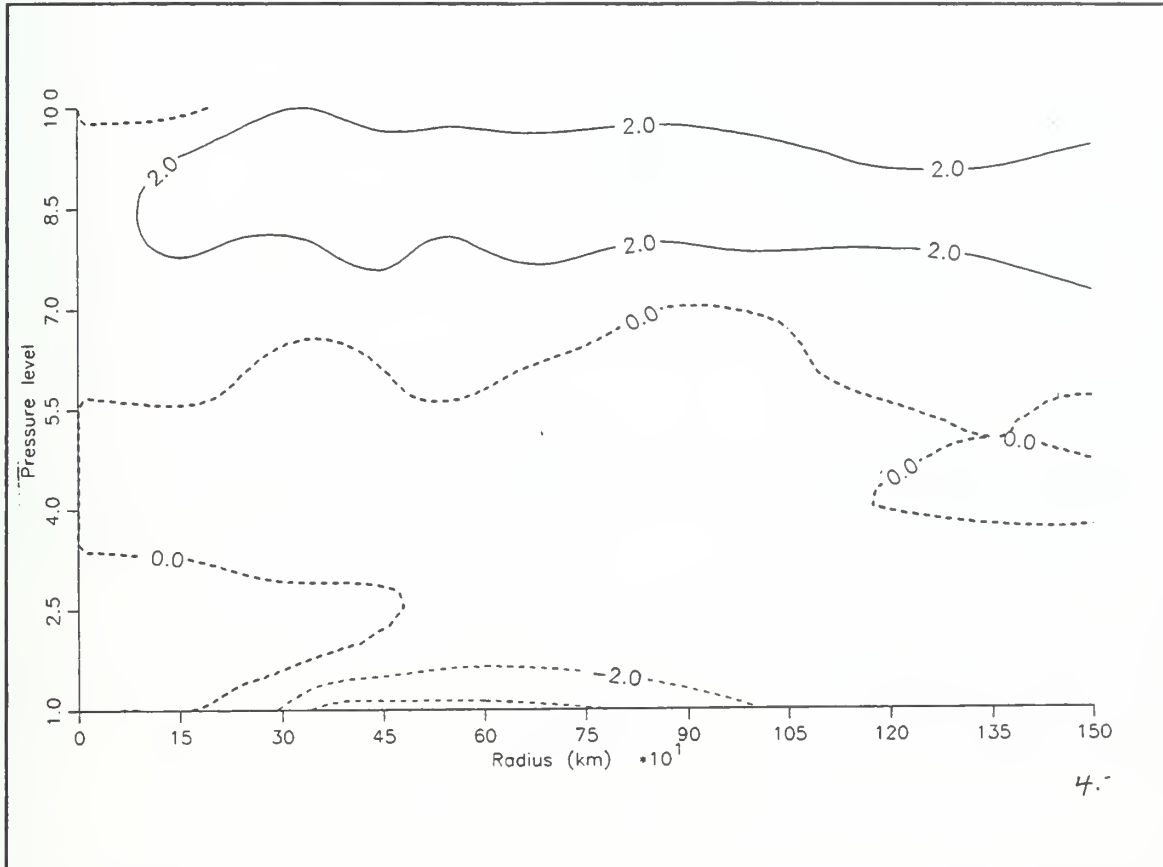


Fig. 4.30. Radial winds as in Figure 4.11, except at 12 UTC 16 September, as calculated by 4DDA analysis.

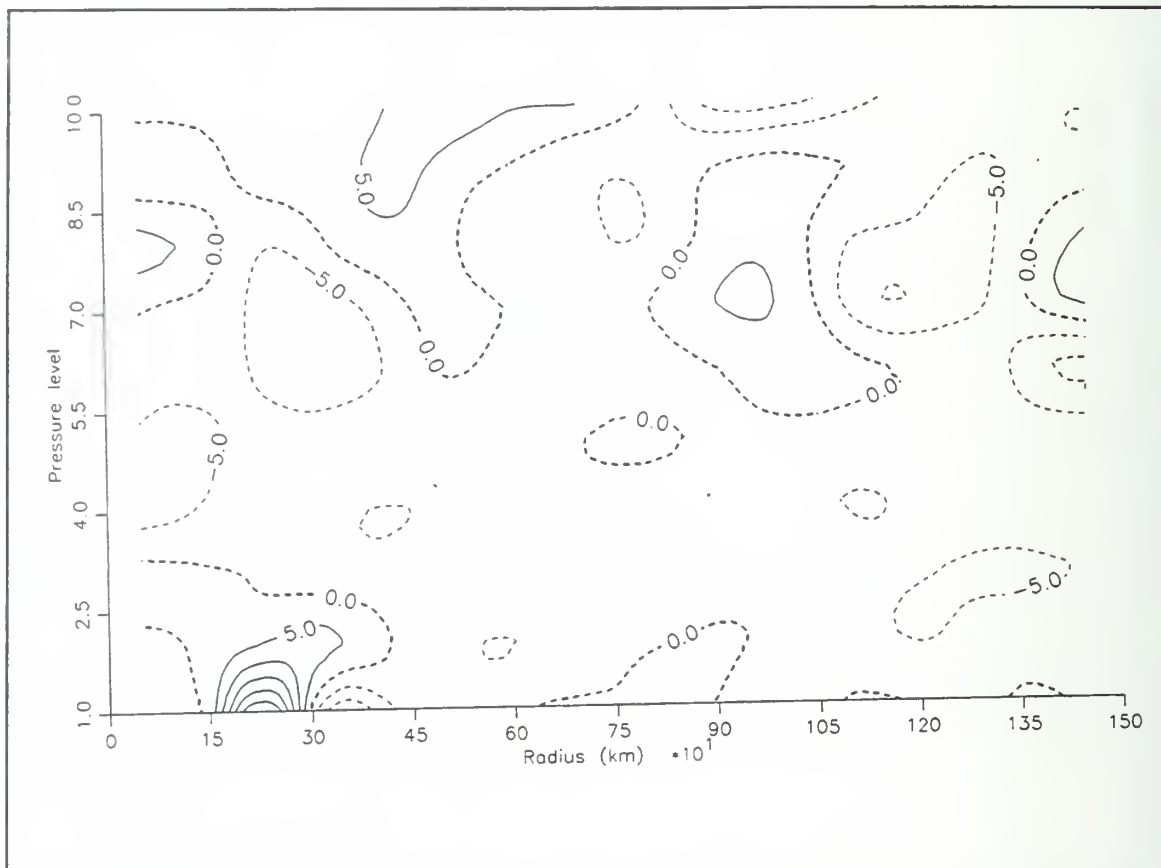


Fig. 4.31. EFC values as in Figure 4.16, except at 12 UTC 16 September, as calculated by 4DDA analysis.

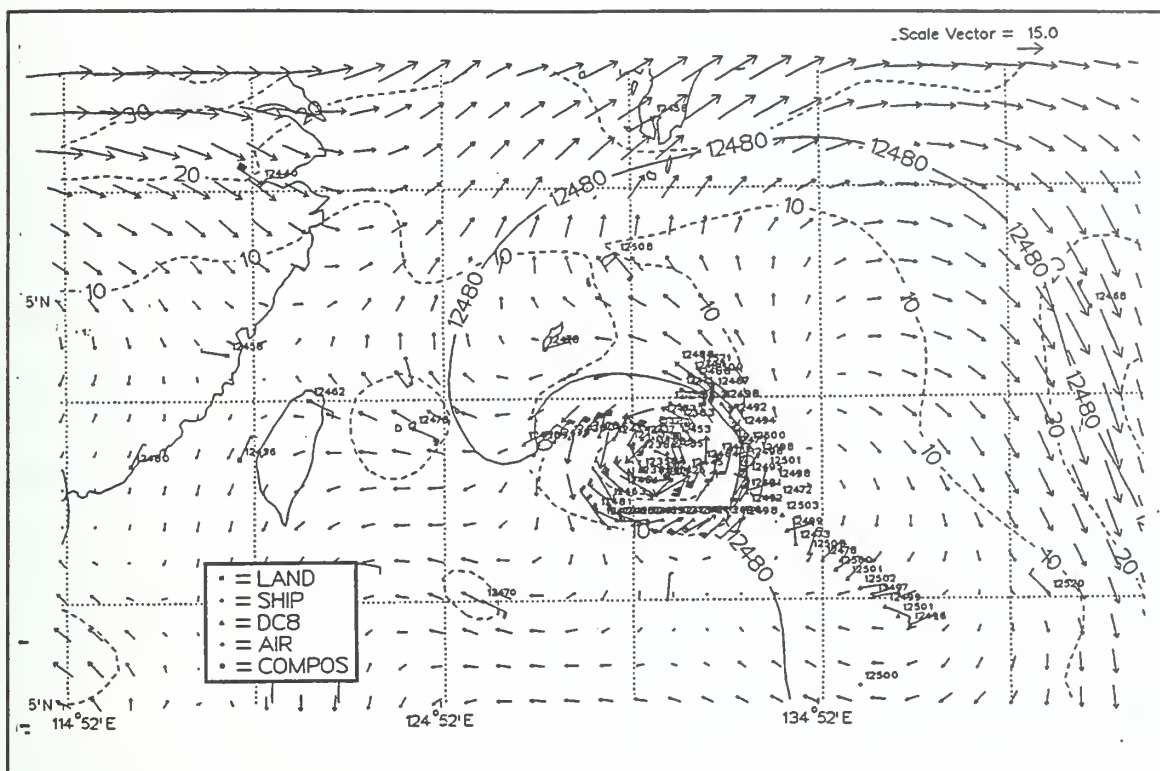


Fig. 4.32. 200 mb observations and MQ analysis isotach and height fields at 06 UTC 16 September. Contour intervals as in Figure 4.4. Types of observations (see inset for symbols) are as in Figures 2.1 and 2.2.

cyclones in other basins (e.g., Hawkins and Rubsam 1968), and indicate low tangential vertical wind shear near the center of Flo. The DC-8 observations also depict well the 200 mb anticyclone about 300 km east-southeast of Flo.

The \bar{v}_L values continue to contract the cyclonic winds towards Flo in the upper troposphere. The 0 m s^{-1} isopleth contracts from 550 km at 12 UTC 15 September (Figure 4.24) to 450 km 24 h later (Figure 4.29a). Outer radius anticyclonic tangential winds continue to increase; the magnitude of the wind at 1500 km radius from Flo increases from 10 m s^{-1} to over 16 m s^{-1} by 12 UTC 16 September.

The influence the NASA DC-8 dropwindsondes had on the MQ analysis can be seen in a comparison of \bar{v}_L between 06 UTC 16 September and 6 h later (Figures 4.33a and 4.29a). The dropwindsonde observations provided the data required for the MQ analysis to depict the maximum winds within 200 km of the center at the surface and within 50 km (or one gridpoint) of the storm center at 200 mb. While the tangential wind maxima of 20 m s^{-1} are still significantly below the estimated storm intensity (59 m s^{-1}), small vertical shear values are found between the lower troposphere and the outflow layer, which is a characteristic of intense tropical cyclones. When the DC-8 dropwindsonde observations are not available (e.g., 12 UTC 16 September), the lower tropospheric wind maximum is depicted over 300 km from the center.

A comparison of the 4DDA analyses of \bar{v}_L for the same times (Figures 4.33b and 4.29b) shows some of the strengths and limitations of the OI-based analysis compared to the MQ analysis. While the 4DDA analysis of \bar{v}_L at 06 UTC depicts a smoother vertical structure than the MQ analysis, the 4DDA analyzes the lower-tropospheric wind maximum 300 km from the center, and the upper-tropospheric maximum is 150 km from the storm center. Also the maximum magnitude of \bar{v}_L at 200 mb is analyzed at 10 m s^{-1} , which is one-half the Multi-quadric analysis-analyzed magnitude. However, the 4DDA analysis provides greater consistency in vertical structure, and is able to use the available observations to influence the analysis above 200 mb. This difference is apparent when comparing Figures 4.33 a and b. However, the differences in the two analyses beyond 300 km are slight.

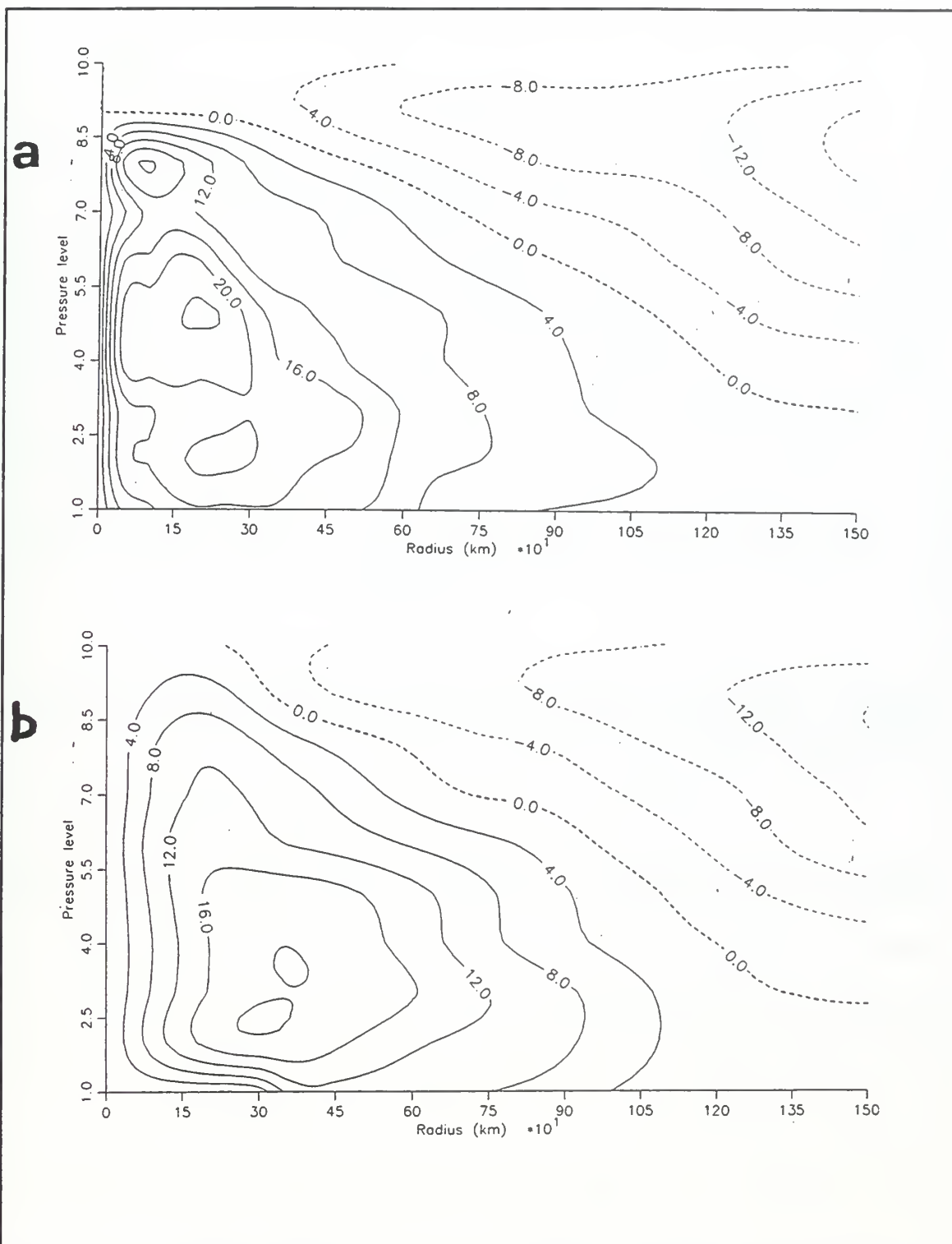


Fig. 4.33. Tangential winds as in Figure 4.7, except at 06 UTC 16 September, as calculated by (a) MQ analysis, and (b) 4DDA analysis.

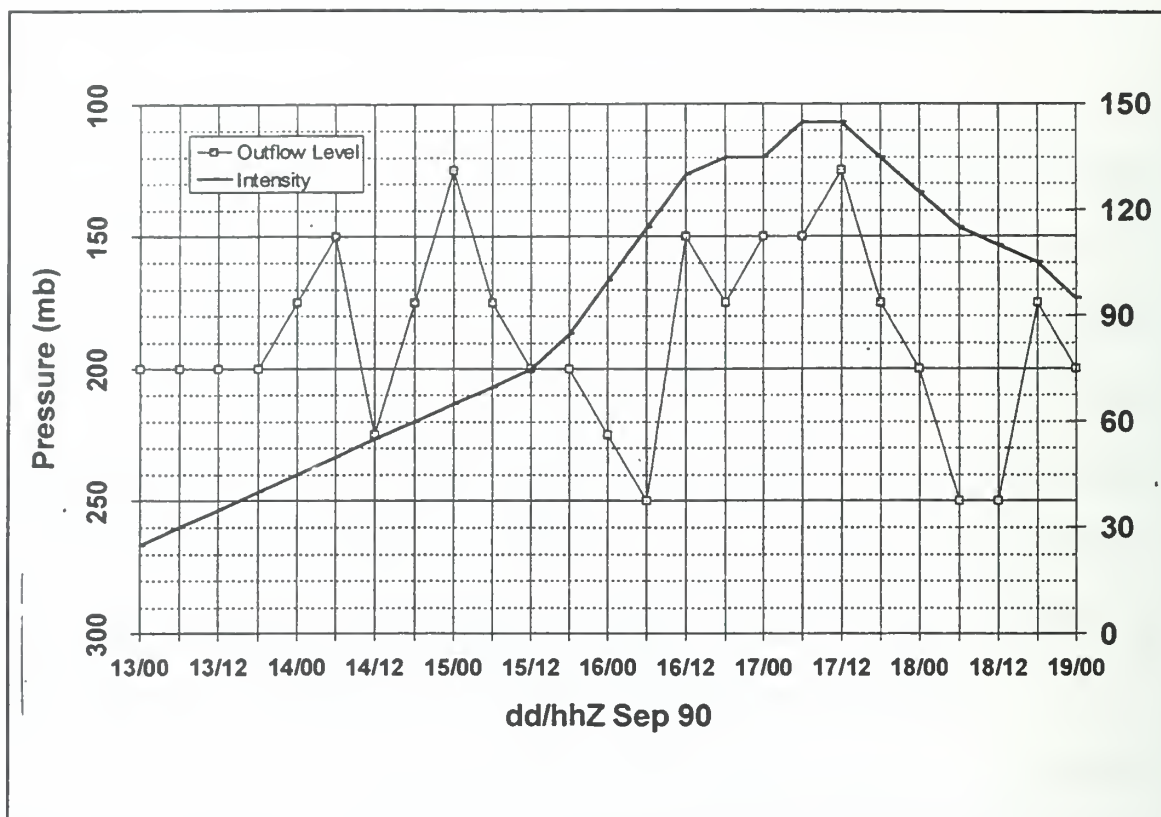


Fig. 4.34. Height (mb) of outflow (\bar{u}_L) at 450 km radius from Typhoon Flo. Storm intensity (heavy solid) is given on right vertical axis.

While the upper-tropospheric tangential wind profile changed little during Flo's rapid intensification, the upper-tropospheric radial winds (\bar{u}_L) exhibited significant variations with time (Figure 4.34). At 12 UTC 15 September (not shown), the primary outflow layer has lowered to 200 mb, with maximum outflow $> 5 \text{ m s}^{-1}$ at radii between 300 and 500 km from Flo. By 18 UTC, the magnitude of the outflow increased to greater than 5 m s^{-1} between 250 and 750 km from Flo on the 4DDA analysis (Figure 4.35b), while the MQ analysis (Figure 4.35a), unconstrained by dynamics, has an outflow magnitude $> 8 \text{ m s}^{-1}$ at the 450 km radius.

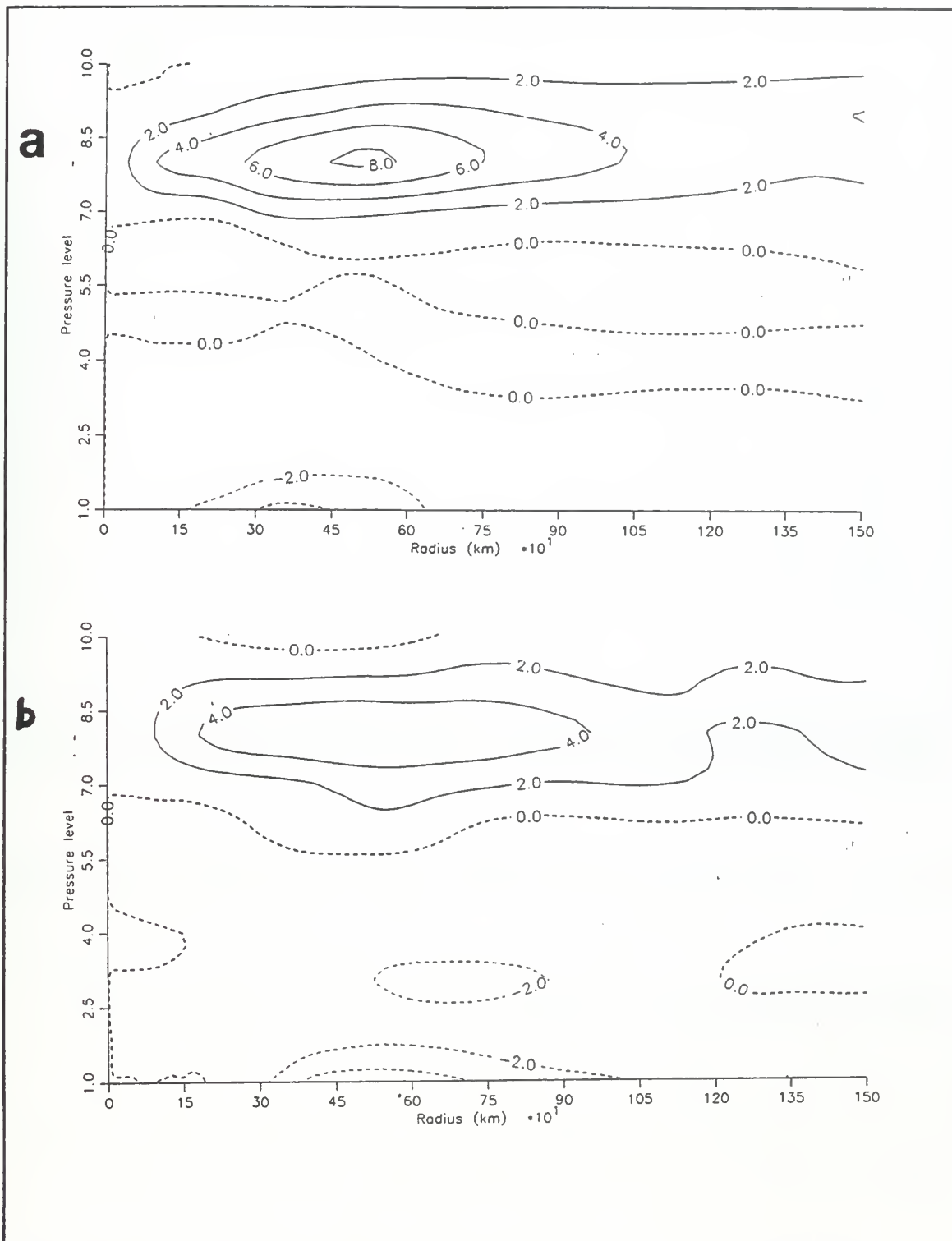


Fig. 4.35 Radial winds as in Figure 4.11, except at 18 UTC 15 September, as calculated by (a) MQ analysis, and (b) 4DDA analysis.

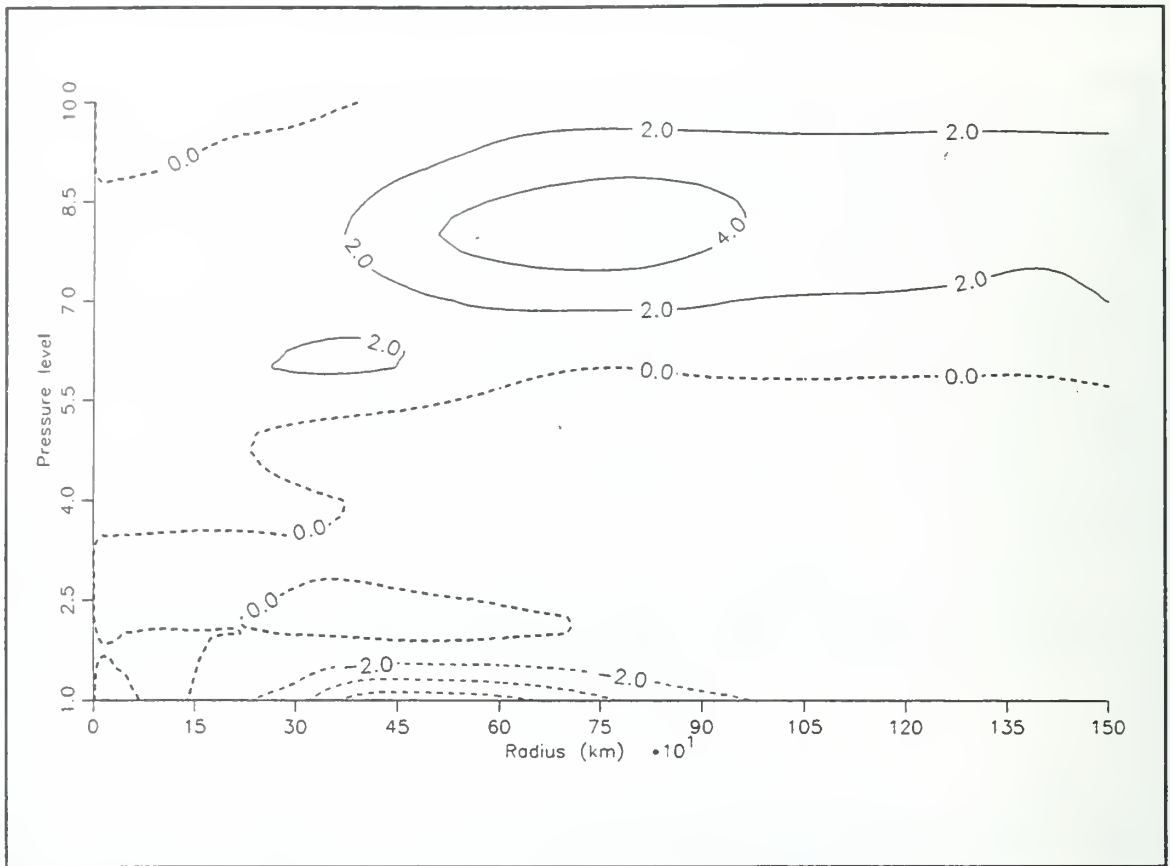


Fig. 4.36. Radial winds as in Figure 4.11, except at 00 UTC 16 September, as calculated by 4DDA analysis.

At 00 UTC 16 September (Figure 4.36), the main outflow channel has lowered to 300 mb, then rose to 200 mb at 600 km from the storm. This pattern continued through 06 UTC. By 12 UTC 16 September (Figure 4.30), the outflow level had again risen to about 150 mb. This time variation in the vertical structure of the outflow has been previously documented for Flo during the Super Typhoon stage (Merrill and Velden 1996). However, this vertical oscillation in Flo's outflow appears to have

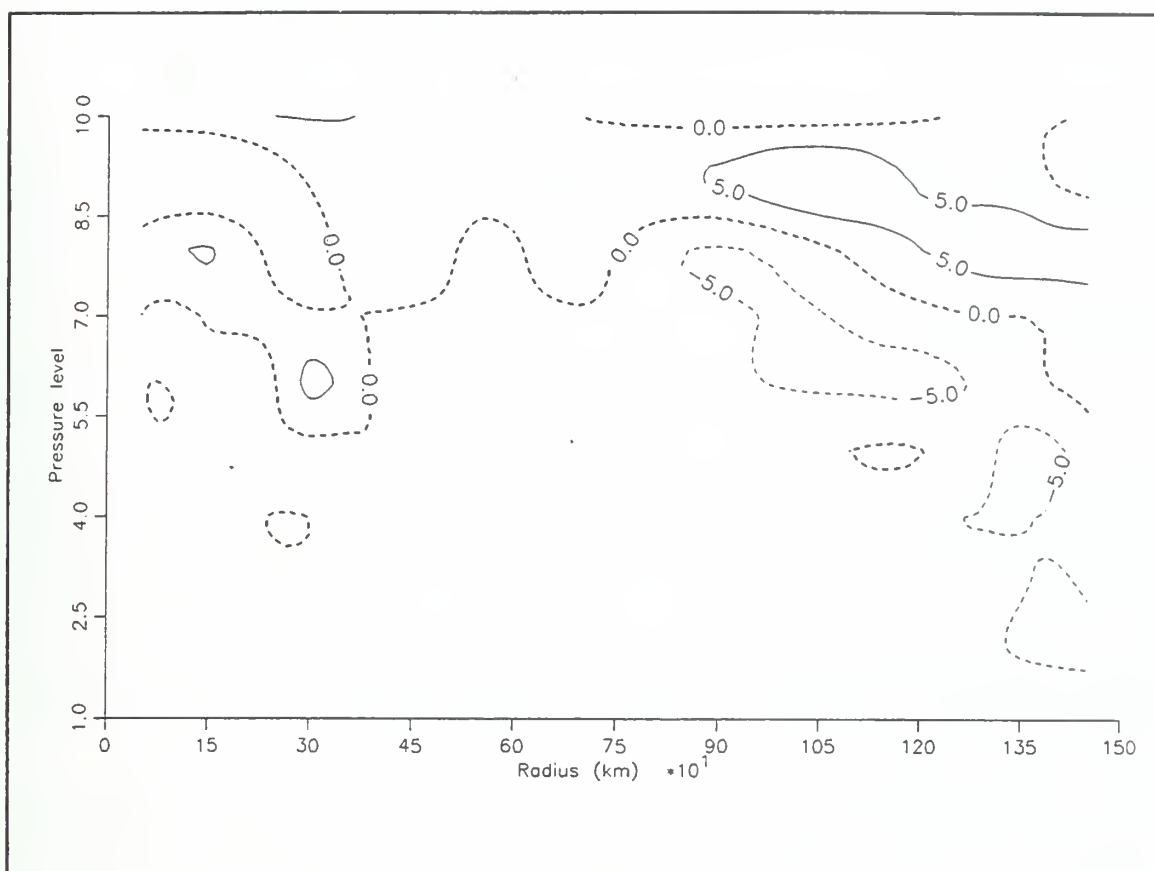


Fig. 4.37. EFC values as in Figure 4.16, except at 00 UTC 16 September, as calculated by MQ analysis.

occurred throughout Flo's existence, not just in the rapid intensification and Super Typhoon phases.

The EFC pattern (e.g., Figures 4.31, 4.37) continues as described in the contraction phase. That is, areas of positive EFC are isolated (in both time and space), and weaker than those observed in the forcing phase (e.g., Figure 4.16). The EFC maximum that was between 800 and 1000 km during the forcing phase probably reached the center of Flo by 00 UTC 16 September (Figure 4.14a). While this inward

shift (first described by Molinari and Vollaro 1989) is evident in the forcing and contraction phase, the positive EFC is not clearly evident at 18 UTC 15 September. This inward shift of positive EFC is also evident in the MQ analysis (Figure 4.14b), but is difficult to follow in parts of the contraction phase and during the early portion of the rapid intensification phase.

Several explanations for this lack of temporal continuity in the EFC calculations are briefly explored: lack of data to describe adequately the upper-tropospheric wind fields; the analysis scheme not "drawing to" the observations; error in the analysis field; and interaction with Flo's convection. The observations at 200 mb (Figure 4.38) have good spatial coverage, primarily because of the reprocessed cloud-track winds. These observations are especially plentiful in an arc around Flo that extends from the southwest clockwise to the east. The available data should be sufficient to capture any eddy flux interaction between Flo and either the anticyclone or TUTT cell to the east or the jet to the northwest. Both the 4DDA (not shown) and MQ (Figure 4.38) analyses for 18 UTC 15 September have assimilated the available observations with no obvious differences between the analyses and the observations.

Molinari and Vollaro (1989) showed how sensitive eddy momentum flux calculations are as a function of radius from the storm. Due to an area-weighted calculation performed on a cylindrical grid, noise in the data is damped as function of the radius squared. Using typical rawinsonde speed and direction errors, Molinari and Vollaro showed that EFC values within 300 km of a storm were questionable, data

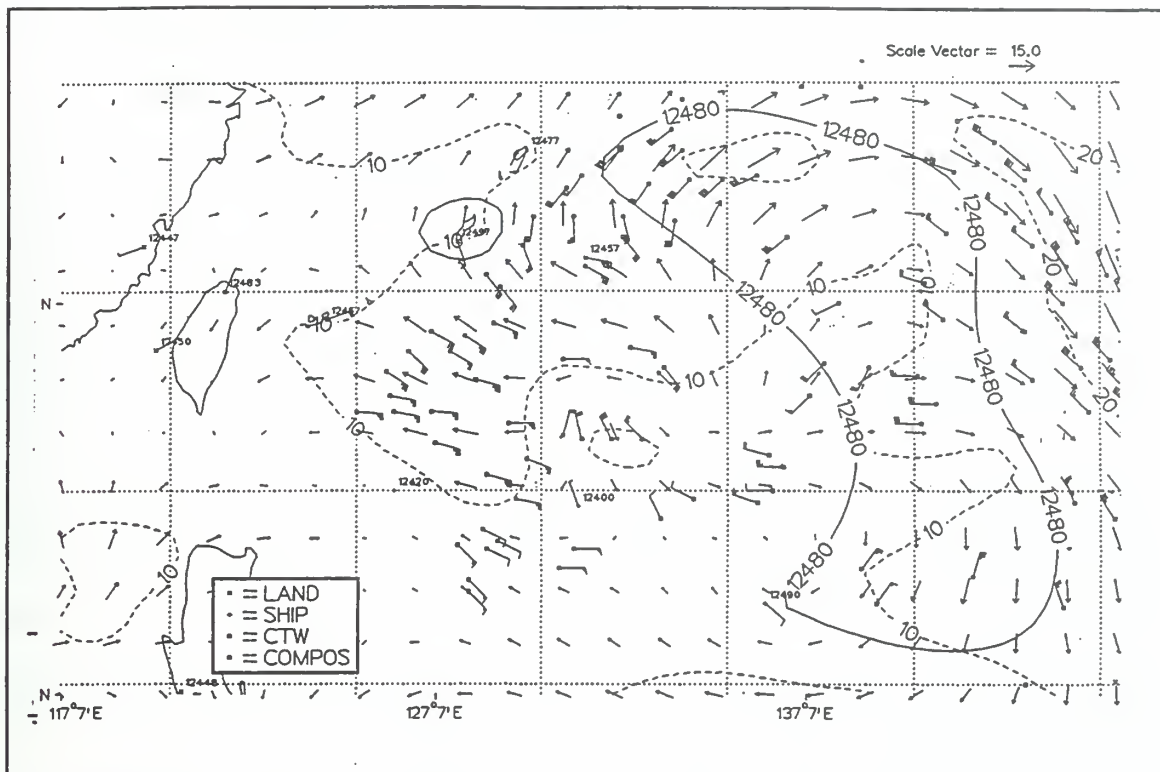


Fig. 4.38. MQ analysis at 200 mb as in Figure 4.32, except at 18 UTC 15 September.

between 300-800 km should be interpreted with caution, and EFM RAM values beyond 800 km were the most reliable. The radius-time plots of EFC for both the 4DDA and MQ analyses (Figures 4.14a-b) show most of the "noise" appears to be inside of 200 km, which is consistent with Molinari and Vollaro's calculations.

Even if one could remove the errors in the observations and analyses, an open question is how EFC interacts with the outer rainbands surrounding the eyewall. While this study does not attempt to address that question, it should be kept in mind when interpreting EFC calculations within 300-500 km of Flo's center.

In summary, calculations of EFC at small radii (< 300 km) should be interpreted with substantial caution. Even where multiple (primarily reprocessed cloud-track wind) observations are at present and the analyses "drew to" the observations, the error in these observations may cause significant variation in the EFC calculations. Also, the dynamics of the interaction between the EFC and the outer convection bands is not known. So while the inward shift in EFC described above may have contributed to Flo's rapid intensification, it is not possible to validate conclusively that hypothesis. Even with detailed, high resolution upper-tropospheric wind measurements as in this study, the exact relationship between EFC and subsequent tropical cyclone intensity changes remains elusive. This analysis based upon the TCM-90 dataset removes the possibility that the reason for conflicting conclusions regarding the role of EFC is due to a lack of upper-tropospheric observations. Instead, it appears that the underlying interactions between the EFC and the tropical cyclone are indirect and potentially complex.

The 850 mb - 200 mb vertical wind shear (Figure 4.18) decreases sharply from 7 m s^{-1} at 12 UTC 15 September to less than 3 m s^{-1} just 6 h later. The 850 - 200 mb wind shear remains at 2 to 3 m s^{-1} through 06 UTC 16 September, then increases to between 3 (Multi-quadric analysis) and 5 (4DDA) m s^{-1} at 12 UTC. These low vertical shear values are consistent with the widely published model of tropospheric wind shear inversely correlated to tropical cyclone formation and intensification (e.g., Simpson *et al.* 1969, Gray 1975, DeMaria *et al.* 1993). However, the discussion of

Typhoon Ed will document similarly small ($< 5 \text{ m s}^{-1}$) values of vertical wind shear with little or no increase in storm intensity. In summary, low tropospheric wind shear appears to be a necessary, but not sufficient condition for tropical cyclones to intensify rapidly over open, warm waters.

Of note were the wind shear magnitudes between 300 and 150 mb (Figure 4.19). During Flo's rapid intensification, these values fell from 5 to about 2 m s^{-1} . In fact, the upper tropospheric (300 mb to 150 mb) wind shear is highly inversely correlated (-0.92) to the intensity from the time Flo reached typhoon strength (00 UTC 15 September) until the storm attained peak intensity (06 UTC 17 September). While this decrease in wind shear is not a precursor of rapid intensification, such a negative correlation was not observed between Ed's upper-tropospheric vertical wind shear and intensity. In fact, the correlation between Ed's upper-tropospheric vertical shear and intensity between the time Ed reached typhoon strength (00 UTC 14 September) and Ed's maximum intensity (45 m s^{-1} at 00 UTC 17 September) was weakly positive (0.23). Physically, Flo's negative correlation of intensity with vertical wind shear can be interpreted as evidence of the cyclonic circulation building up to the tropopause as the storm intensified, thus providing a uniform flow (i.e., low vertical shear) in the 300 - 150 mb layer. This high-level, uniform cyclonic circulation appeared to not occur with Ed.

c. *Super Typhoon Phase (12 UTC 16 September through 18 UTC 17 September)*

In contrast to the quiescent phase, Flo's intensity in the Super Typhoon Phase varied only between 67 and 75 m s⁻¹. However, significant changes occurred in the upper-tropospheric wind field, and the associated EFC. The interaction between Flo's outflow and the mid-latitude trough to the northwest increased throughout the period. By 18 UTC 17 September, the trough had become the primary large-scale feature with which Flo interacted. The outflow jet again rose to the 150 mb level and \bar{u}_L increased in magnitude from 3-5 m s⁻¹ at 12 UTC 16 September (Figure 4.37) to 6-8 m s⁻¹ 24 h later (Figure 4.39). Whereas 200 mb EFC magnitudes are less than 8 m s⁻¹/day at the beginning of the phase (Figure 4.31), EFC had increased to 12 (24) m s⁻¹/day by the end of the Super Typhoon Phase, as calculated by the 4DDA (MQ) analysis (Figure 4.40). Unlike the large EFC values for Flo that were confined to the upper-troposphere in the forcing phase, these strongly positive EFCs had extended down through the mid-troposphere to 400 mb. That is, they are associated with the interaction of Flo and the mid-latitude trough, rather than the tropical features (i.e., trailing anticyclone and TUTT cell) with which Flo has previously interacted.

At the beginning of the Super Typhoon Phase, a substantial portion of Flo's 200-mb outflow merges with the mid-latitude jet southwest of Kyushu, then splits with the jet south of Honshu, curves anticyclonically, then flows south and cyclonically into the TUTT cell 1800 km east-southeast of Flo. Winds on the west side of the TUTT are still in excess of 30 m s⁻¹. This pattern, which is shown schematically in Figure 4.41, continues through 06 UTC 17 September (Flo's maximum intensity of 75 m s⁻¹), with the

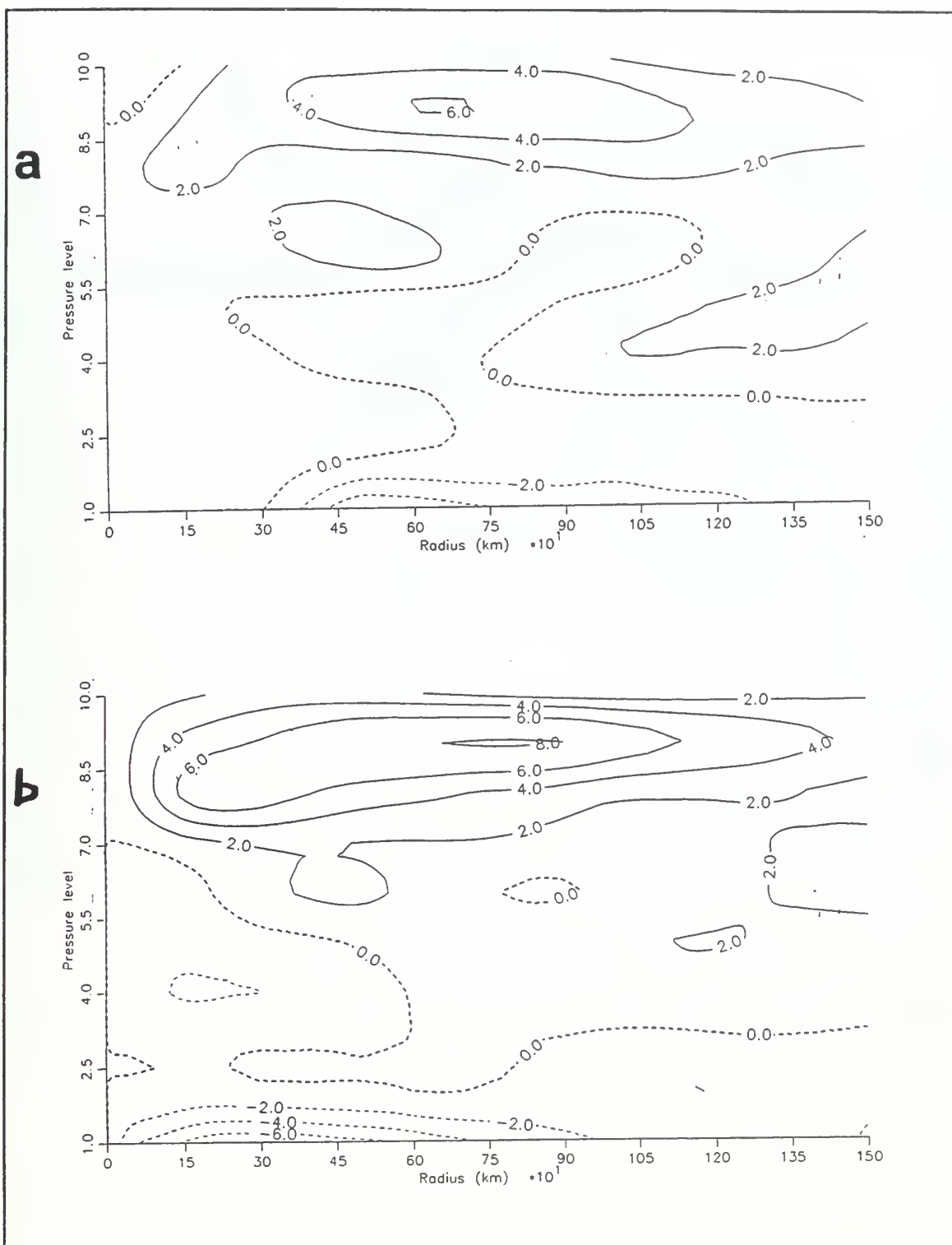


Fig. 4.39. Radial winds as in Figure 4.11, except at 12 UTC 17 September, as calculated by (a) 4DDA analysis, and (b) MQ analysis.

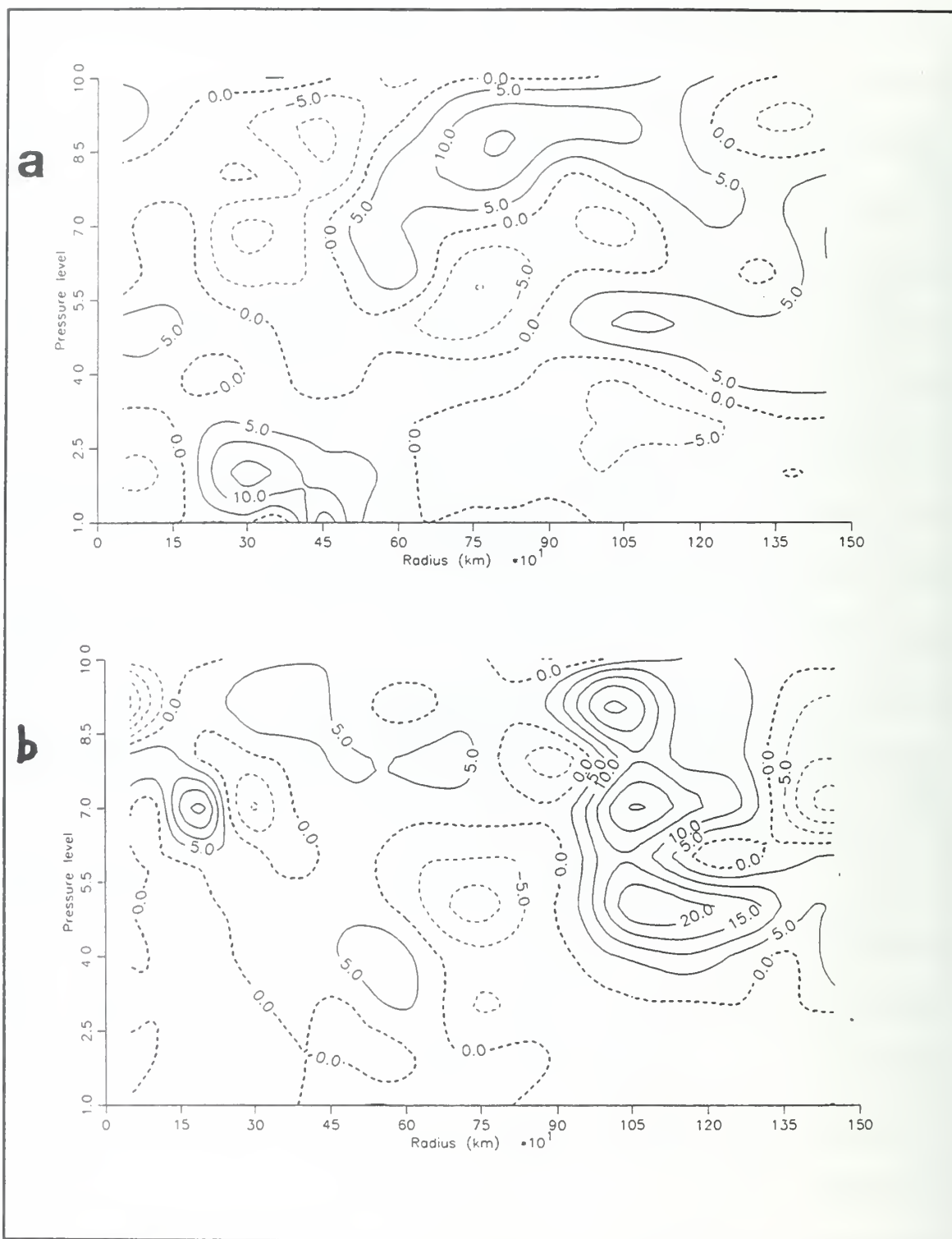


Fig. 4.40. EFC values as in Figure 4.16, except at 18 UTC 17 September, as calculated by (a) 4DDA analysis, and (b) MQ analysis.

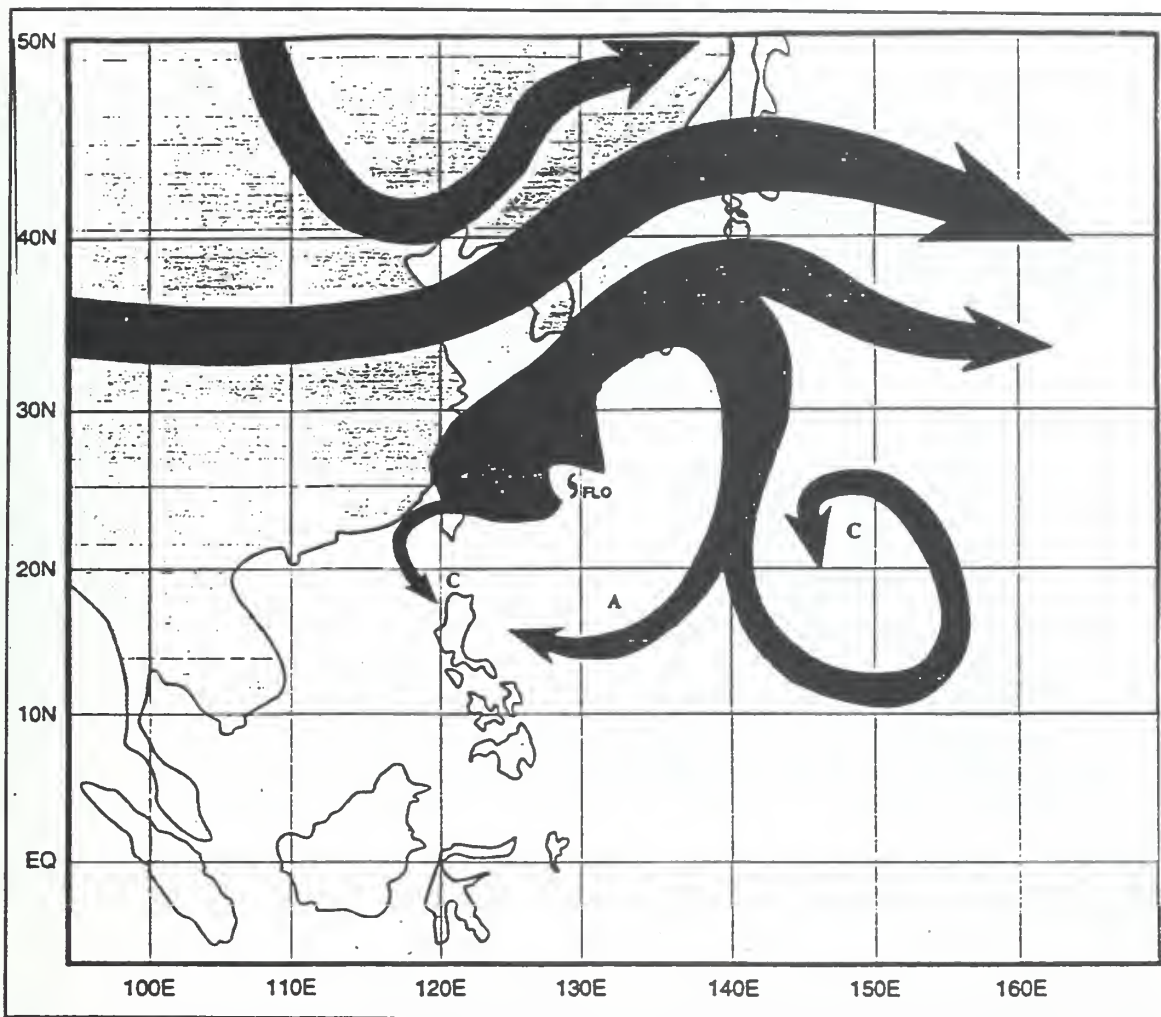


Fig. 4.41. Schematic of outflow trajectories as in Figure 4.23, except at 00 UTC 17 September.

interaction of the outflow, jet, and TUTT cell becoming increasingly meridional, and assumes an "inverted S" shape.

By 12 UTC 17 September (Figure 4.42), almost all of Flo's outflow is initially merging with the jet, before a portion of the jet splits east of Tokyo and flows south to the TUTT cell. Some of this outflow splits from the southwest quadrant of the

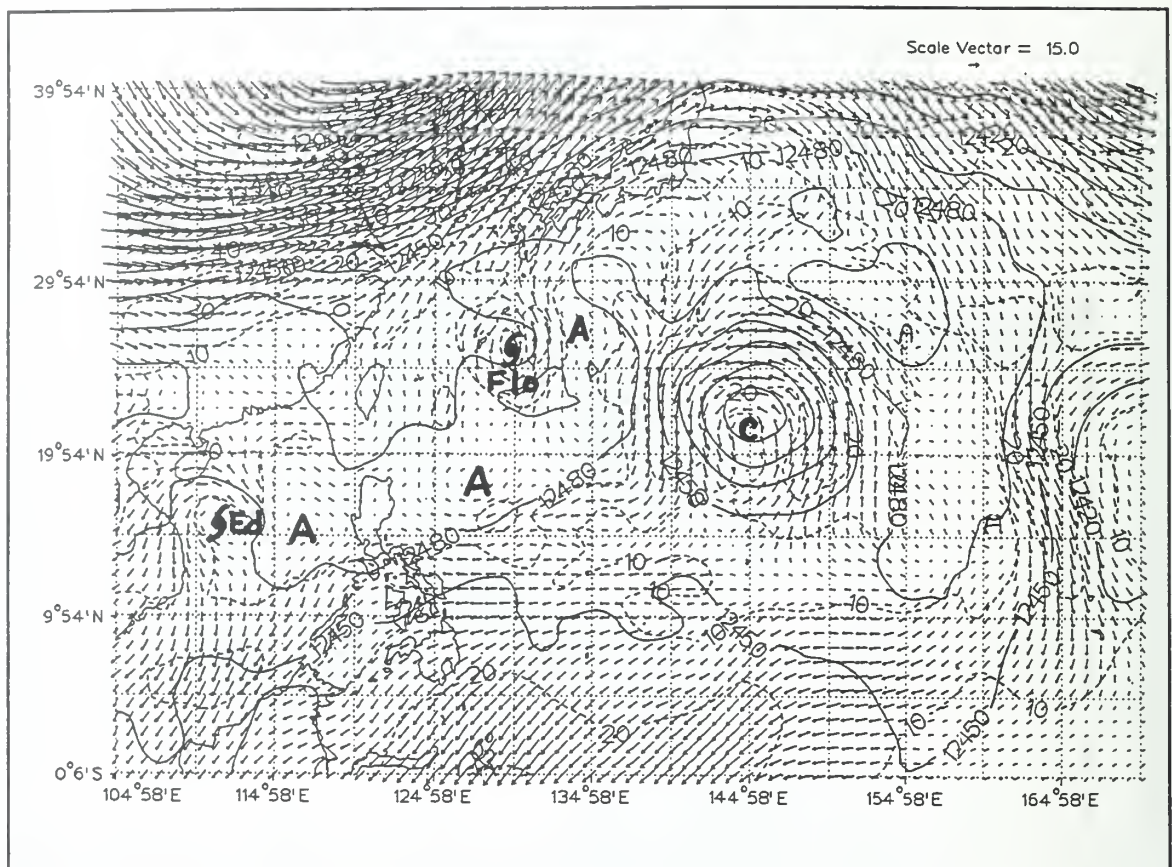


Fig. 4.42 4DDA Analysis as in Figure 4.4, except at 12 UTC 17 September.

TUTT, and flows west-southwest across the Philippine Sea and south of Flo. This is schematically shown in Figure 4.43. The greatly increased interaction between the jet and Flo's outflow between 00 and 12 UTC occurred as Flo was tracking north at 3.5 m s^{-1} , and a short-wave trough moved southeastward from Siberia and across the Yellow Sea, which caused the jet to assume a more north-south orientation. By 18 UTC, the interaction between Flo and the TUTT cell had greatly diminished, as virtually all the outflow merged with the jet and did not split off to flow around the TUTT cell.

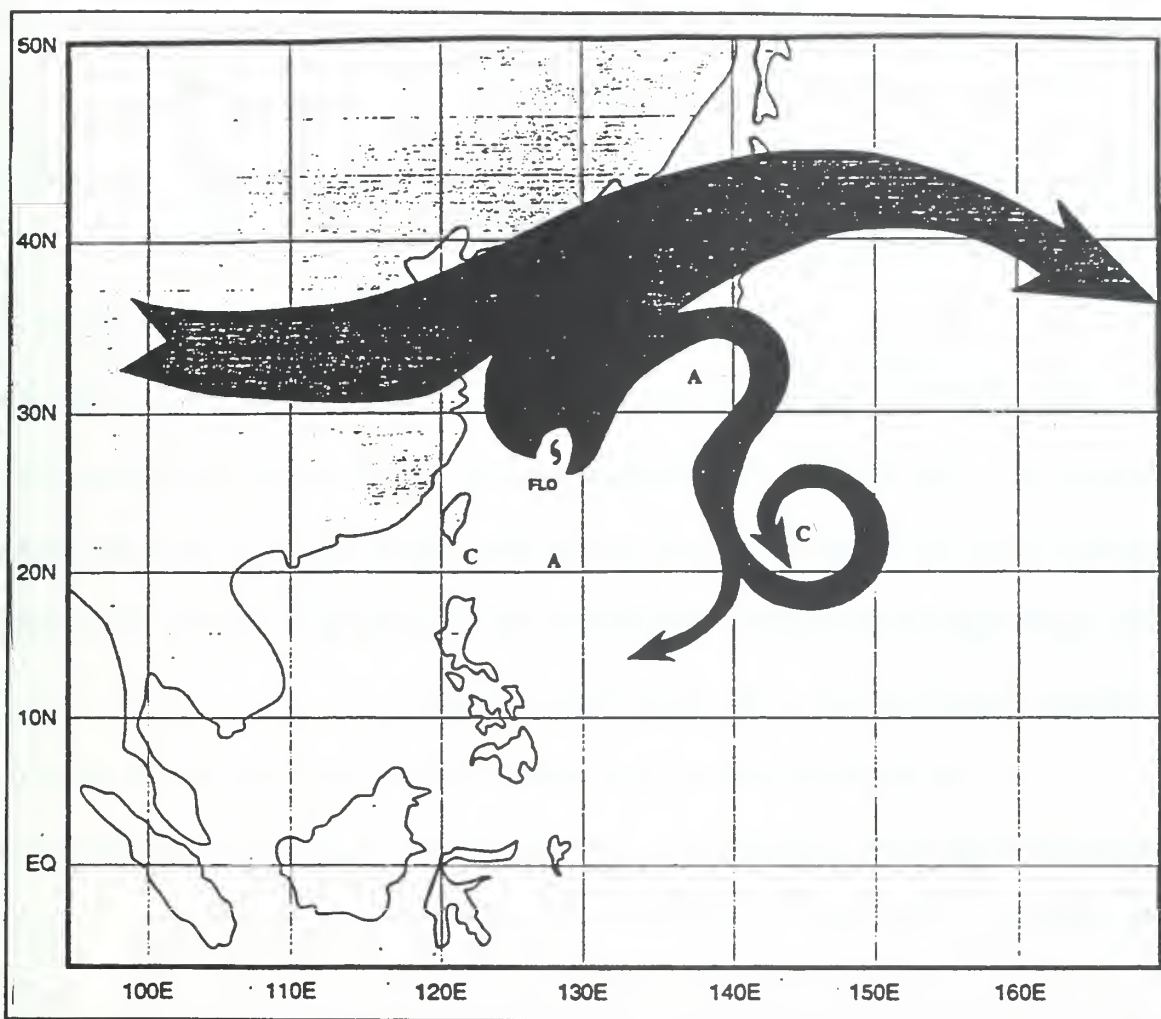


Fig. 4.43. Schematic of outflow trajectory as in Figure 4.23, except at 12 UTC 17 September.

Of note is the significant component of the wind blowing across the isoheights at 200 mb north of Flo, especially in the region of Kyushu and South Korea, even though this is north of 30°N where the atmosphere is normally in large-scale geostrophic balance. This cross-isoheight wind flow is first observed at 06 UTC 17 September, and continues through 12 UTC 18 September. It is depicted in both the

4DDA (e.g., Figure 4.42) and MQ analyses (not shown) despite the geostrophic constraints applied in both analyses. Although beyond the scope of this study, these analyses demonstrate the complex dynamics that occur when two energetic systems of different spatial scales merge.

Both the 4DDA (Figure 4.44a) and MQ analyses (Figure 4.44b) of \bar{v}_L continue to depict the increasingly anticyclonic winds at outer radii as Flo nears the mid-latitude jet. The 06 UTC 17 September analyses which include observations from another NASA DC-8 flight, have low vertical shear within 200 km of the storm center. The 4DDA analysis has cyclonic winds around Flo extending up to 100 mb. This pattern continues through the end of the Super Typhoon phase.

As mentioned above, Flo's primary outflow level rose to 150 mb at the beginning of the Super Typhoon Phase, and remained at that level throughout the period (Figure 4.34). At 06 UTC 17 September, a significant difference exists between the two analyses in the strength of the outflow. While the 4DDA analysis (Figure 4.45a) depicts weak ($< 4 \text{ m s}^{-1}$) outflow, the MQ analysis (Figure 4.45b) has outflow in excess of 7 m s^{-1} about 1000 km from Flo. The 150 mb winds south of Tokyo about 900-1200 km from Flo split from the mid-latitude jet and turn south toward the TUTT, and are about 5 m s^{-1} weaker in the MQ analysis than the 4DDA analysis. Also, the 4DDA analysis depicts the 150 mb winds over eastern China about 10 m s^{-1} stronger than the MQ

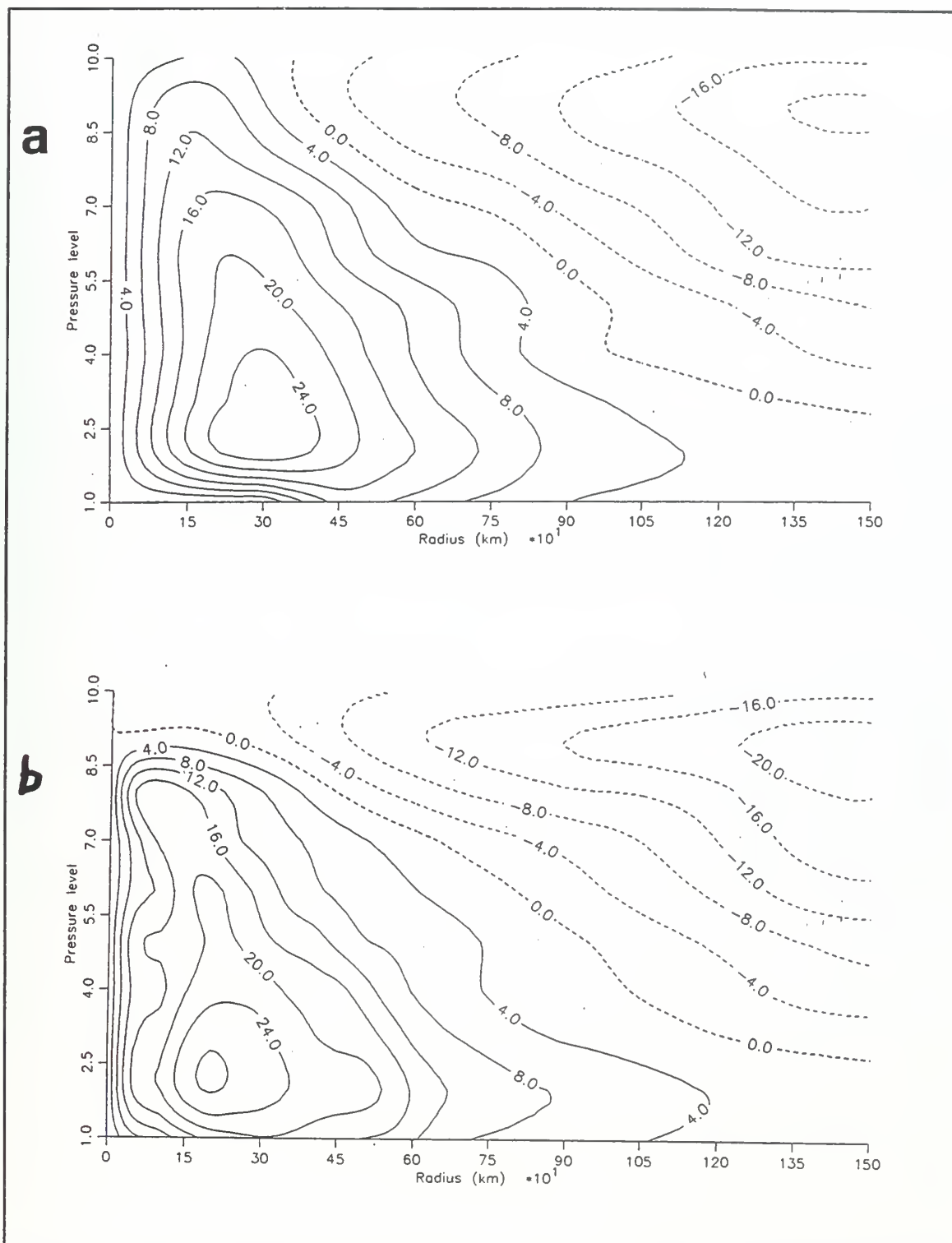


Fig. 4.44 Tangential winds as in Figure 4.7, except at 06 UTC 17 September, as calculated by (a) 4DDA analysis and (b) MQ analysis.

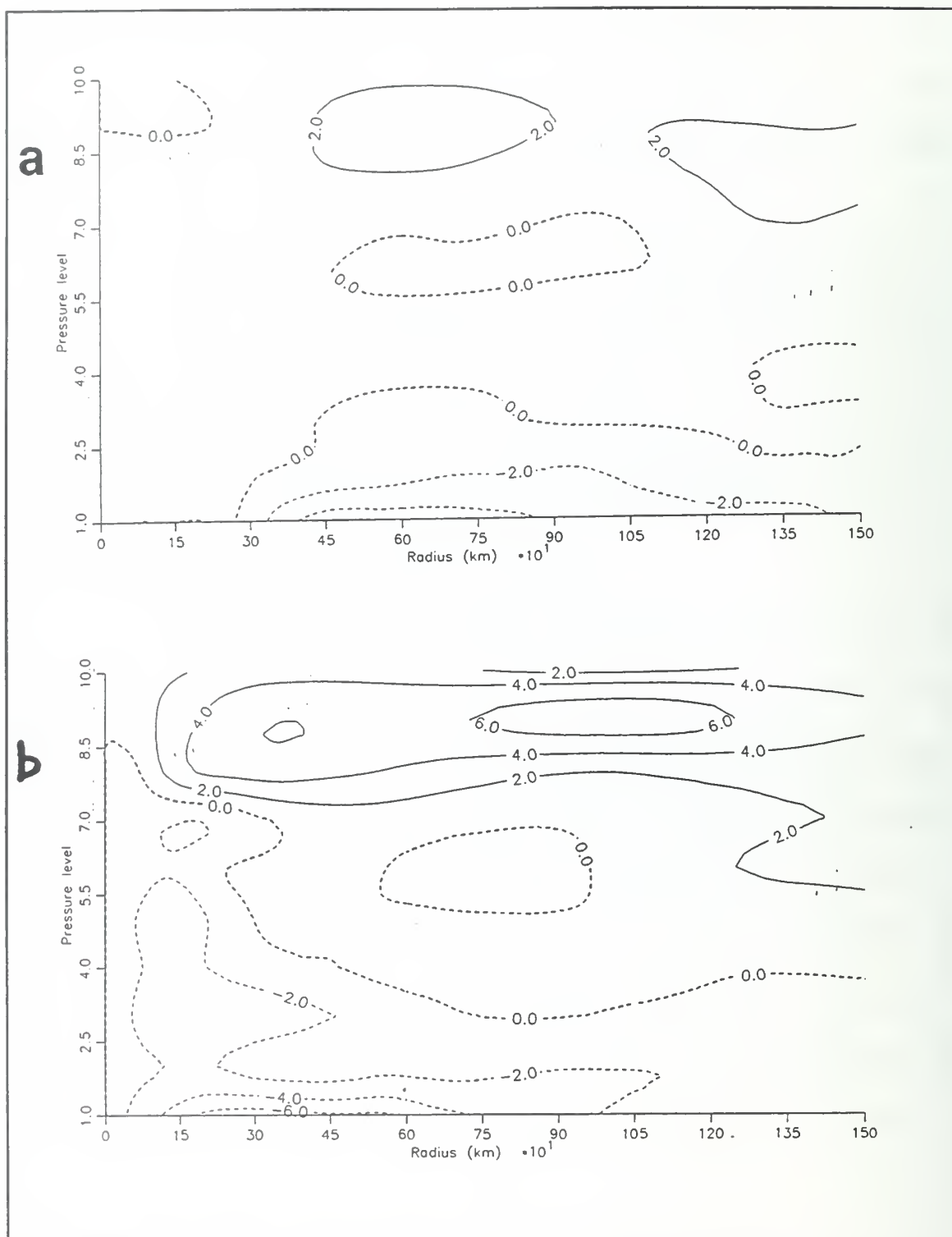


Fig. 4.45. Radial winds as in Figure 4.11, except at 06 UTC 17 September, as calculated by (a) 4DDA analysis and (b) MQ analysis.

analysis. Since neither analysis has observations in these locations, it is not possible to determine which analysis is "correct."

After 06 UTC 17 September, the \bar{u}_L analyses are similar, with both the 4DDA and MQ analyses having the primary outflow jet at 150 mb, with the magnitude of \bar{u}_L between 5 and 8 m s⁻¹. At 12 UTC 17 September, the analyses also show 1 to 2 m s⁻¹ **outflow** down to 500 mb beyond 900 km from Flo (Figure 4.39a and b). Even though Flo is at its maximum intensity (75 m s⁻¹), the classic tropical cyclone "in-up-out" transverse circulation is becoming disrupted by the mid-latitude trough, and is starting to become an "in and out" circulation. Based on these calculations, it is hypothesized that the sustained divergence away from the storm center will lessen the potential amount of sensible heat and moisture fluxes available to the eyewall. Therefore, the inner core deep convection will decrease, the transverse circulation will decrease, and the tropical cyclone will weaken.

Pressure-radius plots of EFC show small values within 1500 km of Flo through 00 UTC 17 September. From 06 to 12 UTC 17 September, the pattern becomes more complex with isolated areas of moderate (> 15 m s⁻¹/day) of positive and negative EFC. The EFC maxima are now occurring primarily in the mid-troposphere, as opposed to the upper troposphere (e.g., Figure 4.46a and b). This mid-level forcing of the transverse circulation is hypothesized to produce the "in and out" vice "in-up-out" circulation described above and shown schematically in Figure 4.47. That is, the mid-latitude trough to the north and west of Flo is a negative influence on Flo's intensity,

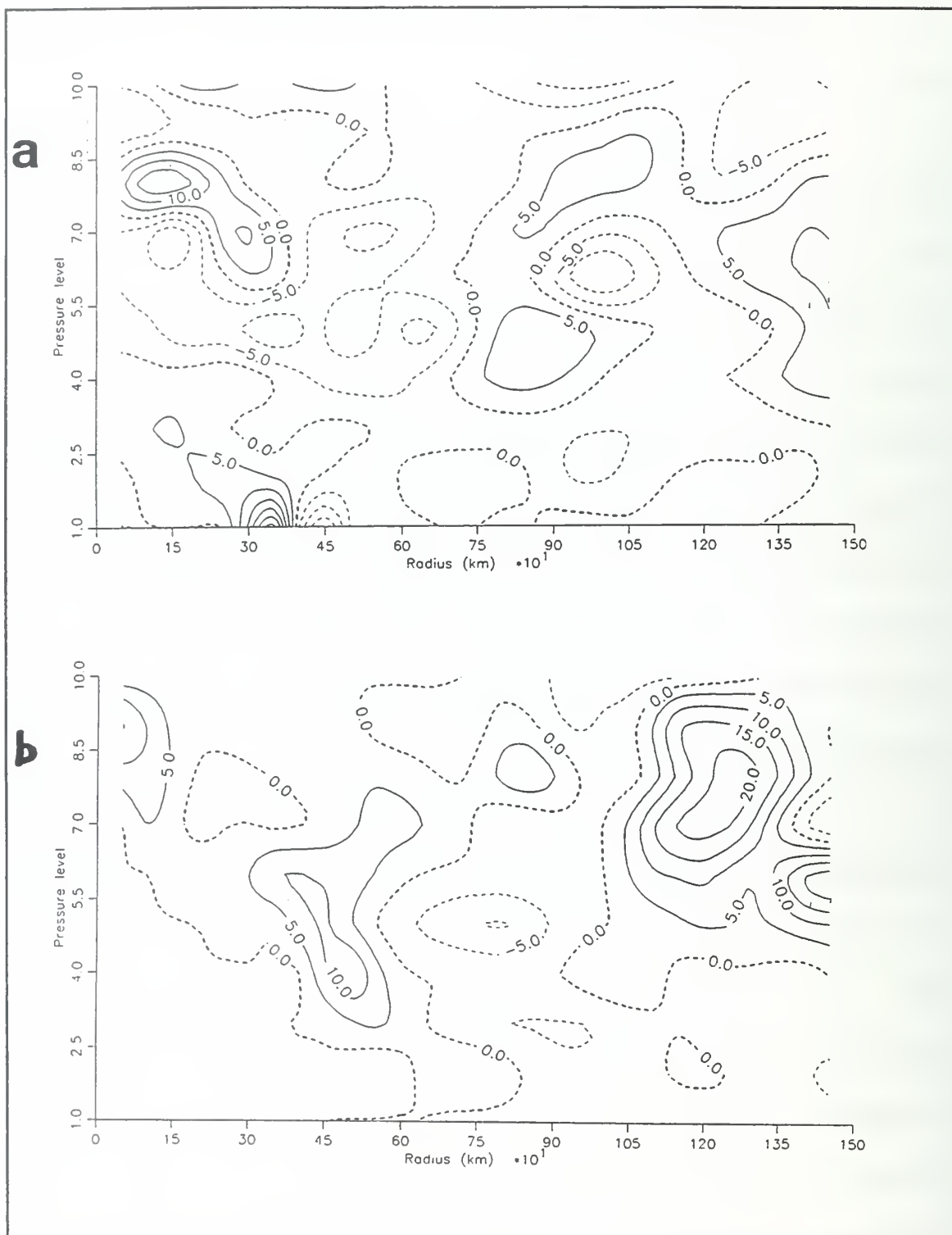


Fig. 4.46. EFC values as in Figure 4.16, except at 12 UTC 17 September, as calculated by (a) 4DDA analysis, and (b) MQ analysis.

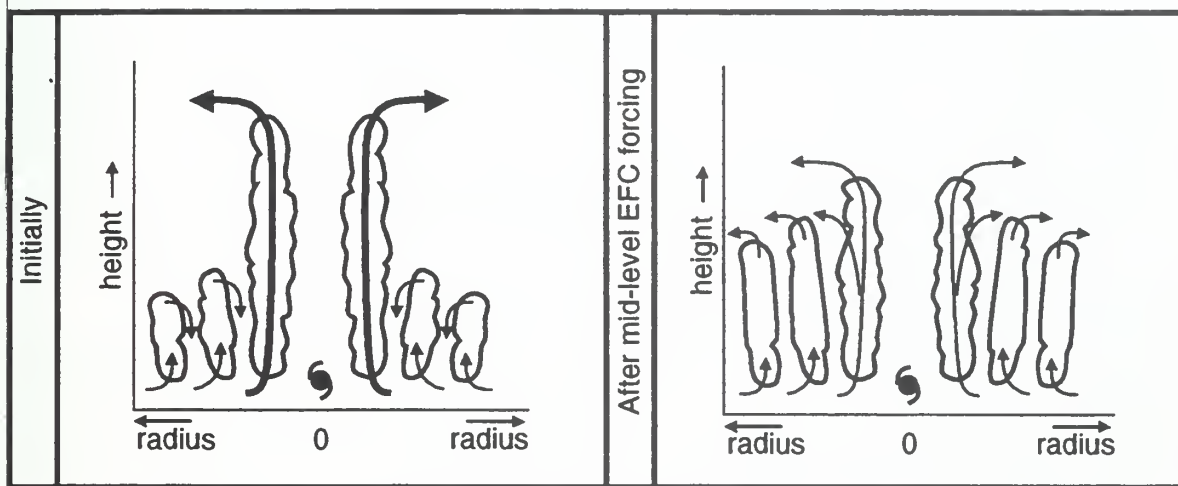


Fig. 4.47. Schematic of proposed interaction between mid-level EFC and the storm transverse circulation.

even prior to considering any vertical wind shear. This significant shift in the spatial distribution of EFC starts at 06 UTC 17 September (the time Flo initially reached its maximum intensity) and continues for the remainder of the IOP.

The 300-150 mb vertical shear values (Figure 4.19) remain very low ($< 3 \text{ m s}^{-1}$ in both analyses) for the entire Super Typhoon Phase, which indicates the upper tropospheric cyclonic circulation is well established, and "coupled" with the 300 mb wind field. However, the 850-200 mb wind shear (Figures 4.18) has significant variability throughout the Super Typhoon Phase, especially as calculated by the 4DDA analysis. For example, the vertical shear values increase by a factor of two to $5\text{--}6 \text{ m s}^{-1}$ from 00 UTC to 18 UTC 16 September. The wind shear then rapidly decreases to 1 m s^{-1} at 00 UTC 17 September, and then steadily increases to over 6 m s^{-1} by 18 UTC. These values are no higher than those observed during Flo's initial intensification, and when averaged over time, are only 0.5 m s^{-1} higher than the wind shear values calculated during the rapid intensification phase.

In summary, the EFC and \bar{u}_L values indicate significant mid-tropospheric interaction begins to occur with the mid-latitude trough to the west and north of Flo while Flo reaches its peak intensity. These interactions start to degrade the efficient transverse "in-up-out" circulation within the storm. It is proposed that the transverse circulation starts to become "in and out", which lessens the amount of convection and latent heat release occurring within Flo's eyewall, and subsequently weakens the storm.

This occurred in a vertical wind shear environment that is not significantly different from that in which Flo initially, and then rapidly intensified.

d. Mid-latitude Interaction Phase (00 UTC 18 September to 00 UTC 19 September)

As Flo continues to move northeast at $4\text{--}6\text{ m s}^{-1}$, the storm is embedded in the mid-latitude trough moving east across eastern China and the Yellow Sea. The outflow is primarily to the north, and quickly merges with the mid-latitude jet. At the beginning of this phase, a secondary outflow jet to the south curves anticyclonically to the southeast. Some of this outflow merges with the TUTT cell that is now 1200 km east-southeast of Flo, while the remainder of the outflow continues an anticyclonic curve to the west before merging with the tropical easterly jet over the Philippine Sea.

By 12 UTC 18 September, the distance between the northeast-moving Flo and the westward-moving TUTT has decreased to 800 km. The TUTT is becoming deformed by the mid-latitude jet as a short-wave trough approaches the western Yellow Sea. The $30\text{--}50\text{ m s}^{-1}$ southerly 200 mb winds over the Korea Strait and southern South Korea accelerate into the jet up to 30° to the left (down-gradient) of the geostrophic flow (Figure 4.48). While this feature is described by the few land station reports in this area, the reprocessed cloud-track winds allow both analysis schemes to correctly depict this significant large-scale ageostrophic flow. When such a flow occurs in the right-entrance quadrant of a jet, the induced large-scale upward motion may assist the transition of a tropical cyclone to an energetic mid-latitude system. Klein (1997) has illustrated cases

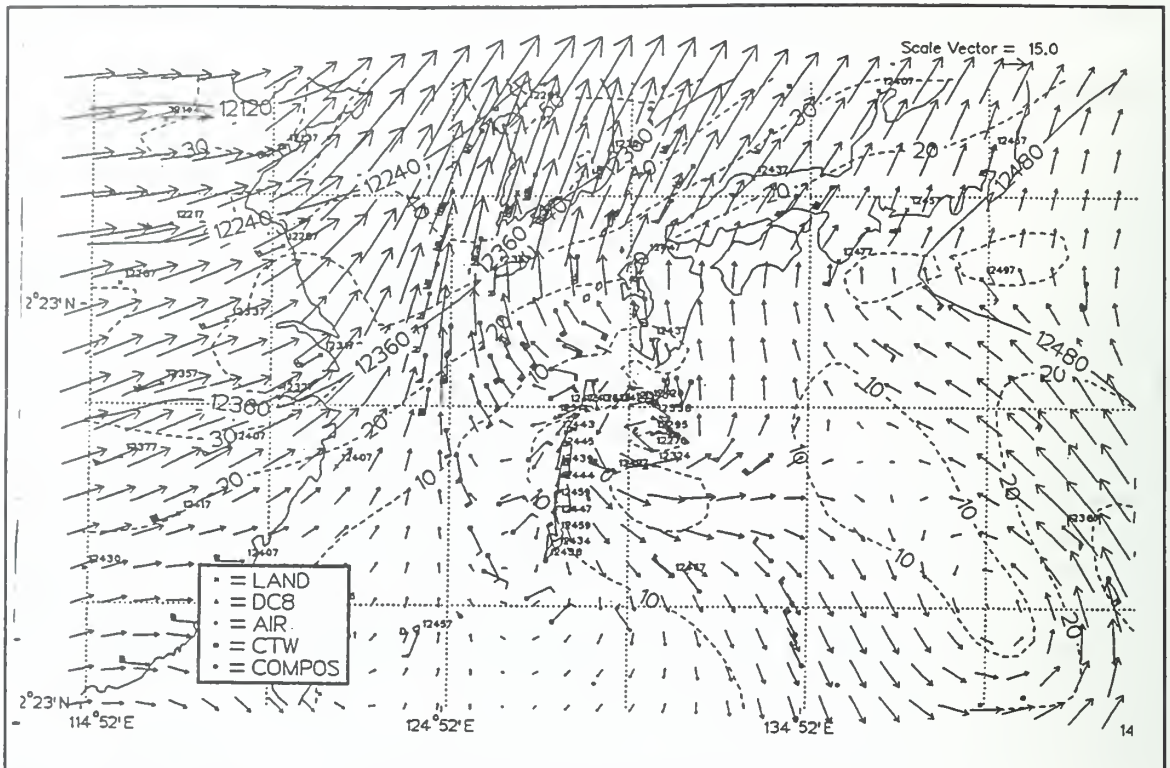


Fig. 4.48. MQ analysis as in Figure 4.32, except at 12 UTC 18 September.

of extratropical transition in the western North Pacific that involved a similar acceleration of an outflow jet into the right-rear quadrant of a mid-latitude jet.

By 00 UTC 19 September, Flo is embedded in the southern edge of the jet about 200 km east of Kyushu, and is becoming increasingly difficult to identify as a discrete system at 200 mb. The TUTT cell in the vicinity of 30°N, 140°E has dissipated. Even though upper-level winds of Flo are less distinct from the surrounding environment, the typhoon still has an intensity of 46 m s^{-1} . The JTWC reclassifies Flo as an extratropical cyclone 30 h later at 06 UTC 20 September.

Through 12 UTC 18 September, the MQ and 4DDA analyses of \bar{v}_L display attributes similar to those observed in the Super Typhoon Phase. That is, the analyses depict the maximum \bar{v}_L within 300 km in the lower troposphere, sloping inwards to within 150 km of the storm center at the outflow level. The MQ analysis continues to fully assimilate the high spatial resolution dropwindsonde observations when they are available (e.g., Figure 4.49a). At inner radii, the MQ analysis depicts \bar{v}_L magnitudes nearly twice that in the 4DDA analysis (Figure 4.49b), although the MQ analysis values are still too low in the inner core by at least a factor of two. As has previously been noted, the 4DDA analysis is able to extend the aircraft and reprocessed cloud-track winds up to 150 mb and higher, while the Multi-quadric analysis relies on the NOGAPS background fields at times and in places where no observations are available.

An example of \bar{v}_L during Flo's transition from a typhoon to an extratropical cyclone is shown in Figure 4.50. Below 500 mb, the positive \bar{v}_L is assuming a more horizontal structure, which implies greater vertical shear as Flo transitions to an extratropical cyclone. Above 500 mb and within 300 km of the center, Flo maintains the vertically oriented maximum of \bar{v}_L , although the magnitude of \bar{v}_L at 150 mb has decreased from 7.5 m s^{-1} at 06 UTC 18 September to about 3 m s^{-1} 18 h later. Although speculation, this evolution may imply that the inner-core, deep convection is "decoupling" from the outer wind field.

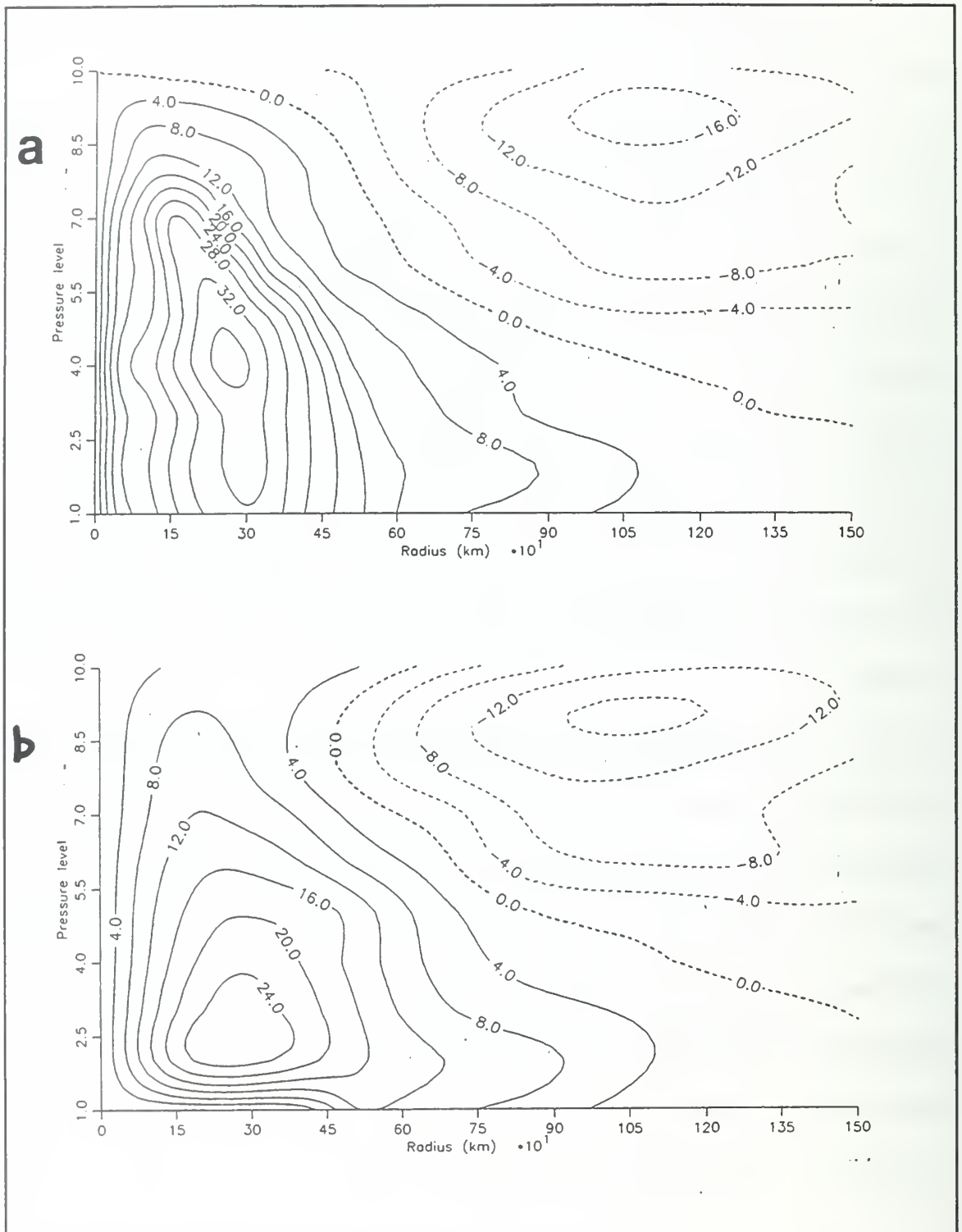


Fig. 4.49. Tangential winds as in Figure 4.7, except at 06 UTC 18 September, as calculated by (a) MQ analysis and (b) 4DDA analysis.

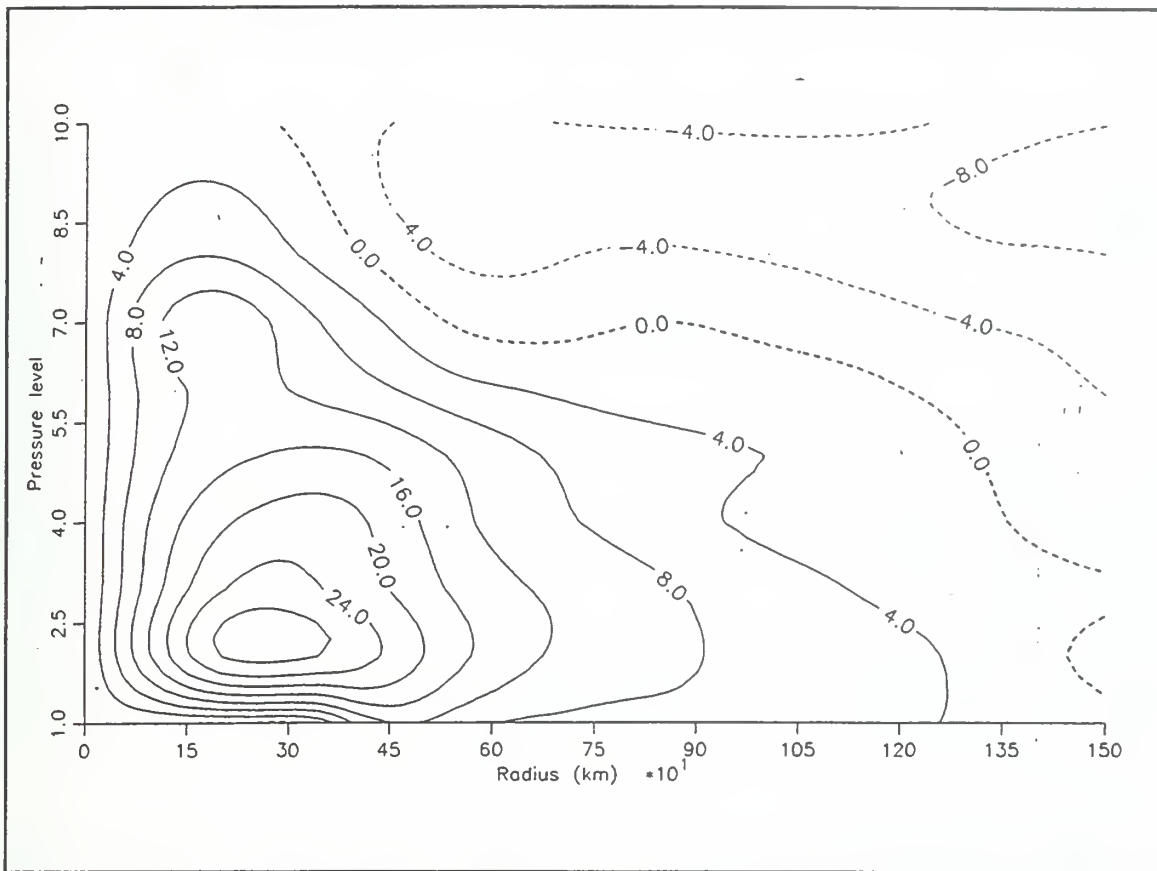


Fig. 4.50. Tangential winds as in Figure 4.7, except at 00 UTC 19 September, as calculated by 4DDA analysis.

At the beginning of the Mid-latitude Interaction Phase, the pressure-radius plots of \bar{u}_L are also similar to those described in the Super Typhoon Phase. The outflow originates at 150 mb, and then gradually descends to 200 mb at about 1000 km radius from Flo. Starting at 06 UTC 18 September, this pattern changes to a more complex outflow structure. Strong outflow ($7\text{--}9\text{ m s}^{-1}$) still originates from 150 mb (e.g., Figure 4.51a and b) near the typhoon center, then descends more rapidly to 200 mb at a radius of 700 km. In addition, moderate outflow ($2\text{--}4\text{ m s}^{-1}$) occurs at 500 mb at a radius to

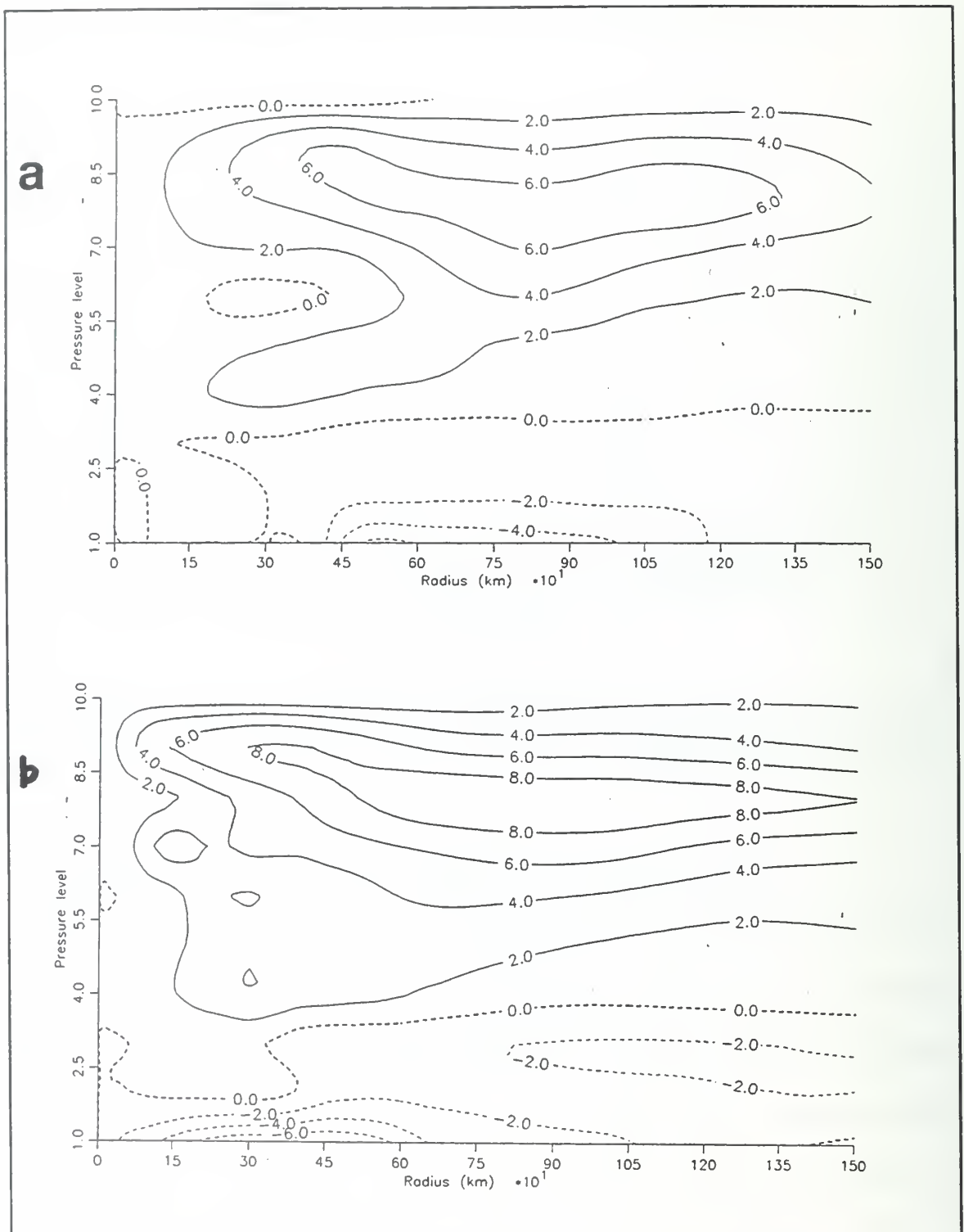


Fig. 4.51 Radial winds as in Figure 4.11, except at 18 UTC 18 September, as calculated by (a) 4DDA analysis and (b) MQ analysis.

200-500 km. Both analyses have outflows at all radii above 700 mb, which contrasts to the early portion of the IOP (e.g., Figures 4.12, 4.25) when the outflow is restricted to heights above 250 mb. It is proposed that the "short-circuiting" of the typhoon transverse circulation, and **not** vertical wind shear, is the primary reason for the 35% decrease in intensity between 12 UTC 17 September (75 m s^{-1}) and 00 UTC 19 September (49 m s^{-1}).

Unlike the horizontal, upper-tropospheric orientation of the positive EFC in the forcing phase (e.g., Figures 4.16 and 4.17), the EFC are oriented vertically at 00 UTC 18 September (Figure 4.52). After 00 UTC, the interaction with the mid-latitude jet produces widespread, deep positive EFC (Figure 4.53). These positive EFC values in the mid-troposphere down to 500 mb are believed to create the mid-tropospheric outflow discussed above, and are therefore instrumental in weakening the typhoon.

Wind shear between 850 and 200 mb (Figure 4.18) steadily increases throughout this final phase of Flo, and reaches about 9 m s^{-1} by 00 UTC 19 September. This value is no higher than that observed prior to 00 UTC 14 September, when Flo was intensifying at a rate of $10 \text{ m s}^{-1}/\text{day}$. During this phase, the value of the 850-300 mb wind shear increased from 4 m s^{-1} to over 10 m s^{-1} and was greater than the magnitude of the 850-200 mb wind shear at all times except one after 18 UTC 17 September. This contrasts to the forcing period, in which the 850-300 mb wind shear was less than half the 850-200 mb wind shear through 12 UTC 13 September. This difference can be

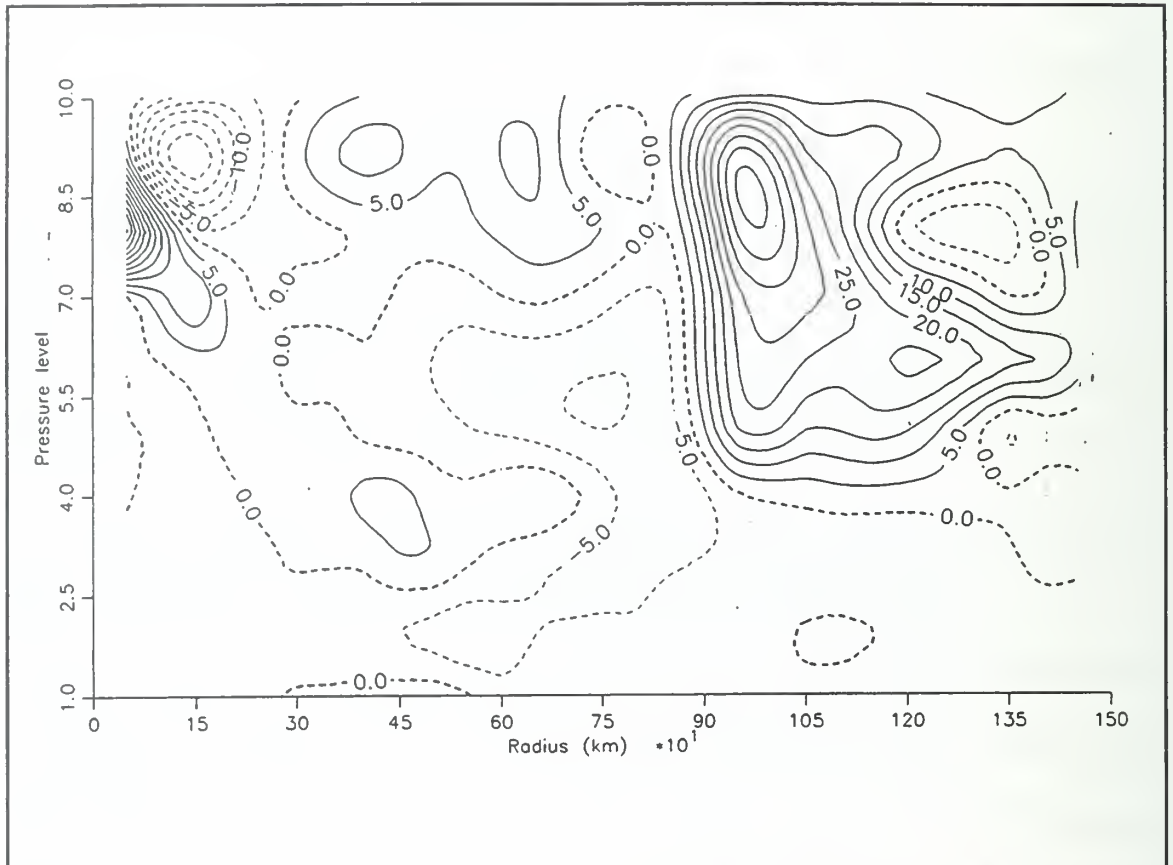


Fig. 4.52. EFC values as in Figure 4.16, except at 00 UTC 18 September, as calculated by MQ analysis.

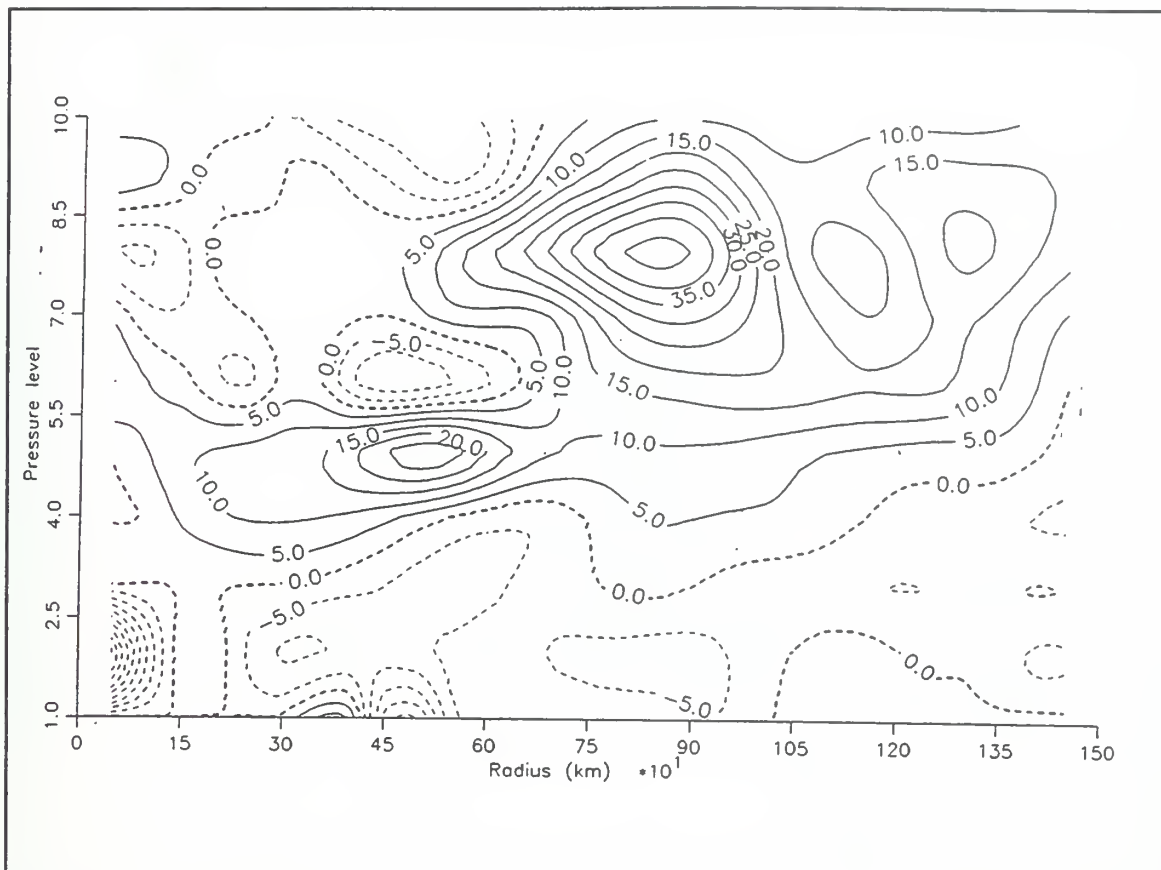


Fig. 4.53. EFC values as in Figure 4.16, except at 12 UTC 18 September, as calculated by 4DDA analysis.

explained by the interaction with the mid-latitude jet, and may have resulted in increased "ventilation" of Flo's inner core.

The interaction between Flo and the mid-latitude jet also appeared to alter the vertical structure of the storm-relative vertical wind shear. Although the magnitude of the 850-200 mb wind shear is very similar ($\pm 1 \text{ m s}^{-1}$) at both 18 UTC 13 September and 06 UTC 18 September, the structure of the relative wind shear is completely different. Whereas most of the vertical shear at 18 UTC 13 September (Figure 4.54) is

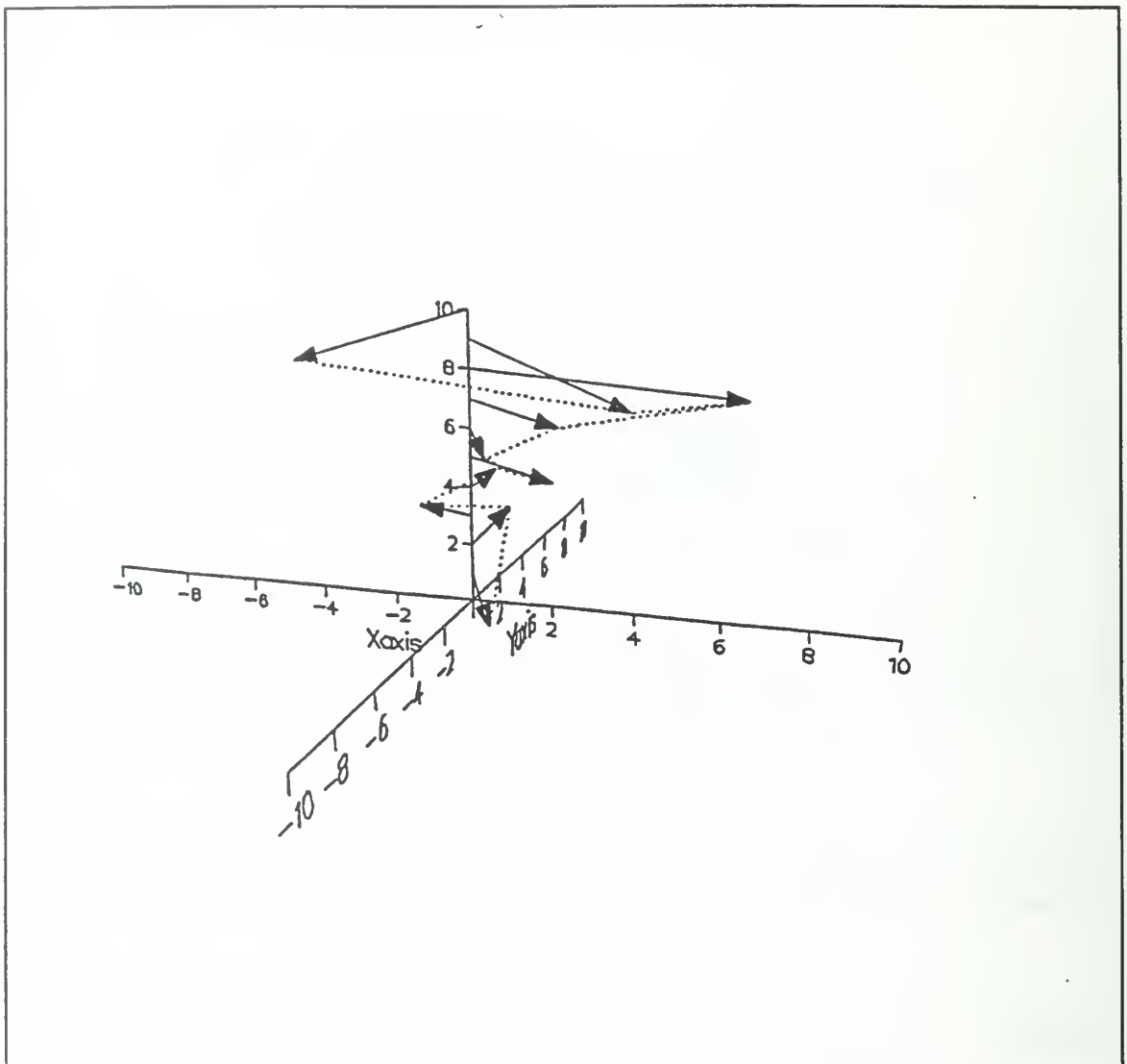


Fig. 4.54. Storm-relative wind (m s^{-1}) azimuthally-averaged between 200 km and 600 km around Typhoon Flo at 18 UTC 13 September at each pressure level, as calculated by 4DDA analysis. Positive X axis (Y axis) values represent easterly (northerly) wind relative to Flo. Negative X axis (Y axis) values represent westerly (southerly) wind relative to Flo. Vertical axis represents pressure levels as in Figure 4.7. Dotted lines connect storm-relative winds at adjacent pressure levels.

concentrated at 200 mb and 150 mb, the vertical shear at 06 UTC 18 September (Figure 4.55) is distributed throughout the troposphere, with minima at 500 mb and 150 mb. It

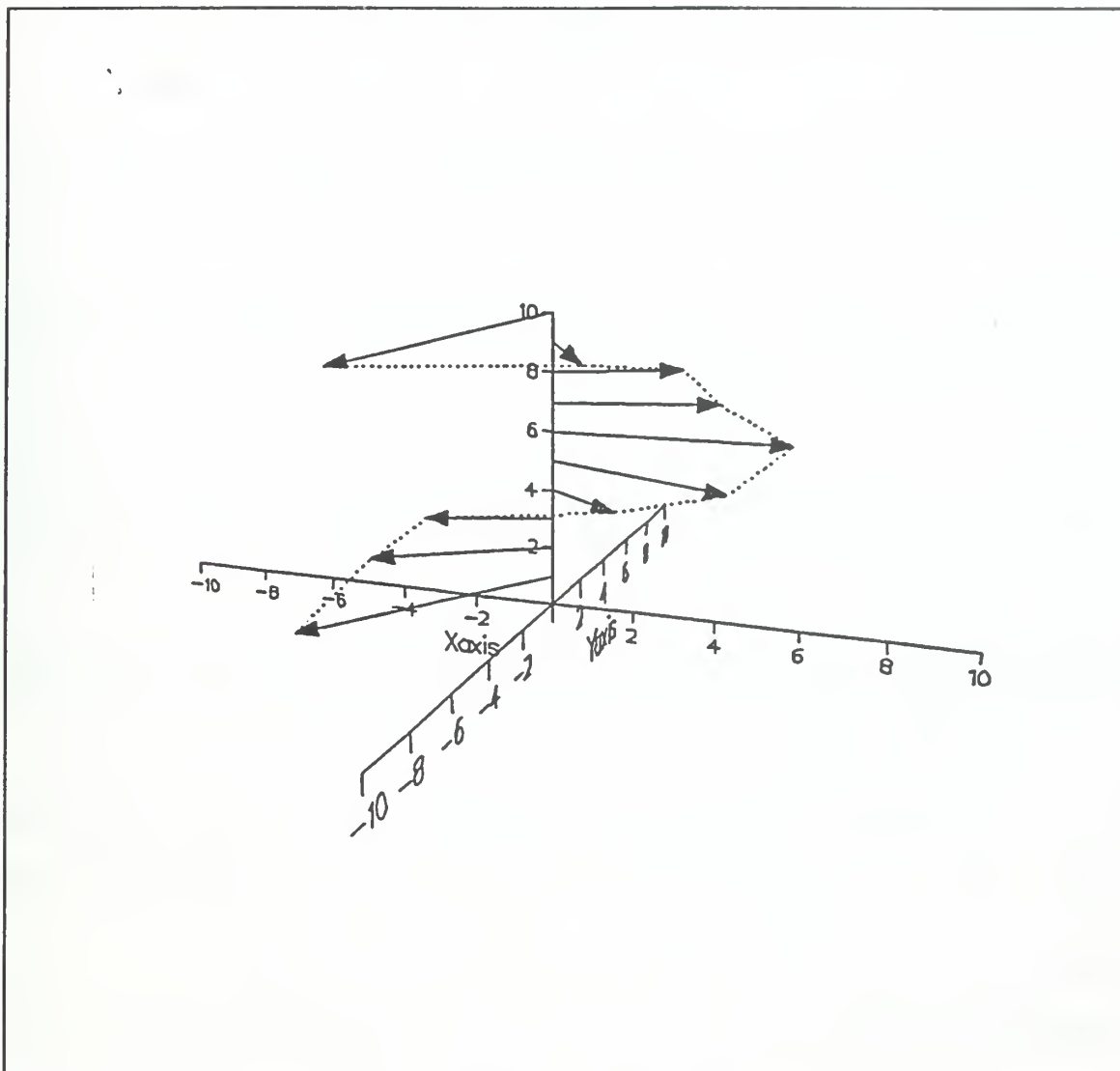


Fig. 4.55. As in Figure 4.48, except at 06 UTC 18 September.

is possible that directional shear (Figure 4.55) has a greater negative effect on Flo than does speed wind shear concentrated at 200 mb (Figure 4.54), although the "ventilation" theory predicts both of these wind regimes would be harmful to storm intensification because the required upper-tropospheric warm core would become decoupled from the lower levels of the storm. Elsberry and Jeffries (1996) hypothesized that wind shear

concentrated in a shallow, upper-tropospheric layer (e.g., Figure 4.54) may be more easily deflected by the outflow of a developing tropical cyclone than wind shear with significant values throughout the troposphere (Figure 4.55). Elsberry and Jeffries also proposed that using an analysis scheme that "draws to" the highly divergent outflow structure near a tropical cyclone may better capture the deflection of the environmental flow around the inner-core convection.

To test this hypothesis, the 4DDA and MQ values of the 850-200 mb wind shear from 00 UTC 13 September to 06 UTC 14 September were compared. The mean value for the 4DDA (MQ) 850-200 mb wind shear for this period was 9.4 (4.8) m s⁻¹/day. Using a standard *t* statistic, the MQ wind shear was statistically significantly lower at the 95% confidence level, consistent with Elsberry and Jeffries' hypothesis.

DeMaria (1996) proposed an alternate explanation of the effects of wind shear. Using a two-layer diagnostic balance model and a potential vorticity (PV) framework, he reasoned that wind shear vertically tilts the upper- and lower-level positive PV anomalies. For the mass field to remain in balance, the thermal field adjusts by creating a warm, midlevel potential temperature anomaly. This mid-level warming may reduce the amount and intensity of convection near the storm center, and thus weaken the tropical cyclone. DeMaria also shows that the PV anomalies rotate around each other. After one-half of a rotation, the vertical shear reduces the tilt, which in turn reduces the mid-level potential temperature anomaly. This negative feedback acts as a "restoring force" on the system. He shows that the magnitude of this feedback depends

upon the Rossby penetration depth. DeMaria shows that the "restoring force" is proportional to latitude and the storm's horizontal scale, and is inversely proportional to the static stability. Thus, DeMaria reasons that higher latitude, larger, and more intense tropical cyclones (a good description of Flo during its mid-latitude interaction phase) should be more resistant to wind shear than low latitude, small, relatively weak systems. By this reasoning, Flo should have been less affected by the $5\text{--}9\text{ m s}^{-1}$ wind shear in the interaction phase than the storm would have been by similar wind shear magnitudes during the forcing and quiescent phases when Flo steadily intensified.

This study does not suggest that wind shear is a positive factor in tropical cyclone intensification, but that the interaction between the environmental wind shear and tropical cyclone is a complex, three-dimensional process. Taking the magnitude of winds at only two levels (a technique normally used by necessity because of the lack of mid-level observations) may be too simplistic to capture the physics.

In summary, Flo weakened 30% from 00 UTC 18 September to 00 UTC 19 September, while it was still over warm water and away from land. The weakening was almost certainly because of the interaction with the mid-latitude jet. The hypothesis is that the primary cause of Flo's weakening was not from the wind shear, but indirectly from the strong, sustained mid-tropospheric EFC fluxes. These fluxes were believed to be instrumental in developing outflow at mid-levels. This sustained, mid-level outflow changed the typhoon's secondary circulation from an "in-up-out" pattern to an "in and out" pattern, and thereby decreased the storm intensity.

4. Typhoon Ed

As described by JTWC (1990), Typhoon Ed formed from a disturbance over the Marshall Islands, then moved towards the northwest until it reached approximately 20°N east of the Marianas Islands (Figure 1.2). Ed reached tropical storm strength at 06 UTC 11 September 1990 about 300 km west of the northern Marianas Islands. Ed tracked westward at 6-7 m s⁻¹ across the northern Philippine Sea, and reached typhoon intensity at 00 UTC 14 September, about 300 km east-northeast of Luzon. In response to the subtropical ridge building westward, Ed moved west-southwest into the South China Sea until 00 UTC 17 September and reached a maximum intensity of 46 m s⁻¹ by 18 UTC 16 September. Ed then tracked to the west, and then northwest at 3-4 m s⁻¹ until it made landfall along the coast of central Vietnam at 18 UTC 18 September.

Although Ed existed at the same time as Flo, and tracked over the Philippine Sea with a similar (28.0 - 28.5°C) SST as Flo encountered, Ed never rapidly intensified (Figure 4.56). The most rapid intensification of Ed was 10 m s⁻¹/6 h in the 12 h prior to 00 UTC 14 September just prior to reaching typhoon strength. The following sections will examine the wind, vertical wind shear, and eddy flux fields, and contrast these fields to those of Super Typhoon Flo.

a. Total Wind Field

While the upper-tropospheric winds in the vicinity of Flo appeared very "connected" with the storm from the initial stages of the development, the 200-mb wind field over Ed appears to have had little interaction with the tropical storm.

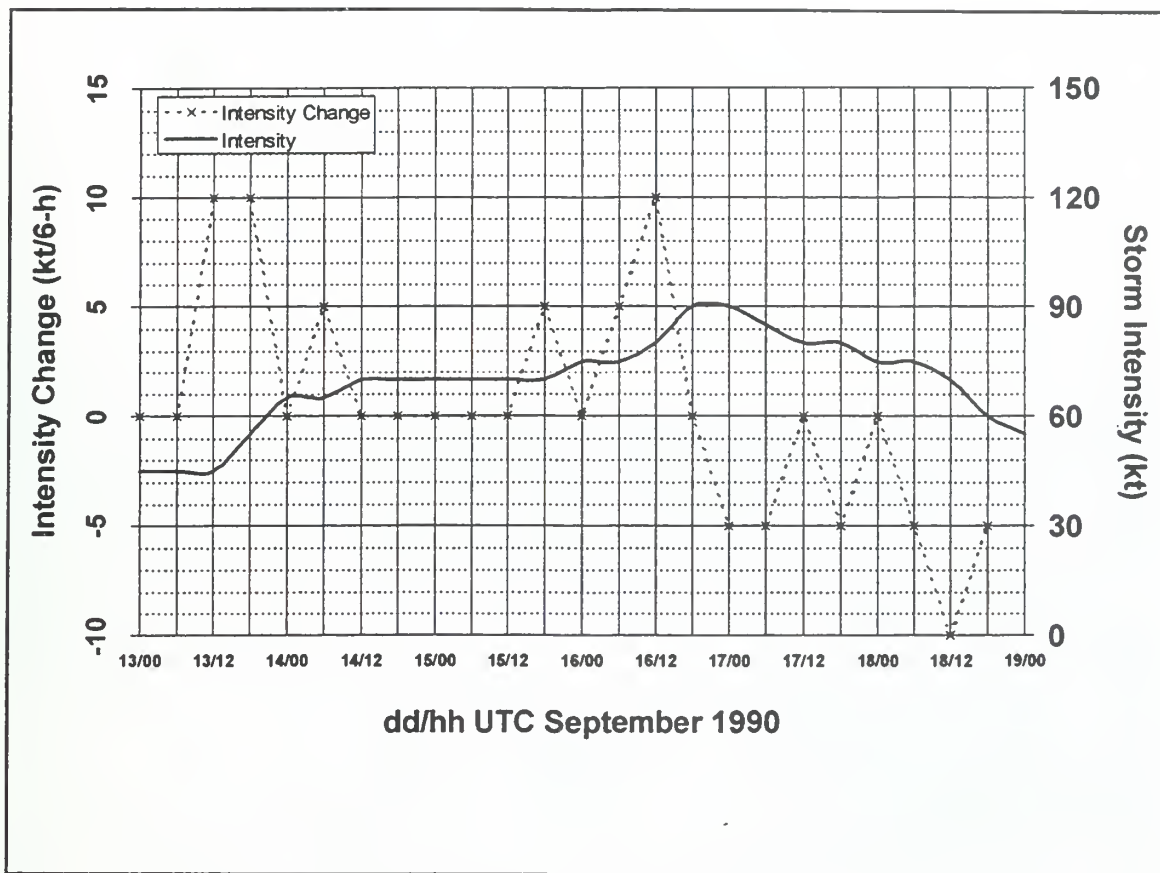


Fig. 4.56. Intensity (kt) and rate of 6-h intensity change (kt) for Typhoon Ed.

Unidirectional east-northeast winds of $10\text{--}15\text{ m s}^{-1}$ are present over Ed (Figure 4.57), with a small anticyclone about 300 km southeast of the storm. This pattern continues even when Ed reaches typhoon strength at 00 UTC 14 September.

By 12 UTC 15 September, 36 h after Ed became a typhoon, both the 4DDA and MQ analyses depict a small-scale cyclonic circulation over Ed at 200 mb (Figure 4.58a and b). However, almost all of the outflow quickly merges into the prevailing northeasterly winds and flows across the South China Sea. This pattern is evident until Ed makes landfall at 18 UTC 18 September.

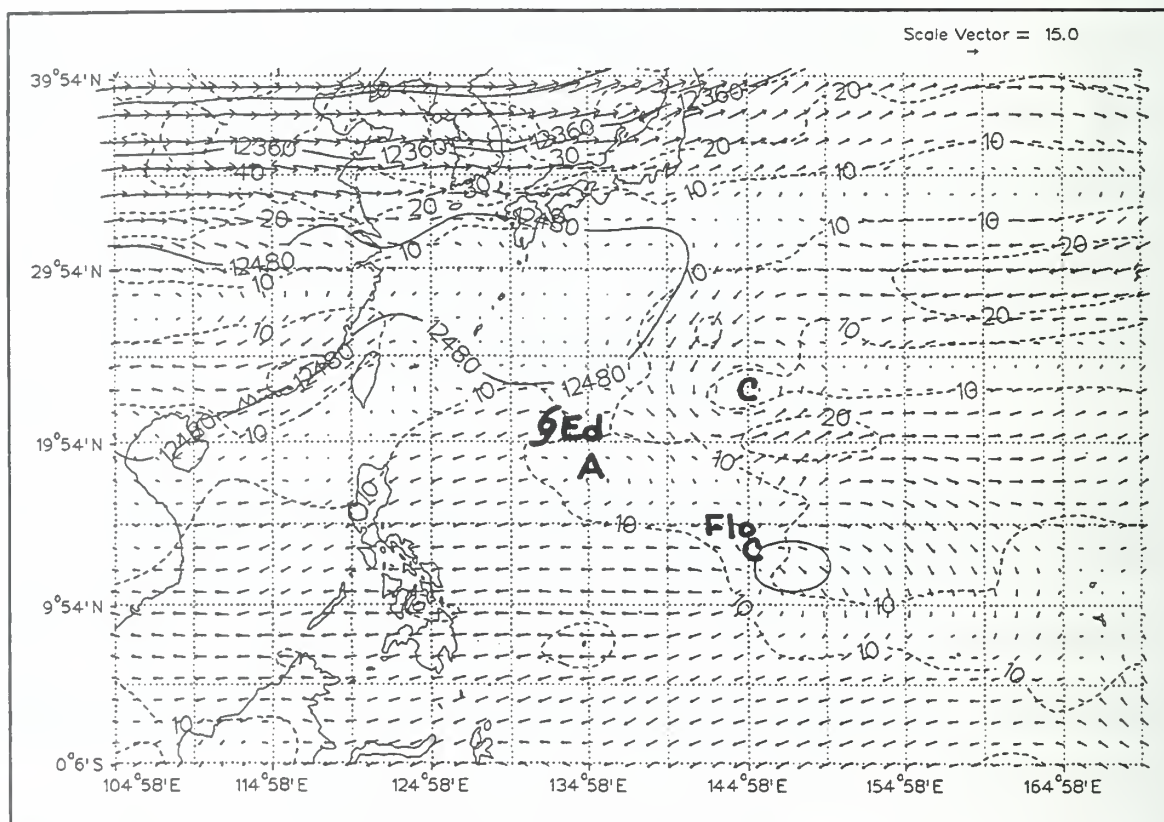


Fig. 4.57. MQ analysis at 200 mb as in Figure 4.5, except at 00 UTC 13 September.

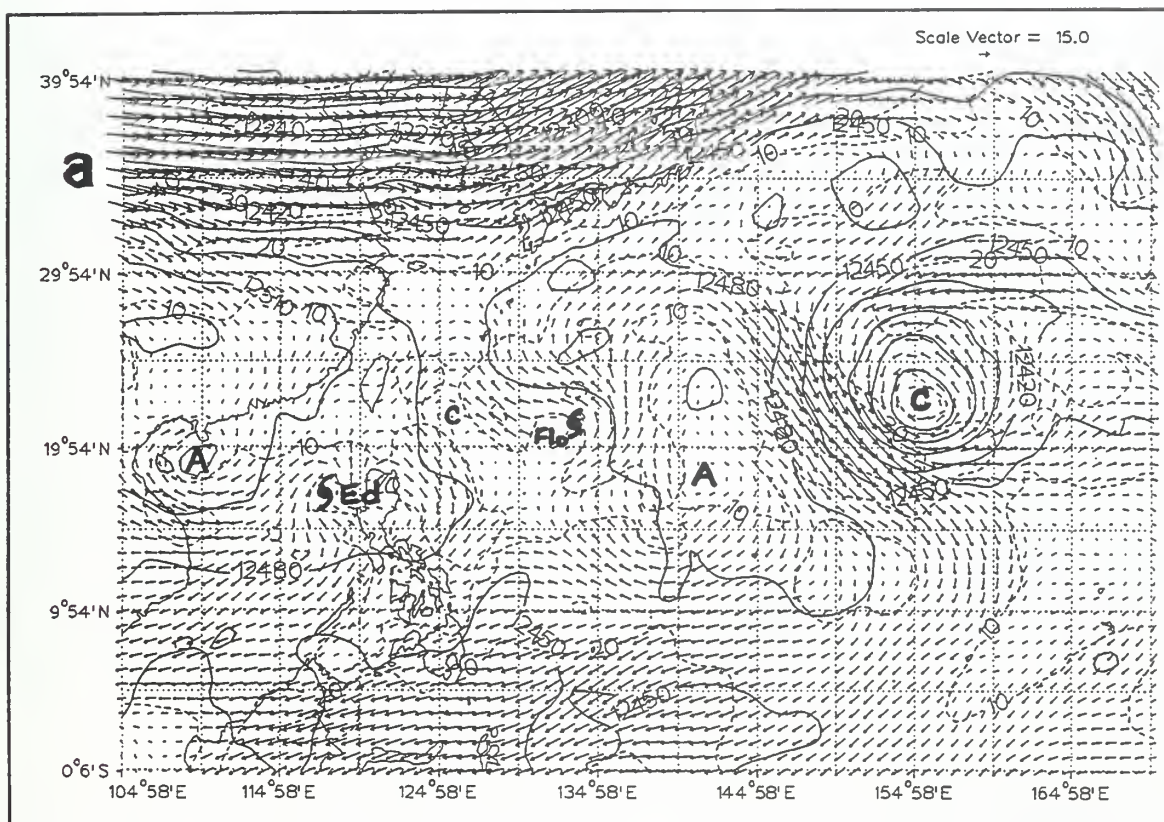


Fig. 4.58. Analysis at 200 mb as in Figure 4.5, except at 12 UTC 15 September, as calculated by (a) 4DDA analysis and (b) MQ analysis.

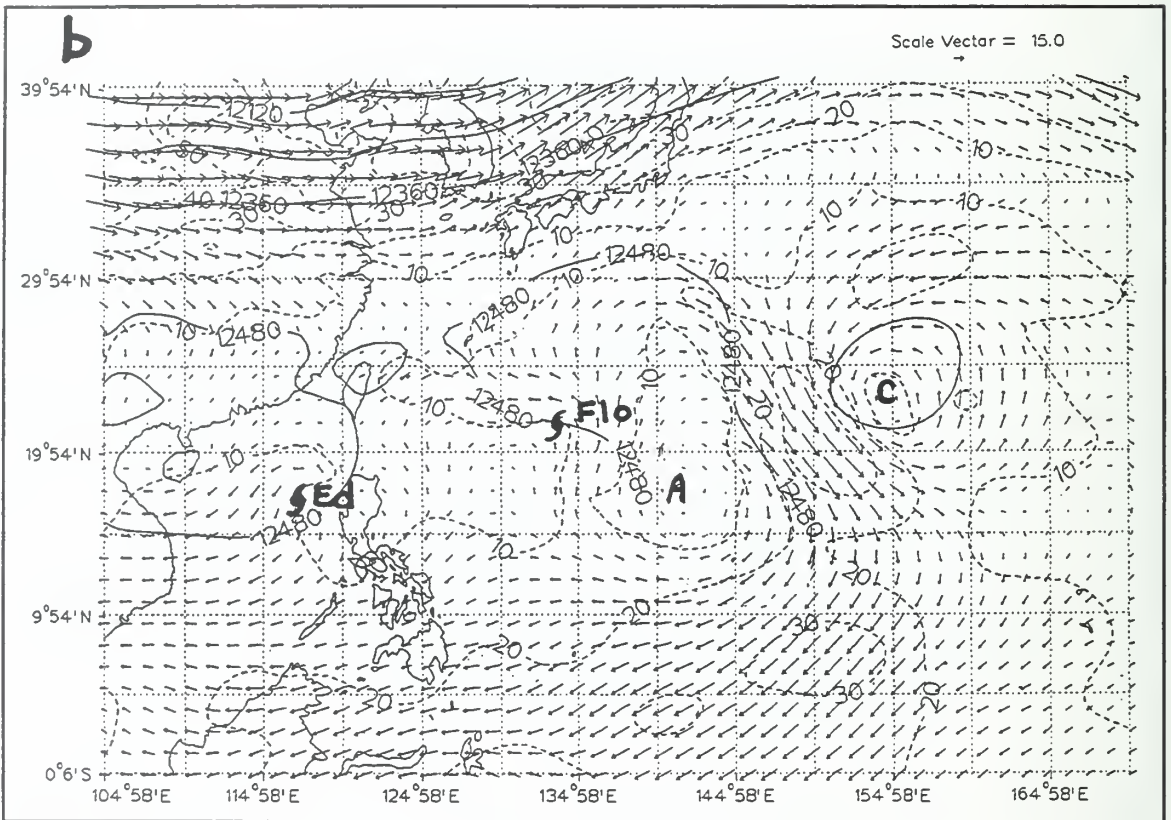


Fig. 4.58. Continued.

In summary, Ed's outflow can be characterized as a single channel, equatorward outflow. As discussed by Chen and Gray (1986), this is the most common outflow pattern for western North Pacific typhoons.

b. Tangential and Radial Winds

Radius-time plots of the 200 mb tangential and radial winds (Figures 4.59 and 4.60) have only minor changes with respect to time throughout the IOP. In contrast to Flo, no tangential "cyclonic burst" or steady increase in the outer radii anticyclonic winds is detected. Rather, little evidence of any cyclonic winds greater than 4 m s^{-1} is found above 250 mb until 12 UTC 14 September when Ed attained an intensity of 36 m s^{-1} . Starting at this time, 200-mb \bar{v}_L winds are observed to be cyclonic out to a radius of 500-650 km. This pattern is maintained until Ed makes landfall. Beyond this radius, \bar{v}_L is typically between -4 and -8 m s^{-1} , with little variation in time. This contrasts to Flo's radius-time plot of 200 mb \bar{v}_L (Figure 4.6a-b) that had the cyclonic wind burst, followed by a cyclonic wind contraction and increasingly anticyclonic winds at Flo's outer radii.

As in the radius-time plot of \bar{v}_L , little variation is analyzed with time in the magnitude of 200 mb \bar{u}_L (Figure 4.60). After 00 UTC 14 September (when Ed reached typhoon strength), \bar{u}_L was greater than 4 m s^{-1} out to nearly 1000 km, and there were three times (12 UTC 14 September, 12-18 UTC 15 September, and most of 17 September) when \bar{u}_L was greater than 6 m s^{-1} between 300 and 800 km. Contrary to expectations, these periods of increased divergence do not directly correlate with changes in the storm intensity. Whereas Ed maintained an intensity of 36 m s^{-1} , during the first

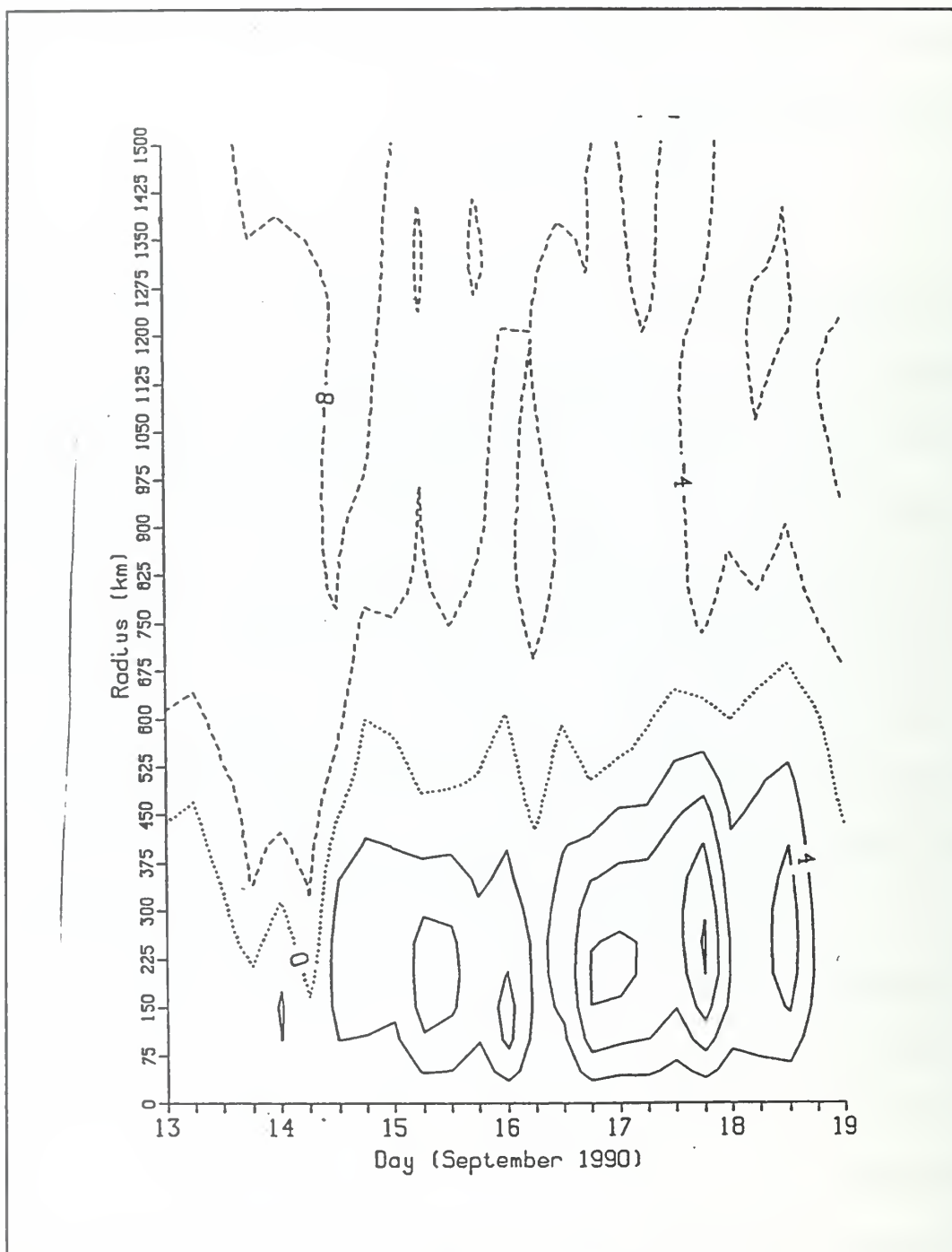


Fig. 4.59. Tangential winds as in Figure 4.6, except for Typhoon Ed, as calculated by 4DDA analysis.

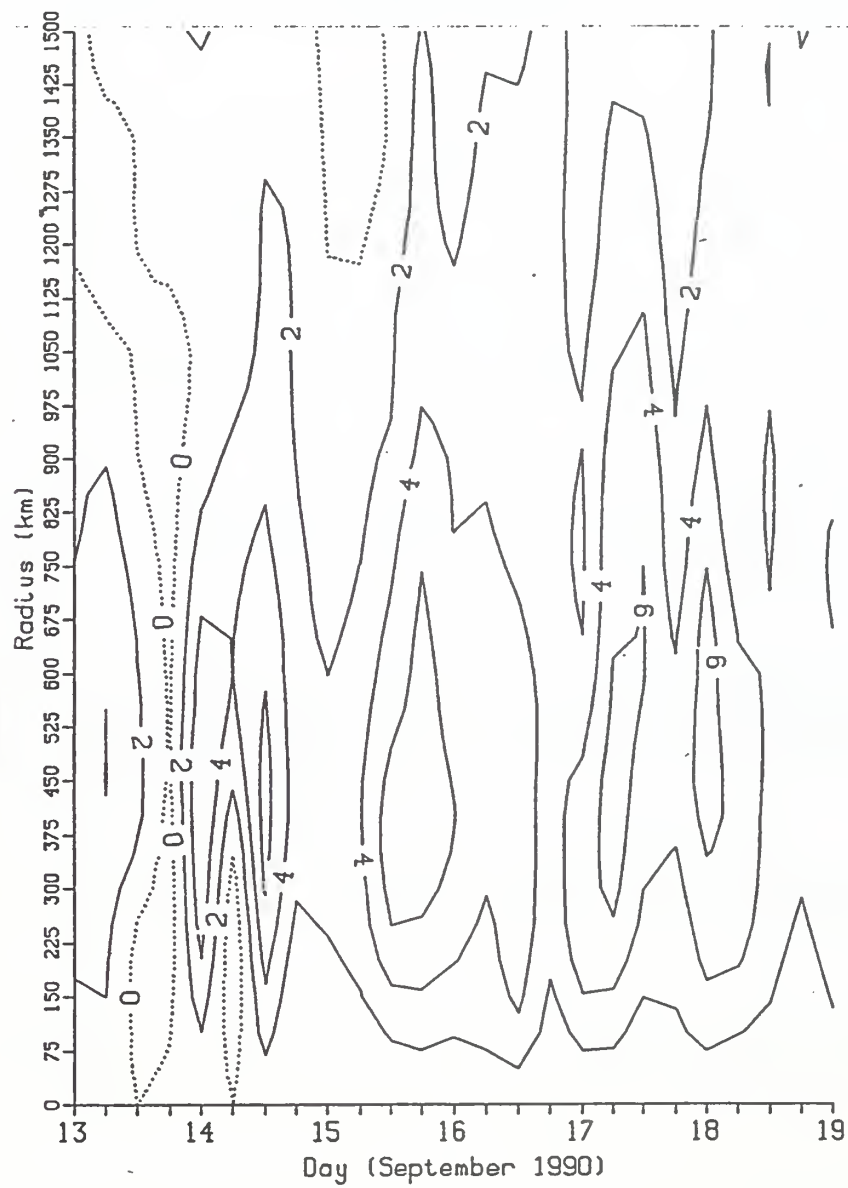


Fig. 4.60. Radial winds as in Figure 4.10, except for Typhoon Ed, as calculated by 4DDA analysis.

and second periods, the storm actually weakened by 5 m s^{-1} during the final period of enhanced divergence.

The time evolution of the average radial wind in \bar{u}_L created by Ed is substantially different from that in Flo. The 200 mb radius-time plot of \bar{u}_L for Flo (Figure 4.10) has only two periods when significant areas of \bar{u}_L greater than 6 m s^{-1} are analyzed: during the forcing phase prior to 00 UTC 14 September, and in the mid-latitude interaction phase after 18 UTC 17 September. While Flo underwent rapid deepening, \bar{u}_L decreased from less than 6 m s^{-1} to less than 4 m s^{-1} . For much of the time when Flo was a Super Typhoon, \bar{u}_L was less than 2 m s^{-1} . Neither Ed nor Flo exhibit the expected positive correlation between the amount of upper-tropospheric divergence and either present storm intensity or rate of intensification.

Based upon Ed's and Flo's \bar{u}_L observations during Ed and Flo, it is hypothesized that the amount of divergence is inversely proportional to the "efficiency" of the storm, relative to the total storm convection. That is, an efficient storm has a greater proportion of its energy in the tangential wind component vice the radial wind. In Flo's case, the forcing by the EFC's early in the life cycle (described above) provided the mechanism for Flo to convert more of its energy release into a combination of increasing the tangential wind, and raising the height of the warm core anomaly. An efficient (inefficient) storm is hypothesized to have less (more) wind shear over the storm

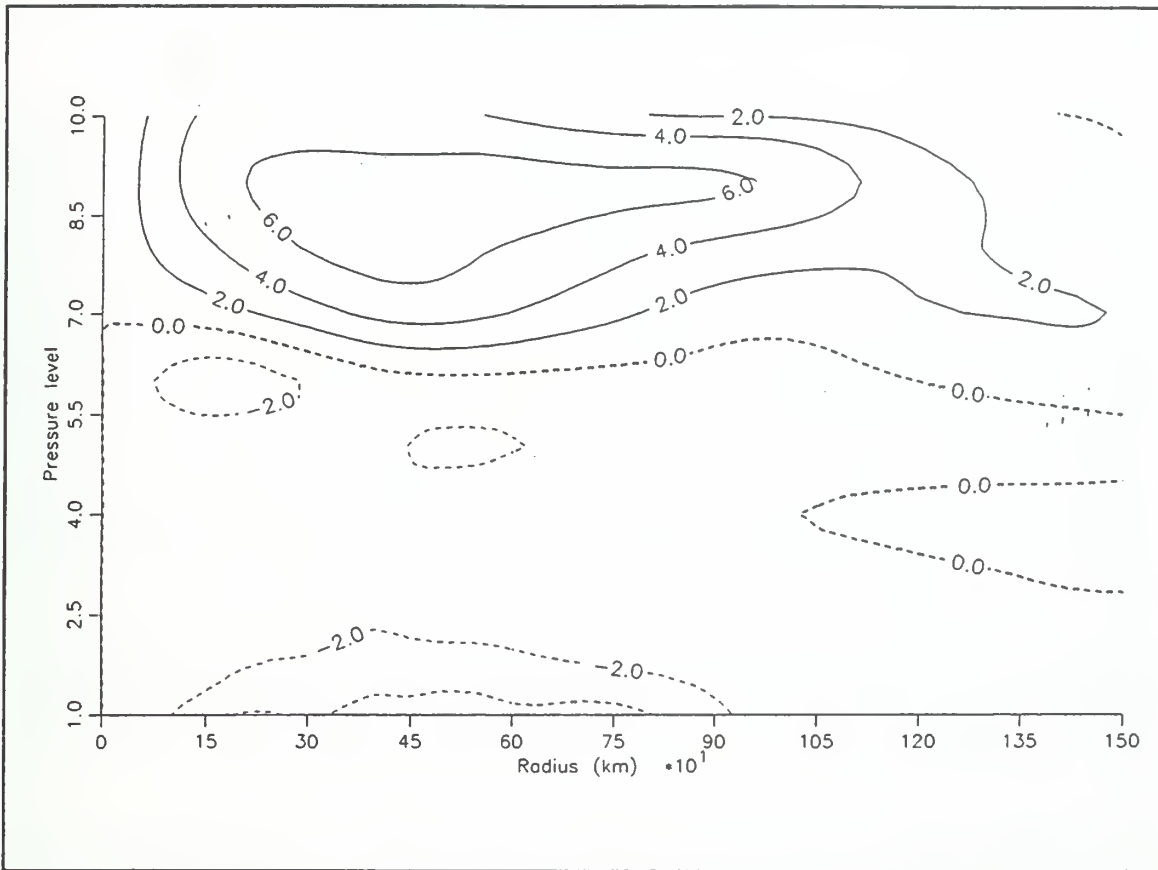


Fig. 4.61. Radial winds as in Figure 4.11, except at 12 UTC 14 September for Typhoon Ed, as calculated by 4DDA analysis.

inner core and to maximize (minimize) the positive temperature anomaly in the tropopause above the storm. This hypothesis can be tested as additional tropical cyclone data sets with high quality upper-tropospheric winds and temperatures become available.

Pressure-radius plots of \bar{u}_L indicate variations in the pressure level of the maximum outflow, which is similar to that observed in Flo. From 00 UTC 14 September through 18 UTC 15 September (e.g., Figure 4.61), the maximum outflow is concentrated at 150 mb. As Ed reaches maximum intensity on 16 September, the level

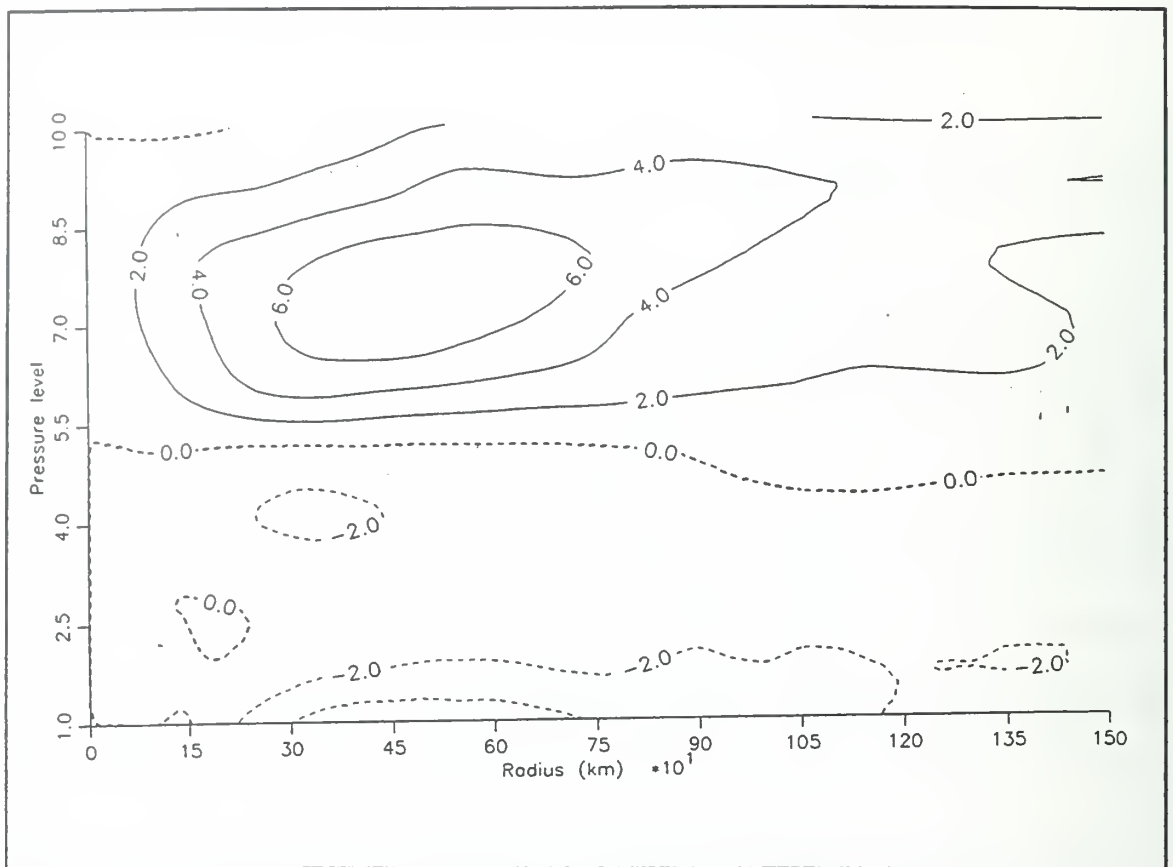


Fig. 4.62. Radial winds as in Figure 4.11, except at 00 UTC 18 September for Typhoon Ed, as calculated by 4DDA analysis.

of maximum outflow varies between 200 and 150 mb. As the storm weakens, the outflow character changes from a narrow vertical ribbon to a broader upper-tropospheric flow. Simultaneously, the level of maximum outflow decreases to 250 mb (e.g., Figure 4.62). Although Ed did not interact with a mid-latitude trough as it weakened, a common characteristic with Flo was an increase in the vertical extent of the outflow, and an implied weakening of the transverse circulation as both storms decreased in intensity.

c. *Relative Angular Momentum Eddy Flux Convergence*

Some significant differences between radius-time plot of 200-mb EFC calculated from the 4DDA and MQ analyses (Figures 4.63a and b) are evident. For example, the 4DDA-derived EFC has a possible inward transport of positive EFC that begins with an area of 5-10 $\text{m s}^{-1}/\text{day}$ at 1050-1350 km radius at 06 UTC 14 September and is followed 30 h later by an area of 10-15 $\text{m s}^{-1}/\text{day}$ at a radius of 400-650 km from Ed. For these times and radii, the MQ-derived EFCs are near zero. An examination of the 200 mb total wind fields for 12 UTC 15 September (Figures 4.58a and b) shows that the major difference in the analyses is about 500-600 km east-northeast of Ed, which is just east of Luzon. The 4DDA analysis depicts northwesterly winds in excess of 10 m s^{-1} for this region, while the Multi-quadric analysis has light northwesterly winds. Although dozens of CTW observations for this area are found at 150 mb (Figure 4.64), no 200-mb wind observations exist. Consequently, the MQ analysis is substantially weighted towards the NOGAPS first-guess wind field. The OI scheme in the 4DDA analysis uses the observations at 150 mb to infer the stronger winds at 200 mb. Therefore, the remainder of this section will discuss the 4DDA-derived EFC.

Pressure-radius plots of EFC (e.g., Figure 4.65) show substantial positive values throughout the troposphere above 500 mb on 14, 16, and 17 September, with mean 200 mb EFC values of 5-10 $\text{m s}^{-1}/\text{day}$. Prior to 06 UTC 14 September and after 12 UTC 17 September, the mean EFC was near zero $\text{m s}^{-1}/\text{day}$. This contrasts with

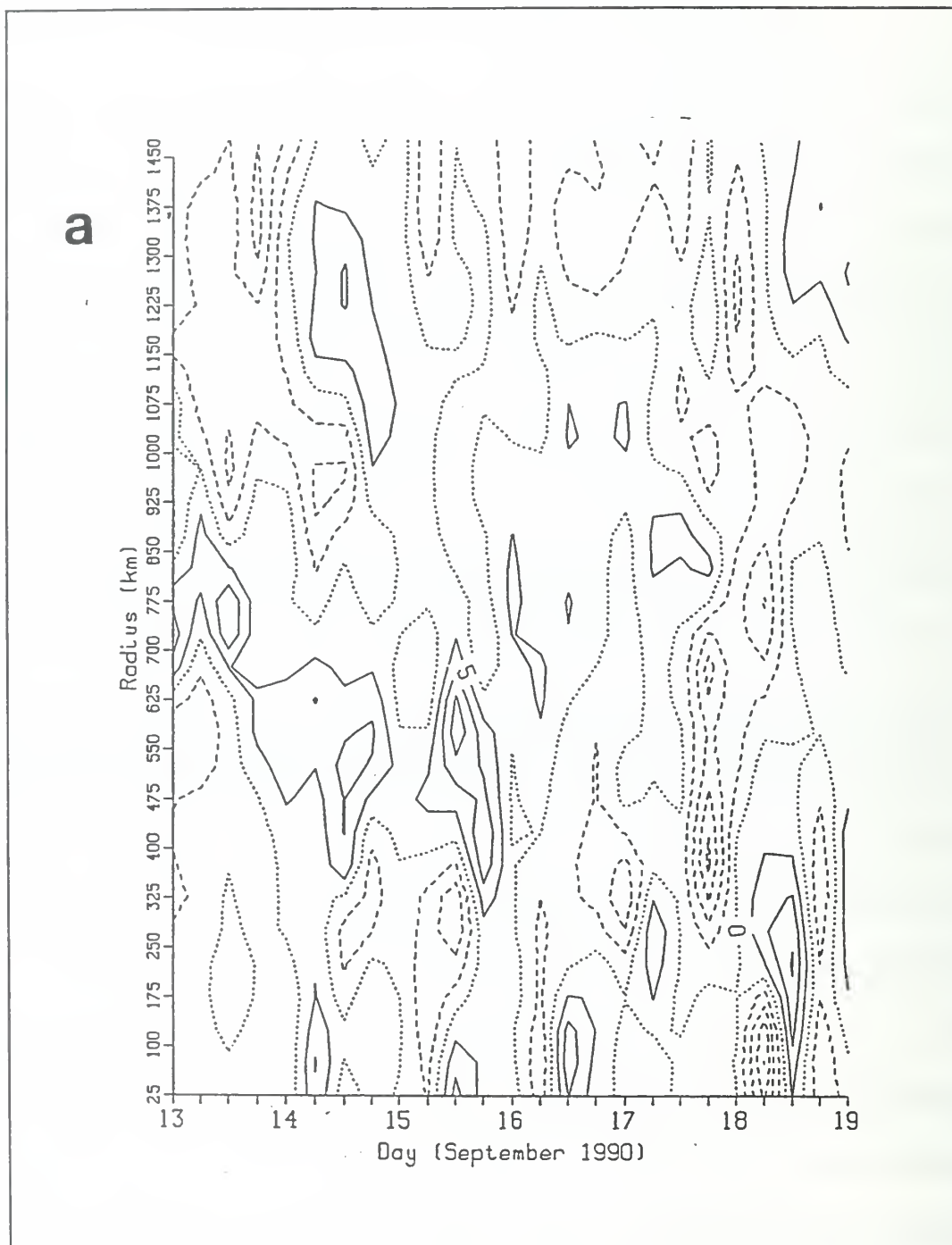


Fig. 4.63. EFC values as in Figure 4.14, except for Typhoon Ed, as calculated by (a) 4DDA analysis and (b) MQ analysis.

b

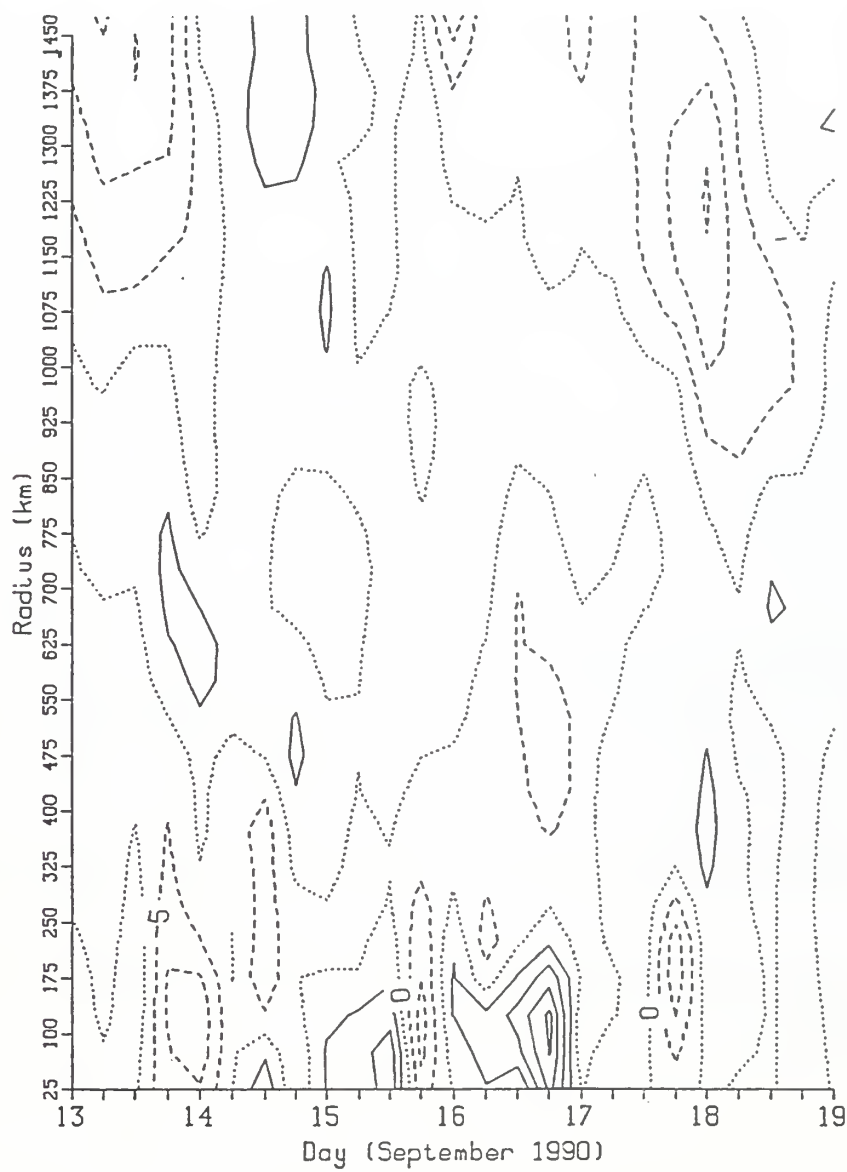


Fig. 4.63. Continued.

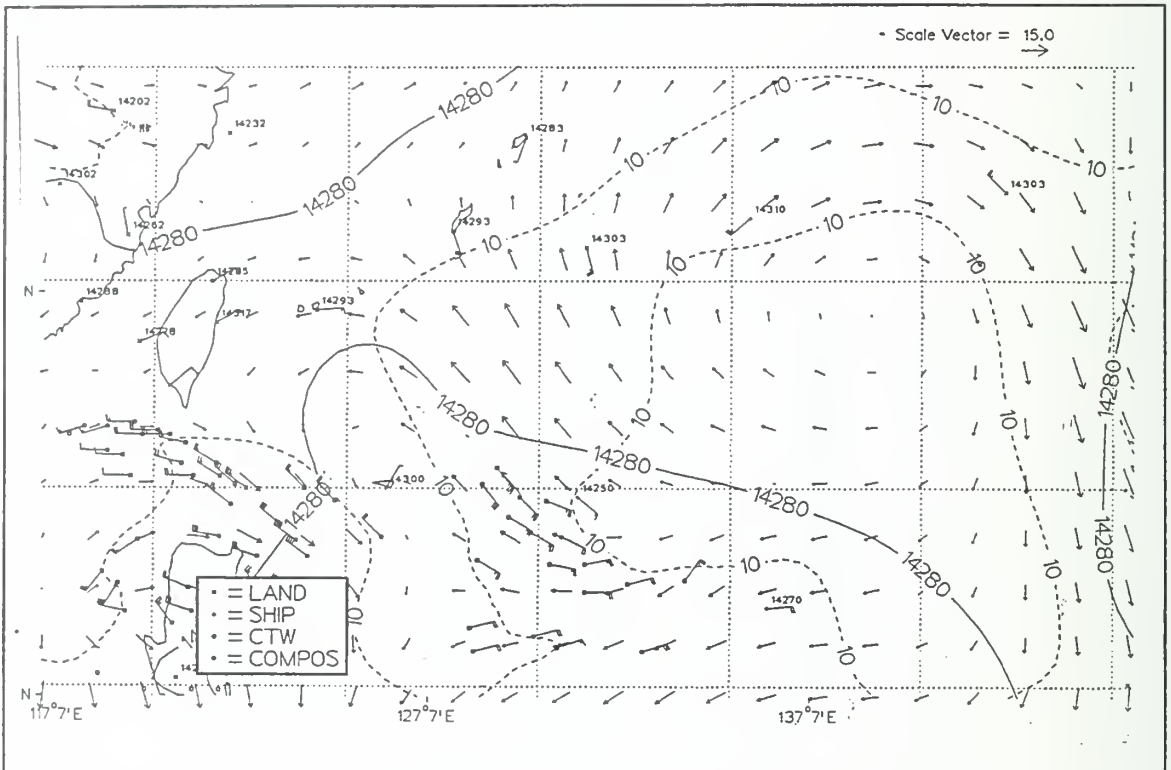


Fig. 4.64. Observations and MQ analyses as in Figure 4.32, except for 150 mb at 12 UTC 15 September.

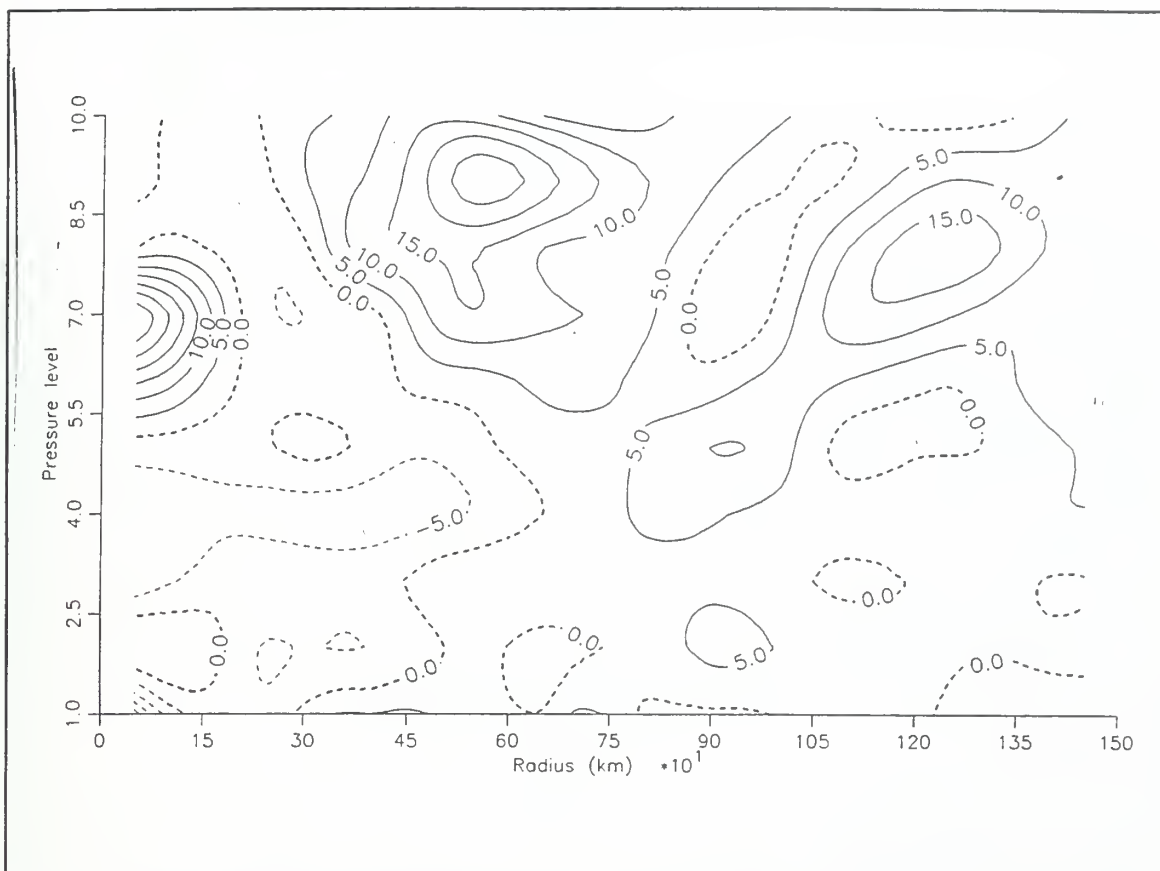


Fig. 4.65. EFC values as in Figure 4.16, except for Typhoon Ed at 12 UTC 14 September, as calculated by 4DDA analysis.

Flo's forcing phase, when the mean EFCs were stronger (10 and $20 \text{ m s}^{-1}/\text{day}$) and were concentrated in the upper troposphere.

The EFC values on 15 September most closely resemble the pattern analyzed for Flo. That is, the region of positive EFC is above 250 mb , and extends from the center of Flo out to 1500 km (Figure 4.66). Although it may be a coincidence, Ed intensified by 10 m s^{-1} in 24 h commencing at 18 UTC 15 September.

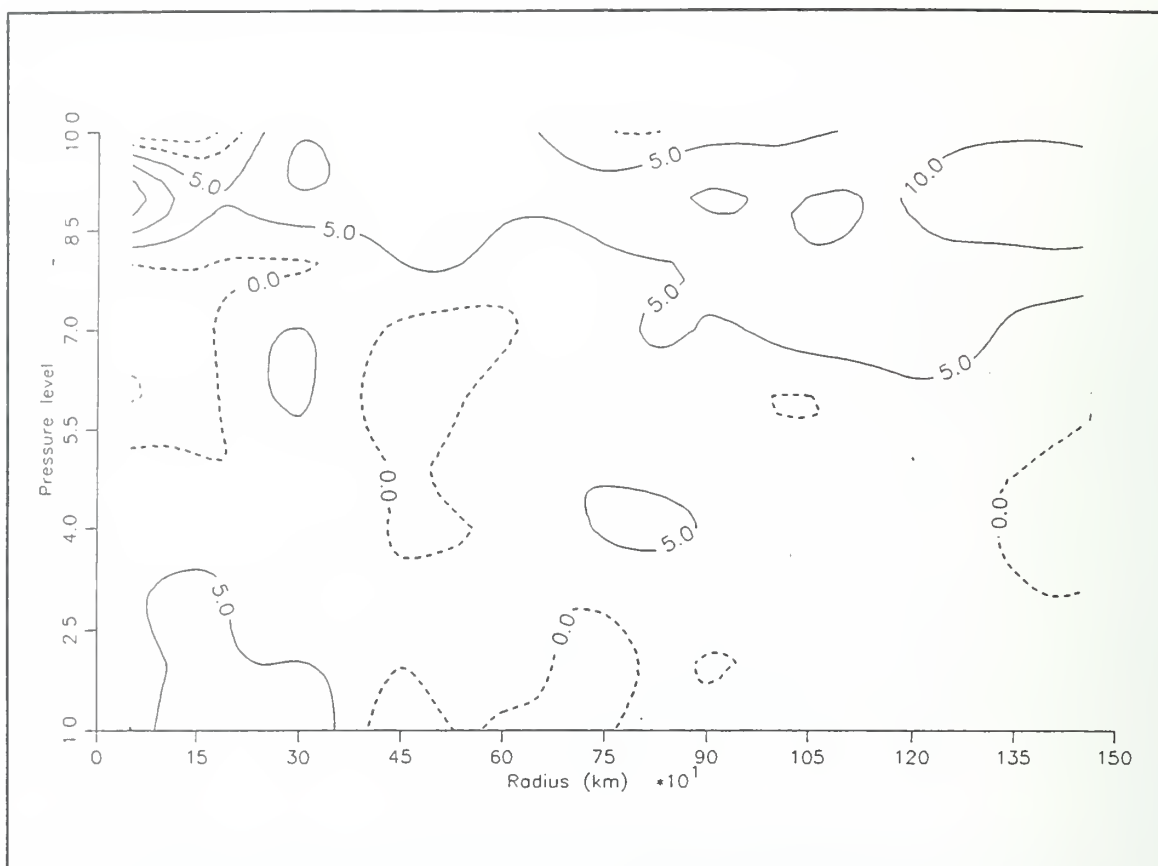


Fig. 4.66. EFC values as in Figure 4.65, except at 00 UTC 15 September, as calculated by 4DDA analysis.

In summary, the EFC calculations of both Typhoons Ed and Flo lend evidence to the conclusion that the **vertical structure** and temporal length of forcing of the EFC may be significant to any subsequent intensification. Based on these case studies, factors that appear to be favorable for intensification are sustained (> 12 h), strong ($> 10 \text{ m s}^{-1}/\text{day}$) EFC forcing concentrated above 250 mb and extending over substantial radii from the storm.

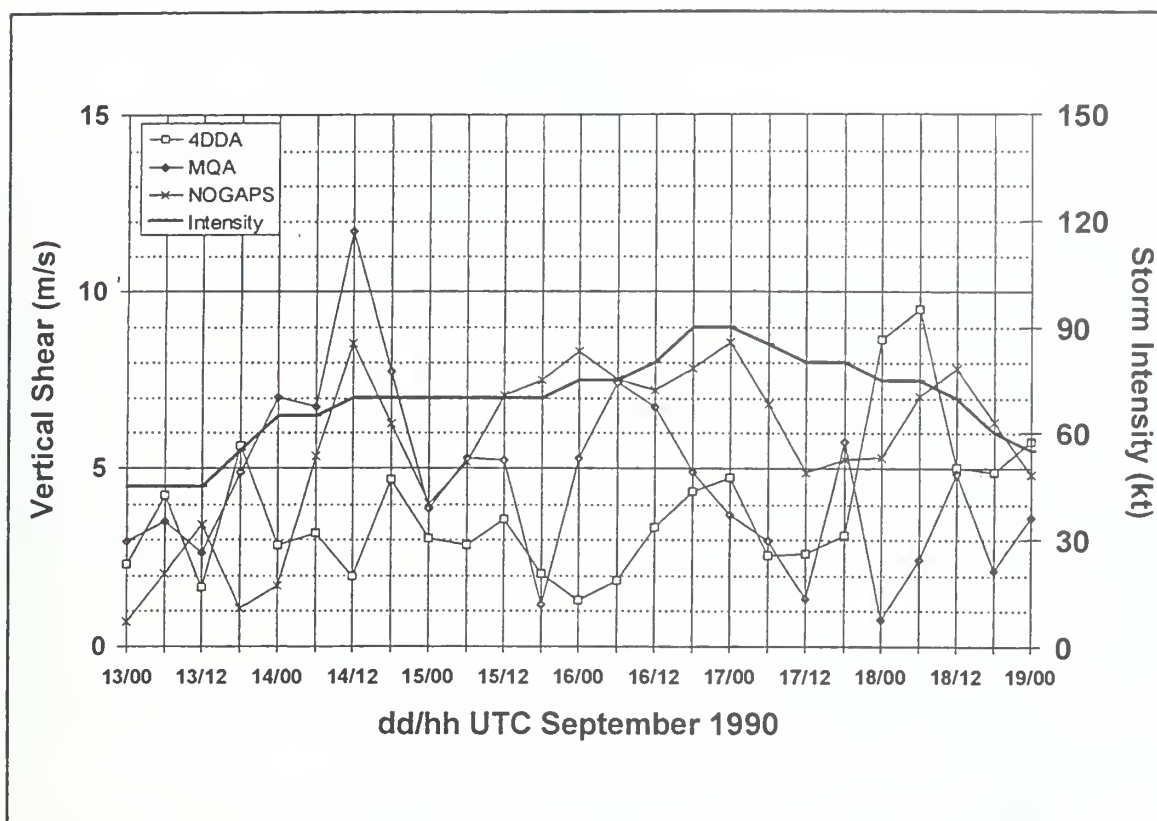


Fig. 4.67. Vertical wind shear as in Figure 4.18, except for Typhoon Ed.

d. Vertical Wind Shear

The vertical wind shear was calculated for Typhoon Ed using the same method as described above for Flo. The 850-200 mb wind shears using the 4DDA, MQ, and NOGAPS analyses are shown in Figure 4.67. While the agreement is generally good, the MQ analysis wind shear at 12 UTC 14 September is nearly 5 m s^{-1} higher than the wind shear using the 4DDA analysis. Unfortunately, few 200 mb observations were available within 600 km of Ed at this time. However, the vertical shear maxima at 12 UTC 14 September, 06 UTC 16 September, and 18 UTC 17 September are similar in both analyses.

| Layer (mb) Analysis | | Vertical Shear Magnitude | | | |
|---------------------|------|--------------------------|--------------------|------------|--------------------|
| | | Flo | | Ed | |
| | | Mean Shear | Standard Deviation | Mean Shear | Standard Deviation |
| 850-500 | 4DDA | 4.0 | 2.4 | 3.7 | 2.1 |
| 850-500 | MQ | 2.4* | 1.1 | 2.1* | 1.3 |
| 850-300 | 4DDA | 5.5 | 2.5 | 3.3 | 1.7 |
| 850-300 | MQ | 3.8 | 2.0 | 2.9 | 1.4 |
| 850-200 | 4DDA | 6.1 | 3.1 | 4.5 | 2.1 |
| 800-200 | MQ | 4.1 | 2.2 | 4.7 | 2.5 |
| 300-200 | 4DDA | 3.7 | 2.5 | 3.8 | 1.7 |
| 300-200 | MQ | 3.6 | 2.3 | 5.2 | 2.9 |
| 300-150 | 4DDA | 4.8 | 3.4 | 5.7 | 2.4 |
| 300-150 | MQ | 4.9 | 2.9 | 7.3 | 2.8 |

*mean shear calculated using MQ analyses is statistically lower than mean shear calculated using 4DDA analyses.

Table 4.2. 4DDA AND ETA-DERIVED MEAN VERTICAL WIND SHEAR (m s^{-1}) AND STANDARD DEVIATION (m s^{-1}) FOR SELECTED LAYERS.

Using the 4DDA analysis, the 850-200 mb wind shear over the life of Ed averaged 4.5 m s^{-1} , or only 74% of the average wind shear for Flo (Table 4.2). While this vertical wind shear in Ed is not statistically different (at the 95% confidence interval) from that in Flo, perhaps due to the small sample size, it is emphasized that low wind shear and high SST values were not sufficient to cause Ed to deepen rapidly. This result provides evidence that the large-scale environment may actively enhance (through sustained, upper-tropospheric EFC that "forces" an environment in which the inner-core

vertical wind shear and horizontal temperature gradients are minimized) tropical cyclone intensification, rather than simply hinder development through varying magnitudes of wind shear as has been previously argued (e.g., Merrill 1988).

Another characteristic of the Ed vertical shear analysis is the weak **positive** correlation with the storm intensity. As will be shown in following section, the correlation between the 850-200 mb wind shear and storm intensity are statistically significant (at the 95% level) for the 6-, 12-, and 18-h future storm intensities. However, correlations between wind shear and intensity change are near zero. That is, the wind shear could not be used as a predictor to determine the rate of either intensification or weakening experienced by Ed at 6, 12, or 24 h in the future.

Again, these results do not imply that vertical shear is beneficial for tropical cyclones. Rather, the low values of wind shear observed throughout the Ed evolution appear to have little positive or negative impact on the storm. Clearly, these low vertical shears were not sufficient to cause Ed to deepen rapidly. The conclusion is that low wind shear is a necessary, but not a sufficient, condition for rapid tropical cyclone intensification.

D. CORRELATION BETWEEN PHYSICAL PARAMETERS AND STORM INTENSITY AND INTENSITY CHANGE

The 50 km gridded 4DDA and MQ analyses allow numerous correlations to be calculated between various physical parameters and TC intensity or intensity change. These correlations were calculated for radial and tangential wind, EFC, absolute vorticity, and vertical wind shear. All variables were derived in a storm-moving,

cylindrical coordinate system. For all variables except wind shear, correlations were calculated by pressure level (850, 700, 500, 400, 300, 250, 200, and 150 mb) and by radius (from 50 km to 1500 km in 50 km increments). In addition, an area-weighted (400 km - 1200 km) value of the parameter was calculated. These parameters were correlated with both intensity and future 6-h intensity change from 00 h to 48 h in 6-h increments. The 850-500, 850-300, 850-200, 300-250, 300-200, and 300-150 mb vertical wind shear values averaged between 200 and 600 km radius were also correlated with current and future (00 to 48 h) storm intensity and intensity change. Correlations were not calculated for any time after a storm had made landfall.

These correlations must be interpreted with substantial caution. Time and space correlations taken from 6-h analyses at gridpoints only 50 km apart, respectively, are not independent observations. The existence of a particular correlation in one dataset does not necessarily imply a physical relationship between that parameter and storm intensity. The purpose of conducting this portion of the study is to examine thoroughly the dataset for clues to physical relationships that might not otherwise be detected. Any such relationship that is evident in multiple storms is particularly interesting.

Independent datasets from Typhoons Ed and Flo were used to search for any common correlations. As described in Elsberry *et al.* (1990), the TCM-90 experiment also conducted IOPs during Typhoons Yancy (Figure 4.68) and Zola (Figure 4.69). These two storms have been analyzed only by the 4DDA analysis. A 50 km gridded dataset was produced. The intent here was not a detailed study of Typhoons Yancy and

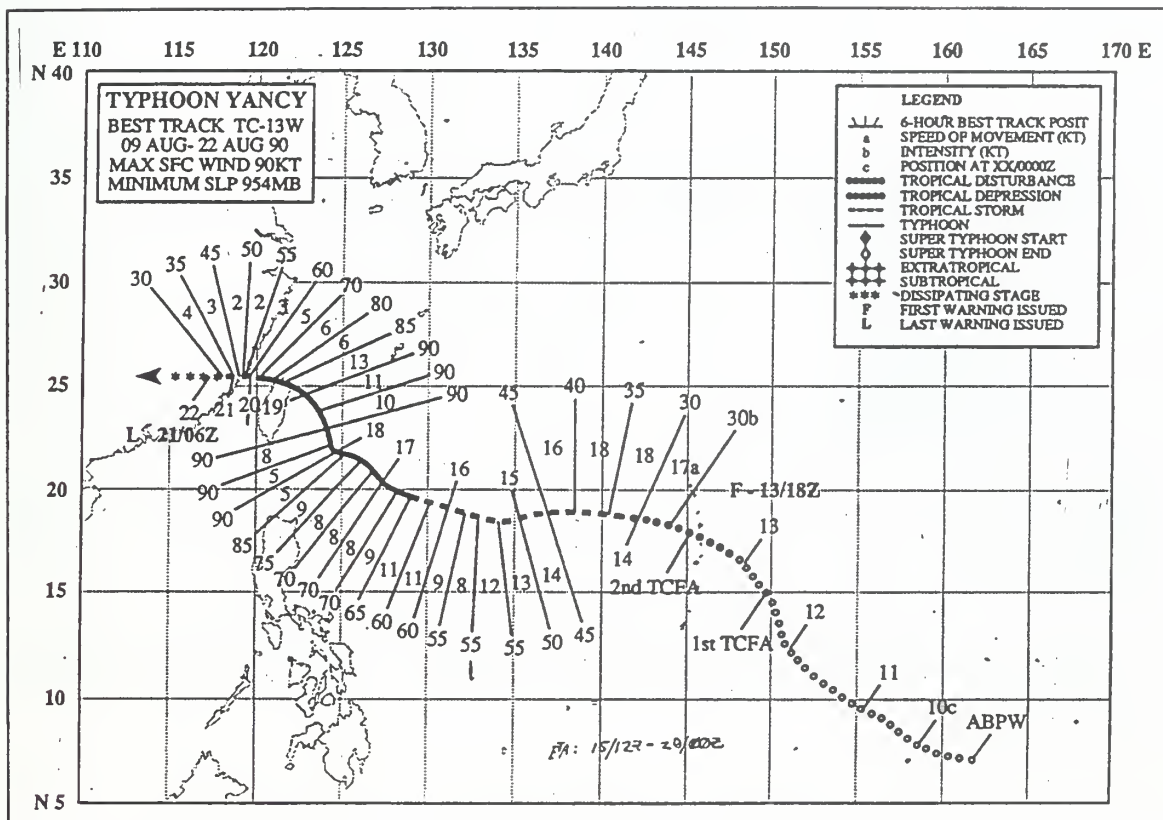


Fig. 4.68. Best-track information for Typhoon Yancy from Annual Tropical Cyclone Report (JTWC 1990).

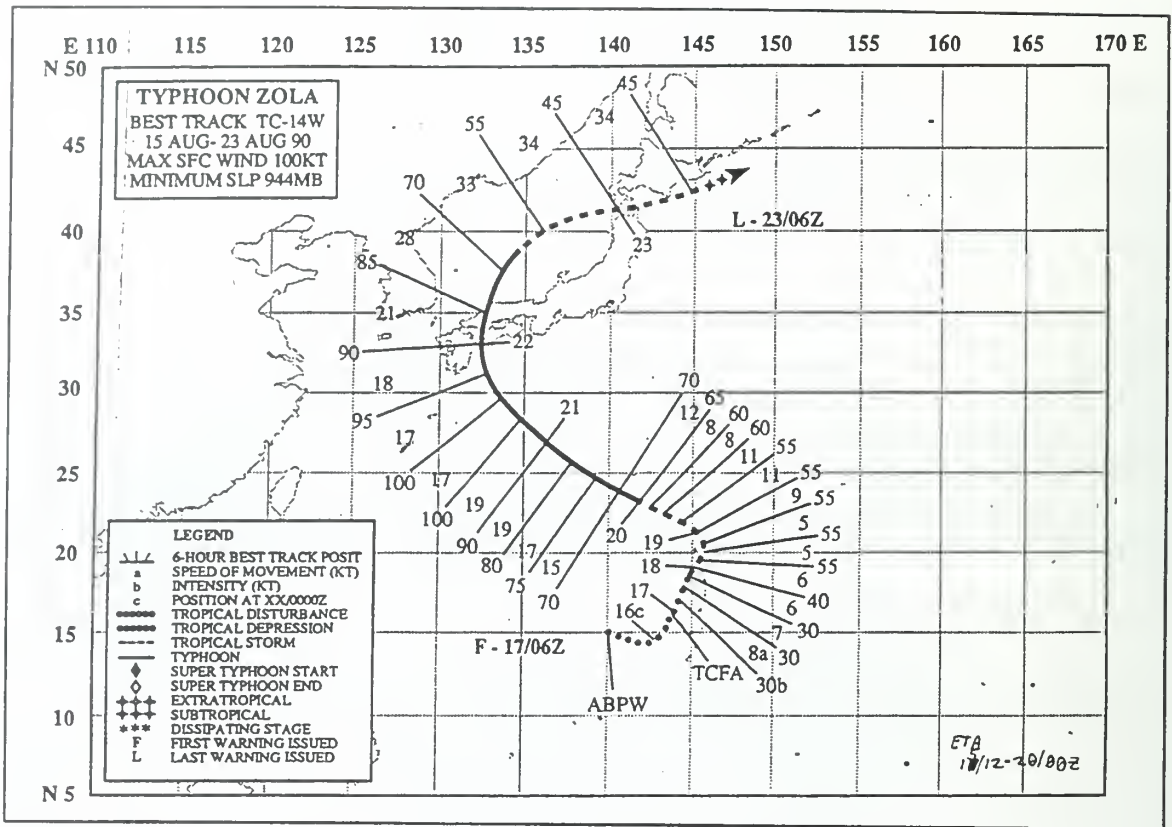


Fig. 4.69. Best track information for Typhoon Zola from Annual Tropical Cyclone Report (JTWC) (1990).

Zola *per se*, but rather to test the general applicability of any correlations common to both Ed and Flo.

1. Relative Angular Momentum Eddy Flux Convergence

Summaries of the 4DDA 400-1200 km area-averaged correlation of 200 mb EFC in the upper troposphere with 12-, 24-, 36-, and 48-h intensity and rate of intensity change for Ed and Flo are given in Tables 4.3 and 4.4, respectively. While the 200-mb EFC over the 400-1200 km area correlation with the 48 h intensity for Ed is 0.77 ($R^2 = 59\%$), the same correlations for Flo are weakly negative. Conversely, while the 200-mb

| A | | | | | | |
|----------|-------|---------|---------|----------|-----------|----------|
| | # Obs | 300-600 | 600-900 | 900-1200 | 1200-1500 | 400-1200 |
| 0h | 22 | 0.06 | 0.04 | 0.67 | 0.47 | 0.45 |
| 12h | 20 | 0.17 | 0.36 | 0.60 | 0.44 | 0.55 |
| 24h | 18 | 0.32 | 0.49 | 0.45 | 0.25 | 0.51 |
| 36h | 16 | 0.44 | 0.43 | 0.43 | 0.27 | 0.53 |
| 48h | 14 | 0.51 | 0.25 | 0.83 | 0.65 | 0.77 |

| B | | | | | | |
|----------|-------|---------|---------|----------|-----------|----------|
| | # Obs | 300-600 | 600-900 | 900-1200 | 1200-1500 | 400-1200 |
| 0h | 21 | 0.18 | 0.15 | -0.29 | -0.23 | -0.11 |
| 12h | 19 | -0.17 | -0.16 | -0.40 | -0.54 | -0.37 |
| 24h | 17 | 0.17 | -0.01 | -0.09 | 0.05 | 0 |
| 36h | 15 | -0.14 | -0.29 | 0.22 | 0.20 | 0.06 |
| 48h | 13 | 0.18 | 0.15 | -0.14 | 0.20 | 0 |

Table 4.3. CORRELATION BETWEEN ED EFC AND 0-, 12-, 24-, 36-, AND 48-H (A) INTENSITY AND (B) INTENSITY CHANGE FOR THE FOLLOWING RADII: 300-600 KM, 600-900 KM, 900-1200 KM, 1200-1500 KM, AND 400-1200 KM.

EFC correlation with the 48-h intensity change for Flo is also 0.77, the correlation value for Ed is zero! These correlations typify the dilemma researchers have experienced while attempting to generalize the effect EFC has on TC intensification, and have led some (e.g., Fitzpatrick 1997, Merrill and Velden 1996) to question the impact EFC has in causing rapid development of tropical cyclones.

| A | | | | | | |
|----------|-------|---------|---------|----------|-----------|----------|
| | # Obs | 300-600 | 600-900 | 900-1200 | 1200-1500 | 400-1200 |
| 0h | 25 | -0.05 | -0.35 | -0.39 | -0.21 | -.38 |
| 12h | 25 | -0.10 | -0.54 | -0.58 | -0.40 | -.59 |
| 24h | 23 | -0.19 | -0.61 | -0.75 | -0.55 | -.78 |
| 36h | 21 | -0.22 | -0.66 | -0.59 | -0.52 | -.66 |
| 48h | 19 | -0.03 | -0.26 | -0.24 | -0.32 | -.26 |

| B | | | | | | |
|----------|-------|---------|---------|----------|-----------|----------|
| | # Obs | 300-600 | 600-900 | 900-1200 | 1200-1500 | 400-1200 |
| 0h | 25 | -0.06 | -0.37 | -0.40 | -0.38 | -0.41 |
| 12h | 24 | -0.07 | -0.06 | 0 | -0.28 | -0.04 |
| 24h | 22 | -0.07 | 0.42 | 0.43 | 0.14 | 0.42 |
| 36h | 20 | 0.26 | 0.73 | 0.60 | 0.33 | 0.69 |
| 48h | 18 | 0.15 | 0.70 | 0.77 | 0.63 | 0.77 |

Table 4.4. CORRELATIONS AS IN TABLE 4.3, EXCEPT FOR TYPHOON FLO EFC.

As discussed earlier, the vertical structure of the EFC appears to be important. While the area-weighted average of 200 mb EFC for Flo was between $10\text{--}20\text{ m}^{-1}\text{ s}^{-1}/\text{day}$ from 00 UTC 13 September through 06 UTC 14 September (the forcing phase), the EFC values were in excess of $20\text{ m}^{-1}\text{ s}^{-1}/\text{day}$ after 06 UTC 18 September. However, the vertical structure of the EFC was significantly different. In the forcing phase of Flo, the large values of EFC were concentrated in a relatively shallow horizontal layer in the upper troposphere. In the mid-latitude interaction phase, the large values of EFC

extended down through the mid-troposphere. This deep layer of large EFC values appeared to be associated with an increase the convection outside the inner core that resulted in greater divergence. This is believed to contribute to a "short-circuiting" of the in-up-out secondary circulation, and, in conjunction with moderate (but not extreme) vertical wind shear values, may have weakened the typhoon.

The role of the EFC in the forcing phase of Flo is believed to be one of "pre-conditioning" the tropical cyclone environment. That is, the EFC values significantly increased the upper-tropospheric cyclonic winds (the "cyclonic wind burst"), and thereby reducing the vertical tangential wind shear $\left(\frac{\partial \bar{v}_L}{\partial p} \right)$. A thermal wind argument would imply that a reduction in $\frac{\partial \bar{v}_L}{\partial p}$ would lead to a reduction in $\frac{\partial T}{\partial r}$, and an increase in the convective instability. The upper-tropospheric EFC in Flo's forcing phase may have been particularly effective at increasing the upper-level cyclonic winds due to the low values of $\bar{\zeta}_a$ ($< 6 * 10^{-5} \text{ s}^{-1}$) analyzed at 200 mb by both 4DDA and MQ schemes between 300 km and 1200 km of Flo's center.

The conclusion is that the EFC has not directly "spun up" the tropical cyclone, but has assisted in creating an environment where strong, deep convection may exist. As shown by Fitzpatrick (1997), such convection is a statistically significant precursor to rapid intensification. This is the first study that has documented a cyclonic wind burst at 200 mb and related its formation to sustained (30 h), strong upper-level EFCs.

| A | | | | | | |
|----------|-------|---------|---------|----------|-----------|----------|
| | # Obs | 300-600 | 600-900 | 900-1200 | 1200-1500 | 400-1200 |
| 0h | 22 | 0.63 | 0.63 | 0.49 | 0.46 | 0.66 |
| 12h | 20 | 0.37 | 0.50 | 0.53 | 0.42 | 0.56 |
| 24h | 18 | 0.43 | 0.53 | 0.45 | 0.55 | 0.54 |
| 36h | 16 | 0.57 | 0.44 | 0.16 | 0.43 | 0.38 |
| 48h | 14 | 0.62 | 0.33 | -0.32 | -0.23 | 0.14 |

| B | | | | | | |
|----------|-------|---------|---------|----------|-----------|----------|
| | # Obs | 300-600 | 600-900 | 900-1200 | 1200-1500 | 400-1200 |
| 0h | 21 | -0.59 | -0.33 | -0.11 | -0.21 | -0.32 |
| 12h | 19 | -0.20 | -0.18 | -0.25 | -0.03 | -0.24 |
| 24h | 17 | 0.06 | -0.11 | -0.40 | -0.25 | -0.26 |
| 36h | 15 | 0 | -0.01 | -0.31 | -0.53 | -0.20 |
| 48h | 13 | -0.53 | -0.74 | -0.56 | -0.58 | -0.76 |

Table 4.5. CORRELATIONS AS IN TABLE 4.3, EXCEPT FOR TYPHOON ED TANGENTIAL WIND (\bar{v}_L).

2. Tangential Wind

The correlations between the upper-tropospheric 4DDA tangential and radial winds and the respective storm intensity for Ed and Flo were examined. The correlation coefficients between the 200 mb tangential wind (\bar{v}_L) and storm intensity are given in Tables 4.5 and 4.6 for Ed and Flo, respectively. While the correlations between \bar{v}_L and future intensity for Ed are weakly positive (r^2 values less than 40%), the correlation

between (400 km - 1200 km) \bar{v}_L and the 12-h future intensity for Flo is -0.84 ($r^2 = 71\%$). That correlation increases to -0.90 when calculated for \bar{v}_L between 1200 km - 1500 km.

These high correlations result from the rapidly increasing magnitude of the anticyclonic \bar{v}_L that forms immediately following the forcing phase, and continues through 06 UTC 17 September, which is when Flo reached maximum intensity. As discussed by Merrill and Velden (1996), this increasingly anticyclonic flow is evidence

| A | | | | | | |
|----------|-------|---------|---------|----------|-----------|----------|
| | # Obs | 300-600 | 600-900 | 900-1200 | 1200-1500 | 400-1200 |
| 0h | 25 | -0.12 | -0.80 | -0.87 | -0.90 | -0.84 |
| 12h | 25 | -0.04 | -0.66 | -0.71 | -0.89 | -0.69 |
| 24h | 23 | 0.05 | -0.42 | -0.42 | -0.71 | -0.42 |
| 36h | 21 | 0.24 | -0.12 | -0.10 | -0.39 | -0.09 |
| 48h | 19 | 0.52 | 0.28 | 0.30 | 0.05 | 0.33 |

| B | | | | | | |
|----------|-------|---------|---------|----------|-----------|----------|
| | # Obs | 300-600 | 600-900 | 900-1200 | 1200-1500 | 400-1200 |
| 0h | 25 | 0.19 | 0.51 | 0.55 | 0.20 | 0.54 |
| 12h | 24 | 0.23 | 0.68 | 0.79 | 0.54 | 0.75 |
| 24h | 22 | 0.36 | 0.79 | 0.75 | 0.68 | 0.79 |
| 36h | 20 | 0.31 | 0.79 | 0.83 | 0.84 | 0.82 |
| 48h | 18 | 0.11 | 0.67 | 0.65 | 0.75 | 0.65 |

Table 4.6. CORRELATIONS AS IN TABLE 4.3, EXCEPT FOR TYPHOON FLO TANGENTIAL WIND (\bar{v}_L).

of the storm outflow as it circulates around the developing warm core. Therefore, this high correlation is consistent with a robustly developing tropical cyclone, but should not be considered an independent "precursor" of rapid development. However, the increase in anticyclonic \bar{v}_L during the quiescent and initial part of the Super Typhoon phase indirectly demonstrates the importance of the forcing phase, and its associated EFC. That is, if the high level (between 100 and 150 mb) warm core does not form, it is less likely that the tangential winds will subsequently become rapidly anticyclonic.

In contrast to the strong negative correlation for Flo between \bar{v}_L and 12-h intensity, the relationship between \bar{v}_L and 12-h intensity for Ed is weakly positive, with an r^2 value of 31% for 200 mb \bar{v}_L . As no strong anticyclone developed in conjunction with Ed, this implies that Ed had no strong high-level warm core. This interpretation is consistent with the composite of the thermal differences (Figure 4.3) discussed earlier this chapter. Compared to the evolution in Flo, Ed never completed a forcing stage. Whereas the failure to establish a high-level warm core may not preclude a tropical cyclone from reaching typhoon intensity, successful completion of the forcing phase appears to be necessary for rapid development.

3. Radial Wind

Correlations between 24-h intensity and the outer (400 km - 1200 km) radii 200 mb \bar{u}_L are positive for Typhoon Ed, with 40% of the variance explained (Table 4.7). However, the same correlation for Super Typhoon Flo (Table 4.8) was negative, and explained over 50% of the storm intensity variations! The relationship between the outer

A

| | # Obs | 300-600 | 600-900 | 900-1200 | 1200-1500 | 400-1200 |
|-----|-------|---------|---------|----------|-----------|----------|
| 0h | 22 | 0.44 | 0.41 | 0.65 | 0.59 | 0.55 |
| 12h | 20 | 0.40 | 0.39 | 0.61 | 0.69 | 0.53 |
| 24h | 18 | 0.52 | 0.52 | 0.69 | 0.51 | 0.63 |
| 36h | 16 | 0.49 | 0.35 | 0.42 | -0.02 | 0.43 |
| 48h | 14 | 0.17 | 0.09 | 0.22 | 0.06 | 0.17 |

B

| | # Obs | 300-600 | 600-900 | 900-1200 | 1200-1500 | 400-1200 |
|-----|-------|---------|---------|----------|-----------|----------|
| 0h | 21 | -0.40 | -0.27 | -0.23 | 0.11 | -0.28 |
| 12h | 19 | -0.15 | -0.14 | -0.31 | -0.55 | -0.24 |
| 24h | 17 | 0.01 | -0.13 | -0.35 | -0.47 | -0.21 |
| 36h | 15 | -0.53 | -0.49 | -0.47 | -0.38 | -0.52 |
| 48h | 13 | -0.11 | 0.03 | 0.02 | 0.30 | 0 |

Table 4.7. CORRELATIONS AS IN TABLE 4.3, EXCEPT FOR TYPHOON ED RADIAL WIND (\bar{u}_L).

A

| | # Obs | 300-600 | 600-900 | 900-1200 | 1200-1500 | 400-1200 |
|-----|-------|---------|---------|----------|-----------|----------|
| 0h | 25 | -0.43 | -0.41 | -0.46 | -0.54 | -.46 |
| 12h | 25 | -0.51 | -0.55 | -0.65 | -0.73 | -.62 |
| 24h | 23 | -0.56 | -0.67 | -0.78 | -0.80 | -.74 |
| 36h | 21 | -0.52 | -0.62 | -0.68 | -0.69 | -.67 |
| 48h | 19 | -0.34 | -0.42 | -0.41 | -0.40 | -.43 |

B

| | # Obs | 300-600 | 600-900 | 900-1200 | 1200-1500 | 400-1200 |
|-----|-------|---------|---------|----------|-----------|----------|
| 0h | 25 | -0.14 | -0.24 | -0.30 | -0.30 | -0.27 |
| 12h | 24 | 0.09 | -0.10 | -0.14 | -0.02 | -0.10 |
| 24h | 22 | 0.11 | 0.20 | 0.31 | 0.36 | 0.25 |
| 36h | 20 | 0.40 | 0.46 | 0.52 | 0.48 | 0.50 |
| 48h | 18 | 0.31 | 0.50 | 0.66 | 0.74 | 0.58 |

Table 4.8. CORRELATIONS AS IN TABLE 4.3, EXCEPT FOR TYPHOON FLO RADIAL WIND (\bar{u}_L).

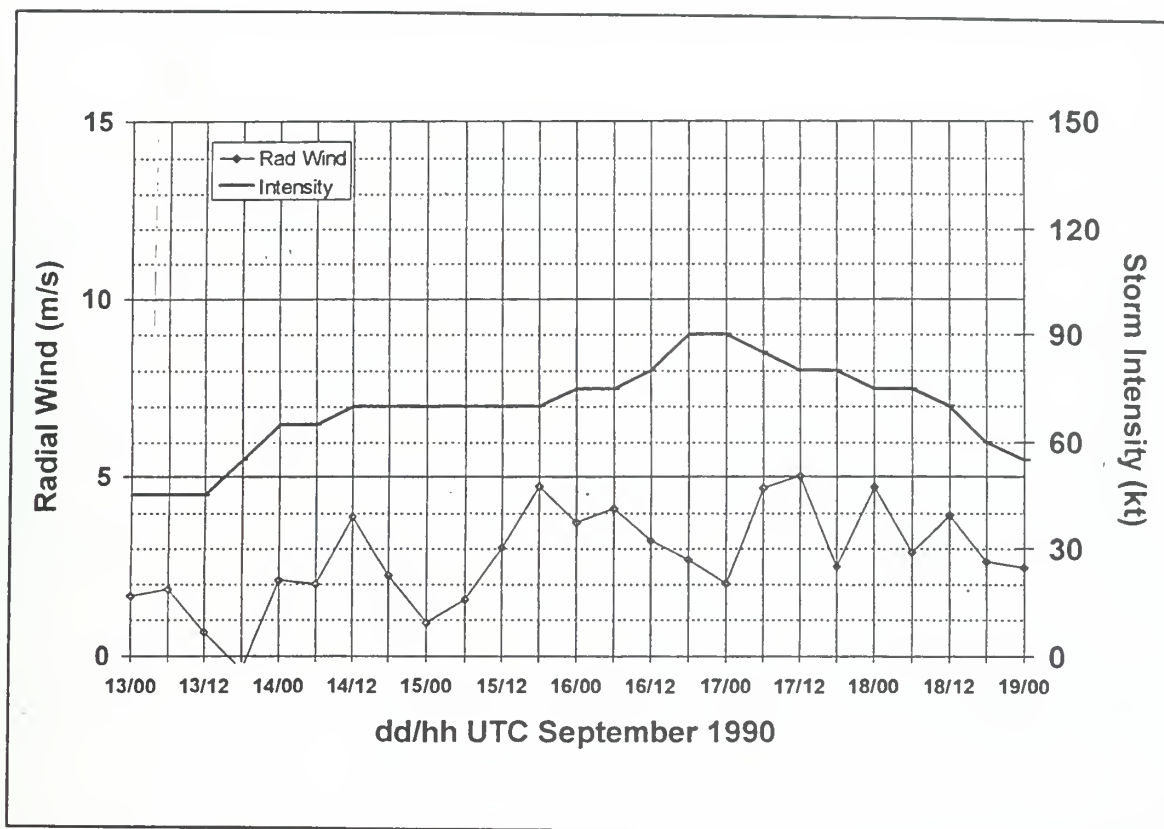


Fig. 4.70. 200 mb \bar{u}_L (m s^{-1}) averaged between 400 km and 1200 km and intensity (kt) for Typhoon Ed, as calculated by 4DDA analysis.

radii 200 mb \bar{u}_L and 24-h intensity are shown in Figures 4.70 and 4.71 for Ed and Flo, respectively. The outer radii \bar{u}_L values for Ed were between 0 and 2 m s^{-1} until the storm intensified from 39 to 46 m s^{-1} , at which time \bar{u}_L increased to 2-3 m s^{-1} . Conversely, outer radii \bar{u}_L values for Flo were 3-8 m s^{-1} in the forcing phase (through 12 UTC 14 September), and then decreased to less than 4 m s^{-1} throughout the rapid intensification and Super Typhoon phases. This minimum in observed \bar{u}_L is consistent with the Merrill and Velden (1996) isentropic analysis of the Flo outflow (Figure 4.72).

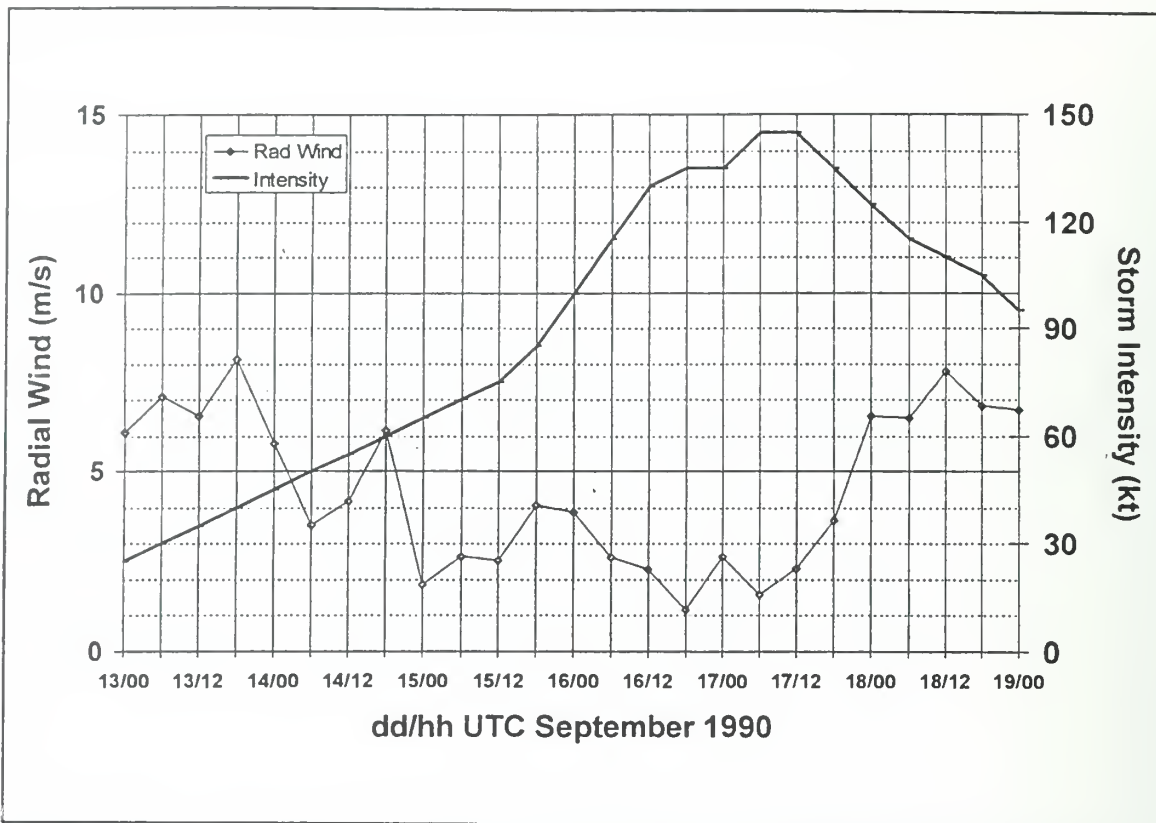


Fig. 4.71. Radial winds and intensity as in Figure 4.70, except for Typhoon Flo.

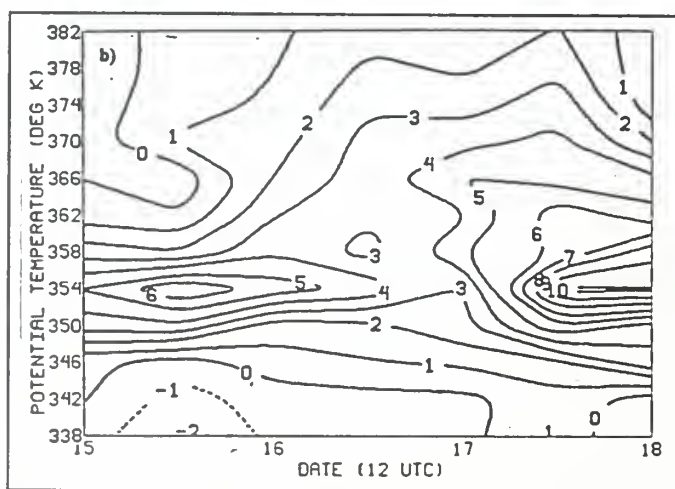


Fig. 4.72. Time - potential temperature section of u_L at 666 km radius computed from rawinsonde and CTW data (From Merrill and Velden 1996, Figure 6b).

Commencing with the mid-latitude interaction phase, the outer radii \bar{u}_L values steadily increased, and were 6-8 m s⁻¹ by 00 UTC 18 September.

These calculations demonstrate that the outflow \bar{u}_L , and thus divergence, are not proportional to typhoon intensity. This lack of a correlation implies that storm intensity depends upon the organization of convection in the typhoon, rather than the absolute amount of divergence. The large magnitude of \bar{u}_L in the Flo forcing phase may be a result of the enhanced secondary circulation forced by strong, sustained EFC. As the external forcing decreases and the high-level warm core develops, the storm outflow appears to become more "efficient", and develops well-defined outflow channels that are reflected by the sharp increase in anticyclonic \bar{v}_L . \bar{u}_L then increases again in the mid-latitude interaction phase, as the mid-latitude trough-induced mid-level EFC disrupts the existing secondary circulation, which leads to the storm weakening.

Conversely, the outer radii (400-1200 km) 200 mb \bar{u}_L values for Ed (Figure 4.70) are less than 2 m s⁻¹ until 18 UTC 15 September. This observation is consistent with the 400-1200 km mean EFC values being less than 10 m s⁻¹/day for the duration of the storm. That is, little (if any) external forcing existed, so only minimal divergence was available to focus.

| Storm | 4DDA Analysis | MQ Analysis |
|-------|---------------|-------------|
| Ed | 0.86 | 0.92 |
| Flo | 0.82 | 0.71 |
| Yancy | 0.91 | --- |
| Zola | 0.81 | --- |

Table 4.9. CORRELATION BETWEEN 500 MB ζ_a AVERAGED BETWEEN 500 - 700 KM AND 48-h STORM INTENSITY.

4. Absolute Vorticity

While the analyses for Ed and Flo have produced very different future intensity correlations with EFC, \bar{v}_L , and \bar{u}_L , the correlation between mid-level (500 mb), mid-radii (500-700 km) azimuthally-averaged absolute vorticity ($\bar{\zeta}_a$) and 48-h future intensity is of similar sign and magnitude for both storms. This correlation was also found for Typhoons Yancy and Zola (Table 4.9). Of all the correlations examined, this was the only one common to all four storms. In each case, the $\bar{\zeta}_a$ correlation explained at least 66% of the variance of the storm 48-h intensity.

This result compares favorably with the Fitzpatrick (1997) result that no more than 38% of the 48-h intensity variance may be explained by a single variable when using climatological, synoptic wind, and satellite infrared data as predictors. Fitzpatrick's 48-h multiple regression analysis explained about 60% of the total 48-h intensity variance. The most significant predictor in Fitzpatrick's single and multiple regressions was the difference between the storm intensity and the MPI as determined by the observed SST. While this predictor may be statistically crucial, it does not help

distinguish between a rapidly deepening storm (Flo) and a slow developer (Ed) when both form over uniformly warm waters in the western North Pacific basin.

While this strong positive correlation is an intriguing and unexpected result, it should be viewed with substantial caution. Few unique TCM-90 observations were available at 400 and 500 mb to enhance either the 4DDA or MQ analyses. Although this result was common to all four storms examined, this is still a very small sample size. Such a high correlation is unexpected because of the high inertial stability in the lower and mid-troposphere. As discussed by Holland and Merrill (1984), this inertial stability significantly restricts the direct influence of any lower-troposphere environmental forcing on the storm inner core.

The correlation between the mid-level vorticity and Flo's 48 h intensity (Figure 4.73) might be explained by the storm intensifying and expanding radially through 00 UTC 15 September, then contracting just prior to rapid intensification. However, the 500 mb \bar{v}_L values calculated between 500 and 700 km only vary between 9-14 m s⁻¹ throughout the IOP, and do not correlate with the $\bar{\zeta}_a$. Also, the vorticity maximum for Ed (Figure 4.74) occurred at 06 UTC 15 September while the storm was at a steady intensity of 36 m s⁻¹. The 06 UTC 15 September 500 mb total wind field (not shown) does not depict any areal expansion of Ed, nor is there any obvious contraction at later times.

An alternate hypothesis may consider this mid-level, outer core vorticity as another source of environmental forcing. While the momentum convergence required

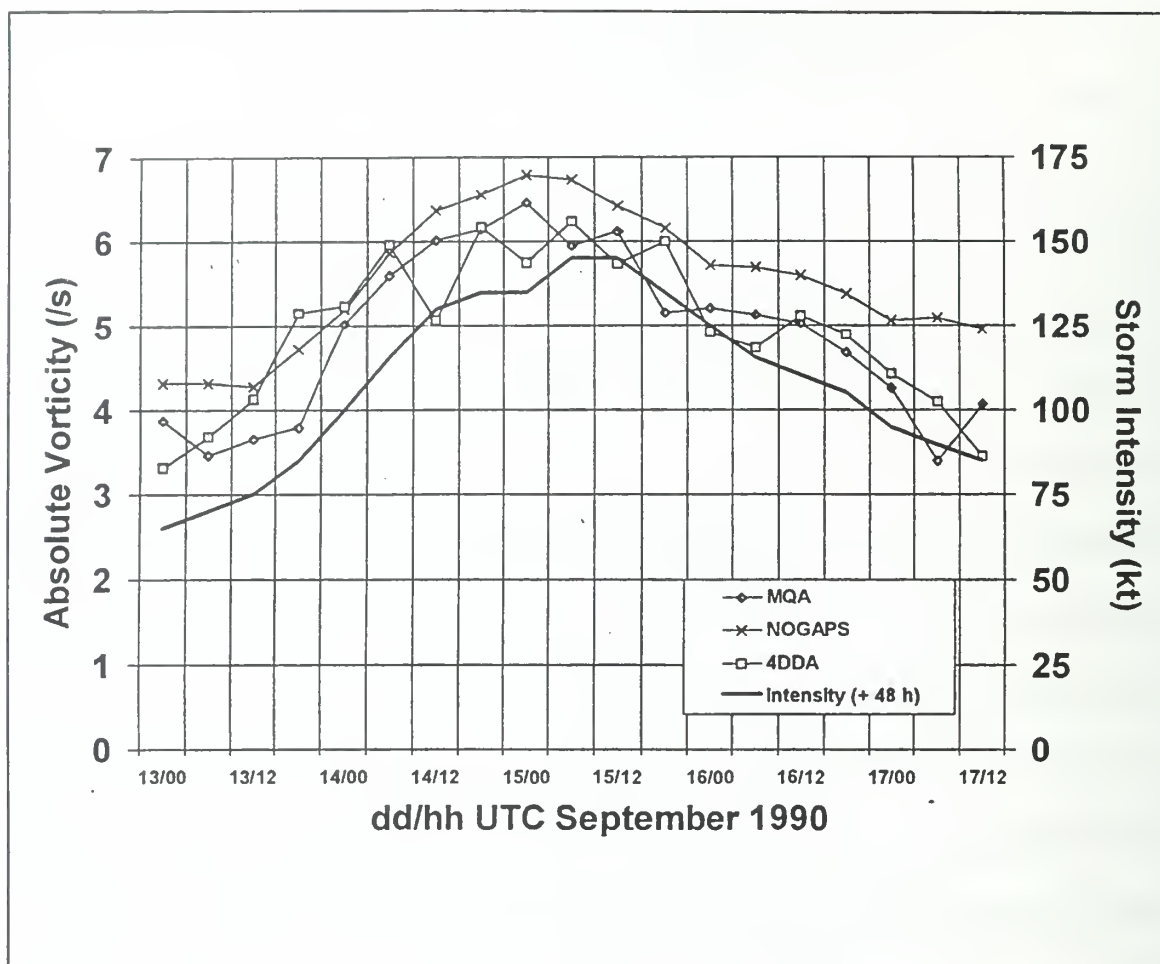


Fig. 4.73. 500 mb absolute vorticity $\bar{\zeta}_a$ (s^{-1}) averaged between 500 km and 700 km and intensity (kt) 48 h after that time for Typhoon Flo.

to increase the intensity (at a small radius of maximum winds) is small relative to the forcing required to change the storm size or strength (Holland and Merrill 1984), this vorticity forcing may propagate inwards similar to the manner in which convective rings contract (Willoughby 1990). The $\bar{\zeta}_a$ effect on storm intensity is likely modified by the previously discussed environmental factors (wind shear, vertical structure of the warm core, structure of the radial winds). It may be possible that the 57% increase in 500-mb

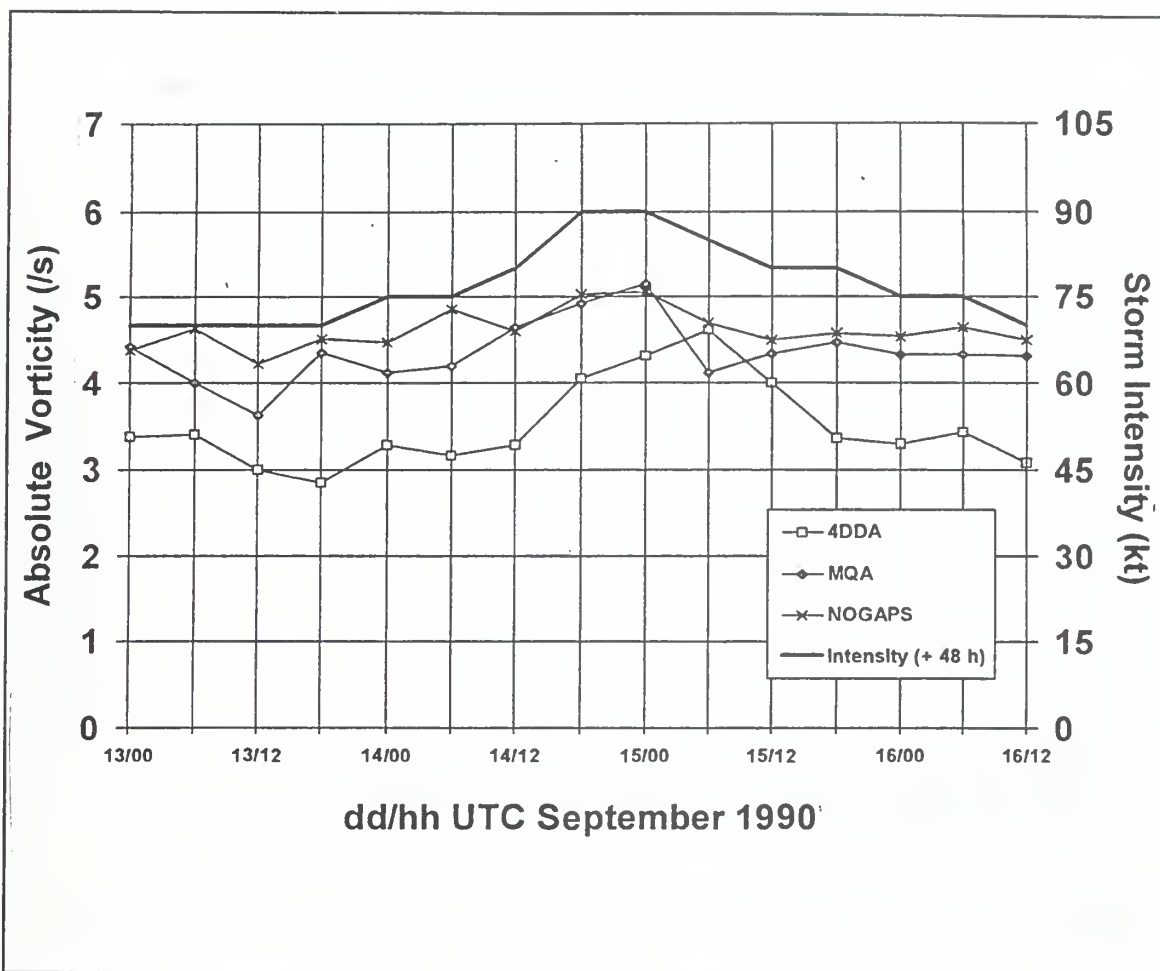


Fig. 4.74. As in Figure 4.73, except for Typhoon Ed.

vorticity for Flo between 00 and 18 UTC 13 September helped create the forcing that concentrated the convection that then formed the high-level warm core, and created a favorable environment for Flo's subsequent rapid intensification. It is not clear if the strong, sustained EFC and consequent increase in 200 mb cyclonic \bar{v}_L affected the mid-level $\bar{\zeta}_a$ field.

Even though the mid-tropospheric data are relatively sparse in this experiment, the consistently positive correlation calculated from these four storms warrants additional

| Analysis | Layer(mb) | 0-h | 12-h | 24-h | 36-h | 48-h |
|----------|-----------|-------|-------|-------|-------|------|
| 4DDA | 850-500 | 0.14 | -0.09 | -0.34 | -0.28 | 0.06 |
| MQ | 850-500 | 0.11 | -0.11 | 0 | 0.46 | 0.40 |
| 4DDA | 850-300 | 0.18 | 0.24 | -0.12 | 0.15 | 0.36 |
| MQ | 850-300 | -0.21 | -0.26 | -0.26 | -0.14 | 0.35 |
| 4DDA | 850-200 | 0.40 | 0.56 | 0.41 | 0.21 | 0.24 |
| MQ | 800-200 | 0.06 | 0.21 | -0.06 | -0.04 | 0.20 |
| 4DDA | 300-200 | 0.29 | 0.46 | 0.08 | 0.04 | 0.13 |
| MQ | 300-200 | 0.22 | 0.18 | -0.19 | 0.04 | 0.41 |
| 4DDA | 300-150 | 0.26 | 0.44 | 0.17 | 0.11 | 0.40 |
| MQ | 300-150 | 0.47 | 0.28 | 0.20 | 0.35 | 0.70 |

Table 4.10. CORRELATION BETWEEN TYPHOON ED VERTICAL WIND SHEAR AT SELECTED LAYERS (MB) AND AVERAGED BETWEEN 200 - 600 KM, AND FUTURE STORM INTENSITY.

research. Recent techniques to remotely observe mid-tropospheric winds (e.g., Velden *et al.* 1997) may assist in determining if these correlations really exist, and, if they do, what the role of mid-level vorticity may be in typhoon intensification.

E. WIND SHEAR

The vertical wind shear was calculated for the 850-500 mb, 850-300 mb, 850-200 mb, 300-200 mb, and 300-150 mb layers. These vertical wind shear values were then correlated with the future intensity values of Ed and Flo (Tables 4.10-4.11).

For both storms, the correlations between 850-500 mb or 850-300 mb wind shear and future intensities are weak. However, the correlation for Flo between the 850-200

| Analysis | Layers (mb) | 0h | 12h | 24h | 36h | 48h |
|----------|-------------|-------|-------|-------|-------|-------|
| 4DDA | 850-500 | -0.13 | -0.26 | -0.36 | -0.36 | -0.15 |
| MQ | 850-500 | -0.17 | -0.37 | -0.48 | -0.38 | -0.04 |
| 4DDA | 850-300 | -0.09 | -0.22 | -0.24 | -0.07 | 0.31 |
| MQ | 850-300 | -0.13 | -0.25 | -0.27 | 0 | 0.27 |
| 4DDA | 850-200 | -0.50 | -0.63 | -0.64 | -0.70 | -0.53 |
| MQ | 800-200 | -0.34 | -0.42 | -0.31 | -0.23 | -0.04 |
| 4DDA | 300-200 | -0.65 | -0.73 | -0.74 | -0.70 | -0.54 |
| MQ | 300-200 | -0.48 | -0.46 | -0.40 | -0.21 | -0.14 |
| 4DDA | 300-150 | -0.81 | -0.78 | -0.74 | -0.53 | -0.38 |
| MQ | 300-150 | -0.70 | -0.72 | -0.66 | -0.43 | -0.23 |

Table 4.11. CORRELATION AS IN TABLE 4.10, EXCEPT FOR TYPHOON FLO.

mb wind shear and Flo's 36-h intensity is -0.71. This result linking lower tropospheric vertical shear with higher storm intensity is in line with expectations. However, it does not show whether the lower vertical shears are a result of a more benign large-scale environment, or if the typhoon outflow has deflected the environmental wind shear around the deep convection, as discussed by Elsberry and Jeffries (1996).

An unexpected result was that the 850-200 mb wind shear correlation with the intensity for Typhoon Ed is **positive**, with a value of +0.56 for the 12-h intensity. As previously discussed, the mean 850-200 mb wind shear associated with Typhoon Ed was 27% less than that associated with Flo. While vertical shear values for Ed and Flo are

not statistically different at a 95% confidence level, these data support the conclusion that low values of wind shear, while necessary for rapid intensification, are not sufficient to trigger the rapid intensification. A study by Fitzpatrick (1997) provides some statistical evidence to support this conclusion. Using operational, 2.5° resolution data, Fitzpatrick performed a multiple regression analysis relating storm intensity to climaticological, synoptic, and satellite-derived parameters for 66 western North Pacific tropical cyclones. He concluded that low vertical wind shear values do not distinguish between slowly and rapidly intensifying tropical cyclones.

A significant difference is also found between Ed and Flo correlations between upper-tropospheric vertical wind shear and storm intensity. While the correlations are weak and positive for Ed, strong negative correlations are calculated between the 300-200 (300-150) mb vertical shear and the 24 (00) hour intensity of Flo. The correlation between present intensity and the 300-150 mb wind shear implies that as Flo intensifies, the shear between these two levels is reduced. This shear value decreased over 65% between 00 UTC 13 September and 18 UTC 14 September, which is 6 h after the completion of the forcing phase. This vertical shear reduction was likely caused by the sustained upper-level EFC that increased the axisymmetric cyclonic tangential wind. An alternate explanation is that Flo moved into a region of very low 300-150 mb wind shear and subsequently rapidly intensified. However, comparison of 300-150 mb wind shear values for Ed and Flo (Figures 4.75 and 4.19) shows that while Flo intensified prior to 12 UTC 14 September with shear values greater than 8 m s^{-1} , Ed weakened after 00 UTC

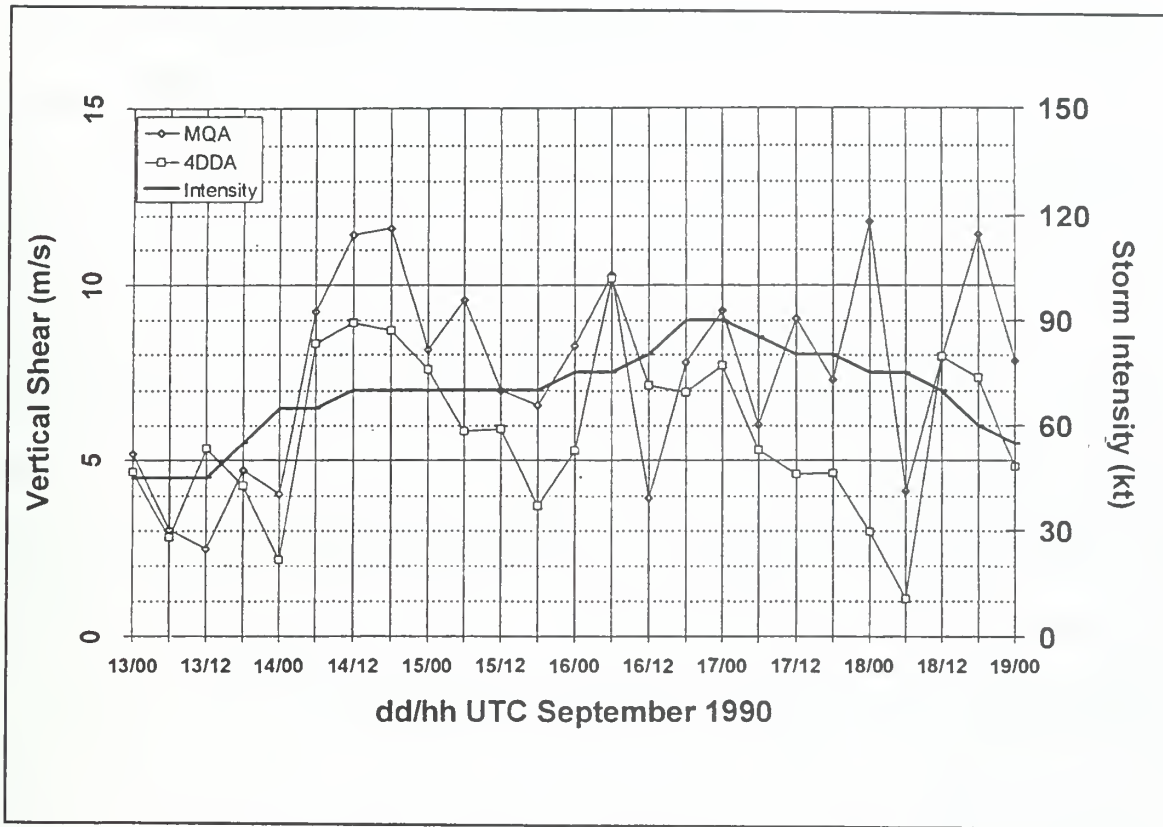


Fig. 4.75. As in Figure 4.19, except for Typhoon Ed.

17 September when sustained 300-150 mb shear values were no greater than 5 m s^{-1} . In conclusion, small upper-tropospheric wind shear values do not appear to be sufficient to cause rapid intensification.

The correlations between 300-200 mb wind shear and future tropical cyclone intensity are very similar to the correlations with the 850-200 mb winds. This is true for both Ed and Flo. Although the sample size is very small, this result supports a conclusion that the vertical wind shear may be most significant at pressure levels co-located with the maximum positive temperature anomaly. In addition, if the tropical wind shear is actually concentrated in a shallow layer just below the tropical cyclone

outflow, rather than evenly distributed throughout the troposphere (Elsberry and Jeffries 1996), the 300-200 mb or 300-150 mb vertical wind shear calculation should capture most of the vertical shear "signal."

F. SUMMARY

Two independent analyses based upon high-resolution TCM-90 observations provide a detailed description, especially in the upper troposphere, of the time-varying structure of Typhoons Ed and Flo. The tangential and radial winds, EFC, and vertical wind shear were closely examined using a cylindrical coordinate system that moved with the individual storm. In addition, correlation coefficients were calculated between the above-listed parameters, absolute vorticity, and the future intensity of each storm.

An original hypothesis for this research stated that outflow-level EFC was a dominant forcing mechanism for future tropical cyclone intensity change. Previous studies that had found either no relationship, or only a weak relationship, between EFC and tropical cyclone intensity had used operational, low (typically 2.5° latitude/longitude) spatial resolution model winds that poorly characterized tropical cyclone outflow layer structure. Therefore it was proposed that EFC values calculated from a high spatial resolution data set, would be highly correlated with future tropical cyclone intensity.

Even with high spatial resolution data in TCM-90, a universal, positive correlation between EFC and future storm intensity was not found. Two possible reasons are suggested for this lack of correlation. First, EFC associated with a mid-latitude trough has a vertical structure that extends down into the mid-troposphere, whereas the EFC

associated with tropical features (e.g., a TUTT cell) is concentrated in the upper troposphere. The mid-level EFC leads to divergence and convection away from the storm inner core, and reduces the efficiency of the "in-up-out" secondary circulation. We have shown that it is equally important to examine the vertical structure of the EFC values as it is to calculate the EFC upper-troposphere magnitudes.

Second, the influence of EFC on tropical cyclone intensity may be indirect (Figure 4.20). That is, sustained, strong EFC is one method of environmental forcing to maximize the efficiency of the convection in the inner core. The EFC, when concentrated in the upper-troposphere, may increase the cyclonic \bar{v}_L and potentially produce a "cyclonic wind burst," which in turn decreases $\frac{\partial \bar{v}_L}{\partial p}$. The decrease in vertical wind shear implies, through thermal wind considerations, a decrease in $\frac{\partial \bar{T}}{\partial r}$. However, the tropical storm is still a warm-core system. The proposed effect would shift the warm core upward to the tropopause and lower stratosphere. This thermal and wind distribution maximizes the efficiency of the secondary circulation, and, for a given amount of latent and sensible heat input, produces the most efficient (intense) tropical cyclone.

This study has reached three significant conclusions concerning the effect of vertical wind shear, and its effect on tropical cyclones. First, we have demonstrated that low values of vertical wind shear and high SSTs are not sufficient environmental factors by themselves to guarantee rapid development. Typhoon Ed never rapidly intensified despite having consistently lower 850 mb - 200 mb vertical shear values than those

calculated for Super Typhoon Flo. While it may be demonstrated that high values of vertical shear are not favorable for tropical cyclone development, the absence of shear does not mandate rapid development.

Second, the routine calculation of the 300 mb - 150 mb shear in a storm-relative, cylindrical coordinate system may provide operational forecasters information relating the degree of "coupling" between a tropical cyclone and the upper-troposphere circulation. Although additional studies are required to confirm the relationship, the data from Super Typhoon Flo appear to show that a tightly coupled system (combined with a favorable large-scale wind shear and SST environment) has a significantly greater potential to deepen rapidly. That is, the 300 mb - 150 mb vertical shear could be used as a "proxy" to measure the effects of any EFC-induced reduction in shear and subsequent alteration in the thermal structure, without having to measure directly either the upper-troposphere temperatures or calculate and interpret the EFC values. The required high-resolution wind data are currently available to the operational community.

Third, we have shown that the interaction of a tropical cyclone with a mid-latitude trough may be much more complex than simply an increased value in vertical wind shear. The vertical shear values encountered by Flo as a mature typhoon were about the same magnitude as those calculated when the storm was steadily intensifying, although the vertical structure of the shear was quite different. It is hypothesized that the reason Flo weakened upon interacting with the mid-latitude trough was due to the associated mid-troposphere EFC enhancing outflow well below the upper-troposphere. This broad

tropospheric outflow effectively "short circuited" the deep transverse circulation required to maintain the storm intensity.

Another potentially significant finding was the high direct correlation between 500 mb $\bar{\zeta}_a$ averaged between 500 km - 700 km and the future 48-h storm intensity. This correlation was observed for both Ed and Flo using the 4DDA, MQ, and NOGAPS analyses. The correlation was also observed for Typhoons Yancy and Zola using the 4DDA analyses. Although the TCM-90 dataset has few additional observations at 500 mb, this correlation is sufficiently high for a variety of tropical cyclones to warrant further research.

Finally, we have demonstrated that both the 4DDA and MQ analyses, although derived by independent means, provided useful, valid, and generally similar depictions of the typhoon dynamics and subsequent correlations with storm intensity (Table 4.12). Specifically, we conclude that the 4DDA assimilation scheme "follows" the observations sufficiently closely to accurately portray regions of substantial divergence in the storm outflow region. The 4DDA technique uses information from observations in both space and time to provide greater temporal and spatial consistency to its analyses of the variables and spatial scales of interest in this study than does the MQ analysis. However, the MQ provides a more faithful depiction of the atmosphere near the storm center when there were multiple (e.g., aircraft) observations. Consequently, the vertical shear calculations from the MQ analysis appeared to be somewhat more realistic than those derived from the 4DDA analysis.

| | | Flo | | | Ed | | |
|-----|------|---------------|----------------|--------|---------------|----------------|--------|
| | | Tang. Wind | Radial Wind | EFC | Tang. Wind | Radial Wind | EFC |
| 00h | 4DDA | - / + | 0 / 0 | 0 / 0 | + / 0 | + / 0 | 0 / 0 |
| | MQ | - / + | 0 / 0 | 0 / 0 | + / 0 | + / 0 | 0 / 0 |
| 12h | 4DDA | - / ++ | - / 0 | - / 0 | + / 0 | + / 0 | + / 0 |
| | MQ | - / + | 0 / 0 | - / 0 | + / 0 | + / 0 | 0 / 0 |
| 24h | 4DDA | 0 / ++ | - / 0 | - / 0 | + / 0 | + / 0 | + / 0 |
| | MQ | 0 / ++ | - / 0 | - / 0 | + / 0 | 0 / 0 | 0 / 0 |
| 36h | 4DDA | 0 / ++ | - / + | - / + | 0 / 0 | 0 / - | + / 0 |
| | MQ | 0 / ++ | - / 0 | - / + | 0 / 0 | 0 / - | + / 0 |
| 48h | 4DDA | 0 / + | 0 / + | 0 / ++ | 0 / - | 0 / 0 | ++ / 0 |
| | MQ | 0 / + | - / 0 | 0 / ++ | 0 / - | 0 / 0 | + / 0 |

| Legend | | |
|---------|----|--------------|
| | ++ | ≥ 0.75 |
| 0.75 > | + | ≥ 0.50 |
| -0.50 > | 0 | > 0.50 |
| -0.50 > | - | > -0.75 |
| | -- | ≤ -0.75 |

Table 4.12. SUMMARY OF CORRELATIONS BETWEEN 0-, 12-, 24-, 36-, AND 48-h STORM INTENSITY AND RATE OF INTENSITY CHANGE AND AZIMUTHALLY-AVERAGED TANGENTIAL AND RADIAL WIND, AND EFC, AS CALCULATED BY 4DDA AND MQ ANALYSES. SYMBOL ON LEFT IS FOR CORRELATION WITH STORM INTENSITY, SYMBOL ON RIGHT IS FOR CORRELATION WITH STORM INTENSITY CHANGE. SYMBOLS AS IN INSET.

In summary, the author recommends using a 4DDA-type analysis, when available, for studies involving tropical cyclone interaction with the environment, but perform a MQ analysis in regions of moderate or high data density when it is important to capture the details of the storm structure, such as vertical shear calculations. If it is not practical to use a 4DDA scheme, and there are observations at the level(s) of interest, the MQ method should provide a reliable analysis.

V. SUMMARY, CONCLUSIONS AND RECOMMENDATIONS

A. SUMMARY

Despite the importance of the intensity forecast, the consensus among operational forecasters and research meteorologists is that operational forecasts are little, if any, better than an intensity forecast based upon persistence and climatology (Elsberry *et al.* 1992). Recent comments from operational forecasters (e.g., Avila 1998) indicate that intensity forecasts have improved little since 1990. Both operational (Avila 1998) and research (Elsberry *et al.* 1992) meteorologists state that the most significant intensity forecast challenge is to understand, and ultimately predict, periods of tropical cyclone rapid intensification. This study tested the hypothesis that EFC events are detectable for, and correlated with, rapid intensification events.

One of the goals of this study was to develop a MQ analysis scheme that draws closely to the observations and may be used as an independent comparison to high-resolution model-based (4DDA) analyses. The MQ method was chosen over more traditional successive-correction schemes based on the results of Franke (1982) and Nuss and Titley (1994). Both studies showed that the MQ method reduced RMS values by 30-50% over the RMS values achieved with successive correction schemes. The MQ method produces fields that are both infinitely differentiable and pleasing to the eye, and thus emulates the work of an experienced synoptic analyst. Obtaining a realistic structure in the vicinity of the TC was possible in this static analysis only after making the

decision to analyze the region near the storm in a cylindrical coordinate system, and then blend the azimuthally-averaged winds into the Cartesian coordinate system with increasing distance from the storm.

The second objective of this study was to examine the interactions between the large-scale environment and the tropical cyclones for insight as to why Flo rapidly intensified and achieved its MPI, while Ed did neither, despite both storms developing and moving over water of similar SST ($\approx 28^{\circ}\text{C}$) values. Although the TCM-90 experiment was not designed specifically to examine the inner-core structure of each storm at high temporal and spatial resolution, the 4DDA analyses were used to examine the azimuthally-averaged thermal structure. Compositing Ed and Flo's temperatures for six times at which the storms had identical or very similar intensities showed Flo's near-core troposphere to be less stable (and thereby enhance convection) than Ed's. In the 4DDA composite, Flo's upper-troposphere temperatures were substantially ($\approx 2^{\circ}\text{C}$) higher than Ed's. This analyzed difference in thermal structure occurred **prior to** Flo's rapid intensification. Such a thermal structure is consistent with Gray's (1992) hypothesis that stronger, intensifying tropical cyclones maintain a cooler, more convectively-unstable eyewall, but still have a warm core by concentrating the warming as high as possible.

Two independent analyses based upon high-resolution TCM-90 observations provide a detailed description, especially in the upper troposphere, of the time-varying structure of Typhoons Ed and Flo. The tangential and radial winds, EFC, and vertical

wind shear were closely examined in a cylindrical coordinate system that moved with the individual storm. In addition, correlation coefficients were calculated between the above-listed parameters, absolute vorticity, and the future intensity of each storm.

B. CONCLUSIONS

This research has provided advances in two areas: objective mesoscale analysis, and understanding the dynamics of tropical cyclone rapid intensification.

1. Objective Mesoscale Analysis

The MQ analysis has been shown to provide an alternate, plausible depiction of the tropical atmosphere. That is, the MQ analysis compares favorably with the Rucker (1992) subjective analyses, agrees well with observations as indicated by the small RMS values, and provides realistic depictions of the azimuthally-averaged wind components. Using the NOGAPS analysis as a first guess and analyzing increments allows the MQ analysis to retain dynamic information inherent in a competitive global NWP system, and yet extracts information from a high spatial and temporal resolution TCM-90 dataset. Because the MQ analysis lacks the constraints of an OI analysis, it draws more closely to the observations than the 4DDA analysis. If the observations are reliable, this is considered to be an advantage near the tropical cyclone where the dynamical properties may deviate considerably from the type of conditions for which the OI coefficients of the 4DDA analyses have been derived.

Both the 4DDA and MQ analyses, although derived by independent means, have been demonstrated to provide useful, valid, and generally similar depictions of the

typhoon dynamics and subsequent correlations with storm intensity (Table 4.12). Specifically, the 4DDA assimilation scheme "follows" the observations sufficiently closely to portray accurately regions of substantial divergence in the storm outflow region. The analysis of observations in both space and time allowed the 4DDA scheme to provide better temporal consistency of the variables and spatial scales of interest in this study than did the MQ analysis. However, the MQ analysis provides a more faithful depiction of the atmosphere near the storm center when multiple (e.g., aircraft) observations were available. Consequently, the vertical shear calculations from the MQ analysis appeared to be somewhat more realistic than those derived from the 4DDA. In summary, the author recommends using a 4DDA-type analysis, when available, for studies involving tropical cyclone interaction with the environment, but perform a MQ analysis in regions of moderate or high data density when it is important to capture the details of the storm structure, such as vertical shear calculations. If it is not practical to use a 4DDA scheme, and there are observations at the level(s) of interest, the MQ method should provide a reliable analysis.

Development of meteorological applications of the MQ technique, as originally described by Nuss and Titley (1994) and applied in this study, is an important contribution to various disciplines within meteorology that require objective, mesoscale analyses. Since the Nuss and Titley publication, the MQ technique has been applied in a variety of meteorological situations, including tropical regions (e.g., Harr *et al.* 1996, Elsberry and Jeffries 1996), polar regions (Bresch *et al.* 1997), radiation (e.g., Zhong

and Doran 1997), hydrologic (Ghan *et al.* 1997), and satellite (Hirschberg *et al.* 1997) analyses.

2. Tropical Cyclone Intensification Dynamics New Findings

The analysis techniques described above applied to the TCM-90 dataset reveal several characteristics of a rapidly intensifying typhoon that have not been previously described. Although there is high confidence in the analysis procedures applied to Typhoon Flo, the single case of a rapidly intensifying typhoons implies that caution should be used in generalizing these results.

The most unusual dynamic result was finding the existence of the "cyclonic wind burst" extending beyond 1000 km radius at 200 mb (Figures 4.6 and 4.21) during the forcing phase for Typhoon Flo. This feature appears to be the result of strong, sustained EFC in the upper troposphere.

EFC values should be calculated for multiple levels of the atmosphere, rather than just at 200 mb. The EFC calculations for Typhoon Flo showed an evolving EFC structure throughout the troposphere. During the forcing phase (e.g., Figure 4.17), moderate to strong positive EFCs are concentrated in the upper troposphere. During the quiescent phase (e.g., Figure 4.27), EFCs are generally weak throughout the troposphere. In the super typhoon phase (e.g., Figure 4.46), EFCs are still weak, although there is evidence of increase mid-tropospheric positive EFCs beyond 1200 km, associated with the mid-latitude trough. By the mid-latitude interaction phase (e.g., Figure 4.53), strong positive EFCs are evident above 500 mb. These changes in vertical

structure affect the forcing of the transverse circulation as in Eq. (1.1). If EFCs are only calculated at a single level, such has been the case in several statistical studies (e.g., Fitzpatrick 1997), the differentiation between positive values of EFC in the upper troposphere only (favorable to enhance the secondary circulation) versus positive EFCs throughout the troposphere (less favorable) may not be made.

The composite of azimuthally-averaged temperature differences for six separate times between Ed and Flo when both were either tropical storm or minimal typhoon strength (Figure 4.3) was a significant thermodynamic result. The temperature composite showed that Flo had developed a warmer core near the tropopause, and was less stable than Ed in the upper troposphere **prior to** the beginning of the rapid intensification period. This result indicates that the less-stable thermal structures of intense tropical cyclones (as discussed by Gray 1992) may create the conditions required for the intensification, rather than result from an intense storm.

Another dynamic feature of note was the vertical variations in the level and directional orientation of maximum outflow. While Flo was a Super Typhoon, the outflow layer rose from 200 mb to 150 mb. This finding is consistent with the results of Merrill and Velden (1996). However, the outflow variation documented while Flo was a Super Typhoon also occurred in other periods. For example, five separate changes in the level of maximum outflow at 450 km radius are apparent using the 4DDA analysis (Figure 4.34).

What may be more important than the level of the outflow at a specific radius is the continually evolving and dynamic change in structure of the azimuthally-averaged radial wind. The outflow structure of Flo progresses from a band of strong upper-tropospheric outflow and significant mid-tropospheric inflow (Figure 4.12) to very high-level outflow (Figure 4.25), to weak outflow with no mid-tropospheric inflow at maximum storm intensity (Figure 4.45), and finally to a structure with very broad outflow above 500 mb (Figure 4.51). These changes in the outflow levels may be a reflection of short-term fluctuations in the strength of the eyewall convection. Unfortunately, no obvious correlation is found between the level of the outflow to either intensity, intensity change, EFC, or the magnitude of the radial wind. However, the level of maximum outflow remained above 200 mb from 12 UTC 16 September through 18 UTC 17 September while the intensity of Flo was above 66 m s^{-1} .

An interesting result for Typhoons Flo and Ed was the high correlation of the mid-troposphere azimuthally-averaged absolute vorticity ($\overline{\zeta_a}$) with the 48-h future intensity of the tropical cyclone (Table 4.9). This result should be viewed with caution due to the paucity of mid-tropospheric observations in the TCM-90 (and virtually any other tropical) dataset. However, the correlations applied not only to Typhoons Ed and Flo, but also to Typhoons Yancy and Zola, for which gridded 4DDA data were also available. If future studies verify this correlation, this result may have significant applicability to operational forecasting of tropical cyclone intensity.

Vertical wind shear for a variety of levels was calculated for Typhoons Ed and Flo. As in the case of the outflow jet structure, the vertical shear structure varied significantly with time (e.g., Figures 4.54 and 4.55). Of special note, the 850 - 200 mb vertical wind shear for Typhoon Ed was **less than** the vertical shear calculated for Typhoon Flo. This result implies that low vertical shear, although necessary for significant storm development is not, by itself, a sufficient dynamic factor to ensure rapid intensification.

The high negative correlation between the 300 - 150 mb vertical shear and 00-h intensity calculated for Typhoon Flo (-0.81 based on the 4DDA) may indicate the degree to which the cyclonic circulation near the storm center built into the upper troposphere as Flo intensified. This is consistent with a thermodynamic stability difference in Flo that supports deeper convection, and the sustained EFC forcing of a more cyclonic upper-tropospheric tangential wind. The same correlation for Typhoon Ed is +0.26, which indicates the upper-tropospheric vertical shear was nearly independent of Ed's intensity.

When the vertical shear for Typhoon Flo is calculated in a coordinate system moving with the storm (Figure 4.18), it is evident that the vertical shear magnitudes are no greater when the storm is significantly weakening (after 18 UTC 17 September) than when the storm is steadily increasing in intensity. This result supports the conclusion that vertical shear, although important, is not the only atmospheric factor that should be considered with regard to tropical cyclone intensification. The result also questions the

common hypothesis that tropical cyclones interacting with mid-latitude troughs weaken exclusively because of increased vertical shear.

a. Proposed View of Tropical Cyclone Intensification and Weakening

To account for the above results, the following model is proposed for tropical cyclone potential rapid intensification and weakening as a result of interaction with a mid-latitude trough. First, the following conditions are necessary, but not sufficient for rapid intensification to occur: the storm must be over open water, have an intensity below its MPI, and also be in a relatively low vertical shear environment.

The potential for rapid intensification is enhanced when the thermal structure near the eyewall is altered to become less stable in the troposphere, with the warm core closer to the tropopause (that is, higher in the atmosphere) than normal. One way this may occur is by "pre-conditioning" the atmosphere with strong, positive, sustained EFC in the upper troposphere, and weak EFC in the middle and lower troposphere. This EFC forcing when concentrated in the upper troposphere may increase the cyclonic \bar{v}_L and potentially produce a "cyclonic wind burst," which in turn decreases $\frac{\partial \bar{v}_L}{\partial p}$. The decrease in vertical wind shear implies, through thermal wind considerations, a decrease in $\frac{\partial \bar{T}}{\partial r}$. Since the tropical storm is a warm-core system, the proposed effect would shift the warm core upward to the tropopause and lower stratosphere. This thermal and wind distribution maximizes the efficiency of the secondary circulation and, for a given amount of boundary layer latent and sensible heat input, produces the most efficient (intense) tropical cyclone. In addition, the large upper-troposphere EFC forcing

may also directly enhance the mid-tropospheric inflow, and increase the total storm absolute angular momentum. Possible evidence of this may be the high correlation between mid-tropospheric $\overline{\zeta_a}$ and the future storm intensity.

Once the storm is "pre-conditioned" (initially defined as at least 12 h of positive 200-mb $\overline{v_L}$, averaged between 400-1200 km radius), it is sufficient, and perhaps even necessary, to have the storm move into a "quiescent" environment. That is, an environment that supports a MPI greater than the current storm intensity, and without significant vertical wind shear or strong EFC at any level. With the thermal structure favorable for convection from the surface to the tropopause, the storm may then deepen until it reaches its MPI. The eyewall contraction process (Willoughby *et al.* 1982, Willoughby 1990) may also be enhanced during this phase.

Questions that still remain with this conceptual model include: Is a quiescent environment required, or can the storm rapidly intensify with concurrent strong synoptic forcing? How long of a period of initial forcing is required? How important is the vertical structure of the EFC relative to the absolute magnitude of the EFC? What is the relationship between the storm's inertial stability and the effectiveness of the EFC? Are there "windows of intensification opportunity," when the forcing most effective? That is, is a given amount of forcing most effective when the system is at weak or strong tropical storm strength, or at some other intensity? These are all questions for future research.

The interaction of a tropical cyclone with a mid-latitude trough may be much more complex than simply an increased value in vertical wind shear. It is hypothesized that tropical cyclones may weaken upon interacting with the mid-latitude trough primarily due to the associated mid-troposphere EFC causing outflow below the upper troposphere, and secondarily by an increase in the vertical shear. This deep tropospheric outflow effectively "short circuits" the secondary circulation required to maintain the storm intensity, and produces an "in and out" circulation versus an "in-up-out" transverse circulation that is conducive to intense tropical cyclones.

In summary, tropical cyclone intensity, and rapid intensification episodes in particular, result from a complex interaction of ocean (including the mixed layer) **and atmospheric** forcing. Although the high spatial-resolution data in TCM-90 did not provide evidence of a universal, positive correlation between EFC and future storm intensity, the relationships between the EFC, tangential and radial winds and vertical shear was much more complex. While tropical cyclone forecasters and research meteorologists for decades have had to rely on data typically taken at 200- and 850-mb, this study shows that the vertical structure of shear, EFC, absolute vorticity and tangential and radial winds analyzed in a cylindrical coordinate system moving with the storm may be crucial to understand, and ultimately predict, tropical cyclone intensity.

b. Typhoons Yancy and Zola

Unfortunately, Typhoon Flo is the only case of rapid intensification during the TCM-90 field experiment. However, 200-mb EFC, tangential and radial winds, and

vertical wind shears were calculated for Typhoons Yancy and Zola. These calculations will be related to the conceptual model discussed above. While two additional, non-rapidly intensifying storms in no way constitutes a true independent sample, these storms also have high quality, gridded data (i.e., 4DDA analyses based upon the TCM-90 dataset) available.

Typhoon Yancy was a very large storm (Elsberry *et al.* 1990) that formed in the monsoon trough, reached tropical storm strength on 14 August, then moved northwest and west, and interacted with Taiwan prior to making landfall over China on 20 August (Figure 4.68). The 400-1200 km radius 200-mb EFC values (Figure 5.1) were positive between 00 UTC 17 August and 12 UTC 18 August, which meets the definition of "cyclonic wind burst." The wind burst had been preceded by 30 h of moderate ($5 - 15 \text{ m s}^{-1}/\text{day}$) EFC, also at 200-mb between 400 - 1200 km radius. While Yancy intensified 10 m s^{-1} in 18 h (between 06 UTC 17 August and 00 UTC 18 August) during the cyclonic wind burst, Yancy never intensified after 00 UTC 18 August.

Several factors may have prevented significant intensification of Yancy. The 300 - 150 mb vertical shear (not shown) increased from 3 m s^{-1} at 00 UTC 18 August to 10 m s^{-1} 12 h later. During this time period, the storm slowed to $< 3 \text{ m s}^{-1}$. This slow movement, combined with the $> 1500 \text{ km}$ radius of strong winds (Elsberry *et al.* 1990), may have reduced the SST, and thus the MPI. This large storm was also interacting with the mountainous terrain of Taiwan. Although the 200-mb EFC values averaged close to zero after 00 UTC 18 August, a complex vertical structure was present

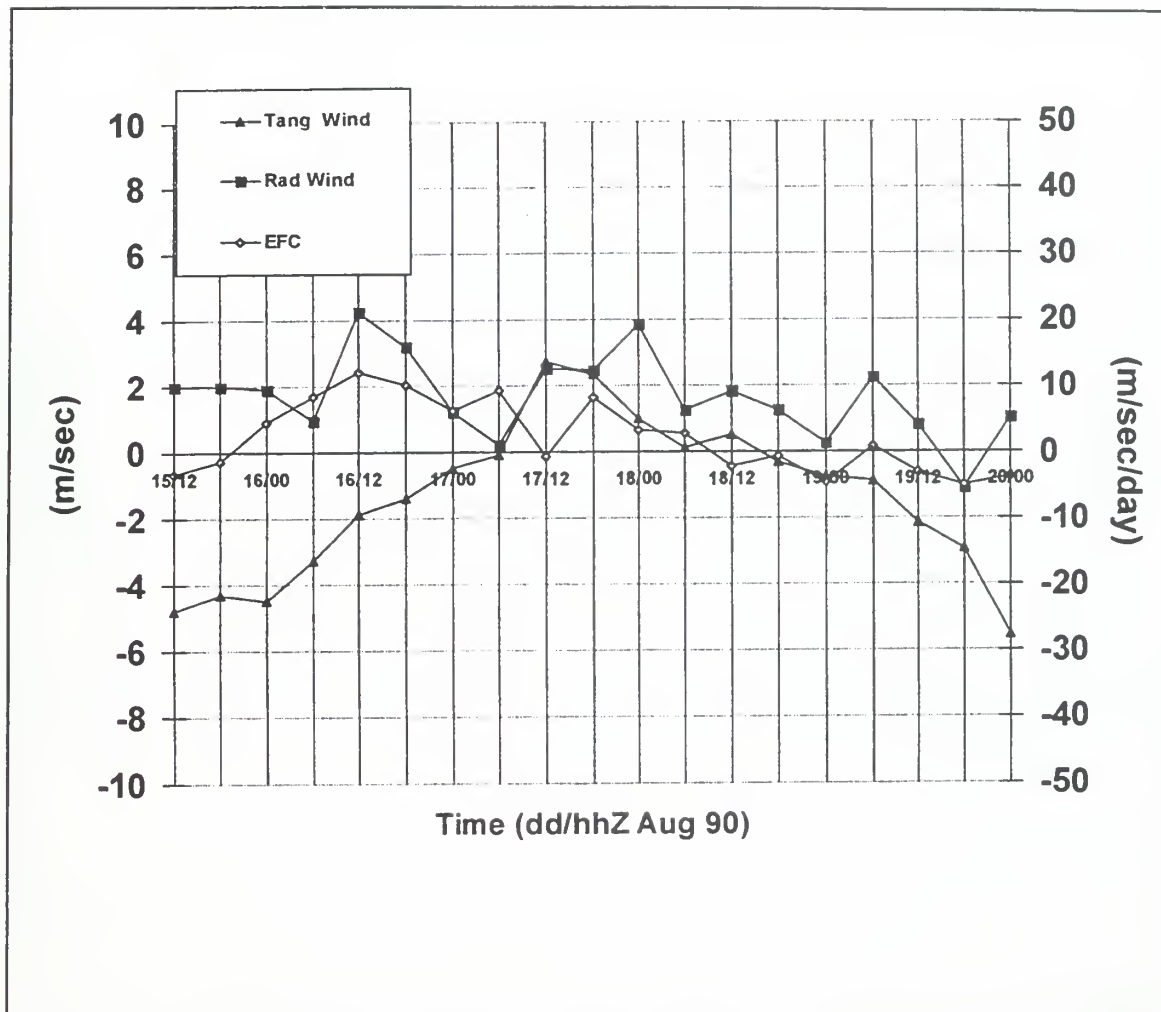


Fig. 5.1. Tangential and radial winds, and EFC values as in Figure 4.21, except for Typhoon Yancy.

(not shown) until the storm made landfall. Finally, the large radius of Yancy may have prevented relatively small forcing ($< 15 \text{ m s}^{-1}/\text{day}$) from having a significant effect on the angular momentum distribution of the storm.

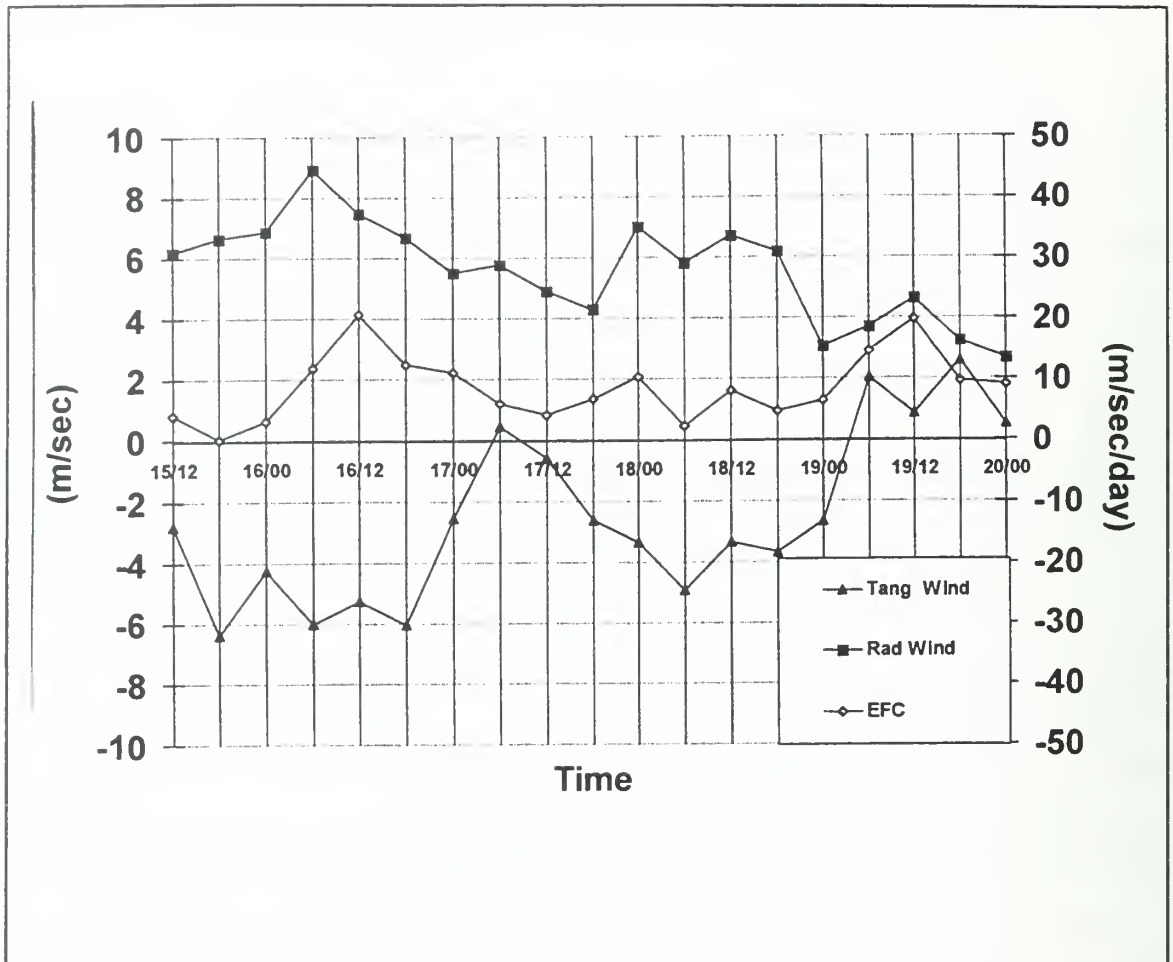


Fig. 5.2. Tangential and radial winds, and EFC values as in Figure 4.21, except for Typhoon Zola.

Typhoon Zola (Figure 4.69) experienced strong ($> 15 \text{ m s}^{-1}/\text{day}$) EFC forcing at 200 mb during two periods (Figure 5.2). The first time was at 12 UTC 16 August when the storm intensity was only 10 m s^{-1} . The azimuthally-averaged 200-mb tangential wind increased from -6 m s^{-1} on 18 UTC 16 August to about $+1 \text{ m s}^{-1}$ 12 h later. Although this does not meet the strict definition of a cyclonic wind burst, it represents a significant increase in the cyclonic component of the 200 mb \bar{v}_L . Zola then

increased in intensity from 15 m s^{-1} at 18 UTC 17 August to 28 m s^{-1} in the following 12 h.

The second strong EFC forcing occurred between 06 and 12 UTC 19 September, and a "cyclonic wind burst" commenced at 06 UTC 19 August and lasted for 18 h. Simultaneously, both the 300 - 150 mb and 850 - 200 mb vertical wind shears (not shown) decreased by at least a factor of two. Although the IOP ended at 00 UTC 20 August, Zola intensified 20 m s^{-1} in 36 h between 18 UTC 19 August and 06 UTC 21 August before interacting with a mid-latitude trough south of Honshu.

While it cannot be shown that Zola interacted with a "quiescent environment" after 00 UTC 20 August, both the 00 UTC 20 August pressure-radius EFC plot (not shown) and vertical shear calculations indicate that the storm was entering a low shear, low EFC environment. In summary, Zola experienced "fast intensification" (Fitzpatrick 1997) twice. Both times were preceded by strong EFC events, and subsequent significant increases in the cyclonic value of $200 \text{ mb } \bar{v}_L$.

3. Recommendations

As in most observational studies, additional cases are required to determine if the storms studied here were "typical" with respect to their intensity evolution. This research suggests three areas for which observations should be targeted. A method is required to measure the thermal characteristics of the storm in the vicinity of the eyewall. It is important to determine if the changes in thermal structure actually precede the rapid intensification, or are a result of the storm deepening. Additional mid-tropospheric

observations are required to prove or disprove the correlation between 500-mb $\overline{\zeta_a}$ and future intensity change. Finally, additional wind observations are required to measure accurately the three-dimensional structure of the EFC, outflow, and inflow.

Numerical modeling studies of tropical cyclone interaction with mid-latitude features may help quantify the amount of weakening caused by vertical wind shear and "short-circuiting" of the transverse circulation, and quantify the effect of different vertical structures of wind shear. Modeling studies may also help to refine the conceptual model proposed above by examining: (i) length of time and amount of forcing required to "pre-condition" the storm; (ii) the importance (if any) of a quiescent period after the forcing phase; (iii) the relationship between storm size, inertial stability, and upper-tropospheric forcing; and (iv) the role of mid-level vorticity in tropical cyclone intensification?

Forecasters require the tools to calculate easily quantitative, storm-relative, cylindrical fields such as EFC, $\overline{v_L}$, $\overline{u_L}$, $\overline{\zeta_a}$, near-core thermal fields, and vertical wind shear at various levels in real-time. Perhaps most importantly, this research may provide the beginning of a conceptual framework by which to understand, and correctly forecast, tropical cyclones that have the potential to deepen rapidly.

APPENDIX A. QUALITY CONTROL PROCEDURES

A. INTRODUCTION

Quality control (QC) procedures were stringently applied in this study. Much effort was spent in obtaining the best-possible dataset, given the distribution and accuracy of the combined real-time and delayed TCM-90 observations. Much of the QC is based upon the procedures employed for the real-time NOGAPS database (Baker 1992).

Although all data were evaluated for gross errors, the static QC checks concentrated on the rawinsonde and LDW data. These data were not necessarily less accurate than other sources, but data at multiple levels allowed vertical consistency checks to be applied.

B. METHOD

Over 85% of the rawinsonde data passed through the real-time NOGAPS static QC checks (Baker 1992) and had QC flags assigned to the wind, height and temperature data. These flags indicated whether the data were accepted, rejected, or labeled as suspect. About 6% of the height observations, 2.5% of the temperature observations, and 1.3% of the mandatory level wind observations were flagged as either erroneous or suspect data. Over 2000 of the 34 500 observations during IOPs 5-7 required further processing.

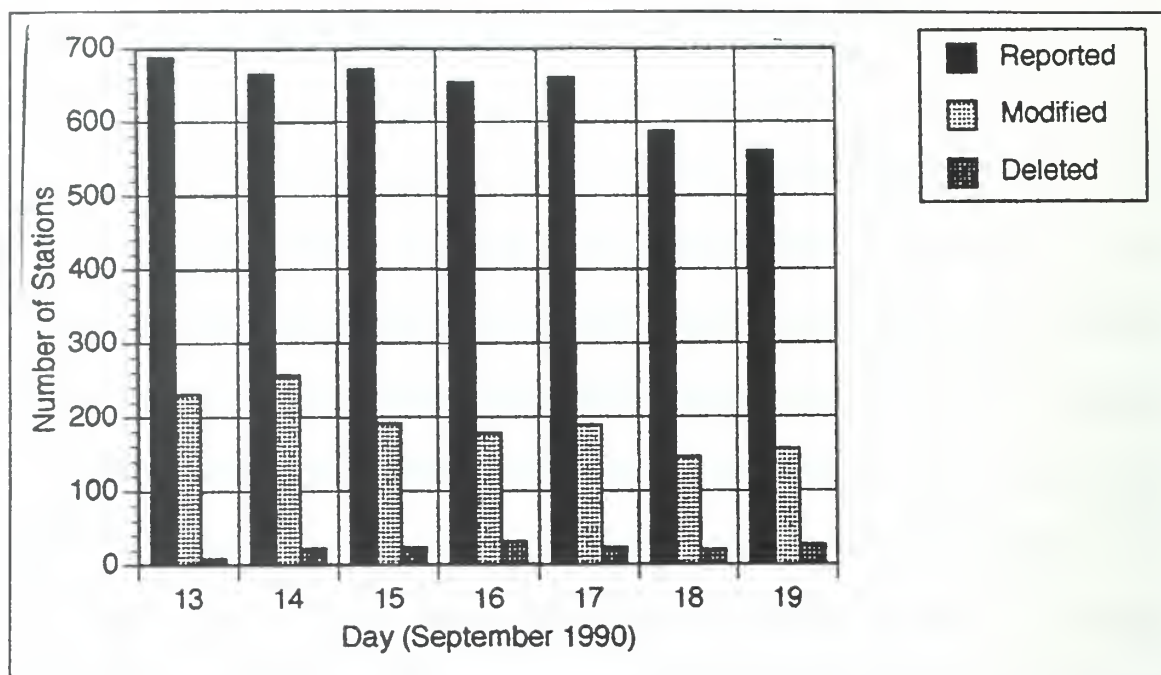


Fig. A-1. Number of rawinsonde observations reported, modified, and rejected (see inset for symbols) by static quality-control procedures.

Each real-time rawinsonde that had at least one non-normal flag assigned was output in both tabular and skew-T format. These observations were individually evaluated, and a decision was made to accept the observation (*i.e.*, override the QC flag), modify the observation (*e.g.*, correct for a communications error) or reject the observation. The objective was to fix as many observations as possible to maximize the data available for analysis. If one or two levels in the observation were incorrect, but the remainder of the observation appeared reasonable, then the observation was retained, and only the bad levels were removed or corrected. The numbers of rawinsonde observations collected, modified and rejected by day during IOPs 5-7 are shown in Figure A-1. About 25% of the rawinsondes were modified by this manual QC approach.

| Reported Height (m) | Maximum Allowed Difference (m) |
|---------------------|--------------------------------|
| < 6000 | 20 |
| 6000-15000 | 30 |
| > 15000 | 40 |

Table A1. MAXIMUM TOLERANCE (m) BETWEEN OBSERVED HEIGHTS (m) AND LOCALLY-CALCULATED HYDROSTATIC HEIGHTS (m) FOR A GIVEN REPORTED HEIGHT. IF DIFFERENCE IS GREATER THAN MAXIMUM TOLERANCE, THEN THE OBSERVATION IS FLAGGED FOR CORRECTIVE ACTION.

After the suspect and erroneous observations had been manually examined and corrected, the FGGE files were modified to reflect the changes in the data. The original data were not deleted, but were copied into another record with an identical station header. Manually modified data were denoted by a "*" in the appropriate QC column.

Once the FGGE files were modified, the data were checked by a program that:

- Checked for gross errors.
- Performed a hydrostatic check to ensure that the mass and temperature observations were within tolerance (Table A1). If the difference exceeded these threshold values, the program would: (i) calculate and insert the hydrostatically correct height, given the temperature and dew point profile; (ii)

allow the user to manually correct the height; or (iii) allow the current height to be maintained.

- Checked the temperature lapse rates and output any super-adiabatic layers, or layers with large temperature inversions.
- Checked the vertical shear of the wind observations. Although this check is based on the procedure described in Baker (1992), it was extended to include vertical shear checks of the significant level, as well as mandatory level observations.

These checks included the gross error and hydrostatic checks already performed by the NOGAPS QC system for two reasons. First, 10-15% of the rawinsondes were not received in real time (Harr *et al.* 1991), and therefore had not been subjected to the FNOC QC checks. Second, this check ensured that any data-entry mistakes made while correcting the initial errors would be detected.

As before, the observations flagged as suspect or erroneous by the local QC program were output in tabular form and plotted on a skew-T diagram. The required changes were made, and the data were again checked by the local QC program. This iterative process continued for all times until no errors were flagged in the static checks (Figure A-2).

C. SUMMARY

The initial QC checks were designed to eliminate gross errors from all data sources, and to ensure that rawinsonde and LDW data contained vertically consistent temperature and height fields, and were free from unreasonable temperature lapse rates or vertical wind shears. Suspect data were manually checked and corrected (when possible). Both mandatory and significant level data were subjected to the height, wind

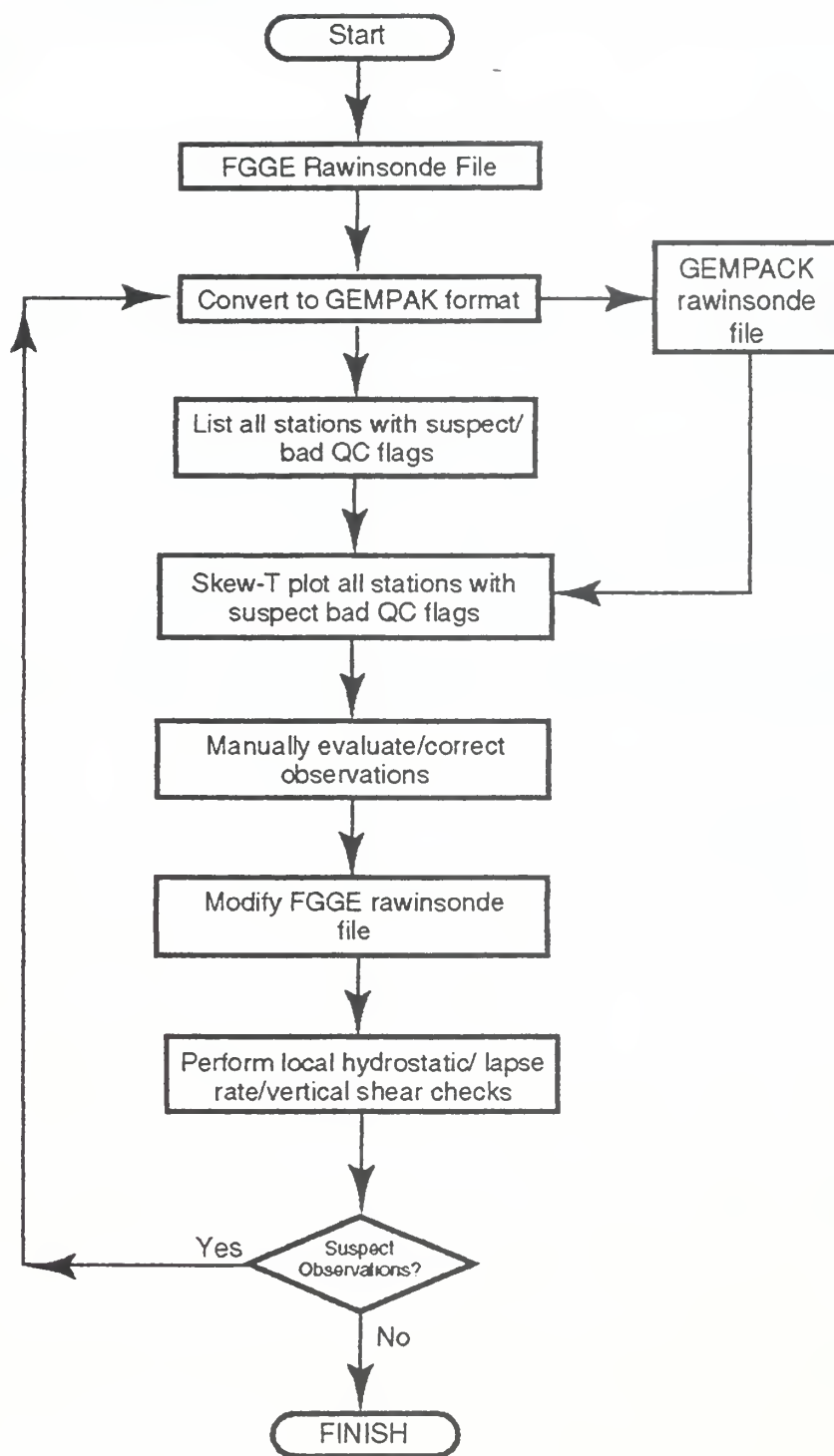


Fig. A-2. Flow diagram of static quality-control procedures followed prior to MQ analysis.

and temperature QC checks. The goal was to maximize both the amount and the quality of data available to the MQ objective analysis.

The QC flags applied by the operational FNMOC QC system detected virtually all the errors in the real-time rawinsonde data. However, the FNMOC QC system occasionally flagged data as erroneous or suspect one level above or below the location of the actual problem. Also, the operational QC system sometimes indicated that the temperature data were suspect when the heights were in error, and vice versa. Although the primarily manual QC system used for the MQ analysis was effective, future work should attempt to automate most of this system, while retaining the ability to detect errors at the actual heights and in the correct parameter (temperature or height).

APPENDIX B. INITIAL DATA PROCESSING

A. METHOD

All the TCM-90 observations used in this study had been previously collected and converted into FGGE-IIB format. Details of the data collection and archiving process can be found in Harr *et al.* (1991). These data were loaded onto the NPS Meteorology Department VAX computer, and converted into General Meteorological data assimilation, analysis, and display software Package (GEMPAK) data format. The GEMPAK format was chosen to facilitate Skew-T plots of rawinsonde and LORAN dropwindsonde data, and to easily plot the different data types on mandatory pressure-level charts.

Prior to converting the data to GEMPAK, some initial processing was required. Data other than land-based rawinsonde stations required the assignment of a station number to identify the station during the subsequent QC processing. Specific steps prior to storing the data in GEMPAK format are listed below.

1. Rawinsonde Data

Several Taiwan stations (WMO station numbers 46685, 46734, 46747, 46780) intermittently reported their winds in dm s^{-1} instead of m s^{-1} . These times had to be identified and the winds converted to m s^{-1} . As noted in Harr *et al.* (1991), some stations in Taiwan are reported simultaneously by both Taiwan and mainland China. These reports are not always identical, and it is impossible to determine which report is correct. The TCM-90 dataset contained both the Taiwanese and Chinese observations.

Both observations were accepted by the MQ analysis scheme and, if less than 25 km apart, were composited into one single observation.

2. Reprocessed Cloud-Tracked Winds

No special processing was required for the reprocessed cloud-tracked wind (CTW) observations.

3. Operational Cloud-Tracked Winds

The operational cloud-tracked winds (CTO) observations were added to the MQ dataset only if the observation was outside the domain of the CTW observations (Figure 2.7). Thus, the CTO observations were generally restricted to a region between 160°E and the dateline. A few CTO observations were also located over the Indian Ocean.

4. Commercial Aircraft Reports

Commercial aircraft (AIREP) observations were typically reported at flight levels. Since flight levels above 18 000 ft were based upon a standard atmosphere, the reported aircraft altitude was only an approximation of the true vertical position of the observation. Despite that limitation, AIREP winds ± 3 h of the analysis time were moved to the nearest mandatory pressure level. Since aircraft tend to report at fixed points in space (Goerss and Phoebus 1992), occasionally more than one report was at the same location and pressure level. Prior to conversion to GEMPAK, these observations were simply averaged and recorded as a single AIREP observation. Unlike the time-weighted FNOC analysis procedure (Goerss and Phoebus 1992), all the co-

located aircraft observations within ± 3 h received equal weight when producing the composite AIREP.

5. DC-8 Flight-Level Observations

The DC-8 observations ± 3 h of an analysis time were moved to the nearest mandatory pressure level. As described in Chapter 2, adjustment of the height observations was performed using preliminary MQ analyses to determine the mean temperature of the layer between the observation and the mandatory pressure level.

The locations of the DC-8 flight-level observations were not adjusted to account for the motion of Typhoon Flo because observations within 300 km of Flo were normally made within 90 minutes of the analysis time. Assuming a typhoon speed of 5 m s^{-1} (actual mean speed was about 4 m s^{-1} during the period that the DC-8 aircraft flew missions into Flo), the observations would be displaced no more than 7.5 km. Since the analysis grid is 50 km, this displacement would not have significantly affected the outcome of the analysis.

B. FINAL STEP

After the observations were converted into GEMPAK format, the observations underwent the QC procedures described in Appendix A. Once the gross errors had been removed and the observations were vertically consistent, the GEMPAK files were scanned for the mandatory-level height, wind and temperature observations. These data were converted to ASCII format, and then ported to the AMDAHL computer for the MQ analysis.

APPENDIX C. NINE-POINT TROPICAL CYCLONE BOGUS PROCEDURE

A more extensive nine-point tropical cyclone bogus was also developed as an alternate representation of the TC in the MQ analyses. This full bogus explicitly determined the location, intensity and size of the tropical cyclone. Best-track position and intensity information was used to determine the central height bogus. The eight height bogus observations equally distributed around a circle of radius of 300 km were calculated from the azimuthally-averaged height field near the TC using the MQ scheme with an alignment bogus.

The central heights were determined by converting the best-track intensity estimate to a minimum sea-level pressure (MSLP) using the empirical relationship between the maximum sustained winds and MSLP described in Atkinson and Holliday (1977). Given the MSLP, the heights were calculated at the mandatory pressure levels using the hydrostatic relationship. To account for the warm core found in the tropical cyclone, a positive temperature anomaly (Table C1) was added to the MQ temperature analysis at the center of the TC. This temperature anomaly was based upon an analysis by Hawkins and Rubsam (1968) of Hurricane Hilda (1964). The NASA DC-8 temperature observations in the eye of Flo at 0600 UTC 17 September agreed well with the 200 mb temperature anomaly analyzed for Hurricane Hilda. Therefore, the temperature anomalies were normalized by the intensity of Flo at 0600 UTC 17

| Pressure (mb) | Anomalies (°C) |
|---------------|----------------|
| 1000 | 3.0 |
| 850 | 5.0 |
| 700 | 10.0 |
| 500 | 12.0 |
| 400 | 13.0 |
| 300 | 16.0 |
| 250 | 16.0 |
| 200 | 13.0 |
| 150 | 2.0 |
| 100 | 0.0 |

Table C1. TEMPERATURE ANOMALY (°C) ASSUMED TO EXIST IN EYE OF A 75 m s^{-1} TROPICAL CYCLONE FOR A GIVEN PRESSURE LEVEL (mb), BASED ON TEMPERATURE ANOMALIES OBSERVED IN HURRICANE HILDA BY HAWKINS AND RUBSAM (1968).

September (75 m s^{-1}). For example, if the best-track intensity estimate was 37.5 m s^{-1} , then the temperature anomaly added to the previously analyzed temperature was one-half that listed in Table C1. The positive temperature anomaly ensured that the bogus

typhoon had a warm core, and that the magnitude of the geopotential height increments decreased with decreasing pressure (increasing heights).

The three techniques for representing the position and intensity of Typhoon Flo are illustrated in Figure C-1 for the 850 mb pressure level at 00 UTC 15 September, when Flo was estimated to have maximum surface winds of about 33 m s^{-1} (JTWc 1990). In the no-bogus case (Figure C-1a), no observations were available within 300 km of the center of the storm, the central height at 850 mb was greater than 1410 m, and maximum winds were $20\text{-}25 \text{ m s}^{-1}$ to the north and east of the storm center. With a single alignment-bogus point inserted (Figure C-1b), the central height was reduced to less than 1410 m, but there was little change in the wind profile near Typhoon Flo. The nine-point bogus method (Figure C-1c) decreased the central height at 850 mb to less than 1230 m, and increased the winds to $20\text{-}30 \text{ m s}^{-1}$ near Flo. Although the nine-point bogus appeared to be reasonable given 50 km horizontal grid spacing, no observations were available to confirm this conclusion.

As discussed in Chapter II, the alignment-bogus method was chosen rather than the nine-point bogus procedure, since the objective of the locally-produced analyses was to produce analyses with as few external assumptions as possible.

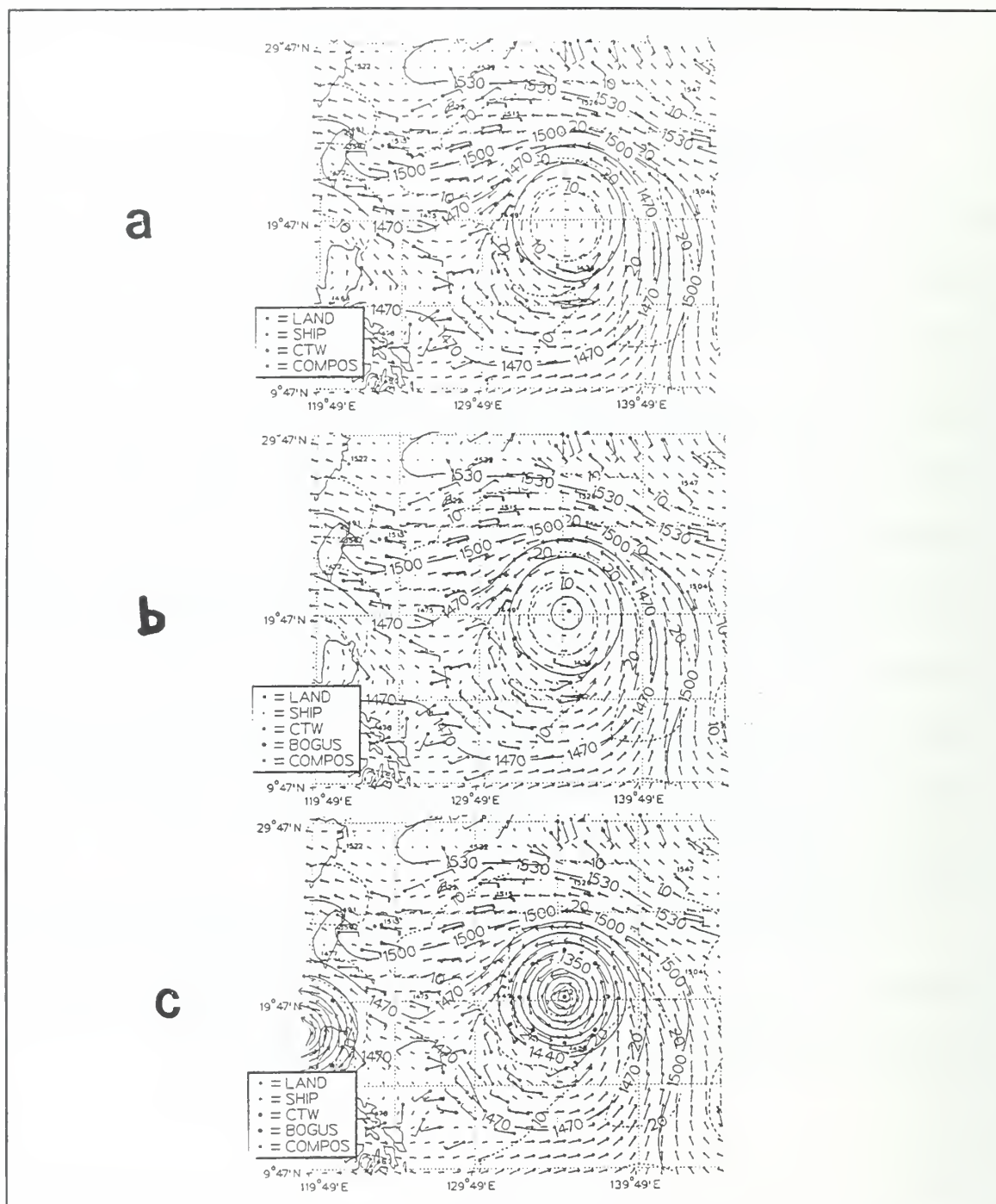


Fig. C-1. MQ analysis of 850 mb heights (m, contour interval 30 m), wind (m s⁻¹, scale vector in upper right), and isotachs (dashed, contour interval 10 m s⁻¹) at 00 UTC 15 September for (a) no-bogus option, (b) alignment-bogus option, and (c) nine-point bogus option. Notice the similarity of the analyses beyond 400 km radius in Typhoon Flo. Typhoon Ed is on lower left edge of chart, west-northwest of Luzon.

LIST OF REFERENCES

- Anthes, R. A., 1982: *Tropical Cyclones--Their Evolution, Structure, and Effects*. *Meteor. Monogr.*, **19** (41), Amer. Meteor. Soc., 208 pp.
- Atkinson, G. D., and C. R. Holliday, 1977: Tropical cyclone minimum sea level pressure maximum sustained wind relationship for the western North Pacific. *Mon. Wea. Rev.*, **105**, 421-427.
- Avila, L. A., 1998: Forecasting tropical cyclone intensity changes: An operational challenge. Preprints, *Symposium on Tropical Cyclone Intensity Change*, Phoenix, AZ, Amer. Meteor. Soc., 1-3.
- Baker, N. L., 1992: Quality control for the Navy operational atmospheric database. *Wea. Forecasting*, **7**, 250-261.
- Barker, E. H., 1992: Design of the Navy's multivariate optimum interpolation analysis system. *Wea. Forecasting*, **7**, 220-231.
- Bayler, G., and H. Lewit, 1992: The Navy operational global and regional atmospheric prediction systems at the Fleet Numerical Oceanography Center. *Wea. Forecasting*, **7**, 273-279.
- Barnes, S. L., 1973: Mesoscale objective analysis using weighted time-series observations. NOAA Tech. Memo. ERL NSSL-62, National Severe Storms Laboratory, Norman, 60 pp. [NTIS COM-73-10781.]
- Bender, M. A., 1997: The effect of relative flow on the asymmetric structure in the interior of hurricanes. *J. Atmos. Sci.*, **54**, 703-724.
- Bergman, K., 1979: Multivariate analysis of temperatures and winds using optimum interpolation. *Mon. Wea. Rev.*, **107**, 1423-1444.
- Bosart, L. F., C. S. Velden, and P. G. Black, 1998: Environmental influences on the rapid intensification stage of Hurricane Opal (1995) over the Gulf of Mexico. Preprints, *Symposium on Tropical Cyclone Intensity Change*, Phoenix, AZ, Amer. Meteor. Soc., 105-112.

- Bracken, W. E., and L. F. Bosart, 1998: Multiple development aspects of Hurricane Opal (1995). Preprints, *Symposium on Tropical Cyclone Intensity Change*, Phoenix, AZ, Amer. Meteor. Soc., 99-104.
- Bresch, J. F., R. J. Reed, and M. D. Albright, 1997: A polar-low development over the Bering Sea: Analysis, numerical simulation, and sensitivity experiments. *Mon. Wea. Rev.*, **125**, 3109-3130.
- Carr, L. E., III, and R. L. Elsberry, 1990: Observational evidence for predictions of tropical cyclone propagation relative to steering. *J. Atmos. Sci.*, **47**, 542-546.
- Carr, L. E., III, and R. L. Elsberry, 1992: Analytical tropical cyclone asymmetric circulation for barotropic model initial conditions. *Mon. Wea. Rev.*, **120**, 644-652.
- Carr, L. E., III, and R. L. Elsberry, 1994: Systematic and integrated approach to tropical cyclone track forecasting. Part I. Approach overview and description of meteorological basis. Tech. Rep. NPS-MR-94-002. Naval Postgraduate School, Monterey, CA 93943, 273 pp.
- Challa, M., and R. L. Pfeffer, 1980: Effects of eddy fluxes of angular momentum on model hurricane development. *J. Atmos. Sci.*, **37**, 1603-1618.
- Challa, M., and R. L. Pfeffer, 1990: The formation of Atlantic hurricanes from cloud clusters and depressions. *J. Atmos. Sci.*, **47**, 909-927.
- Chan, J. C.-L., and R. T. Williams, 1987: Analytical and numerical studies of the beta-effect in tropical cyclone motion. Part I: Zero mean flow. *J. Atmos. Sci.*, **44**, 1257-1264.
- Charney, J. G., and A. Eliassen, 1964: On the growth of the hurricane depression. *J. Atmos. Sci.*, **36**, 2617-2630.
- Charney, J. G., M. Halem, and R. Jastrow, 1969: Use of incomplete historical data to infer the present state of the atmosphere. *J. Atmos. Sci.*, **26**, 1160-1163.
- Chen, L., and W. M. Gray, 1986: Global view of the upper level outflow patterns associated with tropical cyclone intensity change during FGGE. Dept. of Atmos. Sci. Paper No. 392, Colorado State Univ., Ft. Collins, CO, 80523, 126 pp.
- Clune, W. M., P. A. Harr, and L. R. Brody, 1992: The man-machine mix in operational product quality control and verification at Fleet Numerical Meteorology Oceanography Center. *Wea. Forecasting*, **7**, 280-287.

- Cressman, G. P., 1959: An operational objective analysis system. *Mon. Wea. Rev.*, **87**, 367-374.
- Dey, C. H., 1989: The evolution of objective analysis methodology at the National Meteorological Center. *Wea. Forecasting*, **4**, 297-312.
- DeMaria, M., 1996: The effect of vertical shear on tropical cyclone intensity change. *J. Atmos. Sci.*, **53**, 2076-2086.
- DeMaria, M., and J. D. Pickle, 1988: A simplified system of equations for simulation of tropical cyclones. *J. Atmos. Sci.*, **45**, 1542-1554.
- DeMaria, M., and M. Huber, 1998: The effect of vertical shear on tropical cyclone intensity change: An historical perspective. Preprints, *Symposium on Tropical Cyclone Intensity Change*, Phoenix, AZ, Amer. Meteor. Soc., 22-29.
- DeMaria, M., J.-J. Baik and J. Kaplan, 1993: Upper-level angular momentum fluxes and tropical cyclone intensity change. *J. Atmos. Sci.*, **50**, 1133-1147.
- Durst, C. S., and R. C. Sutcliffe, 1938: The importance of vertical motion in the development of tropical revolving storms. *Quart. J. Roy. Meteor. Soc.*, **64**, 75-91.
- Dvorak, V. F., 1984: Tropical cyclone intensity analysis using satellite data. NOAA Technical Report NESDIS 11, U.S. Department of Commerce, Washington, D.C., 47 pp.
- Eliassen, A., 1951: Slow thermally and frictionally controlled meridional circulation in a circular vortex. *Astrophys. Norv.*, **5**, 19-60.
- Elsberry, R. L., 1987: Observations and analyses of tropical cyclones. Chap.1, *A Global View of Tropical Cyclones*, R. L. Elsberry, Ed., Office of Naval Research, 1-12.
- Elsberry, R. L., 1990: International experiments to study tropical cyclones in the western North Pacific. *Bull. Amer. Meteor. Soc.*, **71**, 1305-1316.
- Elsberry, R. L., 1998: Thoughts on why statistical tropical cyclone intensity forecasts have so little skill. Preprints, *Symposium on Tropical Cyclone Intensity Change*, Phoenix, AZ, Amer. Meteor. Soc., 4-10.
- Elsberry, R. L., and R. F. Abbey, Jr., 1991: Recent advances in understanding tropical cyclone motion. Technical Report NPS-MR-91-003, Naval Postgraduate School, Monterey CA 93943, 92 pp.

- Elsberry, R. L., and R. H. Bohner, Jr., 1992: Three-component decompositions of tropical cyclone wind fields: Relation to tropical cyclone motion. *Preprints, ICSU/WMO International Symposium on Tropical Cyclone Disasters*, Beijing, China.
- Elsberry, R. L., and R. Jeffries, 1996: Vertical wind shear influences on tropical cyclone formation and intensification during TCM-92 and TCM-93. *Mon. Wea. Rev.*, **124**, 1374-1387.
- Elsberry, R. L., B. C. Diehl, J. C.-L. Chan, P. A. Harr, G. J. Holland, M. Lander, T. Neta and D. Thom, 1990: ONR tropical cyclone motion research initiative: Field experiment Summary. Technical Report NPS-MR-91-001, Naval Postgraduate School, Monterey CA 93943, 106 pp.
- Elsberry, R. L., G. J. Holland, H. Gerrish, M. DeMaria, C. P. Guard, and K. Emanuel, 1992: Is there any hope for tropical cyclone intensity prediction?--A panel discussion. *Bull. Amer. Meteor. Soc.*, **73**, 264-275.
- Elsberry, R. L., P. H. Dobos, and D. W. Titley, 1993: Extraction of large-scale environmental flow components from the TCM-90 analyses: Implications for tropical cyclone motion studies. *Preprints, 20th Conference on Hurricanes and Tropical Meteorology*, San Antonio TX, Amer. Meteor. Soc., 4 pp.
- Emanuel, K. A., 1986: An air-sea interaction theory for tropical cyclones. Part I: Steady-state maintenance. *J. Atmos. Sci.*, **43**, 585-604.
- Emanuel, K. A., 1988: The maximum intensity of hurricanes. *J. Atmos. Sci.*, **45**, 1143-1155.
- Emanuel, K. A., 1998: Theoretical and numerical modeling inferences on the feedback of ocean dynamics on hurricane intensity. *Preprints, Symposium on Tropical Cyclone Intensity Change*, Phoenix, AZ, Amer. Meteor. Soc., 154-160.
- Evans, J. L., 1993: Sensitivity of tropical cyclone intensity to sea surface temperature. *J. Climate*, **6**, 1133-1140.
- Fiorino, M., and R. L. Elsberry, 1989: Some aspects of vortex structure in tropical cyclone motion. *J. Atmos. Sci.*, **46**, 979-990.
- Fitzpatrick, P. J., 1997: Understanding and forecasting tropical cyclone intensity change with the Typhoon Intensity Prediction Scheme (TIPS). *Wea. Forecasting*, **12**, 826-846.

- Frank, W. M., 1982: Large-scale characteristics of tropical cyclones. *Mon. Wea. Rev.*, **110**, 572-586.
- Franke, R., 1982: Scattered data interpolation: Tests of some methods. *Math. Comp.*, **38**, 181-200.
- Franke, R., 1985: Sources of error in objective analysis. *Mon. Wea. Rev.*, **113**, 260-270.
- Gandin, L., 1963: Objective analysis of meteorological fields. *Gidrometeorologicheskoe Isdatel'stvo*, Leningrad. Translated from Russian, Israel Program for Scientific Translation, Jerusalem, 1965, 242 pp.
- Ghan, S. J., J. C. Liljegren, W. J. Shaw, J. H. Hubbe, and J. C. Doran, 1997: Influence of subgrid variability on surface hydrology. *J. Climate*, **10**, 3157-3166.
- Goerss, J. S., and P. A. Phoebus, 1992: The Navy's operational atmospheric analysis. *Wea. Forecasting*, **7**, 232-249.
- Goerss, J. S., L. Brody, and R. Jeffries, 1991: Assimilation of tropical cyclone observations into the Navy operational global atmospheric prediction system. Preprints, *Ninth Conf. Num. Wea. Prediction*, Denver CO, Amer. Meteor. Soc., 638-641.
- Gray, W. M., 1968: Global view of the origin of tropical disturbances and storms. *Mon. Wea. Rev.*, **96**, 669-700.
- Gray, W. M., 1975: Tropical cyclone genesis. Dept. of Atmos. Sci. Paper No. 323, Colorado State University, Ft. Collins CO, 121 pp.
- Gray, W. M., 1992: Tropical cyclone formation and intensity change. *ICSU/WMO International Symposium on Tropical Cyclone Disasters*, Beijing, 19 pp.
- Guymer, L., 1978: Operational application of satellite imagery to synoptic analysis in the Southern Hemisphere. Tech. Rep. No. 26, Bureau of Meteorology, Melbourne, Australia, 87 pp.
- Haltiner, G. J., and R. T. Williams, 1980: *Numerical Prediction and Dynamic Meteorology*, Second Edition. John Wiley and Sons, 477 pp.
- Hardy, R. L., 1971: Multiquadric equations of topography and other irregular surfaces. *J. Geophys. Res.*, **76**, 1905-1915.

- Hardy, R. L., 1990: Theory and applications of the multiquadric-biharmonic method. *Computers Math. Applic.*, **19**, 163-208.
- Harr, P. A., and R. L. Elsberry, 1993: Variability of tropical cyclone track characteristics and large-scale circulation regimes over the western Pacific Ocean. Preprints, *20th Conference on Hurricanes and Tropical Meteorology*, San Antonio TX, Amer. Meteor. Soc.
- Harr, P. A., T. Neta, and R. L. Elsberry, 1991: ONR Tropical Cyclone Motion Research Initiative: Data users guide to observations. Technical Report NPS-MR-91-002, Naval Postgraduate School, Monterey CA 93943, 124 pp.
- Harr, P. A., R. L. Elsberry, and J. C. Chan, 1996: Transformation of a large monsoon depression to a tropical storm during TCM-93. *Mon. Wea. Rev.*, **124**, 2625-2643.
- Hawkins, H. F., and D. T. Rubsam, 1968: Hurricane Hilda, 1964: II, The structure and budgets of the hurricane on October 1, 1964. *Mon. Wea. Rev.*, **99**, 427-434.
- Hess, S. L., 1979: *Introduction to Theoretical Meteorology*. Reprint Edition. Robert E. Krieger Publishing Co., Inc., 362 pp.
- Hibbard, W. L. and D. A. Santek, 1989: Visualizing large data sets in the earth sciences. *IEEE Computer*, **22**, 53-57.
- Hirschberg, P. A., M. C. Parke, C. H. Wash, and M. Mickelinc, 1997: The usefulness of MSU3 analyses as a forecasting aid: A statistical study. *Wea. Forecasting*, **12**, 324-346.
- Hoke, J. E., N. A. Phillips, G. J. DiMego, J. J. Tuccillo, and J. G. Sela, 1989: The regional analysis and forecast system of the National Meteorological Center. *Wea. Forecasting*, **4**, 323-334.
- Holland, G. J., 1983: Angular momentum transports in tropical cyclones. *Quart. J. Roy. Meteor. Soc.*, **109**, 187-209.
- Holland, G. J., 1987: Mature structure and structure change. Chap. 2, *A Global View of Tropical Cyclones*, R. L. Elsberry, Ed., Office of Naval Research, 13-52.
- Holland, G. J., 1997: The maximum potential intensity of tropical cyclones. *J. Atmos. Sci.*, **54**, 2519-2541.
- Holland, G. J., and R. T. Merrill, 1984: On the dynamics of tropical cyclone structure changes. *Quart. J. Roy. Meteor. Soc.*, **110**, 723-745.

- Holland, G. J., and Y. Wang, 1998: On the relative roles of lateral interactions and thermodynamics in tropical cyclone intensification. Preprints, *Symposium on Tropical Cyclone Intensity Change*, Phoenix, AZ, Amer. Meteor. Soc., 171-175.
- Holton, J. R., 1979: *An Introduction to Dynamic Meteorology*. Second Edition. Academic Press, 391 pp.
- Jancic, Z. I., 1990: The step-mountain coordinate: Physical package. *Mon. Wea. Rev.*, **118**, 1429-1443.
- JTWC, 1990: Annual tropical cyclone report. Joint Typhoon Warning Center, Guam, Mariana Islands.
- Julian, P. R., 1991: RADCOR91--The new radiosonde radiation error correction procedure. Office Note No. 374, National Meteorological Center, Washington D.C., 36 pp.
- Klein, P. M., 1997: Extratropical transition of western North Pacific tropical cyclones. M.S. Thesis, Naval Postgraduate School, Monterey, CA 93943, 101 pp.
- Landsea, C. S., J. Kaplan, and M. DeMaria, 1998: The differing roles of the large-scale environment in the intensity change of recent Atlantic hurricanes. Preprints, *Symposium on Tropical Cyclone Intensity Change*, Phoenix, AZ, Amer. Meteor. Soc., 113-114.
- Levitus, S., 1982: *Climatological Atlas of the World Ocean*. NOAA Prof. Paper 13, 173 pp. [Available from the U.S. Government Printing Office, Washington D.C. 20402]
- May, D. A., M. M. Parmeter, D. S. Olszewski, and B. D. McKenzie, 1998: Operational processing of satellite sea surface temperature retrievals at the Naval Oceanographic Office. *Bull. Amer. Meteor. Soc.*, **79**, 397-407.
- Merrill, R. T., 1987: An experiment in statistical prediction of tropical cyclone intensity change. NOAA Tech. Memo. NWS NHC-22, 21 pp.
- Merrill, R. T., 1988: Environmental influences on hurricane intensification. *J. Atmos. Sci.*, **45**, 1678-1687.
- Merrill, R. T., 1989: On generalizing the theory of tropical cyclones to include environmental influences. Preprints, *18th Conf. on Hurricanes and Tropical Meteorology*, San Diego, CA, Amer. Meteor. Soc., J19-J20.

- Merrill, R. T., and C. S. Velden, 1996: A three-dimensional analysis of the outflow layer of Supertyphoon Flo (1990). *Mon. Wea. Rev.*, **124**, 47-63.
- Mesinger, F., 1984: A blocking technique for representation of mountains in atmospheric models. *Riv. Meteor. Aeronautica*, **44**, 195-202.
- Miller, B. I., 1958: On the maximum intensity of hurricanes. *J. Meteor.*, **15**, 184-195.
- Molinari, J., 1998: Hurricane-trough interactions: How do they work? Preprints, *Symposium on Tropical Cyclone Intensity Change*, Phoenix, AZ, Amer. Meteor. Soc., 169-170.
- Molinari, J., and S. Skubis, 1985: Evolution of the surface wind field in an intensifying tropical cyclone. *J. Atmos. Sci.*, **42**, 2865-2879.
- Molinari, J., and D. Vollaro, 1989: External influences on hurricane intensity. Part I: Outflow layer eddy momentum fluxes. *J. Atmos. Sci.*, **46**, 1093-1105.
- Molinari, J., and D. Vollaro, 1990: External influences on hurricane intensity. Part II: Vertical structure and response of the hurricane vortex. *J. Atmos. Sci.*, **47**, 1902-1918.
- Molinari, J., Vollaro, D. and S. Skubis, 1993: Application of the Eliassen balanced model to real-data tropical cyclones. *Mon. Wea. Rev.*, **121**, 2409-2419.
- Nelson, C. A., and W. T. Aldinger, 1992: An overview of Fleet Numerical Oceanography Center operations and products. *Wea. Forecasting*, **7**, 204-219.
- Nuss, W. A., and D. W. Titley, 1994: Use of multiquadric interpolation for meteorological objective analysis. *Mon. Wea. Rev.*, **122**, 1611-1631.
- O'Brien, J. J., 1970: Alternative solutions to the classical vertical velocity problem. *J. Appl. Meteor.*, **9**, 197-293.
- Palmén, E., 1948: On the formation and structure of tropical hurricanes. *Geophysica*, **3**, 26-38.
- Peterson, R. A., G. J. DiMego, J. E. Hoke, K. E. Mitchell, J. P. Gerrity, R. L. Wobus, H.-M. H. Juang, and M. J. Pecnick, 1991: Changes to NMC's regional analysis and forecasting system. *Wea. Forecasting*, **6**, 133-141.

- Pfeffer, R. L., and M. Challa, 1981: A numerical study of the role of eddy fluxes of momentum in the development of Atlantic hurricanes. *J. Atmos. Sci.*, **38**, 2393-2398.
- Pfeffer, R. L., and M. Challa, 1991: Formation of Atlantic hurricanes from cloud clusters and depressions. Preprints, *19th Conf. on Hurricanes and Tropical Meteorology*, Miami, FL, Amer. Meteor. Soc., 214-216.
- Riehl, H., 1950: A model of hurricane formation. *J. Appl. Phys.*, **21**, 917-925.
- Rogers, E., S. J. Lord, D. G. Deaven and G. J. DiMego, 1992: Data assimilation and forecasting for the Tropical Cyclone Motion experiment at the National Meteorological Center. General Sciences Corp., Laurel MD, 22 pp.
- Rosmond, T. E., 1992: The design and testing of the Navy operational global atmospheric prediction system. *Wea. Forecasting*, **7**, 262-272.
- Rucker, J. H., 1992: Upper-tropospheric forcing of the intensification rates of tropical cyclones Flo and Ed based on TCM-90 observations. M.S. Thesis, Naval Postgraduate School, Monterey CA 93943, 201 pp.
- Sadler, J. C., 1978: Midseason typhoon development and intensity changes and the tropical upper-tropospheric trough. *Mon. Wea. Rev.*, **106**, 1137-1152.
- Sanders, J. F., 1984: Framework for a national mitigation program in the Philippines. Science Applications Inter. Corp., Monterey CA, 40 pp.
- Sawyer, J. S., 1947: Notes on the theory of tropical cyclones. *Quart. J. Roy. Meteor. Soc.*, **73**, 101-126.
- Schiavone, J. A., and T. V. Papathomas, 1990: Visualizing meteorological data. *Bull. Amer. Meteor. Soc.*, **71**, 1012-1020.
- Schmidlin, F. J., 1991: Derivation and application of temperature corrections for the United States radiosonde. Preprints, *Seventh Symp. Meteor. Observations and Instrumentation*, New Orleans, LA, Amer. Meteor. Soc., 227-231.
- Shapiro, L. J., and H. E. Willoughby, 1982: The response of balanced hurricanes to local sources of heat and momentum. *J. Atmos. Sci.*, **39**, 378-394.

- Shay, L. K., G. J. Goni, F. D. Marks, J. J. Cione, and P. G. Black, 1998: Role of warm ocean features on intensity change: Hurricane Opal. Preprints, *Symposium on Tropical Cyclone Intensity Change*, Phoenix, AZ, Amer. Meteor. Soc., 131-138.
- Simpson, R. H., and H. Riehl, 1958: Mid-tropospheric ventilation as a constraint on hurricane development and maintenance. *Proc. Tech. Conf. on Hurr.*, Miami Beach FL, Amer. Meteor. Soc., D4.1-D4.10.
- Simpson, R. H., N. Frank, D. Schideler, and H. M. Johnson, 1969: Atlantic tropical disturbances of 1966. *Mon. Wea. Rev.*, **97**, 240-255.
- Skubis, S., and J. Molinari, 1987: Angular momentum variation in a translating cyclone. *Quart. J. Roy. Meteor. Soc.*, **113**, 1041-1048.
- Southern, R. L., 1987: Tropical cyclone warning and mitigation systems Chap. 6, *A Global View of Tropical Cyclones*, R. L. Elsberry, Ed., Office of Naval Research, 147-185.
- Velden, C. S., C. M. Hayden, S. J. Nieman, W. P. Menzel, S. Wanzong, and J. S. Goerss, 1997: Upper-tropospheric winds derived from geostationary satellite water vapor observations. *Bull. Amer. Meteor. Soc.*, **78**, 173-195.
- Wahba, G., and J. Wendelberger, 1980: Some new mathematical methods for variational objective analysis using splines and cross validation. *Mon. Wea. Rev.*, **108**, 1122-1143.
- Warren, S. W., 1993: Ensemble forecasting techniques in medium range forecasting. M.S. Thesis, Naval Postgraduate School, Monterey, CA 93943, 111 pp.
- Willoughby, H. E., 1988: The dynamics of the tropical cyclone core. *Aust. Meteor. Mag.*, **36**, 183-191.
- Willoughby, H. E., 1990: Temporal changes of the primary circulation in tropical cyclones. *J. Atmos. Sci.*, **47**, 242-264.
- Willoughby, H. E., J. A. Clos, and, M. G. Shoreibah, 1982: Concentric eyewalls, secondary wind maxima, and the evolution of the hurricane vortex. *J. Atmos. Sci.*, **39**, 395-411.
- Zehr, R. M., 1992: Tropical cyclogenesis in the western North Pacific. NOAA Tech. Rep., NESDIS 61, Dept. of Commerce, Washington, D.C., 181 pp.

- Zehr, R. M., 1998: Vertical wind shear and tropical cyclone intensity. Preprints, *Symposium on Tropical Cyclone Intensity Change*, Phoenix, AZ, Amer. Meteor. Soc., 124-128.
- Zhong, S., and J. C. Doran, 1997: A study of the effects of spatially varying fluxes on cloud formation and boundary layer properties using data from the Southern Great Plains cloud and radiation testbed. *J. Climate*, **10**, 327-341.

INITIAL DISTRIBUTION LIST

1. Defense Technical Information Center 2
8735 John J. Kingman Rd. Ste 0944
Ft. Belvoir VA 22060-6218

2. Dudley Knox Library 2
Naval Postgraduate School
411 Dyer Rd
Monterey CA 93943-5101

3. Professor R. L. Elsberry (MR/Es) 1
Naval Postgraduate School
Monterey CA 93943

4. Professor C. H. Wash (MR/Wx) 1
Naval Postgraduate School
Monterey CA 93943

5. Professor W. A. Nuss (MR/Nu) 1
Naval Postgraduate School
Monterey CA 93943

6. Dr. Hugh E. Willoughby 1
HRD/AOML
4301 Rickenbacker Causeway
Miami FL 33149-1097

7. Dr. P. Harr (MR/Hp) 1
Naval Postgraduate School
Monterey CA 93943

8. Dr. L. Carr (MR/Cr) 1
Naval Postgraduate School
Monterey CA 93943

9. Ms. J. Sandidge 1
Code 7341
Remote Sensing Applications Branch
Naval Research Laboratory
Stennis Space Center MS 39529-5004

10. CDR David Titley 1
PSC 473, Box 528
FPO AP 96349-5555
11. Dr. R. Abbey 1
Office of Naval Research, Code 322
800 N. Quincy St.
Arlington VA 22217
12. Commanding Officer 1
Naval Pacific Meteorology and Oceanography Center
Box 113
Pearl Harbor HI 96860
13. Commanding Officer 1
Naval Pacific Meteorology and Oceanography Center West
PSC 498 Box 2
FPO AP 96536-0051

DUDLEY KNOX LIBRARY



3 2768 00347028 7